Fuel Cell Handbook
(Sixth Edition)

DOE/NETL-2002/1179

By
EG&G Technical Services, Inc.
Science Applications International Corporation

Under Contract No. DE-AM26-99FT40575

U.S. Department of Energy
Office of Fossil Energy
National Energy Technology Laboratory
P.O. Box 880
Morgantown, West Virginia 26507-0880

November 2002

DISCLAIMER

This report was prepared as an account of work sponsored by an agency of the United States Government. Neither the United States Government nor any agency thereof, nor any of their employees, makes any warranty, express or implied, or assumes any legal liability or responsibility for the accuracy, completeness, or usefulness of any information, apparatus, product, or process disclosed, or represents that its use would not infringe privately owned rights. Reference herein to any specific commercial product, process, or service by trade name, trademark, manufacturer, or otherwise does not necessarily constitute or imply its endorsement, recommendation, or favoring by the United States Government or any agency thereof. The views and opinions of authors expressed herein do not necessarily state or reflect those of the United States Government or any agency thereof.

Available to DOE and DOE contractors from the Office of Scientific and Technical Information, P.O. Box 62, 175 Oak Ridge Turnpike, Oak Ridge, TN 37831; prices available at (423) 576-8401, fax: (423) 576-5725, E-mail: reports@adonis.osti.gov

Available to the public from the National Technical Information Service, U.S. Department of Commerce, 5285 Port Royal Road, Springfield, VA 22161; phone orders accepted at (703) 487-4650.

TABLE OF CONTENTS

Section	Title	Page
1.	**TECHNOLOGY OVERVIEW**	**1-1**
1.1	FUEL CELL DESCRIPTION	1-1
1.2	CELL STACKING	1-7
1.3	FUEL CELL PLANT DESCRIPTION	1-8
1.4	CHARACTERISTICS	1-9
1.5	ADVANTAGES/DISADVANTAGES	1-11
1.6	APPLICATIONS, DEMONSTRATIONS, AND STATUS	1-13
1.6.1	Stationary Electric Power	1-13
1.6.2	Distributed Generation	1-22
1.6.3	Vehicle Motive Power	1-25
1.6.4	Space and Other Closed Environment Power	1-27
1.6.5	Fuel Cell Auxiliary Power Systems	1-27
1.6.6	Derivative Applications	1-36
1.7	REFERENCES	1-36
2.	**FUEL CELL PERFORMANCE**	**2-1**
2.1	GIBBS FREE ENERGY AND NERNST POTENTIAL	2-1
2.1.1	Ideal Performance	2-4
2.1.2	Cell Energy Balance	2-6
2.1.3	Cell Efficiency	2-7
2.1.4	Efficiency Comparison to Heat Engines	2-9
2.1.5	Actual Performance	2-9
2.1.6	Fuel Cell Performance Variables	2-14
2.2	COMPUTER MODELS	2-22
2.2.1	System Models	2-22
2.2.2	Mechanistic Models	2-24
2.3	REFERENCES	2-26
3.	**POLYMER ELECTROLYTE FUEL CELLS**	**3-1**
3.1	CELL COMPONENTS	3-1
3.1.1	State-of-the-Art Components	3-6
3.1.2	Development Components	3-11
3.2	PERFORMANCE	3-13
3.3	DIRECT METHANOL PROTON EXCHANGE FUEL CELL	3-16
3.4	REFERENCES	3-17
4.	**ALKALINE FUEL CELL**	**4-1**
4.1	CELL COMPONENTS	4-5
4.1.1	State-of-the-Art Components	4-5
4.1.2	Development Components	4-6
4.2	PERFORMANCE	4-7
4.2.1	Effect of Pressure	4-8
4.2.2	Effect of Temperature	4-9
4.2.3	Effect of Impurities	4-11
4.2.4	Effects of Current Density	4-12
4.2.5	Effects of Cell Life	4-14
4.3	SUMMARY OF EQUATIONS FOR AFC	4-14

4.4 REFERENCES 4-16

5. PHOSPHORIC ACID FUEL CELL 5-1

5.1 CELL COMPONENTS 5-2
5.1.1 State-of-the-Art Components 5-2
5.1.2 Development Components 5-6
5.2 PERFORMANCE 5-11
5.2.1 Effect of Pressure 5-12
5.2.2 Effect of Temperature 5-13
5.2.3 Effect of Reactant Gas Composition and Utilization 5-14
5.2.4 Effect of Impurities 5-16
5.2.5 Effects of Current Density 5-19
5.2.6 Effects of Cell Life 5-20
5.3 SUMMARY OF EQUATIONS FOR PAFC 5-21
5.4 REFERENCES 5-22

6. MOLTEN CARBONATE FUEL CELL 6-1

6.1 CELL COMPONENTS 6-4
6.1.1 State-of-the-Art Componments 6-4
6.1.2 Development Components 6-9
6.2 PERFORMANCE 6-13
6.2.1 Effect of Pressure 6-15
6.2.2 Effect of Temperature 6-19
6.2.3 Effect of Reactant Gas Composition and Utilization 6-21
6.2.4 Effect of Impurities 6-25
6.2.5 Effects of Current Density 6-30
6.2.6 Effects of Cell Life 6-30
6.2.7 Internal Reforming 6-30
6.3 SUMMARY OF EQUATIONS FOR MCFC 6-34
6.4 REFERENCES 6-38

7. SOLID OXIDE FUEL CELL 7-1

7.1 CELL COMPONENTS 7-1
7.1.1 State-of-the-Art Components 7-1
7.1.2 Cell Configuration Options 7-12
7.1.3 Development Status 7-17
7.2 PERFORMANCE 7-25
7.2.1 Effect of Pressure 7-26
7.2.2 Effect of Temperature 7-27
7.2.3 Effect of Reactant Gas Composition and Utilization 7-29
7.2.4 Effect of Impurities 7-32
7.2.5 Effect of Current Density 7-34
7.2.6 Effect of Cell Life 7-34
7.3 SUMMARY OF EQUATIONS FOR SOFC 7-35
7.4 REFERENCES 7-35

8. FUEL CELL SYSTEMS 8-1

8.1 SYSTEM PROCESSES 8-2
8.1.1 Fuel Processing 8-2
8.2 POWER CONDITIONING 8-27
8.2.1 Introduction to Fuel Cell Power Conditioning Systems 8-27

8.2.2 Fuel Cell Power Conversion for Supplying a Dedicated / Stand-Alone Load . 8-60
8.2.3 Fuel Cell Power Conversion for Supplying Backup Power (UPS) to a Load Connected to a Local Utility ... 8-72
8.2.4 Fuel Cell Power Conversion for Supplying a Load Operating in Parallel With the Local Utility ... 8-79
8.2.5 Fuel Cell Power Conversion for Connecting Directly to the Local Utility ... 8-80
8.2.6 Power Conditioners for Automotive Fuel Cells ... 8-82
8.2.7 Power Conversion Architectures for a Fuel Cell Turbine Hybrid Interfaced to Local Utility ... 8-84
8.2.8 Fuel Cell Ripple Current ... 8-87
8.2.9 System Issues: Power Conversion Size, Cost ... 8-88
8.3 REFERENCES (SECTIONS 8.1 AND 8.2) ... 8-89
8.4 SYSTEM OPTIMIZATION ... 8-93
8.4.1 Pressure ... 8-93
8.4.2 Temperature ... 8-95
8.4.3 Utilization ... 8-96
8.4.4 Heat Recovery ... 8-97
8.4.5 Miscellaneous ... 8-98
8.4.6 Concluding Remarks on System Optimization ... 8-98
8.5 FUEL CELL SYSTEM DESIGNS ... 8-99
8.5.1 Natural Gas Fueled PEFC System ... 8-99
8.5.2 Natural Gas Fueled PAFC System ... 8-100
8.5.3 Natural Gas Fueled Internally Reformed MCFC System ... 8-103
8.5.4 Natural Gas Fueled Pressurized SOFC System ... 8-104
8.5.5 Natural Gas Fueled Multi-Stage Solid State Power Plant System ... 8-109
8.5.6 Coal Fueled SOFC System (Vision 21) ... 8-113
8.5.7 Power Generation by Combined Fuel Cell and Gas Turbine System ... 8-116
8.5.8 Heat and Fuel Recovery Cycles ... 8-117
8.6 FUEL CELL NETWORKS ... 8-129
8.6.1 Molten Carbonate Fuel Cell Networks: Principles, Analysis and Performance ... 8-129
8.6.2 MCFC Network ... 8-133
8.6.3 Recycle Scheme ... 8-133
8.6.4 Reactant Conditioning Between Stacks in Series ... 8-133
8.6.5 Higher Total Reactant Utilization ... 8-134
8.6.6 Disadvantages of MCFC Networks ... 8-135
8.6.7 Comparison of Performance ... 8-135
8.6.8 Conclusions ... 8-136
8.7 HYBRIDS ... 8-136
8.7.1 Technology ... 8-136
8.7.2 Projects ... 8-138
8.7.3 World's First Hybrid Project ... 8-140
8.7.4 Hybrid Electric Vehicles (HEV) ... 8-140
8.8 REFERENCES ... 8-142

9. SAMPLE CALCULATIONS ... 9-1

9.1 UNIT OPERATIONS ... 9-1
9.1.1 Fuel Cell Calculations ... 9-1
9.1.2 Fuel Processing Calculations ... 9-13
9.1.3 Power Conditioners ... 9-16
9.1.4 Others ... 9-16

9.2 SYSTEM ISSUES 9-17
9.2.1 Efficiency Calculations 9-17
9.2.2 Thermodynamic Considerations 9-19
9.3 SUPPORTING CALCULATIONS 9-22
9.4 COST CALCULATIONS 9-26
9.4.1 Cost of Electricity 9-26
9.4.2 Capital Cost Development 9-27
9.5 COMMON CONVERSION FACTORS 9-28
9.6 AUTOMOTIVE DESIGN CALCULATIONS 9-29
9.7 REFERENCES 9-30

10. APPENDIX 10-1

10.1 EQUILIBRIUM CONSTANTS 10-1
10.2 CONTAMINANTS FROM COAL GASIFICATION 10-2
10.3 SELECTED MAJOR FUEL CELL REFERENCES, 1993 TO PRESENT 10-4
10.4 LIST OF SYMBOLS 10-11
10.5 FUEL CELL RELATED CODES AND STANDARDS 10-14
10.5.1 Introduction 10-14
10.5.2 Organizations 10-15
10.5.3 Codes & Standards 10-17
10.5.4 Codes and Standards for Fuel Cell Manufacturers 10-18
10.5.5 Codes and Standards for the Installation of Fuel Cells 10-19
10.5.6 Codes and Standards for Fuel Cell Vehicles 10-19
10.5.7 Application Permits 10-20
10.5.8 References 10-21
10.6 FUEL CELL FIELD SITE DATA 10-21
10.6.1 Worldwide Sites 10-21
10.6.2 DoD Field Sites 10-23
10.6.3 IFC Field Units 10-24
10.6.4 FuelCell Energy 10-24
10.6.5 Siemens Westinghouse 10-24
10.7 HYDROGEN 10-32
10.7.1 Introduction 10-32
10.7.2 Hydrogen Production 10-33
10.7.3 DOE's Hydrogen Research 10-35
10.7.4 Hydrogen Storage 10-36
10.7.5 Barriers 10-36
10.8 THE OFFICE OF ENERGY EFFICIENCY AND RENEWABLE ENERGY WORK IN FUEL CELLS 10-37
10.8.1 The Office of Industrial Technologies 10-38
10.8.2 The Office of Transportation Technologies 10-39
10.8.3 The Office of Power Technologies 10-44
10.8.4 Office of Building Technology, State and Community Programs 10-46
10.9 RARE EARTH MINERALS 10-47
10.9.1 Introduction 10-47
10.9.2 Demand 10-49
10.10 REFERENCES 10-49

INDEX 11-1

LIST OF FIGURES

Figure	Title	Page
Figure 1-1	Schematic of an Individual Fuel Cell	1-1
Figure 1-2	Simplified Fuel Cell Schematic	1-2
Figure 1-3	External Reforming and Internal Reforming MCFC System Comparison	1-6
Figure 1-4	Expanded View of a Basic Fuel Cell Repeated Unit in a Fuel Cell Stack	1-8
Figure 1-5	Fuel Cell Power Plant Major Processes	1-9
Figure 1-6	Relative Emissions of PAFC Fuel Cell Power Plants Compared to Stringent Los Angeles Basin Requirements	1-10
Figure 1-7	PC-25 Fuel Cell	1-14
Figure 1-8	Combining the SOFC with a Gas Turbine Engine to Improve Efficiency	1-19
Figure 1-9	Overview of Fuel Cell Activities Aimed at APU Applications	1-28
Figure 1-10	Overview of APU Applications	1-28
Figure 1-11	Overview of typical system requirements	1-29
Figure 1-12	Stage of development for fuel cells for APU applications	1-30
Figure 1-13	Overview of subsystems and components for SOFC and PEFC systems	1-32
Figure 1-14	Simplified System process flow diagram of pre-reformer/SOFC system	1-33
Figure 1-15	Multilevel system modeling approach.	1-34
Figure 1-16	Projected cost structure of a 5kWnet APU SOFC system. Gasoline fueled POX reformer, Fuel cell operating at 300mW/cm^2, 0.7 V, 90 % fuel utilization, 500,000 units per year production volume	1-36
Figure 2-1	H_2/O_2 Fuel Cell Ideal Potential as a Function of Temperature	2-5
Figure 2-2	Ideal and Actual Fuel Cell Voltage/Current Characteristic	2-9
Figure 2-3	Example of a Tafel Plot	2-10
Figure 2-4	Contribution to Polarization of Anode and Cathode	2-14
Figure 2-5	Flexibility of Operating Points According to Cell Parameters	2-15
Figure 2-6	Voltage/Power Relationship	2-16
Figure 2-7	Dependence of the Initial Operating Cell Voltage of Typical Fuel Cells on Temperature	2-18
Figure 2-8	The Variation in the Reversible Cell Voltage as a Function of Reactant Utilization	2-20
Figure 3-1a	Schematic of Representative PEFC	3-2
Figure 3-1b	Single Cell Structure of Representative PEFC	3-2
Figure 3-2	PEFC Schematic	3-7
Figure 3-3	Polarization Curves for 3M 7 Layer MEA	3-8
Figure 3-4	Endurance Test Results for Gore Primea 56 MEA at Three Current Densities	3-9
Figure 3-5	Multi-Cell Stack Performance on Dow Membrane	3-11
Figure 3-6	Effect on PEFC Performances of Bleeding Oxygen into the Anode Compartment	3-13
Figure 3-7	Evolutionary Changes in PEFCs Performance (a) H_2/O_2, (b) H_2/Air, (c) Reformate Fuel/Air, (d) H_2/unkown	3-14
Figure 3-8	Influence of O_2 Pressure on PEFCs Performance	3-15
Figure 3-9	Cell Performance with Carbon Monoxide in Reformed Fuel	3-16
Figure 3-10	Single Cell Direct Methanol Fuel Cell Data	3-17

Figure 4-1 Principles of Operation of H_2/O_2 Alkaline Fuel Cell, Immobilized Electrolyte 4-4
Figure 4-2 Principles of Operation of H_2/Air Alkaline Fuel Cell, Circulating Electrolyte 4-4
Figure 4-3 Evolutionary Changes in the Performance of AFCs 4-8
Figure 4-4 Reversible Voltage of the Hydrogen-Oxygen Cell 4-9
Figure 4-5 Influence of Temperature on O_2, (air) Reduction in 12 N KOH. 4-10
Figure 4-6 Influence of Temperature on the AFC Cell Voltage 4-11
Figure 4-7 Degradation in AFC Electrode Potential with CO_2 Containing and CO_2 Free Air 4-12
Figure 4-8 iR-Free Electrode Performance with O_2 and Air in 9 N KOH at 55-60°C. 4-13
Figure 4-9 iR Free Electrode Performance with O_2 and Air in 12N KOH at 65°C. 4-14
Figure 4-10 Reference for Alkaline Cell Performance 4-15
Figure 5-1 Principles of Operation of Phosphoric Acid Fuel Cell 5-2
Figure 5-2 Improvement in the Performance of H_2-Rich Fuel/Air PAFCs 5-6
Figure 5-3 Advanced Water-Cooled PAFC Performance 5-8
Figure 5-4 Effect of Temperature: Ultra-High Surface Area Pt Catalyst. Fuel: H_2, H_2 + 200 ppm H_2S and Simulated Coal Gas 5-14
Figure 5-5 Polarization at Cathode (0.52 mg Pt/cm^2) as a Function of O_2 Utilization, which is Increased by Decreasing the Flow Rate of the Oxidant at Atmospheric Pressure 100% H_3PO_4, 191°C, 300 mA/cm^2, 1 atm. 5-15
Figure 5-6 Influence of CO and Fuel Gas Composition on the Performance of Pt Anodes in 100% H_3PO_4 at 180°C. 10% Pt Supported on Vulcan XC-72, 0.5 mg Pt/cm^2. Dew Point, 57°. Curve 1, 100% H_2; Curves 2-6, 70% H_2 and CO_2/CO Contents (mol%) Specified 5-18
Figure 5-7 Effect of H_2S Concentration: Ultra-High Surface Area Pt Catalyst 5-19
Figure 5-8 Reference Performances at 8.2 atm and Ambient Pressure. Cells from Full Size Power Plant 5-22
Figure 6-1 Principals of Operation of Molten Carbonate Fuel Cells 6-2
Figure 6-2 Dynamic Equilibrium in Porous MCFC Cell Elements 6-4
Figure 6-3 Progress in the Generic Performance of MCFCs on Reformate Gas and Air 6-6
Figure 6-4 Effect of Oxidant Gas Composition on MCFC Cathode Performance at 650°C 6-14
Figure 6-5 Voltage and Power Output of a 1.0/m^2 19 cell MCFC Stack after 960 Hours at 965°C and 1 atm, Fuel Utilization, 75% 6-15
Figure 6-6 Influence of Cell Pressure on the Performance of a 70.5 cm^2 MCFC at 650°C 6-18
Figure 6-7 Influence of Pressure on Voltage Gain 6-19
Figure 6-8 Effect of CO_2/O_2 Ratio on Cathode Performance in an MCFC, Oxygen Pressure is 0.15 atm 6-22
Figure 6-9 Influence of Reactant Gas Utilization on the Average Cell Voltage of an MCFC Stack 6-23
Figure 6-10 Dependence of Cell Voltage on Fuel Utilization 6-25

Figure 6-11 Influence of 5 ppm H_2S on the Performance of a Bench Scale MCFC (10 cm x 10 cm) at 650°C, Fuel Gas (10% H_2/5% CO_2/10% H_2O/75% He) at 25% H_2 Utilization 6-29
Figure 6-12 IIR/DIR Operating Concept, Molten Carbonate Fuel Cell Design 6-31
Figure 6-13 CH_4 Conversion as a Function of Fuel Utilization in a DIR Fuel Cell 6-33
Figure 6-14 Voltage Current Characteristics of a 3kW, Five Cell DIR Stack with 5,016 cm^2 Cells Operating on 80/20% H_2/CO_2 and Methane 6-33
Figure 6-15 Performance Data of a 0.37m^2 2 kW Internally Reformed MCFC Stack at 650°C and 1 atm 6-34
Figure 6-16 Average Cell Voltage of a 0.37m^2 2 kW Internally Reformed MCFC Stack at 650°C and 1 atm. Fuel, 100% CH_4, Oxidant, 12% CO_2/9% O_2/77% N_2 6-35
Figure 6-17 Model Predicted and Constant Flow Polarization Data Comparison 6-37
Figure 7-1 Single Cell Structure-Electrolyte and Anode Supported Cell 7-2
Figure 7-2 Thermal Expansion Behavior of Stack Materials 7-3
Figure 7-3 Electrolyte Conductivity as a Function of Temperature 7-4
Figure 7-4 PSOFC with a Cross-Flow Stack Configuration 7-5
Figure 7-5 Planar Solid Oxide Fuel Cell Stack 7-6
Figure 7-6 Stability of Metal Oxides in Stainless Steels 7-6
Figure 7-7 Observed Leak Rates for Advanced and "Standard" Mica Seals 7-9
Figure 7-8 Tubular and Planar Cell Configurations 7-11
Figure 7-9 Cross Section of a Tubular Cell 7-11
Figure 7-10 Gas Manifold Design for a Tubular SOFC 7-16
Figure 7-11 Cell-to-Cell Connections in a Tubular SOFC 7-16
Figure 7-12 Single Cell Performance of LSGM Electrolyte 7-20
Figure 7-13 Effect of Oxidant Composition on a High Performance Anode-Supported Cell 7-21
Figure 7-14 Performance of PSOFC at Reduced Temperatures 7-23
Figure 7-15 Projected Performance of Seal-less Planar Design with Current Seal-less Cylindrical Design 7-24
Figure 7-16 Planar Seal-less Design 7-24
Figure 7-17 Effect of Pressure on AES Cell Performance at 1,000°C 7-27
Figure 7-18 Two-Cell Stack Performance with 67% H_2 + 22% CO + 11% H_2O/Air 7-28
Figure 7-19 Two Cell Stack Performance with 97% H_2 and 3% H_2O/Air 7-29
Figure 7-20 Cell Performance at 1,000°C with Pure Oxygen (o) and Air (Δ) Both at 25% Utilization 7-30
Figure 7-21 Influence of Gas Composition of the Theoretical Open-Circuit Potential of SOFC at 1,000°C 7-31
Figure 7-22 Variation in Cell Voltage as a Function of Fuel Utilization and Temperature 7-32
Figure 7-23 SOFC Performance at 1,000°C and 350 mA/cm^2, 85% Fuel Utilization and 25% Air Utilization 7-33
Figure 7-24 Voltage-Current Characteristics of an AES Cell 7-34
Figure 8-1 A Rudimentary Fuel Cell Power System Schematic 8-1
Figure 8-2 Representative Fuel Processing Steps & Temperatures 8-3
Figure 8-3 "Well-To-Wheel" Efficiency For Various Vehicle Scenarios 8-9
Figure 8-4 Carbon Deposition Mapping of Methane 8-24
Figure 8-5 Carbon Deposition Mapping of Octane 8-24

Figure 8-6 Block diagram of a fuel cell power system 8-28
Figure 8-7 Block Diagram of a typical Fuel Cell Power Conditioning Stage 8-29
Figure 8-8a Typical fuel cell voltage / current characteristics 8-29
Figure 8-8b Fuel cell, power vs. current curve 8-30
Figure 8-9 Diode symbol and volt-ampere characteristics 8-31
Figure 8-10 Thyristor symbol and volt-ampere characteristics 8-32
Figure 8-11a Power MOSFET symbol, (b) Normalized volt-ampere characteristics 8-33
Figure 8-12 Silicon cross-section of an IGBT with its equivalent circuit and symbol 8-34
Figure 8-13 Preferred application of IGBTs and MOSFETs 8-34
Figure 8-14a A 4.5kV, 3kA IGCT and the gate drive unit. 8-36
Figure 8-14b A 30MW Medium voltage power management system and the 9MVA IGCT power electronic building block (51) 8-36
Figure 8-15 Single switch boost converter schematic 8-37
Figure 8-16 Boost converter states 8-38
Figure 8-17 Idealized boost converter waveforms 8-38
Figure 8-18 Voltage gain as a function of duty cycle. 8-39
Figure 8-19 Closed loop control 8-40
Figure 8-20 Current waveform. 8-41
Figure 8-21a Push-pull DC-DC Converter 8-42
Figure 8-21b Push-pull DC-DC converter with voltage doubling center-tapped DC output 8-43
Figure 8-22a Flyback current fed push-pull topology. Clamp diode D_3 is connected to the output 8-44
Figure 8-22b Flyback current fed push-pull topology. Clamp diode D_3 is connected to the input 8-44
Figure 8-23a Full bridge DC to DC Converter 8-45
Figure 8-23b A Buck current-fed full bridge DC to DC converter 8-45
Figure 8-24a Inverter block diagram 8-46
Figure 8-24b Basic half bridge PWM inverter 8-46
Figure 8-24 Single inverter basic operation 8-47
Figure 8-25 Pulse width modulation 8-48
Figure 8-26a Single Phase full bridge DC to AC Inverter 8-50
Figure 8-26b 8-50
Figure 8-26c 8-50
Figure 8-26d Full bridge inverter output voltage V_{AB} and its frequency spectrum. 8-51
Figure 8-27 Dual output voltage inverter with four switches 8-52
Figure 8-28a Dual voltage inverter output voltage & current on phase V_{An} for linear load 8-53
Figure 8-28b Dual voltage inverter output voltage & current on phase V_{An} for nonlinear load 8-53
Figure 8-29a Six switch dual output voltage inverter topology 8-54
Figure 8-29b Output voltage V_{an} 8-54
Figure 8-29c Filtered output voltage V_{an} and V_{bn} 8-54
Figure 8-30 Three phase PWM signal generation 8-56
Figure 8-31a Three phase inverter supplying a three phase R-L load. 8-57
Figure 8-31b Three phase inverter waveforms 8-57
Figure 8-31c Dc-link current I_{dc} 8-57
Figure 8-31d Frequency spectrum of I_{dc} 8-57

Figure 8-32a Three phase 4-wire DC to AC Inverter topology with a center-tapped dc-link 8-58
Figure 8-32b Three phase 4-wire DC to AC Inverter topology with 8-IGBT devices 8-58
Figure 8-33a Circuit topology of neutral point clamped (NPC) inverter topology 8-59
Figure 8-33b Phase "a" to dc-link midpoint "o" voltage 8-60
Figure 8-33c NPC Inverter line to line output voltage (V_{AB}) after the L-C filter 8-60
Figure 8-34a Block diagram of a typical fuel cell powered unit for supplying a load 8-62
Figure 8-34b Block diagram of the power conditioning stage with line frequency transformer 8-62
Figure 8-34c Circuit topology of the power conditioning stage with line frequency transformer 8-62
Figure 8-35a Block diagram of the power conditioning stage with high frequency isolation transformer within the DC-DC converter stage 8-63
Figure 8-35b Circuit topology of the power conditioning stage with high frequency isolation transformer within the DC-DC converter stage 8-63
Figure 8-36a Block diagram of the power conditioning scheme with fewer power conversion stages in series path of the power flow 8-63
Figure 8-36b Circuit topology of the power conditioning scheme with fewer power conversion stages in series path of the power flow 8-64
Figure 8-36c Fuel cell power conditioner control system for powering dedicated loads 8-64
Figure 8-37 Motorola SG3525A Control chip for push-pull DC-DC converter stage 8-67
Figure 8-38 DC-AC Inverter Output Filter 8-69
Figure 8-39 Equivalent Circuit for a Non-Linear Load 8-70
Figure 8-40a Texas A&M Inverter operating on DOE NETL Fuel Cell on August 14, 2001 8-71
Figure 8-40b Inverter output voltage waveform when running off the fuel cell at NETL on August 14, 2001 8-71
Figure 8-40c Inverter output waveforms (voltage & current) when supplying 8 00W/phase. Both Phase-A and Phase-B were loaded equally. 8-72
Figure 8-40d Inverter output waveforms with Phase A on 800W/phase and Phase B on 150W switching power supply load. 8-72
Figure 8-40e Inverter output waveforms (voltage & current) when a step change in load was applied from 360W to 610W on Phase A 8-72
Figure 8-40f Inverter output waveforms (voltage & current) when a step change in load was applied from 610W to 360W on Phase A. 8-72
Figure 8-41 One line diagram of a modular fuel cell power conversion system for supplying backup power (UPS) to a load connected to a local utility 8-74
Figure 8-42 Modular power conditioning circuit topology employing two fuel cell power sources to supply a load via a line frequency isolation transformer 8-74
Figure 8-43 Modular power conditioning circuit topology employing two fuel cell power sources using a higher voltage (400V) dc-link 8-75
Figure 8-44 Fuel cell supplying a load parallel with the utility 8-80
Figure 8-45 Fuel cell power conditioner control system for supplying power to the utility 8-81
Figure 8-46 A typical fuel cell vehicle system 8-82
Figure 8-47 Power conditioning unit for fuel cell hybrid vehicle 8-83

Figure 8-48 Fuel cell power conditioner control system 8-84
Figure 8-49 Power conditioning architecture for the 250kW fuel cell turbine hybrid system 8-85
Figure 8-50 Alternative power conditioning architecture for the fuel cell turbine hybrid system with shared dc-link 8-86
Figure 8-51 Possible medium voltage power conditioning topology for megawatt range hybrid fuel cell systems 8-87
Figure 8-52 Representative cost of power conditioning as a function of power and dc-link voltage 8-89
Figure 8-53 Optimization Flexibility in a Fuel Cell Power System 8-94
Figure 8-54 Natural Gas Fueled PEFC Power Plant 8-99
Figure 8-55 Natural Gas fueled PAFC Power System 8-101
Figure 8-56 Natural Gas Fueled MCFC Power System 8-103
Figure 8-57 Schematic for a 4.5 MW Pressurized SOFC 8-105
Figure 8-58 Schematic for a 4 MW Solid State Fuel Cell System 8-110
Figure 8-59 Schematic for a 500 MW Class Coal Fueled Pressurized SOFC 8-113
Figure 8-60 Regenerative Brayton Cycle Fuel Cell Power System 8-118
Figure 8-61 Combined Brayton-Rankine Cycle Fuel Cell Power Generation System 8-121
Figure 8-62 Combined Brayton-Rankine Cycle Thermodynamics 8-122
Figure 8-63 T-Q Plot for Heat Recovery Steam Generator 8-123
Figure 8-64 Fuel Cell Rankine Cycle Arrangement 8-124
Figure 8-65 T-Q Plot of Heat Recovery from Hot Exhaust Gas 8-125
Figure 8-66 MCFC System Designs 8-130
Figure 8-67 Stacks in Series Approach Reversibility 8-131
Figure 8-68 MCFC Network 8-134
Figure 8-69 Estimated performance of Power Generation Systems 8-137
Figure 8-70 Diagram of a Proposed Siemens-Westinghouse Hybrid System 8-138
Figure 10-1 Equilibrium Constants (Partial Pressures in MPa) for (a) Water Gas Shift, (b) Methane Formation, (c) Carbon Deposition (Boudouard Reaction), and (d) Methane Decomposition 10-2

LIST OF TABLES AND EXAMPLES

Table	Title	Page
Table 1-1	Summary of Major Differences of the Fuel Cell Types	1-5
Table 1-2	Summary of Major Fuel Constituents Impact on PEFC, AFC, PAFC, MCFC, and SOFC	1-11
Table 1-3	Attributes of Selected Distributed Generation Systems	1-22
Table 2-1	Electrochemical Reactions in Fuel Cells	2-4
Table 2-2	Fuel Cell Reactions and the Corresponding Nernst Equations	2-4
Table 2-3	Ideal Voltage as a Function of Cell Temperature	2-6
Table 2-4	Outlet Gas Composition as a Function of Utilization in MCFC at 650°C	2-21
Table 5-1	Evolution of Cell Component Technology for Phosphoric Acid Fuel Cells	5-4
Table 5-2	Advanced PAFC Performance	5-8
Table 5-3	Dependence of k(T) on Temperature	5-17
Table 6-1	Evolution of Cell Component Technology for Molten Carbonate Fuel Cells	6-5
Table 6-2	Amount in Mol% of Additives to Provide Optimum Performance	6-11
Table 6-3	Qualitative Tolerance Levels for Individual Contaminants in Isothermal Bench-Scale Carbonate Fuel Cells	6-13
Table 6-4	Equilibrium Composition of Fuel Gas and Reversible Cell Potential as a Function of Temperature	6-20
Table 6-5	Influence of Fuel Gas Composition on Reversible Anode Potential at 650°C	6-24
Table 6-6	Contaminants from Coal-Derived Fuel Gas and Their Potential Effect on MCFCs	6-26
Table 6-7	Gas Composition and Contaminants from Air-Blown Coal Gasifier After Hot Gas Cleanup, and Tolerance Limit of MCFCs to Contaminants	6-27
Table 7-1	Recent Technology Advances on Planar Cells and Potential Benefits	7-8
Table 7-2	Evolution of Cell Component Technology for Tubular Solid Oxide Fuel Cells	7-10
Table 7-3	Leading PSOFC Developers – World Wide	7-18
Table 7-4	U.S. Participants Involved in PSOFC Research and Development	7-19
Table 7-5	K Values for ΔV_T	7-28
Table 8-1	Calculated Thermoneutral Oxygen-to-Fuel Molar Ratios (x_o) and Maximum Theoretical Efficiencies (at x_o) for Common Fuels	8-16
Table 8-2	Typical Steam Reformed Natural Gas Reformate	8-17
Table 8-3	Typical Partial Oxidation Reformed Fuel Oil Reformate	8-19
Table 8-4	Typical Coal Gas Compositions for Selected Oxygen-Blown Gasifiers	8-21
Table 8-5	Comparison of high voltage devices	8-36
Table 8-6	Harmonics of v_{Ao} assuming m_f is large	8-49
Table 8-7	Comparison between Figure 8-27 and Figure 8-29a dual output voltage inverters for 120V/240V single phase output with a common neutral	8-55
Table 8-8	Specifications of a typical fuel cell power-conditioning unit for stand-alone domestic (US) loads	8-61
Table 8-9	Example specifications for the 1kW fuel cell powered back power (UPS) unit	8-73
Table 8-10	Specifications of 500W PEFC Stack available from Avista Labs	8-74

Table 8-11 Stream Properties for the Natural Gas Fueled Pressurized PAFC 8-101
Table 8-12 Operating/Design Parameters for the NG fueled PAFC 8-102
Table 8-13 Performance Summary for the NG fueled PAFC..... 8-102
Table 8-14 Operating/Design Parameters for the NG Fueled IR-MCFC 8-104
Table 8-15 Overall Performance Summary for the NG Fueled IR-MCFC 8-104
Table 8-16 Stream Properties for the Natural Gas Fueled Pressurized SOFC 8-106
Table 8-17 Operating/Design Parameters for the NG Fueled Pressurized SOFC 8-107
Table 8-18 Overall Performance Summary for the NG Fueled Pressurized SOFC 8-108
Table 8-19 Heron Gas Turbine Parameters 8-108
Table 8-20 Example Fuel Utilization in a Multi-Stage Fuel Cell Module 8-109
Table 8-21 Stream Properties for the Natural Gas Fueled Solid State Fuel Cell Power Plant System..... 8-110
Table 8-22 Operating/Design Parameters for the NG fueled Multi-Stage Fuel Cell System 8-112
Table 8-23 Overall Performance Summary for the NG fueled Multi-Stage Fuel Cell System 8-112
Table 8-24 Stream Properties for the 500 MW Class Coal Gas Fueled Cascaded SOFC.. 8-114
Table 8-25 Coal Analysis 8-115
Table 8-26 Operating/Design Parameters for the Coal Fueled Pressurized SOFC 8-116
Table 8-27 Overall Performance Summary for the Coal Fueled Pressurized SOFC 8-116
Table 8-28 Performance Calculations for a Pressurized, High Temperature Fuel Cell (SOFC) with a Regenerative Brayton Bottoming Cycle; Approach Delta T=30F 8-119
Table 8-29 Performance Computations for Various High Temperature Fuel Cell (SOFC) Heat Recovery Arrangements..... 8-120
Table 9-1 HHV Contribution of Common Gas Constituents 9-24
Table 9-2 Distributive Estimating Factors..... 9-27
Table10-1 Typical Contaminant Levels Obtained from Selected Coal Gasification Processes..... 10-3
Table 10-2 Summary of Related Codes and Standards 10-17
Table 10-3 DoD Field Site..... 10-25
Table 10-4 IFC Field Units..... 10-27
Table 10-5 FuelCell Energy Field Site 10-30
Table 10-6 Siemens Westinghouse SOFC Field Units..... 10-31
Table 10-7 Hydrogen Producers[1]..... 10-34
Table 10-8 World Mine Production and Reserves 10-48
Table 10-9 Rhodia Rare Earth Oxide Prices in 2,000 10-48

FORWARD

Fuel cells are an important technology for a potentially wide variety of applications including micropower, auxiliary power, transportation power, stationary power for buildings and other distributed generation applications, and central power. These applications will be in a large number of industries worldwide.

In this Sixth Edition of the Fuel Cell Handbook, we have included over 5,000 fuel cell patent abstracts and their claims. In addition, the handbook features a new fuel cell power conditioning section, and overviews on the hydrogen industry and rare earth minerals market. Finally, an updated list of fuel cell URLs is included in the Appendix and an updated index assists the reader in locating specific information quickly.

It is an important task that NETL undertakes to provide you with this handbook. We realize it is an important educational and informational tool for a wide audience. We welcome suggestions to improve the handbook.

Mark C. Williams

Strategic Center for Natural Gas
National Energy Technology Laboratory

PREFACE

The last edition of the Fuel Cell Handbook was published in November, 2000. Since that time, polymer electrolyte fuel cells, molten carbonate fuel cells, and solid oxide fuel cells have been demonstrated at commercial size. The previously-demonstrated phosphoric acid fuel cells have entered the marketplace with over 250 fuel cells in 19 countries around the world. Highlighting this commercial entry, the phosphoric acid power plant fleet has demonstrated 95+% availability, and one plant has completed over 50,000 hours of operation. Fourteen additional plants have operated over 35,000 hours; several of those have passed 40,000 hours of operation.

Early expectations of very low emissions and relatively high efficiencies have been met in power plants with each type of fuel cell. Fuel flexibility has been demonstrated using natural gas, propane, landfill gas, anaerobic digester gas, military logistic fuels, and coal gas, greatly expanding market opportunities. Transportation markets worldwide have shown remarkable interest in fuel cells; nearly every major vehicle manufacturer in the U.S., Europe, and the Far East is supporting development.

Still in its infancy, fuel cell technology development offers further opportunities for significant performance and cost improvements. To achieve 100% successful commercial-scale demonstration, more aggressive pre-testing may be needed to ensure more robust cell technologies. Deficiencies in funding for research and development and for commercial demonstration place tremendous pressure on fuel cell developers.

This Handbook provides a foundation in fuel cells for persons wanting a better understanding of the technology, its benefits, and the systems issues that influence its application. Trends in technology are discussed, including next-generation concepts that promise ultra-high efficiency and low cost, while providing exceptionally clean power plant systems. Section 1 summarizes fuel cell progress since the last edition, and includes existing power plant nameplate data. Section 2 addresses the thermodynamics of fuel cells to provide an understanding of fuel cell operation. Sections 3 through 7 describe the five major fuel cell types and their performance. Polymer electrolyte, alkaline, phosphoric acid, molten carbonate, and solid oxide fuel cell technology descriptions have been updated from the previous edition. Manufacturers are focusing on reducing fuel cell life cycle costs. In this edition, we have included over 5,000 fuel cell patent abstracts and their claims. In addition, the handbook features a new fuel cell power conditioning section, and overviews on the hydrogen industry and rare earth minerals market.

An updated list of fuel cell URLs is included in the Appendix.

ACKNOWLEDGEMENTS

The authors of this edition of the Fuel Cell Handbook acknowledge the cooperation of the fuel cell community for their contributions to this Handbook. Many colleagues provided data, information, references, valuable suggestions, and constructive comments that were incorporated into the Handbook. In particular, we would like to acknowledge the contributions of the following individuals: R. Kumar of Argonne National Laboratory, M. Farooque of FuelCell Energy, B. Ernst of Plug Power, , P. Enjeti of Texas A&M University, D. Archer of Carnegie Mellon University, J. Hirschenhofer, M. Cifrain and UTC Fuel Cells.

C. Hitchings, SAIC, provided technical editing and final layout of the Handbook.

The authors wish to thank M. Williams, R. Dennis, and N. Holcombe of the U.S. Department of Energy, National Energy Technology Laboratory, for their support and encouragement, and for providing the opportunity to enhance the quality of this Handbook.

This work was supported by the U.S. Department of Energy, National Energy Technology Laboratory, under Contract DE-AM21-94MC31166.

1. TECHNOLOGY OVERVIEW

1.1 Fuel Cell Description

Fuel cells are electrochemical devices that convert the chemical energy of a reaction directly into electrical energy. The basic physical structure, or building block, of a fuel cell consists of an electrolyte layer in contact with a porous anode and cathode on either side. A schematic representation of a fuel cell with the reactant/product gases and the ion conduction flow directions through the cell is shown in Figure 1-1.

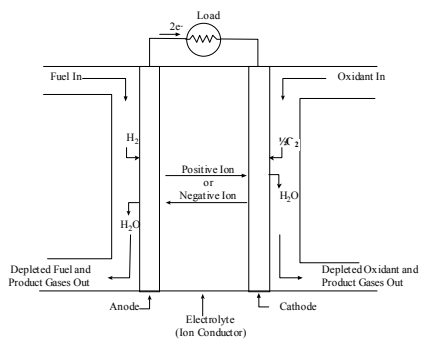

Figure 1-1 Schematic of an Individual Fuel Cell

In a typical fuel cell, gaseous fuels are fed continuously to the anode (negative electrode) and an oxidant (i.e., oxygen from air) is fed continuously to the cathode (positive electrode); the electrochemical reactions take place at the electrodes to produce an electric current. A fuel cell, although having components and characteristics similar to those of a typical battery, differs in several respects. The battery is an energy storage device. The maximum energy available is determined by the amount of chemical reactant stored within the battery itself. The battery will cease to produce electrical energy when the chemical reactants are consumed (i.e., discharged). In a secondary battery, the reactants are regenerated by recharging, which involves putting energy into the battery from an external source. The fuel cell, on the other hand, is an energy conversion device that theoretically has the capability of producing electrical energy for as long as fuel and oxidant are supplied to the electrodes. Figure 1-2 is a simplified diagram that demonstrates how the fuel cell works. In reality, degradation, primarily corrosion, or malfunction of components limits the practical operating life of fuel cells.

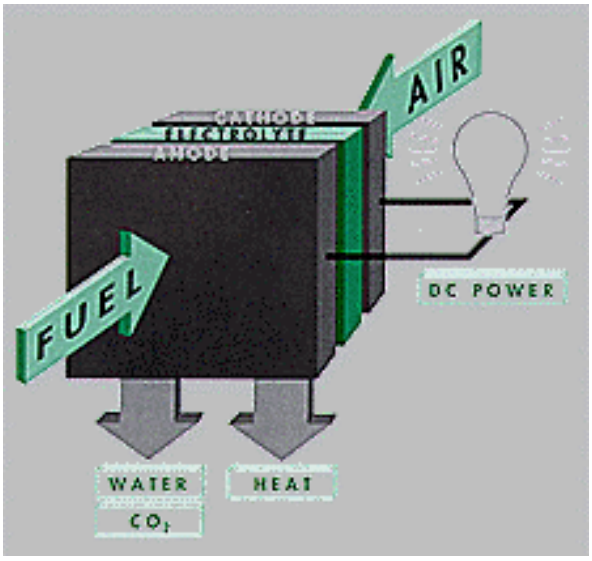

Figure 1-2 Simplified Fuel Cell Schematic

Note that an ion specie and its transport direction can differ, influencing the site of water production and removal. The ion can be either a positive or a negative ion, meaning that the ion carries either a positive or negative charge (surplus or deficit of electrons). The fuel or oxidant gases flow past the surface of the anode or cathode opposite the electrolyte and generate electrical energy by the electrochemical oxidation of fuel, usually hydrogen, and the electrochemical reduction of the oxidant, usually oxygen. Appleby and Foulkes (1) have noted that, in theory, any substance capable of chemical oxidation that can be supplied continuously (as a fluid) can be burned galvanically as fuel at the anode of a fuel cell. Similarly, the oxidant can be any fluid that can be reduced at a sufficient rate. Gaseous hydrogen has become the fuel of choice for most applications, because of its high reactivity when suitable catalysts are used, its ability to be produced from hydrocarbons for terrestrial applications, and its high energy density when stored cryogenically for closed environment applications, such as in space. Similarly, the most common oxidant is gaseous oxygen, which is readily and economically available from air for terrestrial applications, and again easily stored in a closed environment. A three-phase interface is established among the reactants, electrolyte, and catalyst in the region of the porous electrode. The nature of this interface plays a critical role in the electrochemical performance of a fuel cell, particularly in those fuel cells with liquid electrolytes. In such fuel cells, the reactant gases diffuse through a thin electrolyte film that wets portions of the porous electrode and react electrochemically on their respective electrode surface. If the porous electrode contains an excessive amount of electrolyte, the electrode may "flood" and restrict the transport of gaseous species in the electrolyte phase to the reaction sites. The consequence is a reduction in the electrochemical performance of the porous electrode. Thus, a delicate balance must be maintained among the electrode, electrolyte, and gaseous phases in the porous electrode structure. Much of the recent effort in development of fuel cell technology has been devoted to reducing the thickness of cell components while refining and improving the electrode structure and the electrolyte phase, with the aim of obtaining a higher and more stable electrochemical performance while lowering cost.

The electrolyte not only transports dissolved reactants to the electrode, but also conducts ionic charge between the electrodes and thereby completes the cell electric circuit, as illustrated in Figure 1-1. It also provides a physical barrier to prevent the fuel and oxidant gas streams from directly mixing.

The functions of porous electrodes in fuel cells are: 1) to provide a surface site where gas/liquid ionization or de-ionization reactions can take place, 2) to conduct ions away from or into the three-phase interface once they are formed (so an electrode must be made of materials that have good electrical conductance), and 3) to provide a physical barrier that separates the bulk gas phase and the electrolyte. A corollary of Item 1 is that, in order to increase the rates of reactions, the electrode material should be catalytic as well as conductive, porous rather than solid. The catalytic function of electrodes is more important in lower temperature fuel cells and less so in high-temperature fuel cells because ionization reaction rates increase with temperature. It is also a corollary that the porous electrodes must be permeable to both electrolyte and gases, but not such that the media can be easily "flooded" by the electrolyte or "dried" by the gases in a one-sided manner.

A variety of fuel cells are in different stages of development. They can be classified by use of diverse categories, depending on the combination of type of fuel and oxidant, whether the fuel is processed outside (external reforming) or inside (internal reforming) the fuel cell, the type of electrolyte, the temperature of operation, whether the reactants are fed to the cell by internal or external manifolds, etc. The most common classification of fuel cells is by the type of electrolyte used in the cells and includes 1) polymer electrolyte fuel cell (PEFC), 2) alkaline fuel cell (AFC), 3) phosphoric acid fuel cell (PAFC), 4) molten carbonate fuel cell (MCFC), and 5) solid oxide fuel cell (SOFC). These fuel cells are listed in the order of approximate operating temperature, ranging from ~80°C for PEFC, ~100°C for AFC, ~200°C for PAFC, ~650°C for MCFC, ~600-1000°C for SOFC. The operating temperature and useful life of a fuel cell dictate the physicochemical and thermomechanical properties of materials used in the cell components (i.e., electrodes, electrolyte, interconnect, current collector, etc.). Aqueous electrolytes are limited to temperatures of about 200°C or lower because of their high water vapor pressure and rapid degradation at higher temperatures. The operating temperature also plays an important role in dictating the type of fuel that can be used in a fuel cell. The low-temperature fuel cells with aqueous electrolytes are, in most practical applications, restricted to hydrogen as a fuel. In high-temperature fuel cells, CO and even CH_4 can be used because of the inherently rapid electrode kinetics and the lesser need for high catalytic activity at high temperature.

A brief description of various electrolyte cells of interest follows. A detailed description of these fuel cells may be found in Sections 3 through 7.

Polymer Electrolyte Fuel Cell (PEFC): The electrolyte in this fuel cell is an ion exchange membrane (fluorinated sulfonic acid polymer or other similar polymer) that is an excellent proton conductor. The only liquid in this fuel cell is water; thus, corrosion problems are minimal. Water management in the membrane is critical for efficient performance; the fuel cell must operate under conditions where the byproduct water does not evaporate faster than it is produced because the membrane must be hydrated. Because of the limitation on the operating temperature imposed by the polymer, usually less than 120°C, and because of problems with

water balance, a H_2-rich fuel is used. Higher catalyst loading (Pt in most cases) than that used in PAFCs is required for both the anode and cathode. Because CO "poisons" the catalyst, the fuel may contain no CO.

Alkaline Fuel Cell (AFC): The electrolyte in this fuel cell is concentrated (85 wt%) KOH in fuel cells operated at high temperature (~250°C), or less concentrated (35-50 wt%) KOH for lower temperature (<120°C) operation. The electrolyte is retained in a matrix (usually asbestos), and a wide range of electrocatalysts can be used (e.g., Ni, Ag, metal oxides, spinels, and noble metals). The fuel supply is limited to non-reactive constituents except for hydrogen. CO is a poison, and CO_2 will react with the KOH to form K_2CO_3, thus altering the electrolyte. Even the small amount of CO_2 in air is detrimental to the alkaline cell.

Phosphoric Acid Fuel Cell (PAFC): Phosphoric acid concentrated to 100% is used for the electrolyte in this fuel cell, which operates at 150 to 220°C. At lower temperatures, phosphoric acid is a poor ionic conductor, and CO poisoning of the Pt electrocatalyst in the anode becomes severe. The relative stability of concentrated phosphoric acid is high compared to other common acids; consequently the PAFC is capable of operating at the high end of the acid temperature range (100 to 220°C). In addition, the use of concentrated acid (100%) minimizes the water vapor pressure so water management in the cell is not difficult. The matrix universally used to retain the acid is silicon carbide (1), and the electrocatalyst in both the anode and cathode is Pt.

Molten Carbonate Fuel Cell (MCFC): The electrolyte in this fuel cell is usually a combination of alkali carbonates, which is retained in a ceramic matrix of $LiAlO_2$. The fuel cell operates at 600 to 700°C where the alkali carbonates form a highly conductive molten salt, with carbonate ions providing ionic conduction. At the high operating temperatures in MCFCs, Ni (anode) and nickel oxide (cathode) are adequate to promote reaction. Noble metals are not required.

Solid Oxide Fuel Cell (SOFC): The electrolyte in this fuel cell is a solid, nonporous metal oxide, usually Y_2O_3-stabilized ZrO_2. The cell operates at 600-1000°C where ionic conduction by oxygen ions takes place. Typically, the anode is Co-ZrO_2 or Ni-ZrO_2 cermet, and the cathode is Sr-doped $LaMnO_3$.

In low-temperature fuel cells (PEFC, AFC, PAFC), protons or hydroxyl ions are the major charge carriers in the electrolyte, whereas in the high-temperature fuel cells (MCFC and SOFC) carbonate ions and oxygen ions are the charge carriers, respectively. Detailed discussions of these different types of fuel cells are presented in Sections 3 through 7. Major differences between the various cells are shown in Table 1-1.

Table 1-1 Summary of Major Differences of the Fuel Cell Types

	PEFC	AFC	PAFC	MCFC	SOFC
Electrolyte	Ion Exchange Membranes	Mobilized or Immobilized Potassium Hydroxide	Immobilized Liquid Phosphoric Acid	Immobilized Liquid Molten Carbonate	Ceramic
Operating Temperature	80°C	65°C - 220°C	205°C	650°	600-1000°C
Charge Carrier	H^+	OH^-	H^+	$CO3^=$	$O^=$
External Reformer for CH_4 (below)	Yes	Yes	Yes	No	No
Prime Cell Components	Carbon-based	Carbon-based	Graphite-based	Stainless-based	Ceramic
Catalyst	Platinum	Platinum	Platinum	Nickel	Perovskites
Product Water Management	Evaporative	Evaporative	Evaporative	Gaseous Product	Gaseous Product
Product Heat Management	Process Gas + Independent Cooling Medium	Process Gas + Electrolyte Circulation	Process Gas + Independent Cooling Medium	Internal Reforming + Process Gas	Internal Reforming + Process Gas

Even though the electrolyte has become the predominant means of characterizing a cell, another important distinction is the method used to produce hydrogen for the cell reaction. Hydrogen can be reformed from natural gas and steam in the presence of a catalyst starting at a temperature of ~760°C. The reaction is endothermic. MCFC, and SOFC operating temperatures are high enough that reforming reactions can occur within the cell, a process referred to as internal reforming. Figure 1-3 compares internal reforming and external reforming MCFCs. The reforming reaction is driven by the decrease in hydrogen as the cell produces power. This internal reforming can be beneficial to system efficiency because there is an effective transfer of heat from the exothermic cell reaction to satisfy the endothermic reforming reaction. A reforming catalyst is needed adjacent to the anode gas chamber for the reaction to occur. The cost of an external reformer is eliminated and system efficiency is improved, but at the expense of a more complex cell configuration and increased maintenance issues. This provides developers of high-temperature cells a choice of an external reforming or internal reforming approach. Section 6 will show that the present internal reforming MCFC is limited to ambient pressure operation, whereas external reforming MCFC can operate at pressures up to 3 atmospheres. The slow rate of the reforming reaction makes internal reforming impractical in the lower temperature cells. Instead, a separate external reformer is used.

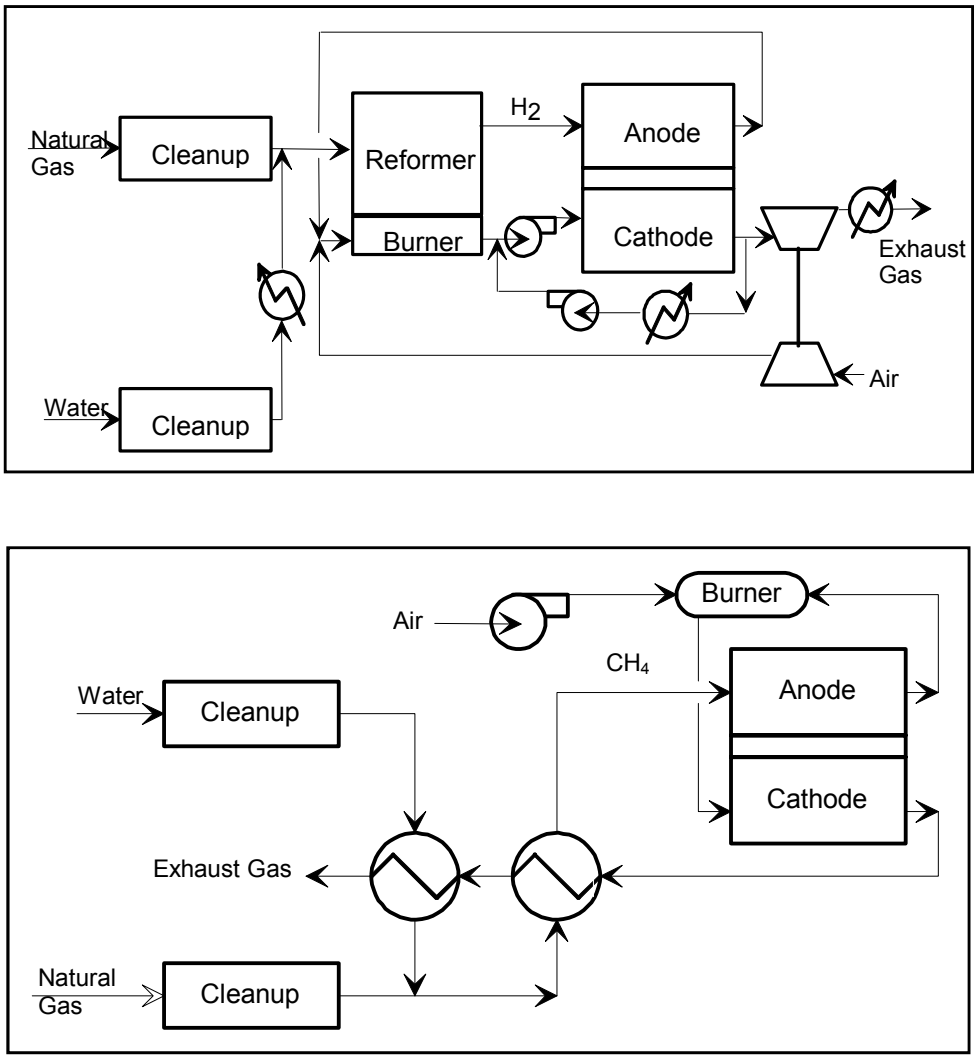

Figure 1-3 External Reforming and Internal Reforming MCFC System Comparison

Porous electrodes, mentioned several times above, are key to good electrode performance. The reason for this is that the current densities obtained from smooth electrodes are usually in the range of a single digit mA/cm^2 or less because of rate-limiting issues such as the available area of the reaction sites. Porous electrodes achieve much higher current densities. These high current densities are possible because the electrode has a high surface area relative to the geometric plate area that significantly increases the number of reaction sites, and the optimized electrode structure has favorable mass transport properties. In an idealized porous electrode, high current densities at reasonable polarization are obtained when the liquid (electrolyte) layer on the electrode surface is sufficiently thin that it does not significantly impede the transport of reactants to the electroactive sites, and a stable three-phase (gas/electrolyte/electrode surface) interface is established. When an excessive amount of electrolyte is present in the porous electrode structure, the electrode is considered to be "flooded" and the concentration polarization increases to a large value.

The porous electrodes used in low-temperature fuel cells consist of a composite structure that contains platinum (Pt) electrocatalyst on a high surface area carbon black and a PTFE (polytetrafluoroethylene) binder. Such electrodes for acid and alkaline fuel cells are described by Kordesch, et al. (3). In these porous electrodes, PTFE is hydrophobic (acts as a wet proofing agent) and serves as the gas permeable phase, and carbon black is an electron conductor that provides a high surface area to support the electrocatalyst. Platinum serves as the electrocatalyst, which promotes the rate of electrochemical reactions (oxidation/reduction) for a given surface area. The carbon black is also somewhat hydrophobic, depending on the surface properties of the material. The composite structure of PTFE and carbon establishes an extensive three-phase interface in the porous electrode, which is the benchmark of PTFE bonded electrodes. Some interesting results have been reported by Japanese workers on higher performance gas diffusion electrodes for phosphoric acid fuel cells (see Section 5.1.2).

In MCFCs, which operate at relatively high temperature, no materials are known that wet-proof a porous structure against ingress by molten carbonates. Consequently, the technology used to obtain a stable three-phase interface in MCFC porous electrodes is different from that used in PAFCs. In the MCFC, the stable interface is achieved in the electrodes by carefully tailoring the pore structures of the electrodes and the electrolyte matrix ($LiA1O_2$) so that capillary forces establish a dynamic equilibrium in the different porous structures. Pigeaud, et al. (4) provide a discussion of porous electrodes for MCFCs.

In a SOFC, there is no liquid electrolyte present that is susceptible to movement in the porous electrode structure, and electrode flooding is not a problem. Consequently, the three-phase interface that is necessary for efficient electrochemical reaction involves two solid phases (solid electrolyte/electrode) and a gas phase. A critical requirement of porous electrodes for SOFC is that they are sufficiently thin and porous to provide an extensive electrode/electrolyte interfacial region for electrochemical reaction.

1.2 Cell Stacking

Additional components of a cell are best described by using a typical cell schematic, Figure 1-4. This figure depicts a PAFC. As with batteries, individual fuel cells must be combined to produce appreciable voltage levels and so are joined by interconnects. Because of the configuration of a flat plate cell, Figure 1-4, the interconnect becomes a separator plate with two functions: 1) to provide an electrical series connection between adjacent cells, specifically for flat plate cells, and 2) to provide a gas barrier that separates the fuel and oxidant of adjacent cells. The interconnect of a solid oxide fuel cell is a special case, and the reader is referred to Section 7 for its slightly altered function. All interconnects must be an electrical conductor and impermeable to gases. Other important parts of the cell are 1) the structure for distributing the reactant gases across the electrode surface and which serves as mechanical support, shown as ribs in Figure 1-4, 2) electrolyte reservoirs for liquid electrolyte cells to replenish electrolyte lost over life, and 3) current collectors (not shown) that provide a path for the current between the electrodes and the separator of flat plate cells. Other arrangements of gas flow and current flow are used in fuel cell stack designs, and are mentioned in Sections 3 through 7 for the various type cells.

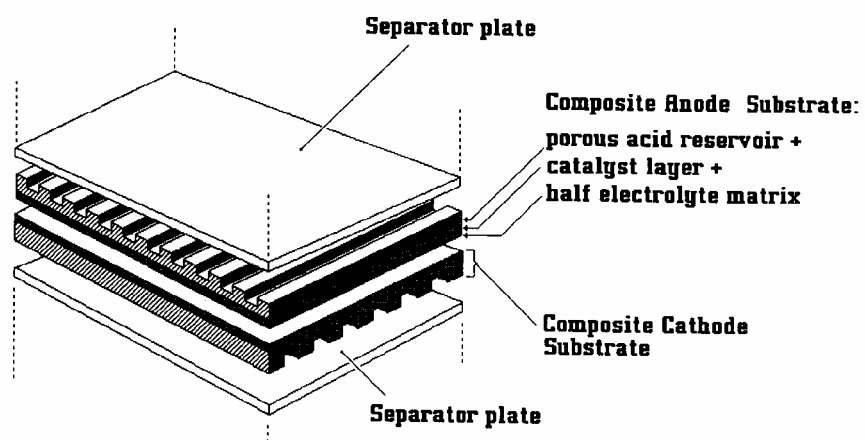

Figure 1-4 Expanded View of a Basic Fuel Cell Repeated Unit in a Fuel Cell Stack (1)

1.3 Fuel Cell Plant Description

As shown in Figure 1-1, the fuel cell combines hydrogen produced from the fuel and oxygen from the air to produce dc power, water, and heat. In cases where CO and CH_4 react in the cell to produce hydrogen, CO_2 is also a product. These reactions must be carried out at a suitable temperature and pressure for fuel cell operation. A system must be built around the fuel cell to supply air and clean fuel, convert the power to a more usable form such as grid quality ac power, and remove the depleted reactants and heat that are produced by the reactions in the cells.
Figure 1-5 shows a simple rendition of a fuel cell power plant. Beginning with fuel processing, a conventional fuel (natural gas, other gaseous hydrocarbons, methanol, naphtha, or coal) is cleaned, then converted into a gas containing hydrogen. Energy conversion occurs when dc electricity is generated by means of individual cells combined in stacks or bundles. A varying number of cells or stacks can be matched to a particular power application. Finally, power conditioning converts the electric power from dc into regulated dc or ac for consumer use. Section 8.1 describes the processes of a fuel cell power plant system.

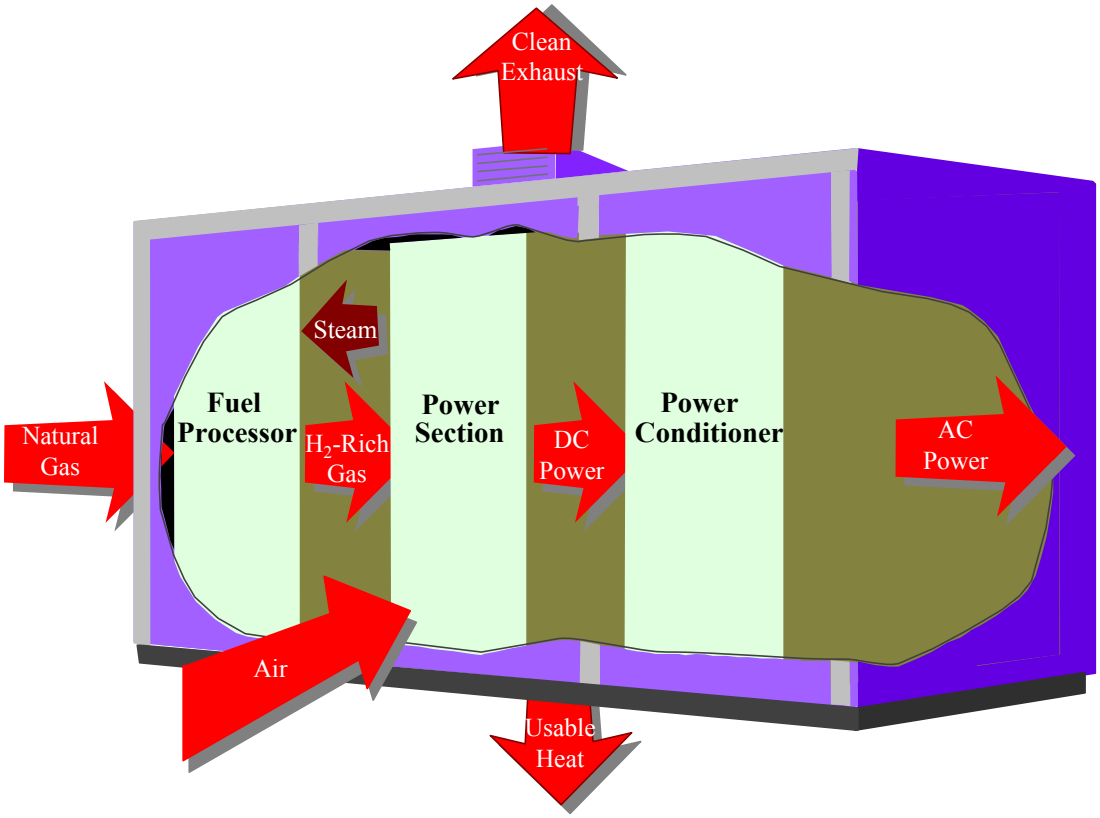

Figure 1-5 Fuel Cell Power Plant Major Processes

1.4 Characteristics

Fuel cells have many characteristics that make them favorable as energy conversion devices. Two that have been instrumental in driving the interest for terrestrial application of the technology are the combination of relatively high efficiency and very low environmental intrusion (virtually no acid gas or solid emissions). Efficiencies of present fuel cell plants are in the range of 40 to 55% based on the lower heating value (LHV) of the fuel. Hybrid fuel cell/reheat gas turbine cycles that offer efficiencies greater than 70% LHV, using demonstrated cell performance, have been proposed. Figure 1-6 illustrates demonstrated low emissions of installed PAFC units compared to the Los Angeles Basin (South Coast Air Quality Management District) requirements, the strictest requirements in the U.S. Measured emissions from the PAFC unit are < 1 ppm of NOx, 4 ppm of CO, and <1 ppm of reactive organic gases (non-methane) (5). In addition, fuel cells operate at a constant temperature, and the heat from the electrochemical reaction is available for cogeneration applications. Because fuel cells operate at nearly constant efficiency, independent of size, small fuel cell plants operate nearly as efficiently as large ones.[1] Thus, fuel cell power plants can be configured in a wide range of electrical output, ranging from watts to megawatts. Fuel cells are quiet and, even though fuel flexible, they are sensitive to certain fuel contaminants that must be minimized in the fuel gas. Table 1-2 summarizes the impact of the major constituents within fuel gases on the various fuel cells. The reader is referred to Sections 3 through 7 for detail on trace contaminants. The two major impediments to the

[1]. The fuel processor efficiency is size dependent; therefore, small fuel cell power plants using externally reformed hydrocarbon fuels would have a lower overall system efficiency.

widespread use of fuel cells are 1) high initial cost and 2) high-temperature cell endurance. These two aspects are the major focus of manufacturers' technological efforts.

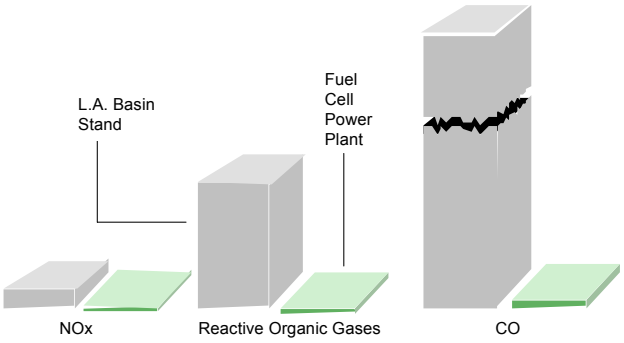

Figure 1-6 Relative Emissions of PAFC Fuel Cell Power Plants Compared to Stringent Los Angeles Basin Requirements

Other characteristics that fuel cells and fuel cell plants offer are

- Direct energy conversion (no combustion).
- No moving parts in the energy converter.
- Quiet.
- Demonstrated high availability of lower temperature units.
- Siting ability.
- Fuel flexibility.
- Demonstrated endurance/reliability of lower temperature units.
- Good performance at off-design load operation.
- Modular installations to match load and increase reliability.
- Remote/unattended operation.
- Size flexibility.
- Rapid load following capability.

General negative features of fuel cells include

- Market entry cost high; N^{th} cost goals not demonstrated.
- Unfamiliar technology to the power industry.
- No infrastructure.

Table 1-2 Summary of Major Fuel Constituents Impact on PEFC, AFC, PAFC, MCFC, and SOFC

Gas Species	PEFC	AFC	PAFC	MCFC	SOFC
H_2	Fuel	Fuel	Fuel	Fuel	Fuel
CO	Poison (reversible) (50 ppm per stack)	Poison	Poison (<0.5%)	Fuel[a]	Fuel
CH_4	Diluent	Poison	Diluent	Diluent[b]	Fuel[a]
CO_2 & H_2O	Diluent	Poison	Diluent	Diluent	Diluent
S as (H_2S & COS)	No Studies to date (11)	Poison	Poison (<50 ppm)	Poison (<0.5 ppm)	Poison (<1.0 ppm)

[a] In reality, CO, with H_2O, shifts to H_2 and CO_2, and CH_4, with H_2O, reforms to H_2 and CO faster than reacting as a fuel at the electrode.

[b] A fuel in the internal reforming MCFC.

1.5 Advantages/Disadvantages

The fuel cell types addressed in this handbook have significantly different operating regimes. As a result, their materials of construction, fabrication techniques, and system requirements differ. These distinctions result in individual advantages and disadvantages that govern the potential of the various cells to be used for different applications.

PEFC: The PEFC, like the SOFC, has a solid electrolyte. As a result, this cell exhibits excellent resistance to gas crossover. In contrast to the SOFC, the cell operates at a low 80°C. This results in a capability to bring the cell to its operating temperature quickly, but the rejected heat cannot be used for cogeneration or additional power. Test results have shown that the cell can operate at very high current densities compared to the other cells. However, heat and water management issues may limit the operating power density of a practical system. The PEFC tolerance for CO is in the low ppm level for low temperature PEFC but can be in many thousands of ppm for emerging high temperature PEFC designs.

AFC: The AFC was one of the first modern fuel cells to be developed, beginning in 1960. The application at that time was to provide on-board electric power for the Apollo space vehicle. Desirable attributes of the AFC include its excellent performance on hydrogen (H_2) and oxygen (O_2) compared to other candidate fuel cells due to its active O_2 electrode kinetics and its flexibility to use a wide range of electrocatalysts, an attribute that provides development flexibility. Once development was in progress for space application, terrestrial applications began to be investigated. Developers recognized that pure hydrogen would be required in the fuel stream, because CO_2 in any reformed fuel reacts with the KOH electrolyte to form a carbonate, reducing the electrolyte's ion mobility. Pure H_2 could be supplied to the anode by passing a reformed, H_2-rich fuel stream by a precious metal (palladium/silver) membrane. The H_2 molecule is able to pass through the membrane by absorption and mass transfer, and into the fuel cell anode. However, a significant pressure differential is required across the membrane and the membrane is

prohibitive in cost. Even the small amount of CO_2 in ambient air, the source of O_2 for the reaction, must be scrubbed. At the time, U.S. investigations determined that scrubbing of the small amount of CO_2 within the air, coupled with purification of the hydrogen, was not cost effective and that terrestrial application of the AFC could be limited to special applications, such as closed environments, at best. Major R&D on AFC is no longer done in the U.S. but recent development in Europe has created renewed interest in this fuel cell type.

PAFC: The CO_2 in the reformed fuel gas stream and the air does not react with the electrolyte in a phosphoric acid fuel cell, but is a diluent. This attribute and the relatively low temperature of the PAFC made it a prime, early candidate for terrestrial application. Although its cell performance is somewhat lower than the alkaline cell because of the cathode's slow oxygen reaction rate, and although the cell still requires hydrocarbon fuels to be reformed into a H_2-rich gas, the PAFC system efficiency improved because of its higher temperature environment and less complex fuel conversion (no membrane and attendant pressure drop). The need for scrubbing CO_2 from the process air is also eliminated. The rejected heat from the cell is hot enough in temperature to heat water or air in a system operating at atmospheric pressure. Some steam is available in PAFCs, a key point in expanding cogeneration applications.

PAFC systems achieve about 37 to 42% electrical efficiency (based on the LHV of natural gas). This is at the low end of the efficiency goal for fuel cell power plants. PAFCs use high cost precious metal catalysts such as platinum. The fuel has to be reformed external to the cell, and CO has to be shifted by a water gas shift reaction to below 3 to 5 vol% at the inlet to the fuel cell anode or it will affect the catalyst. These limitations have prompted development of the alternate, higher temperature cells, MCFC and SOFC.

MCFC: Many of the disadvantages of the lower temperature as well as higher temperature cells can be alleviated with the higher operating temperature MCFC (approximately 650°C). This temperature level results in several benefits: the cell can be made of commonly available sheet metals that can be stamped for less costly fabrication, the cell reactions occur with nickel catalysts rather than with expensive precious metal catalysts, reforming can take place within the cell provided a reforming catalyst is added (results in a large efficiency gain), CO is a directly usable fuel, and the rejected heat is of sufficiently high temperature to drive a gas turbine and/or produce a high pressure steam for use in a steam turbine or for cogeneration. Another advantage of the MCFC is that it operates efficiently with CO_2-containing fuels such as bio-fuel derived gases. This benefit is derived from the cathode performance enhancement resulting from CO_2 enrichment.

The MCFC has some disadvantages, however: the electrolyte is very corrosive and mobile, and a source of CO_2 is required at the cathode (usually recycled from anode exhaust) to form the carbonate ion. Sulfur tolerance is controlled by the reforming catalyst and is low, which is the same for the reforming catalyst in all cells. Operation requires use of stainless steel as the cell hardware material. The higher temperatures promote material problems, particularly mechanical stability that impacts life.

SOFC: The SOFC is the fuel cell with the longest continuous development period, starting in the late 1950s, several years before the AFC. Because the electrolyte is solid, the cell can be cast

into flexible shapes, such as tubular, planar, or monolithic. The solid ceramic construction of the cell also alleviates any cell hardware corrosion problems characterized by the liquid electrolyte cells and has the advantage of being impervious to gas cross-over from one electrode to the other. The absence of liquid also eliminates the problem of electrolyte movement or flooding in the electrodes. The kinetics of the cell are fast, and CO is a directly useable fuel as it is in the MCFC. There is no requirement for CO_2 at the cathode as with the MCFC. At the temperature of presently operating SOFCs (~1000°C), fuel can be reformed within the cell. The temperature of an SOFC is significantly higher than that of the MCFC. However, some of the rejected heat from an SOFC is needed for preheating the incoming process air.

The high temperature of the SOFC has its drawbacks. There are thermal expansion mismatches among materials, and sealing between cells is difficult in the flat plate configurations. The high operating temperature places severe constraints on materials selection, and results in difficult fabrication processes. The SOFC also exhibits a high electrical resistivity in the electrolyte, which results in a lower cell performance than the MCFC by approximately 100 mV. Researchers would like to develop cells at a reduced temperature of 650°C, but the electrical resistivity of the presently-used solid electrolyte material would increase.

Developers are using the advantages of fuel cells to identify early applications and addressing research and development issues to expand applications (see Sections 3 through 7).

1.6 Applications, Demonstrations, and Status

The characteristics, advantages, and disadvantages summarized in the previous section form the basis for selection of the candidate fuel cell types to respond to a variety of application needs. The major applications for fuel cells are as stationary electric power plants, including cogeneration units, as motive power for vehicles, and as on-board electric power for space vehicles or other closed environments. Derivative applications will be summarized.

1.6.1 Stationary Electric Power

One of the characteristics of fuel cell systems is that their efficiency is nearly unaffected by size. This means that small, relatively high efficiency power plants can be developed, thus avoiding the higher cost exposure associated with large plant development. As a result, initial stationary plant development has focused on several hundred kW to low MW capacity plants. Smaller plants (several hundred kW to 1 to 2 MW) can be sited at the user's facility and are suited for cogeneration operation, that is, the plants produce electricity and thermal energy. Larger, dispersed plants (1 to 10 MW) are likely to be used for distributed generation. The plants are fueled primarily with natural gas. Once these plants are commercialized and price improvements materialize, fuel cells will be considered for large base-load plants because of their high efficiency. The base-load plants could be fueled by natural gas or coal. The fuel product from a coal gasifier, once cleaned, is compatible for use with fuel cells. Systems integration studies show that high temperature fuel cells closely match coal gasifier operation.

Operation of complete, self-contained, stationary plants continues to be demonstrated using PEFC, AFC, PAFC, MCFC, and SOFC technology. Demonstrations of these technologies that occurred before 2000 were addressed in previous editions of the Fuel Cell Handbook and in the literature of the period. Recent U.S. manufacturer experience with these various fuel cell tech-

nologies has produced timely information. A case in point is the 200 kW PAFC on-site plant, the PC-25, that is the first to enter the commercial market (see Figure 1-7).

Figure 1-7 PC-25 Fuel Cell

The plant was developed by United Technologies Fuel Cells, a division of United Technologies Corporation (UTC). The plants are built by UTC Fuel Cells. The Toshiba Corporation of Japan and Ansaldo SpA of Italy are partners with UTC Fuel Cells. The on-site plant is proving to be an economic and beneficial addition to the operating systems of commercial buildings and industrial facilities because it is superior to conventional technologies in reliability, efficiency, environmental impact, and ease of siting. Because the PC-25 is the first available commercial unit, it serves as a model for fuel cell application. Because of its attributes, the PC-25 is being installed in various applications, such as hospitals, hotels, large office buildings, manufacturing sites, wastewater treatment plants, and institutions, to meet the following requirements:

- On-site energy
- Continuous power – backup
- Uninterrupted power supply
- Premium power quality
- Independent power source

Characteristics of the plant are as follows:

- Power Capacity 0 to 200 kW with natural gas fuel (-30 to 45°C, up to 1500 m)
- Voltage and Phasing 480/277 volts at 60 Hz ; 400/230 volts at 50 Hz

• Thermal Energy (Cogeneration)	740,000 kJ/hour at 60°C (700,000 Btu/hour heat at 140°F); module provides 369,000 kJ/hour at 120°C (350,000Btu/hour at 250°F) and 369,000 kJ/hour at 60°C
• Electric Connection	Grid-connected for on-line service and grid-independent for on-site premium service
• Power Factor	Adjustable between 0.85 to 1.0
• Transient Overload	None
• Grid Voltage Unbalance	1%
• Grid Frequency Range	+/-3%
• Voltage Harmonic Limits	<3%
• Plant Dimensions	3 m (10 ft) wide by 3 m (10 ft) high by 5.5 m (18 ft) long, not including a small fan cooling module (5)
• Plant Weight	17,230 kg (38,000 lb)

UTC Fuel Cells: Results from the operating units as of August, 2002 are as follows: total fleet operation stands at more than 5.3 million hours. The plants achieve 40% LHV electric efficiency, and overall use of the fuel energy approaches 80% for cogeneration applications (6). Operations confirm that rejected heat from the initial PAFC plants can be used for heating water, space heating, and low pressure steam. One plant has completed over 50,000 hours of operation, and a number of plants have operated over 40,000 hours (6). Fourteen additional plants have operated over 35,000 hours. The longest continuous run stands at 9,500 hours for a unit purchased by Tokyo Gas for use in a Japanese office building (9). This plant ended its duration record because it had to be shut down for mandated maintenance. It is estimated at this time that cell stacks can achieve a life of 5 to 7 years. The fleet has attained an average of over 95% availability. The latest model, the PC-25C, is expected to achieve over 96%. The plants have operated on natural gas, propane, butane, landfill gas (10,11), hydrogen (12), and gas from anaerobic digestors (13). Emissions are so low (see Figure 1-6) that the plant is exempt from air permitting in the South Coast and Bay Area (California) Air Quality Management Districts, which have the most stringent limits in the U.S. The sound pressure level is 62 dBA at 9 meters (30 feet) from the unit. The PC-25 has been subjected to ambient conditions varying from -32°C to +49°C and altitudes from sea level to 1600 meters (~1 mile). Impressive ramp rates result from the solid state electronics. The PC-25 can be ramped at 10 kW/sec up or down in the grid connected mode. The ramp rate for the grid independent mode is idle to full power in ~one cycle or essentially one-step instantaneous from idle to 200 kW. Following the initial ramp to full power, the unit can adjust at an 80 kW/sec ramp up or down in one cycle.

The fuel cell stacks are made and assembled into units at an 80,000 ft^2 facility located in South Windsor, Connecticut. Low cost/high volume production depends on directly insertable sub-assemblies as complete units and highly automatic processes such as robotic component handling and assembly. The stack assembly is grouped in a modified spoke arrangement to allow for individual manufacturing requirements of each of the cell components while bringing them in a continuous flow to a central stacking elevator (14).

UTC Fuel Cells had the best sales year in 2001, selling 23 of its PC25 units. Other notable events that occurred in 2001 were:

- A Hyundai Santa Fe powered by 75-kW UTC PEFC scored best in class in two key performance tests at the Michelin Challenge Bibendum, an annual event where new automotive technologies are evaluated by independent judges.
- Shell Hydrogen and UTC Fuel Cells established HydrogenSource, LLC, a fuel-processing joint venture.
- UTC Fuel Cells and Buderus Heiztechnik agreed to jointly develop and market residential fuel cells in Europe.

New field and planned installations announced since the previous fuel cell handbook are discussed below.

UTC Fuel Cells announced that a PC25™ unit will be installed at the Rebekah Baines Johnson Health Center in Austin, Texas. The 200-kilowatt unit will produce electricity and provide heat for producing hot water. The electricity produced by this unit is fed into the Austin Energy electric grid, making it the first fuel cell in Texas to feed power to the grid.

Seven PC25™ units will be installed at the Verizon facility on Long Island, New York to provide primary power for critical call-routing center. The combined fuel cells will produce 1.4 megawatts of electricity. Verizon also plans to install four natural gas-powered generators to operate in parallel with the fuel cells as a hybrid system that can generate up to 4.4 megawatts of electrical power.

UTC Fuel Cells will install a PC25™ unit Rio de Janeiro, Brazil. Petrobras, Brazil's oil, gas, and energy company, will install the fuel cell at its research and development center. The unit will be the fourth installed in South America, where UTC Fuel Cells is represented by Sieco S.A., a provider of premium power equipment and services based in Argentina.

The New York Power Authority purchased eight PC25™ units. The units will produce power for, and reduce emissions from, wastewater treatment plants in Brooklyn, Staten Bronx, and Queens. The units will run off anaerobic digester gas, a byproduct of the treatment process that would otherwise be burned with no energy recovery.

Ballard Generation Systems: Ballard Generation Systems, a subsidiary of Ballard Power Systems, produces a PEFC stationary on-site plant. It has these characteristics:

- Power Capacity 250 kW with natural gas fuel
- Electric Efficiency 40% LHV
- Thermal Energy 854,600 kJ/hour at 74°C (810,000 Btu/hour at 165°F)
- Plant Dimensions 2.4 m (8 ft) wide by 2.4 m (8 ft) high by 5.7 m (18.5 ft) long
- Plant Weight 12,100 kg (26,700 lb)

Ballard completed 10- and 60-kW engineering prototypes stationary fuel cell power generators in 2001. Ballard, Shell Hydrogen, and Westcoast Energy established a private capital joint venture to help build early stage fuel cell systems. Ballard launched the Nexa™, a portable 1.2 kW power module, in September 2001. Ballard is also selling carbon fiber products for gas diffusion

layers for proton exchange membrane fuel cells (PEFC's). Highlights of Ballard's fuel cell sales are shown below.

One of Ballard's 250 kW generator units completed a 2-year field trail in Basel, Switzerland. Of the remaining eight other 250 kW stationary generators, four are in field tests, two are being prepared for site acceptance testing, one has completed the test program, and one has yet to be sited.

Ballard and EBARA Corporation reached an agreement to develop a pilot-scale plant for manufacturing processes and equipment for fuel cell membranes. During an 18-month development period, EBARA will construct and demonstrate capabilities for manufacturing Ballard's BAM Grafted Proton Exchange Membrane.

Ballard continues to develop a next generation prototype 1 kW cogeneration stationary system for the Japanese residential market.

FuelCell Energy (FCE): FCE reached 50 MW manufacturing capacity, and plans to expand its manufacturing capacity to 400 MW in 2004. The focus of the utility demonstrations and FCE's fuel cell development program is the commercialization of 300 kilowatt, 1.5 megawatt, and 3 megawatt MCFC plants.

- Power Capacity 3.0 MW net AC
- Electric efficiency 57% (LHV) on natural gas
- Voltage and Phasing Voltage is site dependent, 3 phase 60 Hz
- Thermal energy ~4.2 million kJ/hour (~4 million Btu/hour)
- Availability 95%

Field trials employing FCE's commercial MCFC design are being planned at a number of sites. Some are discussed below.

FCE and PPL Energy Services announced that a DFC® unit will be installed at Ocean County College, New Jersey. The unit will operate in a cogeneration mode supplying heat and power.

FCE will demonstrate a two-megawatt size unit on coal-derived syngas from the Wabash River Integrated Gasification Combined Cycle facility located in West Terre Haute, Indiana. The unit will operate at FCE's Torrington facility on natural gas before it is shipped to the site in the second half of 2003.

FCE installed a 1 MW DFC® power plant at the King Country wastewater treatment facility in Renton, Washington. The two year demonstration project is cost-shared equally by FCE and King County through a cooperative grant to the County from the U.S. Environmental Protection Agency (EPA). Operations are expected to commence during the third quarter of 2002. The project will demonstrate that wastewater treatment systems can generate sufficient quantities of gas to supply the fuel cell plant. The King County municipal wastewater treatment system uses an anaerobic digester process to stabilize solids and reduce microorganisms, and produces a methane-rich gas that can be fed to the DFC® power plant.

FCE's partner in Europe, the MTU Friedrichshafen GmbH unit of DaimlerChrysler, placed a 250 kW DFC® unit at the Rhon-Klinkum Hospital in Bad Neustadt. The power plant is connected to the internal system of the hospital, and will also provide heat energy.

In July 2001, FCE began operations of a DFC® power plant integrated with a Capstone Turbine Corporation modified Model 330 microturbine. The power plant is designed to operate in a dual mode: as a standalone fuel cell system or in combination with the microturbine.

FCE installed a 250 kW DFC® power unit at the Los Angeles Department of Water and Power headquarters the fourth quarter of 2001. A second unit was installed the second quarter 2002. Since the DFC® power plant operates without producing measurable nitrogen and sulfur emissions, it can be readily sited in the middle of Los Angeles.

FCE and Marubeni plans to place a 250 kW DFC® power plant in Asia at the Kirin brewery plant outside Tokyo Japan. The fuel cell will operate in cogeneration mode, using a methane-like digester gas produced from the brewery effluent.

FCE announced that it is installing a 250 kW DFC® power plant at the University of Connecticut.

FCE and its partner, PPL Energy Plus, a subsidiary of PPL Corporation, announced that they are providing two DFC® power plants for installation at New Jersey hotels owned by Starwood Hotels & Resorts Worldwide, Inc. PPL and Starwood Hotels have signed an agreement to install, own and operate one 250-kilowatt DFC® fuel cell power plant at the Sheraton Parsippany Hotel and another at the Sheraton Edison Raritan Center.

FCE received an order from PPL Spectrum, Inc., a subsidiary of PPL Corp., for the purchase of a 250 kW DFC® power plant for installation at the United States Coast Guard Air Station Cape Cod located in Bourne, MA. The power plant will provide electricity and heating to the base, which includes barracks, hangars, and administrative buildings.

Siemens Westinghouse Power Corporation (SWPC): SWPC selected the Pittsburgh, Pennsylvania area for expansion of its stationary fuel cell business. The 22-acre site located in Munhall, Allegheny County will have a 430,000-ft^2 manufacturing facility; SWPC plans to deploy its fuel cell product line in commercial market by fall 2003. SWPC has three SOFC systems employing tubular cell technology operating on user sites. All were produced in their Pittsburgh, Pennsylvania facility. The capacities of the systems are 220 kilowatts, 100 kilowatts, and 25 kilowatts.

The 220 kilowatt fuel cell/gas turbine power plant operating at the University of California's National Fuel Cell Research Center located in Irvine, California is the world's first SOFC/gas turbine system. The hybrid power plant consists of a 200 kilowatt fuel cell generator pressurized at about 3.5 atmospheres in combination with a 20 kilowatt two-shaft gas turbine. The system was first run at the Pittsburgh facility and started operating at Irvine in June 2000. As of January, 2002, the system has operated for 900+ hours and has demonstrated 53 percent

electrical efficiency. Efficiency goals for the SOFC/gas turbine hybrids should be in the 60-70 percent range.

The nominal 100 kW 50 Hz unit first operated at the NUON District Heating site in Westvoort, the Netherlands. EDB/ELSAM, a consortium of Dutch and Danish Energy distribution companies, sponsored the unit. Site acceptance was completed by February 6, 1998. The system delivered 109 kW ac to the grid for 16,667 hours. The electrical efficiency was 46%, plus the plant supplied 64 kW of hot water into the local district heating system. In March 2001, the system was moved from the Netherlands to a site in Essen, Germany for operation by the German utility RWE. As of January 2002, the system has operated in Essen for an additional 3,700+ hours, for a total of 20,000+ hours.

The 25 kilowatt system at the National Fuel Cell Research Center has operated more than 9,000 hours on a variety of fuels including natural gas, diesel, and jet fuel. The system was restarted in August 2000 after being idle for two years. It started up with no difficulty. An earlier SWPC test unit in the 25 kW range operated for more than 13,000 hours, with a non-stop run over 6500 hours. Tokyo Gas and Osaka Gas of Japan sponsored this system.

The Siemens Westinghouse SOFC is planning two major product lines with a series of product designs in each line. The first product will be a 250 kW cogeneration system operating at atmospheric pressure. This will be followed by a pressurized SOFC/gas turbine hybrid of approximately 0.5 MW. After the initial production, larger systems are expected as well. Also, a system capable of separating CO_2 from the exhaust is planned as an eventual option to other products.

The commercialization plan is focused on an initial offering of a hybrid fuel cell/gas turbine plant. The fuel cell module replaces the combustion chamber of the gas turbine engine. Figure 1-8 shows the benefit behind this combined plant approach. Additional details are provided in Section 7. As a result of the hybrid approach, the 1 MW early commercial unit is expected to attain ~60% efficiency LHV when operating on natural gas.

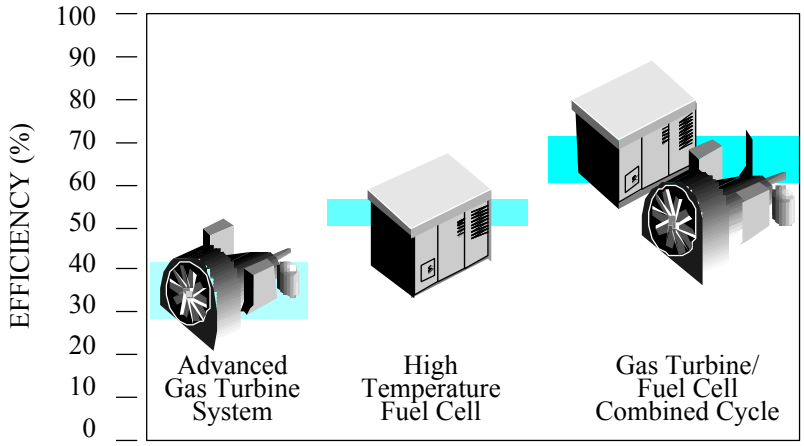

Figure 1-8 Combining the SOFC with a Gas Turbine Engine to Improve Efficiency

Siemens Westinghouse is planning a number of tests on power plants that are prototypes of future products. All systems employ the tubular SOFC concept and most are combined with gas turbines in a hybrid configuration. Capacities of these systems are 250 kilowatts atmospheric, 300 kilowatt class hybrid, and 1 megawatt class hybrid. They are to operate at various sites in the U.S., Canada, and Europe. Some of them are discussed below.

A 250 kilowatt atmospheric system is planned for a Toronto, Ontario, Canada site. The system will be operated by Ontario Power Technologies (formerly Ontario Hydro). The unit will supply 145 kilowatts of heat to the site heating system. Electric efficiency is expected to be about 47% (LHV). Operation of the combined heat and power system is expected in 2002.

Operation of a 230 kilowatt class hybrid system is planned for Essen, Germany. The utility RWE will operate the system. Efficiency of the system will be about 57% (LHV). Operation is expected in 2002.

A 230 kilowatt class hybrid system is planned to operate near Milan, Italy. Edison SpA will operate the power plant. Efficiency will be about 57% (LHV). Operation is expected to begin in 2002.

A 250 kilowatt system is planned for a site in Norway. The system will be operated by Norske Shell to demonstrate that CO_2 can be economically recovered. The CO_2 recovery technology is being developed by Shell Hydrogen. The CO_2 could be sequestered in underground reservoirs or could be used for special applications such as fish farms or agricultural greenhouses. The test system will be sited at a fish hatchery. The system is expected to begin operation in 2003.

An eventual market for fuel cells is the large (100 to 300 MW), base-loaded, stationary plants operating on coal or natural gas. Another related, early opportunity may be in repowering older, existing plants with high-temperature fuel cells (19). MCFCs and SOFCs, coupled with coal gasifiers, have the best attributes to compete for the large, base load market. The rejected heat from the fuel cell can be used to produce steam for the existing plant's turbines. Studies showing the potential of high-temperature fuel cells for plants of this size have been performed (see Section 8). These plants are expected to attain from 50 to 60% efficiency based on the HHV of the fuel. Coal gasifiers produce a fuel gas product requiring cleaning to the stringent requirements of the fuel cells' electrochemical environment, a costly process. The trend of environmental regulations has also been towards more stringent cleanup. If this trend continues, coal-fired technologies will be subject to increased cleanup costs that may worsen process economics. This will improve the competitive position of plants based on the fuel cell approach. Fuel cell systems will emit less than target emissions limits. U.S. developers have begun investigating the viability of coal gas fuel to MCFCs and SOFCs (20,21,22). An FCE 20 kW MCFC stack was tested for a total of 4,000 hours, of which 3,900 hours was conducted at Plaquemine, LA, using coal gas as well as pipeline gas. The test included 1,500 hours of operation using 9,142 kJ/m^3 syngas from a slip stream of a 2,180 tonne/day Destec entrained gasifier. The fuel processing system incorporated cold gas cleanup for bulk removal of H_2S and other contaminants, allowing the 21 kW MCFC stack to demonstrate that the FCE technology can operate on either natural gas or coal gas.

User groups have organized together with the manufacturers in stationary plant development programs. The groups are listed below:

• PAFC, IFC	The North American Fuel Cell Owners Group
• MCFC, FCE	The Fuel Cell Commercialization Group
• SOFC, Siemens Westinghouse	SOFC Commercialization Association (SOCA)

These groups provide invaluable information from a user viewpoint about fuel cell technology for stationary power plant application. They can be contacted though the manufacturers.

A series of standards is being developed to facilitate the application of stationary fuel cell technology power plants. Standard development activities presently underway are

• Design and Manufacturing Standard	ANSI Z21.83/CGA 12.10
• Interconnect Standards for Interfacing	Revive/Revise ANSI/IEEE Std 1001-1988
• Performance Test	ASME PTC50, Fuel Cell Performance Code Committee
• Emergency Generator Standards	NFPA 70,110
• Installation Standard	Review NFPA TC 850

MILITARY APPLICATIONS

The military finds certain characteristics of fuel cell power plants desirable for field duty. Foremost, a fuel cell unit is quiet and has a low heat profile so can be close to the front line. It can be scaled to various sizes, from a few kW backpack to larger mobile power plant. The main drawback for the military is that the existing infrastructure is limited to logistic fuels. Logistic fuels (defined as easily transportable and stored, and compatible with military uses) are difficult to convert to hydrogen for fuel cell use. The burden of changing the fuel infrastructure to accommodate lighter fuels, normally used in fuel cells, is far greater than the benefits fuel cells offer the military. The Advanced Research Projects Agency of DOD funded several projects to investigate adapting logistics fuels to fuel cell use.

IFC conducted testing of a 100 kW mobile electric power plant (MEP) with the logistic fuels of JP-8 and DF-2. An auto-thermal reformer that achieved 98% conversion was used to convert the logistic fuel to a methane rich fuel.

FCE tested a lab-scale carbonate fuel cell stack on a model diesel-like fuel (Exxsol) using an adiabatic pre-reformer to convert the liquid fuel to methane in 1991 to 1993. In 1995 and 1996, FCE verified a 32 kW MCFC stack operation on jet fuel (JP-8) and diesel (DF-2) in system integrated tests using the diesel-to-methane adiabatic pre-reformer approach. Test results showed that there was a 5% power derating compared to natural gas operation.

The 25 kW SOFC power unit (see Siemens Westinghouse, above) was fitted with a pre-reformer similar to the FCE and operated with JP-8 (766 hours) and DF-2 (1555 hours) while the unit was installed at FCE's Highgrove Station.

SOFCo, a limited partnership of Babcock and Wilcox (a McDermott International Company) and Ceramatec (an Elkem company), has tested a planar SOFC unit for the MEP program that will operate on logistic fuels. Honeywell tested their MEP unit on logistic fuel.

All demonstrations showed that fuel cell units can be operated with military logistic fuels (18).

The utility applications for DOD refers to power plants that serve the load of a particular population and range in size from a few megawatts for distributed power generation to 100+ MW. Electricity purchased from local utilities is expensive. Master metering and large air-conditioning loads can cause the demand portion of the electric bill to be more than 50 % of the total bill. There is significant potential for improving the security of electrical power supplied by using onsite power generation. The increased concern of environmental issues has made producing clean power desirable and mandatory. In addition, most central heat plants on U.S. military installations are nearing the end of their useful life: there are opportunities to replace outdated existing equipment with modern technologies.

1.6.2 Distributed Generation

Distributed generation is small, modular power systems that are sited at or near their point of use. The typical system is less than 30 MW, used for generation or storage, and extremely clean. Examples of technologies used in distributed generation include proven gas turbines and reciprocating engines, biomass-based generators, concentrating solar power and photovoltaic systems, fuel cells, wind turbines, micro-turbines, and flywheel storage devices. See Table 1-3 for size and efficiencies of selected systems.

Table 1-3 Attributes of Selected Distributed Generation Systems

Type	Size	Efficiency, %
Reciprocating Engines	50 kW – 6 MW	33 – 37
Micro turbines	10 kW – 300 kW	20 – 30
Phosphoric Acid Fuel Cell (PAFC)	50 kW – 1 MW	40
Solid Oxide Fuel Cell (SOFC)	5 kW – 3 MW	45 – 65
Proton Exchange Fuel Cell (PEFC)	<1 kW – 1 MW	34 – 36
Photovoltaics (PV)	1 kW – 1 MW	NA
Wind Turbines	150 kW – 500 kW	NA
Hybrid Renewable	<1 kW – 1 MW	40 – 50

The market for distributed generation is aimed at customers dependent on reliable energy, such as hospitals, manufacturing plants, grocery stores, restaurants, and banking facilities. There is currently over 15 GW of distributed power generation operating in the U.S. Over the next decade, the domestic market for distributed generation, in terms of installed capacity to meet the demand, is estimated to be 5-6 GW per year. The projected global market capacity increases are estimated to be 20 GW per year (23). Several factors have played a role in the rise in demand for distributed generation. Utility restructuring is one of the factors. Energy suppliers must now take on the financial risk of capacity additions. This leads to less capital intensive projects and

shorter construction periods. Also, energy suppliers are increasing capacity factors on existing plants rather than installing new capacity, which places pressure on reserve margins. This increases the possibility of forced outages, thereby increasing the concern for reliable service. There is also a demand for capacity additions that offer high efficiency and use of renewables as the pressure for enhanced environmental performance increases (23).

There are many applications for distributed generation systems. They include:

- Peak shaving - Power costs fluctuate hour by hour depending upon demand and generation, therefore customers would select to use distributed generation during relatively high-cost on-peak periods.
- Combined heat and power (CHP) (Cogeneration) –The thermal energy created while converting fuel to electricity would be utilized for heat in addition to electricity in remote areas and electricity and heat for sites that have a 24 hour thermal/electric demand.
- Grid support – Strategic placement of distributed generation can provide system benefits and preclude the need for expensive upgrades and provide electricity in regions where small increments of new baseload capacity is needed.
- Standby power – Power during system outages is provided by a distributed generation system until service can be restored. This is used for customers that require reliable back-up power for health or safety reasons, companies with voltage sensitive equipment, or where outage costs are unacceptably high.
- Remote/Stand alone – The user is isolated from the grid either by choice or circumstance. The purpose is for remote applications and mobile units to supply electricity where needed.

Benefits and Obstacles:

Distributed generation systems have small footprints, are modular and mobile making them very flexible in use. The systems provide benefits at the customer level, the supplier level, and the national level. Benefits to the customer include high power quality, improved reliability, and flexibility to react to electricity price spikes. Supplier benefits include avoiding investments in transmission and distribution (T&D) capacity upgrades by locating power where it is most needed and opening new markets in remote areas. At the national level, the market for distributed generation establishes a new industry, boosting the economy. The improved efficiencies also reduce greenhouse gas emissions.

However, there are also a number of barriers and obstacles to overcome before distributed generation can become a mainstream service. These barriers include technical, economic, institutional, and regulatory issues. Many of the proposed technologies have not yet entered the market and will need to meet performance and pricing targets before entry. Questions have also risen on requirements for connection to the grid. Lack of standardized procedures creates delays and discourages customer-owned projects. Siting, permitting, and environmental regulations can also delay and increase the costs of distributed generation projects.

In 1998, the Department of Energy created a Distributed Power Program to focus on market barriers and other issues, which are prohibiting the growth of distributed generation systems. Under the leadership of the National Renewable Energy Laboratory (NREL), a collaboration of national laboratories and industry partners have been creating new standards and identifying and

removing regulatory barriers. The goals of the program include 1) Strategic research, 2) System Integration, and 3) Mitigation of regulatory and institutional barriers (24).

Fuel Cells:
Fuel cells, one of the emerging technologies in distributed generation, have been hindered by high initial costs. However, costs are expected to decline as manufacturing capacity and capability increase and designs and integration improve. The fuel cell systems offer many potential benefits as a distributed generation system. They are small and modular, and capital costs are relatively insensitive to scale. This makes them ideal candidates for diverse applications where they can be matched to meet specific load requirements. The systems are unobtrusive with very low noise levels and have negligible air emissions. These qualities enable them to be placed close to the source of power demand. Fuel cells also offer higher efficiencies than conventional plants. The efficiencies can be enhanced by utilizing the quality waste heat derived from the fuel cell reactions for combined heat and power and combined-cycle applications.

Phosphoric acid fuel cells have successfully been commercialized. Second generation fuel cells, including solid oxide fuel cells and molten carbonate fuel cells, are expected to make market entry by 2002. Research is ongoing in areas such as fuel options and new ceramic materials. Different manufacturing techniques are also being sought to help reduce capital costs. Proton exchange membrane fuel cells are still in the development and testing phase.

Projects:
There are currently several projects in the distributed generation market underway with various fuel cell developers and utility companies. These projects are helping to drive costs down and bring the fuel cells closer to commercialization. Below is a summary of some of the projects.

IdaTech LLC (formerly Northwest Power Systems), of Bend, Oregon, an Idacorp subsidiary, delivered the first of 110 planned fuel cell systems to the Bonneville Power Administration (BPA), Portland, Oregon in June 2000. The BPA program is part of a fuel cell test and development phase intended to commercialize fuel cell systems for home and small commercial applications by 2003.

Avista Labs, an affiliate of Avista Corp., of Spokane, Washington, received a U.S. patent in March 2000 that covers 162 claims for its modular, cartridge-based proton exchange membrane fuel cell. The fuel cell cartridges can be removed and replaced while the power system continues to operate. Additional elements of the patented system include proprietary designs that simplify the humidifying and cooling systems, resulting in lower manufacturing costs and higher efficiency. Currently, Avista has 75 fuel cells installed at 20 sites around the U.S. and Brazil.

Bewag AG's Treptow heating plant, located in Berlin, Germany received a 250 kW PEFC unit in April 2000 from Ballard Generation Systems, a subsidiary of Ballard Power System, of Burnaby, BC, Canada.

Plug Power, Inc, of Latham, NY delivered more than 106 5-kW grid-parallel systems, through October 2001. Deliveries include 44 units to New York State Research & Development

Authority and 57 units to the Long Island Power Authority. Plug Power has also sent units to 1) Kubota, a diversified Japanese Manufacturing and distribution company, 2) Oak Ridge National Laboratory, 3) Vaillant GmbH in Germany, and 4) a 50-kW unit to Air Products and Chemicals.

Energy USA, a subsidiary of NiSource Inc, of Merrillville, Ind formed a joint venture with Institute of Gas Technology called Mosiac Energy LLC. They designed fuel cells for the core of the home's energy-generating system to be used in a Chesterton, Indiana housing development. Space heating and other household needs will be provided by the byproduct heat production.

UTC Fuel Cells, of South Windsor, Connecticut, has the most commercially advanced fuel cell for electricity generation, the PC25, a 200-kW phosphoric acid fuel cell (PAFC). UTC Fuel Cells has over 250 fuel cells in 19 countries delivered around the world.

Siemens Westinghouse, of Pittsburgh, PA has manufactured the largest tubular solid oxide fuel cell (SOFC) system. The Dutch/Danish consortium EDB/Elsam operates the system, which supplies 110 kW of electricity to the grid and 64 kW to the city of Westervoort, Netherlands district heating system. The efficiency is about 46% with exhaust gas values for NO_X, SO_X, CO and VHC under 1 ppm each. Commercial units ranging in size from 250 to 1000 kW are expected in 2004. Siemens Westingtonhouse installed a 250 kW unit at the National Fuel Cell Center.

The Los Angeles Department of Water and Power (LADWP) is investing $1.5 million to develop and install a 250 kW molten carbonate fuel cell (MCFC) powerplant. FCE, of Danbury, Connecticut will supply the fuel cell. The goals of the project include testing and demonstrating the feasibility of the technology to generate electricity for the LADWP system.

In early 2000, FCE's DFC® went into a joint public/private development with NETL. This system uses internal conversion of the natural-gas fuel to hydrogen, as opposed to an external unit. This reduces costs and creates efficient use of excess heat. The DFC® system has already passed 8600 hours and a one-year milestone at FCE's headquarters.

In 2001, FCE delivered a 250 kW DFC® power plant to the Mercedes-Benz manufacturing facility in Tuscaloosa, AL. The fuel cell is tied into the existing power distribution system.

MILITARY APPLICATIONS

The Navy is studying the concept of all electric ships. These new ships will not have a central engine room and long drive shafts. The ships will depend on redundancy of generator capacity for combat survival, rather than protection of a centralized engine room.

1.6.3 Vehicle Motive Power

Since the late 1980s, there has been a strong push to develop fuel cells for use in light-duty and heavy-duty vehicle propulsion. A major drive for this development is the need for clean, efficient cars, trucks, and buses that can operate on conventional fuels (gasoline, diesel), as well as renewable and alternative fuels (hydrogen, methanol, ethanol, natural gas, and other hydrocarbons). With hydrogen as the on-board fuel, such vehicles would be zero emission vehicles. With on-board fuels other than hydrogen, the fuel cell systems would use an appropriate fuel

processor to convert the fuel to hydrogen, yielding vehicle power trains with very low acid gas emissions and high efficiencies. Further, such vehicles offer the advantages of electric drive and low maintenance because of the few critical moving parts. This development is being sponsored by various governments in North America, Europe, and Japan, as well as by major automobile manufacturers worldwide. Several fuel cell-powered cars, vans, and buses have operated on hydrogen and methanol.

In the early 1970s, K. Kordesch modified a 1961 Austin A-40 two-door, four-passenger sedan to an air-hydrogen fuel cell/battery hybrid car (23). This vehicle used a 6-kW alkaline fuel cell in conjunction with lead acid batteries, and operated on hydrogen carried in compressed gas cylinders mounted on the roof. The car was operated on public roads for three years and about 21,000 km.

In 1994 and 1995, H-Power (Belleville, New Jersey) headed a team that built three PAFC/battery hybrid transit buses (24,25). These 9 meter (30 foot), 25 seat (with space for two wheel chairs) buses used a 50 kW fuel cell and a 100 kW, 180 amp-hour nickel cadmium battery.

The major activity in transportation fuel cell development has focused on the polymer electrolyte fuel cell (PEFC). In 1993, Ballard Power Systems (Burnaby, British Columbia, Canada) demonstrated a 10 m (32 foot) light-duty transit bus with a 120 kW fuel cell system, followed by a 200 kW, 12 meter (40 foot) heavy-duty transit bus in 1995 (26). These buses use no traction batteries. They operate on compressed hydrogen as the on-board fuel. In 1997, Ballard provided 205 kW (275 HP) PEFC units for a small fleet of hydrogen-fueled, full-size transit buses for demonstrations in Chicago, Illinois, and Vancouver, British Columbia. Working in collaboration with Ballard, Daimler-Benz built a series of PEFC-powered vehicles, ranging from passenger cars to buses (27). The first such vehicles were hydrogen-fueled. A methanol-fueled PEFC A-class car unveiled by Daimler-Benz in 1997 has a 640 km (400 mile) range. Plans are to offer a commercial vehicle by 2004. A hydrogen-fueled (metal hydride for hydrogen storage), fuel cell/battery hybrid passenger car was built by Toyota in 1996, followed in 1997 by a methanol-fueled car built on the same (RAV4) platform (28).

In February 2002, UTC Fuel Cells and Nissan signed an agreement to develop fuel cells and fuel cell components for vehicles. Renault, Nissan's alliance partner, is also participating in the development projects. UTC Fuel Cells will provide proprietary ambient-pressure proton exchange membrane fuel cell technology.

Ballard's fuel cell engine powered DaimlerChrysler's NECAR 5 fuel cell vehicle in a 13-day, 3,000-mile endurance test across the United States. The drive provided Ballard and DaimlerChrysler with testing experience in a variety of conditions.

Toyota Motor Corp. and Honda Motor Co. have announced they will advance their initial vehicle introduction plans for fuel cell vehicles to late in 2002 from 2003. Honda achieved a significant milestone for its product launch by receiving both CARB and EPA certification of its zero emission FCX-V4 automobile. This is the first vehicle to receive such certification. Ballard's fuel cell powered this Honda vehicle.

Other major automobile manufacturers, including General Motors, Volkswagen, Volvo, Chrysler, Nissan, and Ford, have also announced plans to build prototype polymer electrolyte fuel cell vehicles operating on hydrogen, methanol, or gasoline (29). IFC and Plug Power in the U.S., and Ballard Power Systems of Canada (15), are involved in separate programs to build 50 to 100 kW fuel cell systems for vehicle motive power. Other fuel cell manufacturers are involved in similar vehicle programs. Some are developing fuel cell-powered utility vehicles, golf carts, etc. (30,31).

MILITARY APPLICATIONS

The U.S. Army plans to reduce battlefield fuel consumption 75% by the year 2020. This will make supplying combat units easier, while also making it easier to protect supply lines. The future Army must reduce its vehicle exhaust emissions during peacetime. The Army owns a large number of vehicles equipped with non-emission controlled diesel engines, and will still own a significant number of these engines in 2020. One example of military-sponsored research is the all-electric tank with an electromagnetic rail gun. The gun would use a powerful magnetic field to propel a small armor-piercing projectile to hypersonic speeds. Such a vehicle would be fast, quiet, and capable of firing flurries of rounds at multiple targets.

1.6.4 Space and Other Closed Environment Power

The application of fuel cells in the space program (1 kW PEFC in the Gemini program and 1.5 kW AFC in the Apollo program) was demonstrated in the 1960s. More recently, three 12 kW AFC units have been used for at least 87 missions with 65,000 hours flight time in the Space Shuttle Orbiter. In these space applications, the fuel cells use pure reactant gases. IFC has produced a H_2/O_2 30 kW unit for the Navy's Lockheed Deep Quest vehicle. It operates at depths of 1500 meters (5000 feet). Ballard Power Systems has produced an 80 kW PEFC unit for submarine use (methanol fueled) and for portable power systems.

1.6.5 Fuel Cell Auxiliary Power Systems

In addition to high-profile fuel cell applications such as automotive propulsion and distributed power generation, the use of fuel cells as auxiliary power units (APUs) for vehicles has received considerable attention (see Figure 1-9). APU applications may be an attractive market because it offers a true mass-market opportunity that does not require the challenging performance and low cost required for propulsion systems for vehicles. In this section, a discussion of the technical performance requirements for such fuel cell APUs, as well as the current status of the technology and the implications for fuel cell system configuration and cost is given.

Participants	Application	Size range	Fuel /Fuel Cell type	Nature of Activity
BMW, International Fuel Cells[1]	passenger car, BMW 7-series	5kW net	Hydrogen, Atmospheric PEFC	Demonstration
Ballard, Daimler-Chrysler[2]	Class 8 Freightliner heavy-duty Century Class S/T truck cab	1.4 kW net for 8000 BTU/h A/C unit	Hydrogen, PEFC	Demonstration
BMW, Delphi, Global Thermoelectric[3]	passenger car	1-5kW net	Gasoline, SOFC	Technology development program

1. "Fuel Cell Auxiliary Power Unit – Innovation for the Electric Supply of Passenger Cars?" J. Tachtler et al. BMW Group, SAE 2000-01-0374, Society of Automotive Engineers, 2000.
2. "Freightliner unveils prototype fuel cell to power cab amenities," O. B. Patten, Roadstaronline.com news, July 20, 2000.
3. Company press releases, 1999.

Figure 1-9 Overview of Fuel Cell Activities Aimed at APU Applications

Auxiliary power units are devices that can provide all or part of the non-propulsion power for vehicles. Such units are already in widespread use in a range of vehicle types and for a variety of applications, in which they provide a number of potential benefits (see Figure 1-10). Although each of these applications could provide attractive future markets for fuel cells, this section will focus on application to on-road vehicles (specifically trucks).

Vehicles Types	Loads Serviced	Potential Benefits
• Heavy-duty & utility trucks • Airplanes • Trains • Yachts & Ships • Recreational vehicles • Automobiles & light trucks (not commercial yet)	• Space conditioning • Refrigeration • Lighting and other cabin amenities • Communication and information equipment • Entertainment (TV, radio)	• Can operate when main engine unavailable • Reduce emissions and noise while parked • Extend life of main engine • Improve power generation efficiency when parked

Figure 1-10 Overview of APU Applications

In 1997, the Office of Naval Research initiated an advanced development program to demonstrate a ship service fuel cell power generation module. The ship service generator supplies the electrical power requirements of the ship. This program will provide the basis for a new fuel cell-based design that will be an attractive option for the future Navy surface ships. This program will provide the Navy with a ship service that is more efficient and incorporates a distributive power system that will remain operating even if the engine is destroyed.

Fuel cells can serve as a generator, battery charger, battery replacements and heat supply. They can adapt to most environments, even locations in Arctic and Antarctic regions.
One effort, being run in collaboration with the Army Research Office, has demonstrated a prototype fuel cell designed to replace in many applications a popular military standard battery.

The target application is the Army's BA-5590 primary (i.e., use-once-and-dispose) lithium battery. The Army purchases approximately 350,000 of these batteries every year at a cost of approximately $100 per battery, including almost $30 per battery for disposal. Fuel cells, on the other hand, are not thrown away after each use but can be reused hundreds of times. Mission weight savings of factors of 10 or more are projected. The prototype fuel cell, which has the same size and delivers the same power as a battery, has been tested in all orientations and under simulated adverse weather conditions, and was enthusiastically received by Army senior management.

System Performance Requirements

A key reason for interest in fuel cell APU applications is that there may be a good fit between APU requirements and fuel cell system characteristics. Fuel cells could be efficient and quiet, and APUs do have the load following requirements and physical size and weight constraints associated with propulsion applications. However, in order to understand the system requirements for fuel cell APUs, it is critical to understand the required functionality (refer to Figure 1-10) as well as competing technologies. To provide the functionality of interest, and to be competitive with internal combustion engine (ICE) driven APUs, fuel cell APUs must meet various requirements; an overview is provided in Figure 1-11.

Key Parameter	*Typical Requirements*	*Expected fuel cell performance*
Power output	12 – 42 V DC is acceptable for most applications, 110 / 220 V AC may be desirable for powering power tools etc.	DC power output simplifies the power conditioning and control for fuel cells
System Capacity	1 – 5 kW for light duty vehicles and truck cabins up to 15 kW for truck refrigeration	Fits expected range for PEFCs and probably also advanced SOFCs
System Efficiency	More than 15-25% based on LHV	Efficiency target should be achievable, even in smallest capacity range
Operating life and reliability	Greater than about 5,000 hours stack life, with regular service intervals less than once every 1,000 hours	Insufficient data available to assess whether this is a challenge or not

Figure 1-11 Overview of typical system requirements

Fuel cell APUs will likely have to operate on gasoline, and for trucks preferably on diesel fuel, in order to match the infrastructure available, and preferably to be able to share on-board storage tanks with the main engine. The small amount of fuel involved in fueling APUs would likely not justify the establishment of a specialized infrastructure (e.g. a hydrogen infrastructure) for APUs alone. Similarly, fuel cell APUs should be water self-sufficient, as the need to carry water for the APU would be a major inconvenience to the operator, and would require additional space and associated equipment.

In addition to the requirement for stationary operation mentioned in Figure 1-11, fuel cell APUs must be able to provide power rapidly after start-up, and must be able to follow loads. While the use of batteries to accomplish this is almost a given, a system start-up time of about ten minutes or less will likely be required to arrive at a reasonable overall package.

Finally, fuel cell APUs are clean. These attributes may well be the key competitive advantage that fuel cell APUs have over conventional APUs, and hence their performance must more than match that of internal combustion engines APUs.

Technology Status

Active technology development efforts in both PEFC and planar SOFC technology, driven primarily by the interest in distributed generation and automotive propulsion markets, have achieved significant progress in the development of these technologies. For distributed power applications, refined and even early commercial prototypes are being constructed.
However, in the case of planar SOFC a distinction must be made between different types of SOFC technologies. Neither the tubular nor the electrolyte supported SOFC technology is suitable for APU applications due to their very high operating temperature, large size and weight. Only the electrode supported planar SOFC technology may be applicable to APU applications. Since it has only been developed over the past nine years, as opposed to several decades for PEFC and other SOFC technologies, it has not developed as far, although it appears to be catching up quickly (See Figure 1-12).

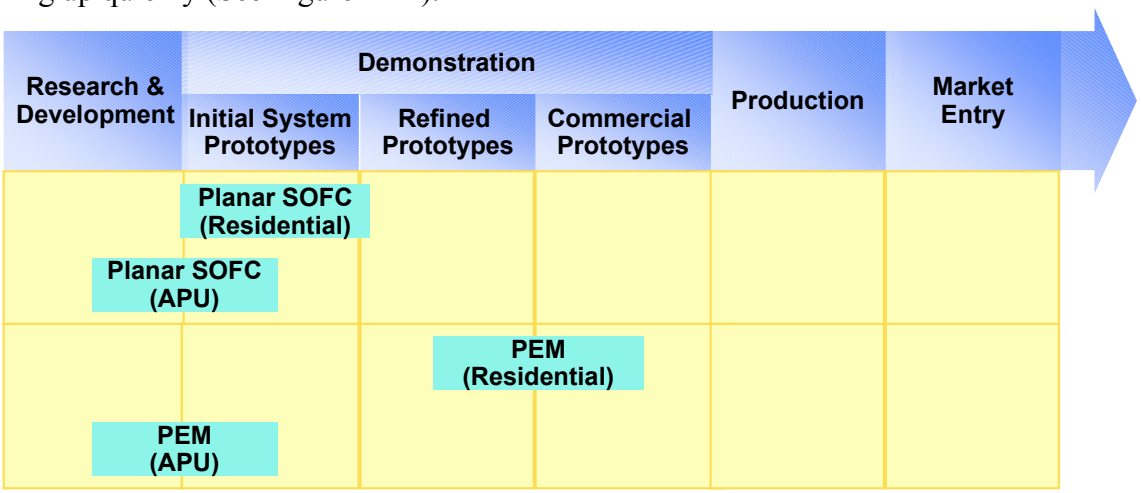

Figure 1-12 Stage of development for fuel cells for APU applications

Fuel cell APU applications could benefit significantly from the development of distributed generation systems, especially from residential scale systems, because of the similarity in scale and duty cycle. However, distributed generation systems are designed mostly for operation on natural gas, and do not face as stringent weight and volume requirements as APU applications. As a result, fuel cell APUs are in the early initial system prototype stage.

Several developers, including Nuvera, Honeywell, and Plug Power are active in the development for residential PEFC power systems. Most of the PEFC system technology can be adapted for

APU application, except that a fuel processor capable of handling transportation fuels is required. However, most of the players in the residential PEFC field are also engaged in the development of PEFC systems for automotive propulsion applications, which are targeting the ability to utilize transportation fuels for PEFC systems.

Relatively few developers of SOFC technology have paid attention to non-stationary markets. All are focused on small to medium sized distributed generation and on-site generation markets. Only Global Thermoelectric (Calgary, Canada) has been active in the application of its technology to APUs. A recent study conducted a detailed conceptual design and cost estimate of a 5-kWnet SOFC-based truck APU and concluded that, provided continued improvement in several technology areas, planar SOFCs could ultimately become a realistic option for this mass-market application.

System Configuration and Technology Issues

Based on the system requirements discussed above, fuel cell APUs will consist of a fuel processor, a stack system and the balance of plant. Figure 1-13 lists the components required in SOFC and PEFC based systems. The components needed in a PEFC system for APU applications are similar to that needed in residential power. The main issue for components for PEFC-based systems is the minimization or elimination of the use of external supplied water. For both PEFC and SOFC systems, start-up batteries (either existing or dedicated units) will be needed since external electric power is not available.

Detailed cost and design studies for both PEFC and SOFC systems at sizes ranging from 5kW to 1 MW were made that point to the fundamental differences between PEFC and SOFC technology that impact the system design and by implication the cost structure. These differences will be discussed in the following paragraphs.

The main components in a SOFC APU are the fuel cell stack, the fuel processor, and the thermal management system. In addition, there are several balance of plant components, which are listed in Figure 1-13. The relatively simple reformer design is possible because the SOFC stack operates at high temperatures (around 800°C) and is capable of utilizing both carbon monoxide and certain hydrocarbons as fuel. Since both the anode and cathode exhaust at temperatures of 600-850°C, high temperature recuperators are required to maintain system efficiency. These recuperators are made of expensive materials (high temperature reducing and oxidizing atmosphere), making it an expensive component in the system. However, if hydrocarbons are converted inside the stack, this leads to a less exothermic overall reaction so that the stack cooling requirements are reduced.

Further system simplification would occur if a sulfur-free fuel was used or if the fuel cell were sulfur tolerant. In that case, the fuel can be provided directly from the reformer to the fuel cell. In order to minimize system volume, (and minimize the associated system weight and start-up time) integration of the system components is a key design issue. By recycling the entire anode tailgas to provide steam, a water management system can be avoided, though a hot gas recirculation system is required.

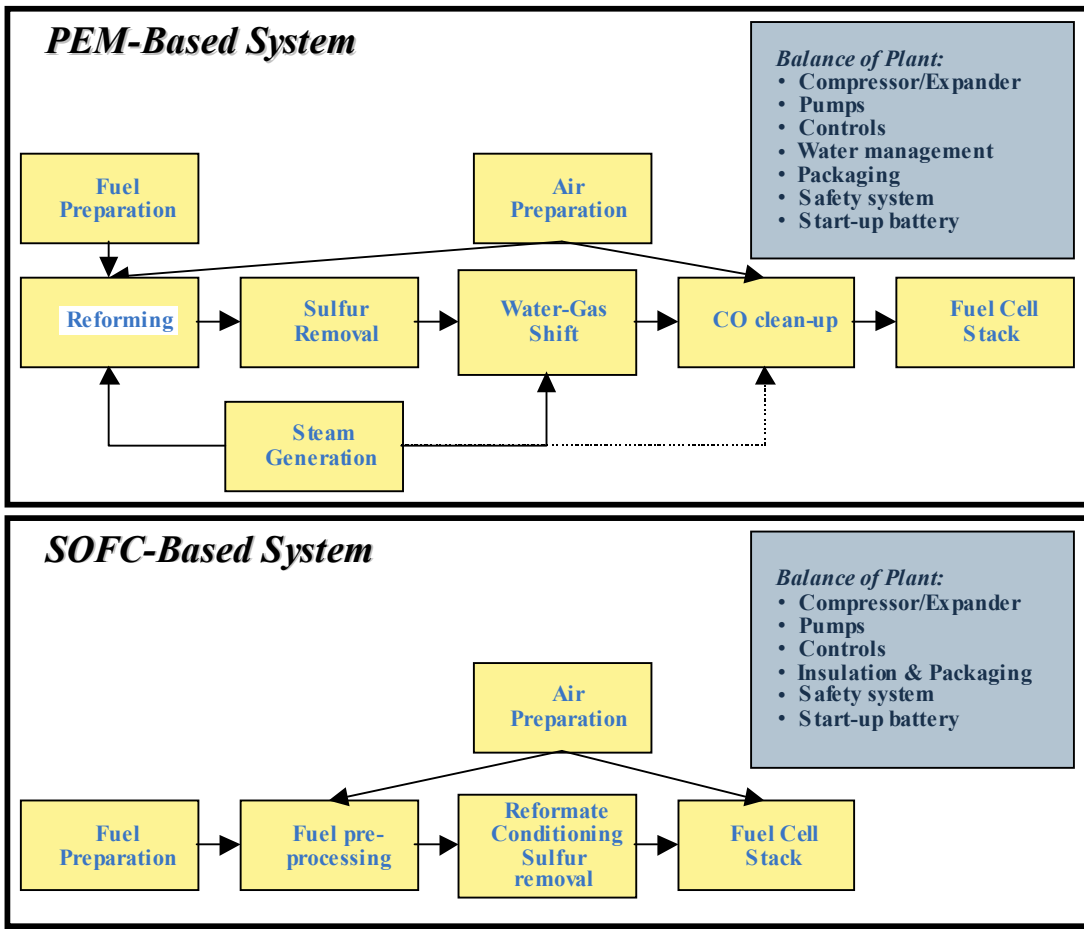

Figure 1-13. Overview of subsystems and components for SOFC and PEFC systems

Figure 1-14 shows a simplified layout for an SOFC-based APU. The air for reformer operation and cathode requirements is compressed in a single compressor and then split between the unit operations. The external water supply shown in Figure 1-14 will most likely not be needed; the anode recycle stream provides water. Unreacted anode tail gas is recuperated in a tail gas burner. Additional energy is available in a SOFC system from enthalpy recovery from tail gas effluent streams that are typically 400-600°C. Current thinking is that reformers for transportation fuel based SOFC APUs will be of the exothermic type (i.e. partial oxidation or autothermal reforming), as no viable steam reformers are available for such fuels.

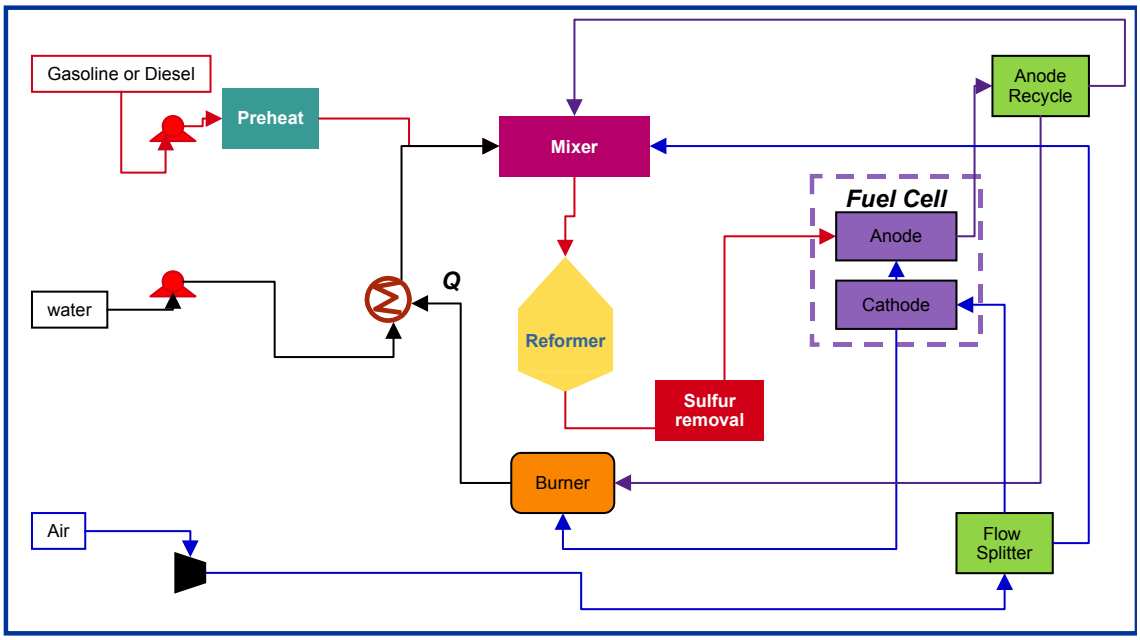

Figure 1-14. Simplified System process flow diagram of pre-reformer/SOFC system

Due to the operating requirements of PEFC stack technology, shift reactors and a carbon monoxide removal step are required to produce reformate of sufficient quality. Similarly, the stack operating temperature and its humidity requirements require a water management system as well as radiators for heat rejection. Some developers are developing pressurized systems to the benefit from higher reactant partial pressures on both anode and cathode. Fuel processing for PEFC APU systems is identical to that needed in residential power or propulsion applications. The additional issue for PEFC is the minimization of steam needed for the fuel processor system. Since an APU is a mobile and/or remote unit, the need for external sources of water should be minimized. The reformate stream is further diluted by additional steam, if that water is not removed prior to the fuel cell stack.

Another design integration issue in PEFC systems is water management for hydrating the electrolyte and providing the necessary steam for reforming and water-gas shift operations. Additional steam may be required for the CO clean-up device. Some reformate-based PEFC systems are run under pressure to increase the partial pressure of reactants for the PEFC anode and cathode, increasing efficiency. Pressure operation also aids in heat integration for the internal generation of steam at pressures greater than atmospheric (i.e. steam generated at temperatures greater than 100°C). PEFC system integration involves the integration of a reformer (either exothermic or endothermic overall, ~850-1000°C), shift reactors (exothermic, 150-500°C), CO-cleanup (primarily exothermic, 50-200°C), and the fuel cell stack (exothermic, 80°C). Each reaction zone operates at a significantly different temperature, thus providing a challenge for system integration and heat rejection. To alleviate some of these drawbacks, and further reduce the cost of the PEFC systems, developers are now investigating the possibility of using higher temperature membranes (e.g. operating slightly above 100°C). This would increase the carbon monoxide tolerance, potentially simplifying the fuel processor design, and simplify the heat rejection.

The power requirements for auxiliary power applications require smaller fuel cell stack duties. The heat losses for a SOFC stack operating at a smaller power duty are a larger proportion of the gross rating than in a stationary power application. Insulation, required for specified system skin temperature requirements, could conceivably result in a large proportion of the total system volume. Integration of the high temperature components is important in order to reduce the system volume and insulation requirements. SOFC APU systems will require inexpensive high performance insulation materials to decrease both system volume and cost.

System Cost Considerations

As for any new class of product, total cost of ownership and operation of fuel cells will be a critical factor in their commercialization, along with the offered functionality and performance. This total cost of ownership typically has several components for power systems such as fuel cells. These components include fuel cost, other operating costs such as maintenance cost, and the first cost of the equipment. This first cost has a significant impact on fuel cells' competitiveness.

The main component of a fuel cell's first cost is the manufacturing cost, which is strongly related to the physical configuration and embodiment of the system, as well as to the manufacturing methods used. System configuration and design in turn are directly related to the desired system functionality and performance, while the manufacturing methods used are strongly linked to the anticipated production volume.

Arthur D. Little has carried out cost structure studies for a variety of fuel cell technologies for a wide range of applications, including SOFC tubular, planar, and PEFC technologies. Because phenomena at many levels of abstraction have a significant impact on performance and cost, they have developed a multi-level system performance and cost modeling approach (see Figure 1-15). At the most elementary level, it includes fundamental chemical reaction/reactor models for the fuel processor and fuel cell as one-dimensional systems.

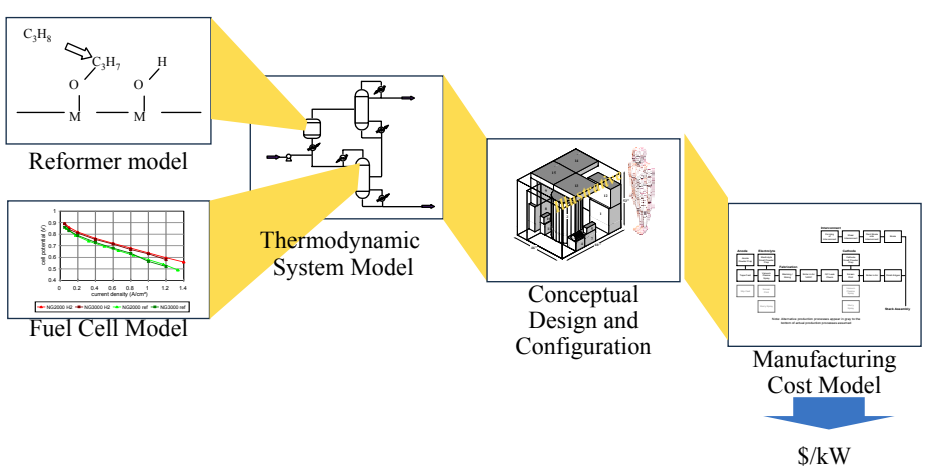

Figure 1-15 Multilevel system modeling approach.

Each of the detailed sub-models feed into the thermodynamic system model, and provides sizing information directly to the conceptual design and configuration. The thermodynamic system

model provides a technical hub for the multi-level approach. It provides inputs on the required flow rates and heat duties in the system. Sizing information, together with information from the thermodynamic model then flows to the conceptual design.

SOFC System Cost Structure

The main difference in SOFC stack cost structure as compared to PEFC cost relates to the simpler system configuration of the SOFC-based system. This is mainly due to the fact that SOFC stacks do not contain the type of high-cost precious metals that PEFCs contain. This is off-set in part by the relatively complex manufacturing process required for the manufacture of the SOFC electrode electrolyte plates and by the somewhat lower power density in SOFC systems. Low temperature operation (enabled with electrode supported planar configuration) enables the use of low cost metallic interconnects which can be manufactured with conventional metal forming operations.

The balance of plant contains all the direct stack support systems, reformer, compressors, pumps, and the recuperating heat exchangers. Its cost is low by comparison to the PEFC because of the simplicity of the reformer. However, the cost of the recuperating heat exchangers partially offsets that.

To provide some perspective on the viability of SOFCs in APU applications from a cost perspective, NETL sponsored an estimate of the cost structure of small-scale (5 kW), simple-cycle SOFC anode-supported system, operated on gasoline. The estimated manufacturing cost for such systems (see Figure 1-16) could well be close to that estimated for comparable PEFC systems, while providing somewhat higher system efficiency.

While the stack, insulation and stack balance in this simple-cycle system is a key component, the balance of plant is also an important factor. The stack cost again mainly depends on the achievable power density. Small systems like these will likely not be operated under high pressure. While this simplifies the design and reduces cost for compressors and expanders (which are not readily available at low cost for this size range in any case) it might also negatively affect the power density achievable.

One of the key challenges with small-scale SOFC systems is to overcome heat losses. The higher the heat losses are, the more recuperation is required to maintain the fuel cell within an acceptable operating temperature range and hence to ensure good performance.

The large fraction of cost related to balance of plant issues is mainly due to the very small scale of this system, which results in a significant reverse economy of scale. While design work is still ongoing, it is anticipated that the cost structure of this system will change rapidly to reduce the cost of balance of plant further, and further improve the competitiveness of these systems.

SOFC System Cost Structure:

Manufacturing Costs: $350-550/kW

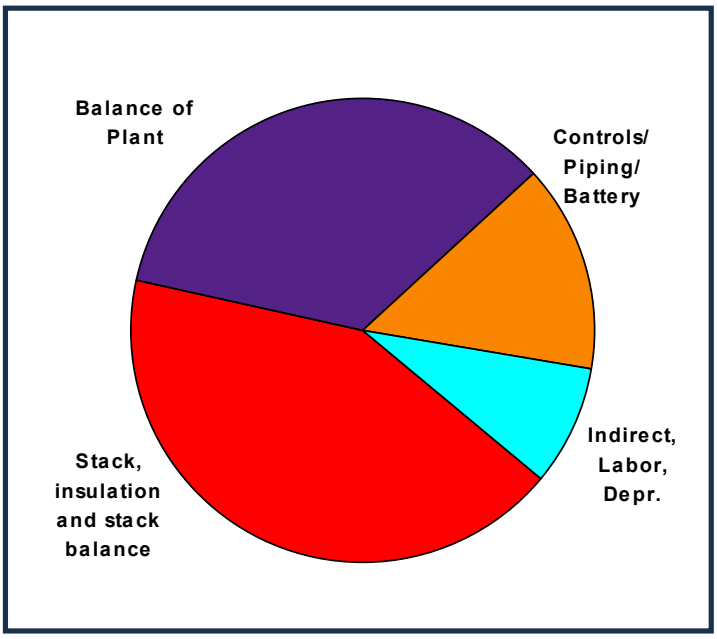

Figure 1-16. Projected cost structure of a 5kWnet APU SOFC system. Gasoline fueled POX reformer, Fuel cell operating at 300mW/cm^2, 0.7 V, 90 % fuel utilization, 500,000 units per year production volume.

Outlook and Conclusions

In conclusion, both PEFC and SOFC have the potential to meet the allowable cost targets, provided successful demonstrations prove the technology. It is critical however, that for the current technologies to be commercially successful, especially in small-capacity markets, high production volumes will have to be reached. APU applications might provide such markets. It is similarly critical that the technologies be demonstrated to perform and achieve the projected performance targets, and demonstrate long life. These are the challenges ahead for the fuel cell industry in the APU market segment.

1.6.6 Derivative Applications

Because of the modular nature of fuel cells, they are attractive for use in small portable units, ranging in size from 5 W or smaller to 100 W power levels. Examples of uses include the Ballard fuel cell, demonstrating 20 hour operation of a portable power unit (32), and an IFC military backpack. There has also been technology transfer from fuel cell system components. The best example is a joint IFC and Praxair, Inc. venture to develop a unit that converts natural gas to 99.999% pure hydrogen based on using fuel cell reformer technology and pressure swing adsorption process.

1.7 References

1. A.J. Appleby, F.R. Foulkes, *Fuel Cell Handbook*, Van Nostrand Reinhold, New York, NY, 1989.

2. *Report of the DOE Advanced Fuel-Cell Commercialization Working Group*, Edited by S.S. Penner, DOE/ER/0643, prepared by the DOE Advanced Fuel Cell Working Group (AFC2WG) or the United States Department of Energy under Contract No. DEFG03-93ER30213, March 1995.
3. K. Kordesch, J. Gsellmann, S. Jahangir, M. Schautz, in *Proceedings of the Symposium on Porous Electrodes: Theory and Practice,* Edited by H.C. Maru, T. Katan, M.G. Klein, The Electrochemical Society, Inc., Pennington, NJ, p. 163, 1984.
4. A. Pigeaud, H.C. Maru, L. Paetsch, J. Doyon, R. Bernard, in *Proceedings of the Symposium on Porous Electrodes: Theory and Practice,* Edited by H.C. Maru, T. Katan, M.G. Klein, The Electrochemical Society, Inc., Pennington, NJ, p. 234, 1984.
5. J.M. King, N. Ishikawa, "Phosphoric Acid Fuel Cell Power Plant Improvements and Commercial Fleet Experience," Nov. 96 Fuel Cell Seminar.
6. www.utcfuelcells.com.
7. Communications with IFC, August 24, 2000.
8. K. Yokota, et al., "GOI 11 MW FC Plant Operation Interim Report," in *Fuel Cell Program and Abstracts*, 1992 Fuel Cell Seminar, Tucson, AZ, November 29-December 2, 1992.
9. ONSI Press Release, "Fuel Cell Sets World Record; Runs 9,500 Hours Nonstop," May 20, 1997.
10. Northeast Utilities System Press Release, "Converting Landfill Gas into Electricity is an Environmental Plus," June 24, 1996.
11. "Groton's Tidy Machine," Public Power, March-April 1997.
12. ONSI Press Release, "World's First Hydrogen Fueled Fuel Cell Begins Operation in Hamburg, Germany," November 7, 1997.
13. "Anaerobic Gas Fuel Cell Shows Promise," Modern Power Systems, June 1997.
14. E.W. Hall, W.C. Riley, G.J. Sandelli, "PC25™ Product and Manufacturing Experience," IFC, Fuel Cell Seminar, November 1996.
15. www.ballard.com, 1998.
16. www.fuelcellenergy.com.
17. Information supplied by ERC for the Fuel Cell Handbook.
18. M.M. Piwetz, J.S. Larsen, T.S. Christensen, "Hydrodesulfurization and Pre-reforming of Logistic Fuels for Use in Fuel Cell Applications," *Fuel Cell Seminar Program and Abstracts*, Courtesy Associates, Inc., November 1996.
19. Westinghouse Electric Corporation, Bechtel Group, Inc., "Solid Oxide Fuel Cell Repowering of Highgrove Station Unit 1, Final Report," prepared for Southern California Edison Research Center, March 1992.
20. ERC, "Effects of Coal-Derived Trace Species on the Performance of Molten Carbonate Fuel Cells," topical report prepared for U.S. DOE/METC, DOE/MC/25009-T26, October 1991.
21. N. Maskalick, "Contaminant Effects in Solid Oxide Fuel Cells," in *Agenda and Abstracts*, Joint Contractors Meeting, *Fuel Cells and Coal-Fired Heat Engines Conference*, U.S. DOE/METC, August 3-5, 1993.
22. D.M. Rastler, C. Keeler, C.V. Chang, "Demonstration of a Carbonate on Coal Derived Gas," Report 15, in *An EPRI/GRI Fuel Cell Workshop on Technology Research and Development*. Stonehart Associates, Madison, CT, 1993.
23. Distributed Generation, Securing America's Future with Reliable, Flexible Power," U.S. Department of Energy, Office of Fossil Energy, National Energy Technology Center, October 1999.

24. U. S. Department of Energy's Office of Energy Efficiency and Renewable Energy webpage, http://www.eren.doe.gov/distributedpower Giovando, CarolAnn, "Distributed resources carve out a niche in competitive markets," *Power*, July/August 2000, pp. 46 – 57.
25. K.V. Kordesch, "City Car with H_2-Air Fuel Cell and Lead Battery," *6th Intersociety Energy Conversion Engineering Conference*, SAE Paper No. 719015, 1971.
26. A. Kaufman, "Phosphoric Acid Fuel Cell Bus Development," *Proceedings of the Annual Automotive Technology Development Contractors' Coordination Meeting*, Dearborn, MI, October 24-27, 1994, SAE Proceedings Volume P-289, pp. 289-293, 1995.
27. R.R. Wimmer, "Fuel Cell Transit Bus Testing & Development at Georgetown University," *Proceedings of the Thirty Second Intersociety Energy Conversion Engineering Conference*, July 27-August 1, 1997, Honolulu, HI, pp. 825-830, 1997.
28. N.C. Otto, P.F. Howard, "Transportation Engine Commercialization at Ballard Power Systems," *Program and Abstracts 1996 Fuel Cell Seminar*, November 17-20, 1996, Orlando, FL, pp. 559-562.
29. F. Panik, "Fuel Cells for Vehicle Application in Cars - Bringing the Future Closer," J. Power Sources, 71, 36-38, 1998.
30. S. Kawatsu, "Advanced PEFC Development for Fuel Cell Powered Vehicles," J. Power Sources, 71, 150-155, 1998.
31. *Fuel-Cell Technology: Powering the Future*, Electric Line, November/December 1996.
32. M. Graham, F. Barbir, F. Marken, M. Nadal, "Fuel Cell Power System for Utility Vehicle," *Program and Abstracts 1996 Fuel Cell Seminar*, November 17-20, 1996, Orlando, FL, pp. 571-574.
33. P.A. Lehman, C.E. Chamberlin, "Design and Performance of a Prototype Fuel Cell Powered Vehicle," *Program and Abstracts 1996 Fuel Cell Seminar*, November 17-20, 1996, Orlando, FL, pp. 567-570.
34. J. Leslie, "Dawn of the Hydrogen Age," Wired (magazine), October 1997

2. FUEL CELL PERFORMANCE

The purpose of this section is to describe the chemical and thermodynamic operation of fuel cells, i.e., how operating conditions affect the performance of fuel cells. The impact of variables such as temperature, pressure, and gas constituents on fuel cell performance must be assessed to predict how the cells operate to produce power. Understanding the impacts of these variables allows fuel cell developers to optimize their design of the modular units, and it allows process engineers to maximize the performance of systems applications.

A logical first step in understanding the operation of a fuel cell is to define its ideal performance. Once the ideal performance is determined, parasitic losses can be calculated and then deducted from the ideal performance to describe the actual operation.

2.1 Gibbs Free Energy and Nernst Potential

Total energy is composed of two types of energy: 1) free energy, G and 2) unavailable energy, TS. Free energy earns its name because it is energy that is available (or free) for conversion into usable work. The unavailable energy is lost due to the increased disorder, or entropy, of the system. The maximum electrical work (W_{el}) obtainable in a fuel cell operating at constant temperature and pressure is given by the change in (Gibbs) free energy (ΔG) of the electrochemical reaction:

$$W_{el} = \Delta G = -n \mathcal{F} E \qquad (2\text{-}1)$$

where n is the number of electrons participating in the reaction, **F** is Faraday's constant (96,487 coulombs/g-mole electron), and **E** is the ideal potential of the cell. For reactants and products in their standard states, then

$$\Delta G^\circ = -n F E^\circ \qquad (2\text{-}2)$$

where the superscript represents standard state conditions (25°C or 298°K and 1 atm).

For a fuel cell, the maximum work available is related to the free energy of reaction, whereas the enthalpy (heat) of reaction is the pertinent quantity in the case of thermal conversion (such as a heat engine). For the state function

$$\Delta G = \Delta H - T\Delta S \qquad (2\text{-}3)$$

the difference between ΔG and ΔH is proportional to the change in entropy (ΔS). The maximum amount of electrical energy available is ΔG, as mentioned above, and the total thermal energy available is ΔH. The amount of heat that is produced by a fuel cell operating reversibly is $T\Delta S$. Reactions in fuel cells that have negative entropy change generate heat, while those with positive entropy change may extract heat from their surroundings if the irreversible generation of heat is smaller than the reversible absorption of heat.

The reversible potential of a fuel cell at temperature T is calculated from ΔG for the cell reaction at that temperature. This potential can be computed from the heat capacities (C_p) of the species involved as a function of T and from values of both $\Delta S°$ and $\Delta H°$ at the reference temperature, usually 298K. Empirically, the heat capacity of a species, as a function of T, can be expressed as

$$C_p = a + bT + cT^2 \qquad (2\text{-}4)$$

where a, b, and c are empirical constants. The specific enthalpy for any species present during the reaction is given by

$$\underline{H}_i = \Delta\underline{H}_i^o + \int_{298}^{T} C_{pi}\, dT \qquad (2\text{-}5)$$

and, at constant pressure

$$\underline{S}_i = \Delta\underline{S}_i^o + \int_{298}^{T} \frac{C_{pi}}{T}\, dT \qquad (2\text{-}6)$$

then it follows that

$$\Delta H = \sum_i n_i \underline{H}_i \Big|_{out} - \sum_i n_i \underline{H}_i \Big|_{in} \qquad (2\text{-}7)$$

and

$$\Delta S = \sum_i n_i \underline{S}_i \Big|_{out} - \sum_i n_i \underline{S}_i \Big|_{in} \qquad (2\text{-}8)$$

The coefficients a, b, and c (see Table 9-3), as well as ΔS° and ΔH°, are available from standard reference tables, and may be used to calculate ΔH and ΔS. From these values it is then possible to calculate ΔG and E.

Instead of using the coefficients a, b, and c, it is modern practice to rely on tables, such as JANAF Thermochemical Tables (4) to provide Cp, ΔH, ΔS, and ΔG over a range of temperatures for all species present in the reaction.

For the general cell reaction,

$$\alpha A + \beta B \rightarrow cC + \delta D \qquad (2\text{-}9)$$

the free energy change can be expressed by the equation:

$$\Delta G = \Delta G^\circ + RT \ln \frac{[C]^c [D]^\delta}{[A]^\alpha [B]^\beta} \qquad (2\text{-}10)$$

When Equations (2-1) and (2-2) are substituted in Equation (2-10),

$$E = E^\circ + \frac{RT}{n\mathcal{F}} \ln \frac{[A]^\alpha [B]^\beta}{[C]^c [D]^\delta} \qquad (2\text{-}11)$$

or

$$E = E^\circ + \frac{RT}{n\mathcal{F}} \ln \frac{\Pi\ [\text{reactant activity}]}{\Pi\ [\text{product activity}]} \qquad (2\text{-}12)$$

which is the general form of the Nernst equation. For the overall cell reaction, the cell potential increases with an increase in the activity (concentration) of reactants and a decrease in the activity of products.

2.1.1 Ideal Performance

The ideal performance of a fuel cell is defined by its Nernst potential, E, which is the ideal cell voltage. The overall reactions for various types of fuel cells are presented in Table 2-1. The corresponding Nernst equations for those reactions are provided in Table 2-2.

Table 2-1 Electrochemical Reactions in Fuel Cells

Fuel Cell	Anode Reaction	Cathode Reaction
Proton Exchange Membrane and Phosphoric Acid	$H_2 \rightarrow 2H^+ + 2e^-$	$\frac{1}{2} O_2 + 2H^+ + 2e^- \rightarrow H_2O$
Alkaline	$H_2 + 2(OH)^- \rightarrow 2H_2O + 2e^-$	$\frac{1}{2} O_2 + H_2O + 2e^- \rightarrow 2(OH)^-$
Molten Carbonate	$H_2 + CO_3^= \rightarrow H_2O + CO_2 + 2e^-$ $CO + CO_3^= \rightarrow 2CO_2 + 2e^-$	$\frac{1}{2} O_2 + CO_2 + 2e^- \rightarrow CO_3^=$
Solid Oxide	$H_2 + O^= \rightarrow H_2O + 2e^-$ $CO + O^= \rightarrow CO_2 + 2e^-$ $CH_4 + 4O^= \rightarrow 2H_2O + CO_2 + 8e^-$	$\frac{1}{2} O_2 + 2e^- \rightarrow O^=$

CO - carbon monoxide	e^- - electron	H_2O - water
CO_2 - carbon dioxide	H^+ - hydrogen ion	O_2 - oxygen
$CO_3^=$ - carbonate ion	H_2 - hydrogen	OH^- - hydroxyl ion

The Nernst equation provides a relationship between the ideal standard potential (E°) for the cell reaction and the ideal equilibrium potential (E) at other temperatures and partial pressures of reactants and products. Once the ideal potential at standard conditions is known, the ideal voltage can be determined at other temperatures and pressures through the use of these Nernst equations. According to the Nernst equation for the hydrogen reaction, the ideal cell potential at a given temperature can be increased by operating at higher reactant pressures, and improvements in fuel cell performance have, in fact, been observed at higher pressures. This will be further demonstrated in Sections 3 through 7 for the various types of fuel cells.

The reaction of H_2 and O_2 produces H_2O. When a carbon-containing fuel is involved in the anode reaction, CO_2 is also produced. For MCFCs, CO_2 is required in the cathode reaction to maintain an invariant carbonate concentration in the electrolyte. Because CO_2 is produced at the anode and consumed at the cathode in MCFCs, and because the concentrations in the anode and cathode feed streams are not necessarily equal, the CO_2 partial pressures for both electrode reactions are present in the second Nernst equation shown in Table 2-2.

Table 2-2 Fuel Cell Reactions and the Corresponding Nernst Equations

Cell Reactions*	Nernst Equation
$H_2 + \frac{1}{2}O_2 \rightarrow H_2O$	$E = E° + (RT/2\mathcal{F}) \ln [P_{H_2} / P_{H_2O}] + (RT/2\mathcal{F}) \ln [P_{O_2}^{1/2}]$

$H_2 + \frac{1}{2}O_2 + CO_{2(c)} \rightarrow H_2O + CO_{2(a)}$	$E = E° + (RT/2\mathcal{F}) \ln [P_{H_2} / P_{H_2O}(P_{CO_2})_{(a)}] + (RT/2\mathcal{F}) \ln [P_{O_2}^{1/2} (P_{CO_2})_{(c)}]$
$CO + \frac{1}{2}O_2 \rightarrow CO_2$	$E = E° + (RT/2\mathcal{F}) \ln [P_{CO} / P_{CO_2}] + (RT/2\mathcal{F}) \ln [P_{O_2}^{1/2}]$
$CH_4 + 2O_2 \rightarrow 2H_2O + CO_2$	$E = E° + (RT/8\mathcal{F}) \ln [P_{CH_4} / P_{H_2O}^2 P_{CO_2}] + (RT/8\mathcal{F}) \ln [P_{O_2}^2]$

(a) - anode
(c) - cathode
E - equilibrium potential
F - Faraday's constant
P - gas pressure
R - universal gas constant
T - temperature (absolute)
* - The cell reactions are obtained from the anode and cathode reactions listed in Table 2-1.

The ideal standard potential (E^o) for a fuel cell in which H_2 and O_2 react is 1.229 volts with liquid water product, or 1.18 volts with gaseous water product. This value is shown in numerous chemistry texts (1) as the oxidation potential of H_2. The potential is the change in Gibbs free energy resulting from the reaction between hydrogen and oxygen. The difference between 1.229 volts and 1.18 volts represents the latent heat of vaporization of water at standard conditions.

Figure 2-1 shows the relation of E to cell temperature. Because the figure shows the potential of higher temperature cells, the ideal potential corresponds to a reaction where the water product is in a gaseous state. Hence, E is 1.18 volts at standard conditions when considering gaseous water product.

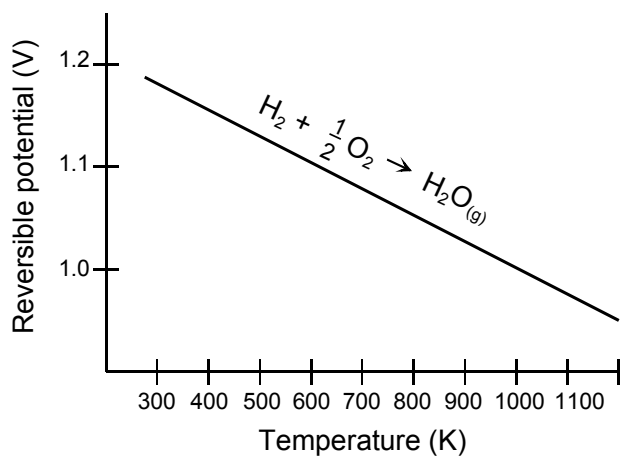

Figure 2-1 H_2/O_2 Fuel Cell Ideal Potential as a Function of Temperature

The impact of temperature on the ideal voltage, E, for the oxidation of hydrogen is also shown in Table 2-3 for the various types of fuel cells. Each case assumes gaseous products as its basis.

Table 2-3 Ideal Voltage as a Function of Cell Temperature

Temperature	25°C (298K)	80°C (353K)	100°C (373K)	205°C (478K)	650°C (923K)	1100°C (1373K)
Cell Type		PEFC	AFC	PAFC	MCFC	TSOFC
Ideal Voltage	1.18	1.17		1.14	1.03	0.91

The ideal performance of a fuel cell depends on the electrochemical reactions that occur between different fuels and oxygen as summarized in Table 2-1. Low-temperature fuel cells (PEFC, AFC, and PAFC) require noble metal electrocatalysts to achieve practical reaction rates at the anode and cathode, and H_2 is the only acceptable fuel. With high-temperature fuel cells (MCFC and TSOFC), the requirements for catalysis are relaxed, and the number of potential fuels expands. While carbon monoxide "poisons" a noble metal anode catalyst such as platinum (Pt) in low-temperature fuel cells, it competes with H_2 as a reactant in high-temperature fuel cells where non-noble metal catalysts such as nickel (Ni) can be used.

Note that H_2, CO, and CH_4 are shown in Table 2-1 as undergoing anodic oxidation. In actuality, insignificant direct oxidation of the CO and CH_4 may occur. It is common systems analysis practice to assume that H_2, the more readily oxidized fuel, is produced by CO and CH_4 reacting, at equilibrium, with H_2O through the water gas shift and steam reforming reactions, respectively. The H_2 calculated to be produced from CO and CH_4, along with any H_2 in the fuel supply stream, is referred to as equivalent H_2. The temperature and catalyst of state-of-the-art MCFCs provide the proper environment for the water gas shift reaction to produce H_2 and CO_2 from CO and H_2O. An MCFC that reacts only H_2 and CO is known as an external reforming (ER) MCFC. In an internal reforming (IR) MCFC, the reforming reaction to produce H_2 and CO_2 from CH_4 and H_2O can occur if a reforming catalyst is placed in proximity to the anode to promote the reaction. The direct oxidation of CO and CH_4 in a high-temperature SOFC is feasible without the catalyst, but again the direct oxidation of these fuels is not as favorable as the water gas shift of CO to H_2 and reforming of CH_4 to H_2. These are critical arguments in determining the equations to describe the electrical characteristics and the energy balance of the various types of cells. It is fortunate that converting CO and CH_4 to equivalent H_2, then reacting within the cell simplifies the prediction of the electrochemical behavior of the fuel cell.

2.1.2 Cell Energy Balance

The discussion above can be used to formulate a mass and energy balance around a fuel cell to describe its electrical performance. The energy balance around the fuel cell is based on the energy absorbing/releasing processes (e.g., power produced, reactions, heat loss) that occur in the cell. As a result, the energy balance varies for the different types of cells because of the differences in reactions that occur according to cell type.

In general, the cell energy balance states that the enthalpy flow of the reactants entering the cell will equal the enthalpy flow of the products leaving the cell plus the sum of three terms: 1) the net heat generated by physical and chemical processes within the cell, 2) the dc power output from the cell, and 3) the rate of heat loss from the cell to its surroundings.

Component enthalpies are readily available on a per mass basis from data tables such as JANAF (4). Product enthalpy usually includes the heat of formation in published tables. A typical energy balance determines the cell exit temperature knowing the reactant composition, the feed stream temperatures, H_2 and O_2 utilization, the expected power produced, and a percent heat loss. The exit constituents are calculated from the fuel cell reactions as illustrated in Example 9-3, Section 9.

2.1.3 Cell Efficiency

The thermal efficiency of an energy conversion device is defined as the amount of useful energy produced relative to the change in stored chemical energy (commonly referred to as thermal energy) that is released when a fuel reacts with an oxidant.

$$\eta = \frac{\text{Useful Energy}}{\Delta H} \qquad (2\text{-}13)$$

Hydrogen (a fuel) and oxygen (an oxidant) can exist in each other's presence at room temperature, but given sufficient activation energy, they explode violently. This reaction occurs spontaneously at 580°C, but can be initiated below 580°C by providing a flame, such as in a heat engine. A catalyst and an electrolyte, such as in a fuel cell, can sustain reaction between H_2 and O_2 at temperatures lower than 580°C. Note that the rate of reaction is controlled and limited because the permeable electrolyte physically separates the fuel from the oxidant. The heat engine process is thermal; the fuel cell process is electrochemical. Differences in these two methods of producing useful energy are the reason for increased efficiency in the fuel cell.

In the ideal case of an electrochemical converter, such as a fuel cell, the change in Gibbs free energy, ΔG, of the reaction is available as useful electric energy at the temperature of the conversion. The ideal efficiency of a fuel cell, operating reversibly, is then

$$\eta = \frac{\Delta G}{\Delta H} \qquad (2\text{-}14)$$

The most widely used efficiency of a fuel cell is based on the change in the standard free energy for the cell reaction

$$H_2 + 1/2O_2 \rightarrow H_2O(1) \qquad (2\text{-}15)$$

given by

$$\Delta G_r^o = G_{H_2o(\lambda)}^o - G_{H_2}^o - \frac{1}{2} G_{o_2}^o \tag{2-16}$$

where the product water is in liquid form. At standard conditions of 25°C (298°K) and 1 atmosphere, the thermal energy (ΔH) in the hydrogen/oxygen reaction is 285.8 kJ/mole, and the free energy available for useful work is 237.1 kJ/mole. Thus, the thermal efficiency of an ideal fuel cell operating reversibly on pure hydrogen and oxygen at standard conditions would be:

$$\eta_{ideal} = \frac{237.1}{285.8} = 0.83 \tag{2-17}$$

The efficiency of an actual fuel cell can be expressed in terms of the ratio of the operating cell voltage to the ideal cell voltage. The actual cell voltage is less than the ideal cell voltage because of losses associated with cell polarization and the iR loss, which will be discussed below. The thermal efficiency of the fuel cell can then be written in terms of the actual cell voltage:

$$\eta = \frac{\text{Useful Energy}}{\Delta H} = \frac{\text{Useful Power}}{(\Delta G/0.83)} = \frac{\text{Volts}_{actual} \text{ x Current}}{\text{Volts}_{ideal} \text{ x Current / 0.83}} = \frac{(0.83)(V_{actual})}{V_{ideal}} \tag{2-18}$$

As mentioned previously, the ideal voltage of a cell operating reversibly on pure hydrogen and oxygen at 1 atm pressure and 25ºC is 1.229 V. Thus, the thermal efficiency of an actual fuel cell operating at a voltage of V_{cell}, based on the higher heating value of hydrogen, is given by

$$\eta_{ideal} = 0.83 \text{ x } V_{cell} / V_{ideal} = 0.83 \text{ x } V_{cell} / 1.229 = 0.675 \text{ x } V_{cell} \tag{2-19}$$

A fuel cell can be operated at different current densities, expressed as mA/cm^2 or A/ft^2. The corresponding cell voltage then determines the fuel cell efficiency. Decreasing the current density increases the cell voltage, thereby increasing the fuel cell efficiency. The trade-off is that as the current density is decreased, the active cell area must be increased to obtain the requisite amount of power. Thus, designing the fuel cell for higher efficiency increases the capital cost, but decreases the fuel cost.

Two additional aspects of efficiency are of interest: 1) the effects of integrating a fuel cell into a complete system that accepts readily available fuels like natural gas and produces grid quality ac power (see Section 8), and 2) issues arising when comparing fuel cell efficiency with heat engine efficiency, which will be discussed next.

2.1.4 Efficiency Comparison to Heat Engines

If a fuel cell is compared to an equivalent efficiency heat engine, the fuel cell does not need to achieve the large temperature differential to achieve the same Carnot cycle efficiency as the heat engine (5). This is because of the added energy gained from Gibbs free energy as opposed to simply the thermal energy. The resulting freedom from large temperature differentials in the fuel cell provides a great benefit because it relaxes material temperature problems when trying to achieve comparable efficiency.

2.1.5 Actual Performance

The actual cell potential is decreased from its equilibrium potential because of irreversible losses, as shown in Figure 2-2[2]. Multiple phenomena contribute to irreversible losses in an actual fuel cell. The losses, which are called polarization, overpotential, or overvoltage (η), originate primarily from three sources: 1) activation polarization (η_{act}), 2) ohmic polarization (η_{ohm}), and 3) concentration polarization (η_{conc}). These losses result in a cell voltage (V) that is less than its ideal potential, E (V = E - Losses).

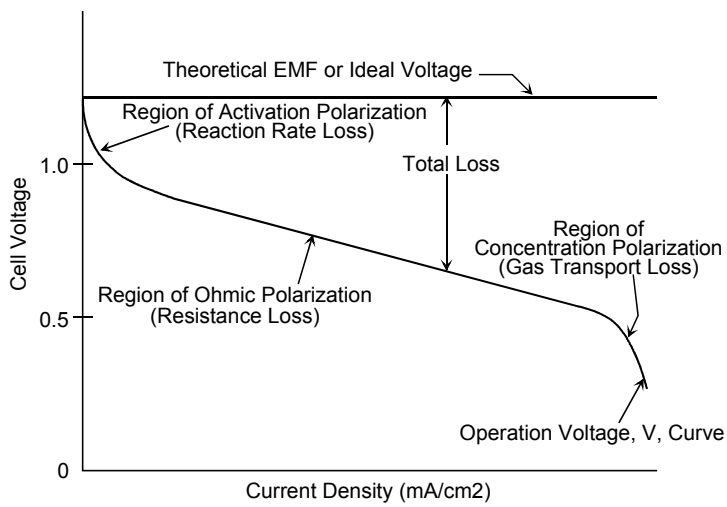

Figure 2-2 Ideal and Actual Fuel Cell Voltage/Current Characteristic

The activation polarization loss is dominant at low current density. At this point, electronic barriers must be overcome prior to current and ion flow. Activation losses increase as current increases. Ohmic polarization (loss) varies directly with current, increasing over the entire range of current because cell resistance remains essentially constant. Gas transport losses occur over the entire range of current density, but these losses become prominent at high limiting currents where it becomes difficult to provide enough reactant flow to the cell reaction sites.

Activation Polarization: Activation polarization is present when the rate of an electrochemical reaction at an electrode surface is controlled by sluggish electrode kinetics. In other words, activation polarization is directly related to the rates of electrochemical reactions. There is a

[2] Activation region and concentration region are more representative of low-temperature fuel cells.

close similarity between electrochemical and chemical reactions in that both involve an activation energy that must be overcome by the reacting species. In the case of an electrochemical reaction with $\eta_{act} \geq$ 50-100 mV, it is customary to express the voltage drop due to activation polarization by a semi-empirical equation, called the Tafel equation (2). The equation for activation polarization is shown by Equation (2-20):

$$\eta_{act} = \frac{RT}{\alpha n \mathcal{F}} \ln \frac{i}{i_o} \qquad (2\text{-}20)$$

where α is the electron transfer coefficient of the reaction at the electrode being addressed, and i_o is the exchange current density. Tafel plots, such as in Figure 2-3, provide a visual understanding of the activation polarization of a fuel cell. They are used to measure the exchange current density, given by the extrapolated intercept at $\eta_{act} = 0$ which is a measure of the maximum current that can be extracted at negligible polarization (5), and the transfer coefficient (from the slope).

The usual form of the Tafel equation that can be easily expressed by a Tafel Plot is

$$\eta_{act} = a + b \ln i \qquad (2\text{-}21)$$

where $a = (-RT/\alpha nF) \ln i_o$ and $b = RT/\alpha nF$. The term b is called the Tafel slope, and is obtained from the slope of a plot of η_{act} as a function of ln i. There exists a strong incentive to develop electrocatalysts that yield a lower Tafel slope for electrochemical reactions so that increases in current density result only in nominal increases in activation polarization.

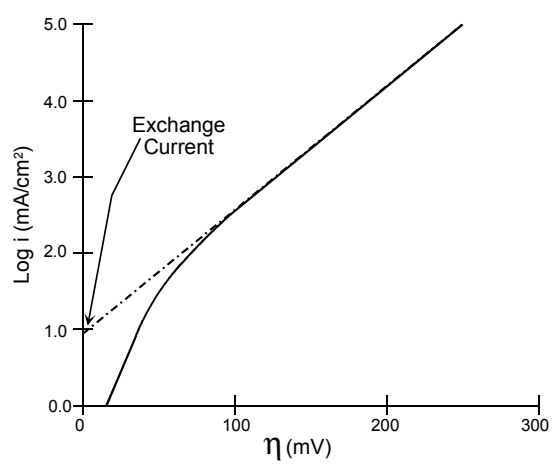

Figure 2-3 Example of a Tafel Plot

The simplified description presented here did not consider processes that give rise to activation polarization, except for attributing it to sluggish electrode kinetics. Processes involving absorption of reactant species, transfer of electrons across the double layer, desorption of product species, and the nature of the electrode surface all contribute to activation polarization.

Ohmic Polarization: Ohmic losses occur because of resistance to the flow of ions in the electrolyte and resistance to flow of electrons through the electrode. The dominant ohmic losses through the electrolyte are reduced by decreasing the electrode separation and enhancing the ionic conductivity of the electrolyte. Because both the electrolyte and fuel cell electrodes obey Ohm's law, the ohmic losses can be expressed by the equation

$$\eta_{ohm} = iR \qquad (2\text{-}22)$$

where i is the current flowing through the cell, and R is the total cell resistance, which includes electronic, ionic, and contact resistance.

Concentration Polarization: As a reactant is consumed at the electrode by electrochemical reaction, there is a loss of potential due to the inability of the surrounding material to maintain the initial concentration of the bulk fluid. That is, a concentration gradient is formed. Several processes may contribute to concentration polarization: slow diffusion in the gas phase in the electrode pores, solution/dissolution of reactants and products into and out of the electrolyte, or diffusion of reactants and products through the electrolyte to and from the electrochemical reaction site. At practical current densities, slow transport of reactants and products to and from the electrochemical reaction site is a major contributor to concentration polarization.

The rate of mass transport to an electrode surface in many cases can be described by Fick's first law of diffusion:

$$i = \frac{n\mathcal{F}D\,(C_B - C_S)}{\delta} \qquad (2\text{-}23)$$

where D is the diffusion coefficient of the reacting species, C_B is its bulk concentration, C_S is its surface concentration, and δ is the thickness of the diffusion layer. The limiting current (i_L) is a measure of the maximum rate at which a reactant can be supplied to an electrode, and it occurs when $C_S = 0$, i.e.,

$$i_L = \frac{n\mathcal{F}DC_B}{\delta} \qquad (2\text{-}24)$$

By appropriate manipulation of Equations (2-23) and (2-24),

$$\frac{C_S}{C_B} = 1 - \frac{i}{i_L} \qquad (2\text{-}25)$$

The Nernst equation for the reactant species at equilibrium conditions, or when no current is flowing, is

$$E_{i=0} = E^\circ + \frac{RT}{n\mathcal{F}} \ln C_B \qquad (2\text{-}26)$$

When current is flowing, the surface concentration becomes less than the bulk concentration, and the Nernst equation becomes

$$E = E^\circ + \frac{RT}{n\mathcal{F}} \ln C_S \qquad (2\text{-}27)$$

The potential difference (ΔE) produced by a concentration change at the electrode is called the concentration polarization:

$$\Delta E = \eta_{conc} = \frac{RT}{n\mathcal{F}} \ln \frac{C_S}{C_B} \qquad (2\text{-}28)$$

Upon substituting Equation (2-25) in (2-28), the concentration polarization is given by the equation

$$\eta_{conc} = \frac{RT}{n\mathcal{F}} \ln \left(1 - \frac{i}{i_L}\right) \qquad (2\text{-}29)$$

In this analysis of concentration polarization, the activation polarization is assumed to be negligible. The charge transfer reaction has such a high exchange current density that the activation polarization is negligible in comparison with the concentration polarization (most appropriate for the high temperature cells).

Summing of Electrode Polarization: Activation and concentration polarization can exist at both the positive (cathode) and negative (anode) electrodes in fuel cells. The total polarization at these electrodes is the sum of η_{act} and η_{conc}, or

$$\eta_{anode} = \eta_{act,a} + \eta_{conc,a} \tag{2-30}$$

and

$$\eta_{cathode} = \eta_{act,c} + \eta_{conc,c} \tag{2-31}$$

The effect of polarization is to shift the potential of the electrode ($E_{electrode}$) to a new value ($V_{electrode}$):

$$V_{electrode} = E_{electrode} \pm \left| \eta_{electrode} \right| \tag{2-32}$$

For the anode,

$$V_{anode} = E_{anode} + \left| \eta_{anode} \right| \tag{2-33}$$

and for the cathode,

$$V_{cathode} = E_{cathode} - \left| \eta_{cathode} \right| \tag{2-34}$$

The net result of current flow in a fuel cell is to increase the anode potential and to decrease the cathode potential, thereby reducing the cell voltage. Figure 2-4 illustrates the contribution to polarization of the two half cells for a PAFC. The reference point (zero polarization) is hydrogen. These shapes of the polarization curves are typical of other types of fuel cells as well.

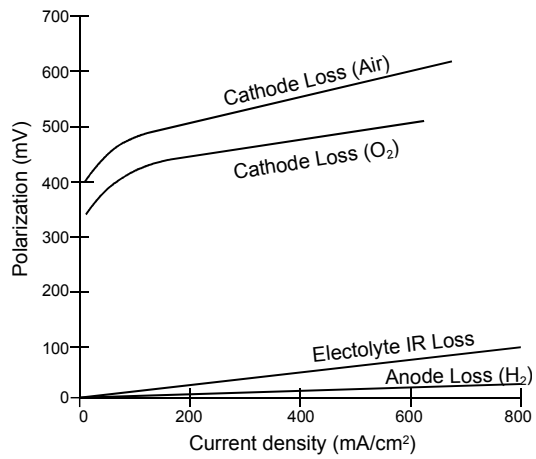

Figure 2-4 Contribution to Polarization of Anode and Cathode

Summing of Cell Voltage: The cell voltage includes the contribution of the anode and cathode potentials and ohmic polarization:

$$V_{cell} = V_{cathode} - V_{anode} - iR \qquad (2\text{-}35)$$

When Equations (2-33) and (2-34) are substituted in Equation (2-35)

$$V_{cell} = E_{cathode} - \left| \eta_{cathode} \right| - (E_{anode} + \left| \eta_{anode} \right|) - iR \qquad (2\text{-}36)$$

or

$$V_{cell} = \Delta E_e - \left| \eta_{cathode} \right| - \left| \eta_{anode} \right| - iR \qquad (2\text{-}37)$$

where $\Delta E_e = E_{cathode} - E_{anode}$. Equation (2-37) shows that current flow in a fuel cell results in a decrease in the cell voltage because of losses by electrode and ohmic polarizations. The goal of fuel cell developers is to minimize the polarization so that V_{cell} approaches ΔE_e. This goal is approached by modifications to fuel cell design (improvement in electrode structures, better electrocatalysts, more conductive electrolyte, thinner cell components, etc.). For a given cell design, it is possible to improve the cell performance by modifying the operating conditions (e.g., higher gas pressure, higher temperature, change in gas composition to lower the gas impurity concentration). However, for any fuel cell, compromises exist between achieving higher performance by operating at higher temperature or pressure and the problems associated with the stability/durability of cell components encountered at the more severe conditions.

2.1.6 Fuel Cell Performance Variables

The performance of fuel cells is affected by operating variables (e.g., temperature, pressure, gas composition, reactant utilizations, current density) and other factors (impurities, cell life) that

influence the ideal cell potential and the magnitude of the voltage losses described above. Any number of operating points can be selected for application of a fuel cell in a practical system, as illustrated by Figure 2-5.

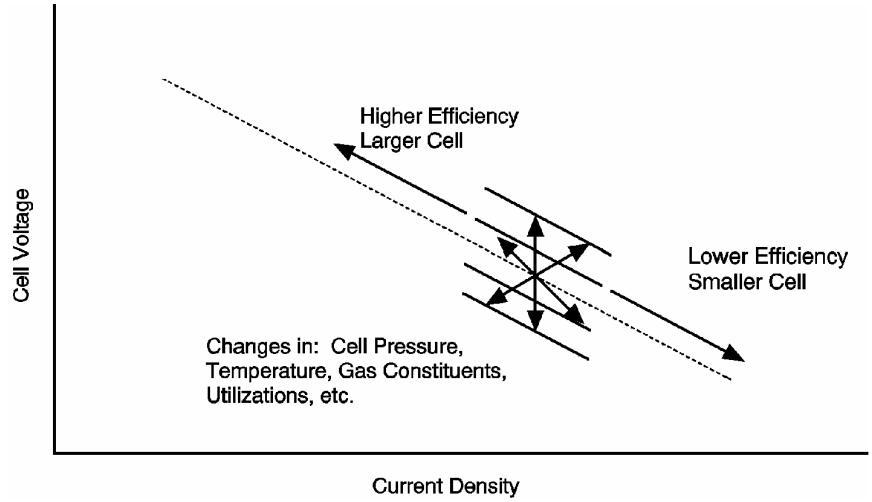

Figure 2-5 Flexibility of Operating Points According to Cell Parameters

Figure 2-5 represents the characteristics of a fuel cell once its physical design is set. Changing the cell operating parameters (temperature and pressure) can have either a beneficial or a detrimental impact on fuel cell performance and on the performance of other system components. These effects may be offsetting. Changes in operating conditions may lower the cost of the cell, but increase the cost of the surrounding system. Usually, compromises in the operating parameters are necessary to meet the application requirements, obtain lowest system cost, and achieve acceptable cell life. Operating conditions are based on defining specific system requirements, such as power level, voltage, or system weight. From this and through interrelated systems studies, the power, voltage, and current requirements of the fuel cell stack and individual cells are determined. It is a matter of selecting a cell operating point (cell voltage and related current density) as shown by Figure 2-5 until the design requirements are satisfied (such as lowest cost, lightest unit, highest power density). For example, a design point at high current density will allow a smaller cell size at lower capital cost to be used for the stack, but a lower system efficiency results (because of the lower cell voltage) and attendant higher operating cost. This type of operating point would be typified by a vehicle application where light weight and small volume, as well as efficiency, are important drivers for cost effectiveness. Cells capable of higher current density would be of prime interest. Operating at a lower current density, but higher voltage (higher efficiency, lower operating cost) would be more suitable for stationary power plant operation. Operating at a higher pressure will increase cell performance and lower cost. However, there will be a higher parasitic power to compress the reactants, and the cell stack pressure vessel and piping will have to withstand the greater pressure. This adds cost. It is evident that the selection of the cell design point interacts with the application objectives. These will be discussed further in Section 8.

Figure 2-6 presents the same information as Figure 2-5, but in a way to highlight another aspect of determining the cell design point. It would seem logical to design the cell to operate at the maximum power density that peaks at a higher current density (right of the figure). However,

operation at the higher power densities will mean operation at lower cell voltages or lower cell efficiency. Setting operation near the peak power density can cause instability in control because the system will have a tendency to oscillate between higher and lower current densities around the peak. It is usual practice to operate the cell to the left side of the power density peak and at a point that yields a compromise between low operating cost (high cell efficiency that occurs at high voltage/low current density) and low capital cost (less cell area that occurs at low voltage/high current density).

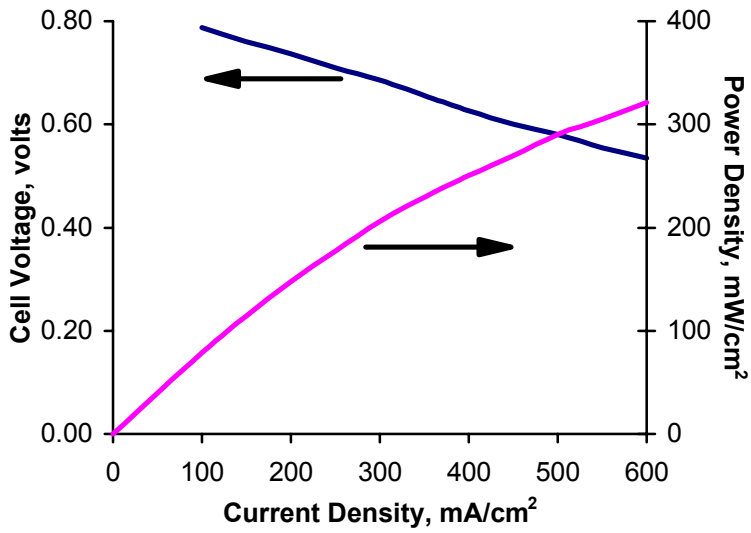

Figure 2-6 Voltage/Power Relationship

It is interesting to observe that the resulting characteristic provides the fuel cell with a benefit that is unique among other energy conversion technologies: the fuel cell efficiency increases at part load conditions.[3] Other components within the fuel cell system operate at lower component efficiencies as the system's load is reduced. The combination of increased fuel cell efficiency and lower supporting component efficiencies can result in a rather flat trace of total system efficiency as the load is reduced. Alternative energy conversion techniques experience a loss of efficiency as the power load is reduced. This loss, coupled with the same supporting component losses of efficiency that the fuel cell system experiences, causes lower total efficiencies as the load is reduced. This gives the fuel cell system a fuel cost advantage for part load applications.

The equations describing performance variables, which will be developed in Sections 3 through 7, address changes in cell performance as a function of major operating conditions to allow the reader to perform quantitative parametric analysis. The following discussion provides basic insight into the effects of some operating parameters.

[3]. Constraints can limit the degree of part load operation of a fuel cell. For example, a PAFC is limited to operation below approximately 0.85 volts because of entering into a corrosion region.

Temperature and Pressure: The effect of temperature and pressure on the ideal potential (E) of a fuel cell can be analyzed on the basis of changes in the Gibbs free energy with temperature and pressure.

$$\left(\frac{\partial E}{\partial T}\right)_P = \frac{\Delta S}{nF} \qquad (2\text{-}38)$$

or

$$\left(\frac{\partial E}{\partial P}\right)_T = \frac{-\Delta V}{nF} \qquad (2\text{-}39)$$

Because the entropy change for the H_2/O_2 reaction is negative, the reversible potential of the H_2/O_2 fuel cell decreases with an increase in temperature by 0.84 mV/°C (assuming reaction product is liquid water). For the same reaction, the volume change is negative; therefore, the reversible potential increases with an increase in pressure.

The effect of temperature on the actual voltage of fuel cells is quite different from the reversible potential. This is represented schematically in Figure 2-7, which presents initial (i.e., early in life) performance data from typical operating cells and the dependence of the reversible potential of H_2/O_2 fuel cells on temperature (3). The cell voltages of PEFCs, PAFCs, and MCFCs show a strong, positive dependence on temperature.[4] The reversible potential decreases with increasing temperature, but the operating voltages of these fuel cells actually increase with an increase in operating temperature. PEFCs, however, exhibit a maximum in operating voltage,[5] as in Figure 2-7. The lower operating temperature of state-of-the-art TSOFCs is limited to about 1000°C (1832°F) because the ohmic resistance of the solid electrolyte increases rapidly as the temperature decreases. The cell is limited by material concerns and fabrication processes at temperatures above 1000°C. The other types of fuel cells typically operate at voltages considerably below the reversible cell voltage. The increase in performance is due to changes in the types of primary polarizations affecting the cell as temperature varies. An increase in the operating temperature is beneficial to fuel cell performance because of the increase in reaction rate, higher mass transfer rate, and usually lower cell resistance arising from the higher ionic conductivity of the electrolyte. In addition, the CO tolerance of electrocatalysts in low-temperature fuel cells improves as the operating temperature increases. These factors combine to reduce the polarization at higher temperatures.

---

[4]. The cell voltages are not taken at equal current densities. Absolute cell voltage should not be compared.

[5]. The cell voltage of PEFCs goes through a maximum as a function of temperature because of the difficulties with water management at higher temperature. It may be possible to adjust operating conditions so that the PEFC voltage will increase up to a temperature of ~140°C, the point at which the membrane degrades rapidly.

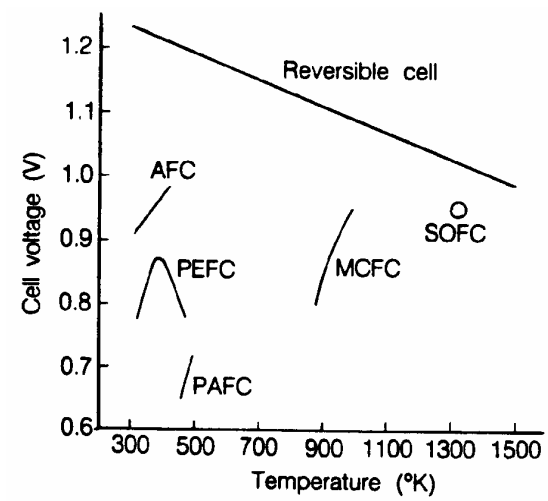

Figure 2-7 Dependence of the Initial Operating Cell Voltage of Typical Fuel Cells on Temperature (1)

On the negative side, materials problems related to corrosion, electrode degradation, electrocatalyst sintering and recrystallization, and electrolyte loss by evaporation are all accelerated at higher temperatures.

An increase in operating pressure has several beneficial effects on fuel cell performance because the reactant partial pressure, gas solubility, and mass transfer rates are higher. In addition, electrolyte loss by evaporation is reduced at higher operating pressures. Increased pressure also tends to increase system efficiencies. However, there are compromises such as thicker piping and additional expense for pressurization. Section 7.2.1 addresses system aspects of pressurization. The benefits of increased pressure must be balanced against hardware and materials problems, as well as parasitic power costs. In particular, higher pressures increase material problems in MCFCs (see Section 6.1), pressure differentials must be minimized to prevent reactant gas leakage through the electrolyte and seals, and high pressure favors carbon deposition and methane formation in the fuel gas.

Reactant Utilization and Gas Composition: Reactant utilization and gas composition have major impacts on fuel cell efficiency. It is apparent from the Nernst equations in Table 2-2 that fuel and oxidant gases containing higher partial pressures of electrochemical reactants produce a higher cell voltage. Utilization (U) refers to the fraction of the total fuel or oxidant introduced into a fuel cell that reacts electrochemically. In low-temperature fuel cells, determining the fuel utilization is relatively straightforward when H_2 is the fuel, because it is the only reactant involved in the electrochemical reaction,[6] i.e.

$$U_f = \frac{H_{2,in} - H_{2,out}}{H_{2,in}} = \frac{H_{2,\,consumed}}{H_{2,in}} \qquad (2\text{-}40)$$

[6]. Assumes no gas cross-over or leakage out of the cell.

where $H_{2,in}$ and $H_{2,out}$ are the flow rates of H_2 at the inlet and outlet of the fuel cell, respectively. However, hydrogen can be consumed by various other pathways, such as by chemical reaction (i.e., with O_2 and cell components) and loss via leakage out of the cell. These pathways increase the apparent utilization of hydrogen without contributing to the electrical energy produced by the fuel cell. A similar type of calculation is used to determine the oxidant utilization. For the cathode in MCFCs, two reactant gases, O_2 and CO_2, are utilized in the electrochemical reaction. The oxidant utilization should be based on the limiting reactant. Frequently O_2, which is readily available from make-up air, is present in excess, and CO_2 is the limiting reactant.

A significant advantage of high-temperature fuel cells such as MCFCs is their ability to use CO as a fuel. The anodic oxidation of CO in an operating MCFC is slow compared to the anodic oxidation of H_2; thus, the direct oxidation of CO is not favored. However, the water gas shift reaction

$$CO + H_2O = H_2 + CO_2 \qquad (2\text{-}41)$$

reaches equilibrium rapidly in MCFCs at temperatures as low as 650°C (1200°F) to produce H_2.[7] As H_2 is consumed, the reaction is driven to the right because both H_2O and CO_2 are produced in equal quantities in the anodic reaction. Because of the shift reaction, fuel utilization in MCFCs can exceed the value for H_2 utilization, based on the inlet H_2 concentration. For example, for an anode gas composition of 34% H_2, 22% H_2O, 13% CO, 18% CO_2, and 12% N_2, a fuel utilization of 80% (i.e., equivalent to 110% H_2 utilization) can be achieved even though this would require 10% more H_2 (total of 37.6%) than is available in the original fuel. The high fuel utilization is possible because the shift reaction provides the necessary additional H_2 that is oxidized at the anode. In this case, the fuel utilization is defined by

$$U_f = \frac{H_{2,\,consumed}}{H_{2,in} + CO_{in}} \qquad (2\text{-}42)$$

where the H_2 consumed originates from the H_2 present at the fuel cell inlet ($H_{2,in}$) and any H_2 produced in the cell by the water gas shift reaction (CO_{in}).

Gas composition changes between the inlet and outlet of a fuel cell, caused by the electrochemical reaction, lead to reduced cell voltages. This voltage reduction arises because the cell voltage adjusts to the lowest electrode potential given by the Nernst equation for the various gas compositions at the exit of the anode and cathode chambers. Because electrodes are usually good electronic conductors and isopotential surfaces, the cell voltage can not exceed the minimum (local) value of the Nernst potential. In the case of a fuel cell with the flow of fuel and oxidant in the same direction (i.e., co-flow), the minimum Nernst potential occurs at the cell outlet. When the

[7]. Example 9-5 in Section 9 illustrates how to determine the amount of H_2 produced by the shift reaction.

gas flows are counterflow or crossflow, determining the location of the minimum potential is not straightforward.

The MCFC provides a good example to illustrate the influence of the extent of reactant utilization on the electrode potential. An analysis of the gas composition at the fuel cell outlet as a function of utilization at the anode and cathode is presented in Example 9-5. The Nernst equation can be expressed in terms of the mole fraction of the gases (X_i) at the fuel cell outlet:

$$E = E^o + \frac{RT}{2F} \ln \frac{X_{H_2} X_{O_2}^{1/2} X_{CO_2,\text{cathode}} P^{1/2}}{X_{H_2O,\text{anode}} X_{CO_2,\text{anode}}} \qquad (2\text{-}43)$$

where P is the cell gas pressure. The second term on the right side of Equation (2-43), the so-called Nernst term, reflects the change in the reversible potential as a function of reactant utilization, gas composition, and pressure. Figure 2-8 illustrates the change in reversible cell potential calculated as a function of utilization using Equation (2-43).

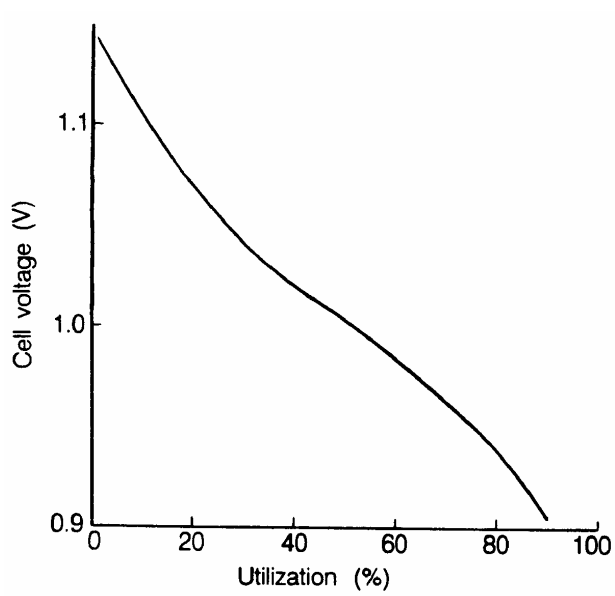

Figure 2-8 The Variation in the Reversible Cell Voltage as a Function of Reactant Utilization

(Fuel and oxidant utilizations equal) in a MCFC at 650°C and 1 atm. Fuel gas: 80% H_2/20% CO_2 saturated with H_2O at 25°C; oxidant gas: 60% CO_2/30% O_2/10% inert)

The reversible potential at 650°C (1200°F) and 1 atmosphere pressure is plotted as a function of reactant utilization (fuel and oxidant utilizations are equal) for inlet gas compositions of 80% H_2/20% CO_2 saturated with H_2O at 25°C (77°F) (fuel gas[8]) and 60% CO_2/30% O_2/10% inerts (oxidant gas); gas compositions and utilizations are listed in Table 2-4. Note that the oxidant

[8]. Anode inlet composition is 64.5% H_2/6.4% CO_2/13% CO/16.1% H_2O after equilibration by water gas shift reaction.

composition is based on a gas of 2/1 CO_2 to O_2. The gas is not representative of the cathode inlet gas of a modern system, but is used for illustrative purposes only. The mole fractions of H_2 and CO in the fuel gas decrease as the utilization increases, and the mole fractions of H_2O and CO_2 show the opposite trend. At the cathode, the mole fractions of O_2 and CO_2 decrease with an increase in utilization because they are both consumed in the electrochemical reaction. The reversible cell potential plotted in Figure 2-8 is calculated from the equilibrium compositions for the water gas shift reaction at the cell outlet. An analysis of the data in the figure indicates that a change in utilization from 20% to 80% will cause a decrease in the reversible potential of about 0.158 V. These results show that MCFCs operating at high utilization will suffer a large voltage loss because of the magnitude of the Nernst term.

An analysis by Cairns and Liebhafsky (3) for a H_2/air fuel cell shows that a change in the gas composition that produces a 60 mV change in the reversible cell potential near room temperature corresponds to a 300 mV change at 1200°C (2192°F). Thus, gas composition changes are more significant in high temperature fuel cells.

Table 2-4 Outlet Gas Composition as a Function of Utilization in MCFC at 650°C

Gas		Utilization[a] (%)			
	0	25	50	75	90
Anode[b]					
X_{H2}	0.645	0.410	0.216	0.089	0.033
X_{CO2}	0.064	0.139	0.262	0.375	0.436
X_{CO}	0.130	0.078	0.063	0.033	0.013
X_{H2O}	0.161	0.378	0.458	0.502	0.519
Cathode[c]					
X_{CO2}	0.600	0.581	0.545	0.461	0.316
X_{O2}	0.300	0.290	0.273	0.231	0.158

a - Same utilization for fuel and oxidant. Gas compositions are given in mole fractions.
b - 80% H_2/20% CO_2 saturated with H_2O at 25°C. Fuel gas compositions are based on compositions for water-gas shift equilibrium.
c - 30% O_2/60% CO_2/10% inert gas. Gas is not representative of a modern system cathode inlet gas, but used for illustrative purposes only.

Current Density: The effects on performance of increasing current density were addressed in Section 2.6. That section described how activation, ohmic, and concentration losses occur as the current is changed. Figure 2-2 is a simplified depiction of how these losses affect the shape of the cell voltage-current characteristic. As current is initially drawn, sluggish kinetics (activation losses) cause a decrease in cell voltage. At high current densities, there is an inability to diffuse enough reactants to the reaction sites (concentration losses) so the cell experiences a sharp

performance decrease through reactant starvation. There also may be an associated problem of diffusing the reaction products from the cell.

Ohmic losses predominate in normal fuel cell operation. These losses can be expressed as iR losses where i is the current and R is the summation of internal resistances within the cell, Equation (2-22). As is readily evident from the equation, the ohmic loss and hence voltage change is a direct function of current (current density multiplied by cell area).

2.2 Computer Models

Computer models are useful for conducting tests at various operating conditions and involving various materials in a search for optimal design performance. Computer models enable preliminary investigations without the need to construct and operate demonstration-scale equipment, which is both costly and time-consuming. They enable researchers to predict cell performance as multiple operating conditions are changed, such as temperature, pressure, and gas composition. The constitutive equations presented in the previous sections represent the backbone of these computer models.

Systems models vs. mechanistic models
Depending on the needs of the researcher, either a systems model or a mechanistic model can be used to investigate a technology development issue. Systems models are typically macroscopic in nature and use basic design parameters and operating conditions to compute overall performance. These models solve mass and energy balances at various temperatures, pressures, fuel compositions, and other design setpoints from which the overall voltage, power output, and area can be calculated. This information can then be used to optimize performance characteristics such as thermal efficiency or cost.

Mechanistic models, on the other hand, are formulated to investigate minute details of fuel cell operation to address particular design issues. These design issues may include thermal transients during start-up or shut-down, mass transport through the electrolyte and electrodes, or effects of cell geometry. Mechanistic models are much more complex than systems models, requiring additional physical dimensions of the cell, additional physical properties, and generally the solution to systems of partial differential equations.

Large, complex computer codes, often proprietary, have been written to simulate fuel cell performance for both systems studies and mechanistic models. A brief overview of very few of the publicly-available codes, developed through government support, is provided in the following paragraphs. This discussion is not meant to endorse any software, but rather to provide a flavor of representative applications of software to design issues.

2.2.1 System Models

Unit Operations Models for Process Analysis using ASPEN
DOE's National Energy Technology Laboratory has been engaged in the development of systems models for fuel cells for over 15 years. The models were originally intended for use in applications of stationary power generation designs to optimize process performance and to evaluate process alternatives. Hence, the models were designed to work within DOE's ASPEN

process simulator and later ported to the commercial version of this product, ASPEN Plus. ASPEN is a sophisticated software application developed to model a wide variety of chemical processes. It contains a library of unit operations models that simulate process equipment and processing steps, and it has a chemical component data bank that contains physical property parameters that are used to compute thermodynamic properties, including phase and chemical equilibrium.

The first general purpose fuel cell model was a Nernst-limited model designed to compute the maximum attainable fuel cell voltage as a function of the cell operating conditions, inlet stream compositions, and desired fuel utilization. Subsequently,
customized unit operations models were developed to simulate the operation of solid oxide (internal reforming), molten carbonate (both external and internal reforming), phosphoric acid, and proton exchange fuel cell (PEFC). These fuel cell models are lumped parameter models based on empirical performance equations. As operation deviates from the setpoint conditions at a "reference" state, a voltage adjustment is applied to account for perturbations. Separate voltage adjustments are applied for current density, temperature, pressure, fuel utilization, fuel composition, oxidant utilization, oxidant composition, cell lifetime, and production year. These models were developed in a collaborative effort by DOE's National Energy Technology Laboratory and the National Renewable Energy Laboratory.

Stand-alone fuel cell power systems have been investigated, as well as hybrid systems using a wide variety of fuels and process configurations. Some of the systems analysis studies that have been conducted using these fuel cell models are described in Section 8.

Argonne's GCTool

Argonne National Laboratory developed the General Computational Toolkit (GCTool) specifically for designing, analyzing, and comparing fuel cell systems and other power plant configurations, including automotive, space-based, and stationary power systems. A library of models for subcomponents and physical property tables is available, and users can add empirical models of subcomponents as needed. Four different types of fuel cell models are included: proton exchange, molten carbonate, phosphoric acid, and solid oxide. Other process equipment models include heat exchangers, reactors (including reformers), and vehicle systems. The physical property models include multiphase chemical equilibrium. Mathematical utilities include a nonlinear equation solver, a constrained nonlinear optimizer, an integrator, and an ordinary differential equation solver.

GCTool has been used to analyze a variety of PEFC systems using different fuels, fuel storage methods, and fuel processing techniques. Examples include compressed hydrogen, metal hydride, glass microsphere, and sponge-iron hydrogen storage systems. Fuel processing alternatives have included reformers for methanol, natural gas, and gasoline using either partial oxidation or steam reforming.

Researchers have examined atmospheric and pressurize PEFC automotive systems. These analyses included the identification of key constraints and operational analysis for off-design operation, system dynamic and transient performance, and the effects of operation at extreme temperatures.

NREL's Advisor 2002
The National Renewable Energy Laboratory created ADVISOR (Advanced VehIcle SimulatOR) to analyze transportation applications. The model assesses the performance and fuel economy of conventional, electric, hybrid, and fuel cell vehicles. The user can evaluate component and vehicle specifications such as electric motors, batteries, engines, and fuel cells. ADVISOR simulates the vehicle's performance under different driving conditions. Industry partnerships contributed state-of-the-art algorithms to ensure the accuracy of the model. For example, detailed electrical analysis is made possible by co-simulation links to Avant's Saber and Ansoft's SIMPLORER. Transient air conditioning analysis is possible by co-simulation with C&R Technologies' SINDA/FLUINT. Michelin provided data for a tire rolling resistance model, and Maxwell provided data for an ultracapacitor energy storage model.

2.2.2 Mechanistic Models

NETL's 3-D Analysis
The National Energy Technology Laboratory (NETL) developed an accurate, 3-dimensional computational fluid dynamics (CFD) model to simulate the performance of fuel cells so that design advances can proceed rapidly without the need for time-consuming build-and-test efforts. As opposed to systems models, 3-dimensional CFD models can address critical issues such as thermal stress distribution, an important consideration related to cell life. Such a model accounts for the distribution of fuel consumption throughout the cell; distribution which, in turn, depends upon the complex flow patterns within the cell.

CFD analysis computes local fluid velocity, pressure, and temperature throughout the region of interest for problems with complex geometries and boundary conditions. By coupling the CFD-predicted fluid flow behavior with the electrochemistry and accompanying thermodynamics occurring in fuel cells, detailed predictions are possible. Improved knowledge of temperature and flow conditions at all points in the fuel cell lead to improved design and performance of the unit.

Based on the successful initial validation with established 1-dimensional codes, NETL researchers now perform sophisticated 3-dimensional simulations using FLUENT, a commercially available product . One configuration studied was tubular solid oxide fuel cell (TSOFC) technology, including a support tube on the cathode side of the cell. Six chemical species were tracked in the simulation: H_2, CO_2, CO, O_2, H_2O, and N_2. Fluid dynamics, heat transfer, electrochemistry, and the potential field in electrode and interconnect regions were all simulated. Voltage losses due to chemical kinetics, ohmic conduction, and diffusion were accounted for in the model.

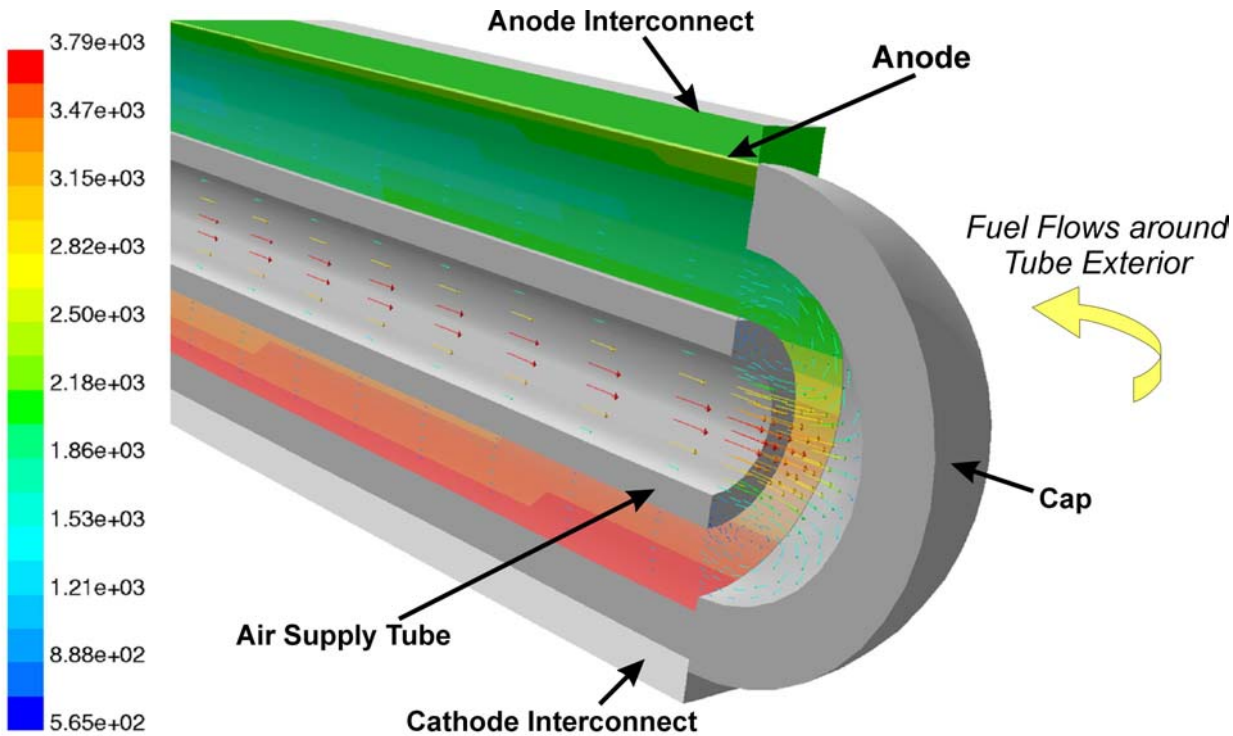

CAPTION: Current density is shown on the electrolyte and air-flow velocity vectors are shown for the cap-end of the tubular fuel cell. Cathode and support tube layers have been removed for clarity. Results indicate that current density and fuel consumption vary significantly along the electrolyte surface as hydrogen fuel is consumed and current flows around the electrodes between interconnect regions. Peak temperature occurs about one-third of the axial distance along the tube from the cap end.

NETL's CFD research demonstrates two major points. First, CFD analysis provides results that agree well with one-dimensional codes that have been validated experimentally. Second, CFD can provide the detailed temperature and chemical species information needed to develop improved fuel cell designs. The output of the FLUENT-based fuel cell model has been coupled to finite element-based stress analysis software to model thermal stresses in the porous and solid regions of the cell. Fuel cell designers will find these capabilities useful in solving some of the most intractable and time-consuming issues facing them. For these reasons, CFD simulation is expected to play a major role in the development of lower-cost, higher-efficiency fuel cell designs.

Further enhancement of the design tool is continuing. The next steps are to validate the model with experimental data and then to extend the model to stack analysis. NETL is now operating SOFC test facilities to generate detailed model validation data using well-characterized SOFC test specimens. These steps should make it possible to create a model that will accurately predict the performance of cells and stacks so that critical design information, such as the distribution of cell and stack stresses, can be provided to the fuel cell design engineer.

2.3 References

1. P.W. Atkins, "Physical Chemistry," 3rd Edition, W.H. Freeman and Company, New York, NY, 1986.
2. S.N. Simons, R.B. King and P.R. Prokopius, in *Symposium Proceedings Fuel Cells Technology Status and Applications*, Figure 1, p. 46, Edited by E.H. Camara, Institute of Gas Technology, Chicago, IL, 45, 1982.
3. E.J. Cairns and H.A. Liebhafsky, *Energy Conversion,* p. 9**,** 63, 1969.
4. M.W. Chase, et al., "JANAF Thermochemical Tables," Third Edition, American Chemical Society and the American Institute of Physics for the National Bureau of Standards (now National Institute of Standards and Technology), 1985.
5. "Fuel Cell Handbook," J. Appleby and F. Foulkes, Texas A&M University, Van Nostrand Reinhold, New York (out of print),republished by Krieger Publishing Co., Melbourne, FL, 1989.
6. W. Stanley Angrist, "Direct Energy Conversion," Third Edition, Allyn and Bacon, Inc. Boston, MA, date of publication unknown.

3. POLYMER ELECTROLYTE FUEL CELLS

Polymer electrolyte membrane fuel cells (PEFC)[9] are able to efficiently generate high power densities, thereby making the technology attractive for motive and stationary applications. Specifically, the weight, volume, and ultimately cost are the primary factors for acceptance. PEFC technology differentiates itself from other fuel cell technologies in that a solid phase polymer membrane is used as the cell separator/electrolyte. Because the cell separator is a polymer film, issues such as sealing, assembly, and handling are less complex than most other fuel cell systems. The need to handle liquids, including corrosive acids and bases, are eliminated in this system. Furthermore, the site responsible for proton transport is chemically bonded to the polymer itself, thereby eliminating materials issues. PEFCs typically operate at low temperatures (60° - 80° C), allowing for faster startup and immediate response to changes in the demand for power. The PEFC is attractive for transportation applications, and is a major competitor for stationary power applications less than 100kW. References (1) and (2) provide excellent overviews and more technical information for PEFCs.

3.1 Cell Components

Typical cell components within a PEFC stack include: 1) the ion exchange membrane; 2) an electrically conductive porous backing layer; 3) a catalyst layer (the electrodes) sandwiched between the backing layer and the membrane, and 4) cell plate hardware shown in a double sided (bi-polar) configuration that delivers the fuel and oxidant to the reactive sites via flow channels, see Figures 3-1a and 3-1b. Typically, the electrodes can be cast as thin films that can be either transferred to the membrane or applied directly to the membrane. Alternatively, the catalyst-electrode layer may be deposited onto the backing layer, then bonded to the membrane.

9. Polymer electrolyte fuel cells are referred to by several acronyms; a common one is PEFC.

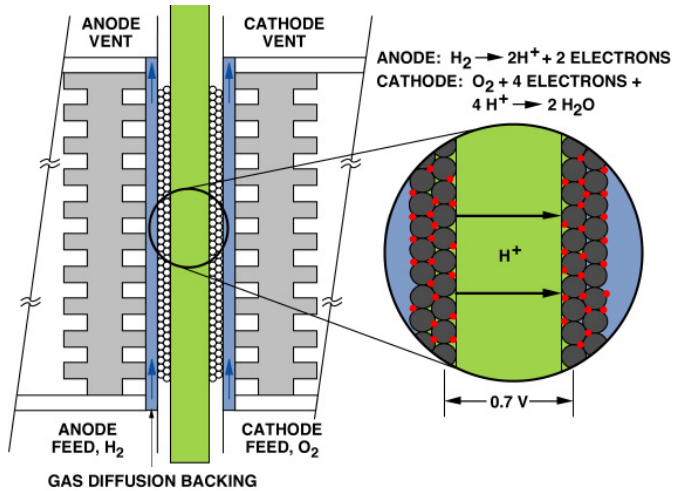

Figure 3-1a Schematic of Representative PEFC (3)

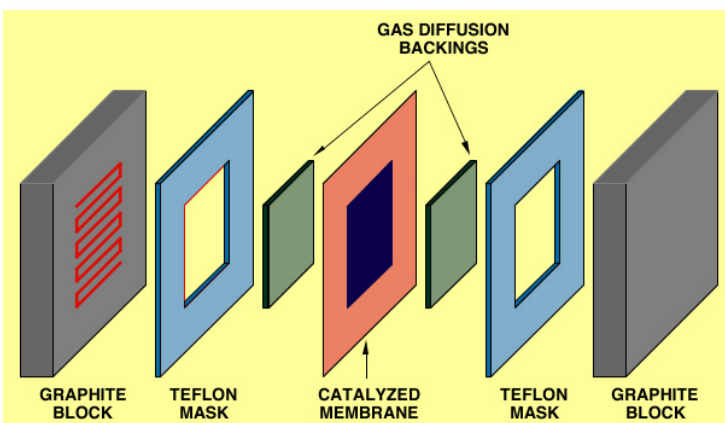

Figure 3-1b Single Cell Structure of Representative PEFC (3)

Membrane

Organic-based cation exchange membranes in fuel cells were originally conceived by William T. Grubbs (4) in 1959. That initial effort eventually led to development of the perfluorosulfonic acid polymer used in today's systems. The function of the ion exchange membrane is to provide a conductive path while at the same time separating the reactant gases. The material is an electrical insulator. As a result, ion conduction takes place via ionic groups within the polymer structure. Ion transport at such sites is highly dependent on the bound and free water associated with those sites.

A commonly used material, Nafion®[10] is a polymer that falls within the perfluorosulfonic acid family. It is characterized by a backbone structure that is Teflon®-like, i.e., polytetrafluoroethylene, and which has bonded to it a perfluorinated side chain that has a terminal sulfonic acid group (SO_3^-). It is through the regular repeating of the sulfonic acid sites on the side chains that ionic transport characteristics are attained. For the most part, the number of sulfonic acid sites dictates the ionic conductivity of such systems. Even though the bulk of the polymer is fluorinated, imparting a highly hydrophobic character to the bulk of the membrane, the sulfonic acid sites are hydrophyllic. The degree of water content a membrane can attain is proportional to the ionic sites and, as a result, the significant properties of the membrane (conductivity, gas permeability, and mechanical properties) are dictated by water content (5).

Porous Backing Layer

The polymer membrane is sandwiched between two sheets of porous backing media. The function of the backing layer[11] is to: 1) act as a gas diffuser; 2) provide mechanical support, and 3) provide an electrical pathway for electrons. The backing layer is typically carbon-based, and may be in cloth form, a non-woven pressed carbon fiber configuration, or simply a felt-like material. The layer incorporates a hydrophobic material, such as polytetrafluoroethylene. The function of polytetrafluoroethylene is to prevent water from "pooling" within the pore volume of the backing layer so that gases freely contact the catalyst sites. Furthermore, it facilitates product water removal on the cathode as it creates a non-wetting surface within the passages of the backing material.

Electrode-Catalyst Layer

In intimate contact with the membrane and the backing layer is a catalyst layer. This catalyst layer, integral with its binder, forms the electrode. The catalyst and binder electrode structure is either applied to the membrane or else applied to the backing layer. In either case, the degree of intimacy of the catalyst particles and the membrane is critical for optimal proton mobility. The binder performs multiple functions. In one case, it "fixes" the catalyst particles within a layered structure, while a second function is to contribute to the overall architecture of the electrode. This architecture has a direct bearing on performance.

There are two schools of thought on the electrode composition, in particular, the binder. In the original hydrophobic, porous, gaseous electrodes developed by Union Carbide and later advanced by General Electric, the Dow Chemical Company, and others, the binder was polytetrafluoroethylene: a non-wetting component within the electrode itself. The second school of electrode science developed a hydrophyllic electrode in which the binder is perfluorosulfonic acid. The driver for this development was to enhance the membrane/catalyst contact to minimize the platinum loading requirements (6).

The catalyst is platinum-based for both the anode and cathode. To promote hydrogen oxidation, the anode uses either pure platinum metal catalyst or a supported platinum catalyst, typically on carbon or graphite for pure hydrogen feed streams. For other fuels, such as a reformate (containing H_2, CO_2, CO, and N_2), the desired catalyst is an alloy of platinum containing

10. Nafion is a registered trademark of the E.I. DuPont Company.
11. Commonly referred to as the gas diffusion layer (GDL) even though it has additional functions.

ruthenium. Oxygen reduction reaction at the cathode may use either the platinum metal or the supported catalyst.

The electrochemical reactions of the PEFC are similar to those of the PAFC[12]: molecular hydrogen at the anode is oxidized to provide protons, while at the same time freeing two electrons that pass through an external "electrical" circuit to reach the cathode. The voltages at each electrode, due to the hydrogen oxidation potential and the oxygen reduction potential, form a voltage gradient of approximately 1 volt (dependent on conditions) at open circuit, i.e., zero current draw. It is this potential that drives the proton through the membrane. As the proton is "pulled" through the membrane, it drags with it a certain number of water molecules. The proton will react with oxygen to form water at the catalyst sites on the cathode.

Because of the intrinsic nature of the materials used, the polymer membrane fuel cell operates at temperatures less than 100°C, typically in the 60 – 80°C range. When compared to other fuel cells, PEFC technology has been capable of very high current densities: while most technologies can operate up to approximately 1 amp/cm^2, the polymer membrane cell has operated at up to 4 amps/cm^2 (7). This ability is due primarily to the membrane used. Other desirable attributes include fast start capability and rapid response times to load changes. Because of the high power density capability, smaller, lighter-weight stacks are possible (8). Other beneficial attributes of the cell include no corrosive fluid hazard and lower sensitivity to orientation. As a result, the PEFC is particularly suited for vehicular power application. Transportation applications suggest that the fuel of choice might be of comparable energy density to gasoline, although hydrogen storage on-board in the form of pressurized gas and the partial oxidation of gasoline (9) are being considered. The PEFC is also being considered widely for stationary power applications, perhaps using natural gas or other hydrogen-rich gases.

The low operating temperature of a PEFC has both advantages and disadvantages. Low temperature operation is advantageous because the cell can start from ambient conditions quickly, especially when pure hydrogen fuel is available. It is a disadvantage in carbon monoxide-containing fuel streams, because carbon will attack the platinum catalyst sites, masking the catalytic activity and reducing cell performance.[13] The effect is reversible by flowing a CO-free gas over the electrode. To minimize the CO poisoning, operating temperatures must be greater than 120°C, at which point there is a reduction in chemisorption and electro-oxidation. Due to CO affecting the anode, only a few ppm of CO can be tolerated at 80°C. Because reformed and shifted hydrocarbons contain about one percent of CO, a mechanism to eliminate CO in the fuel gas is needed. This can be accomplished with preferential oxidation (PROX) that selectively oxidizes CO over H_2 using a precious metal catalyst. The low operating temperature also means that little, if any, heat is available from the fuel cell for endothermic reforming (10, 11).

Recent PEFC development has focused on operation in the 160°C range using a new ion exchange membrane, polybenzimidizole (PBI) (12). The higher operating temperature eliminates CO poisoning by eliminating CO occlusion of the platinum sites. Also, this operating regime provides higher quality heat for possible use in stationary combined heat/power (CHP)

---

12. Equations 5-1, 5-2, and 5-3 for the PAFC apply as well to the PEFC.
13. Referred to as poisoning in catalysis literature.

applications. Because PBI requires significantly lower water content to facilitate proton transport, an additional benefit is that water management is dramatically simplified (13, 14).

Both temperature and pressure have a significant influence on cell performance. Present cells operate at 80°C over a range of 0.0010 - 1.0 MPa (~0.1 - 150 psig). Nominally, 0.285 MPa (25 psig) (8) is used for some transportation applications. Using appropriate current collectors and supporting structure, polymer electrolyte fuel cells and electrolysis cells should be capable of operating at pressures up to 3000 psi and differential pressures up to 500 psi (15).

Water Management

Due to operation at less than 100°C and atmospheric pressure, water is produced as a liquid. A critical requirement is to maintain high water content in the electrolyte to ensure high ionic conductivity. Maintaining high water content is particularly critical when operating at high current densities (approximately 1 A/cm^2) because mass transport issues associated with water formation and distribution limit cell output. The ionic conductivity of the electrolyte is higher when the membrane is fully saturated: this impacts the overall efficiency of the fuel cell. Without adequate water management, an imbalance will occur between water production and water removal from the cell.

Water content is determined by the balance of water[14] during operation. Contributing factors to water transport are the water drag through the cell, back-diffusion from the cathode, and the diffusion of water in the fuel stream through the anode. Water transport is not only a function of the operating conditions[14] but a function of the characteristics of the membrane and the electrodes. Water drag refers to the amount of water that is pulled by osmotic action along with the proton (16). One estimate is that between 1 - 2.5 molecules are dragged with each proton (17). As a result, transported water can be envisioned as a hydrated proton, $H(H_2O)n$. During operation, a concentration gradient may form whereby the anode is drier than the cathode. Under these conditions, there is a back-diffusion of water from the cathode to the anode. Membrane thickness is also a factor in that the thinner the membrane, the greater the transport of water back to the anode. Under ideal conditions, there should be a net zero (17, 18) water exchange. References (19) and (20) can be reviewed for specific modeling information, but suffice it to say that if too much water is available, the electrodes may be flooded and reactants may be diluted; while if too little, the membrane may be dehydrated. Adherence of the membrane to the electrode will be adversely affected if dehydration occurs. Intimate contact between the electrodes and the electrolyte membrane is important because there is no free liquid electrolyte to form a conducting bridge. Operation under dry conditions will severely impact membrane lifetime (21).

Reliable forms of water management have been developed based on continuous flow field design and appropriate operating adjustments. If more water is exhausted than produced, then humidification of the incoming anode gas becomes important (19). If there is too much humidification, however, the electrode floods, which causes problems with gas diffusion to the electrode. A temperature rise between the inlet and outlet of the flow field increases evaporation

14. A smaller current, larger reactant flow, lower humidity, higher temperature, or lower pressure will result in a water deficit. A higher current, smaller reactant flow, higher humidity, lower temperature, or higher pressure will lead to a water surplus.

to maintain water content in the cell. There also have been attempts to control the water in the cell using external wicking connected to the membrane to either drain or supply water by capillary action.

One PEFC developer (22) devised an alternative plate structure that provides passive water control. Product water is removed by two mechanisms: 1) transport of liquid water through the porous bipolar plate into the coolant, and 2) evaporation into the reactant gas streams. The cell is similar in basic design to other PEFCs with membrane, catalysts, substrates, and bipolar plate components. However, there is a difference in construction and composition of the bipolar plate: it is made of porous graphite. During operation, the pores are filled with liquid water that communicates directly with the coolant stream. Product water flows from the cathode through the pores into the coolant stream (a small pressure gradient between reactant and the coolant stream is needed). The water in the coolant stream is then routed to a reservoir. Removal of water by the porous membrane results in the reactant flow stream being free of any obstructions (liquid water). The flooded pores serve a second purpose of supplying water to the incoming reactant gases and humidifying those gases. This prevents drying of the membrane, a common failure mode, particularly at the anode. Control of the amount of area used to humidify the inlet gases has eliminated the need to pre-humidify the reactant gases.

Reasons for removing the water through the porous plate are: 1) there is less water in the spent reactant streams; 2) this approach reduces parasitic power needs of the oxidant exhaust condenser; 3) the cell can operate at high utilizations that further reduce water in the reactant streams; 4) higher temperatures can be used with higher utilizations so that the radiator can be smaller,[15] and 5) the control system is simplified.

3.1.1 State-of-the-Art Components

An accelerated interest in polymer electrolyte fuel cells within the decade has led to improvements in both cost and performance. Development has reached the point where both motive and stationary power applications are nearing an acceptable cost for commercial markets. PEFC operation at ambient pressure has been validated by more than 25,000 hours with a six-cell stack without forced air flow, humidification, or active cooling (23). Complete fuel cell systems have been demonstrated for a number of transportation applications including public transit buses and passenger automobiles. For stationary applications, a factory-produced residential power system has operated unattended for over 1,000,000 kWhrs (24). Recent development has focused on cost reduction and high-volume manufacture for the catalyst, membranes, and bipolar plates. This coincides with ongoing research to increase power density, improve water management, operate at ambient conditions, tolerate reformed fuel, and extend stack life.

Manufacturing details of the Plug Power cell and stack design are proprietary, but the literature provides some information on the cell and stack design. Example schematics for the cross-section and a current collecting plate are shown in Figure 3-2 (25, 26). An approach for sealing the cell with flat gaskets is shown (Label 402) but there are many alternatives with gaskets and plates having different shapes and grooves, respectively. The plate shows the flow path for one of

15. Higher average temperature operaton is possible because of the reduction of hot spots within the cell. Water will evaporate through the porous plate in the vicinity of a hot spot. Conversely, a local cool spot can produce a concentration of water. This water is quickly removed through the porous plate.

the reactants from the inlet to the outlet manifold. The other side of the plate (not shown) would have channels either for coolant flow or the other reactant.

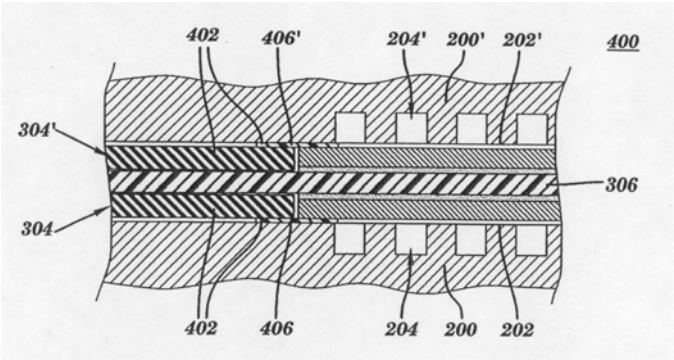

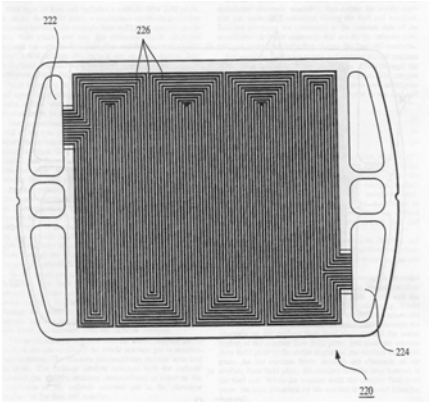

Figure 3-2 PEFC Schematic (25, 26)

The standard electrolyte material in PEFCs belongs to the fully fluorinated Teflon®-based family similar to that produced by E.I. DuPont de Nemours for space application in the mid-1960s. The membrane is characterized by its equivalent weight (inversely proportional to the ion exchange capacity). A typical equivalent weight range is 800 – 1100 milliequivalents per dry gram of polymer. The type used most often in the past was a melt-extruded membrane manufactured by DuPont and sold under the label Nafion® No. 117. The perfluorosulfonic acid family of membranes exhibits exceptionally high chemical and thermal stability, and is stable against chemical attack in strong bases, strong oxidizing and reducing acids, Cl_2, H_2, and O_2 at temperatures up to 125°C (27). Nafion consists of a fluoropolymer backbone, similar to Teflon®, upon which sulfonic acid groups are chemically bonded (23, 28). Nafion membranes have exhibited long life in selected applications, operating conditions, and electrochemical applications. In selected fuel cell tests and water electrolysis systems, lifetimes of over 50,000 hours have been demonstrated. The Dow Chemical Company produced an electrolyte membrane, the XUS 13204.10, that contained a polymeric structure similar to that of Nafion, except that the side chain length was shortened (29). As a result, the membrane properties were significantly impacted, including a higher degree of water interactions within the membrane. This translated to lower electrical resistance and permited higher current densities than the Nafion membrane, particularly when used in thinner form (30). These short side-chain membranes exhibited good performance and stability, but are no longer being supplied by Dow. Furthermore, due to Nafion's present expense and other engineering issues, new alternative membranes are being developed by a number of different companies.

Progress in manufacturing techniques has been made as well. Although melt-extruded films were the norm, the industry is moving to a solution-cast film process to reduce costs and improve manufacturing throughput efficiency. In this process, the ionic form of the polymer is solubilized in an alcoholic solution, such as propanol, and then fabricated into a film of desired thickness. The conversion of the non-ionic polymer to an ionic phase, ready for use in a fuel cell, is carried out prior to the solubilization step.

Another advancement in membrane technology is that of using an internal support layer to enhance the mechanical properties of the membrane films, especially as the membrane thickness is decreased. The Primea 55 and 56 series membranes manufactured by W.L. Gore are examples of such internally-supported membranes.

Typically, electrodes can be cast as thin films and transferred to the membrane or applied directly to the membrane. Alternatively, the catalyst-electrode layer may be deposited onto the gas diffusion layer (GDL), then bonded to the membrane. Low platinum loading electrodes (≤ 1.0 mg Pt/cm^2 total on the anode and the cathode) are regularly used and have performed as well as earlier, higher platinum loading electrodes (2.0 - 4.0 mg Pt/cm^2). These electrodes, which have been produced using a high-volume manufacturing process, have achieved nearly 600 mA/cm^2 at 0.7 V on reformate. A number of companies globally are developing such electrodes. An example of electrode performance is shown in Figure 3-3. The figure depicts the performance of a standard 100 cm^2 7-layer membrane/electrode assembly (MEA) manufactured by the 3M Corporation operating on hydrogen and reformate at 70°C (31). Recent advances in MEA performance and durability have led to tests with reformate in excess of 10,000 hours with the 3M 7-layer MEA. This MEA is produced using high-speed, continuous, automated assembly equipment.

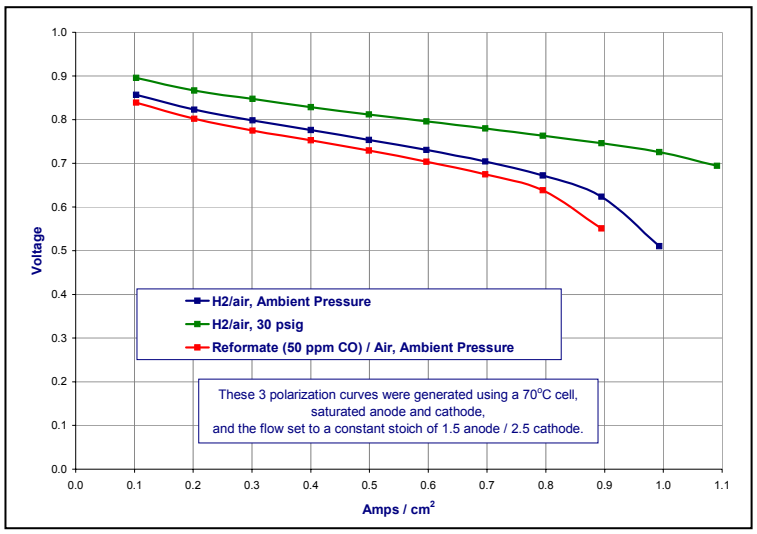

Figure 3-3 Polarization Curves for 3M 7 Layer MEA (31)

Much progress has been made towards PEFC commercialization. Figure 3-4, from Gore Fuel Cell Technologies, demonstrates the company's newest commercial offering, PRIMEA® Series 56 MEA that has demonstrated over 15,000 hours of cell operation (32).

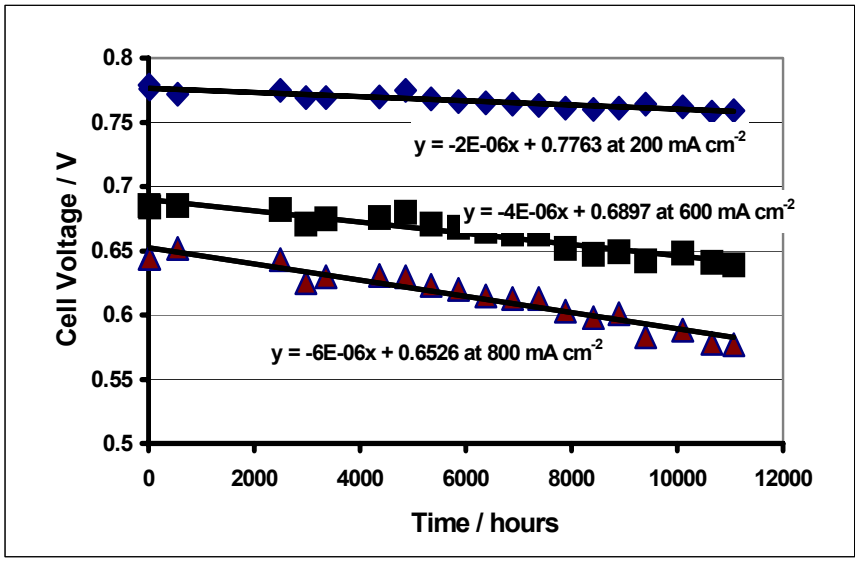

Figure 3-4 Endurance Test Results for Gore Primea 56 MEA at Three Current Densities

To improve effectiveness of the platinum catalyst, a soluble form of the polymer is incorporated into the pores of the carbon support structure. This increases the interface between the electrocatalyst and the solid polymer electrolyte. Two methods are used to incorporate the polymer solution within the catalyst. In Type A, the polymer is introduced after fabrication of the electrode; in Type B, it is introduced before fabrication.

Most PEFCs presently use cast carbon composite plates for current collection and distribution, gas distribution, and thermal management. Cooling is accomplished using a circulating fluid, usually water that is pumped through integrated coolers within the stack. The temperature rise across the cell is kept to less than 10°C. In one configuration, water-cooling and humidification are in series, which results in the need for high quality water. The cooling unit of a cell can be integrated to supply reactants to the MEA, remove reaction products from the cell, and seal off the various media against each other and the outside.

The primary contaminants of a PEFC are carbon monoxide (CO) and sulfur (S). Carbon dioxide (CO_2) and unreacted hydrocarbon fuel act as diluents. Reformed hydrocarbon fuels typically contain at least 1% CO. Even small amounts of CO in the gas stream, however, will preferentially adsorb on the platinum catalyst and block hydrogen from the catalyst sites. Tests indicate that as little as 10 ppm of CO in the gas stream impacts cell performance (33, 34). Fuel processing can reduce CO content to several ppm, but there are system costs associated with increased fuel purification. Platinum/ruthenium catalysts with intrinsic tolerance to CO have been developed. These electrodes have been shown to tolerate CO up to 200 ppm (35). Although much less significant than the catalyst poisoning by CO, anode performance is adversely affected by the reaction of CO_2 with adsorbed hydrides on platinum. This reaction is the electrochemical equivalent of the water gas shift reaction.

A number of approaches can be used to purify reformate fuel. These include pressure swing adsorption, membrane separation, methanation, and selective oxidation. Although selective oxidation does not remove CO_2, it is usually the preferred method for CO removal because of the parasitic system loads and energy required by other methods. In selective oxidation, the reformed fuel is mixed with air or oxygen either before the fuel is fed to the cell or within the stack itself. Current selective oxidation technology can reduce CO levels to <10 ppm. Another approach involves the use of a selective oxidation catalyst that is placed between the fuel stream inlet and the anode catalyst. Introducing an air bleed to the fuel stream, however, appears to be the most effective way to reduce CO to an acceptable level. Research to find approaches and materials that better tolerate impurities in the fuel continues today.

A number of technical and cost issues face polymer electrolyte fuel cells at the present stage of development (33, 36, 37, 38, 39). These concern the cell membrane, cathode performance, and cell heating limits. The membranes used in present cells are expensive, and available only in limited ranges of thickness and specific ionic conductivity. Lower-cost membranes that exhibit low resistivity are needed. This is particularly important for transportation applications characterized by high current density operation. Less expensive membranes promote lower-cost PEFCs, and thinner membranes with lower resistivities could contribute to power density improvement (39). It is estimated that the present cost of membranes could fall (by one order of magnitude) if market demand increased significantly (by two orders of magnitude) (22).

There is some question of whether higher catalyst effectiveness is needed even though new research has resulted in loading being reduced to less than 1 mg/cm^2. Some researchers cite a need for higher catalyst effectiveness, while others state that because only 10% of the cell material cost is tied up in catalyst, it is better to maintain high catalyst loading and instead concentrate on the design of an effective MEA (40).

Improved cathode performance, when operating on air at high current densities, is needed. At high current densities, there is a limiting gas permeability and ionic conductivity within the catalyst layer. A nitrogen blanket forming on the gas side of the cathode is suspected of creating additional limitations (3). There is a need to develop a cathode that lessens the impact of the nitrogen blanket, allows an increase in cell pressure of the cell, and increases the ionic conductivity.

Local heat dissipation problems limit stack operation with air at a current density of approximately 2 A/cm^2. Single cells have shown the capability to operate at higher current densities on pure oxygen. It may be possible to increase current density and power density through better cooling schemes.

Although not an individual cell technology issue, one developer (41) uses hot, swappable, modular power cartridge architecture. This patented technology is claimed to be more reliable because servicing can be accomplished quickly and easily by simply swapping out one cell cartridge for another, while the stack continues to create power. In addition to providing superior reliability and ease of use, the cartridge-based architecture tends to minimize the vulnerability of damage to the proton exchange membranes. The inherent advantages of this design include self-hydration, air cooling, and the ability to operate at low pressure.

3.1.2 Development Components

The primary focus of ongoing research has been to improve performance and reduce cost. The principal areas of development are improved cell membranes, CO removal from the fuel stream, and improved electrode design. There has been a move toward operation with zero humidification at ambient pressure, increased cell temperature, and direct fuel use. DuPont now produces a membrane of 2 mils or less thickness that performs (at lower current densities) similar to the Dow Chemical Company membrane, the XUS 13204.10 depicted in the top curve of Figure 3-5 (42). There is ongoing work to investigate alternative membranes and MEAs that not only exhibit durability and high performance, but also can be manufactured inexpensively in high volume.

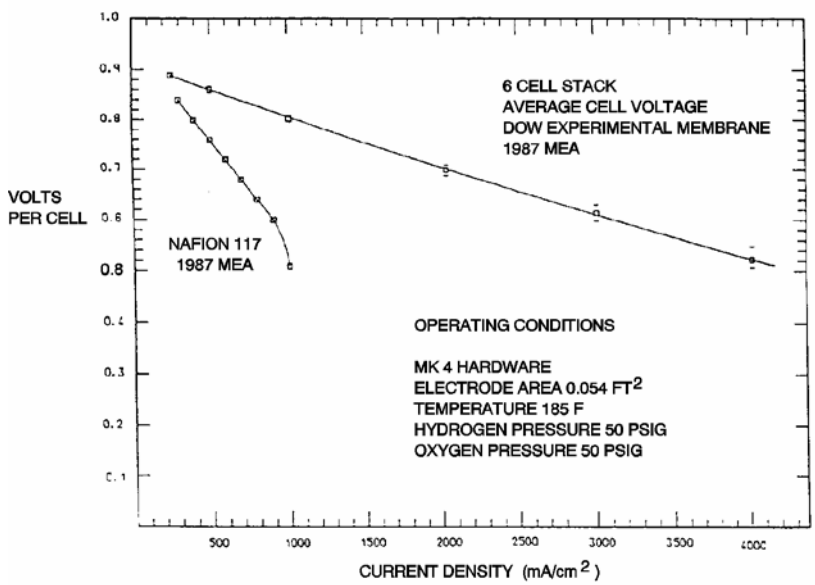

Figure 3-5 Multi-Cell Stack Performance on Dow Membrane (30)

PEFCs were originally made with an unimpregnated electrode/Nafion electrolyte interface. This was later replaced by a proton conductor that was impregnated into the active layer of the electrode. This allowed reduced catalyst loading to 0.4 mg/cm^2 while obtaining high power density (15). The standard "Prototech" electrodes contained 10% Pt on carbon supports. Using higher surface area carbon-supported catalysts, researchers have tested electrodes with even lower platinum loading, but having performance comparable to conventional electrodes. Los Alamos National Laboratory has tested a cathode with 0.12 mg Pt/cm^2 loading, and Texas A&M University has tested a cathode with 0.05 mg Pt/cm^2 loading. Another example of low catalyst loadings is the work carried out at Deutsches Zentrum fur Luft- und Raumfahrt (43) in which loadings as low as 0.07 mg/cm^2 were applied to the membrane using a dry process. The binder was a Teflon-like material.

Another approach has been developed to fabricate electrodes with loading as low as 0.1 mg Pt/cm^2 (44). The electrode structure was improved by increasing the contact area

between the electrolyte and the platinum clusters. The advantages of this approach were that a thinner catalyst layer of 2 - 3 microns and a uniform mix of catalyst and polymer were produced. For example, a cell with a Pt loading of 0.07 - 0.13 mg/cm^2 was fabricated. The cell generated 3 A/cm^2 at > 0.4V on pressurized O_2, and 0.65 V at 1 A/cm^2 on pressurized air (44, 45).

Stable performance was demonstrated over 4,000 hours with Nafion membrane cells having 0.13 mg Pt/cm^2 catalyst loading and cell conditions of 2.4 atmospheres H_2, 5.1 atmospheres air, and 80°C (4,000 hour performance was 0.5 V at 600 mA/cm^2). Water management was stable, particularly after thinner membranes of somewhat lower equivalent weight became available. Some performance losses may have been caused by slow anode catalyst deactivation, but the platinum catalyst "ripening" phenomenon was not considered to contribute significantly to the long-term performance losses observed in PEFCs (3).

Other research has focused on developing low-cost, lightweight, graphite carbon-based materials that can be used in place of expensive, high-purity graphite bi-polar plates. Plated metals, such as aluminum and stainless steel, are also under consideration for this application, but these materials are typically inferior to graphite plates because of contact resistance and durability concerns (23). Conductive plastic and composite bi-polar plates have met with significant success in the laboratory, and have even reached commercial production. The time line for the development of a vinyl ester configuration is shown in Reference (46) for a material that has reached almost 100 /ohm-cm conductivity.

Selective oxidation is able to decrease CO in a methanol reformed gas (anode fuel supply stream) from 1% to approximately 10 ppm using a platinum/alumina catalyst. The resulting performance of the anode catalyst, though satisfactory, is impacted even by this low amount of CO. Research at Los Alamos National Laboratory has demonstrated an approach to remedy this problem by bleeding a small amount of air or oxygen into the anode compartment. Figure 3-6 shows that performance equivalent to that obtained on pure hydrogen can be achieved using this approach. It is assumed that this approach would also apply to reformed natural gas that incorporated water gas shift to obtain CO levels of 1% entering the fuel cell. This approach results in a loss of fuel, which should not exceed 4% provided that the reformed fuel gas can be limited to 1% CO (3). Another approach is to develop a CO-tolerant anode catalyst such as the platinum/ruthenium electrodes currently under consideration. Platinum/ruthenium anodes have allowed cells to operate, with a low-level air bleed, for over 3,000 continuous hours on reformate fuel containing 10 ppm CO (15).

There is considerable interest in extending PEFC technology to direct methanol and formaldehyde electro-oxidation (47, 48) using Pt-based bi-metallic catalyst. Tests have been conducted with gas diffusion-type Vulcan XC-72/Toray support electrodes with Pt/Sn (0.5 mg/cm^2, 8% Sn) and Pt/Ru (0.5 mg/cm^2, 50% Ru). The electrodes have Teflon content of 20% in the catalyst layer.

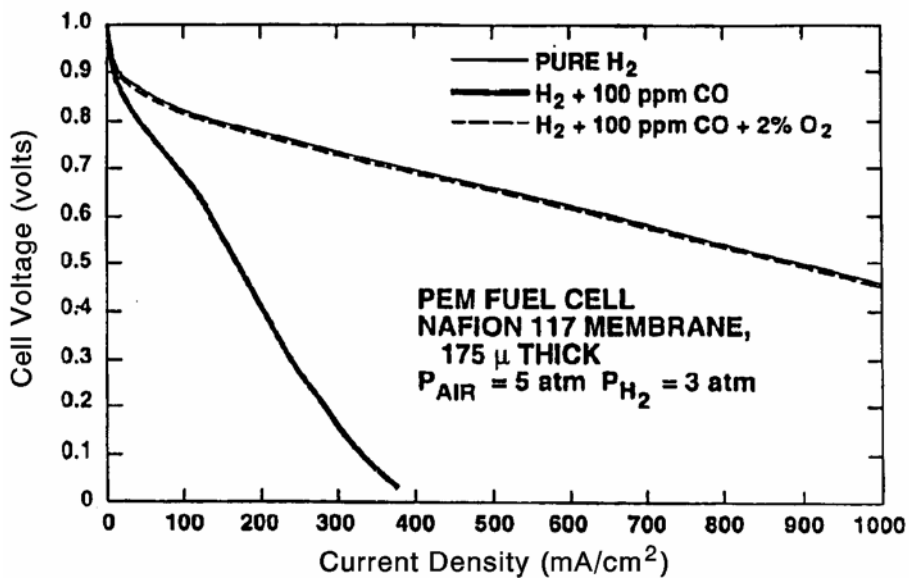

Figure 3-6 Effect on PEFC Performances of Bleeding Oxygen into the Anode Compartment (3)

3.2 Performance

A summary of the performance levels achieved with PEFCs since the mid-1960s is presented in Figure 3-7. Because of changes in operating conditions involving pressure, temperature, reactant gases, and other parameters, a wide range of performance levels can be obtained. The performance of the PEFC in the U.S. Gemini Space Program was 37 mA/cm^2 at 0.78 V in a 32-cell stack that typically operated at 50°C and 2 atmospheres (1). Current technology yields performance levels that are vastly superior. Results from Los Alamos National Laboratory show that 0.78 V at about 200 mA/cm^2 (3 atmospheres H_2 and 5 atmospheres air) can be obtained at 80°C in PEFCs containing a Nafion membrane and electrodes with a platinum loading of 0.4 mg/cm^2. Further details on PEFC performance developments with Nafion membranes are presented by Watkins, et al. (49).

Operating temperature has a significant influence on PEFC performance. An increase in temperature decreases the ohmic resistance of the electrolyte. In addition, mass transport limitations are reduced at higher temperatures. The overall result is an improvement in cell performance. Experimental data (53, 50, 51) suggest a voltage gain in the range of 1.1 - 2.5 mV for each degree (°C) of temperature increase. Operating at higher temperatures also reduces the chemisorption of CO. Improving the cell performance through an increase in temperature, however, is limited by the vapor pressure of water in the ion exchange membrane due to the membrane's susceptibility to dehydration and the subsequent loss of ionic conductivity.

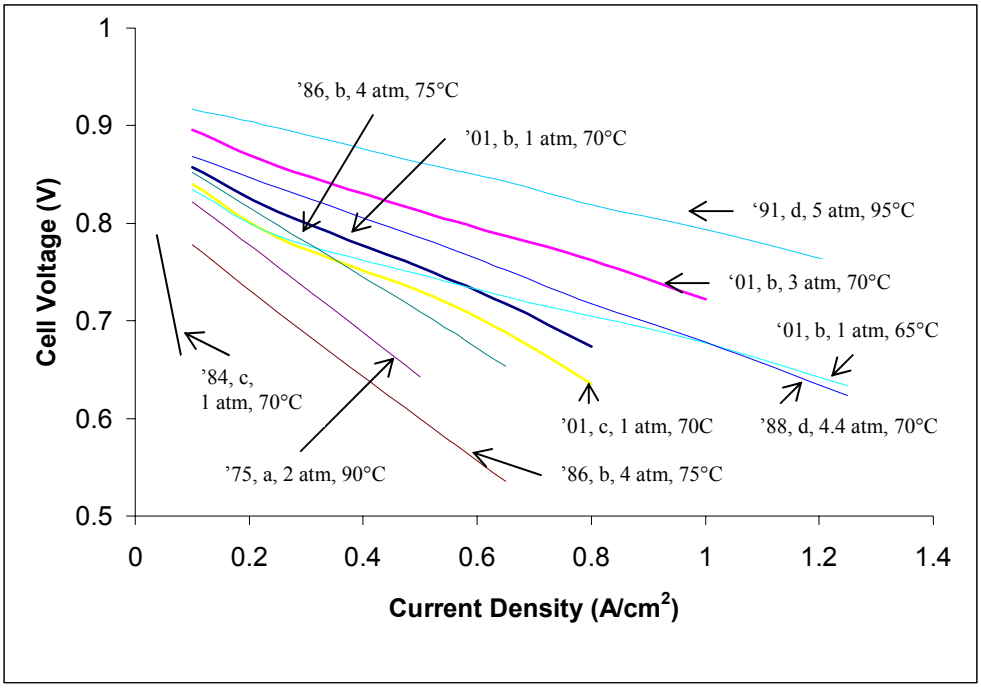

Figure 3-7 Evolutionary Changes in PEFCs Performance (a) H_2/O_2, (b) H_2/Air, (c) Reformate Fuel/Air, (d) H_2/unkown [19, 22, 31, 52, 53]

Operating pressure also impacts cell performance. The influence of oxygen pressure on the performance of a PEFC at 93°C is illustrated in Figure 3-8 (54). An increase in oxygen pressure from 30 to 135 psig (3 to 10.2 atmospheres) produces an increase of 42 mV in the cell voltage at 215 mA/cm^2. According to the Nernst equation, the increase in the reversible cathode potential that is expected for this increase in oxygen pressure is about 12 mV, which is considerably less than the measured value. When the temperature of the cell is increased to 104°C, the cell voltage increases by 0.054 V for the same increase in oxygen pressure. Additional data suggest an even greater pressure effect. A PEFC at 50°C and 500 mA/cm^2 (53) exhibited a voltage gain of 83 mV for an increase in pressure from 1 to 5 atmospheres. Another PEFC at 80°C and 431 mA/cm^2 (50) showed a voltage gain of 22 mV for a small pressure increase from 2.4 to 3.4 atmospheres. These results demonstrate that an increase in the pressure of oxygen results in a significant reduction in polarization at the cathode. Performance improvements due to increased pressure must be balanced against the energy required to pressurize the reactant gases. The overall system must be optimized according to output, efficiency, cost, and size.

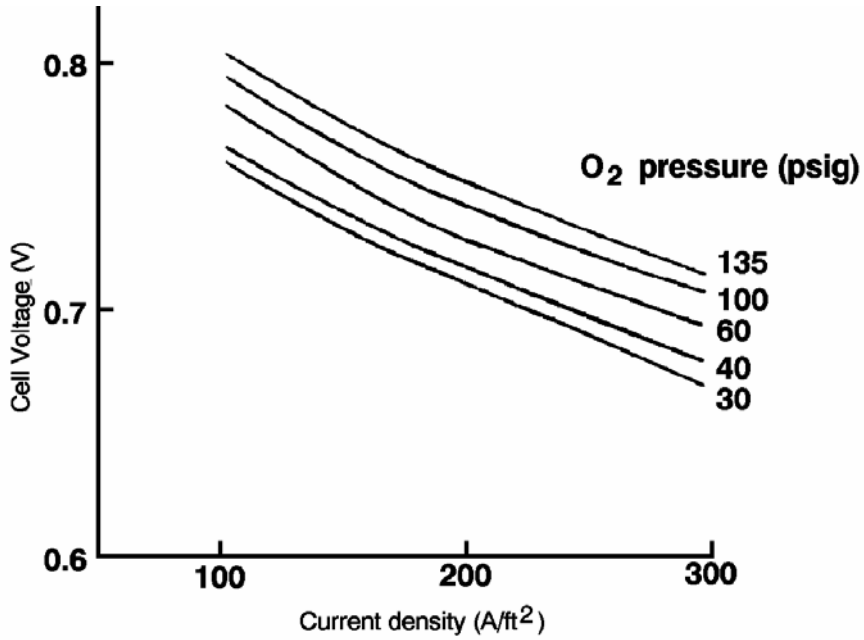

Figure 3-8 Influence of O_2 Pressure on PEFCs Performance (93°C, Electrode Loadings of 2 mg/cm^2 Pt, H_2 Fuel at 3 Atmospheres) [(54) Figure 29, p. 49]

Lifetime performance degradation is a key performance parameter in a fuel cell, but the causes of degradation are not fully understood. The sources of voltage decay are kinetic (or activation) loss, ohmic (or resistive) loss, loss of mass transport, and loss of reformate tolerance (23).

Presently, the major focus of R&D on PEFC technology is to develop a fuel cell for terrestrial transportation, which requires the development of low-cost cell components. Reformed methanol is expected to be a major fuel source for PEFCs in transportation applications. Because the operating temperature of PEFCs is much lower than that of PAFCs, poisoning of the anode electrocatalyst by CO from steam reformed methanol is a concern. The performance achieved with a proprietary anode in a PEFC with four different concentrations of CO in the fuel gas is shown in Figure 3-9. The graph shows that at higher current densities, the poisoning effect of CO is increased. At these higher current densities, the presence of CO in the fuel causes the cell voltage to become unstable and cycle over a wide range. Additional data (34) have suggested that the CO tolerance of a platinum electrocatalyst can be enhanced by increasing either the temperature or the pressure.

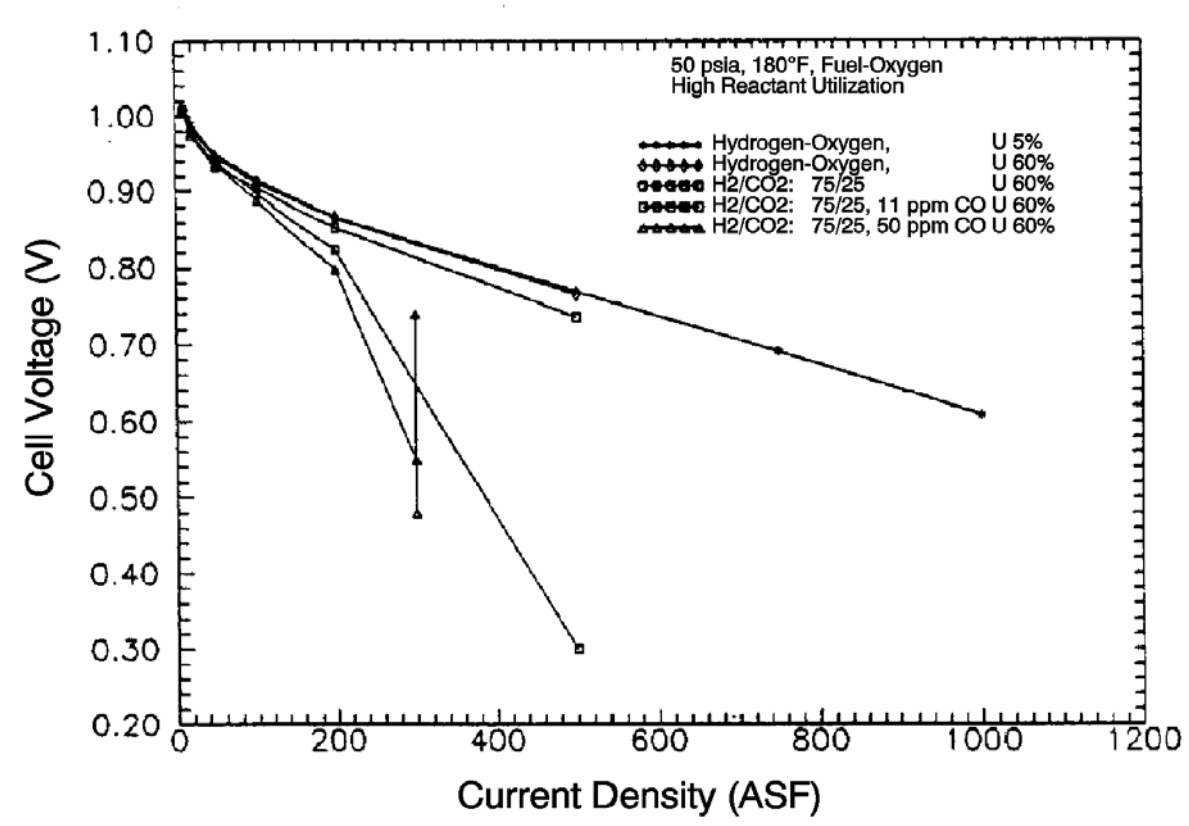

Figure 3-9 Cell Performance with Carbon Monoxide in Reformed Fuel (54)

3.3 Direct Methanol Proton Exchange Fuel Cell

The large potential market for fuel cell vehicle applications has generated a strong interest in a fuel cell that can run directly on methanol. Operation on liquid fuel would assist in rapid introduction of fuel cell technology into commercial markets, because it would greatly simplify the on-board system as well as the infrastructure needed to supply fuel to passenger cars and commercial fleets. Performance levels achieved with a direct methanol PEFC using air are now in the range of 180 - 250 mA/cm^2 (23). Problems with methanol crossover and high overpotentials still inhibit performance. Research has focused on finding more advanced electrolyte materials to combat fuel crossover and more active anode catalysts to promote methanol oxidation. Significant progress has been made over the past few years in both of these key areas.

Improvements in solid polymer electrolyte materials have extended the operating temperature of direct methanol PEFCs from 60°C to almost 100°C. Electro-catalyst developments have focused on materials with higher activity. Researchers at the University of Newcastle upon Tyne have reported over 200 mA/cm^2 at 0.3 V at 80°C with platinum/ruthenium electrodes having platinum loading of 3.0 mg/cm^2. The Jet Propulsion Laboratory in the U.S. has reported over 100 mA/cm^2 at 0.4 V at 60°C with platinum loading of 0.5 mg/cm^2. Recent work at Johnson Matthey has clearly shown that platinum/ruthenium materials possess substantially higher activity than platinum alone (55).

All fuel cells exhibit kinetic losses that cause the electrode reactions to deviate from their theoretical ideal. This is particularly true for a direct methanol PEFC. Eliminating the need for a fuel reformer, however, makes methanol and air PEFCs an attractive alternative to PEFCs that require pure hydrogen as a fuel. The minimum performance goal for direct methanol PEFC commercialization is approximately 200 mW/cm^2 at 0.5 to 0.6 V.

Figure 3-10 summarizes the performance recently achieved by developers.

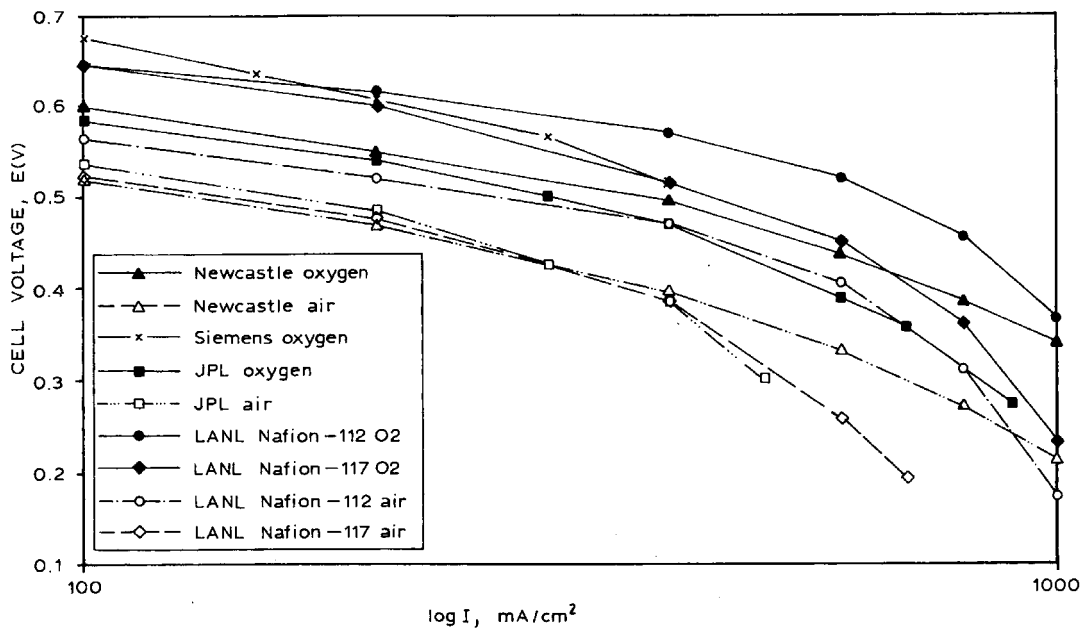

Figure 3-10 Single Cell Direct Methanol Fuel Cell Data (55)

3.4 References

1. A.J. Appleby, E.B. Yeager, *Energy*, pg. 11, 137, 1986.
2. S. Gottesfeld, T. Zawodzinski, PEFC Chapter in Advances in Electrochemical Science and Engineering, Volume 5, edited by R. Alkire, H. Gerischer, D. Kolb, C. Tobias, pp. 197-301, 1998.
3. S. Gottesfeld, "The Polymer Electrolyte Fuel Cell: Materials Issues in a Hydrogen Fueled Power Source," LANL, undated.
4. W.T. Grubb, *Proceedings of the 11th Annual Battery Research and Development Conference*, PSC Publications Committee, Red Bank, NJ, p. 5, 1957; U.S. Patent No. 2,913,511, 1959.
5. G.A. Eisman, Abstracts, "Fuel Cell Technology and Applications," International Seminar, The Netherlands, p. 287, 1987.
6. Peter M. Schutz, A Preliminary Investigation of Radiation Catalysts in Fuel Cells, Master of Science Thesis, Virginia Polytechnic University, Blacksburg, Va., August, 1979 Pg. 59.

7. D. S. Watkins, et al., Abstracts 37th International Power Sources Symposium (The Electrochemical Society) p. 782, 1988.
8. J. C. Amphlett, M. Farahani, R. F. Mann, B. A. Peppley, P. R. Roberge, in *Proceedings of the 26th Intersociety Energy Conversion Engineering Conference*, August 4-9, 1991, Volume 3, Conversion Technologies/Electrochemical Conversion, American Nuclear Society, La Grange, Illinois, p. 624, 1991.
9. W. Teagan, J. Bentley, "Status: ADL/EPYX Fuel Processing Technology," Joint DOE/EPRI/GRI Workshop on Fuel Cell Technology, San Francisco, CA, May 18-20, 1998.
10. M. Krumpelt, K. M. Myles, No. 8, An EPRI/GRI Fuel Cell Workshop on Technology Research and Development, April 13-14, 1993, Stonehart Associates, Madison, Connecticut, 1993.
11. M. Krumpelt, R. Kumar, J. Miller, C. Christianson, in *1992 Fuel Cell Seminar Program and Abstracts*, The Fuel Cell Seminar Organizing Committee, November 29 - December 2, 1992, Tucson, Arizona, p. 35, 1992.
12. R. F. Savinell, J. S. Wainright, M. Litt, "High Temperature Polymer Electrolyte Fuel Cells," The Electrochemical Society, Journal 98-27, p.81.
13. W.D. Ernst, "PEM Technology Development at Plug Power," *2000 Fuel Cell Seminar Program and Abstracts*, Portland Oregon, sponsored by Fuel Cell Seminar Organizing Committee, October 30 – November 2, 2000.
14. Gordon Research Conference, Rhode Island, July 29 - August 3, 2001**.**
15. T.G. Coker, A.B. LaConti, L.J. Nuttall, in *Proceedings of the Symposium on Membranes and Ionic and Electronic Conducting Polymers*, edited by E.G. Yeager, B. Schumm, K. Mauritz, K. Abbey, D. Blankenship, J. Akridge, The Electrochemical Society, Inc., Pennington, NJ, p. 191, 1983.
16. N. Giordano, et al., in *Proceedings 26th Intersociety Energy Conversion Engineering Conference*, August 4-9, 1991, Volume 3, Conversion Technologies/Electrochemical Conversion, American Nuclear Society, La Grange, Illinois, p. 624, 1991.
17. T.A. Zawodzinski, et al., *Journal of Electrochemical Society*, p. 140, 1042, 1993.
18. T.E. Springer, et al., *Journal of Electrochemical Society*, p. 138, 2335, 1991.
19. D.M. Bernardi, *Journal of Electrochemical Society*, p. 137, 3344, 1990.
20. T.E. Springer, M. S. Wilson, S. Gottesfeld, "Modeling and Experimental Diagnostics in Polymer Electrolyte Fuel Cells," submitted to J. ElectroChem. Soc., LA-UR-93-1469 Los Alamos National Laboratory, New Mexico, 1993.
21. R. Baldwin, M. Pham, A. Leonida, J. McElroy, and T. Nalette, Hydrogen-Oxygen Proton Exchange Membrane Fuel Cells and Electrolyzers, Proceedings of the Space Electrochemical Research and Technology (SERT), NASA LEWIS Research Center, Cleveland, Ohio, April, 1989.
22. D.J. Wheeler, J.S. Yi, R. Fredley, D. Yang, T. Patterson Jr., L. VanDine, "Advacements in Fuel cell Stack Technology at International Fuel Cells," International Fuel Cells (now UTC Fuel Cells*), Journal of New Materials for Electrochemical Systems*, 4, 2001.
23. D. Wilkinson, A. Steck, "General Progress in the Research of Solid Polymer Fuel Cell Technology at Ballard," *Proceedings of the Second International Symposium on New Materials for Fuel Cell and Modern Battery Systems*, Montreal, Quebec, Canada, July 6-10, 1997.
24. Communication with Plug Power, August 2002.
25. W.D. Ernst, Patent No. 5,912,088, Plug Power Inc., June 15, 1999.

26. G.S. Eisman, et al., Patent No. 6,280,865, Plug Power Inc., August 28, 2001.
27. W.G.F. Grot, G.E. Munn, P.N. Walmsley, paper presented at the 141st National Meeting of the Electrochemical Society, Inc., Abstract No. 154, Houston, TX, May 7-11, 1972.
28. T. Ralph, "Proton Exchange Membrane Fuel Cells: Progress in Cost Reduction of the Key Components," *Platinum Metals Review*, 41, pp. 102-113, 1997.
29. B.R. Ezzell, B. Carl, and W. Mod, Ion Exchange Membranes for the Chlor Alkali Industry, AIChE Symp. Series, Houston, TX, March 1985, Pg. 49
30. K. Prater, "The Renaissance of the Solid Polymer Fuel Cell," Ballard Power Systems, Inc., Journal of Power Sources, p. 29, 1990.
31. 3M Product Bulletin, date unknown.
32. S. Cleghorn, J. Kolde, W. Liu, "Catalyst Coated Composite Membranes," Chapter 49, *Fuel Cell Reference Book,* to be published, Wiley-VCH, 2002.
33. S. Gottesfeld, "Polymer Electrolyte Fuel Cells: Transportation and Stationary Application," No. 10, in *An EPRI/GRI Fuel Cell Workshop on TechnologyResearch and Development,* April 13-14, 1993, Stonehart Associates, Madison, Connecticut, 1993.
34. "Investigation of Design and Manufacturing Methods for Low-Cost Fabrication of High Efficiency, High Power Density PEM Fuel Cell Power Plant," prepared by International Fuel Cells, Final Report FCR-11320A, June 10, 1991.
35. D. Wilkinson, D. Thompsett, "Materials and Approaches for CO and CO_2 Tolerance for Polymer Electrolyte Membrane Fuel Cells," *Proceedings of the Second International Symposium on New Materials for Fuel Cell and Modern Battery Systems*, pp. 266-285, (Montreal, Quebec, Canada, July 6-10, 1997).
36. "Information Sheet," prepared by the U.S. Department of Energy, Office of Propulsion Systems, Proton Exchange Membrane Fuel Cell Program, DE93000009, November 1992.
37. K. Sikairi, K. Tsurumi, S. Kawaguchi, M. Watanabe, P. Stonehart, in *1992 Fuel Cell Seminar Program and Abstracts*, Tucson, AZ, November 29 - December 2, 1992, sponsored by Fuel Cell Organizing Committee, p. 153, 1992.
38. S. Srinivasan, O.A. Velev, A. Parthasarathy, A.C. Ferriera, S. Mukerjee, M. Wakizoe, Y.W. Rho, Y.T. Kho, A.J. Appleby, in *1992 Fuel Cell Seminar Program and Abstracts*, Tucson, Arizona November 29 - December 2, 1992, sponsored by Fuel Cell Organizing Committee, p. 619, 1992.
39. F.N. Buchi, B. Gupta, M. Rouilly, P.C. Hauser, A. Chapiro, G.G. Scherer, in *27th Intersociety Energy Conversion Engineering Conference Proceedings*, Volume 3, Conversion Technologies/Electrochemical Conversions, San Diego, CA, August 3-7, 1992, published by Society of Automotive Engineers, Inc., Warrendale, PA, 419, 1992.
40. S. Srinivasan, O.A. Velev, A. Partharasarathy, D.J. Manko, and A.J. Appleby, Journal of Power Sources, 36, 299, 1991.
41. Modular Cartridge Technology™ Fact Sheet, prepared for 6th Edition of the Fuel Cell Handbook, Avista Labs, a subsidiary of Avista Corp., August, 2002.
42. T.A. Zawodzinski, T.A. Springer, F. Uribe, S. Gottesfeld, "Characterization of Polymer Electrolytes for Fuel Cell Applications," Solid State Tonics 60, pp. 199-211, North-Holland, 1993.
43. E. Gulzow, M. Schulze, N. Wagner, et al., J. of Power Sources Vol. 86 pages 352-362, 2000.
44. M.S. Wilson, T.E. Springer, T.A. Zawodzinski, S. Gottesfeld, in *26th Intersociety Energy Conversion Engineering Conference Proceedings*, Volume 3, Conversion

Technologies/Electrochemical Conversion, Boston, Massachusetts, August 4-9, 1991, published by Society of Automotive Engineers, Inc., Warrendale, PA, 1991.
45. C. Derouin, T. Springer, F. Uribe, J. Valerio, M. Wilson, T. Zawodzinski, S. Gottesfeld, in *1992 Fuel Cell Seminar Program and Abstracts*, Tucson AZ, November 29 - December 2, 1992, sponsored by Fuel Cell Organizing Committee, p. 615, 1992.
46. J.G. Clulow, F.E. Zappitelli, C.M. Carlstrom, J.L. Zemsky, D.M. Buskirk, M.S. Wilson, “Development of Vinyl Ester/ Graphite Composite Bipolar Plates,” Fuel Cell Technology: Opportunites and Challenges, 2002 AIChE Spring National Meeting, March 10-14, 2002.
47. P.D. Naylor, P.J. Mitchell, P.L. Adcock, in *1992 Fuel Cell Seminar Program and Abstracts*, Tucson, AZ, November 29 - December 2, 1992, sponsored by Fuel Cell Organizing Committee, 575, 1992.
48. S.R. Narayanan, E. Vamos, H. Frank, S. Surampudi, G. Halpert, in *1992 Fuel Cell Seminar Program and Abstracts*, Tucson, AZ, November 29 - December 2, 1992, sponsored by Fuel Cell Organizing Committee, p. 233, 1992.
49. D. Watkins, K. Dircks, E. Epp, A. Harkness, *Proceedings of the 32nd International Power Sources Symposium*, The Electrochemical Society, Inc., Pennington, NJ, p. 590, 1986.
50. J.C. Amphlett, et al., "The Operation of a Solid Polymer Fuel Cell: A Parametric Model," Royal Military College of Canada, no date.
51. K. Ledjeff, et al., "Low Cost Membrane Fuel Cell for Low Power Applications," Fraunhofer-Institute for Solar Energy Systems, *Program and Abstracts, 1992 Fuel Cell Seminar*.
52. J. R. Huff, "Status of Fuel Cell Technologies," *Fuel Cell Seminar Abstracts, Fuel Cell Seminar*, October 26-29, 1986, Tucson, AZ.
53. J. Srmivason, et al., "High Energy Efficiency and High Power Density Proton Exchange Membrane Fuel Cells - Electrode Kinetics and Mass Transport," Journal of Power Sources, p. 36, 1991
54. LaConti, G. Smarz, F. Sribnik, "New Membrane-Catalyst for Solid Polymer Electrolyte Systems," Final Report prepared by Electro-Chem Products, Hamilton Standard for Los Alamos National Laboratory under Contract No. 9-X53-D6272-1, 1986.
55. M. Hogarth, G. Hards, "Direct Methanol Fuel Cells: Technological Advances and Further Requirements," *Platinum Metals Review*, 40, pp. 150-159, 1996.

4. ALKALINE FUEL CELL

The Alkaline Fuel Cell (AFC) was one of the first modern fuel cells to be developed, beginning in 1960. The application at that time was to provide on-board electric power for the Apollo space vehicle. Desirable attributes of the AFC include excellent performance compared to other candidate fuel cells due to its active O_2 electrode kinetics and flexibility to use a wide range of electrocatalysts. The AFC continues to be used: it now provides on-board power for the Space Shuttle Orbiter with cells manufactured by UTC Fuel Cells.

The AFC developed for space application was based, in large part, on work initiated by F.T. Bacon (1) in the 1930s. By 1952, construction and performance testing of a 5-kW alkaline fuel cell, operating on H_2 and O_2, was completed. The fuel cell developed by Bacon operated at 200-240°C with 45% KOH electrolyte. Pressure was maintained at 40 to 55 atm to prevent the electrolyte from boiling. At this relatively high temperature and pressure, performance of the cell was quite good (0.78 volts at 800 mA/cm^2). The anode consisted of a dual-porosity Ni electrode (two-layer structure with porous Ni of 16 μm maximum pore diameter on the electrolyte side and 30 μm pore diameter on the gas side). The cathode consisted of a porous structure of lithiated NiO. The three-phase boundary in the porous electrodes was maintained by a differential gas pressure across the electrode, since a wetproofing agent was not available at that time, i.e., PTFE (polytetrafluoroethylene) as a wetproofing material did not exist, and it would not have been stable in the high temperature alkaline solution (2).

The kinetics of O_2 reduction in alkaline electrolytes are more favorable than in phosphoric acid. Consider a Pt cathode (0.25 mg/cm^2) in 30% KOH at 70°C and in 96% phosphoric acid at 165°C. The cathode potentials (vs. RHE - Reversible Hydrogen Electrode) at 100 mA/cm^2 in these two electrolytes are 0.868 and 0.730 V, respectively, according to data reported by Appleby (Figure 2.15-1 in Reference 3). Various explanations have been advanced for the higher O_2 reduction rates in alkaline electrolytes (4). The practical consequence of the higher performance of Pt cathodes in alkaline electrolytes is that AFCs are capable of higher efficiencies than PAFCs at a given current density, or higher power densities at the same efficiency. Bockris (2) estimates that the efficiency of AFCs fueled by pure H_2 is about 60% HHV, and that of PAFCs is about 50% HHV.

The high performance of the alkaline cell relative to phosphoric acid and other cells leads to the plausibility of developing the technology for terrestrial application. The leading developer of alkaline technology for space application, UTC Fuel Cells, investigated adaptating the

technology to terrestrial, stationary power applications using air as an oxidant in the early 1970s. The predominant drawback with terrestrial applications is that CO_2 in any hydrocarbon fuel or in the air reacts with the ion carrier in the electrolyte. During the 1970s, a high pressure drop platinum/palladium separator was used in the fuel processor to obtain a pure stream of H_2 from reformed hydrocarbon fuels (primarily natural gas for stationary power plants). Similarly, a soda-lime scrubber treated the inlet ambient air stream to minimize CO_2 entering the cell. The expense of the separator and scrubber was deemed uneconomical for commercial development of stationary power plants. Augmenting the issue was a slow build-up of K_2CO_3 due to the minuscule amount of CO_2 escaping the soda-lime scrubber. There was also an issue of component life for stationary power applications. Alkaline cell life (now 2,600 hours on H_2/O_2, but 5,000 hour R&D underway) is suitable for space missions, but too brief for terrestrial, stationary power plants. As a result of the CO_2 issue, UTC Fuel Cells, which uses an immobilized electrolyte, now focuses their alkaline program completely toward space applications with H_2/O_2 as fuel and oxidant.

Union Carbide Corp. (UCC) developed AFCs for terrestrial mobile applications starting in the late 1950s, lasting until the early 1970s. UCC systems used liquid caustic electrolytes; the electrodes were either pitch-bonded carbon plates or plastic-bonded carbon electrodes with a nickel current collector. UCC also built fuel cell systems for the U.S. Army and the U.S. Navy, an alkaline direct hydrazine powered motorcycle, and the "Electrovan" of General Motors. Finally, Professor Karl V. Kordesch built his Austin A-40 car, fitted with UCC fuel cells with lead acid batteries as hybrid. It was demonstrated on public roads for three years. The years of research and development are very well summarized in reference (5) *Brennstoffbatterien*.

Based on the UCC technology, other developers are now pursuing terrestrial applications of alkaline technology due to its high performance, particularly for motive power. The majority of these developers use circulating electrolytes with an external, commercial type soda-lime absorber that promises to resolve the problem of CO_2 in the air stream. The quantity of CO_2 can be limited to a small amount with a circulating electrolyte, versus a continual build-up with an immobilized electrolyte. Life expectancy increases (~5,000 hour life is ample for personal automobile engine life) because the cell is nearly inactive when switched off**.** Hence, only the true operating hours count for the total lifetime. During normal operation, the electrolyte circulates continuously, which has several advantages over an immobilized system: 1) no drying-out of the cell occurs because the water content of the caustic electrolyte remains quite constant everywhere inside the stack; 2) heat management by dedicated heat exchanger compartments in the stack becomes unnecessary - the electrolyte itself works as a cooling liquid inside each cell; 3) accumulated impurities, such as carbonates, are concentrated in the circulating stream and can easily be removed (comparable to a function of oil in today's gasoline engines); 4) the OH^- concentration gradient is highly diminished, and 5) the electrolyte prevents the build-up of gas bubbles between electrodes and electrolyte as they are washed away.

Other attributes are that the alkaline cell could have high reactivity without the need for noble metal catalysts on the cell electrodes; this represents a cost savings (6). Additionally, the radiator of the alkaline cell system should be smaller than the radiator in the competitive PEFC system because of higher alkaline cell temperature and its higher performance.

In stacks using circulating electrolytes, parasitic currents might occur. All cells are connected via the electrolyte stream to all other cells, producing high voltages between the electrodes. Parasitic current not only lowers the stack performance, but can also harm the electrodes. Fortunately, this issue can be resolved easily by using a special electrode frame design with long, narrow electrolyte channels.

Some developers have investigated a direct methanol alkaline cell to circumnavigate hydrocarbon fuel separator issues. These cells exhibit a reduced performance, and have not been as thoroughly investigated as the hydrogen-fueled cells.

The unusual economics for remote power applications (i.e., space, undersea, and military applications) result in the cell itself not being strongly constrained by cost. The consumer and industrial markets, however, require the development of low-cost components if the AFC is to successfully compete with alternative technologies. Much of the recent interest in AFCs for mobile and stationary terrestrial applications has addressed the development of low-cost cell components. In this regard, carbon-based porous electrodes play a prominent role (6). It remains to be demonstrated whether alkaline cells will prove commercially viable for the transportation sector. Reference (7) provides an in-depth view of the development history and the potential of alkaline technology for terrestrial application.

Figures 4-1 and 4-2 depict the operating configuration of the H_2/O_2 alkaline fuel cell (8) and a H_2/air cell (9). In both, the half-cell reactions are:

$$H_2 + 2OH^- \rightarrow 2H_2O + 2e^- \quad \text{(Anode)} \tag{4-1}$$

$$\tfrac{1}{2}O_2 + H_2O + 2e^- \rightarrow 2OH^- \quad \text{(Cathode)} \tag{4-2}$$

Hydroxyl ions, OH^-, are the conducting species in the electrolyte. The equivalent overall cell reaction is:

$$H_2 + \tfrac{1}{2}O_2 \rightarrow H_2O + \text{electric energy} + \text{heat} \tag{4-3}$$

Since KOH has the highest conductance among the alkaline hydroxides, it is the preferred electrolyte.

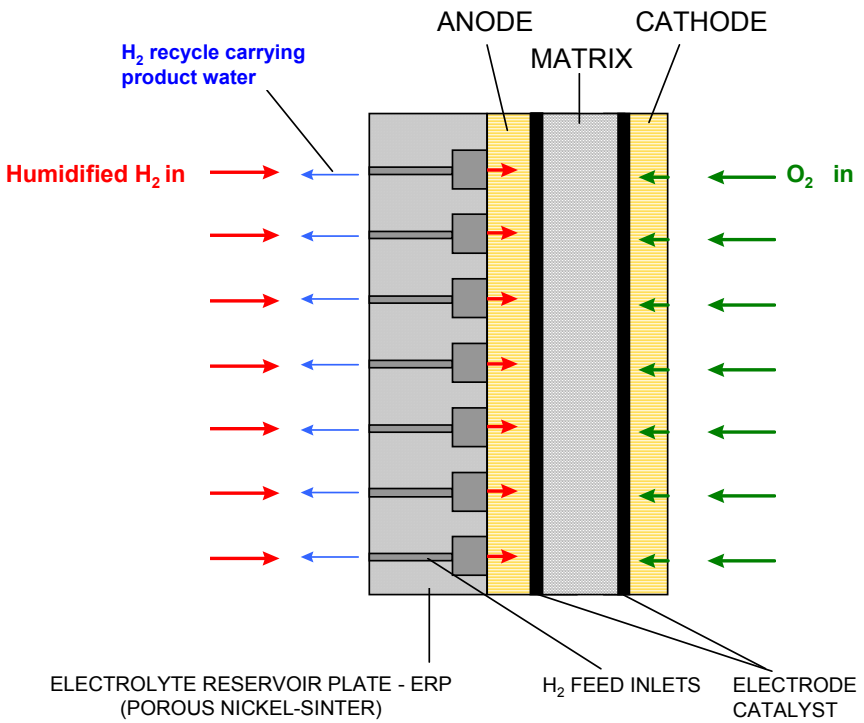

Figure 4-1 Principles of Operation of H_2/O_2 Alkaline Fuel Cell, Immobilized Electrolyte (8)

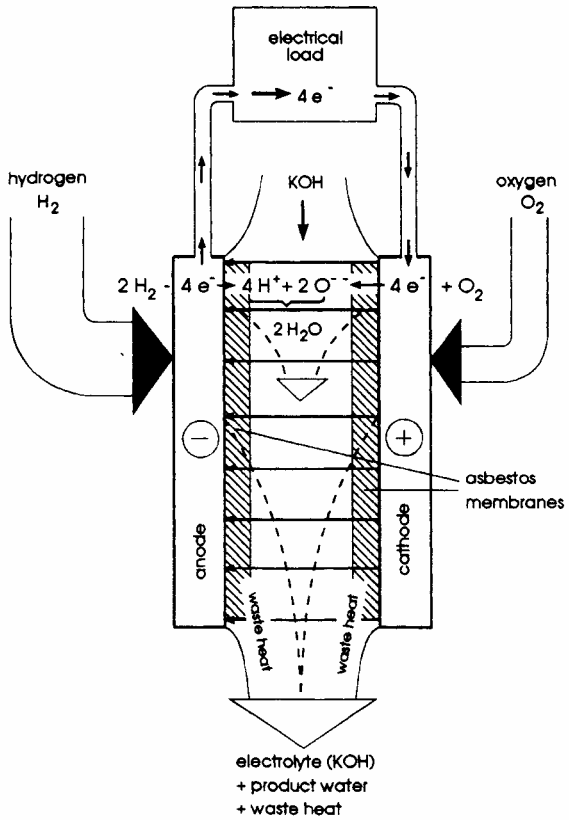

Figure 4-2 Principles of Operation of H_2/Air Alkaline Fuel Cell, Circulating Electrolyte (9)

4.1 Cell Components

4.1.1 State-of-the-Art Components

The concentration of KOH in an immobilized electrolyte typically used in the space program varies from 35-50 wt% KOH for low temperature (<120°C) operation to 85 wt% KOH in cells designed for operation at high temperature (~260°C). The electrolyte is retained in a matrix (usually asbestos), and a wide range of electrocatalysts can be used (e.g., Ni, Ag, metal oxides, spinels, and noble metals) to promote reaction.

The cylindrical AFC modules used in the U.S. Apollo Space Program had a 57 cm diameter, a 112 cm height, weighed about 110 kg, produced a peak power of 1.42 kW at 27-31 V, and operated at an average power of 0.6 kW. These cells operated on pure H_2 and O_2 and concentrated electrolyte (85% KOH) at a moderate pressure (4 atmospheres reactant gas pressure) without electrolyte boiling. With this concentrated electrolyte, cell performance was not as high as in the less-concentrated electrolyte; consequently, the operating temperature was increased to 260°C. The typical performance of this AFC cell was 0.85 V at 150 mA/cm^2, comparing favorably to the performance of the Bacon cell operating at about 10 times higher pressure.

The state-of-the-art alkaline fuel cell stacks in the Space Shuttle Orbiter are rectangular with a width of 38 cm, a length of 114 cm, and a height of 35 cm. They weigh 118 kg, produce a peak power of 12 kW at a minimum of 27.5 V (end of life), and operate at an average power of 7 kW. They operate in the same pressure range as the Apollo cells (4 atmospheres), but at a lower temperature (85 to 95°C) and higher current density (0.88 V at 470 mA/cm^2; UTC Fuel Cells has demonstrated 3.4 W/cm^2 at 0.8 V and 4,300 mA/cm^2, Reference (8)). The electrodes contain high loadings of noble metals: 80% Pt - 20% Pd anodes are loaded at 10 mg/cm^2 on Ag-plated Ni screen; 90% Au - 10% Pt cathodes are loaded at 20 mg/cm^2 on Ag-plated Ni screen. Both are bonded with PTFE to achieve high performance at the lower temperature of 85-95°C. A wide variety of materials (e.g., potassium titanate, ceria, asbestos, zirconium phosphate gel) have been used in the micro-porous separators for AFCs. The electrolyte is 35% KOH and is replenished via a reservoir on the anode side. Gold-plated magnesium is used for the bipolar plates. Sheibley and Martin (10) provide a brief survey of the advanced technology components in AFCs for space applications.

An advanced cell configuration for underwater application was developed using high surface area Raney nickel anodes loaded at 120 mg/cm^2 (1-2% Ti) and Raney silver cathodes loaded at 60 mg/cm^2 containing small amounts of Ni, Bi, and Ti (11).

The efforts of Union Carbide Corporation has formed the basis for most of today's terrestrial applications of AFCs with circulating liquid electrolytes. Companies like Da Capo Fuel Cell Ltd. (which bought ZeTek Power (formerly Zevco and Elenco)), Astris Energy, and Apollo Energy System Inc. are developing circulating electrolyte cells for motive and backup power primarily based on that technology. A typical configuration (Apollo, Figure 4-2) uses carbon-based plastic-bonded gas diffusion electrodes with a current collector (nickel) inside. Due to the ease of preparation, the electrodes in present stacks use noble metals loaded to less than 0.5mg/cm^2. The 0.3 cm thick cells are stacked in a monopolar order and are commonly

connected in series via edge connectors. Neither membranes nor bipolar plates are needed. The stacks operate at 75°C, using a 9N KOH electrolyte. The gases are fed at ambient pressure; either pure hydrogen or cracked ammonia is used. Lifetime testing (12) has not been finished, but is >1,000 hours at intermittent operation (a few hours per day).

Several types of catalysts are used or are being considered for the electrodes: 1) noble metals (expensive but simple, and acceptable for low volume stack preparation); 2) "classic" non-noble metals (Silver for the cathode and Raney Nickel for the anode), and 3) spinels and perovskites (often referred to as alternative catalysts, these are being developed because they cost less than the noble metal catalysts).

4.1.2 Development Components

Immobilized electrolyte AFCs, used mostly in space or closed environments, and circulating electrolyte AFCs, used for terrestrial application, face separate and unique development challenges.

H_2/O_2 alkaline technology using immobilized electrolytes is considered to be fully developed. Confidence in the present cell technology is best represented by the fact that there is no back-up electric power on the Space Shuttle Orbiter. Further improvement of the present H_2/O_2 design is not considered to be cost effective with one exception: maintenance cost can be decreased directly by increasing the cell stack life of the Orbiter power plant.

The life-limiting event in the present Orbiter cell is KOH corrosion of the cell frame (cell support). Present stack life is 2,600 hours. The cell stacks have demonstrated capability to reach this life in 110 flights and a total of ~87,000 hours in the Orbiter (July 2002). Present practice is to refurbish the power unit at 2,600 hours by installing a new stack, and cleaning and inspecting the balance of equipment. The stack life is being improved to 5,000 hours by elongating the path length associated with KOH-induced corrosion of the cell frame. A 10 cell short stack has demonstrated the new 5,000 hours concept. The concept is now being qualified in a complete power plant, presently being tested (13).

Electrode development in circulating electrolyte AFCs has concentrated on 1) multi-layered structures with porosity characteristics optimized for flow of liquid electrolytes and gases (H_2 and air), and 2) catalyst development. Another area for concern is the instability of PTFE, which causes weeping of the electrodes. Most developers use noble metal catalysts; some use non-noble catalysts. Spinels and perovskites are being developed in an attempt to lower the cost of the electrodes. Development of low-cost manufacturing processes includes powder mixing and pressing of carbon-based electrodes, sedimentation and spraying, and high-temperature sintering.

AFC electrolyte development has been restricted to KOH water solutions with concentrations ranging from 6-12N. Still, use of less expensive NaOH has been considered. Minimal cost advantages appear to be far outweighed by performance reductions due to wetting angle and lower conductivity. However, NaOH as an electrolyte increases the lifetime of electrodes when CO_2 is present, because sodium carbonate, although less soluble than potassium carbonate, forms much smaller crystals, which do not harm the carbon pores.

Other approaches to increasing life and reducing weight and cost include investigating epoxy resins, polysulfone and ABS (acrylonitrile-butadiene-styrene). Framing techniques under development include injection molding, filter pressing, and welding (14, 15).

Immobilized electrolyte AFCs are highly sensitive to carbon dioxide (CO_2). Non-hydrocarbon hydrogen fuel or pure H_2 can be fed directly to the anode. For example, a carbon-free fuel gas such as cracked ammonia (25% N_2, 75% H_2, and residual NH_3) can be fed directly to the cell. Due to the high diffusion rate of hydrogen compared to nitrogen, only a very small decrease in potential is observed with hydrogen content greater than 25% (at medium current densities). Gas purification is necessary when H_2 is produced from carbon-containing fuel sources (e.g., methanol, gasoline, propane and others). There are many approaches to separate CO_2 from gaseous or liquid streams. Physical separation and chemical separation are the most common methods used. However, CO_2 removal by these methods requires more than one process step to reduce the CO_2 to the limits required by the fuel cell. Two additional methods include cryogenic separation and biological fixation. If liquid hydrogen is used as the fuel for the alkaline fuel cell, a system of heat exchangers can be used to condense the CO_2 out of the air for the oxidant stream. This technique has a potential weight advantage over the soda-lime scrubber. Low-temperature distillation is commonly used for the liquefaction of CO_2 from high purity sources. A new, potentially efficient technique that is being investigated uses capillary condensation to separate gases by selective wicking. Biological separation is promising, but must overcome the challenge of reactivation after shutdown periods.

Another promising CO_2 separation method is membrane separation. This has the advantages of being compact, no moving parts, and the potential for high energy efficiency. Polymer membranes transport gases by solution diffusion, and typically have a low gas flux and are subject to degradation. These membranes are relatively expensive. The main drawbacks of membrane separation are the significant pressure differential that may be required across the membrane and its high cost. The need for a high pressure gradient can be eliminated by using a membrane in which a potential is applied over the membrane. This approach is sometimes referred to as the "sacrificial cell" technique. Another approach is to use a membrane with steam reforming of liquid fuels. Little additional energy is needed to pressurize the liquid fuel and water to the pressure required for separation.

Alkaline cell developers continue to investigate CO_2 separation methods that show economic promise. However, circulating electrolyte is the technology of choice for terrestrial applications.

4.2 Performance

Performance of AFCs since 1960 has undergone many changes, as evident in the performance data in Figure 4-3. H_2/air performance is shown as solid lines, and H_2/O_2 performance is shown as dashed lines. The early AFCs operated at relatively high temperature and pressure to meet the requirements for space applications. More recently, a major focus of the technology is for terrestrial applications in which low-cost components operating at near-ambient temperature and pressure with air as the oxidant are desirable. This shift in fuel cell operating conditions resulted in the lower performance shown in Figure 4-3**.** The figure shows, using dotted lines, H_2/O_2 performance for: 1) the Orbiter with immobilized electrolyte (8), and 2) a circulating electrolyte cell (12).

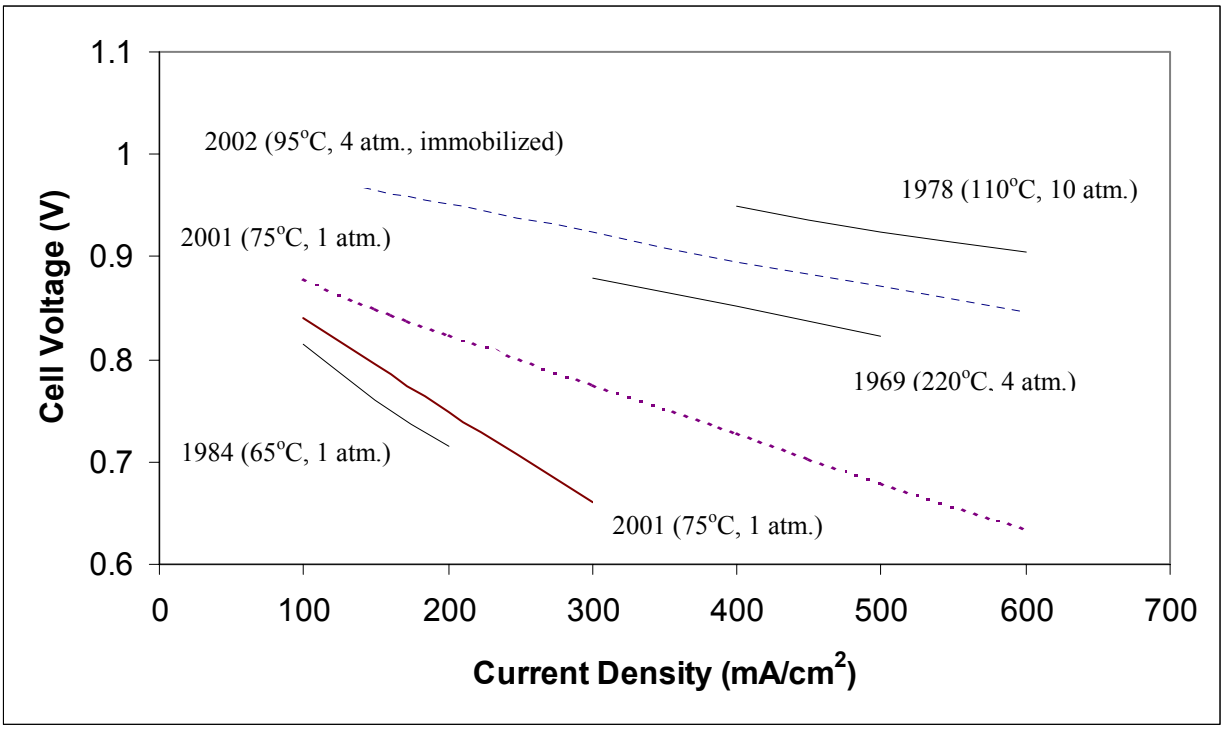

Figure 4-3 Evolutionary Changes in the Performance of AFCs (8, 12, & 16)

The data described in the following paragraphs pertains to the H_2/air cell. Unfortunately, H_2/air performance data is rather dated; there has been a noticeable lack of recent H_2/air data.

4.2.1 Effect of Pressure

AFCs experience the typical enhanced performance with an increase in cell operating pressure. Figure 4-4 plots the increase in reversible e.m.f. (electromotive force) of alkaline cells with pressure over a wide range of temperatures (17). The actual increase in cell open circuit voltage is somewhat less than shown because of the greater gas solubility with increasing pressure that produces higher parasitic current.

At an operating temperature (T), the change in voltage (ΔV_P) as a function of pressure (P) can be expressed fairly accurately using the expression:

$$\Delta V_P \text{ (mV)} = 0.15T \text{ (°K)} \log(P_2/P_1) \qquad (4\text{-}4)$$

over the entire range of pressures and temperatures shown in Fig. 4-4. In this expression, P_2 is the desired performance pressure and P_1 is the reference pressure at which performance is known.

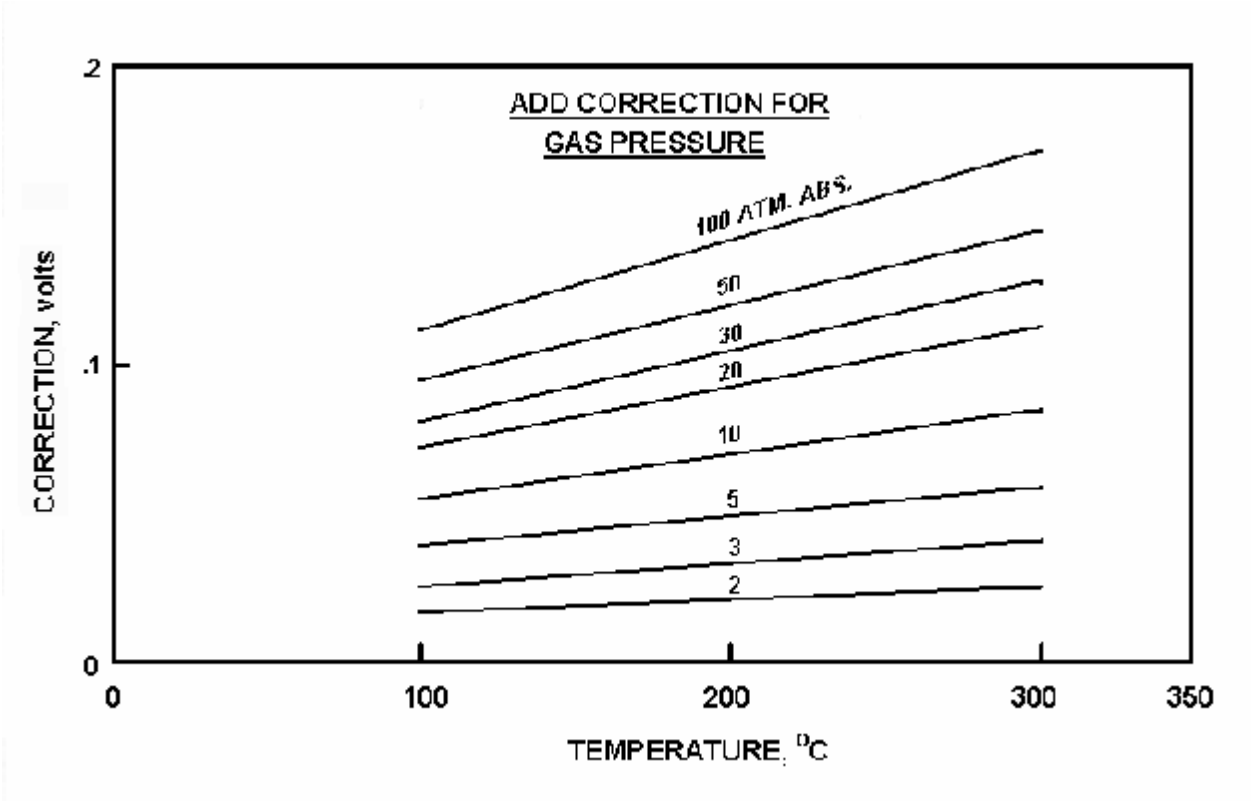

Figure 4-4 Reversible Voltage of the Hydrogen-Oxygen Cell (14)

To achieve faster kinetics, operating temperatures greater than 100°C, accompanied by higher pressures, are used. Spacecraft fuel cells have operated for over 5,000 hours at 200°C at 5 atm achieving HHV efficiencies exceeding 60% (18, 19). It should be noted that a pressure increase beyond about 5 atm produces improvements that are usually outweighed by a significant weight increase required to sustain the higher operating pressure. For space applications, weight is critical. Also, this increase in performance can only be realized in applications where compressed gases are available (such as in space vehicles or submarines). In all other cases, compressors are needed. Compressors are not only noisy, but incur parasitic power that lowers the system efficiency (20). An increase of overall efficiency when using compressors in simple cycles is very unlikely.

4.2.2 Effect of Temperature

Section 2.1 describes that the reversible cell potential for a fuel cell consuming H_2 and O_2 decreases by 49 mV under standard conditions in which the reaction product is water vapor. However, as is the case in PAFCs, an increase in temperature improves cell performance because activation polarization, mass transfer polarization, and ohmic losses are reduced.

The improvement in performance with cell temperature of catalyzed carbon-based (0.5 mg Pt/cm^2) porous cathodes is illustrated in Figure 4-5 (21). As expected, the electrode potential at a given current density decreases at lower temperatures, and the decrease is more significant at higher current densities. In the temperature range of 60-90°C, the cathode performance increases by about 0.5 mV/°C at 50-150 mA/cm^2.

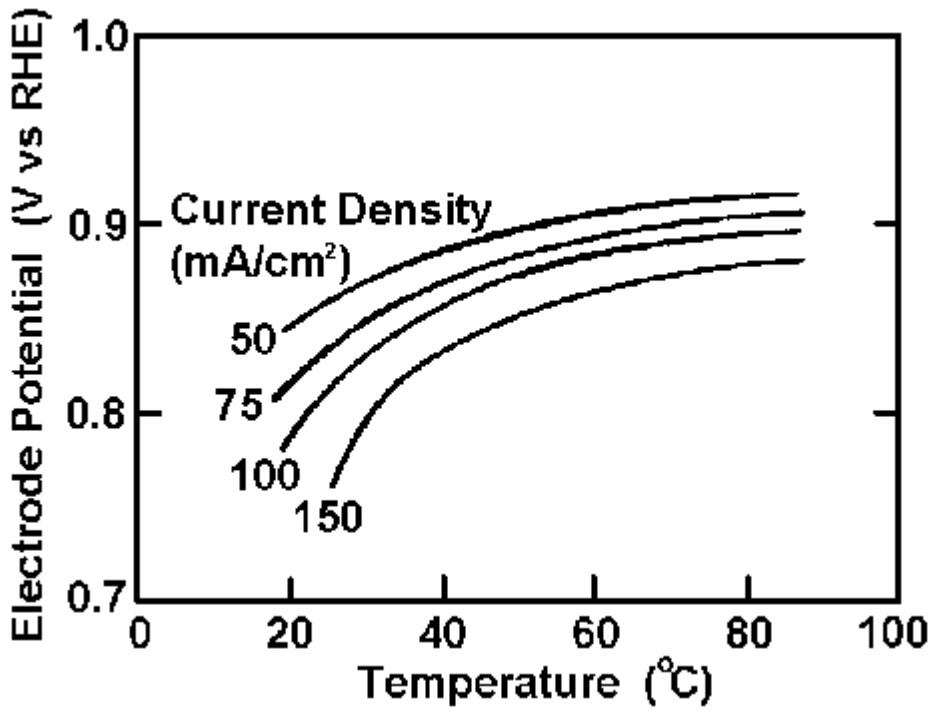

Figure 4-5 Influence of Temperature on O_2, (air) Reduction in 12 N KOH.
Source: Fig. 10, p. 324, Reference (21).

Early data by Clark, et al. (22) indicated a temperature coefficient for AFCs operating between 50-70°C of about 3 mV/°C at 50 mA/cm^2, and cells with higher polarization had higher temperature coefficients under load. Later measurements by McBreen, et al. (23) on H_2/air single cells (289 cm^2 active area, carbon-based Pd anode and Pt cathode) with 50% KOH showed that the temperature coefficient above 60°C was considerably lower than that obtained at lower temperatures, as shown in Figure 4-6. The McBreen data suggest the following expressions for evaluating the change in voltage (ΔV_T) as a function of temperature (T) at 100 mA/cm^2:

$$\Delta V_t \text{ (mV)} = 4.0\ (T_2 - T_1) \qquad \text{for } T < 63°C \tag{4-5}$$

or

$$\Delta V_t \text{ (mV)} = 0.7\ (T_2 - T_1) \qquad \text{for } T > 63°C \tag{4-6}$$

Alkaline cells exhibit reasonable performance when operating at low temperatures (room temperature up to about 70°C). This is because the conductivity of KOH solutions is relatively high at low temperatures. For instance, an alkaline fuel cell designed to operate at 70°C will reduce to only half power level when its operating temperature is reduced to room temperature (24).

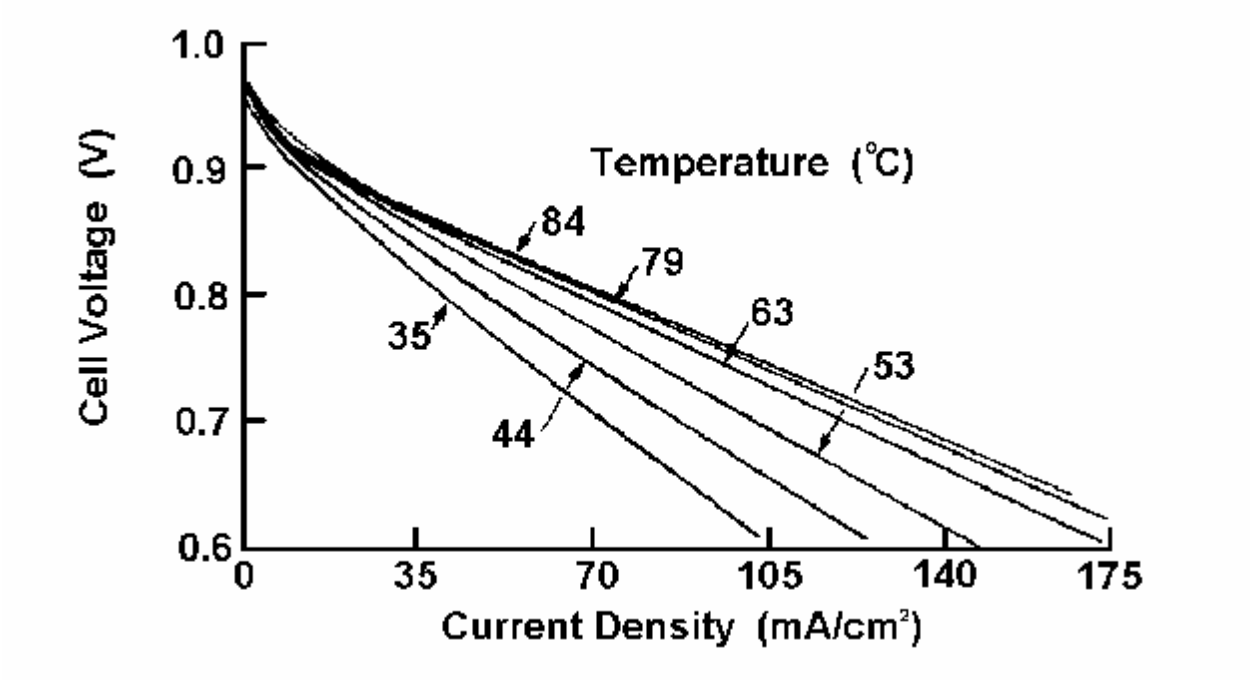

Figure 4-6 Influence of Temperature on the AFC Cell Voltage
Source: Figure 6, p. 889, reference (23).

4.2.3 Effect of Impurities

Carbon dioxide was the only impurity of concern in the data surveyed. AFCs with immobilized electrolytes suffer a considerable performance loss with reformed fuels containing CO_2 and from the presence of CO_2 in air (typically ~350 ppm CO_2 in ambient air). The negative impact of CO_2 arises from its reaction with OH^-

$$CO_2 + 2OH^- \rightarrow CO_3^= + H_2O \qquad (4\text{-}7)$$

producing the following effects: 1) reduced OH^- concentration, interfering with kinetics; 2) electrolyte viscosity increase, resulting in lower diffusion rate and lower limiting currents; 3) precipitation of carbonate salts in the porous electrode, reducing mass transport; 4) reduced oxygen solubility, and 5) reduced electrolyte conductivity.

In the case of circulating liquid electrolytes, the situation is not as critical, but is still significant. The influence of CO_2 on air cathodes (0.2 mg Pt/cm^2 supported on carbon black) in 6N KOH at 50°C can be ascertained by analysis of the performance data presented in Figure 4-7 (25). To obtain these data, the electrodes were operated continuously at 32 mA/cm^2, and current-voltage performance curves were periodically measured. Performance in both CO_2-free air and CO_2-containing air showed evidence of degradation with time. However, with CO_2-free air the performance remained much more constant after 2,000-3,000 hours of operation. Later tests, however, showed that this drop in performance was caused purely by mechanical destruction of

the carbon pores by carbonate crystals. Improved electrodes can withstand even high amounts of CO_2 (5%) over many thousands of hours, as proven recently by DLR (Deutsches Zentrum fηr Luft- und Raumfahrt) (26).

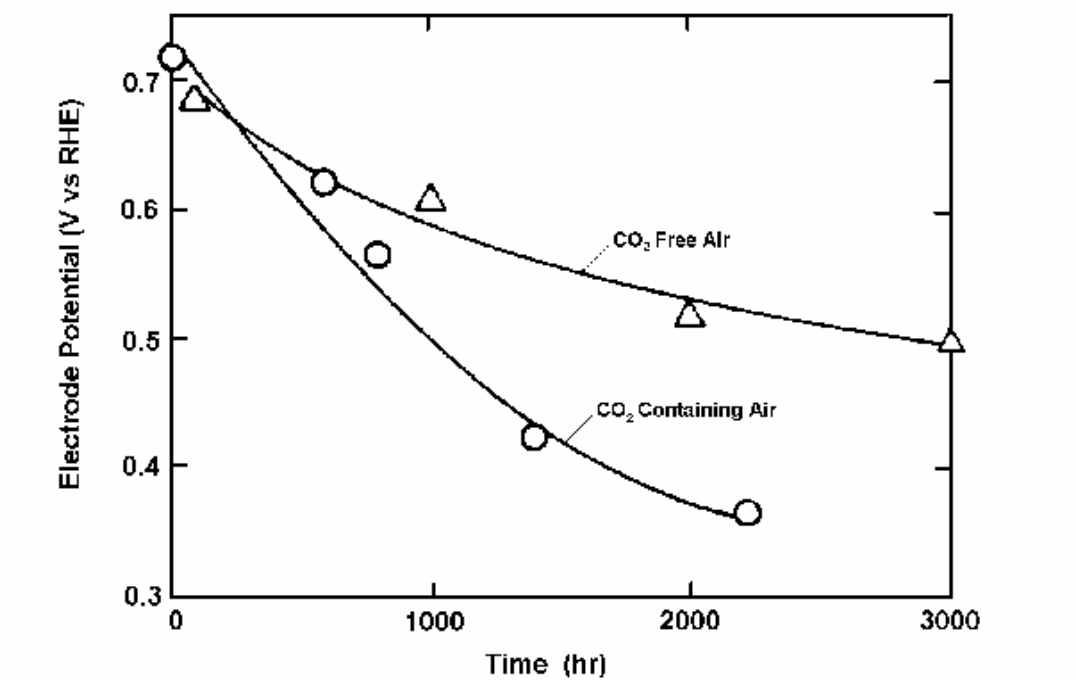

Figure 4-7 Degradation in AFC Electrode Potential with CO_2 Containing and CO_2 Free Air Source: Figure 2, p. 381, Reference (25)

High concentrations of KOH are also detrimental to the life of O_2 electrodes operating with CO_2-containing air, but operating the electrode at higher temperature is beneficial because it increases the solubility of CO_2 in the electrolyte. Hence, modifying the operating conditions can prolong electrode life. Extensive studies by Kordesch, et al. (25) indicate that the operational life of air electrodes (PTFE-bonded carbon electrodes on porous nickel substrates) with CO_2-containing air in 9N KOH at 65°C ranges from 1,600-3,400 hours at a current density of 65 mA/cm^2. The life of these electrodes with CO_2-free air tested under similar conditions ranged from 4,000-5,500 hours. It was reported (2) that a lifetime of 15,000 hours was achieved with AFCs, with failure caused at that time by corrosion of the cell frames.

4.2.4 Effects of Current Density

As in the case with PAFCs, voltage obtained from an AFC is affected by ohmic, activation, and concentration losses. Figure 4-8 presents data obtained in the 1960s (22) that summarizes these effects, excluding electrolyte ohmic (iR) losses, for a catalyzed reaction (0.5-2.0 mg noble metal/cm^2) with carbon-based porous electrodes for H_2 oxidation and O_2 reduction in 9N KOH at 55-60°C. The electrode technology was similar to that employed in the fabrication of PAFC electrodes.

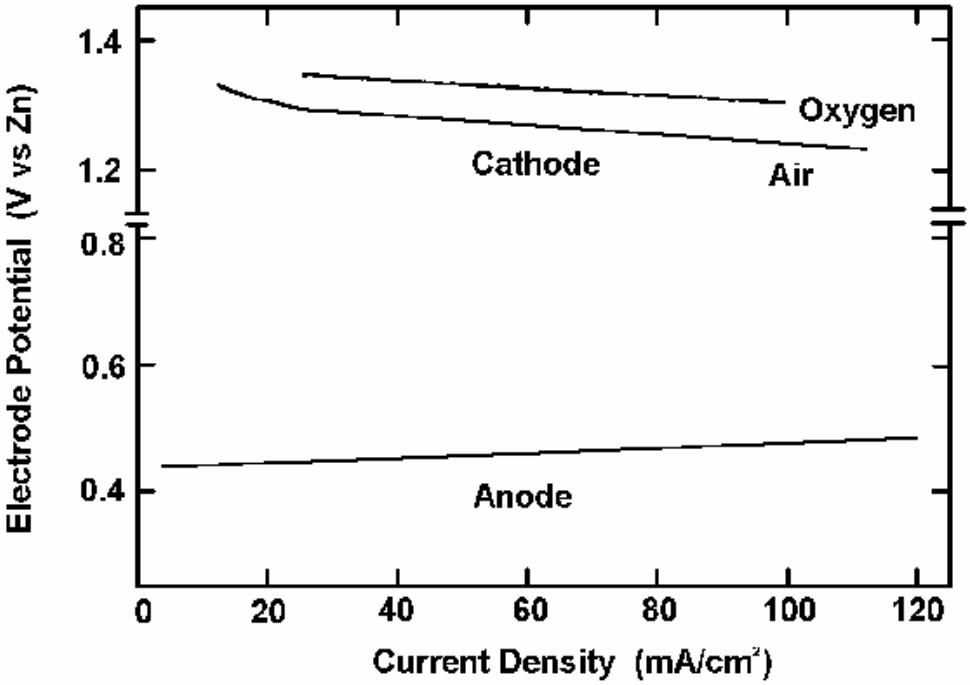

Figure 4-8 iR-Free Electrode Performance with O_2 and Air in 9 N KOH at 55-60°C. Catalyzed (0.5 mg Pt/cm^2 Cathode, 0.5 mg Pt-Rh/cm^2 Anode) Carbon-based Porous Electrodes (22)

The results in Figure 4-8 yield the following current density equations for cells operating in 9N KOH at 55-60°C:

$$\Delta V_J \text{ (mV)} = -0.18\Delta J \qquad \text{for } J = 40 - 100 \text{ mA/cm}^2 \text{ operating in } O_2 \qquad (4\text{-}8)$$

or

$$\Delta V_J \text{ (mV)} = -0.31\Delta J \qquad \text{for } J = 40 - 100 \text{ mA/cm}^2 \text{ operating in air} \qquad (4\text{-}9)$$

where J is in mA/cm^2. The performance of a single cell with supported noble metal electrocatalyst (0.5 mg Pt-Rh/cm^2 anode, 0.5 mg Pt/cm^2 cathode) in 12N KOH at 65°C is shown in Figure 4-9 (21). These results, reported in 1986, are comparable to those obtained in 1965. The iR-free electrode potentials (vs. RHE) at 100 mA/cm^2 in Figure 4-9 are 0.9 V with O_2 and 0.85 V with air. One major difference between the early cathodes and the cathodes in current use is that the limiting current for O_2 reduction from air has been improved (i.e., 100-200 mA/cm^2 improved to >250 mA/cm^2).

These results yield the following equations for cells operating in 12N KOH at 65°C:

$$\Delta V_J \text{ (mV)} = -0.25\Delta J \qquad \text{for } J = 50 - 200 \text{ mA/cm}^2 \text{ operating in } O_2 \qquad (4\text{-}10)$$

or

$$\Delta V_J \text{ (mV)} = -0.47\Delta J \qquad \text{for } J = 50 - 200 \text{ mA/cm}^2 \text{ operating in air.} \qquad (4\text{-}11)$$

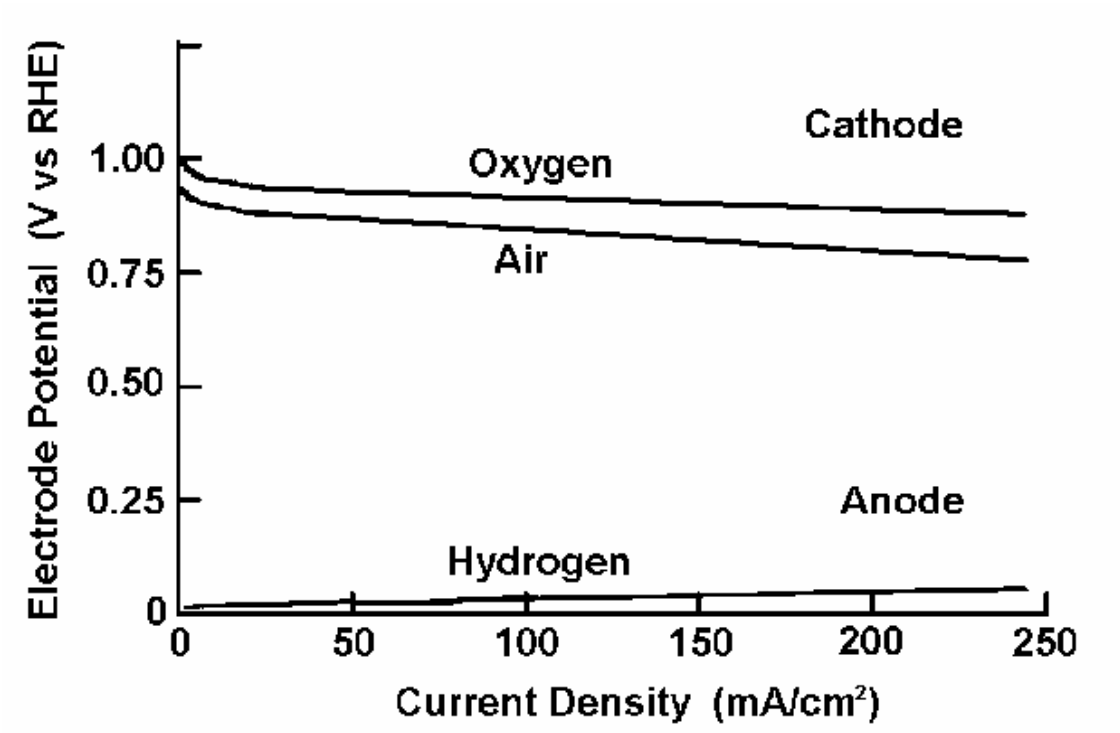

Figure 4-9 iR Free Electrode Performance with O_2 and Air in 12N KOH at 65°C. Catalyzed (0.5 mg Pt/cm^2 Cathode, 0.5 mg Pt-Rh/cm^2 Anode), Carbon-based Porous Electrodes (21).

4.2.5 Effects of Cell Life

The UTC Fuel Cells H_2/O_2 alkaline technology exhibits a degradation of ~25 mV/1,000 hours (13). AFC cell stacks have demonstrated sufficiently stable operation for at least 5,000 hours, with degradation rates of 20 mV per 1,000 hours or less (24). Siemens has reported a total of >8,000 operating hours with approximately 20 units (27). For large scale utility applications, economics demand operating times exceeding 40,000 hours, which presents perhaps the most significant obstacle to commercialization of AFC devices for stationary electric power generation.

4.3 Summary of Equations for AFC

The preceding sections described parametric performance based on various referenced data at different cell conditions. The following set of equations can be used to predict performance only if no better data or basis for estimate is available. Unfortunately, a noticeable lack of recent, published H_2/air data is available to predict performance trends. The equations presented below can be used in conjunction with the measured H_2/air performance shown in Figure 4-10 (12) as a basis for predicting performance at various operating conditions. The Space Shuttle Orbiter performance is included in Figure 4-10 as a reference point for H_2/O_2 performance (8); however,

the trend equations should not be used for H_2/O_2 cells to predict operation at other conditions.

Parameter	Equation	Comments	
Pressure	ΔV_P (mV) = 0.15 T (°K) log (P_2/P_1)	1 atm < P < 100 atm 100 °C < T < 300 °C	(4-4)
Temperature	ΔV_T (mV) = 4.0 (T_2-T_1)	for T < 63°C, at 100 mA/cm^2	(4-5)
Temperature	ΔV_T (mV) = 0.7 (T_2-T_1)	for T > 63°C, at 100 mA/cm^2	(4-6)
Current Density	ΔV_J (mV) = -0.18ΔJ	for J = 40-100 mA/cm^2 operating in O_2 with 9N KOH at 55-60°C.	(4-8)
	ΔV_J (mV) = -0.31ΔJ	for J = 40-100 mA/cm^2 operating in air with 9N KOH at 55-60°C.	(4-9)
	ΔV_J (mV) = -0.25ΔJ	for J = 50-200 mA/cm^2 operating in O_2 with 12N KOH at 65°C.	(4-10)
	ΔV_J (mV) = -0.047ΔJ	for J = 50-200 mA/cm^2 operating in air with 12N KOH at 65°C.	(4-11)
Life Effects	$\Delta V_{Lifetime}$ (mV) = 20 µV per 1,000 hours or less		(4-12)

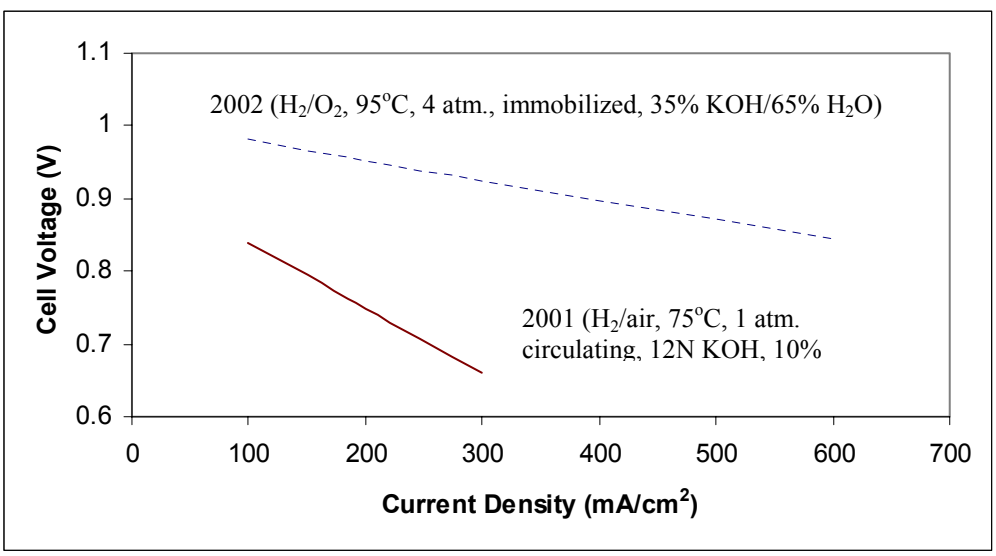

Figure 4-10 Reference for Alkaline Cell Performance

4.4 References

1. F.T. Bacon, *Electrochim. Acta,* 14, 569, 1969.
2. J.O'M Bockris and A.J. Appleby, *Energy*, 11, 95, 1986.
3. A.J. Appleby, *Energy*, 11, 13, 1986.
4. K.F. Blurton and E. McMullin, *Energy Conversion,* 9, 141, 1969.
5. K.V. Kordesch, *Brennstoffbatterien*, Springer-Verlag, New York, 1984.
6. V. Hacker, P. Enzinger, M. Muhr, K. Kordesh, J. Gsellman, M. Cifrain, P. Prenninger, K. Meitz, R. Aronsson, "Advantages of Alkaline Fuel Cell Systems for Mobile Applications," *2000 Fuel Cell Seminar Program and Abstracts*, Portland, OR; sponsored by the Fuel Cell Seminar Organizing Committee, October 30 – November 2, 2000.
7. G.F. McLean, T. Niet, S. Prince-Richard, N.Djilali, "An assessment of alkaline fuel cell technology," University of Victoria, in *International Journal of Hydrogen Energy,* p. 507 – 526, 27 (2002).
8. Communication with UTC Fuel Cells, July, 2002.
9. K. V. Kordesch, G. Simader, "Fuel Cells and Their Applications," Wiley, Weinheim – New York – Tokyo 1996.
10. D.W. Sheibley and R.A. Martin, *Prog. Batteries Solar Cells*, 6, 155, 1987.
11. K. Strasser, *J. Power Sources* 29, 152-153, 1990.
12. M. Cifrain, K. Kordesch, J. Gsellmann, T. Hejze, R. R. Aronson, "Alkaline Fuel Cells with Circulating Electrolytes," Poster presented at *Fuel Cell Seminar 2000,* Portland, Oregon, October 30-November 2, 2000.
13. Meeting with UTC Fuel Cells, June 2002.
14. K. Strasser, *J. Electrochem. Soc.* 127, 2173-2177, 1980.
15. H. van den Broeck, G. van Bogaert, G. Vennekens, L. Vermeeren, F. Vlasselaer, J. Lichtenberg, W. Schlösser, A. Blanchart, *Proc. 22nd IECEC Meeting*, 1005, Philadelphia, 1987.
16. J. Huff, paper presented at the 1986 "Status of Fuel Cell Technologies," *Fuel Cell Seminar Abstracts, Fuel Cell Seminar*, Tucson, AZ, October 26-29, 1986.
17. A.M. Adams, F.T. Bacon and R.G.H. Watson, *Fuel Cells* (W. Mitchell, ed.), Academic Press, New York, 138,1963.
18. S.S. Penner, ed., *Assessment of Research Needs for Advanced Fuel Cells*, DOE/ER/300.60-T1, US DOE, 1985.
19. Fuel Cell Seminar Abstracts, Long Beach, CA; sponsored by the National Fuel Cell Coordinating Group, October 23-26, 1988.
20. J. Larminie, A. Dicks, *"Fuel Cell Systems Explained,"* Wiley, Chichester (GB) 2000.
21. K. Tomantschger, F. McClusky, L. Oporto, A. Reid and K. Kordesch, *J. Power Sources*, 18, 317, 1986.
22. M.B. Clark, W.G. Darland and K.V. Kordesch, *Electrochem. Tech.,* 3, 166, 1965.
23. J. McBreen, G. Kissel, K.V. Kordesch, F. Kulesa, E.J. Taylor, E. Gannon and S. Srinivasan, in *Proceedings of the 15th Intersociety Energy Conversion Engineering Conference*, Volume 2, American Institute of Aeronautics and Astronautics, New York, NY, 886, 1980.
24. J.M.J. Blomen and M.N. Mugerwa ed., *Fuel Cell Systems*, Plenum Press, New York and London, 251, 1993.

25. K. Kordesch, J. Gsellmann and B. Kraetschmer, in *Power Sources*, 9, Edited by J. Thompson, Academic Press, New York, NY, 379, 1983.
26. E. Guelzow, M. Schulze, "Long Time Operation of AFC Electrodes with CO_2 Containing Gases," *8th Ulm ElectroChemical Talks*, Neu-Ulm, Germany, Abstracts p. 68, June 20-21, 2002.
27. K. Strasser, L. Blume and W. Stuhler, *Fuel Cell Seminar Program and Abstracts*, Long Beach, CA; sponsored by the National Fuel Cell Coordinating Group, October 23-26, 1988.

5. PHOSPHORIC ACID FUEL CELL

The phosphoric acid fuel cell (PAFC) was the first fuel cell technology to be commercialized. The number of units built exceeds any other fuel cell technology, with over 85 MW of demonstrators that have been tested, are being tested, or are being fabricated worldwide. Most of the plants are in the 50-200 kW capacity range, but large plants of 1 MW and 5 MW have been built. The largest plant operated to date achieved 11 MW of grid quality ac power (1, 2). Major efforts in the U.S. are concentrated on the improvement of PAFCs for stationary, dispersed power plants and on-site cogeneration power plants. The major industrial participants are UTC Fuel Cells in the U.S. and Fuji Electric Corporation, Toshiba Corporation, and Mitsubishi Electric Corporation in Japan.

Figure 5-1 depicts the operating configuration of the phosphoric acid cell. The electrochemical reactions occurring in PAFCs are

$$H_2 \rightarrow 2\,H^+ + 2\,e^- \qquad (5\text{-}1)$$

at the anode, and

$$\tfrac{1}{2}O_2 + 2H^+ + 2e^- \rightarrow H_2O \qquad (5\text{-}2)$$

at the cathode. The overall cell reaction is

$$\tfrac{1}{2}O_2 + H_2 \rightarrow H_2O \qquad (5\text{-}3)$$

The electrochemical reactions occur on highly dispersed electrocatalyst particles supported on carbon black. Platinum (Pt) or Pt alloys are used as the catalyst at both electrodes.

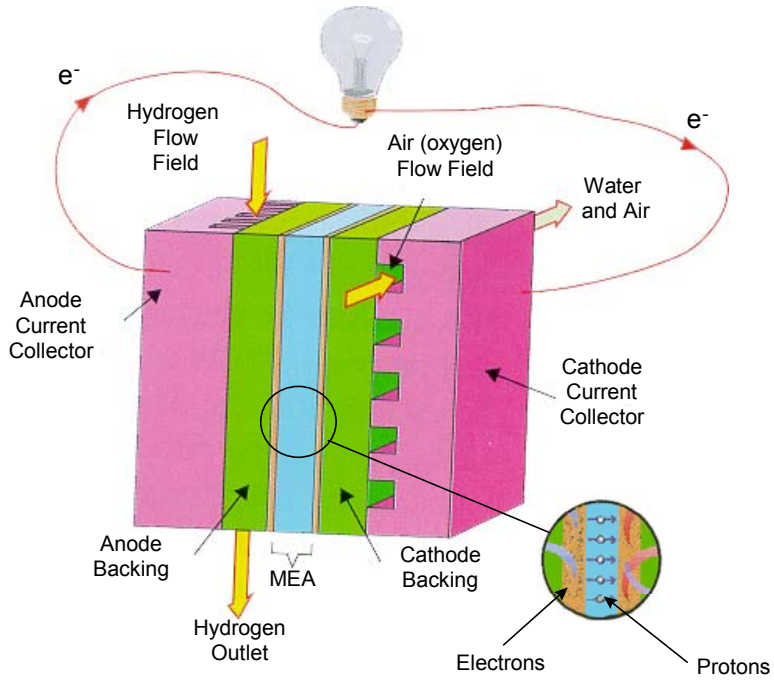

Figure 5-1 Principles of Operation of Phosphoric Acid Fuel Cell (Courtesy of UTC Fuel Cells)

5.1 Cell Components

5.1.1 State-of-the-Art Components

There have been only minor changes in cell design in recent years. The major U.S. manufacturer, UTC Fuel Cells, has concentrated on improving cell stability and life, and in improving the reliability of system components at reduced cost.

The evolution of cell components from 1965 to the present day for PAFCs is summarized in Table 5-1. In the mid-1960s, the conventional porous electrodes were polytetrafluoroethylene (PTFE) - bonded Pt black, and the loadings were about 9 mg Pt/cm^2. During the past two decades, Pt supported on carbon black has replaced Pt black in porous PTFE-bonded electrode structures as the electrocatalyst. A dramatic reduction in Pt loading has also occurred; the loadings[16] are currently about 0.10 mg Pt/cm^2 in the anode and about 0.50 mg Pt/cm^2 in the cathode.

The operating temperatures and acid concentrations of PAFCs have increased to achieve higher cell performance; temperatures of about 200°C (392°F) and acid concentrations of 100% H_3PO_4 are commonly used today. Although the present practice is to operate at atmospheric pressure, the operating pressure of PAFCs surpassed 8 atm in the 11 MW electric utility demonstration

[16]. Assuming a cell voltage of 750 mV at 205 mA/cm^2 (approximate 11 MW design, 8 atmospheres) and the current Pt loadings at the anode and cathode, ~54 g Pt is required per kilowatt of power generated.

plant, confirming an increase in power plant efficiency. However, a number of issues remain whether to design and operate PAFC units at atmospheric vs. pressurized conditions.

Primarily, small, multi-kW PAFC power units that were the focus of initial commercial applications led to atmospheric pressure operation. Although pressurization increased efficiency (lower fuel cost), it complicated the power unit - resulting in higher capital cost. The economic trade-off favored simpler, atmospheric operation for early commercial units.

Another important issue, independent of power unit size, is that pressure promotes corrosion. Phosphoric acid electrolyte (H_3PO_4) produces a vapor. This vapor, which forms over the electrolyte, is corrosive to cell locations other than the active cell area. These cell locations are at a mixed voltage (open circuit and cell voltage), that can be over ~0.8V/C. That is the limit above which corrosion occurs (active area limited to operation under ~0.8 V/C). An increase in cell total pressure causes the partial pressure of the H_3PO_4 vapor to increase, causing increased corrosion in the cell. Cell temperature must also be increased with pressurized conditions to produce steam for the steam reformer (3).

A major breakthrough in PAFC technology that occurred in the late 1960s was the development of carbon black and graphite for cell construction materials; this and other developments are reviewed by Appleby (4) and Kordesch (5). Carbon black and graphite were sufficiently stable to replace the more expensive gold-plated tantalum cell hardware used at the time. The use of high-surface-area graphite to support Pt permitted a dramatic reduction in Pt loading without sacrificing electrode performance. It was reported (4) that "without graphite, a reasonably inexpensive acid fuel cell would be impossible, since no other material combines the necessary properties of electronic conductivity, good corrosion resistance, low density, surface properties (especially in high area form) and, above all, low cost." However, carbon corrosion and Pt dissolution become an issue at cell voltages above ~0.8 V. Consequently, low current densities at cell voltage above 0.8 V and hot idle at open circuit potential should be avoided.

The porous electrodes used in PAFCs have been described extensively in patent literature (6); see also the review by Kordesch (5). These electrodes contain a mixture of electrocatalyst supported on carbon black and a polymeric binder, usually PTFE (30 - 50 wt%). The PTFE binds the carbon black particles together to form an integral, but porous, structure that is supported on a porous graphite substrate. The graphite structure serves as a support for the electrocatalyst layer, as well as the current collector. A typical graphite structure used in PAFCs has an initial porosity of about 90%, which is reduced to about 60% by impregnation with 40 wt% PTFE. This wet-proof graphite structure contains macropores of 3 - 50 μm diameter (median pore diameter of about 12.5 μm) and micropores with a median pore diameter of about 34 Å for gas permeability. The composite structure, consisting of a carbon black/PTFE layer on the graphite substrate, forms a stable, three-phase interface in the fuel cell, with H_3PO_4 electrolyte on one side (electrocatalyst side) and the reactant gas environment on the other.

Table 5-1 Evolution of Cell Component Technology for Phosphoric Acid Fuel Cells

Component	ca. 1965	ca. 1975	Current Status[a]
Anode	PTFE-bonded Pt black	PTFE-bonded Pt/C	PTFE-bonded Pt/C
		Vulcan XC-72[a]	
	9 mg/cm^2	0.25 mg Pt/cm^2	0.25 mg Pt/cm^2
Cathode	PTFE-bonded Pt black	PTFE-bonded Pt/C	PTFE-bonded Pt/C
		Vulcan XC-72[a]	
	9 mg/cm^2	0.5 mg Pt/cm^2	0.5 mg Pt/cm^2
Electrode Support	Ta mesh screen	Graphite Structure	Graphite Structure
Electrolyte Support	Glass fiber paper	PTFE-bonded SiC	PTFE-bonded SiC
Electrolyte	85% H_3PO_4	95% H_3PO_4	100% H_3PO_4
Electrolyte Reservoir		Porous graphite plate.	Porous graphite plate.
Cooler			1 per ~7 cells; imbedded (*SS)* tubes in graphite plate

a. - Over 40,000 hour component life demonstrated in commercial power plants.

A bipolar plate separates the individual cells and electrically connects them in series in a fuel cell stack. In some designs, the bipolar plate also contains gas channels that feed the reactant gases to the porous electrodes and remove the reaction products and inerts. Bipolar plates made from graphite resin mixtures that are carbonized at low temperature (~900°C/1,652°F) are not suitable because of their rapid degradation in PAFC operating environments (7, 8). However, corrosion stability is improved by heat treatment to 2,700°C (4,892°F) (8), i.e., the corrosion current is reduced by two orders of magnitude at 0.8 V in 97% H_3PO_4 at 190°C (374°F) and 4.8 atm (70.5 psi). The all-graphite bipolar plates are sufficiently corrosion-resistant for a projected life of 40,000 hours in PAFCs, but they are still relatively costly to produce.

Several designs for the bipolar plate and ancillary stack components are used by fuel cell developers, and these are described in detail (9, 10, 11, 12). A typical PAFC stack contains cells connected in series to obtain the practical voltage level desired for the load. In such an arrangement, individual cells are stacked with bipolar plates between the cells. The bipolar plates used in early PAFCs consisted of a single piece of graphite with gas channels machined on either side to direct the flow of fuel and oxidant. Currently, both bipolar plates of the previous design and new designs consisting of several components are being considered. In the multi-component bipolar plates, a thin impervious plate separates the reactant gases in adjacent cells in the stack, and

separate porous plates with ribbed channels are used to direct gas flow. In a cell stack, the impervious plate is subdivided into two parts, and each joins one of the porous plates. The electrolyte vaporizes so that a portion of H_3PO_4 escapes from the cell in the air stream over time. An electrolyte reservoir plate (ERP), made of porous graphite, provides enough electrolyte to achieve a 40,000-hour cell life goal (there is no electrolyte replacement). The ERP also accommodates increases in electrolyte volume due to an increase in H_2O, so the porous graphite electrodes don't flood. These fluctuations in electrolyte volume occur during start-up and during transient operation. The porous structure, which allows rapid gas transport, is also used to store additional acid to replenish the supply lost by evaporation during the cell operating life.

In PAFC stacks, provisions must be included to remove heat generated during cell operation. In practice, heat has been removed by either liquid (two-phase water or a dielectric fluid) or gas (air) coolants that are routed through cooling channels located (usually about every fifth cell) in the cell stack. Liquid cooling requires complex manifolds and connections, but better heat removal is achieved than with air-cooling. The advantage of gas cooling is its simplicity, reliability, and relatively low cost. However, the size of the cell is limited, and the air-cooling passages must be much larger than the liquid- cooling passages.

Improvements in state-of-the-art phosphoric acid cells are illustrated by Figure 5-2. Performance by the ~1 m^2 (10 ft^2) short stack, (f), results in a power density of nearly 0.31 W/cm^2.

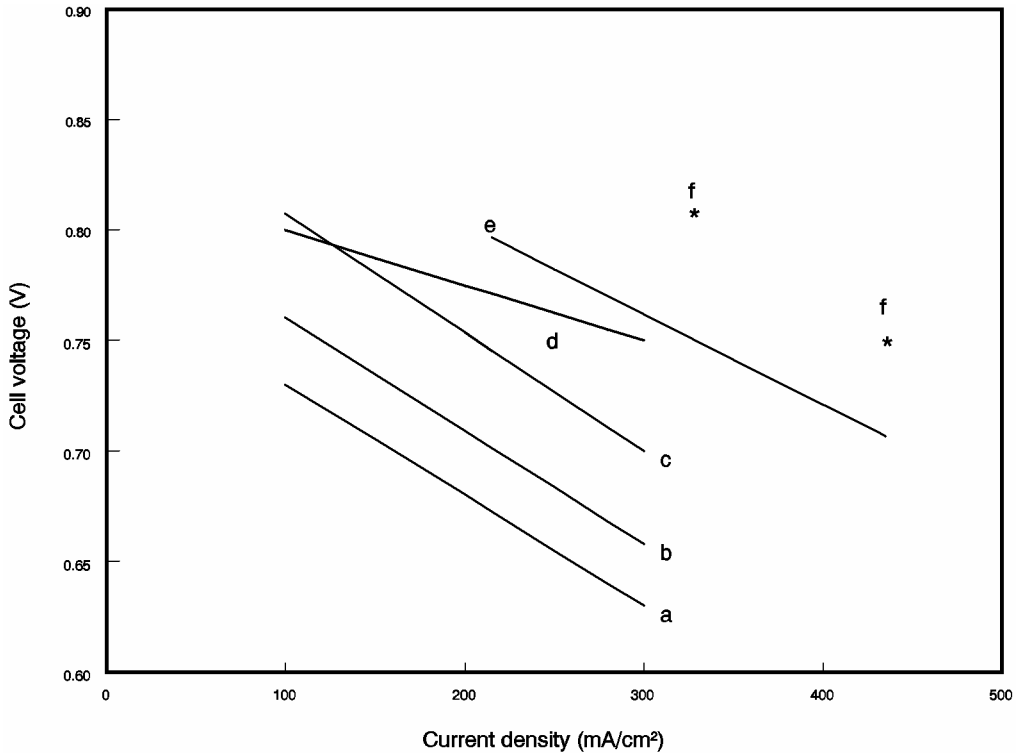

Figure 5-2 Improvement in the Performance of H_2-Rich Fuel/Air PAFCs

a - 1977: 190°C, 3 atm, Pt loading of 0.75 mg/cm^2 on each electrode (13)
b - 1981: 190°C, 3.4 atm, cathode Pt loading of 0.5 mg/cm^2 (14)
c - 1981: 205°C, 6.3 atm, cathode Pt loading of 0.5 mg/cm^2 (14)
d - 1984: 205°C, 8 atm, electrocatalyst loading was not specified (15)
e - 1992: 205°C, 8 atm, 10 ft^2 short stack, 200 hrs, electrocatalyst loading not specified (16)
f - 1992: 205°C, 8 atm, subscale cells, electrocatalyst loading not specified (16)

5.1.2 Development Components

Phosphoric acid electrode/electrolyte technology has now reached a level of maturity at which developers commit resources for commercial capacity, multi-unit demonstrations and pre-prototype installations. UTC Fuel Cells has 25 (200 kW) atmospheric pressure power plants that have operated between 30,000-40,000 hours. Most cell parts are graphite, and there has been no electrolyte replacement over the cell life of 40,000 hours. Grid-independent units undergo extensive cycling. Cell components are manufactured at scale and in large quantities, demonstrating confidence that predicted performance will be met (3). However, further increases in power density and reduced cost are needed to achieve economic competitiveness with other energy technologies, as expressed in the early 1990s (17, 18). Fuel cell developers continue to address these issues.

In 1992, UTC Fuel Cells' predecessor, International Fuel Cells, completed a government-sponsored, advanced water-cooled PAFC development project to improve the performance and reduce the cost of both its atmospheric and pressurized technology for both on-site and utility

applications (16). The project focused on five major activities: 1) produce a conceptual design of a large stack with a goal of 175 W/ft^2 (0.188 W/cm^2), 40,000 hour useful life, and a stack cost of less than $400/kW; 2) test pressurized Configuration "B" single cells developed in a previous program, but improved with proprietary design advances in substrates, electrolyte reservoir plates, catalysts, seals, and electrolyte matrix to demonstrate the 175 W/ft^2 (0.188 W/cm^2) power density goal; 3) test a pressurized short stack with subscale size, improved component cells, and additional improvements in the integral separators and coolers to confirm the stack design; 4) test a pressurized short stack of improved full-size cell components, nominal 10 ft^2 size (approximately 1 m^2), to demonstrate the 175 W/ft^2 (0.188 W/cm^2) power density goal, and 5) test an advanced atmospheric "on-site" power unit stack with the improved components.

A conceptual design of an improved technology stack, operating at 120 psi (8.2 atm) and 405°F (207°C), was produced based on cell and stack development tests. The stack was designed for 355 10 ft^2 (approximately 1 m^2) cells to produce over 1 MW dc power in the same physical envelope as the 670 kW stack used in the 11 MW PAFC plant built for Tokyo Electric Power. The improvements made to the design were tested in single cells and in subscale and full size short stacks.

Table 5-2 summarizes the results. Single cells achieved an initial performance of 0.75 volts/cell at a current density of 400 A/ft^2 (431 mA/cm^2) at 8.2 atm and 207°C. The power density, 300 W/ft^2 (0.323 W/cm^2), was well above the project goal. Several cells were operated to 600 A/ft^2 (645 mA/cm^2), achieving up to 0.66 volts/cell. The flat plate component designs were verified in a subscale stack prior to fabricating the full size short stack. The pressurized short stack of 10 ft^2 cells achieved a performance of 285 W/ft^2 (0.307 W/cm^2). Although the average cell performance, 0.71 volts/cell at 400 A/ft^2 (431 mA/cm^2), was not as high as the single cell tests, the performance was 65% higher than the project goal. Figure 5-3 presents single cell and stack performance data for pressurized operation. The stack was tested for over 3,000 hours. For reference purposes, Tokyo Electric Power Company's 11 MW power plant, operational in 1991, had an average cell performance of approximately 0.75 volts/cell at 190 mA/cm^2 or 0.142 W/cm^2 (19).

Table 5-2 Advanced PAFC Performance

	Average Cell Voltage, V	Current Density mA/cm^2	Power Density W/cm^2
IFC Pressurized:			
Project Goal			0.188
Single Cells	0.75 to 0.66	431 to 645	0.323
	0.71	431	
Full Size Short Stack	0.75	190	0.307
11 MW Reference			0.142
IFC Atmospheric:			
Single Cells	0.75	242	0.182
Full Size Short Stack	0.65	215	0.139
Mitsubishi Electric Atmospheric Single Cells	0.65	300	0.195

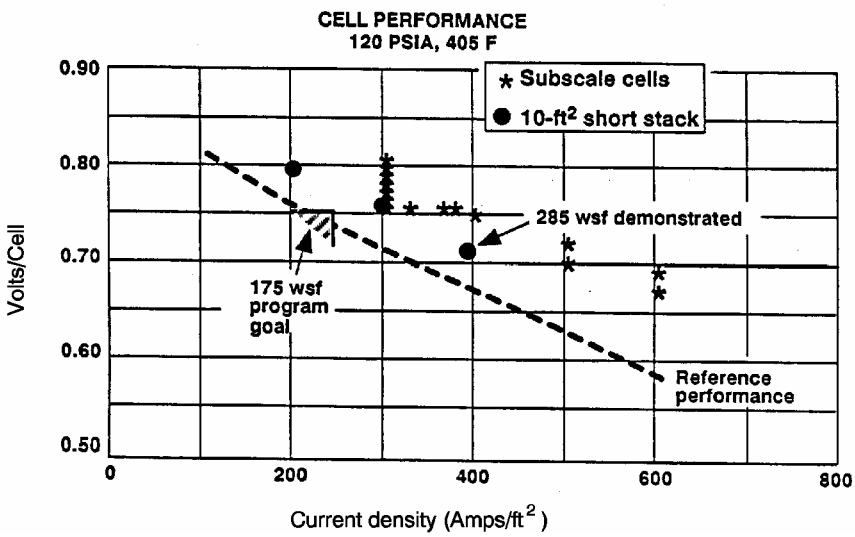

Figure 5-3 Advanced Water-Cooled PAFC Performance (16)

The atmospheric pressure short stack, consisting of 32 cells, obtained an initial performance of 0.65 volts/cell at 200 A/ft^2 (215 mA/cm^2) or 0.139 W/cm^2. The performance degradation rate was less than 4 mV/1,000 hours during the 4,500 hour test. Single cells, tested at atmospheric conditions, achieved a 500 hour performance of approximately 0.75 volts/cell at 225 A/ft^2 (242 mA/cm^2) or 0.182 W/cm^2.

Mitsubishi Electric Corporation investigated alloyed catalysts, processes to produce thinner electrolytes, and increased utilization of the catalyst layer (20). These improvements resulted in an initial atmospheric performance of 0.65 mV at 300 mA/cm^2 or 0.195 W/cm^2, which was higher than the UTC Fuel Cells' performance mentioned above (presented in Table 5-2 for comparison). Note that this performance was obtained using small 100 cm^2 cells and may not yet have been demonstrated with full-scale cells in stacks. Approaches to increase life are to use series fuel gas

flow in the stack to alleviate corrosion, provide well-balanced micropore size reservoirs to avoid electrolyte flooding, and use a high corrosion resistant carbon support for the cathode catalyst. These improvements resulted in the lowest PAFC degradation rate publicly acknowledged: 2 mV/1,000 hours for 10,000 hours at 200-250 mA/cm^2 in a short stack with 3,600 cm^2 area cells. UTC Fuel Cells reported a similar degradation rate in 2002 for power units operating up to 40,000 hours (3).

Several important technology development efforts for which details have been published include catalyst improvements, advanced gas diffusion electrode development, and tests on materials that offer better carbon corrosion protection. Transition metal (e.g., iron, cobalt) organic macrocycles[17] from the families of tetramethoxyphenylporphyrins (TMPP), phthalocyanines (PC), tetraazaannulenes (TAA) and tetraphenylporphyrins (TPP) have been evaluated as O_2-reduction electrocatalysts in PAFCs. One major problem with these organic macrocycles is their limited chemical stability in hot concentrated phosphoric acid. However, after heat treatment of the organic macrocycle (i.e., CoTAA, CoPC, CoTMPP, FePC, FeTMPP) on carbon at about 500-800°C (932-1,472°F), the pyrolyzed residue exhibits electrocatalytic activity that, in some instances, is comparable to that of Pt and has promising stability, at least up to about 100°C/212°F (21). Another successful approach for enhancing the electrocatalysis of O_2 reduction is to alloy Pt with transition metals such as Ti (22), Cr (23), V (24), Zr, and Ta (24). The enhancement in electrocatalytic activity has been explained by a correlation between the optimum nearest-neighbor distance of the elements in the alloy and the bond length in O_2 (25).

Conventional cathode catalysts comprise either platinum or platinum alloys supported on conducting carbon black at 10 wt% platinum. Present platinum loadings on the anode and cathode are 0.1 mg/cm^2 and 0.5 mg/cm^2, respectively (12, 16). It has been suggested by Ito, et al., that the amount of platinum may have been reduced to the extent that it might be cost effective to increase the amount of platinum loading on the cathode (26). However, a problem exists in that fuel cell stack developers have not experienced satisfactory performance improvements when increasing the platinum loading. Johnson Matthey Technology Centre (J-M) presented data that resulted in improved performance nearly in direct proportion to that expected based on the increase in platinum (27). Initial tests by J-M confirmed previous results - that using platinum alloy catalyst with a 10 wt% net platinum loading improves performance. Platinum/nickel alloy catalysts yielded a 49 wt% increase in specific activity over pure platinum. This translated into a 39 mV improvement in the air electrode performance at 200 mA/cm^2.

Johnson Matthey then determined that the platinum loading in the alloyed catalyst could be increased up to 30 wt% while retaining the same amount of platinum without any decrease in specific activity or performance; the amount of nickel, hence the total amount of alloyed catalyst, decreased. Next, J-M researchers increased the amount of platinum from 10 to 30 wt% while keeping the same nickel catalyst loading. The total amount of alloyed catalyst increased in this case. Results showed an additional 36 wt% increase in specific activity, which provided another 41 mV increase at 200 mA/cm^2. The ideal voltage increase would have been 46 mV for this increase in platinum. Thus, the performance increase obtained experimentally was nearly in direct

[17]. See Reference 21 for literature survey.

proportion to the theoretical amount expected. The type of carbon support did not seem to be a major factor, based on using several typical supports during the tests.

The anode of a phosphoric acid fuel cell is subject to a reduction in performance when even low amounts of contaminants are preferentially absorbed on the noble catalysts. Yet, hydrogen-rich fuel gases, other than pure hydrogen, are produced with contaminant levels well in excess of the anode's tolerance limit. Of particular concern are CO, COS, and H_2S in the fuel gas. The fuel stream in a state-of-the-art PAFC anode, operating at approximately 200°C (392°F), must contain 1 vol % or less of CO (12), less than 50 ppmv of COS plus H_2S, and less than 20 ppmv of H_2S (28). Current practice is to place COS and H_2S cleanup systems and CO shift converters prior to the cell (normally in the fuel processor before reforming) to reduce the fuel stream contaminant levels to the required amounts. Giner, Inc. performed experiments to develop a contaminant-tolerant anode catalyst in order to reduce or eliminate the cleanup equipment (29). An anode catalyst, G87A-17-2, was identified that resulted in only a 24 mV loss from reference when exposed to a 75% H_2, 1% CO, 24% CO_2, 80 ppm H_2S gas mixture at 190°C (374°F), 85% fuel utilization, and 200 mA/cm^2. A baseline anode experienced a 36 mV loss from the reference at the same conditions. At 9.2 atm (120 psi) pressure, the anode loss was only 19 mV at 190°C (374°) and 17 mV at 210°C (410°F) (compared with pure H_2) with a gas of 71% H_2, 5% CO, 24% CO_2, and 200 ppm H_2S. Economic studies comparing the tradeoff between decreased cell performance with increased savings in plant cost showed no advantage when the new anode catalyst was used with gas containing 1% CO/200 ppm H_2S. A $7/kW increase resulted with the 5% CO gas (compared to a 1% CO gas) at a 50 MW size. Some savings would result by eliminating the low temperature shift converter. The real value of the catalyst may be its ability to tolerate excessive CO and H_2S concentrations during fuel processor upsets, and to simplify the system by eliminating equipment.

As previously mentioned, state-of-the-art gas diffusion electrodes are configured to provide an electrolyte network and a gas network formed with the mixture of carbon black and PTFE. In the electrodes, carbon black agglomerates, consisting of small primary particles 0.02-0.04 μm, are mixed with much larger PTFE particles of ~0.3 μm. The carbon black surface may not be covered completely by the PTFE because of the large size of conventional PTFE particles. The space in the agglomerates or the space between the agglomerates and PTFE may act as gas networks at the initial stage of operation, but fill with electrolyte eventually because of the small contact angle of carbon black, uncovered with PTFE, to electrolyte (<90°), resulting in the degradation of cell performance. Attempts to solve this flooding problem by increasing the PTFE content have not been successful because of the offset in performance resulting from the reduction of catalyst utilization. Higher performance and longer lifetime of electrodes are intrinsically at odds, and there is a limit to the improvement in performance over life by optimizing PTFE content in the state-of-the-art electrode structures. Watanabe, et al. (30) proposed preparing an electrode utilizing 100% of catalyst clusters, where the functions of gas diffusion electrodes were allotted completely to a hydrophilic, catalyzed carbon black and a wet-proofed carbon black. The former worked as a fine electrolyte network, and the latter worked as a gas-supplying network in a reaction layer. Higher utilization of catalyst clusters and longer life at the reaction layer were expected, compared to state-of-the-art electrodes consisting of the uniform mixture of catalyzed carbon black and PTFE particles. The iR-free electrode potentials for the reduction of oxygen and air at 200 mA/cm^2 on the advanced electrode were 10 mV higher than those of the conventional electrode.

There is a trade-off between high power density and cell life performance. One of the major causes of declining cell performance over its life is that electrode flooding and drying, caused by migration of phosphoric acid between the matrix and the electrodes, occurs during cell load cycling. Researchers at Fuji Electric addressed two approaches to improve cell life performance while keeping power density high (31). In one, the wettability of the cathode and anode were optimized, and in the other a heat treatment was applied to the carbon support for the cathode catalyst. During tests, it was observed that a cell with low cathode wettability and high anode wettability was more than 50 mV higher than a cell with the reverse wetting conditions after 40 start/stop cycles.

The use of carbon black with large surface area to improve platinum dispersion on supports was investigated as a method to increase the power density of a cell (32). However, some large surface area carbon blacks are fairly corrosive in hot potassium acid, resulting in a loss of catalytic activity. The corrosivity of the carbon support affects both the rate of catalyst loss and electrode flooding and, in turn, the life performance of a cell. Furnace black has been heat treated at high temperature by Fuji Electric to increase its resistance to corrosion. It was found that corrosion could be reduced and cell life performance improved by heat treating carbon supports at high temperature, at least to around 3,000°C (5,432°F).

More recently, UTC Fuel Cells cites improvements to achieve 40,000 cell life through better cell temperature control, increasing H_3PO_4 inventory, and incorporating electrolyte reservoir plates in the cell stack (3).

5.2 Performance

There have been only minor changes in documented cell performance since the mid-1980s - mostly due to the operating conditions of the cell. The changes are reported in performance trends shown in this section that were primarily gained from contracts that UTC Fuel Cells had with the Department of Energy or outside institutions. New, proprietary PAFC performance data may likely have been observed by the manufacturer (3).

Cell performance for any fuel cell is a function of pressure, temperature, reactant gas composition, and fuel utilization. In addition, performance can be adversely affected by impurities in both the fuel and oxidant gases.

The sources of polarization in PAFCs (with cathode and anode Pt loadings of 0.5 mg Pt/cm^2, 180°C, 1 atm, 100% H_3PO_4) were discussed in Section 2 and were illustrated as half cell performance in Figure 2-4. From Figure 2-4 it is clear that the major polarization occurs at the cathode, and furthermore, the polarization is greater with air (560 mV at 300 mA/cm^2) than with pure oxygen (480 mV at 300 mA/cm^2) because of dilution of the reactant. The anode exhibits very low polarization (-4 mV/100 mA/cm^2) on pure H_2, and increases when CO is present in the fuel gas. The ohmic (iR) loss in PAFCs is also relatively small, amounting to about 12 mV at 100 mA/cm^2.

Typical PAFCs will generally operate in the range of 100-400 mA/cm^2 at 600-800 mV/cell. Voltage and power constraints arise from increased corrosion of platinum and carbon components at cell potentials above approximately 800 mV.

5.2.1 Effect of Pressure

Even though pressure operation is not being pursued, it is still of interest for possible future development. It is well known that an increase in the cell operating pressure enhances the performance of PAFCs (11, 33, 34). The theoretical change in voltage (ΔV_P) as a function of pressure (P) is expressed as

$$\Delta V_P(\text{mV}) = \frac{(3)(2.3RT)}{2F} \log \frac{P_2}{P_1} \qquad (5\text{-}4)$$

where $\frac{3(2.3RT)}{2F} = 138\ mV$ at 190°C (374°F). Experimental data (35) reported that the effect of pressure on cell performance at 190°C (374°F) and 323 mA/cm^2 is correlated by the equation:

$$\Delta V_P\ (\text{mV}) = 146 \log \frac{P_2}{P_1} \qquad (5\text{-}5)$$

where P_1 and P_2 are different cell pressures. The experimental data (35) also suggest that Equation (5-5) is a reasonable approximation for a temperature range of 177°C $\leq$ T $\leq$ 218°C (351°F $\leq$ T $\leq$ 424°F) and a pressure range of 1 atm $\leq$ P $\leq$ 10 atm (14.7 psi $\leq$ P $\leq$ 147.0 psi). Data from Appleby (14) in Figure 5-2 indicate that the voltage gain observed by increasing the pressure from 3.4 atm (190°C) to 6.3 atm (205°C) is about 44 mV. According to Equation (5-5), the voltage gain calculated for this increase in pressure at 190°C (374°F) is 39 mV[18], which is in reasonable agreement with experimental data in Figure 5-2. Measurements (33) of ΔV_P for an increase in pressure from 4.7 to 9.2 atm (69.1 to 135.2 psia) in a cell at 190°C (374°F) show that ΔV_P is a function of current density, increasing from 35 mV at 100 mA/cm^2 to 42 mV at 400 mA/cm^2 (50% O_2 utilization with air oxidant, 85% H_2 utilization with pure H_2 fuel). From Equation (5-4), ΔV_p is 43 mV for an increase in pressure from 4.7 to 9.2 atm (69.1 to 135.2 psia) at 190°C (374°F), which is very close to the experimental value obtained at 400 mA/cm^2. Other measurements (36) for the same increase in pressure from 4.7 to 9.2 atm (69.1 to 135.2 psia), but at a temperature of 210°C (410°F) show less agreement between the experimental data and Equation (5-4).

The improvement in cell performance at higher pressure and high current density can be attributed to a lower diffusion polarization at the cathode and an increase in the reversible cell potential. In addition, pressurization decreases activation polarization at the cathode because of the increased oxygen and water partial pressures. If the partial pressure of water is allowed to increase, a lower acid concentration will result. This will increase ionic conductivity and bring about a higher exchange current density. The net outcome is a reduction in ohmic losses. It was reported (33) that an increase in cell pressure (100% H_3PO_4, 169°C (336°F)) from 1 to 4.4 atm (14.7 to 64.7 psia) produces a reduction in acid concentration to 97%, and a decrease of about 0.001 ohm in the resistance of a small six cell stack (350 cm^2 electrode area).

---

[18]. The difference in temperature between 190 and 205°C is disregarded so Equation (5-5) is assumed to be valid at both temperatures.

5.2.2 Effect of Temperature

Figure 2-1 shows that the reversible cell potential for PAFCs consuming H_2 and O_2 decreases as the temperature increases by 0.27 mV/°C under standard conditions (product is water vapor). However, as discussed in Section 2, an increase in temperature has a beneficial effect on cell performance because activation polarization, mass transfer polarization, and ohmic losses are reduced.

The kinetics for the reduction of oxygen on Pt improves[19] as the cell temperature increases. At a mid-range operating load (~250 mA/cm^2), the voltage gain (ΔV_T) with increasing temperature of pure H_2 and air is correlated by

$$\Delta V_T \text{ (mV)} = 1.15 \, (T_2 - T_1) \text{ (°C)} \qquad (5\text{-}6)$$

Data suggest that Equation (5-6) is reasonably valid for a temperature range of 180°C $\leq$ T $\leq$ 250°C (356°F $\leq$ T $\leq$ 482°F). It is apparent from this equation that each degree increase in cell temperature should increase performance by 1.15 mV. Other data indicate that the coefficient for Equation (5-6) may be in the range of 0.55 to 0.75, rather than 1.15. Although temperature has only a minimal effect on the H_2 oxidation reaction at the anode, it is important in terms of the amount of CO that can be absorbed by the anode. Figure 5-4 shows that increasing the cell temperature results in increased anode tolerance to CO absorption. A strong temperature effect was also observed using simulated coal gas. Below 200°C (392°F), the cell voltage drop was significant. Experimental data suggest that the effect of contaminants is not additive, indicating that there is an interaction between CO and H_2S (37). Increasing temperature increases performance, but elevated temperature also increases catalyst sintering, component corrosion, electrolyte degradation, and evaporation. UTC Fuel Cells operates its phosphoric acid cells at 207°C (405°F), which is a compromise that allows reasonable performance at a life of 40,000 hours (3).

[19]. The anode shows no significant performance improvement from 140 to 180° on pure H_2, but in the presence of CO, increasing the temperature results in a marked improvement in performance (see discussion in Section 5.2.4).

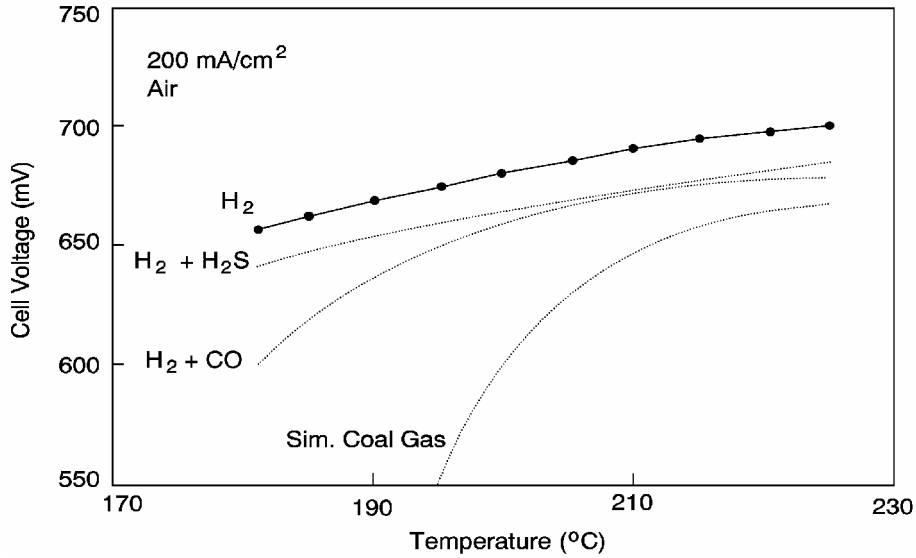

Figure 5-4 Effect of Temperature: Ultra-High Surface Area Pt Catalyst. Fuel: H_2, H_2 + 200 ppm H_2S and Simulated Coal Gas (37)

5.2.3 Effect of Reactant Gas Composition and Utilization

Increasing reactant gas utilization or decreasing inlet concentration results in decreased cell performance due to increased concentration polarization and Nernst losses. These effects are related to the partial pressures of reactant gases and are discussed below.

Oxidant: The oxidant composition and utilization are parameters that affect the cathode performance, as evident in Figure 2-5. Air, which contains ~21% O_2, is the obvious oxidant for terrestrial application PAFCs. The use of air with ~21% O_2 instead of pure O_2 results in a decrease in the current density of about a factor of three at constant electrode potential. The polarization at the cathode increases with an increase in O_2 utilization. Experimental measurements (38) of the change in overpotential ($\Delta\eta_c$) at a PTFE-bonded porous electrode in 100% H_3PO_4 (191°C, atmospheric pressure) as a function of O_2 utilization is plotted in Figure 5-5 in accordance with Equation (5-7):

$$\Delta\eta_c = \eta_c - \eta_{c,\infty} \qquad (5\text{-}7)$$

where η_c and $\eta_{c,\infty}$ are the cathode polarizations at finite and infinite (i.e., high flow rate, close to 0% utilization) flow rates, respectively. The additional polarization attributed to O_2 utilization is reflected in the results, and the magnitude of this loss increases rapidly as the utilization increases. At a nominal O_2 utilization of 50% for prototype PAFC power plants, the additional polarization estimated from the results in Figure 5-5 is 19 mV. Based on experimental data (16, 38, 39), the voltage loss due to a change in oxidant utilization can be described by Equations (5-8) and (5-9):

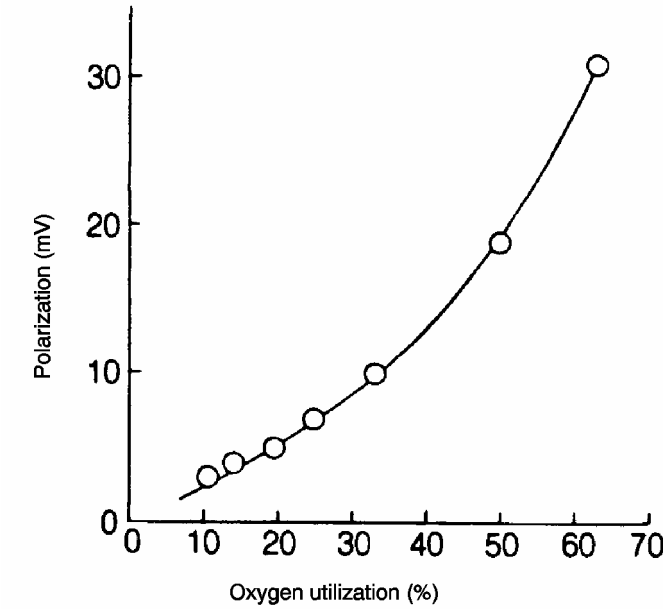

Figure 5-5 Polarization at Cathode (0.52 mg Pt/cm^2) as a Function of O_2 Utilization, which is Increased by Decreasing the Flow Rate of the Oxidant at Atmospheric Pressure 100% H_3PO_4, 191°C, 300 mA/cm^2, 1 atm. (38)

$$\Delta V_{Cathode}(mV) = 148 \log \frac{(\overline{P}_{0_2})_2}{(\overline{P}_{0_2})_1} \quad 0.04 \leq \frac{\overline{P}_{0_2}}{\overline{P}_{Total}} \leq 0.20 \qquad (5\text{-}8)$$

$$\Delta V_{Cathode}(mV) = 96 \log \frac{(\overline{P}_{0_2})_2}{(\overline{P}_{0_2})_1} \quad 0.20 < \frac{\overline{P}_{0_2}}{\overline{P}_{Total}} < 1.00 \qquad (5\text{-}9)$$

where $\overline{P}_{O_2}$ is the average partial pressure of O_2. The use of two equations over the concentration range more accurately correlates actual fuel cell operation. Equation (5-8) will generally apply to fuel cells using air as the oxidant and Equation (5-9) for fuel cells using an O_2-enriched oxidant.

Fuel: Hydrogen for PAFC power plants will typically be produced from conversion of a wide variety of primary fuels such as CH_4 (e.g., natural gas), petroleum products (e.g., naphtha), coal liquids (e.g., CH_3OH), or coal gases. Besides H_2, CO and CO_2 are also produced during conversion of these fuels (unreacted hydrocarbons are also present). These reformed fuels contain low levels of CO (after steam reforming and shift conversion reactions in the fuel processor) that cause anode CO absorption in PAFCs. The CO_2 and unreacted hydrocarbons (e.g., CH_4) are electrochemically inert and act as diluents. Because the anode reaction is nearly reversible, the fuel composition and hydrogen utilization generally do not strongly influence cell performance. The voltage change due to a change in the partial pressure of hydrogen (which can result from a change in either the fuel composition or utilization) can be described by Equation (5-10) (16, 36, 37):

$$\Delta V_{Anode}(mV) = 55 \log \frac{(\overline{P}_{H_2})_2}{(\overline{P}_{H_2})_1} \qquad (5\text{-}10)$$

where $\overline{P}_{H_2}$ is the average partial pressure of H_2. At 190°C (374°F), the presence of 10% CO_2 in H_2 should cause a voltage loss of about 2 mV. Thus, diluents in low concentrations are not expected to have a major effect on electrode performance; however, relative to the total anode polarization (i.e., 3 mV/100 mA/cm^2), the effects are large. It has been reported (16) that with pure H_2, the cell voltage at 215 mA/cm^2 remains nearly constant at H_2 utilizations up to 90%, and then it decreases sharply at H_2 utilizations above this value.

Low utilizations, particularly oxygen utilization, yield high performance. Low utilizations, however, result in poor fuel use. Optimization of this parameter is required. State-of-the-art utilizations are on the order of 85% and 50% for the fuel and oxidant, respectively.

5.2.4 Effect of Impurities

The concentrations of impurities entering the PAFC are very low relative to diluents and reactant gases, but their impact on performance is significant. Some impurities (e.g., sulfur compounds) originate from fuel gas entering the fuel processor and are carried into the fuel cell with the reformed fuel, whereas others (e.g., CO) are produced in the fuel processor.

Carbon Monoxide: The presence of CO in a H_2-rich fuel has a significant effect on anode performance because CO affects Pt electrode catalysts. CO absorption is reported to arise from the dual site replacement of one H_2 molecule by two CO molecules on the Pt surface (40, 41). According to this model, the anodic oxidation current at a fixed overpotential, with (i_{CO}) and without (i_{H_2}) CO present, is given as a function of CO coverage (θ_{CO}) by Equation (5-11):

$$\frac{i_{CO}}{i_{H_2}} = (1 - \theta_{CO})^2 \qquad (5\text{-}11)$$

For $[CO]/[H_2] = 0.025$, $\theta_{CO} = 0.31$ at 190°C (35); therefore, i_{CO} is about 50% of i_{H_2}.

Both temperature and CO concentration have a major influence on the oxidation of H_2 on Pt in CO containing fuel gases. Benjamin, et al. (35) derived Equation (5-12) for the voltage loss resulting from CO absorption as a function of temperature

$$\Delta V_{CO} = k(T)\,([CO]_2 - [CO]_1) \qquad (5\text{-}12)$$

where k(T) is a function of temperature, and $[CO]_1$ and $[CO]_2$ are the mole fractions CO in the fuel gas. The values of k(T) at various temperatures are listed in Table 5-3. Using Equation (5-12) and the data in Table 5-3, it is apparent that for a given change in CO content, ΔV_{CO} is about 8.5 times larger at 163°C (325°F) than at 218°C (424°F). The correlation provided by Equation (5-12) was obtained at 269 mA/cm^2; thus, its use at significantly different current densities may not be

appropriate. In addition, other more recent data (37) suggest a value for k(T) of -2.12 at a temperature of 190°C (374°) rather than -3.54.

Table 5-3 Dependence of k(T) on Temperature

T (°C)	T (°F)	k(T)[a] (mV/%)
163	325	-11.1
177	351	-6.14
190	374	-3.54
204	399	-2.05
218	424	-1.30

a - Based on electrode with 0.35 mg Pt/cm^2, and at 269 mA/cm^2 (35)

The data in Figure 5-6 illustrate the influence of H_2 partial pressure and CO content on the performance of Pt anodes (10% Pt supported on Vulcan XC-72, 0.5 mg Pt/cm^2) in 100% H_3PO_4 at 180°C (356°F) (11). Diluting the H_2 fuel gas with 30% CO_2 produces an additional polarization of about 11 mV at 300 mA/cm^2. The results show that the anode polarization with fuel gases of composition 70% H_2/(30-x)% CO_2/x% CO (x =0, 0.3, 1, 3 and 5) increases considerably as the CO content increases to 5%.

Sulfur Containing Compounds: Hydrogen sulfide and carbonyl sulfide (COS) impurities[20] in fuel gases from fuel processors and coal gasifiers can reduce the effectiveness of fuel cell catalysts. Concentrations of these compounds must also be limited in a power plant's fuel processing section, because the fuel reformer too has catalysts. As a result, sulfur must be removed prior to fuel reforming with the non-sulfur tolerant catalysts now in use in PAFC power plants. It is prudent to be concerned about sulfur effects in the cell, however, because the fuel processor catalyst's tolerance limits may be less than the fuel cell catalyst's or there could be an upset of the fuel processor sulfur guard with sulfur passing through to the cell. The concentration levels of H_2S in an operating PAFC (190-210°C (374-410°F), 9.2 atm (120 psig), 80% H_2 utilization, <325 mA/cm^2) that can be tolerated by Pt anodes without suffering a destructive loss in performance are <50 ppm (H_2S + COS) or <20 ppm (H_2S) (42). Rapid cell failure occurs with fuel gas containing more than 50 ppm H_2S. Sulfur does not affect the cathode, and the impact of sulfur on the anodes can be re-activated by polarization at high potentials (i.e., operating cathode potentials). A synergistic effect between H_2S and CO negatively impacts cell performance. Figure 5-7 (37) shows the effect of H_2S concentration on ΔV with and without 10% CO present in H_2. The ΔV is referenced to performance on pure H_2 in the case of H_2S alone and to performance on H_2 with 10% CO for H_2S and CO. In both cases, at higher H_2S concentrations, the ΔV rises abruptly. This drop in performance occurs above 240 ppm for H_2S alone and above 160 ppm for H_2S with 10% CO.

[20]. Anode gases from coal gasifiers may contain total sulfur of 100 to 200 ppm.

Experimental studies by Chin and Howard (43) indicate that H_2S adsorbs on Pt and blocks the active sites for H_2 oxidation. The following electrochemical reactions, Equations (5-13), (5-14), and (5-15) involving H_2S are postulated to occur on Pt electrodes:

$$Pt + HS^- \rightarrow Pt - HS_{ads} + e^- \qquad (5\text{-}13)$$

$$Pt - H_2S_{ads} \rightarrow Pt - HS_{ads} + H^+ + e^- \qquad (5\text{-}14)$$

$$Pt - HS_{ads} \rightarrow Pt - S_{ads} + H^+ + e^- \qquad (5\text{-}15)$$

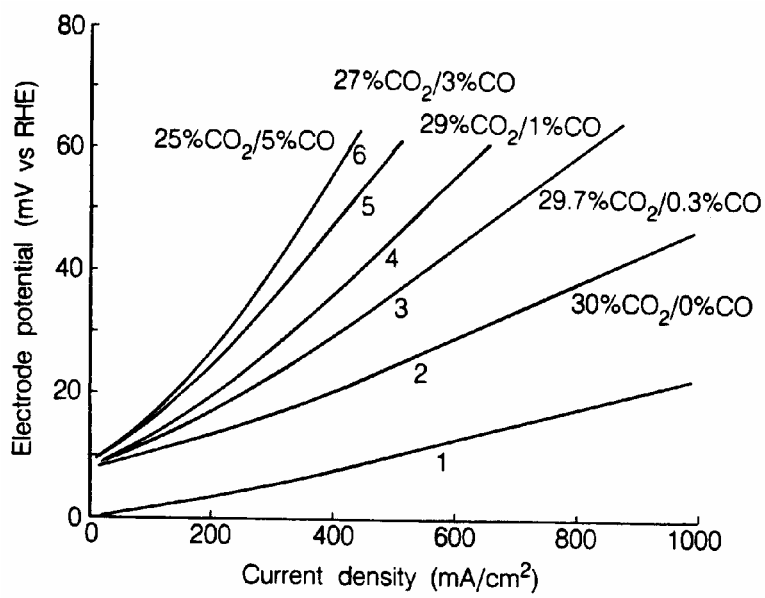

Figure 5-6 Influence of CO and Fuel Gas Composition on the Performance of Pt Anodes in 100% H_3PO_4 at 180°C. 10% Pt Supported on Vulcan XC-72, 0.5 mg Pt/cm^2. Dew Point, 57°. Curve 1, 100% H_2; Curves 2-6, 70% H_2 and CO_2/CO Contents (mol%) Specified (21)

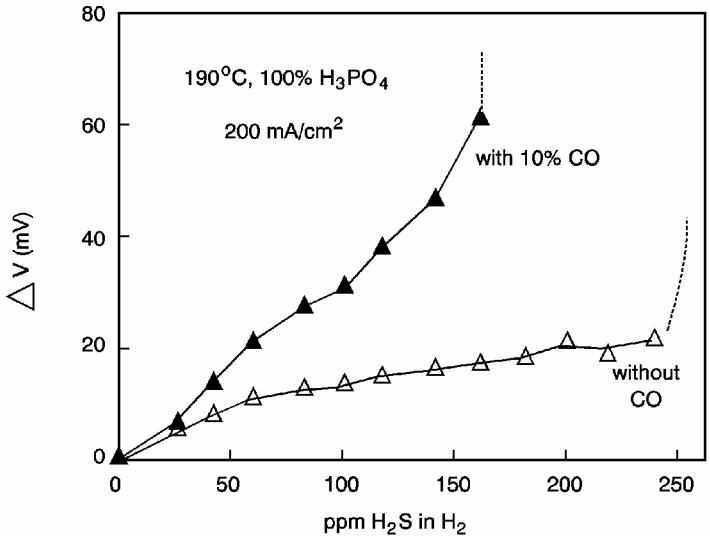

Figure 5-7 Effect of H_2S Concentration: Ultra-High Surface Area Pt Catalyst (37)

Elemental sulfur (in Equation (5-15) is expected on Pt electrodes only at high anodic potentials; at sufficiently high potentials, sulfur is oxidized to SO_2. The extent of catalyst masking by H_2S increases with increasing H_2S concentration, electrode potential, and exposure time. The effect of H_2S, however, decreases with increasing cell temperature.

Other Compounds: The effects of other compounds (such as those containing nitrogen) on PAFC performance has been adequately reviewed by Benjamin, et al. (35). Molecular nitrogen acts as a diluent but other nitrogen compounds (e.g., NH_3, HCN, NO_X) may not be as innocuous. NH_3 in the fuel or oxidant gases reacts with H_3PO_4 to form a phosphate salt, $(NH_4)H_2PO_4$,

$$H_3PO_4 + NH_3 \rightarrow (NH_4)H_2PO_4 \qquad (5\text{-}16)$$

which decreases the rate of O_2 reduction. A concentration of less than 0.2 mol% $(NH_4)H_2PO_4$ must be maintained to avoid unacceptable performance losses (44). Consequently, the amount of molecular nitrogen must be limited to 4% because it will react with hydrogen to form NH_3 (3). The effects of HCN and NO_X on fuel cell performance have not been clearly established.

5.2.5 Effects of Current Density

The voltage that can be obtained from a PAFC is reduced by ohmic, activation, and concentration losses that increase with increasing current density. The magnitude of this loss can be approximated by the following equations:

$$\Delta V_J \text{ (mV)} = -0.53\ \Delta J \qquad \text{for } J = 100 - 200 \text{ mA/cm}^2 \qquad (5\text{-}17)$$

$$\Delta V_J \text{ (mV)} = -0.39\ \Delta J \qquad \text{for } J = 200 - 650 \text{ mA/cm}^2 \qquad (5\text{-}18)$$

The coefficients in these equations were correlated from performance data for cells (45) operating at 120 psia (8.2 atm), 405°F (207°C) (16) with fuel and oxidant utilizations of 85% and 70%, respectively[21], an air fed cathode, and an anode inlet composition of 75% H_2, and 0.5% CO. Similarly, at atmospheric conditions, the magnitude of this loss can be approximated by

$$\Delta V_J \text{ (mV)} = -0.74\ \Delta J \qquad \text{for } J = 50 - 120 \text{ mA/cm}^2 \qquad (5\text{-}19)$$

$$\Delta V_J \text{ (mV)} = -0.45\ \Delta J \qquad \text{for } J = 120 - 215 \text{ mA/cm}^2 \qquad (5\text{-}20)$$

The coefficients in the atmospheric condition equations were derived from performance data for cells (45) operating at 14.7 psia (1 atm) and 400°F (204°C), fuel and oxidant utilizations of 80% and 60%, respectively[21], an air fed cathode, and an anode inlet composition of 75% H_2 and 0.5% CO.

5.2.6 Effects of Cell Life

One of the primary areas of research is in extending cell life. The goal is to maintain the performance of the cell stack during a standard utility application (~40,000 hours). Previous state-of-the-art PAFCs (46, 47, 48) showed the following degradation over time:

$$\Delta V_{lifetime} \text{ (mV)} = -3 \text{ mV/1,000 hours} \qquad (5\text{-}21)$$

UTC Fuel Cells reports that the efficiency of its latest power plants at the beginning of life is 40% LHV. The infant life loss reduces the efficiency quickly to 38%, but then there is a small decrease in efficiency over the next 40,000 hours (expected cell life) resulting in an average efficiency over life of 37% (3). Assuming that the loss in efficiency is due solely to cell voltage loss, the maximum degradation rate can be determined as:

$$\Delta V_{lifetime} \text{ (mV)} = -2 \text{ mV/1,000 hours} \qquad (5\text{-}22)$$

[21]. Assumes graph operating conditions (not provided) are the same as associated text of Ref.15.

5.3 Summary of Equations for PAFC

The preceding sections provide parametric performance based on various referenced data at differing cell conditions. It is suggested that the following set of equations be used unless the reader prefers other data or rationale. Figure 5-8 is provided as reference PAFC performances at ambient pressure and 8.2 atm.

Parameter	Equation	Comments	
Pressure	$\Delta V_P\,(mV) = 146 \log \frac{P_2}{P_1}$	$1\ atm \le P \le 10\ atm$ $177°C \le T \le 218°C$	(5-5)
Temperature	$\Delta V_T\,(mV) = 1.15\,(T_2 - T_1)$	$180°C \le T \le 250°C$	(5-6)
Oxidant	$\Delta V_{Cathode}\,(mV) = 148 \log \frac{(\bar{P}_{0_2})_2}{(\bar{P}_{0_2})_1}$	$0.04 \le \frac{\bar{P}_{0_2}}{\bar{P}_{Total}} \le 0.20$	
	$\Delta V_{cathode}\,(mV) = 96 \log \frac{(\bar{P}_{02})_2}{(\bar{P}_{02})_1}$	$0.20 \le \frac{\bar{P}_{0_2}}{\bar{P}_{Total}} < 1.0$	(5-9)
Fuel	$\Delta V_{anode}\,(mV) = 55 \log \frac{(\bar{P}_{H_2})_2}{(\bar{P}_{H_2})_1}$		(5-10)
CO Absorption Impact	$\Delta V_{CO}\,(mV) = -11.1\,([CO]_2 - [CO]_1)$	163°C	(5-12)
	$\Delta V_{CO}\,(mV) = --6.14\,([CO]_2 - [CO]_1)$	177°C	
	$\Delta V_{CO}\,(mV) = -3.54\,([CO]_2 - [CO]_1)$	190°C	
	$\Delta V_{CO}\,(mV) = -2.05\,([CO]_2 - [CO]_1)$	204°C	
	$\Delta V_{CO}\,(mV) = -1.30\,([CO]_2 - [CO]_1)$	218°C	
Current Density	$\Delta V_J\,(mV) = -0.53\,)\Delta J$ for $J = 100 - 200\ mA/cm^2$, $P = 8.2\ atm$		(5-17)
	$\Delta V_J\,(mV) = -0.39\,)\Delta J$ for $J = 200 - 650\ mA/cm^2$, $P = 8.2\ atm$		(5-18)
	$\Delta V_J\,(mV) = -0.74\,)\Delta J$ for $J = 50 - 120\ mA/cm^2$, $P = 1\ atm$		(5-19)
	$\Delta V_J\,(mV) = -0.45\,)\Delta J$ for $J = 120 - 215\ mA/cm^2$, $P = 1\ atm$		(5-20)
Life Effects	$\Delta V_{lifetime}\,(mV) = -2mV/1{,}000\ hrs.$		(5-22)

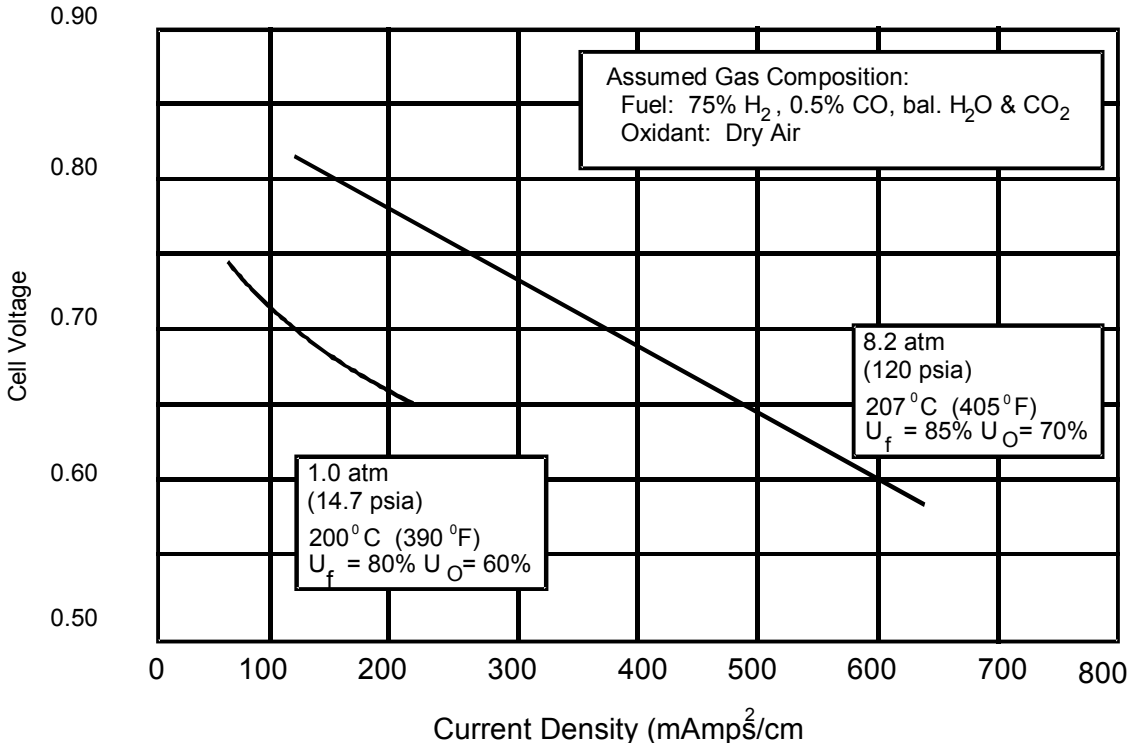

Figure 5-8 Reference Performances at 8.2 atm and Ambient Pressure. Cells from Full Size Power Plant (16)

5.4 References

1. J. Hirschenhofer, "Latest Progress in Fuel Cell Technology," IEEE-Aerospace and Electronic Systems Magazine, 7, November 1992.
2. J. Hirschenhofer, "Status of Fuel Cell Commercialization Efforts," *American Power Conference*, Chicago, IL, April 1993.
3. Meeting with UTC Fuel Cells, June 2002.
4. J. Appleby, in *Proceedings of the Workshop on the Electrochemistry of Carbon*, Edited by S. Sarangapani, J.R. Akridge and B. Schumm, The Electrochemical Society, Inc., Pennington, NJ, p. 251, 1984.
5. K.V. Kordesch, "Survey of Carbon and Its Role in Phosphoric Acid Fuel Cells," BNL 51418, prepared for Brookhaven National Laboratory, December 1979.
6. K. Kinoshita, *Carbon: Electrochemical and Physicochemical Properties*, Wiley Interscience, New York, NY, 1988.
7. L. Christner, J. Ahmad, M. Farooque, in *Proceedings of the Symposium on Corrosion in Batteries and Fuel Cells and Corrosion in Solar Energy Systems,* Edited by C. J. Johnson and S.L. Pohlman, The Electrochemical Society, Inc., Pennington, NJ, p. 140, 1983.
8. P.W.T. Lu, L.L. France, in *Extended Abstracts*, Fall Meeting of The Electrochemical Society, Inc., Volume 84-2, Abstract No. 573, The Electrochemical Society, Inc., Pennington, NJ, p. 837, 1984.

9. M. Warshay, in *The Science and Technology of Coal and Coal Utilization,* Edited by B.R. Cooper, W.A. Ellingson, Plenum Press, New York, NY, p. 339, 1984.
10. P.R. Prokopius, M. Warshay, S.N. Simons, R.B. King, in *Proceedings of the 14th Intersociety Energy Conversion Engineering Conference,* Volume 2, American Chemical Society, Washington, D. C., p. 538, 1979.
11. S.N. Simons, R.B. King, P.R. Prokopius, in *Symposium Proceedings Fuel Cells Technology Status and Applications,* Edited by E. H. Camara, Institute of Gas Technology, Chicago, IL, p. 45, 1982.
12. Communications with IFC, September 2000.
13. A.P. Fickett, in *Proceedings of the Symposium on Electrode Materials and Processes for Energy Conversion and Storage,* Edited by J.D.E. McIntyre, S. Srinivasan and F.G. Will, The Electrochemical Society, Inc. Pennington, NJ, p. 546, 1977.
14. A.J. Appleby, *J. Electroanal, Chem.,* 118**,** 31, 1981.
15. J. Huff, "Status of Fuel Cell Technologies," in *Fuel Cell Seminar Abstracts*, 1986 National Fuel Cell Seminar, Tucson, AZ, October 1986.
16. "Advanced Water-Cooled Phosphoric Acid Fuel Cell Development, Final Report," Report No. DE/MC/24221-3130, International Fuel Cells Corporation for U.S. DOE under Contract DE-AC21-88MC24221, South Windsor, CT, September 1992.
17. N. Giordano, E. Passalacqua, L. Pino, V. Alderucci, P.L. Antonucci, "Catalyst and Electrochemistry in PAFC: A Unifying Approach," in *The International Fuel Cell Conference Proceedings*, NEDO/MITI, Tokyo, Japan, 1992.
18. B. Roland, J. Scholta, H. Wendt, "Phosphoric Acid Fuel Cells - Materials Problems, Process Techniques and Limits of the Technology," in *The International Fuel Cell Conference Proceedings*, NEDO/MITI, Tokyo, Japan, 1992.
19. "Overview of 11 MW Fuel Cell Power Plant," Non-published information from Tokyo Electric Power Company, September 1989.
20. M. Matsumoto, K. Usami, "PAFC Commercialization and Recent Progress of Technology in Mitsubishi Electric," in *The International Fuel Cell Conference Proceedings*, NEDO/MITI, Tokyo, Japan, 1992.
21. J.A.S. Bett, H.R. Kunz, S.W. Smith and L.L. Van Dine, "Investigation of Alloy Catalysts and Redox Catalysts for Phosphoric Acid Electrochemical Systems," FCR-7157F, prepared by International Fuel Cells for Los Alamos National Laboratory under Contract No. 9-X13-D6271-1, 1985.
22. B.C. Beard, P.N. Ross, *J. Electrochem. Soc.,* 133, 1839, 1986.
23. J.T. Glass, G.L. Cahen, G.E. Stoner, E.J. Taylor, *J. Electrochem. Soc.,* 134, 58, 1987.
24. P.N. Ross, "Oxygen Reduction on Supported Pt Alloys and Intermetallic Compounds in Phosphoric Acid," Final Report, EM-1553, prepared under Contract 1200-5 for the Electric Power Research Institute, Palo Alto, CA, September 1980.
25. V. Jalan, J. Giner, in *DECHEMA Monographs,* Volume 102, Edited by J.W. Schultze, VCH Verlagsgesellschaft, Weinheim, West Germany, p. 315, 1986.
26. T. Ito, K. Kato, S. Kamitomai, M. Kamiya, "Organization of Platinum Loading Amount of Carbon-Supported Alloy Cathode for Advanced Phosphoric Acid Fuel Cell," in *Fuel Cell Seminar Abstracts*, 1990 Fuel Cell Seminar, Phoenix, AZ, November 25-28, 1990.
27. J.S. Buchanan, G.A. Hards, L. Keck, R.J. Potter, "Investigation into the Superior Oxygen Reduction Activity of Platinum Alloy Phosphoric Acid Fuel Cell Catalysts," in *Fuel Cell Seminar Abstracts*, Tucson, AZ, November 29-December 2, 1992.

28. K. Kinoshita, F.R. McLarnon, E.J. Cairns, *Fuel Cells, A Handbook*, prepared by Lawrence Berkeley Laboratory for the U.S. Department of Energy under Contract DE-AC03-76F00098, May 1988.
29. N.D. Kackley, S.A. McCatty, J.A. Kosek, "Improved Anode Catalysts for Coal Gas-Fueled Phosphoric Acid Fuel Cells," Final Report DOE/MC/25170-2861, prepared for U.S. Department of Energy under Contract DE-AC21-88MC25170, July 1990.
30. M. Watanabe, C. Shirmura, N. Hara, K. Tsurumi, "An Advanced Gas-Diffusion Electrode for Long-Life and High Performance PAFC," in *The International Fuel Cell Conference Proceedings*, NEDO/MITI, Tokyo, Japan, 1992.
31. M. Aoki, Y. Ueki, H. Enomoto, K. Harashima, "Some Approaches to Improve the Life Performance of Phosphoric Acid Fuel Cell," paper provided to the authors by Fuji Electric Corporate Research and Development, 1992, date of preparation unknown.
32. M. Watanabe, H. Sei, P. Stonehart, *Journal of Electroanalytical Chemistry*. 261, 375, 1989.
33. M. Farooque, "Evaluation of Gas-Cooled Pressurized Phosphoric Acid Fuel Cells for Electric Utility Power Generation," Final Technical Report, NASA CR-168298 prepared by Energy Research Corp. under Contract No. DEN 3-201 for NASA Lewis Research Center, September 1983.
34. J. McBreen, W.E. O'Grady, R. Richter, *J. Electrochem. Soc.,* 131**,** 1215, 1984.
35. T.G. Benjamin, E.H. Camara, L.G. Marianowski, *Handbook of Fuel Cell Performance,* prepared by the Institute of Gas Technology for the United States Department of Energy under Contract No. EC-77-C-03-1545, May 1980.
36. J.M. Feret, "Gas Cooled Fuel Cell Systems Technology Development," Final Report, NASA CR-175047, prepared by Westinghouse Electric Corp. under Contract No. DEN 3-290 for NASA Lewis Research Center, August 1985.
37. V. Jalan, J. Poirier, M. Desai, B. Morrisean, "Development of CO and H_2S Tolerant PAFC Anode Catalysts," in *Proceedings of the Second Annual Fuel Cell Contractors Review Meeting*, 1990.
38. P.W.T. Lu and L. L. France, in *Proceedings of the Symposium on Transport Processes in Electrochemical Systems,* R. S. Yeo, K. Katan and D. T. Chin, The Electrochemical Society, Inc., Pennington, NJ, p. 77, 1982.
39. P.N. Ross, "Anomalous Current Ratios in Phosphoric Acid Fuel Cell Cathodes," LBL-13955; submitted to *J. Electrochem. Soc.*, March 1986.
40. P.Ross, P. Stonehart, *Electrochim. Acta,* 21**,** 441, 1976.
41. W. Vogel, J. Lundquist, P. Ross, P. Stonehart, *Electrochim. Acta,* 20**,** 79, 1975.
42. H.R. Kunz, in *Proceedings of the Symposium on Electrode Materials and Processes for Energy Conversion and Storage,* Edited by J. D. E. McIntyre, S. Srinivasan and F. G. Will, The Electrochemical Society, Inc., Pennington, NJ, p. 607, 1977.
43. D.T. Chin, P.D. Howard, *J. Electrochem. Soc.,* 133, 2447, 1986.
44. S.T. Szymanski, G.A. Gruver, M. Katz, H.R. Kunz, *J. Electrochem. Soc.,* 127, 1440, 1980.
45. F.S. Kemp, IFC, "Status of Development of Water - Cooled Phosphoric Acid Fuel Cells," in *Proceedings of the Second Annual Fuel Cell Contractors Review Meeting*, U.S. DOE/METC, 1990.
46. N. Giordano, "Fuel Cells Activity at CNR, TAE Institute," CNR/TAE, Italy, 1992.
47. "Gas Cooled Fuel Cell Systems Technology Development," Westinghouse/DOE, WAES-TR-92-001, March 1992.
48. K. Harasawa, I. Kanno, I. Masuda, "Fuel Cell R&D and Demonstration Programs at Electric Utilities in Japan," in *Fuel Cell Seminar Abstracts*, Tucson, AZ, November 29-December 2, 1992.

6. MOLTEN CARBONATE FUEL CELL

The molten carbonate fuel cell operates at approximately 650°C (1200°F). The high operating temperature is needed to achieve sufficient conductivity of its carbonate electrolyte, yet allow the use of low-cost metal cell components. A benefit associated with this high temperature is that noble metal catalysts are not required for the cell electrochemical oxidation and reduction processes. Molten carbonate fuel cells are being developed for natural gas and coal-based power plants for industrial, electrical utility, and military applications[22]. Currently, one industrial corporation is actively pursuing the commercialization of MCFCs in the U.S.: FuelCell Energy (FCE). Europe and Japan each have at least one developer pursuing the technology: MTU Friedrichshafen, Ansaldo (Italy), and Ishikawajima-Harima Heavy Industries (Japan).

Figure 6-1 depicts the operating configuration of the molten carbonate fuel cell. The half cell electrochemical reactions are

$$H_2 + CO_3^{=} \rightarrow H_2O + CO_2 + 2e^- \qquad (6\text{-}1)$$

at the anode, and

$$\tfrac{1}{2}O_2 + CO_2 + 2e^- \rightarrow CO_3^{=} \qquad (6\text{-}2)$$

at the cathode. The overall cell reaction[23] is

$$H_2 + \tfrac{1}{2}O_2 + CO_2\ (\text{cathode}) \rightarrow H_2O + CO_2\ (\text{anode}) \qquad (6\text{-}3)$$

[22]. MCFCs operate more efficiently with CO_2 containing bio-fuel derived gases. Performance loss on the anode due to fuel dilution is compensated by cathode side performance enhancement resulting from CO_2 enrichment.

[23]. CO is not directly used by electrochemical oxidation, but produces additional H_2 when combined with water in the water gas shift reaction.

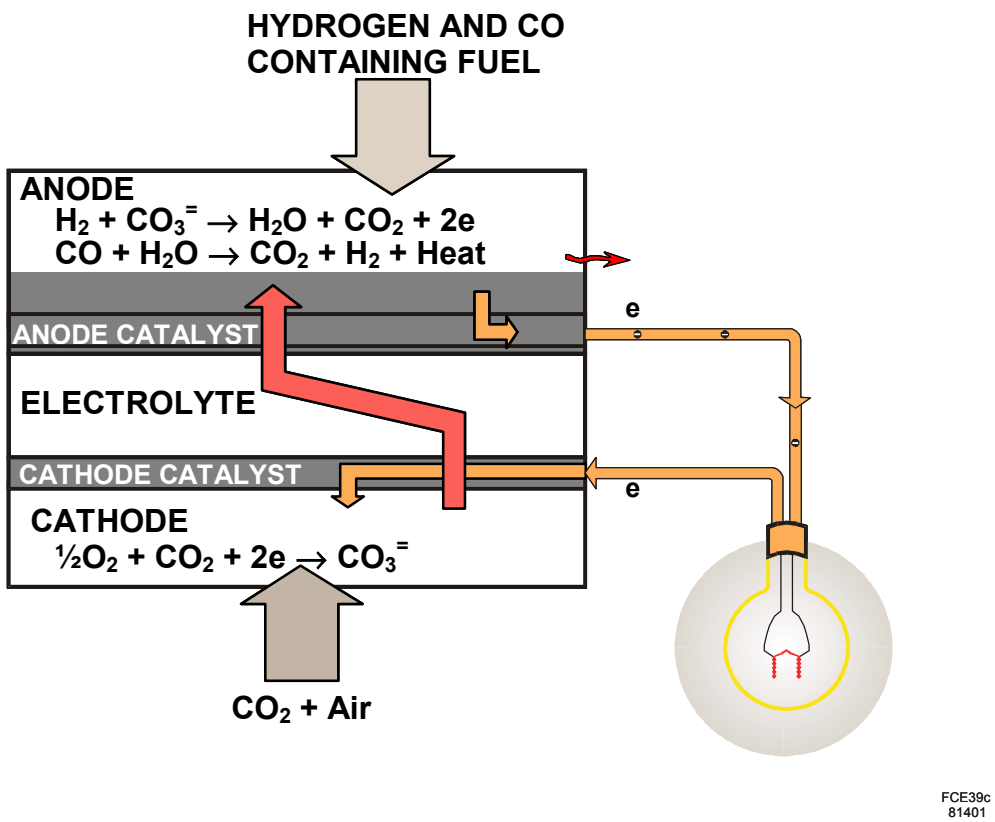

Figure 6-1 Principals of Operation of Molten Carbonate Fuel Cells (FuelCell Energy)

Besides the reaction involving H_2 and O_2 to produce H_2O, Equation 6-3 shows a transfer of CO_2 from the cathode gas stream to the anode gas stream via the $CO_3^=$ ion, with 1 mole CO_2 transferred along with two Faradays of charge, or 2 gram moles of electrons. The reversible potential for an MCFC, taking into account the transfer of CO_2, is given by the equation

$$E = E^\circ + \frac{RT}{2F}\ln\frac{P_{H_2}P_{O_2}^{1/2}}{P_{H_2O}} + \frac{RT}{2F}\ln\frac{P_{CO_{2,c}}}{P_{CO_{2,a}}} \qquad (6\text{-}4)$$

where the subscripts a and c refer to the anode and cathode gas compartments, respectively. When the partial pressures of CO_2 are identical at the anode and cathode, and the electrolyte is invariant, the cell potential depends only on the partial pressures of H_2, O_2, and H_2O. Typically, the CO_2 partial pressures are different in the two electrode compartments and the cell potential is affected accordingly.

The need for CO_2 at the cathode requires some schemes that will either 1) transfer the CO_2 from the anode exit gas to the cathode inlet gas ("CO_2 transfer device"), 2) produce CO_2 by combustion of the anode exhaust gas, which is mixed directly with the cathode inlet gas, or 3) supply CO_2 from

an alternate source. It is usual practice in an MCFC that the CO_2 generated at the anode be routed (external to the cell) to the cathode.

MCFCs differ in many respects from PAFCs because of their higher operating temperature (650 vs. 200°C) and the nature of the electrolyte. The higher operating temperature of MCFCs provides the opportunity to achieve higher overall system efficiencies (potential for heat rates below 7,500 Btu/kWh) and greater flexibility in the use of available fuels.[24] On the other hand, the higher operating temperature places severe demands on the corrosion stability and life of cell components, particularly in the aggressive environment of the molten carbonate electrolyte. Another difference between PAFCs and MCFCs lies in the method used for electrolyte management in the respective cells. In a PAFC, PTFE serves as a binder and wet-proofing agent to maintain the integrity of the electrode structure and to establish a stable electrolyte/gas interface in the porous electrode. The phosphoric acid is retained in a matrix of PTFE and SiC between the anode and cathode. There are no high temperature, wetproofing materials available for use in MCFCs that are comparable to PTFE. Thus, a different approach is required to establish a stable electrolyte/gas interface in MCFC porous electrodes, and this is illustrated schematically in Figure 6-2. The MCFC relies on a balance in capillary pressures to establish the electrolyte interfacial boundaries in the porous electrodes (1, 2, 3). At thermodynamic equilibrium, the diameters of the largest flooded pores in the porous components are related by the equation

$$\frac{\gamma_c \cos\theta_c}{D_c} = \frac{\gamma_e \cos\theta_e}{D_e} = \frac{\gamma_a \cos\theta_a}{D_a} \qquad (6\text{-}5)$$

where γ is the interfacial surface tension, θ is the contact angle of the electrolyte, D is the pore diameter, and the subscripts a, c, and e refer to the anode, cathode and electrolyte matrix, respectively. By properly coordinating the pore diameters in the electrodes with those of the electrolyte matrix, which contains the smallest pores, the electrolyte distribution depicted in Figure 6-2 is established. This arrangement permits the electrolyte matrix to remain completely filled with molten carbonate, while the porous electrodes are partially filled, depending on their pore size distributions. According to the model illustrated in Figure 6-2 and described by Equation (6-5), the electrolyte content in each of the porous components will be determined by the equilibrium pore size (<D>) in that component; pores smaller than <D> will be filled with electrolyte, and pores larger than <D> will remain empty. A reasonable estimate of the volume distribution of electrolyte in the various cell components is obtained from the measured pore-volume-distribution curves and the above relationship for D (2, 3).

Electrolyte management, that is, control over the optimum distribution of molten carbonate electrolyte in the different cell components, is critical for achieving high performance and endurance with MCFCs. Various processes (i.e., consumption by corrosion reactions, potential-driven migration, creepage of salt and salt vaporization) occur, all of which contribute to the redistribution of molten carbonate in MCFCs; these aspects are discussed by Maru, et al. (4) and Kunz (5).

---

[24]. *In situ* reforming of fuels in MCFCs is possible as discussed later in the section.

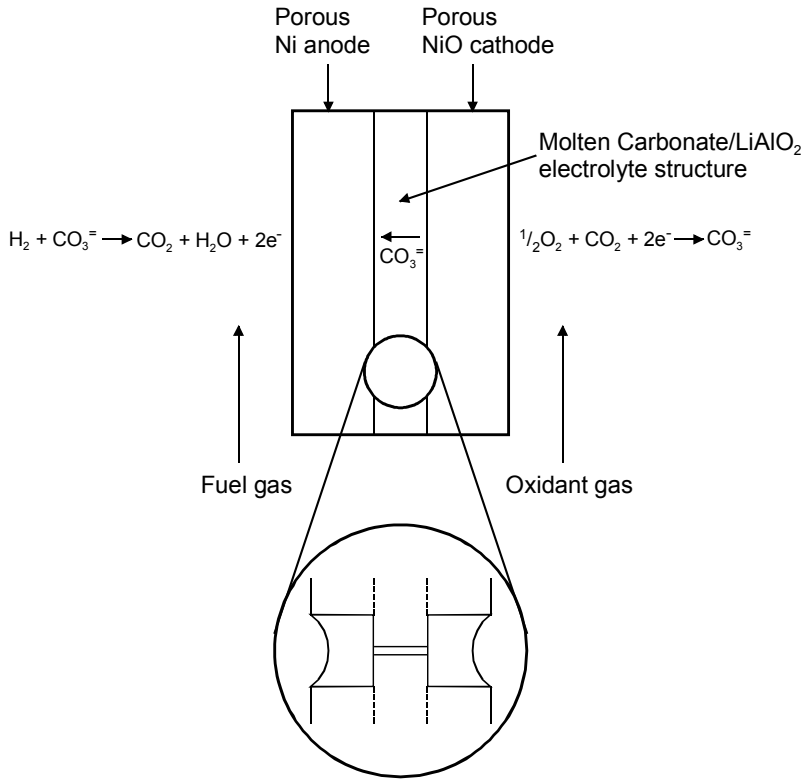

Figure 6-2 Dynamic Equilibrium in Porous MCFC Cell Elements
(Porous electrodes are depicted with pores covered by a thin film of electrolyte)

6.1 Cell Components

6.1.1 State-of-the-Art Componments

The data in Table 6-1 provide a chronology of the evolution in MCFC component technology. In the mid-1960s, electrode materials were, in many cases, precious metals, but the technology soon evolved to use Ni-based alloys at the anode and oxides at the cathode. Since the mid-1970s, the materials for the electrodes and electrolyte (molten carbonate/$LiAlO_2$) have remained essentially unchanged. A major development in the 1980s was the evolution in fabrication of electrolyte structures. Developments in cell components for MCFCs have been reviewed by Maru, et al. (6, 7), Petri and Benjamin (8), and Selman (9). Over the past 28 years, the performance of single cells has improved from about 10 mW/cm^2 to >150 mW/cm^2. During the 1980s, both the performance and endurance of MCFC stacks showed dramatic improvements. The data in Figure 6-3 illustrate the progress that has been made in the performance of single cells, and in the cell voltage of small stacks at 650°C. Several MCFC stack developers have produced cell stacks with cell areas up to 1 m^2. Tall, full-scale U.S. stacks fabricated to date include several FCE 300 plus cell stacks with ~9000 cm^2 cell area producing >250 kW.

Table 6-1 Evolution of Cell Component Technology for Molten Carbonate Fuel Cells

Component	Ca. 1965	Ca. 1975	Current Status
Anode	• Pt, Pd, or Ni	• Ni-10 Cr	• Ni-Cr/Ni-Al/Ni-Al-Cr • 3-6 μm pore size • 45-70% initial porosity • 0.20-1.5 mm thickness • 0.1-1 m^2/g
Cathode	• Ag_2O or lithiated NiO	• lithiated NiO	• lithiated NiO-MgO • 7-15 μm pore size • 70-80% initial porosity • 60-65% after lithiation and oxidation • 0.5-1 mm thickness • 0.5 m^2/g
Electrolyte Support	• MgO	• mixture of α-, β-, and γ-$LiAlO_2$ • 10-20 m^2/g • 1.8 mm thickness	• γ-$LiAlO_2$, α-$LiAlO_2$ • 0.1-12 m^2/g • 0.5-1 mm thickness
Electrolyte[a] (wt%)	• 52 Li-48 Na • 43.5 Li-31.5 Na-25 K • "paste"	• 62 Li-38 K • hot press "tile" • 1.8 mm thickness	• 62 Li-38 K • 60 Li-40 Na 51 Li-48 Na • tape cast • 0.5-1 mm thickness

a - Mole percent of alkali carbonate salt

Specifications for the anode and cathode were obtained from References (6), (10), and (11).

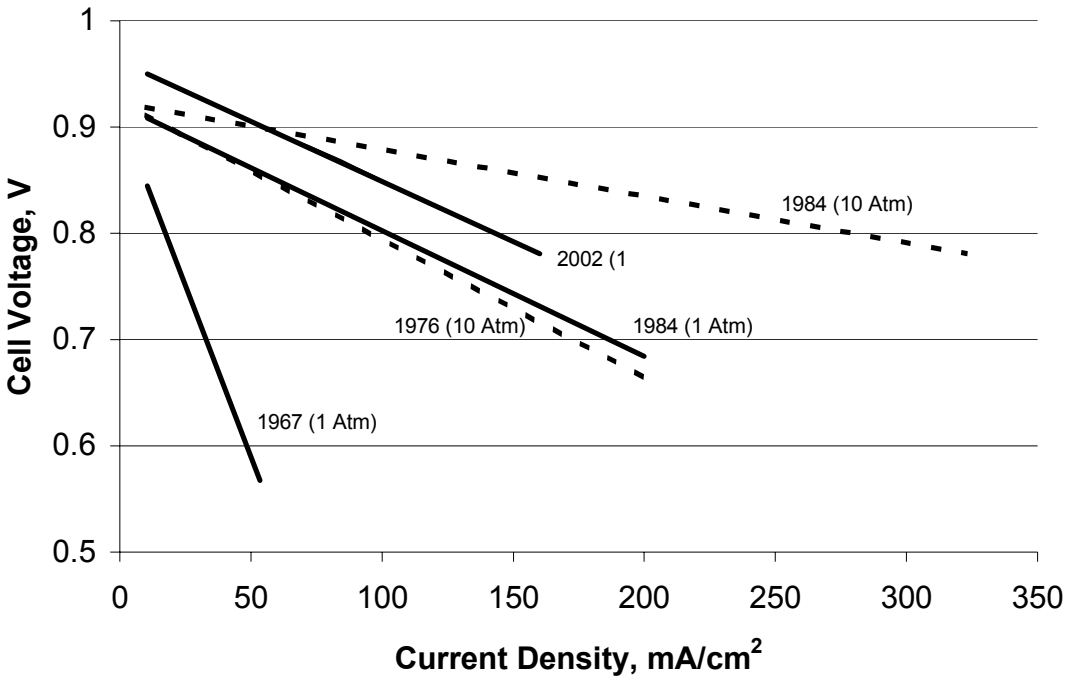

Figure 6-3 Progress in the Generic Performance of MCFCs on Reformate Gas and Air (12, 13)

The conventional process to fabricate electrolyte structures until about 1980 involved hot pressing (about 5,000 psi) mixtures of $LiAlO_2$ and alkali carbonates (typically >50 vol% in liquid state) at temperatures slightly below the melting point of the carbonate salts (e.g., 490°C for electrolyte containing 62 mol% Li_2CO_3-38 mol% K_2CO_3). These electrolyte structures (also called "electrolyte tiles") were relatively thick (1-2 mm) and difficult to produce in large sizes[25] because large tooling and presses were required. The electrolyte structures produced by hot pressing are often characterized by 1) void spaces (<5% porosity), 2) poor uniformity of microstructure, 3) generally poor mechanical strength, and 4) high iR drop. To overcome these shortcomings of hot pressed electrolyte structures, alternative processes such as tape casting (7) and electrophoretic deposition (14) for fabricating thin electrolyte structures were developed. The greatest success to date with an alternative process has been reported with tape casting, which is a common processing technique used by the ceramics industry. This process involves dispersing the ceramic powder in a solvent[26] that contains dissolved binders (usually an organic compound), plasticizers, and additives to yield the proper slip rheology. The slip is cast over a moving smooth substrate, and the desired thickness is established with a doctor blade device. After drying the slip, the "green" structure is assembled into the fuel cell where the organic binder is removed by thermal decomposition, and the absorption of alkali carbonate into the ceramic structure occurs during cell startup. Deposition (14) for fabricating thin electrolyte structures was developed.

---

[25]. The largest electrolyte tile produced by hot pressing was about 1.5 m^2 in area (7).
[26]. An organic solvent is used because $LiAlO_2$ in the slip reacts with H_2O.

The tape casting and electrophoretic deposition processes are amenable to scale-up, and thin electrolyte structures (0.25-0.5 mm) can be produced. The ohmic resistance of an electrolyte structure[27] and the resulting ohmic polarization have a large influence on the operating voltage of MCFCs (15). FCE has stated that the electrolyte matrix encompasses 70% of the ohmic loss (16) of the cell. At a current density of 160 mA/cm^2, the voltage drop (ΔV_{ohm}) of an 0.18 cm thick electrolyte structure, with a specific conductivity of ~0.3/ohm-cm at 650°C, was found to obey the relationship (14),

$$\Delta V_{ohm}\,(V) = 0.5t \qquad (6\text{-}6)$$

where ΔV_{ohm} is in volts and t is the thickness in cm. Later data confirm this result (16). With this equation, it is apparent that a fuel cell with an electrolyte structure of 0.25 cm thickness would operate at a cell voltage that is 35 mV higher than that of an identical cell with an electrolyte structure of 0.18 cm thickness because of the lower ohmic loss. Thus, there is a strong incentive for making thinner electrolyte structures to improve cell performance.

The electrolyte composition affects the performance and endurance of MCFCs in several ways. Higher ionic conductivities, and hence lower ohmic polarization, are achieved with Li-rich electrolytes because of the relative high ionic conductivity of Li_2CO_3 compared to that of Na_2CO_3 and K_2CO_3. However, gas solubility and diffusivity are lower, and corrosion is more rapid in Li_2CO_3.

The major considerations with Ni-based anodes and NiO cathodes are structural stability and NiO dissolution, respectively (9). Sintering and mechanical deformation of the porous Ni-based anode under compressive load lead to performance decay by redistribution of electrolyte in a MCFC stack. The dissolution of NiO in molten carbonate electrolyte became evident when thin electrolyte structures were used. Despite the low solubility of NiO in carbonate electrolytes (~10 ppm), Ni ions diffuse in the electrolyte towards the anode, and metallic Ni can precipitate in regions where a H_2 reducing environment is encountered. The precipitation of Ni provides a sink for Ni ions, and thus promotes the diffusion of dissolved Ni from the cathode. This phenomenon becomes worse at high CO_2 partial pressures (17, 18) because dissolution may involve the following mechanism:

$$NiO + CO_2 \rightarrow Ni^{2+} + CO^{=}_3 \qquad (6\text{-}7)$$

The dissolution of NiO has been correlated to the acid/base properties of the molten carbonate. The basicity of the molten carbonate is defined as equal to -log (activity of $O^{=}$) or -log a_{M_2O}, where a is the activity of the alkali metal oxide M_2O. Based on this definition, acidic oxides are associated with carbonates (e.g., K_2CO_3) that do not dissociate to M_2O, and basic oxides are formed with highly dissociated carbonate salts (e.g., Li_2CO_3). The solubility of NiO in binary

[27]. Electrolyte structures containing 45 wt% $LiAlO_2$ and 55 wt% molten carbonate (62 mol% Li_2CO_3-38 mol% K_2CO_3) have a specific conductivity at 650°C of about 1/3 that of the pure carbonate phase (15).

carbonate melts shows a clear dependence on the acidity/basicity of the melt (19, 20). In relatively acidic melts, NiO dissolution can be expressed by

$$NiO \rightarrow Ni^{2+} + O^{=} \qquad (6\text{-}8)$$

In basic melts, NiO reacts with $O^{=}$ to produce one of two forms of nickelate ions:

$$NiO + O^{=} \rightarrow NiO_2^{=} \qquad (6\text{-}9)$$

$$2NiO + O^{=} + \tfrac{1}{2}O_2 \rightarrow 2NiO_2^{-} \qquad (6\text{-}10)$$

A distinct minimum in NiO solubility is observed in plots of log (NiO solubility) versus basicity (-log a_{M_2O}), which can be demarcated into two branches corresponding to acidic and basic dissolution. Acidic dissolution is represented by a straight line with a slope of +1, and a NiO solubility that decreases with an increase in a_{M_2O}. Basic dissolution is represented by a straight line with a slope of either -1 or -½, corresponding to Equations (6-9) and (6-10), respectively. The CO_2 partial pressure is an important parameter in the dissolution of NiO in carbonate melts because the basicity is directly proportional to log P_{CO_2}. An MCFC usually operates with a molten carbonate electrolyte that is acidic.

Based on 12,000-hour full-size stack tests as well as post-test results, FCE believes that Ni dissolution and subsequent precipitation will not be an issue for the desired 40,000-hour (5-yr) life (21) at atmospheric pressure. But at 10 atm cell pressure, only about 5,000 to 10,000 hours may be possible with currently available NiO cathodes (22). The solubility of NiO in molten carbonates is complicated by its dependence on several parameters: carbonate composition, H_2O partial pressure, CO_2 partial pressure, and temperature. For example, measurements of NiO dissolution by Kaun (23) indicate that solubility is affected by changing the electrolyte composition; a lower solubility is obtained in a Li_2CO_3-K_2CO_3 electrolyte that contains less Li_2CO_3 (i.e., lower solubility in 38 mol% Li_2CO_3-62 mol% K_2CO_3 than in 62 mol% Li_2CO_3-38 mol% K_2CO_3 at 650°C). However, the solubility of Ni increases in the electrolyte with 38 mol% Li_2CO_3 when the temperature decreases, whereas the opposite trend is observed in the electrolyte with 62 mol% Li_2CO_3. Another study reported by Appleby (24) indicates that the solubility of Ni decreases from 9 to 2 ppm by increasing the Li concentration in Li_2CO_3-K_3CO_3 from 62 to 75 wt%, and a lower solubility is obtained in 60 mol% Li_2CO_3-40 mol% Na_2CO_3 at 650°C. The compaction of cathodes became evident in MCFC stacks once the anode creep was eliminated when strengthened by oxide dispersion [i.e., oxide dispersion strengthened (ODS) anode].

The bipolar plates used in MCFC stacks are usually fabricated from thin (~15 mil) sheets of an alloy (e.g., Incoloy 825, 310S or 316L stainless steel) that are coated on one side (i.e., the side

exposed to fuel gases in the anode compartment) with a Ni layer. The Ni layer is stable in the reducing gas environment of the anode compartment, and it provides a conductive surface coating with low contact resistance. Pigeaud et al. describe approaches to circumvent the problems associated with gas leaks and corrosion of bipolar plates (25). Corrosion is largely overcome by application of a coating (about 50 μm thickness) at the vulnerable locations on the bipolar plate. For example, the wet-seal[28] area on the anode side is subject to a high chemical potential gradient because of the fuel gas inside the cell and the ambient environment (usually air) on the outside of the cell, which promotes corrosion (about two orders of magnitude greater than in the cathode wet-seal area (26)). Donado et al. present a general discussion on corrosion in the wet-seal area of MCFCs (27). A thin aluminum coating in the wet-seal area of a bipolar plate provides corrosion protection by forming a protective layer of $LiAlO_2$ after reaction of Al with Li_2CO_3 (28). Such a protective layer would not be useful in areas of the bipolar plate that must permit electronic conduction because $LiAlO_2$ is an insulating material.

A dense and electronically insulating layer of $LiAlO_2$ is not suitable for providing corrosion resistance to the cell current collectors because these components must remain electrically conductive. The typical materials used for this application are 316 stainless steel and Ni plated stainless steels. However, materials with better corrosion resistance are required for long-term operation of MCFCs. Research is continuing to understand the corrosion processes of high-temperature alloys in molten carbonate salts under both fuel gas and oxidizing gas environments (29, 26) and to identify improved alloys (30) for MCFCs. Stainless steels such as Type 310 and 446 have demonstrated better corrosion resistance than Type 316 in corrosion tests (30).

6.1.2 Development Components

MCFC components are limited by several technical considerations (31), particularly those described in Section 6.1.1. Even though present approaches function properly in full size cells at atmospheric pressure, research is addressing alternate cathode materials and electrolytes, performance improvement, life extension beyond the commercialization goal of five years, and cost reduction (32). The studies described in recent literature provide updated information on promising development of the electrodes, the electrolyte matrix, and the capability of the cell to tolerate trace contaminants in the fuel supply. Descriptions of some of this work follow.

Anode: As stated in Section 6.1.1 and Reference (33), state-of-the-art anodes are made of a Ni-Cr/Ni-Al alloy. The Cr was added to eliminate the problem of anode sintering. However, Ni-Cr anodes are susceptible to creep when placed under the torque load required in the stack to minimize contact resistance between components. The Cr in the anode is also lithiated by the electrolyte; then it consumes carbonate. Developers are trying lesser amounts of Cr (8%) to reduce the loss of electrolyte, but some have found that reducing the Cr by 2 percentage points increased creep (34). Several developers have tested Ni-Al alloy anodes that provide creep resistance with minimum electrolyte loss (34, 35, 36). The low creep rate with this alloy is attributed to the formation of $LiAlO_2$ dispersed in Ni (35).

---

[28]. The area of contact between the outer edge of the bipolar plate and the electrolyte structure prevents gas from leaking out of the anode and cathode compartments. The gas seal is formed by compressing the contact area between the electrolyte structure and the bipolar plate so that the liquid film of molten carbonate at operating temperature does not allow gas to permeate through.

Even though chromium and/or aluminum alloys strengthen nickel and provides a stable, non-sintering, creep-resistant anode, electrodes made with Ni are relatively high in cost. Alloys, such as Cu-Al and $LiFeO_2$, have not demonstrated sufficient creep strength or performance. Because of this, present research is focused on reducing the manufacturing cost of the nickel alloy anodes (37).

There is a need for better sulfur tolerance in MCFCs, especially when considering coal operation. The potential benefit for sulfur tolerant cells is to eliminate cleanup equipment that impacts system efficiency. This is especially true if low temperature cleanup is required, because the system efficiency and capital cost suffer when the fuel gas temperature is first reduced, then increased to the cell temperature level. Tests are being conducted on ceramic anodes to alleviate the problems, including sulfur poisoning, being experienced with anodes (31). Anodes are being tested with undoped $LiFeO_2$ and $LiFeO_2$ doped with Mn and Nb. Preliminary testing where several parameters were not strictly controlled showed that the alternative electrodes exhibited poor performance and would not operate over 80 mA/cm^2. At the present time, no alternative anodes have been identified. Instead, future work will focus on tests to better understand material behavior and to develop other alternative materials with emphasis on sulfur tolerance.

***Cathode**:* An acceptable material for cathodes must have adequate electrical conductivity, structural strength, and low dissolution rate in molten alkali carbonates to avoid precipitation of metal in the electrolyte structure. State-of-the art cathodes are made of lithiated NiO (33, 38) that have acceptable conductivity and structural strength. However, in early testing, a predecessor of UTC Fuel Cells found that the nickel dissolved, then precipitated and reformed as dendrites across the electrolyte matrix. This decreased performance and eventual short-circuting of the cell (see Section 6.1.1). Dissolution of the cathode has turned out to be the primary life-limiting constraint of MCFCs, particularly in pressurized operation (35). Developers are investigating approaches to resolve the NiO dissolution issue. For atmospheric cells, developers are looking at increasing the basicity of the electrolyte (use a more basic melt such as $Li/NaCO_3$). Another approach is to lower CO_2 (acidic) partial pressure. To operate at higher pressures (higher CO_2 partial pressure), developers are investigating alternative materials for the cathodes and using additives in the electrolyte to increase its basicity (37).

Initial work on $LiFeO_2$ cathodes showed that electrodes made with this material were very stable chemically under the cathode environment; there was essentially no dissolution (31). However, these electrodes perform poorly compared to the state-of-the-art NiO cathode at atmospheric pressure because of slow kinetics. The electrode shows promise at pressurized operation, so it is still being investigated. Higher performance improvements are expected with Co-doped $LiFeO_2$. It also has been shown that 5 mol% lithium doped NiO with a thickness of 0.02 cm provided a 43 mV overpotential (higher performance) at 160 mA/cm^2 compared to the state-of-the-art NiO cathode. It is assumed that reconfiguring the structure, such as decreasing the agglomerate size, could improve performance.

Another idea for resolving the cathode dissolution problem is to formulate a milder cell environment. This leads to the approach of using additives in the electrolyte to increase its basicity. Small amounts of additives provide similar voltages to those without additives, but larger amounts adversely affect performance (39). Table 6-2 quantifies the limiting amounts of additives.

Table 6-2 Amount in Mol% of Additives to Provide Optimum Performance (39)

	62 MOL% Li_2CO_3/K_2CO_2	52 MOL% Li_2CO_3/NA_2CO_3
$CaCO_3$	0 – 15	0 - 5
$SrCO_3$	0 – 5	0 - 5
$BaCO_3$	0 - 10	0 - 5

Another approach to a milder cell environment is to increase the fraction of Li in the baseline electrolyte or change the electrolyte to Li/Na rather than the baseline 62/38 Li/K melt (29, 39, 40). Within the past 10 years, a lower cost stabilized cathode was developed with a base material cost comparable to the unstabilized cathode (41). A 100 cm^2 cell test of the lower-cost stabilized cathode with a Li/Na electrolyte system completed 10,000 hours of operation.

Electrolyte Matrix: The present electrolyte structure materials are tightly packed, fine α- or γ-$LiAlO_2$ with fiber or particulate reinforcement. Long-term cell testing reveals significant particle growth and γ to α phase transformation, leading to detrimental changes in the pore structure. The particles grow faster at higher temperatures, in low CO_2 gas atmospheres, and in strongly basic melts. The γ phase is stable at > 700°C, whereas the α phase is stable at 600 to 650°C. Such particle growth and phase transformations can be explained by a dissolution - precipitation mechanism. The matrix must also be strong enough to counter operating mechanical and thermal stresses, and still maintain the gas seal. Thermal cycling below the carbonate freezing temperature can induce cracking due to thermo-mechanical stress. Ceramic fiber reinforcement is the most effective for crack deflection, followed by platelet and sphere forms. However, strong, cost effective, and stable ceramic fibers are not yet commercially available. Long-term intense material research may be needed to develop such ceramic fibers. If particle sizes are markedly different, the phase transformation is more controlled by the particle sizes, according to Ostwald ripening where small particles preferentially dissolve and re-precipitate onto larger particles. Therefore, a more uniform particle size distribution is needed to maintain a desired pore structure. The industry trend is to switch from γ-$LiAlO_2$ to α-$LiAlO_2$ for better long-term phase and particle-size stabilities. FCE is developing a low cost $LiAlO_2$, aqueous-base manufacturing system, but must resolve slow drying rate of $LiAlO_2$ and its instability in water (42).

Electrolyte: Present electrolytes have the following chemistry: lithium potassium carbonate, Li_2CO_3/K_2CO_3 (62:38 mol%) for atmospheric pressure operation and lithium sodium carbonate, $LiCO_3/NaCO_3$ (52:48 o 60:40 mol%) that is better for improved cathode stability under pressurized operation and life extension. The electrolyte composition affects electrochemical activity, corrosion, and electrolyte loss rate. Evaporation of the electrolyte is a life-limiting issue for the molten carbonate fuel cell. Li/Na electrolyte is better for higher-pressure operation than Li/K because it gives higher performance. This allows the electrolyte matrix to be made thicker for the same performance relative to the Li/K electrolyte. Thicker electrolytes result in a longer time to shorting by internal precipitation. Li/Na also provides better corrosion resistance to

mitigate acidic cathode dissolution. However, it has lower wettability and greater temperature sensitivity. Additives are being investigated to minimize the temperature sensitivity of Li/Na. The electrolyte has a low vapor pressure at operating temperature and may slowly evaporate. Stack testing has shown that the electrolyte vapor loss is significantly slower than expected from equilibrium. The evaporation loss is projected to have minimal impact on stack life.

***Electrolyte Structure**:* Ohmic losses contribute about a 65 mV loss at the beginning of life, and may increase to as much as 145 mV by 40,000 hours (16). The majority of the voltage loss is in the electrolyte and the cathode components. The electrolyte offers the highest potential for reduction because 70% of the total cell ohmic loss occurs there. FCE investigated increasing the porosity of the electrolyte 5% to reduce the matrix resistance by 15%, and change the melt to Li/Na from Li/K to reduce the matrix resistivity by 40%. Work is continuing on the interaction of the electrolyte with the cathode components. At the present time, an electrolyte loss of 25% of the initial inventory can be projected with a low surface area cathode current collector and with the proper selection of material.

Another area for electrolyte improvement is the ability to prevent gas crossover from one electrode to the other. FCE produced an improved matrix fabrication process providing low temperature binder burnout. FCE reported in 1997 that it had developed a high performance rugged matrix that increases the gas sealing efficiency by approximately a factor of ten better than the design goal (43).

***Electrolyte Migration**:* There is a tendency for the electrolyte to migrate from the positive end of the stack to the negative end of the stack. This may cause the end cells to lose performance compared to the central cells. The electrolyte loss is through the gasket used to couple the external manifolds to the cell stack. The standard gasket material is porous and provides a conduit for electrolyte transfer. A new gasket design incorporating electrolyte flow barriers inside the gasket (US Patent 5,110,692) plus end cell inventory capability offers the potential for reaching 40,000 hours, if only this mode of failure is considered. Stacks with internal manifolding do not require a gasket and may not experience this problem (44).

Bipolar Plate: The present bipolar plate consists of a separator, current collectors, and the wet seal. The separator and current collector is Ni-coated 310S/316L and the wet seal is formed by aluminization of the metal. The plate is exposed to the anode environment of one side and the cathode environment on the other. Low oxygen partial pressure on the anode side of the bipolar plate prevents the formation of a protective oxide coating. After reaction with the thin, creeping electrolyte, heat-resistant alloys form a multi-layered corrosion scale. This condition may be accelerated by carbonization, higher temperature, and higher moisture gas environment. On the cathode side, contact electrical resistance increases as an oxide scale builds up. Electrolyte loss due to corrosion and electrolyte creep also contributes to power decay. Single alloy bipolar current collector materials that function well in both anode and cathode environments need to be developed. Although such development has been attempted, high cost and high ohmic resistance prevent it from being successful. Presently, stainless steels, particularly austenitic stainless steels, are the primary construction materials. More expensive nickel based alloys resist corrosion as well as or only slightly better than austenitic stainless steels. A thermodynamically stable nickel coating is needed to protect the anode side. Unfortunately, electroless nickel

coatings, although dense and uniform in thickness, are expensive and contain detrimental impurities; and electrolytic nickel coatings are not sufficiently dense and uniform in thickness. FCE and others have found that cladding with nickel provides excellent corrosion protection. A nickel cladding of 50 μm thickness is projected for >40,000 hours of life (42).

***Coal Gas Trace Species**:* MCFCs to date have been operated on reformed or simulated natural gas and simulated coal gas. Testing conducted with simulated coal gas has involved the expected individual and multi-trace constituents to better understand coal operation (45).

Table 6-3 shows the contaminants and their impact on MCFC operation. The table denotes the species of concern and what cleanup of the fuel gas is required to operate on coal gas. Confidence in operation with coal will require the use of an actual gasifier product. An FCE MCFC stack was installed (fall of 1993) using a slipstream of an actual coal gasifier to further clarify the issues of operation with trace gases (46).

Table 6-3 Qualitative Tolerance Levels for Individual Contaminants in Isothermal Bench-Scale Carbonate Fuel Cells (46, 47, and 48)
(Only 4 out of the 10 contaminants studied appear to have a significant effect)

CONTAMINANTS (typical ppm in raw coal gas)	REACTION MECHANISM	QUALITATIVE TOLERANCES	CONCLUSIONS
NO NOTICEABLE EFFECTS			
NH_3 (10,000) Cd (5) Hg (1) Sn (3)	$2NH_3 \rightarrow N_2+3H_2$ $Cd+H_2O \rightarrow CdO(s)+H_2$ (Hg Vapor Not Reactive) (Sn(l) Not Volatile)	~1 vol% NH_3 ~30 ppm Cd 35 ppm Hg No Vapor @ 650°C	No Effects No Cell Deposits No TGA Effects No Cell Deposits
MINOR EFFECTS			
Zn (100) Pb (15)	$Zn+H_2O \rightarrow ZnO(s)+H_2$ $Pb+H_2O \rightarrow PbS(s)+H_2$	<15 ppm Zn 1.0 ppm Pb sat'd vapor	No Cell Deposits at 75% Utilization Cell Deposits Possible in Presence of High H_2Se
SIGNIFICANT EFFECTS			
H_2S (15,000) HCl (500) H_2Se (5) As (10)	$xH_2S+Ni \rightarrow NiS_x+xH_2$ $2HCl+K_2CO_3 \rightarrow 2KCl(v)+H_2O/CO_2$ $xH_2Se+Ni \rightarrow NiSe_x+xH_2$ $AsH_3+Ni \rightarrow NiAs(s)+3/2H_2$	<0.5 ppm H_2S <0.1 ppm HCl <0.2 ppm H_2Se <0.1 ppm As	Recoverable Effect Long Term Effects Possible Recoverable Effect Cumulative Long Term Effect

6.2 Performance

Factors affecting the selection of operating conditions are stack size, heat transfer rate, voltage level, load requirement, and cost. The performance curve is defined by cell pressure, temperature, gas composition, and utilization. Typical MCFCs will generally operate in the range of 100 to 200 mA/cm^2 at 750 to 900 mV/cell.

Typical cathode performance curves obtained at 650°C with an oxidant composition (12.6% O_2/18.4% CO_2/69% N_2) that is anticipated for use in MCFCs, and a common baseline composition (33% O_2/67% CO_2) are presented in Figure 6-4 (22, 49). The baseline composition contains O_2

and CO_2 in the stoichiometric ratio that is needed in the electrochemical reaction at the cathode (Equation (6-2)). With this gas composition, little or no diffusion limitations occur in the cathode because the reactants are provided primarily by bulk flow. The other gas composition, which contains a substantial fraction of N_2, yields a cathode performance that is limited dilution by an inert gas.

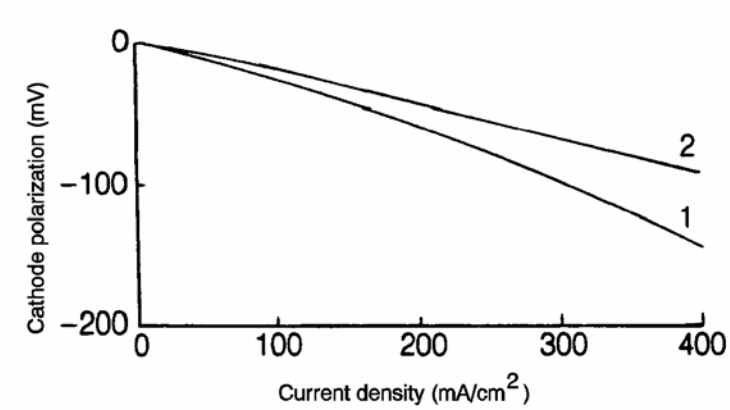

Figure 6-4 Effect of Oxidant Gas Composition on MCFC Cathode Performance at 650°C, (Curve 1, 12.6% O_2/18.4% CO_2/69.0% N_2; Curve 2, 33% O_2/67% CO_2) (47, Figure 3, Pg. 2711)

In the 1980s, the performance of MCFC stacks increased dramatically. During the 1990s, cells as large as 1.0 m^2 are being tested in stacks. Most recently, the focus has been on achieving performance in a stack equivalent to single cell performance. Cells with an electrode area of 0.3 m^2 were routinely tested at ambient and above ambient pressures with improved electrolyte structures made by tape-casting processes (22). Several stacks underwent endurance testing in the range of 7,000 to 10,000 hours. The voltage and power as a function of current density after 960 hours for a 1.0 m^2 stack consisting of 19 cells are shown in Figure 6-5. The data were obtained with the cell stack at 650°C and 1 atmosphere.

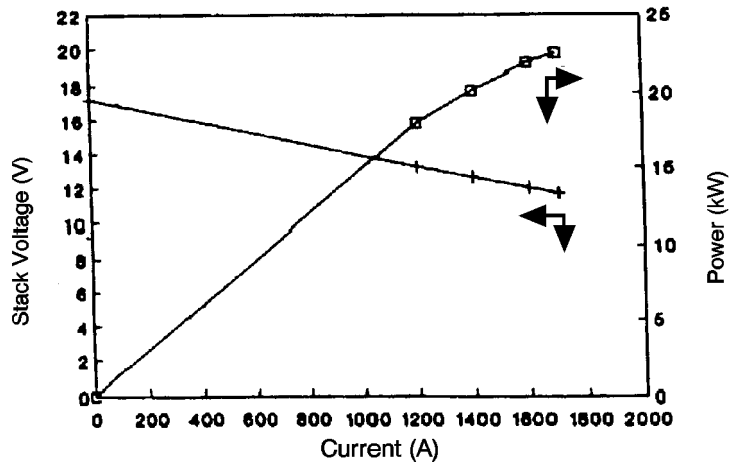

Figure 6-5 Voltage and Power Output of a 1.0/m^2 19 cell MCFC Stack after 960 Hours at 965°C and 1 atm, Fuel Utilization, 75% (50)

The remainder of this section will review operating parameters that affect MCFC performance. Supporting data will be presented as well as equations derived from empirical analysis.

6.2.1 Effect of Pressure

The dependence of reversible cell potential on pressure is evident from the Nernst equation. For a change in pressure from P_1 to P_2, the change in reversible potential (ΔV_p) is given by

$$\Delta V_p = \frac{RT}{2F} \ln \frac{P_{1,a}}{P_{2,a}} + \frac{RT}{2F} \ln \frac{P_{2,c}^{3/2}}{P_{1,c}^{3/2}} \qquad (6\text{-}11)$$

where the subscripts a and c refer to the anode and cathode, respectively. In an MCFC with the anode and cathode compartments at the same pressure (i.e., $P_1=P_{1,a}=P_{1,c}$ and $P_2=P_{2,a}=P_{2,c}$):

$$\Delta V_p = \frac{RT}{2F} \ln \frac{P_1}{P_2} + \frac{RT}{2F} \ln \frac{P_2^{3/2}}{P_1^{3/2}} = \frac{RT}{4F} \ln \frac{P_2}{P_1} \qquad (6\text{-}12)$$

At 650°C

$$\Delta V_p \text{ (mV)} = 20 \ln \frac{P_2}{P_1} = \left(46 \log \frac{P_2}{P_1}\right) \qquad (6\text{-}13)$$

Thus, a tenfold increase in cell pressure corresponds to an increase of 46 mV in the reversible cell potential at 650°C.

Increasing the operating pressure of MCFCs results in enhanced cell voltages because of the increase in the partial pressure of the reactants, increase in gas solubilities, and increase in mass transport rates. Opposing the benefits of increased pressure are the effects of pressure on undesirable side reactions such as carbon deposition (Boudouard reaction):

$$2CO \rightarrow C + CO_2 \qquad (6\text{-}14)$$

and methane formation (methanation)

$$CO + 3H_2 \rightarrow CH_4 + H_2O \qquad (6\text{-}15)$$

In addition, decomposition of CH_4 to carbon and H_2 is possible

$$CH_4 \rightarrow C + 2H_2 \qquad (6\text{-}16)$$

but this reaction is suppressed at higher pressure. According to Le Chatelier's principle, an increase in pressure will favor carbon deposition by Equation (6-14)[29] and methane formation by Equations (6-15) and (6-16) (51). The water-gas shift reaction (52)[30]

$$CO_2 + H_2 \leftrightarrow CO + H_2O \qquad (6\text{-}17)$$

is not affected by an increase in pressure because the number of moles of gaseous reactants and products in the reaction is identical. Carbon deposition in an MCFC is to be avoided because it can lead to plugging of the gas passages in the anode. Methane formation is detrimental to cell performance because the formation of each mole consumes three moles of H_2, which represents a considerable loss of reactant and would reduce power plant efficiency.

The addition of H_2O and CO_2 to the fuel gas modifies the equilibrium gas composition so that the formation of CH_4 is not favored. Increasing the partial pressure of H_2O in the gas stream can

---

[29]. Data from translation of Russian literature (51) indicate the equilibrium constant is almost independent of pressure.

[30]. Data from translation of Russian literature (52) indicate the equilibrium constant K is a function of pressure. In relative terms, if K (627°C) = 1 at 1 atm, it decreases to 0.74K at 500 atm and 0.60K at 1000 atmospheres. At the operating pressures of the MCFC, the equilibrium constant can be considered invariant with pressure.

reduce carbon deposition. The measurements (22) on 10 cm x 10 cm cells at 650°C using simulated gasified coal GF-1 (38% H_2/56% CO/6% CO_2) at 10 atm showed that only a small amount of CH_4 is formed. At open circuit, 1.4 vol% CH_4 (dry gas basis) was detected, and at fuel utilizations of 50 to 85%, 1.2 to 0.5% CH_4 was measured. The experiments with a high CO fuel gas (GF-1) at 10 atmospheres and humidified at 163°C showed no indication of carbon deposition in a subscale MCFC. These studies indicated that CH_4 formation and carbon deposition at the anodes in an MCFC operating on coal-derived fuels can be controlled, and under these conditions, the side reactions would have little influence on power plant efficiency.

Figure 6-6 shows the effect of pressure (3, 5, and 10 atmospheres) and oxidant composition (3.2% CO_2/23.2% O_2/66.3% N_2/7.3% H_2O and 18.2% CO_2/9.2% O_2/65.3% N_2/7.3% H_2O) on the performance of 70.5 cm^2 MCFCs at 650°C (53). The major difference as the CO_2 pressure changes is the change in open circuit potential, which increases with cell pressure and CO_2 content (see Equation (6-11)). At 160 mA/cm^2, ΔV_p is -44 mV for a pressure change from 3 to 10 atmospheres for both oxidant compositions.

Because ΔV_p is a function of the total gas pressure, the gas compositions in Figure 6-6 have little influence on ΔV_p. Based on these results, the effect of cell voltage from a change in pressure can be expressed by the equation

$$\Delta V_p \text{ (mV)} = 84 \log \frac{P_2}{P_1} \qquad \textit{(6-18)}$$

where P_1 and P_2 are different cell pressures. Another analysis by Benjamin, et al. (54) suggests that a coefficient less than 84 may be more applicable. The change in voltage as a function of pressure change was expressed as

$$V_p \text{ (mV)} = 76.5 \log \frac{P_2}{P_1} \qquad \textit{(6-19)}$$

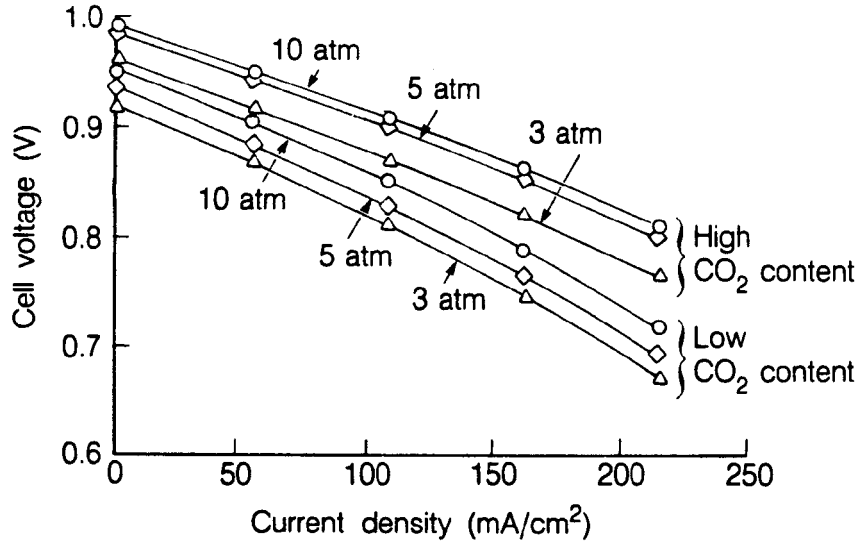

Figure 6-6 Influence of Cell Pressure on the Performance of a 70.5 cm^2 MCFC at 650°C (anode gas, not specified; cathode gases, 23.2% O_2/3.2% CO_2/66.3% N_2/7.3% H_2O and 9.2% O_2/18.2% CO_2/65.3% N_2/7.3% H_2O; 50% CO_2, utilization at 215 mA/cm^2) (53, Figure 4, Pg. 395)

Equation (6-19) was based on a load of 160 mA/cm^2 at a temperature of 650°C. It was also found to be valid for a wide range of fuels and for a pressure range of 1 atmosphere $\leq P \leq$ 10 atmospheres. Other results (55) support this coefficient. Figure 6-7 shows the influence of pressure change on voltage gain for three different stack sizes. These values are for a temperature of 650°C and a constant current density of 150 mA/cm^2 at a fuel utilization of 70%. The line that corresponds to a coefficient of 76.5 falls approximately in the middle of these values. Further improvements in cell performance will lead to changes in the logarithmic coefficient. Additional data (56, 57, 58) indicate that the coefficient may indeed be less than 76.5, but Equation (6-19) appears to represent the effect of pressure change on performance.

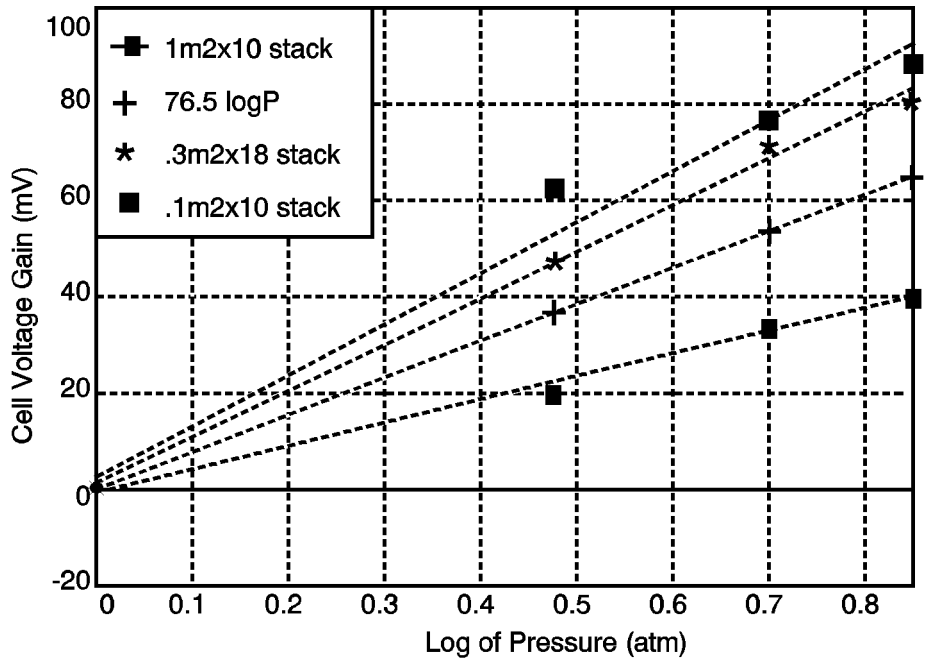

Figure 6-7 Influence of Pressure on Voltage Gain (55)

6.2.2 Effect of Temperature

The influence of temperature on the reversible potential of MCFCs depends on several factors, one of which involves the equilibrium composition of the fuel gas (22, 59, 60, 61).[31] The water gas shift reaction achieves rapid equilibrium[32] at the anode in MCFCs, and consequently CO serves as an indirect source of H_2. The equilibrium constant (K)

$$K = \frac{P_{CO} P_{H_2O}}{P_{H_2} P_{CO_2}} \qquad (6\text{-}20)$$

increases with temperature (see Table 6-4 and Appendix 11.1), and the equilibrium composition changes with temperature and utilization to affect the cell voltage.

The influence of temperature on the voltage of MCFCs is illustrated by the following example. Consider a cell with an oxidant gas mixture of 30% O_2/60% CO_2/10% N_2, and a fuel gas mixture of 80% H_2/20% CO_2. When the fuel gas is saturated with H_2O vapor at 25°C, its composition becomes 77.5% H_2/19.4% CO_2/3.1% H_2O. After considering the equilibrium established by the

---

31. For a fixed gas composition of H_2, H_2O, CO, CO_2, and CH_4 there is a temperature, T_b, below which the exothermic Boudouard reaction is thermodynamically favored, and a temperature, T_m, above which carbon formation by the endothermic decomposition of CH_4 is thermodynamically favored; more extensive details on carbon deposition are found elsewhere (22, 59, 60, 61).

32. The dependence of equilibrium constant on temperature for carbon deposition, methanation, and water gas shift reactions is presented in Appendix 11.1.

water gas shift reaction Equation (6-17), the equilibrium concentrations can be calculated (see Example 9-5 in Section 9) using Equation (6-20) and the equilibrium constant; see for instance, Broers and Treijtel (62). The equilibrium concentrations are substituted into Equation (6-4) to determine E as a function of T.

Table 6-4 Equilibrium Composition of Fuel Gas and Reversible Cell Potential as a Function of Temperature

Parameter[a]	Temperature (°K)		
	800	900	1000
P_{H_2}	0.669	0.649	0.643
P_{CO_2}	0.088	0.068	0.053
P_{CO}	0.106	0.126	0.141
P_{H_2O}	0.137	0.157	0.172
E^b (V)	1.155	1.143	1.133
K^c	0.2474	0.4538	0.7273

a - P is the partial pressure computed from the water gas shift equilibrium of inlet gas with composition77.5% H_2/19.4% CO_2/3.1% H_2O at 1 atmosphere.
b - Cell potential calculated using Nernst equation and cathode gas composition of 30% O_2/60% CO_2/10% N_2.
c - Equilibrium constant for water gas shift reaction from Reference (59).

The results of these calculations are presented in Table 6-4. Inspection of the results shows a change in the equilibrium gas composition with temperature. The partial pressures of CO and H_2O increase at higher T because of the dependence of K on T. The result of the change in gas composition, and the decrease in E° with increasing T, is that E decreases with an increase in T. In an operating cell, the polarization is lower at higher temperatures, and the net result is that a higher cell voltage is obtained at elevated temperatures. The electrode potential measurements (9) in a 3 cm^2 cell[33] show that the polarization at the cathode is greater than at the anode, and that the polarization is reduced more significantly at the cathode with an increase in temperature. At a current density of 160 mA/cm^2, cathode polarization is reduced by about 160 mV when the temperature increases from 550 to 650°C, whereas the corresponding reduction in anode polarization is only about 9 mV (between 600 and 650°C, no significant difference in polarization is observed at the anode).

Baker, et al. (63) investigated the effect of temperature (575 to 650°C) on the initial performance of small cells (8.5 cm^2). With steam-reformed natural gas as the fuel and 30% CO_2/70% air as

[33]. Electrolyte is 55 wt% carbonate eutectic (57 wt% Li_2CO_3, 31 wt% Na_2CO_3, 12 wt% K_2CO_3) and 45 wt% $LiA1O_2$, anode is Co + 10% Cr, cathode is NiO, fuel is 80% H_2/20% CO_2 and oxidant is 30% CO_2/70% air.

the oxidant, the cell voltage[34] at 200 mA/cm^2 decreased by 1.4 mV/° for a reduction in temperature from 650 to 600°C, and 2.16 mV/°C for a decrease from 600 to 575°C. In the temperature range 650 to 700°C, data analysis (58) indicates a relationship of 0.25 mV/°C. The following equations summarize these results.

$$\Delta V_T \text{ (mV)} = 2.16\ (T_2 - T_1) \qquad 575°C \leq T < 600°C \qquad (6\text{-}21)$$

$$\Delta V_T \text{ (mV)} = 1.40\ (T_2 - T_1) \qquad 600°C \leq T < 650°C \qquad (6\text{-}22)$$

$$\Delta V_T \text{ (mV)} = 0.25\ (T_2 - T_1) \qquad 650°C < T \leq 700°C \qquad (6\text{-}23)$$

The two major contributors responsible for the change in cell voltage with temperature are the ohmic polarization and electrode polarization. It appears that in the temperature range of 575 to 650°C, about 1/3 of the total change in cell voltage with decreasing temperature is due to an increase in ohmic polarization, and the remainder from electrode polarization at the anode and cathode. Most MCFC stacks currently operate at an average temperature of 650°C. Most carbonates do not remain molten below 520°C, and as seen by the previous equations, increasing temperature enhances cell performance. Beyond 650°C, however, there are diminishing gains with increased temperature. In addition, there is increased electrolyte loss from evaporation and increased material corrosion. An operating temperature of 650°C thus offers a compromise between high performance and stack life.

6.2.3 Effect of Reactant Gas Composition and Utilization

The voltage of MCFCs varies with the composition of the reactant gases. The effect of reactant gas partial pressure, however, is somewhat difficult to analyze. One reason involves the water gas shift reaction at the anode due to the presence of CO. The other reason is related to the consumption of both CO_2 and O_2 at the cathode. Data (55, 64, 65, 66) show that increasing the reactant gas utilization generally decreases cell performance.

As reactant gases are consumed in an operating cell, the cell voltage decreases in response to the polarization (i.e., activation, concentration) and to the changing gas composition (see discussion in Section 2). These effects are related to the partial pressures of the reactant gases.

Oxidant: The electrochemical reaction at the cathode involves the consumption of two moles CO_2 per mole O_2 (see Equation (6-2)), and this ratio provides the optimum cathode performance. The influence of the $[CO_2]/[O_2]$ ratio on cathode performance is illustrated in Figure 6-8 (46). As this ratio decreases, the cathode performance decreases, and a limiting current is discernible. In the

[34]. Cell was operated at constant flow rate; thus, the utilization changes with current density.

limit where no CO_2 is present in the oxidant feed, the equilibrium involving the dissociation of carbonate ions becomes important.

$$CO_3^{=} \leftrightarrow CO_2 + O^{=} \qquad (6\text{-}24)$$

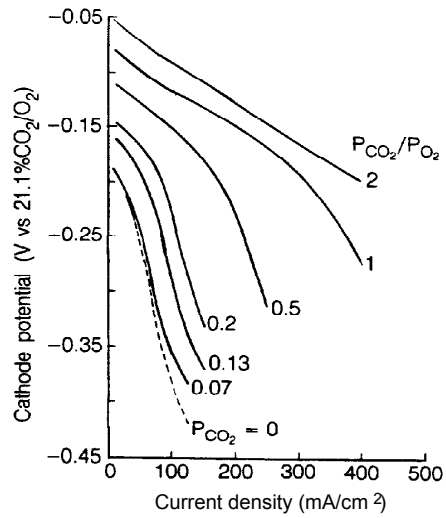

Figure 6-8 Effect of CO_2/O_2 Ratio on Cathode Performance in an MCFC, Oxygen Pressure is 0.15 atm (22, Figure 5-10, Pgs. 5-20)

Under these conditions the cathode performance shows the greatest polarization because of the composition changes that occur in the electrolyte. The change in the average cell voltage of a ten-cell stack as a function of oxidant utilization is illustrated in Figure 6-9. In this stack, the average cell voltage at 172 mA/cm^2 decreases by about 30 mV for a 30 percentage point increase in oxidant (20 to 50%) utilization. Based on this additional data (55, 64, 65), the voltage loss due to a change in oxidant utilization can be described by the following equations:

$$\Delta V_{cathode}\,(mV) = 250 \log \frac{\left(\overline{P}_{CO_2}\ \overline{P}_{O_2}^{\frac{1}{2}}\right)_2}{\left(\overline{P}_{CO_2}\ \overline{P}_{O_2}^{\frac{1}{2}}\right)_1} \qquad \text{for } 0.04 \le \left(\overline{P}_{CO_2}\ \overline{P}_{O_2}^{\frac{1}{2}}\right) \le 0.11 \qquad (6\text{-}25)$$

$$V_{cathode}\,(mV) = 99 \log \frac{\left(\overline{P}_{CO_2}\ \overline{P}_{O_2}^{\frac{1}{2}}\right)_2}{\left(\overline{P}_{CO_2}\ \overline{P}_{O_2}^{\frac{1}{2}}\right)_1} \qquad \text{for } 0.11 < \left(\overline{P}_{CO_2}\ \overline{P}_{O_2}^{\frac{1}{2}}\right) \le 0.38 \qquad (6\text{-}26)$$

where $\overline{P}_{CO_2}$ and $\overline{P}_{O_2}$ are the average partial pressures of CO_2 and O_2 in the system.

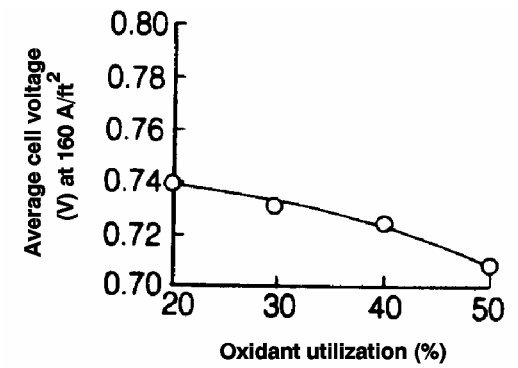

Figure 6-9 Influence of Reactant Gas Utilization on the Average Cell Voltage of an MCFC Stack (67, Figure 4-21, Pgs. 4-24)

Fuel: The data in Table 6-5 from Lu and Selman (68) illustrate the dependence of the anode potential on the composition of five typical fuel gases and two chemical equilibria occurring in the anode compartment.[35] The calculations show the gas compositions and open circuit anode potentials obtained after equilibria by the water gas shift and CH_4 steam reforming reactions are considered. The open circuit anode potential calculated for the gas compositions after equilibration, and experimentally measured, is presented in Table 6-5. The equilibrium gas compositions obtained by the shift and steam reforming reactions clearly show that, in general, the H_2 and CO_2 contents in the dry gas decrease, and CH_4 and CO are present in the equilibrated gases. The anode potential varies as a function of the $[H_2]/[H_2O][CO_2]$ ratio; a higher potential is obtained when this ratio is higher. The results show that the measured potentials agree with the values calculated, assuming that simultaneous equilibria of the shift and the steam reforming reactions reach equilibrium rapidly in the anode compartments of MCFCs.

[35]. No gas phase equilibrium exists between O_2 and CO_2 in the oxidant gas that could alter the composition or cathode potential.

Table 6-5 Influence of Fuel Gas Composition on Reversible Anode Potential at 650°C (68, Table 1, Pg. 385)

Typical Fuel Gas[a]	Gas Composition (mole fraction) H_2	H_2O	CO	CO_2	CH_4	N_2	-E[b] (mV)
Dry gas							
High Btu (53°C)	0.80	-	-	0.20	-	-	1116±3[c]
Intermed. Btu (71°C)	0.74	-	-	0.26	-	-	1071±2[c]
Low Btu 1 (71°C)	0.213	-	0.193	0.104	0.011	0.479	1062±3[c]
Low Btu 2 (60°C)	0.402	-	-	0.399	-	0.199	1030±[c]
Very low Btu (60°C)	0.202	-	-	0.196	-	0.602	1040±[c]
Shift equilibrium							
High Btu (53°)	0.591	0.237	0.096	0.076	-	-	1122[d]
Intermed. Btu (71°C)	0.439	0.385	0.065	0.112	-	-	1075[d]
Low Btu 1 (71°C)	0.215	0.250	0.062	0.141	0.008	0.326	1054[d]
Low Btu 2 (60°C)	0.231	0.288	0.093	0.228	-	0.160	1032[d]
Very low Btu (60°C)	0.128	0.230	0.035	0.123	-	0.484	1042[d]
Shift and Steam-reforming							
High Btu (53°C)	0.555	0.267	0.082	0.077	0.020	-	1113[d]
Intermed. Btu (71°C)	0.428	0.394	0.062	0.112	0.005	-	1073[d]
Low Btu 1 (71°C)	0.230	0.241	0.067	0.138	0.001	0.322	1059[d]
Low Btu 2 (60°C)	0.227	0.290	0.092	0.229	0.001	0.161	1031[d]
Very low Btu (60°C)	0.127	0.230	0.035	0.123	0.0001	0.485	1042[d]

a - Temperature in parenthesis is the humidification temperature
b - Anode potential with respect to 33% O_2/67% CO_2 reference electrode
c - Measured anode potential
d - Calculated anode potential, taking into account the equilibrated gas composition

Further considering the Nernst equation, an analysis shows that the maximum cell potential for a given fuel gas composition is obtained when $[CO_2]/[O_2] = 2$. Furthermore, the addition of inert gases to the cathode, for a given $[CO_2]/[O_2]$ ratio, causes a decrease in the reversible potential. On the other hand, the addition of inert gases to the anode increases the reversible potential for a given $[H_2]/[H_2O][CO_2]$ ratio and oxidant composition. This latter result occurs because two moles of product are diluted for every mole of H_2 reactant. However, the addition of inert gases to either gas stream in an operating cell can lead to an increase in concentration polarization.

Figure 6-10 depicts an average voltage loss for the stack of about 30 mV for a 30% increase in fuel utilization (30 to 60%). This and other data (66) suggest that the voltage loss due to a change in fuel utilization can be described by the following equation:

$$\Delta V_{anode}\,(mV) = 173 \log \frac{\left(\overline{P}_{H_2} / \overline{P}_{CO_2}\,\overline{P}_{H_2O}\right)_2}{\left(\overline{P}_{H_2} / \overline{P}_{CO_2}\,\overline{P}_{H_2O}\right)_1} \qquad (6\text{-}27)$$

where $\overline{P}_{H_2}$, $\overline{P}_{CO_2}$, and $\overline{P}_{H_2O}$ are the average partial pressures of H_2, CO_2, and O_2 in the system.

The above discussion implies that MCFCs should be operated at low reactant gas utilizations to maintain voltage levels, but doing this means inefficient fuel use. As with other fuel cell types, a compromise must be made to optimize overall performance. Typical utilizations are 75 to 85% of the fuel.

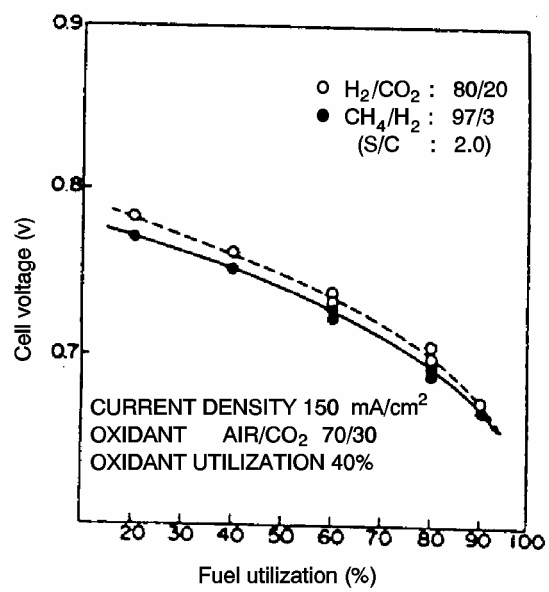

Figure 6-10 Dependence of Cell Voltage on Fuel Utilization (69)

6.2.4 Effect of Impurities

Gasified coal is expected to be the major source of fuel gas for MCFCs, but because coal contains many contaminants in a wide range of concentrations, fuel derived from this source also contains a considerable number of contaminants.[36] A critical concern with these contaminants is the concentration levels that can be tolerated by MCFCs without suffering significant degradation in

[36]. See Table 11.1 for contaminant levels found in fuel gases from various coal gasification processes.

performance or reduction in cell life. A list of possible effects of contaminants from coal-derived fuel gases on MCFCs is summarized in Table 6-6 (70).

Table 6-6 Contaminants from Coal-Derived Fuel Gas and Their Potential Effect on MCFCs (70, Table 1, Pg. 299)

Class	Contaminant	Potential Effect
Particulates	Coal fines, ash	• Plugging of gas passages
Sulfur compounds	H_2S, COS, CS_2, C_4H_4S	• Voltage losses • Reaction with electrolyte via SO_2
Halides	HCl, HF, HBr, $SnCl_2$	• Corrosion • Reaction with electrolyte
Nitrogen compounds	NH_3, HCN, N_2	• Reaction with electrolyte via NO_x
Trace metals	As, Pb, Hg, Cd, Sn Zn, H_2Se, H_2Te, AsH_3	• Deposits on electrode • Reaction with electrolyte
Hydrocarbons	C_6H_6, $C_{10}H_8$, $C_{14}H_{10}$	• Carbon deposition

The typical fuel gas composition and contaminants from an air-blown gasifier that enter the MCFC at 650°C after hot gas cleanup, and the tolerance level of MCFCs to these contaminants are listed in Table 6-7 (58, 71, 72). It is apparent from this example that a wide spectrum of contaminants is present in coal-derived fuel gas. The removal of these contaminants can add considerably to the efficiency. A review of various options for gas cleanup is presented by Anderson and Garrigan (70) and Jalan, et al. (73).

***Sulfur**:* It is well established that sulfur compounds in low parts per million concentrations in fuel gas are detrimental to MCFCs (74, 75, 76, 77, 78). The tolerance of MCFCs to sulfur compounds (74) is strongly dependent on temperature, pressure, gas composition, cell components, and system operation (i.e., recycle, venting, gas cleanup). The principal sulfur compound that has an adverse effect on cell performance is H_2S. At atmospheric pressure and high gas utilization (~75%), <10 ppm H_2S in the fuel can be tolerated at the anode (tolerance level depends on anode gas composition and partial pressure of H_2), and <1 ppm SO_2 is acceptable in the oxidant (74). These concentration limits increase when the temperature increases, but they decrease at increasing pressures.

Table 6-7 Gas Composition and Contaminants from Air-Blown Coal Gasifier After Hot Gas Cleanup, and Tolerance Limit of MCFCs to Contaminants

Fuel Gas[a] (mol%)	Contaminants[b,c]	Content[b,c]	Remarks[b]	Tolerance[c,d] Limit
19.2 CO	Particulates	<0.5 mg/l	Also includes ZnO from H_2S cleanup stage	<0.1 g/l for large particulates >0.3 :m
13.3 H_2	NH_3	2600 ppm		<10,000 ppm
2.6 CH_4	AsH_3	<5 ppm		< 1 ppm
6.1 CO_2	H_2S	<10 ppm	After first-stage cleanup	<0.5 ppm
12.9 H_2O	HCl	500 ppm	Also includes other halides	<10 ppm
45.8 N_2	Trace Metals	<2 ppm	Pb	<1 ppm
		<2 ppm	Cd	30+ ppm
		<2 ppm	Hg	35+ ppm
		<2 ppm	Sn	NA
	Zn	<50 ppm	From H_2S hot cleanup	<20 ppm
	Tar	4000 ppm	Formed during desulfurization cleanup stage	<2000 ppm[e]

a - Humidified fuel gas enters MCFC at 650°C
b - (71, Table 1, Pg. 177)
c - (79)
d - (72)
e - Benzene

The mechanisms by which H_2S affects cell performance have been investigated extensively (75, 76, 77, 78). The adverse effects of H_2S occur because of:

- Chemisorption on Ni surfaces to block active electrochemical sites,
- Poisoning of catalytic reaction sites for the water gas shift reaction, and
- Oxidation to SO_2 in a combustion reaction, and subsequent reaction with carbonate ions in the electrolyte.

The adverse effect of H_2S on the performance of MCFCs is illustrated in Figure 6-11. The cell voltage of a 10 cm x 10 cm cell at 650°C decreases when 5 ppm H_2S is added to the fuel gas (10% H_2/5% CO_2/10% H_2O/75% He), and current is drawn from the cell. The measurements indicate that low concentrations of H_2S do not affect the open circuit potential, but they have a major impact on the cell voltage as the current density is progressively increased. The decrease in cell voltage is not permanent;[37] when fuel gas without H_2S is introduced into the cell, the cell voltage returns to the level for a cell with clean fuel. These results can be explained by the chemical and electrochemical reactions that occur involving H_2S and $S^{=}$. A nickel anode at anodic potentials reacts with H_2S to form nickel sulfide:

$$H_2S + CO_2^{=} \rightarrow H_2O + CO_2 + S^{=} \qquad (6\text{-}28)$$

followed by

$$Ni + xS^{=} \rightarrow NiS_x + 2xe^{-} \qquad (6\text{-}29)$$

When the sulfided anode returns to open circuit, the NiS_x is reduced by H_2:

$$NiS_x + xH_2 \rightarrow Ni + xH_2S \qquad (6\text{-}30)$$

Similarly, when a fuel gas without H_2S is introduced to a sulfided anode, reduction of NiS_x to Ni can also occur. Detailed discussions on the effect of H_2S on cell performance are presented by Vogel and co-workers (75, 76) and Remick (77, 78).

The rapid equilibration of the water gas shift reaction in the anode compartment provides an indirect source of H_2 by the reaction of CO and H_2O. If H_2S poisons the active sites for the shift reaction, this equilibrium might not be established in the cell, and a lower H_2 content than predicted would be expected. Fortunately, the evidence (77, 78) indicates that the shift reaction is not significantly poisoned by H_2S. In fact, Cr used in stabilized-Ni anodes appears to act as a sulfur tolerant catalyst for the water gas shift reaction (78).

The CO_2 required for the cathode reaction is expected to be supplied by recycling the anode gas exhaust (after combustion of the residual H_2) to the cathode. Therefore, any sulfur in the anode effluent will be present at the cathode inlet unless provisions are made for sulfur removal. In the absence of sulfur removal, sulfur enters the cathode inlet as SO_2, which reacts quantitatively (equilibrium constant is 10^{15} to 10^{17}) with carbonate ions to produce alkali sulfates. These sulfate

---

[37]. The effects of H_2S on cell voltage are reversible if H_2S concentrations are present at levels below that required to form nickel sulfide.

ions are transported through the electrolyte structure to the anode during cell operation. At the anode, $SO_4^{=}$ is reduced to $S^{=}$, thus increasing the concentration of $S^{=}$ there.

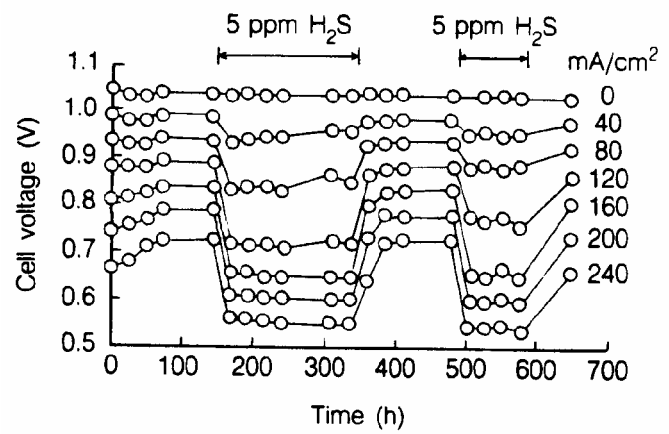

Figure 6-11 Influence of 5 ppm H_2S on the Performance of a Bench Scale MCFC (10 cm x 10 cm) at 650°C, Fuel Gas (10% H_2/5% CO_2/10% H_2O/75% He) at 25% H_2 Utilization (78, Figure 4, Pg. 443)

Based on the present understanding of the effect of sulfur on MCFCs, and with the available cell components, it is projected that long-term operation (40,000 hr) of MCFCs may require fuel gases with sulfur[38] levels of the order 0.01 ppm or less, unless the system is purged of sulfur at periodic intervals or sulfur is scrubbed from the cell burner loop (76). Sulfur tolerance would be approximately 0.5 ppm (see Table 6-3) in the latter case. Considerable effort has been devoted to develop low-cost techniques for sulfur removal, and research and development are continuing (80, 81). The effects of H_2S on cell voltage are reversible if H_2S concentrations are present at levels below which nickel sulfide forms.

Halides: Halogen-containing compounds are destructive to MCFCs because they can lead to severe corrosion of cathode hardware. Thermodynamic calculations (82) show that HCl and HF react with molten carbonates (Li_2CO_3 and K_2CO_3) to form CO_2, H_2O, and the respective alkali halides. Furthermore, the rate of electrolyte loss in the cell is expected to increase because of the high vapor pressure of LiCl and KCl. The concentration of Cl^- species in coal-derived fuels is typically in the range 1 to 500 ppm. It has been suggested (83) that the level of HCl should be kept below 1 ppm in the fuel gas, perhaps below the level of 0.5 ppm (47), but the tolerable level for long-term operation has not been established.

***Nitrogen Compounds*:** Compounds such as NH_3 and HCN do not appear to harm MCFCs (70, 79) in small amounts. However, if NO_x is produced by combustion of the anode effluent in the cell burner loop, it could react irreversibly with the electrolyte in the cathode compartment to form nitrate salts. The projection by Gillis (84) for the NH_3 tolerance level of MCFCs was 0.1 ppm, but Table 6-3 indicates that the level could be increased to 1 vol% (47).

---

[38]. Both COS and CS_2 appear to be equivalent to H_2S in their effect on MCFCs (76).

Solid Particulates: These contaminants can originate from a variety of sources, and their presence is a major concern because they can block gas passages and/or the anode surface. Carbon deposition and conditions that can be used to control its formation have been discussed earlier in this section. Solid particles such as ZnO, which is used for sulfur removal, can be entrained in the fuel gas leaving the desulfurizer. The results by Pigeaud (72) indicate that the tolerance limit of MCFCs to particulates larger than 3 μm diameter is <0.1 g/l.

Other Compounds: Experimental studies indicate that 1 ppm As from gaseous AsH_3 in fuel gas does not affect cell performance, but when the level is increased to 9 ppm As, the cell voltage drops rapidly by about 120 mV at 160 mA/cm^2 (71). Trace metals, such as Pb, Cd, Hg, and Sn in the fuel gas, are of concern because they can deposit on the electrode surface or react with the electrolyte (16). Table 6-3 addresses limits of these trace metals.

6.2.5 Effects of Current Density

The voltage output from an MCFC is reduced by ohmic, activation, and concentration losses that increase with increasing current density. The major loss over the range of current densities of interest is the linear iR loss. The magnitude of this loss (iR) can be described by the following equations (64, 85, 86):

$$\Delta V_J(\text{mV}) = -1.21\Delta J \qquad \text{for } 50 \leq J \leq 150 \qquad (6\text{-}31)$$

$$\Delta V_J(\text{mV}) = -1.76\Delta J \qquad \text{for } 150 \leq J \leq 200 \qquad (6\text{-}32)$$

where J is the current density (mA/cm^2) at which the cell is operating.

6.2.6 Effects of Cell Life

Endurance of the cell stack is a critical issue in the commercialization of MCFCs. Adequate cell performance must be maintained over the desired length of service, quoted by one MCFC developer as being an average potential degradation no greater than 2mV/1,000 hours over a cell stack lifetime of 40,000 hours (29). State-of-the-art MCFCs (55, 64, 66, 87, 88) depict an average degradation over time of

$$\Delta V_{lifetime}(\text{mV}) = -5\text{mV}/1000 \text{ hours} \qquad (6\text{-}33)$$

6.2.7 Internal Reforming

In a conventional fuel cell system, a carbonaceous fuel is fed to a fuel processor where it is steam reformed to produce H_2 (as well as other products, CO and CO_2, for example), which is then introduced into the fuel cell and electrochemically oxidized. The internal reforming molten carbonate fuel cell, however, eliminates the need for a separate fuel processor for reforming

carbonaceous fuels. This concept is practical in high-temperature fuel cells where the steam reforming reaction[39] can be sustained with catalysts. By closely coupling the reforming reaction and the electrochemical oxidation reaction within the fuel cell, the concept of the internal reforming MCFC is realized. The internal reforming MCFC eliminates the need for the external fuel processor. It was recognized early that the internal reforming MCFC approach provides a highly efficient, simple, reliable, and cost effective alternative to the conventional MCFC system (89). Development to date in the U.S. and Japan continues to support this expectation (85, 90).

There are two alternate approaches to internal reforming molten carbonate cells: indirect internal reforming (IIR) and direct internal reforming (DIR). In the first approach, the reformer section is separate, but adjacent to the fuel cell anode. This cell takes advantage of the close-coupled thermal benefit where the exothermic heat of the cell reaction can be used for the endothermic reforming reaction. Another advantage is that the reformer and the cell environments do not have a direct physical effect on each other. A disadvantage is that the conversion of methane to hydrogen is not promoted as well as in the direct approach. In the DIR cell, hydrogen consumption reduces its partial pressure, thus driving the methane reforming reaction, Equation (6-34), to the right. Figure 6-12 depicts one developer's approach where IIR and DIR have been combined.

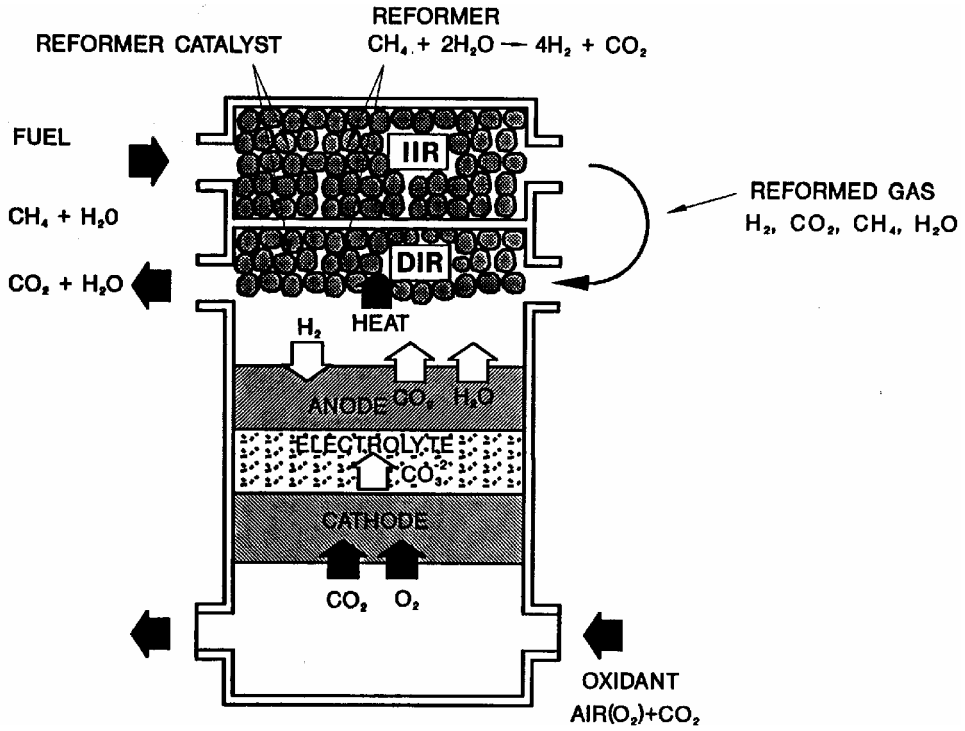

Figure 6-12 IIR/DIR Operating Concept, Molten Carbonate Fuel Cell Design (29)

[39]. Steam reforming of CH_4 is typically performed at 750 to 900°C; thus, at the lower operating temperature of MCFCs, a high activity catalyst is required. Methanol is also a suitable fuel for internal reforming. It does not require an additional catalyst because the Ni-based anode is sufficiently active.

Methane is a common fuel in internal reforming MCFCs, where the steam reforming reaction

$$CH_4 + H_2O \rightarrow CO + 3H_2 \qquad (6\text{-}34)$$

occurs simultaneously with the electrochemical oxidation of hydrogen in the anode compartment. The steam reforming reaction is endothermic, with $\Delta H_{650°C} = 53.87$ kcal/mol (89), whereas the overall fuel cell reaction is exothermic. In an internal reforming MCFC, the heat required for the reaction in Equation (6-34) is supplied by heat from the fuel cell reaction, thus eliminating the need for external heat exchange that is required by a conventional fuel processor. In addition, the product steam from the reaction in Equation (6-1) can be used to enhance the reforming reaction and the water gas shift reaction (Equation (6-17)) to produce additional H_2. The forward direction of the reforming reaction (Equation (6-34)) is favored by high temperature and low pressure; thus, an internal reforming MCFC is best suited to operate near atmospheric pressure.

A supported Ni catalyst (e.g., Ni supported on MgO or $LiAlO_2$) sustains the steam reforming reaction at 650°C to produce sufficient H_2 to meet the needs of the fuel cell. The interrelationship between the conversion of CH_4 to H_2 and its utilization in an internal reforming MCFC at 650°C is illustrated in Figure 6-13. At open circuit, about 83% of the CH_4 was converted to H_2, which corresponds closely to the equilibrium concentration at 650°C. When current is drawn from the cell, H_2 is consumed and H_2O is produced, and the conversion of CH_4 increases and approaches 100% at fuel utilizations greater than about 65%. Thus, by appropriate thermal management and adjustment of H_2 utilization with the rate of CH_4 reforming, a similar performance can be obtained in internal reforming MCFC stacks with natural gas and with synthesized reformate gas containing H_2 and CO_2, Figure 6-14. The concept of internal reforming has been successfully demonstrated for more than 15,000 hours in a 5 kW stack (91 and more than 10,000 hours in a 250 kW stack (92) The performance of the 2 kW stack over time can be seen in Figure 6-15 (64).

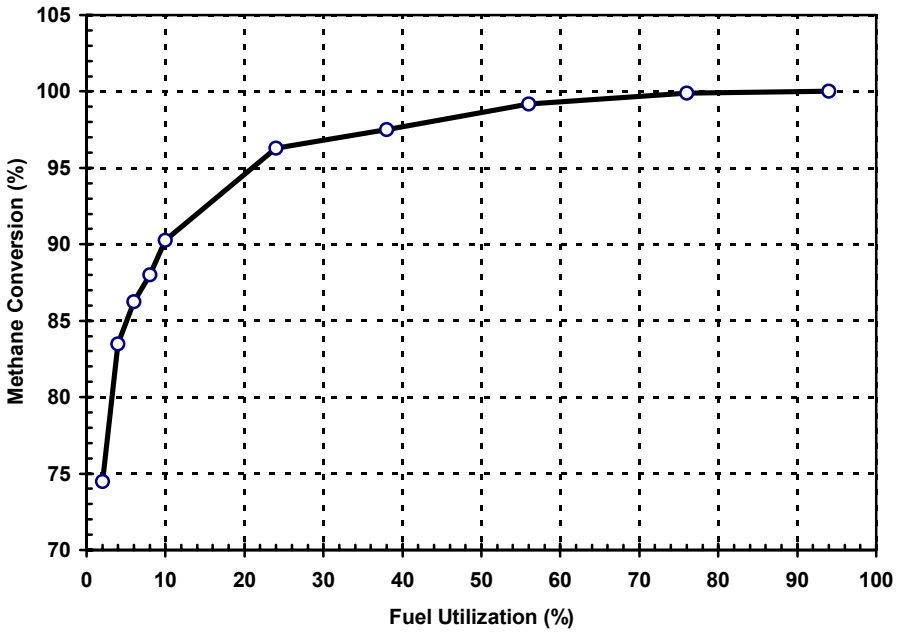

Figure 6-13 CH_4 Conversion as a Function of Fuel Utilization in a DIR Fuel Cell (MCFC at 650°C and 1 atm, steam/carbon ratio = 2.0, >99% methane conversion achieved with fuel utilization > 65% (93)

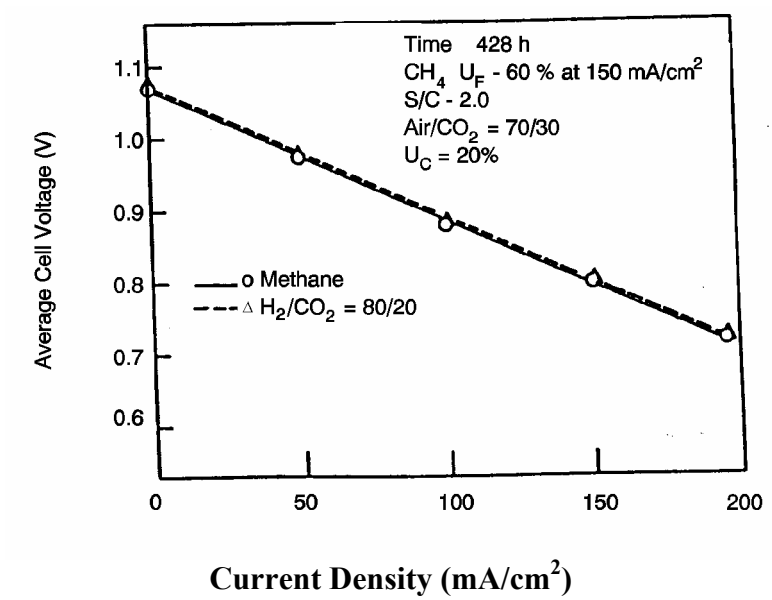

Figure 6-14 Voltage Current Characteristics of a 3kW, Five Cell DIR Stack with 5,016 cm^2 Cells Operating on 80/20% H_2/CO_2 and Methane (85)

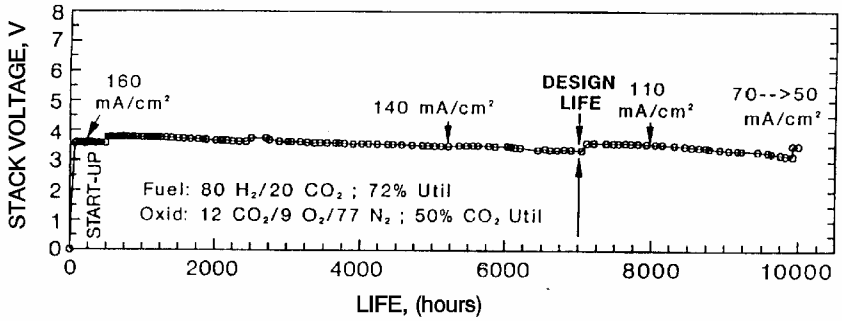

Figure 6-15 Performance Data of a 0.37m^2 2 kW Internally Reformed MCFC Stack at 650°C and 1 atm (94)

Direct Internal Reforming Catalysts: The anode catalyst is deactivated by the alkali carbonates electrolyte-containing environment. Making hardware of a non-wetting metal such as nickel has mitigated electrolyte creepage over the hardware surface towards the catalyst. Presently DIR catalyst deactivation is mainly by the vapor phase alkali species. The deactivation mechanism includes electrolyte-accelerated sintering pore filling/plugging and surface coverage. Making hardware of a non-wetting metal such as nickel has mitigated electrolyte creepage over the hardware surface towards the catalyst. Alkali-resistant supports such as magnesium oxide, calcium aluminate, and α-alumina have been investigated to reduce vapor phase alkali species effects. Results show that these supports undergo different degrees of decay. Ruthenium and rhodium-based catalysts are more stable, but are too costly (95, 96E has identified a more active and stable DIR catalyst (high activity supported Ni), projecting a catalyst life exceeding 40,000 hours and pursuing further enhancement of catalyst life. Another approach is to apply a getter-type barrier to trap the volatile alkali species before they reach the catalysts. A porous Ni or a SiC membrane was placed between the cell internal catalyst and the electrolyte containing components. (37)

6.3 Summary of Equations for MCFC

The preceding sections provide parametric performance based on various referenced data at different operating conditions. It is suggested that the following set of equations could be used for performance adjustments unless the reader prefers other data or correlations. Figure 6-16 is provided as reference MCFC performance.

Parameter	Equation	Comments	
Pressure	$\Delta V_p(mV) = 76.5 \log \frac{P_2}{P_1}$	1 atm $\leq$ P $\leq$ 10 atm	(6-19)
Temperature	$\Delta V_T(mV) = 2.16(T_2 - T_1)$	575°C $\leq$ T < 600°C	(6-21)
	$\Delta V_T(mV) = 1.40(T_2 - T_1)$	600°C $\leq$ T $\leq$ 650°C	(6-22)
	$\Delta V_T(mV) = 0.25(T_2 - T_1)$	650°C < T $\leq$ 700°C	(6-23)
Oxidant	$\Delta V_{cathode}(mV) = 250 \log \frac{(\bar{P}_{CO_2}\ \bar{P}_{O_2}^{1/2})_2}{(P_{CO_2}\ P_{O_2}^{1/2})_1}$	$0.04 \leq (\bar{P}_{CO_2}\ \bar{P}_{O_2}^{1/2}) \leq 0.11$	(6-25)
	$\Delta V_{cathode}(mV) = 99 \log \frac{(\bar{P}_{CO_2}\ \bar{P}_{O_2}^{1/2})_2}{(\bar{P}_{CO_2}\ \bar{P}_{O_2}^{1/2})_1}$	$0.11 \leq (\bar{P}_{CO_2}\ \bar{P}_{O_2}^{1/2}) \leq 0.38$	(6-26)
Fuel	$\Delta V_{anode}(mV) = 173 \log \frac{(\bar{P}_{H_2} / \bar{P}_{CO_2}\ \bar{P}_{H_2O}^{1/2})_2}{(\bar{P}_{H_2} / \bar{P}_{CO_2}\ \bar{P}_{O_2}^{1/2})_1}$		(6-27)
Current Density	$\Delta V_J(mV) = -1.21\ \Delta J$	50 $\leq$ J $\leq$ 150mA/cm^2	(6-31)
	$\Delta V_J(mV) = -1.76\ \Delta J$	150 < J $\leq$ 200mA/cm^2	(6-32)
Life Effects	$\Delta V_{lifetime}(mV) = -5mV/1000$ hours		(6-33)

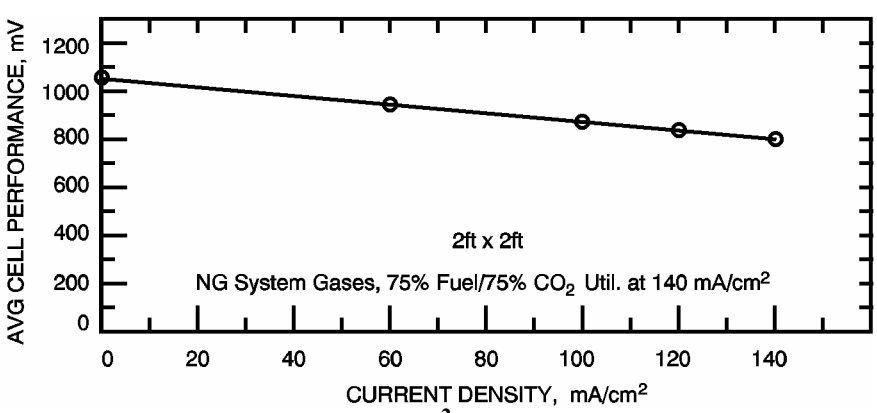

Figure 6-16 Average Cell Voltage of a 0.37m^2 2 kW Internally Reformed MCFC Stack at 650°C and 1 atm. Fuel, 100% CH_4, Oxidant, 12% CO_2/9% O_2/77% N_2

Fuel Cell Energy presented a computer model for predicting carbonate fuel cell performance at different operating conditions. The model was described in detail at the Fourth International Symposium on Carbonate Fuel Cell Technology, Montreal, Canada, 1997 (97). The model equations are listed as follows:

The general voltage versus current density relation is:

$$V = E_{Nernst} - (\eta_a + \eta_c) - \eta_{conc} - iz_r \qquad (6\text{-}41)$$

where

$$V_0 = E_0 + \frac{RT}{2F} \ln \left(\frac{P_{H_2,a}}{P_{CO_2,a}\, P_{H_2O,a}} P_{CO_2,c} \; P_{0_2,c}^{1/2} \right) \qquad (6\text{-}42)$$

At low current density (i<0.04 A/cm^2)

$$\eta_a = \frac{iRT}{2F} \frac{1}{K_a^0} e^{Ea/T} \, p_{H_2}^{\beta-0.5} \, p_{CO_2}^{-\beta} \, p_{H_2O}^{-\beta} \qquad (6\text{-}43)$$

$$\eta_c = \frac{iRT}{2F} \frac{1}{K_a^0} e^{Ec/T} \, p_{CO_2}^{-b_1'} \, p_{O_2}^{-b_2'} \qquad (6\text{-}44)$$

At high current density (i < 0.04A/cm^2)

$$\eta_a = \frac{RT}{2F}\left(a_0 + a_1 \ln p_{H_2} + a_2 \ln p_{CO_2,a} + a_3 \ln p_{H_2O} + a_4/T + a_5 \ln(i)\right) \qquad (6\text{-}45)$$

$$\eta_c = \frac{RT}{2F}\left(b_0 + b_1 \ln p_{CO_2,c} + b_2 \ln p_{o_2} + b_3 / T + b_4 \ln i\right) \qquad (6\text{-}46)$$

and

$$\eta = c_6 \ln(1 - i/i_L) \qquad (6\text{-}47)$$

cell resistance

$$Z_r = Z_0 \exp[c(\frac{1}{T_0} - \frac{1}{T})] \qquad (6\text{-}48)$$

A description of the parameters in the model follows:

V	=	Cell voltage, V
E◦	=	Standard E.M.F., V
R	=	Universal gas constant (8.314 joule/deg-mole)
T	=	Temperature, K
P	=	Partial pressure of gas compositions at anode (a) or cathode (c), atm.
η	=	Polarization, V
i	=	Current density, A/cm^2
z	=	Cell impedance, Ω-cm^2
F	=	Faraday's Constant (96,487 joule/volt - gram equivalent)
a,b,c	=	Parameters determined for experiments

The parameters in the above equations were calibrated from 400 sets of FCE's laboratory-scale test data and were further verified by several large-scale stack experiments. These parameter values may be dependent on the FCE cell design and characteristics and may not be directly applicable to other carbonate technologies. Figure 6-17 is a comparison of the measured data match with the model prediction.

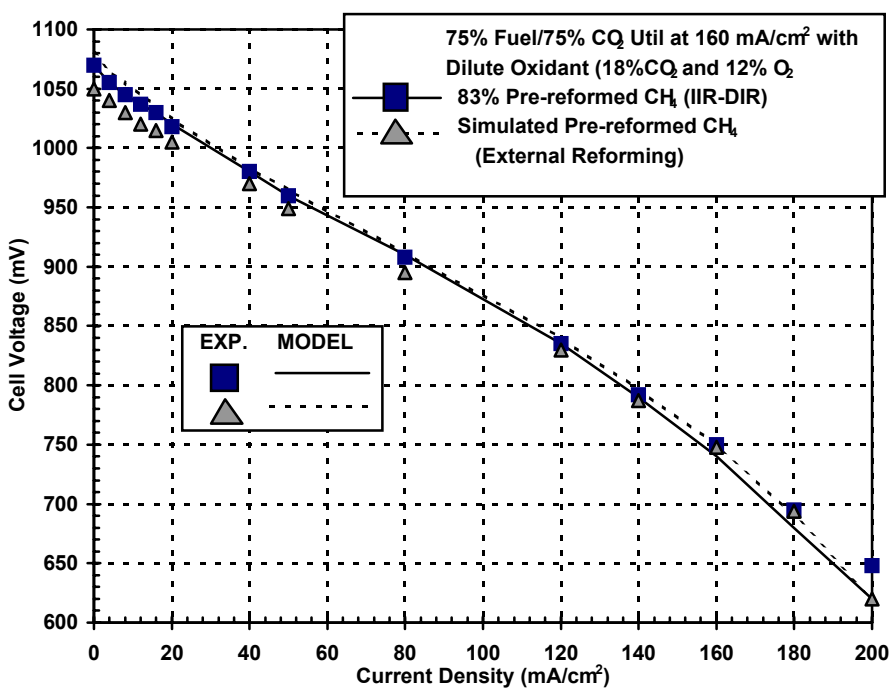

Figure 6-17 Model Predicted and Constant Flow Polarization Data Comparison (98)

6.4 References

1. H.C. Maru, L.G. Marianowski, *Extended Abstracts,* Abstract #31, Fall Meeting of the Electrochemical Society, October 17-22, 1976, Las Vegas, NV, Pg. 82, 1976.R.H.
2. J. Mitteldorf, G. Wilemski, *J. Electrochem. Soc.,* 131, 1784, 1984.
3. R.H. Arendt, *J. Electrochem. Soc.,* 129, 942, 1982.
4. H.C. Maru, A. Pigeaud, R. Chamberlin, G. Wilemski, in *Proceedings of the Symposium on Electrochemical Modeling of Battery, Fuel Cell, and Photoenergy Conversion Systems,* edited by J.R. Selman and H.C. Maru, The Electrochemical Society, Inc., Pennington, NJ, Pg. 398, 1986.
5. H.R. Kunz, *J. Electrochem. Soc.,* 134, 105, 1987.
6. A. Pigeaud, H.C. Maru, L. Paetsch, J. Doyon, R. Bernard, in *Proceedings of the Symposium on Porous Electrodes: Theory and Practices,* edited by H.C. Maru, T. Katan and M.G. Klein, The Electrochemical Society, Inc., Pennington, NJ, Pg. 234, 1984.
7. H.C. Maru, L. Paetsch, A. Pigeaud, in *Proceedings of the Symposium on Molten Carbonate Fuel Cell Technology,* edited by R.J. Selman and T.D. Claar, The Electrochemical Society, Inc., Pennington, NJ, Pg. 20, 1984.
8. R.J. Petri, T.G. Benjamin, in *Proceedings of the 21st Intersociety Energy Conversion Engineering Conference,* Volume 2, American Chemical Society, Washington, DC, Pg. 1156, 1986.
9. R.J. Selman, *Energy,* 11, 153, 1986.
10. M. Farooque, ERC, "Development on Internal Reforming Carbonate Fuel Cell Technology, Final Report," prepared for U.S. DOE/METC, DOE/MC/23274-2941, Pgs. 4-19 - 4-29, October, 1990.
11. FCE correspondence, June 2002
12. R. Huff, "Status of Fuel Cell Technologies," 1986 Fuel Cell Seminar, October 26-29, 1986, Tucson, AZ, 1986.
13. M. Farooque, data from ERC testing, 1992 and 2002.
14. C.E. Baumgartner, V.J. DeCarlo, P.G. Glugla, J.J. Grimaldi, *J. Electrochem. Soc.,* 132, 57, 1985.
15. P.G. Glugla, V.J. DeCarlo, *J. Electrochem. Soc.,* 129, 1745, 1982.
16. C. Yuh, M. Farooque, R. Johnsen, ERC, "Understanding of Carbonate Fuel Cell Resistances in MCFCs," in *Proceedings of the Fourth Annual Fuel Cells Contractors Review Meeting*, U.S. DOE/METC, Pgs. 53 - 57, July, 1992 and FCE correspondence, 2002.
17. C. Baumgartner, *J. Electrochem. Soc.,* 131, 1850, 1984.
18. W.M. Vogel, L.J. Bregoli, H.R. Kunz, S.W. Smith, in *Proceedings of the Symposium on Molten Carbonate Fuel Cell Technology,* edited by R.J. Selman and T.D. Claar, The Electrochemical Society, Inc., Pennington, NJ, Pg. 443, 1984.
19. M.L. Orfield, D.A. Shores, in *Corrosion 86,* Paper No. 88, National Association of Corrosion Engineers, Houston, TX, 1986.
20. D.A. Shores, in *Proceedings of the 22nd Intersociety Energy Conversion Engineering Conference,* Volume 2, American Institute of Aeronautics & Astronautics, New York, NY, Pg. 1023, 1987.
21. Communication with FCE, July 2002.
22. "Development of Improved Molten Carbonate Fuel Cell Technology," Final Report prepared by United Technologies Corp. for the Electric Power Research Institute, Palo Alto, CA, under Contract #RP1085-4, July 1983.

23. T.D. Kaun, in *Proceedings of the Fourth International Symposium on Molten Salts,* edited by M. Blander, D.S. Newman, M.L. Saboungi, G. Mamantov, K. Johnson, The Electrochemical Society, Inc., Pennington, NJ, Pg. 489, 1984.
24. A.J. Appleby, "Advanced Fuel Cells and Their Future Market," *Energy Conservation Strategies,* Progress Series, edited by W.E. Murphy, L.H. Fletcher, American Society of Aeronautics and Astronautics, New York, NY, date unknown.
25. A. Pigeaud, A.J. Skok, P.S. Patel, H.C. Maru, *Thin Solid Films,* 83, 1449, 1981.
26. R.A. Donado, L.G. Marianowski, H.C. Maru, J.R. Selman, *J. Electrochem. Soc.,* 131, 2541, 1984.
27. R.A. Donado, L.G. Marianowski, H.C. Maru, J.R. Selman, *J. Electrochem. Soc.,* 131, 2535, 1984.
28. R.B. Swaroop, J.W. Sim, K. Kinoshita, *J. Electrochem. Soc.,* 125, 1799, 1978
29. M. Farooque, ERC, "Development on Internal Reforming Carbonate Fuel Cell Technology, Final Report," prepared for U.S. DOE/METC, DOE/MC/23274-2941, Pgs.. 3 - 18, October, 1990.
30. D.A. Shores, P. Singh, in *Proceedings of the Symposium on Molten Carbonate Fuel Cell Technology,* edited by R.J. Selman and T. D. Claar, The Electrochemical Society, Inc., Pennington, NJ, Pg. 271, 1984.
31. G. Kucera, K. Myles, A. Brown, M. Roche, D. Chu, E. Indacochea, "ANL's Research and Development of Alternate Components for MCFCs," *in Proceedings of the Fourth Annual Fuel Cells Contractors Review Meeting*, U.S. DOE/METC, July 1992, Pgs. 31 - 41.
32. M Farooque, H.C. Maru, "Carbonate Fuel Cells Overview," *in Proceedings of the American Chemical Society Meeting*, August 2001.
33. N. Minh, "High Temperature Fuel Cells," in *CHEMTECH*, journal published by the American Chemical Society, Vol. 21, No. 1, January, Pgs. 32-37, 1991.
34. Y. Yamamasu, T. Kakihara, E. Kasai, T. Morita, IHI, "Component Development and Durability Test of MCFC," in *The International Fuel Cell Conference Proceedings*, NEDO/MITI, Tokyo, Japan, Pgs. 161-164, 1992.
35. H. Urushibata, T. Murahashi, MELCO, "Life Issues of Molten Carbonate Fuel Cell," in *The International Fuel Cell Conference Proceedings*, NEDO/MITI, Tokyo, Japan, Pgs. 223-226, 1992.
36. S. Takashima, K. Ohtsuka, T. Kara, M. Takeuchi, Y. Fukui, H. Fujimura, Hitachi, "MCFC Stack Technology at Hitachi," in *The International Fuel Cell Conference Proceedings*, NEDO/MITI, Tokyo, Japan, Pgs. 265-268, 1992.
37. C. Yuh, M. Farooque, "Carbonate Fuel Cell Materials," in *Advanced Materials and Processes*, journal published by the American Society of Materials, July, 2002.
38. J. Hirschenhofer, D. Stauffer, R. Engleman, Fuel Cells A Handbook (Revision 3) prepared by Gilbert/Commonwealth, Inc. for the U.S. Department of Energy under Contract No. DE-ACO1-88FE61684, January 1994.
39. K. Tanimoto, Y. Miyazaki, M. Yanagida, S. Tanase, T. Kojima, N. Ohtori, H. Okuyama, T. Kodama, Government Industrial Research Institute, Osaka, "Cell Performance of Molten Carbonate Fuel Cell with Alkali and Alkaline Earth Carbonate Mixtures," in *The International Fuel Cell Conference Proceedings*, NEDO/MITI, Pgs. 185-188, Tokyo, Japan, 1992.
40. K. Ota, S. Mitsushima, K Kato, N. Kamiya, Yokahama National University, "Solubilities of Metal Oxides in Molten Carbonate, " in Proceedings of the Second Symposium on Molten

Carbonate Fuel Cell Technology, Volume 90 - 16, The Electrochemical Society, Inc. Pennington, NJ, Pgs. 318-327, 1990.
41. T. Benjamin, et al., "Status of the M-C Power MCFC Commercialization Program," IECEC-97, Honolulu, Hawaii, July 27 - August 1, 1997.
42. A. Yuh, M. Farooque, "Carbonate Fuel Cell Materials," in *Advanced Materials and Processes*, journal published by the American Society of Materials, July, 2002.
43. H. Maru, et al., "ERC Direct Carbonate Fuel Cell Program Overview," DOE Contractor's Review Meeting, Morgantown, WV, August 26-28, 1997.
44. R.O.Petkus, "Successful Test of a 250 kW Molten Carbonate Fuel Cell Power Generator at Miramar," POWER-GEN International '97, Dallas, TX, December 1997.
45. A. Pigeaud, ERC, and G. Wilemski, Physical Sciences, "Effects of Coal-Derived Trace Species on the Performance of Carbonate Fuel Cells," *in Proceedings of the Fourth Annual Fuel Cells Contractors Review Meeting*, U.S. DOE/METC, Pgs. 42-45, July 1992.
46. D. Rastler, EPRI, G. Devore, Destec Engineering, R. Castle, Haldor Topsoe, C. Chi, ERC, "Demonstration of a Carbonate Fuel Cell Stack on Coal-Derived Gas," *in Fuel Cell Seminar.*
47. "Effects of Coal-Derived Trace Species on the Performance of Molten Carbonate Fuel Cells," Topical Report prepared by Energy Research Corporation for US DOE/METC, DOE/MC/25009-T26, October, 1991.
48. A. Pigeaud, et al., "Trace Contaminant Effects and Emissions with Integrated Coal Gasification and Cleanup," 1994 Fuel Cell Seminar, Pgs. 539-542 (1994).
49. L.J. Bregoli and H.R. Kunz, *J. Electrochem. Soc.,* 129, 2711, 1982.
50. Benjamin et al., "Status of MCFC Technology at M-C Power-1992," 1992 Fuel Cell Seminar Program and Abstracts, 1992.
51. M.G. Gonikberg, *Chemical Equilibria and Reaction Rates at High Pressures,* Translated from Russian by M. Artment, edited by S. Monson, published for the National Science Foundation, Washington, D.C., by the Israel Program for Scientific Translations Jerusalem, Israel, Pg. 58, 1963.
52. M.G. Gonikberg, *Chemical Equilibria and Reaction Rates at High Pressures,* Translated from Russian by M. Artment, edited by S. Monson, published for the National Science Foundation, Washington, DC, by the Israel Program for Scientific Translations, Jerusalem, Israel, Pg. 133, 1963.
53. H.R. Kunz, L.A. Murphy, in *Proceedings of the Symposium on Electrochemical Modeling of Battery, Fuel Cell, and Photoenergy Conversion Systems,* edited by J.R. Selman and H.C. Maru, The Electrochemical Society, Inc., Pennington, NJ, Pg. 379, 1986.
54. T.G. Benjamin, E.H. Camara, L.G. Marianowski, *Handbook of Fuel Cell Performance,* prepared by the Institute of Gas Technology for the United States Department of Energy under Contract No. EC-77-C-03-1545, May 1980.
55. Research and Development on Fuel Cell Power Generation Technology FY1990 Annual Report, NEDO, April 1991.
56. M. Hosalaetal, "IHI Large Site Molten Carbonate Fuel Cell Advancements," *Fuel Cell Program and Abstracts* 1990 Fuel Cell Seminar, Phoenix, AR, November 25-28, 1990.
57. W.H. Johnson, "Molten Carbonate Fuel Cell Technology Improvement," Quarterly Technical Progress Report No. 23 for the Period Ending May, 1990, prepared for US DOE/METC, DOE/MC/23270-2923, September 1990.
58. D.B. Stauffer, et al., "An Aspen/SP MCFC Performance User Block," G/C Report No. 2906, July 1991.

59. J.R. Rostrup-Nielsen, in *Catalysis Science and Technology,* edited by J.R. Anderson and M. Boudart, Springer-Verlag, Berlin, German Democratic Republic, Pg. 1, 1984.
60. H.A. Leibhafsky, E.J. Cairns, *Fuel Cells and Fuel Batteries,* John Wiley and Sons, Inc., New York, NY, Pg. 654, 1968.
61. T.D. Tawari, E. Pigeaud, H.C. Maru, in *Proceedings of the Fifth Annual Contractors Meeting on Contaminant Control in Coal-Derived Gas Streams,* DOE/METC-85/6025, edited by D.C. Cicero and K.E. Markel, U.S. Department of Energy, Morgantown, WV, Pg. 425, January 1986.
62. G.H.J. Broers, B.W. Triejtel, *Advanced Energy Conversion,* 5, 365, 1965.
63. A. Baker, S. Gionfriddo, A. Leonida, H. Maru, P. Patel, "Internal Reforming Natural Gas Fueled Carbonate Fuel Cell Stack," Final Report prepared by Energy Research Corporation for the Gas Research Institute, Chicago, IL, under Contract No. 5081-244-0545, March, 1984.
64. M. Farooque, Data from ERC testing, 1992.
65. S. Kaneko, et al., "Research on On-Site Internal Reforming Molten Carbonate Fuel Cell," 1989 International Gas Research Conference, 1989.
66. M. Farooque, "Development of Internal Reforming Carbonate Fuel Cell Stack Technology," Final Report, DOE/MC/23274-2941, October 1991.
67. J.M. King, A.P. Meyer, C.A. Reiser, C.R. Schroll, "Molten Carbonate Fuel Cell System Verification and Scale-up," EM-4129, final report prepared by United Technologies Corp. for the Electric Power Research Institute, Research Project 1273-1, July 1985.
68. S.H. Lu, J.R. Selman, in *Proceedings of the Symposium on Molten Carbonate Fuel Cell Technology,* edited by R.J. Selman, T.D. Claar, The Electrochemical Society, Inc., Pennington, NJ, Pg. 372, 1984.
69. T. Tanaka, et al., "Research on On-Site Internal-Reforming Molten Carbonate Fuel Cell," 1989 International Gas Research Conference, Pg. 252, 1989.
70. G.L. Anderson, P.C. Garrigan, in *Proceedings of the Symposium on Molten Carbonate Fuel Cell Technology,* edited by R.J. Selman, T.D. Claar, The Electrochemical Society, Inc., Pennington, NJ, Pg. 297, 1984.
71. A. Pigeaud, in *Proceedings of the Sixth Annual Contractors Meeting on Containment Control in Coal-Derived Gas Streams,* DOE/METC-86/6042, edited by K.E. Markel and D.C. Cicero, U.S. Department of Energy, Morgantown, WV, Pg. 176, July 1986.
72. A. Pigeaud, "Study of the Effects of Soot, Particulate and Other Contaminants on Molten Carbonate Fuel Cells Fueled by Coal Gas," Progress Report prepared by Energy Research Corporation for U.S. Department of Energy, Morgantown, WV, under Contract No. DE-AC21-84MC21154, June 1987.
73. V. Jalan, M. Desai, C. Brooks, in *Proceedings of the Symposium on Molten Carbonate Fuel Cell Technology,* edited by R. J. Selman, T. D. Claar, The Electrochemical Society, Inc., Pennington, NJ, Pg. 506, 1984.
74. L.J. Marianowski, *Prog. Batteries & Solar Cells,* 5, 283, 1984.
75. W.V. Vogel and S.W. Smith, *J. Electrochem. Soc.,* 129, 1441, 1982.
76. S.W. Smith, H.R. Kunz, W.M. Vogel and S.J. Szymanski, in *Proceedings of the Symposium on Molten Carbonate Fuel Cell Technology,* edited by R.J. Selman and T.D. Claar, The Electrochemical Society, Inc., Pennington, NJ, Pg. 246, 1984.
77. R.J. Remick, E.H. Camara, paper presented at the Fall Meeting for The Electrochemical Society, Inc., New Orleans, LA, October 7-12, 1984.

78. R.J. Remick, in *Proceedings of the Fourth Annual Contractors Meeting on Contaminant Control in Hot Coal-Derived Gas Streams,* DOE/METC-85/3, edited by K. E. Markel, U.S. Department of Energy, Morgantown, WV, Pg. 440, May 1984.
79. M.C. Williams, D.A. Berry, "Overview of the DOE-Funded Fuel Cell Contaminants R&D Program," Fuel Cell Seminar Program and Abstracts, 1990 Fuel Cell Seminar, Phoenix, AR, November 25-28, 1990.
80. P.S. Patel, S.M. Rich, H.C. Maru, in *Proceedings of the Fourth Annual Contractors Meeting on Contaminant Control in Hot Coal-Derived Gas Streams,* DOE/METC-85/3, edited by K. E. Markel, U.S. Department of Energy, Morgantown, WV, Pg. 425, May 1984.
81. G.L. Anderson, F.O. Berry, G.D. Harmon, R.M. Laurens, R. Biljetina, in *Proceedings of the Fifth Annual Contractors Meeting on Contaminant Control in Coal-Derived Gas Streams,* DOE/METC-85/6025, edited by D.C. Cicero, K.E. Markel, U.S. Department of Energy, Morgantown, WV, Pg. 87, January 1986.
82. T.P. Magee, H.R. Kunz, M. Krasij, H.A. Cole, "The Effects of Halides on the Performance of Coal Gas-Fueled Molten Carbonate Fuel Cell," Semi-Annual Report, October 1986 - March 1987, prepared by International Fuel Cells for the U.S. Department of Energy, Morgantown, WV, under Contract No. DE-AC21-86MC23136, May 1987.
83. G.N. Krishnan, B.J. Wood, G.T. Tong, M.A. Quinlan, in *Proceedings of the Fifth Annual Contractors Meeting on Contaminant Control in Coal-Derived Gas Streams,* DOE/METC-85/6025, edited by D.C. Cicero and K.E. Markel, U.S. Department of Energy, Morgantown, WV, Pg. 448, January 1986.
84. E.A. Gillis, *Chem. Eng. Prog.,* 88, October 1980.
85. T. Tanaka, et al., "Development of Internal Reforming Molten Carbonate Fuel Cell Technology," in *Proceedings of the 25th IECEC*, American Institute of Chemical Engineers, New York, NY, August 1990.
86. M. Miyazaki, T. Okada, H. Ide, S. Matsumoto, T. Shinoki, J. Ohtsuki, "Development of an Indirect Internal Reforming Molten Carbonate Fuel Cell Stack," in the 27th Intersociety Energy Conversion Engineering Conference Proceedings, San Diego, CA, August 3-7, 1992, Pg. 290, 1992.
87. W.H. Johnson, "International Fuel Cells MCFC Technical Accomplishment," in *Proceedings of the Second Annual Fuel Cells Contractor's Review Meeting*, US DOE/METC, May 1990.
88. T. Benjamin, G. Rezniko, R. Donelson, D. Burmeister," IMHEX^R MCFC Stack Scale-Up," in the *Proceedings of the 27th Intersociety Energy Conversion Engineering Conference*, Vol. 3, San Diego, CA, Aug. 3-7, 1992, Pg. 290, 1992.
89. H.C. Maru, B.S. Baker, *Prog. Batteries & Solar Cells*, 5, 264, 1984.
90. M. Faroogue, G. Steinfield, H. Maru, "Comparative Assessment of Coal-Fueled Carbonate Fuel Cell and Competing Technologies," in *Proceedings of the 25th IECEC*, Vol. 3, American Institute of Chemical Engineers, New York, NY, 1990.
91. H.C. Maru and M. Farooque, FCE, “Molten Carbonate Fuel Cell Product Design Improvement,” Prepared for U.S. DOE/DARPA, Annual Report, DE-FC21-95MC31184, Pages 5-9, December 1999.
92. H.C. Maru and M. Farooque, FCE, “Molten Carbonate Fuel Cell Product Design Improvement,” Prepared for U.S. DOE/DARPA, Annual Report, DE-FC21-95MC31184, Pages 4-10, December 2000.
93. ERC correspondence, laboratory data, March 1998.
94. M. Farooque, data from ERC testing, 1992

95. S. Katikaneni, C. Yuh, S. Abens and M. Farooque, "Catalysis Today," 2002 (In Press).
96. S. Katikaneni, C. Yuh and M. Farooque, "The Direct Carbonate Fuel Cell Technology: Advances in Fuel Processing and Internal Reforming," ACS Fuel Chemistry, 46(2) 685-688, Preprints, 2001.
97. J. Ding, et al., "A Computer Model for Direct Carbonate Fuel Cells," Proceedings of the Fourth International Symposium on Carbonate Fuel Cells, 191st Electrochemical Society Meeting, Montreal, May 1997.
98. J. Ding, P. S. Patel, M. Farooque, H. C. Maru, in Carbonate Fuel Cell Technology IV, (eds. J. R. Selman, et al.), The Electrochemical Society, Inc., New Jersey, Pg. 127-138, 1997.

7. SOLID OXIDE FUEL CELL

The solid oxide fuel cell[40] (SOFC) is viable for generating electricity from hydrocarbon fuels. The high operating temperature from 600-1,000°C allows internal reforming, promotes rapid kinetics with non-precious materials, and produces high quality by-product heat for cogeneration or for use in a bottoming cycle. The high temperature of the SOFC, however, places stringent requirements on its materials. The development of suitable low-cost materials and low-cost fabrication of ceramic structures is presently the key technical challenge facing SOFC commercialization.

7.1 Cell Components

SOFC major components include the anode, the cathode, and the electrolyte. Fuel cell stacks contain an electrical interconnect which links individual cells together in series or parallel.

SOFC components must meet certain general requirements in order to be useful. Electrolytes and interconnects must be chemically, morphologically, and dimensionally stable in both oxidizing conditions and reducing conditions. No components may exhibit any significant changes in volume between room temperature and the fabrication temperature. The components must be chemically stable in order to limit chemical interactions with other cell components. They must have similar thermal expansion in order to minimize thermal stresses that may cause cracking and delamination during thermal cycling or fabrication. It is also desirable that fuel cell components have high strength and durability, are easy to fabricate, and are relatively inexpensive.

7.1.1 State-of-the-Art Components

Advances in modern ceramic technology and solid-state science have led to the development of a range of efficient, environmentally-friendly devices for tomorrow's industries and consumers. In particular, many ceramics can be tailored for electrical properties unattainable in metallic or polymer counterparts; these materials are known as electroceramics. One group of electro-ceramics, known alternatively as fast ion conductors, rapid ion conductors, and superionic conductors, are able to support a high flux of ions in the solid state. Materials that rapidly con-

[40]. A broader, more generic name for fuel cells operating at the temperatures described in this section would be "ceramic" fuel cells. The electrolyte of these cells is made primarily from solid ceramic material to survive the high temperature environment. The electrolyte of present SOFCs is oxygen ion conducting. Ceramic cells could also be proton conducting.

duct oxygen ions ($O^{=}$) can be used as solid electrolytes in a number of industrial applications including oxygen gas sensors, oxygen pumps, exhaust catalysts and SOFCs. This section presents the state-of-the-art development of tubular SOFCs and planar solid oxide fuel cells (PSOFCs). The discussion addresses electrolyte thickness, structural support for PSOFCs, electrolyte and electrode material compatibility, stacks, and seals.

Planar SOFCs: Current efforts in PSOFCs can be categorized on the basis of the supporting component of the cathode/electrolyte/anode structure; two approaches are electrode-supported or electrolyte-supported cells. Two basic types of stacking configurations under development are shown in Figure 7-1. Electrolyte-supported cells use yttria stabilized zirconia (YSZ) membranes of $\geq$100 μm thickness. The ohmic contribution, or area-specific resistance (ASR) of the electrolyte at 800°C is in excess of 0.75 Σ-cm^2. This significantly exceeds the usual desirable goal (1) of 0.2 Σ-cm^2 for the entire cell. As such, electrolyte-supported fuel cells are problematic for operation at temperatures below 900°C with reasonable performance. Operation above 900°C necessitates the use of expensive ceramic or high chromium metallic interconnects.

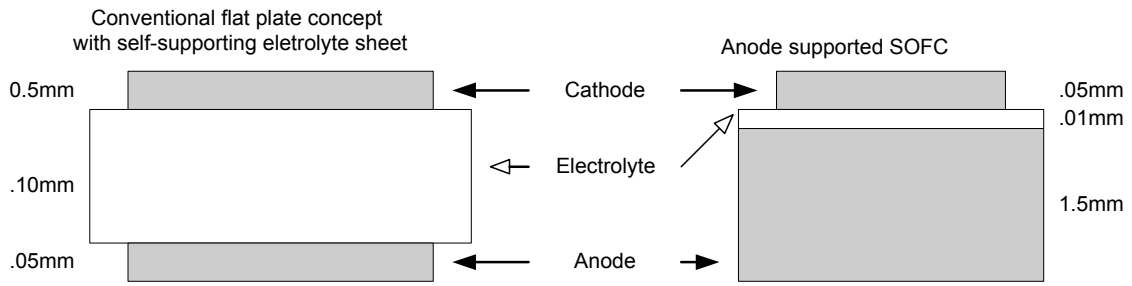

Figure 7-1 Single Cell Structure-Electrolyte and Anode Supported Cell

In electrode-supported cells, the supporting component can either be the anode or the cathode. In these designs, the electrolyte is typically between 5 – 30 μm, while the electrode thickness can be between ~ 250 μm and ~ 2 mm. In the cathode-supported design, the YSZ electrolyte and the lanthanum strontium manganite (LSM) cathode coefficients of thermal expansion (CTE) are well matched, which places no restriction on electrolyte thickness. In anode-supported cells, the CTE of the nickel-containing YSZ anode is greater than that of the YSZ electrolyte. This places an upper limit on the electrolyte thickness, which is typically about 30 μm. The anode-supported cell design offers the following advantages over the cathode-supported design:

- The concentration polarization is lower since the effective diffusivity of the anode gas is typically 3 to 4 times greater than that of air.

- The presence of metallic nickel in the anode leads to a better thermal shock resistance due to its higher thermal conductivity and plasticity.

- Since the required porosity is readily created by reducing NiO to Ni, the desired electrode microstructure can readily be developed in the anode-supported cells.

Figure 7-2 (2,3) demonstrates how the combination of similar CTEs with the anode-supported cell and lower operating temperatures have created the potential for using lower cost stainless steel interconnects. In addition, developers have stated that the combination of metallic interconnects, thick nickel anode, and lower temperatures have facilitated the development of more viable seal designs.

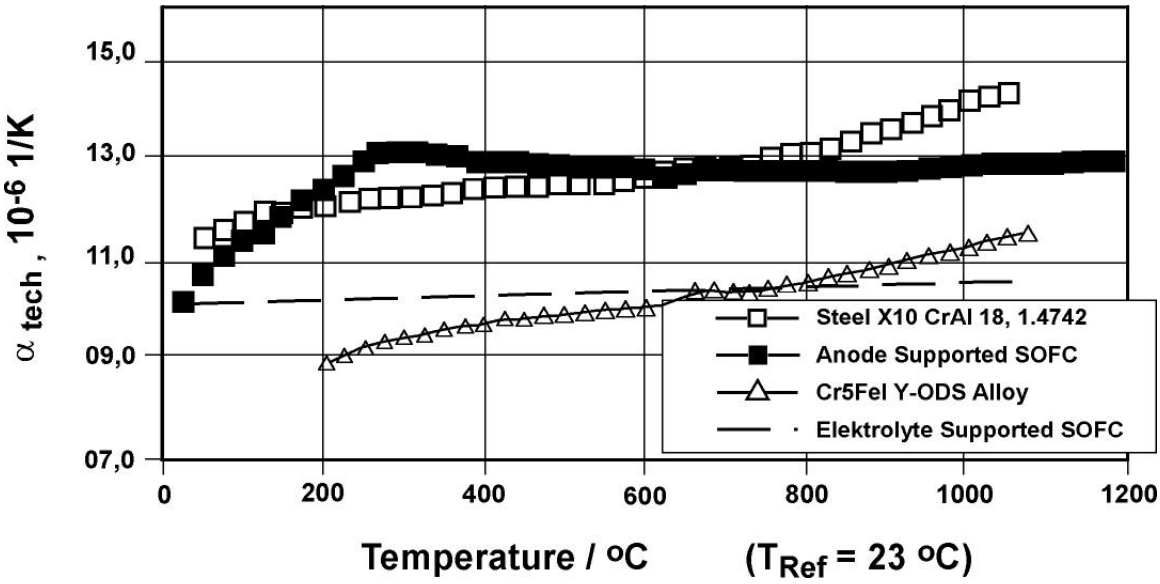

Figure 7-2 Thermal Expansion Behavior of Stack Materials

The YSZ electrolyte has a conductivity of about 10^{-1}/ohm-cm at 1,000°C. In a fuel cell operating with a current density of 250 mA/cm^2 and an electrolyte of 200 µm thickness, the resistance loss in the electrolyte would be 50 mV. The trend in technology development is to decrease the operating temperature of the SOFCs. To operate at 800°C, the electrolyte thickness must be diminished by about an order of magnitude if a reasonable resistance loss is to be maintained. Figure 7-3 (5,6,7) illustrates the relation between conductivity, electrolyte thickness, and temperature for YSZ and several other electrolytes. As shown, scandium doped zirconia (SDZ) is more conductive than YSZ, permitting a further reduction of the operating temperature by 50-100°C. Gadolinium doped ceria is even more conductive, but is partially reduced in hydrogen at temperatures above 600°C; formation of Ce^{+3} ions generates electron holes that make ceria electronically conductive, thus short-circuiting the cell.

A substantially more conductive material that is stable in air and hydrogen was discovered by Goodenough (4). Lanthanum gallate with strontium doping on the A-site of the perovskite and magnesium on the B-site could be used at temperatures as low as 600°C even on a thick electrolyte. Laboratory fuel cells with this new electrolyte have been tested, but the typical challenges of matching the thermal expansion coefficients, mechanical strength, and chemical compatibilities need further development.

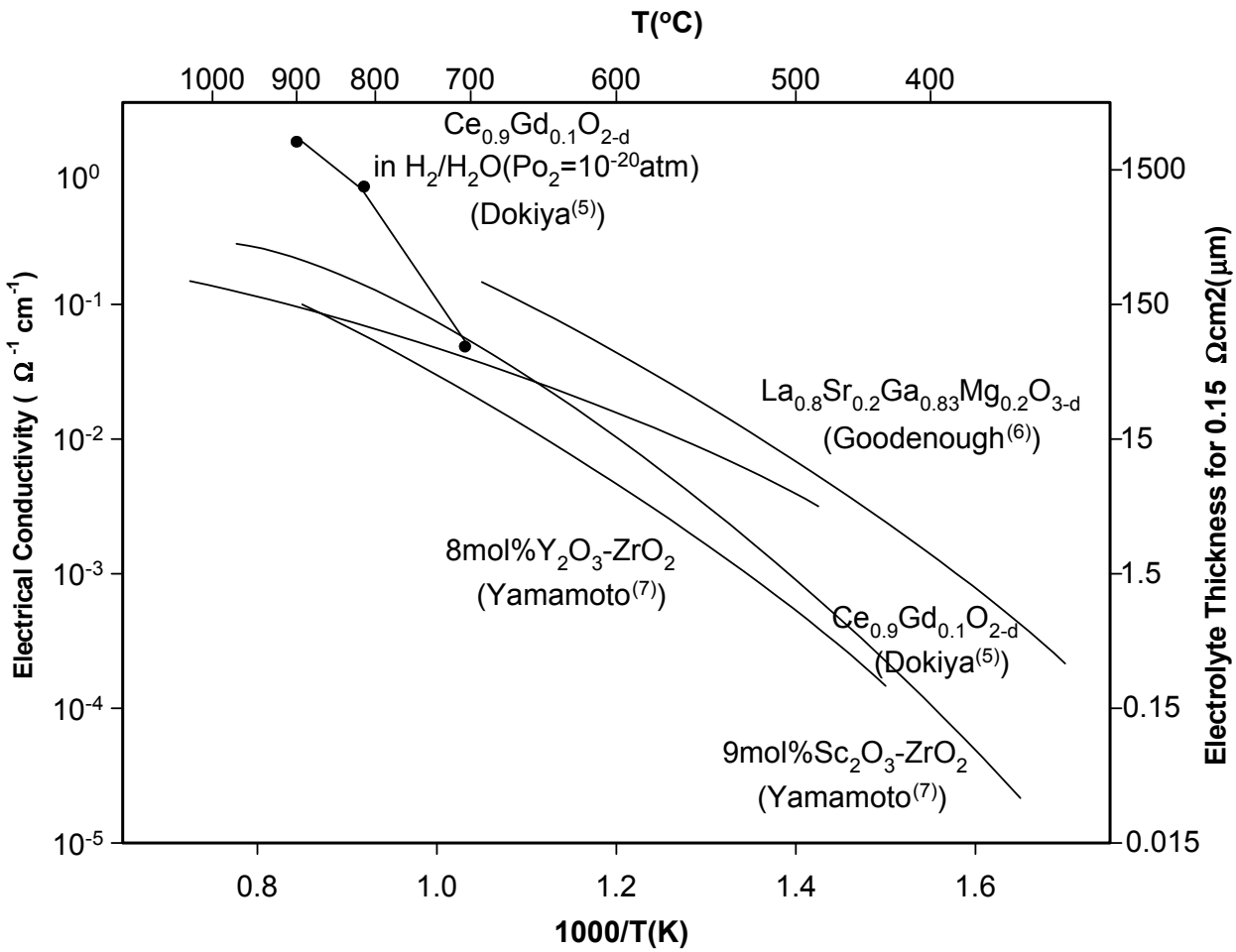

Figure 7-3 Electrolyte Conductivity as a Function of Temperature

A significant advance in the development of intermediate temperature PSOFCs has been the use of metallic "bipolar" interconnects. A bipolar plate is shown in Figure 7-4 (2). The unit shown has a pitch of 5 unit cells per inch. The bipolar plate has several functions, including providing a gas barrier between the anode and cathode, providing a series electrical connector between the anode and cathode, and flow field distribution. In order to be functional, the metallic inter-connect must satisfy a number of requirements, including:

- Impermeability
- Mechanical Strength
- Flexibility/compliance – compensate for CTE differences between ceramic components
- Flatness and dimensional tolerances
- Electrical
- Bulk conductivity
- Contact Resistance
- Pressure Drop (Flow Field Design)
- Manufacturability

- Cost

The bipolar plate is important for the so-called "stacking" of planar fuel cells. In order to produce significant amounts of power, PSOFC elements are assembled into a stack analogous to a multi-layered sandwich.

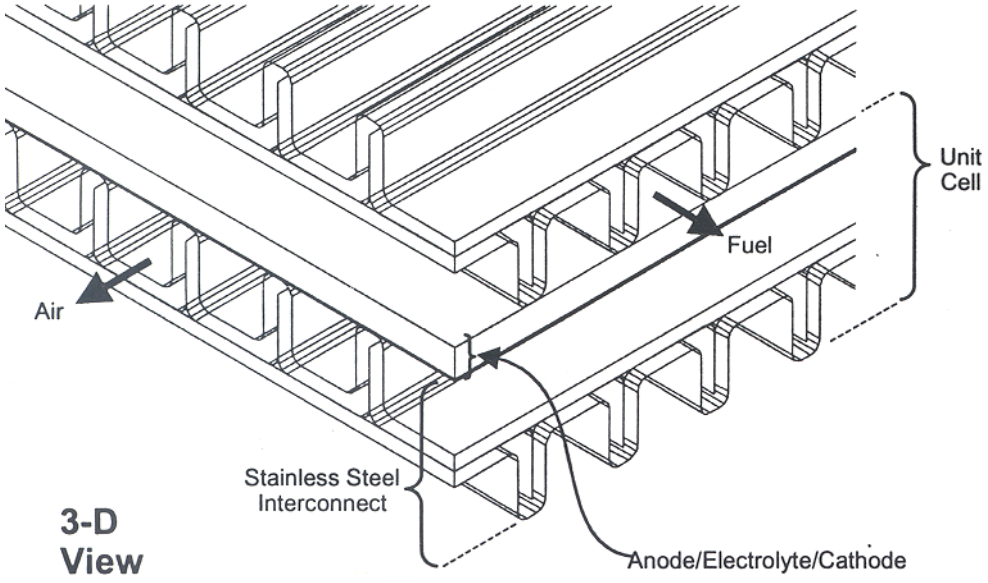

Figure 7-4 PSOFC with a Cross-Flow Stack Configuration

Individual cell assemblies, each including an anode, electrolyte, and cathode are stacked with metal interconnecting plates between them. The metal plates are shaped to permit the flow of fuel and air to the membranes. Figure 7-5 (8) shows a SOFC planar stack. The electrolyte and interconnect layers are made by tape casting. The electrodes are applied by the slurry method, by screen-printing, or by plasma spraying. Fuel cell stacks are formed by layers of unit cells, much like other fuel cell technologies (9). Tests of single cells and two-cell stacks of SOFCs with a planar configuration (5cm diameter) have demonstrated power densities up to 0.12 W/cm^2. One major technical difficulty with these structures is their brittleness in tension; the tensile strength is only about 20% of their compressive strength.

One candidate for use as a metallic interconnect material is ferritic stainless steel. However, a significant issue with this material is evaporation of a chromium hydrous oxide into the electrodes - degrading their performance. This evaporation creates a dilemma between corrosion protection and contact resistance. Stainless steel is protected against oxidation by surface films of chromium oxide, aluminum oxide, or some other stable oxides as shown in Figure 7-6 (2,10). However, only chromium oxide is a good electrical conductor. To solve this problem, surface coatings on steels are being explored which are conductive but contain chromium in a less volatile form.

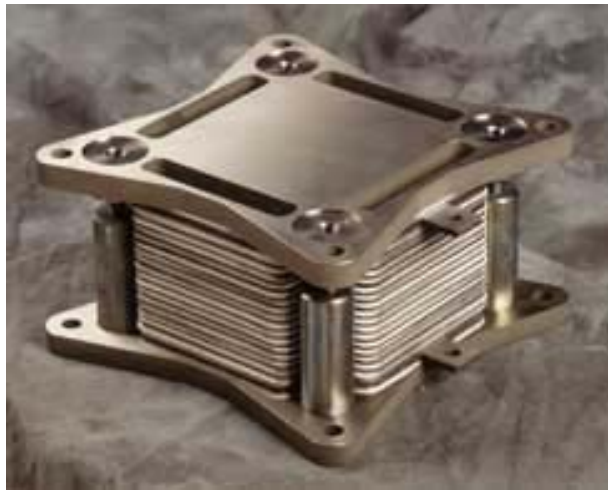

Figure 7-5 Planar Solid Oxide Fuel Cell Stack

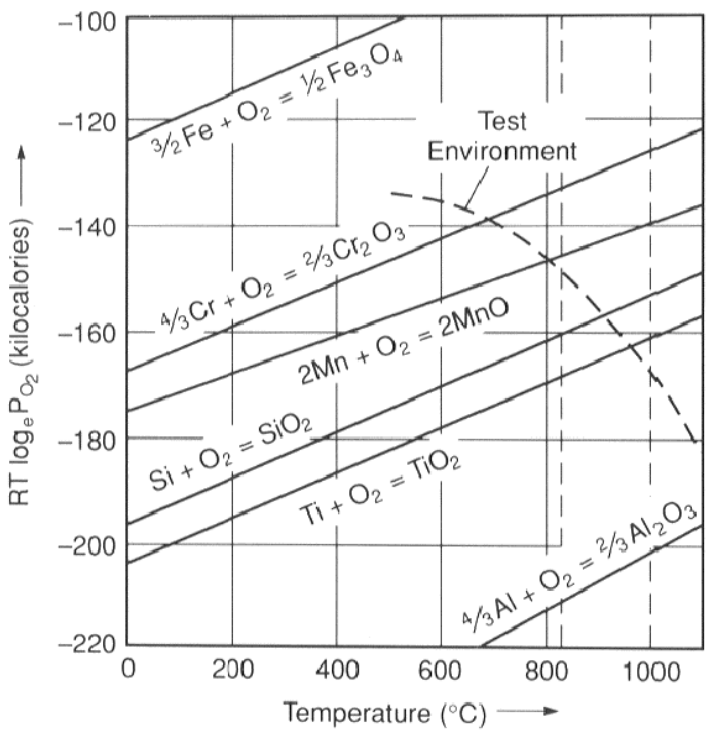

Figure 7-6 Stability of Metal Oxides in Stainless Steels

YSZ is the most commonly-used electrolyte material for SOFCs, oxygen generation systems, and oxygen sensors. YSZ is a preferred electrolyte material for SOFCs because it exhibits predominately ionic conductivity over a wide range of oxygen partial pressures. Colloidal fabrication and co-sintering processes have emerged, whereby YSZ membranes are produced as thin films (~10 μm) on porous electrode structures. These thin-film membranes improve

performance and reduce operating temperatures of SOFCs. To enable these colloidal processes to be successful, finer YSZ powders are needed. These applications require nano-scale powders with BET surface areas of 100 to 120 m^2/g and the use of suspensions ranging from 10 - 40% solid content (11,12).

With respect to cathode materials, the choice depends on the specific ceramic electrolyte material, the desired operating temperature, the electrochemical cell design, and the specific ceramic fabrication methods. Perovskite structured lanthanum strontium manganite (LSM) has been the most frequently-used material for SOFCs, including both planar and tubular. Another perovskite material with similar properties is lanthanum calcium manganite (LCM). Both of these materials offer an excellent thermal expansion match with zirconia electrolytes and provide good performance at temperatures above 800°C. For applications requiring lower temperature operation (600°C to 800°C), a range of alternative perovskite-structured ceramic electrodes are available. These include lanthanum strontium ferrite (LSF), lanthanum strontium cobalt ferrite (LSCF), lanthanum strontium manganese ferrite (LSMF), praseodymium strontium manganite (PSM), and praseodymium strontium manganese ferrite (PSMF). Improved performance of the cathode can be obtained by blending electrolyte material, such as YSZ, samarium doped ceria (SDC) or gadolinium doped ceria (GDC), with the perovskite material, such as LSM or PSFM. The incorporation of electrolyte material into the cathode materials has been shown to improve electrode performance at lower temperatures by increasing the volume of active sites available for electrochemical reactions. The electrolyte composition is typically 40 volume %.

SOFC anodes are fabricated from composite powdered mixtures of electrolyte materials (YSZ, GDC, or SDC) and nickel oxide. The nickel oxide is subsequently reduced to nickel metal prior to operation. The NiO/YSZ anode material is suited for applications with YSZ material, whereas NiO/SDC and NiO/GDC anode materials are best used with ceria-based electrolyte materials. Typical anode materials have nickel contents of approximately 40 volume % after reduction of the nickel oxide to nickel. Depending upon the application, powders have surface areas of 15 – 20 m^2/g for screen-printing and 5 – 10 m^2/g for tape casting.

Based on the above, it can be seen that recent technology development in the PSOFC cell components and materials has been the change to a thinner electrolyte layer, anode-supported cells, the use of metallic interconnect plates, and more conductive materials for electrolytes. A summary of the advantages associated with these advances is presented in Table 7-1 (2). From the table, it can be seen that the shift to thinner electrolytes has created the opportunity to reduce operating temperature and to use metal interconnects while still increasing power density. Development of higher conductivity electrolytes will further enhance these benefits. Developers are also evaluating the anode-supported electrolyte layer with YSZ, a proven material. Higher conductivity electrolytes may allow the use of thicker electrolyte layers at lower temperatures.

Table 7-1 Recent Technology Advances on Planar Cells and Potential Benefits

	Technology Advance	Potential Benefit
Design	Electrode supported **thin electrolyte** unit cells – e.g., anode	• Lower Resistance of Electrolyte • Increased Power Density
System	**Lower temperature** of operation	• Use of Metallic Interconnects and Manifolding Possible
Materials	**Metallic Interconnect Plates**	• Lower Cost • Lower Resistance Interconnect • Mechanical Solution to Thermal Expansion of Stack
Materials	More conductive Electrolyte Materials: Sc – Zr Oxides Ce – Gd Oxides	• Reduced Voltage Drop Across Electrolyte

The requirements for stack seal materials are extremely stringent (13). To avoid stress due to thermal expansion mismatch with adjacent components, the CTE must be similar to that of the other components (typically, in the range of 10-13 x 10^{-6}/°C). Chemical compatibility with the stack components and gaseous constituents of the highly oxidizing and reducing environments is also of primary concern. In addition, the seal should be electrically insulating to prevent shorting within the stack. A principal advantage of glass seals is that the glass composition can be tailored to optimize physical properties such as the CTE. However, several problems remain with regard to the use of glass seals in PSOFCs. The two issues of concern are the brittle nature of glass ceramics, and glasses tend to react with other cell components, such as electrodes, at SOFC operating temperatures.

A possible alternative to glass is the use of compressive, non-bonding seals. This approach permits the individual stack components to freely expand and contract during thermal cycling. However, the use of compressive seals also brings several new challenges to SOFC stack design; a load frame must be included to maintain the desired level of compressive load during operation, and the stack components must be able to withstand the compressive load required for adequate sealing for the lifetime of the stack. This research is in the early stage, and to date has focused on micas (14), which are composed of sheets of silicate platelets (15).

Figure 7-7 presents the results of recently-completed work at DOE's Pacific Northwest National Laboratory (PNNL) (16) that compares the leak rate of advanced compressive seals with those for mica gaskets under moderate compressive loads. As seen from the figure, the advanced compressive seals exhibited leak rates approximately 2 orders of magnitude lower than the simple mica gasket. The tests were conducted in air at 800°C.

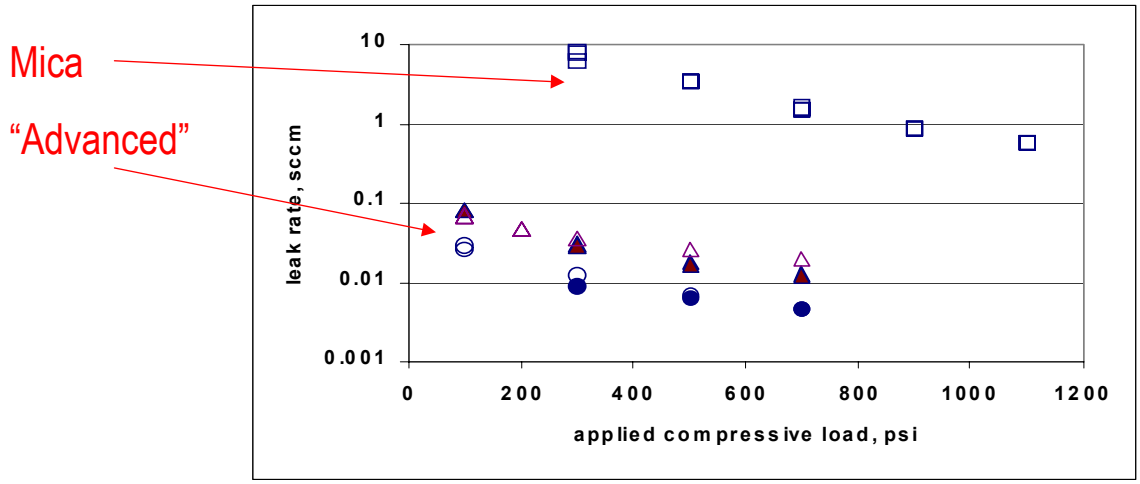

Figure 7-7 Observed Leak Rates for Advanced and "Standard" Mica Seals

Tubular SOFCs: Table 7-2 briefly describes the materials now used in various cell components of the tubular SOFC, and those that were considered during earlier development. Because of the high operating temperatures of the present tubular SOFCs (900 - 1,000°C), materials used in cell components are limited by chemical stability in oxidizing and reducing environments, chemical stability of contacting materials, conductivity, and thermomechanical compatibility.

To make a tubular SOFC, the cathode tube is fabricated first by extrusion and sintering. As shown in the table, it has a porosity of 30 - 40% to permit rapid transport of the reactant and product gases to the cathode/electrolyte interface where the electrochemical reactions occur. The electrolyte is applied to the cathode tubes by electrochemical vapor deposition (EVD), which for many years has been the heart of Siemens Westinghouse technology (17). In this technique, the appropriate metal chloride vapor is introduced on one side of the tube surface, and O_2/H_2O is introduced on the other side. The gas environments on both sides of the tube act to form two galvanic couples, as described in Equations 7-1, 7-2, and 7-3.

$$MeCl_y + \tfrac{1}{2}yO^{=} \rightarrow MeO_{y/2} + \tfrac{1}{2}yCl_2 + ye^- \qquad (7\text{-}1)$$

$$\tfrac{1}{2}O_2 + 2e^- \rightarrow O^{=} \qquad (7\text{-}2)$$

$$H_2O + 2e^- \rightarrow H_2 + O^{=} \qquad (7\text{-}3)$$

Table 7-2 Evolution of Cell Component Technology for Tubular Solid Oxide Fuel Cells

Component	Ca. 1965	Ca. 1975	Current Status [a]
Anode	• Porous Pt	• Ni/ZrO_2 cermet[a]	• Ni/ZrO_2 cermet[b] • Deposit slurry, EVD fixed[c] • 12.5 X 10^{-6} cm/cm°C CTE • ~150 :m thickness • 20-40% porosity
Cathode	• Porous Pt	• Stabilized ZrO_2 impregnated with praseodymium oxide and covered with SnO doped In_2O_3	• Doped lanthanum manganite • Extrusion, sintering • ~2 mm thickness • 11 X 10^{-6} cm/cm°C CTE from room temperature to 1000°C • 30-40% porosity
Electrolyte	• Yttria stabilized ZrO_2 • 0.5-mm thickness	• Yttria stabilized ZrO_2	• Yttria stabilized ZrO_2 (8 mol% Y_2O_3) • EVD[d] • 10.5 X 10^{-6} cm/cm°C CTE from room temperature to 1000°C • 30-40 :m thickness
Cell Interconnect	• Pt	• Mn doped cobalt chromite	• Doped lanthanum chromite • Plasma spray • 10 X 10^{-6} cm/cm°C CTE • ~100 :m thickness

a - Specification for Siemens Westinghouse SOFC
b - Y_2O_3 stabilized ZrO_2
c - "Fixed EVD" means additional ZrO_2 is grown by EVD to fix (attach) the nickel anode to the electrolyte. This process is expected to be replaced.
d - EVD = electrochemical vapor deposition

The net result is the formation of a dense, uniform metal oxide layer in which the deposition rate is controlled by the diffusion rate of ionic species and the concentration of electronic charge carriers. This procedure is used to fabricate the solid YSZ electrolyte.

The anode consists of metallic Ni and Y_2O_3 stabilized ZrO_2 skeleton. The latter serves to inhibit sintering of the metal particles and to provide a CTE comparable to those of the other cell materials. The anode structure is fabricated with a porosity of 20-40% to facilitate mass transport of reactant and product gases.

The cell interconnect (doped lanthanum chromite), on the other hand, must be impervious to fuel and oxidant gases and must possess good electronic conductivity. In addition, the cell interconnect is exposed to both the cathode and anode environments. Thus, it must be chemically stable under O_2 partial pressures of about 1 to 10^{-18} atmospheres at 1,000°C. The interconnect material is applied to the cathode tube as a narrow strip (see Figures 7-8 and 7-9)

prior to depositing the electrolyte by masking the rest of the tube. Similarly, the interconnect strip is masked when the electrolyte is applied.

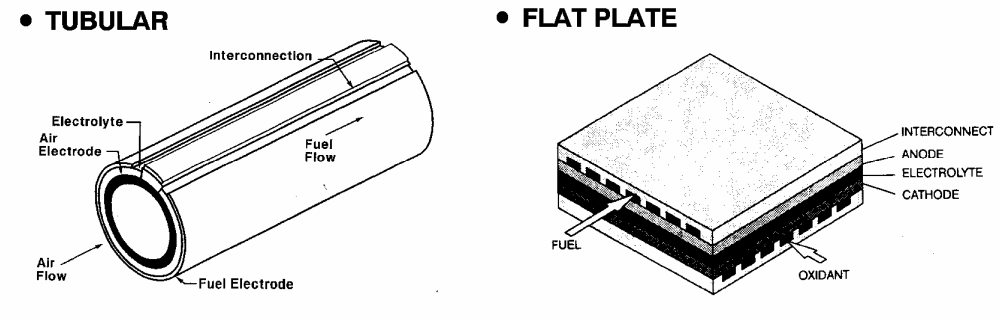

Figure 7-8 Tubular and Planar Cell Configurations

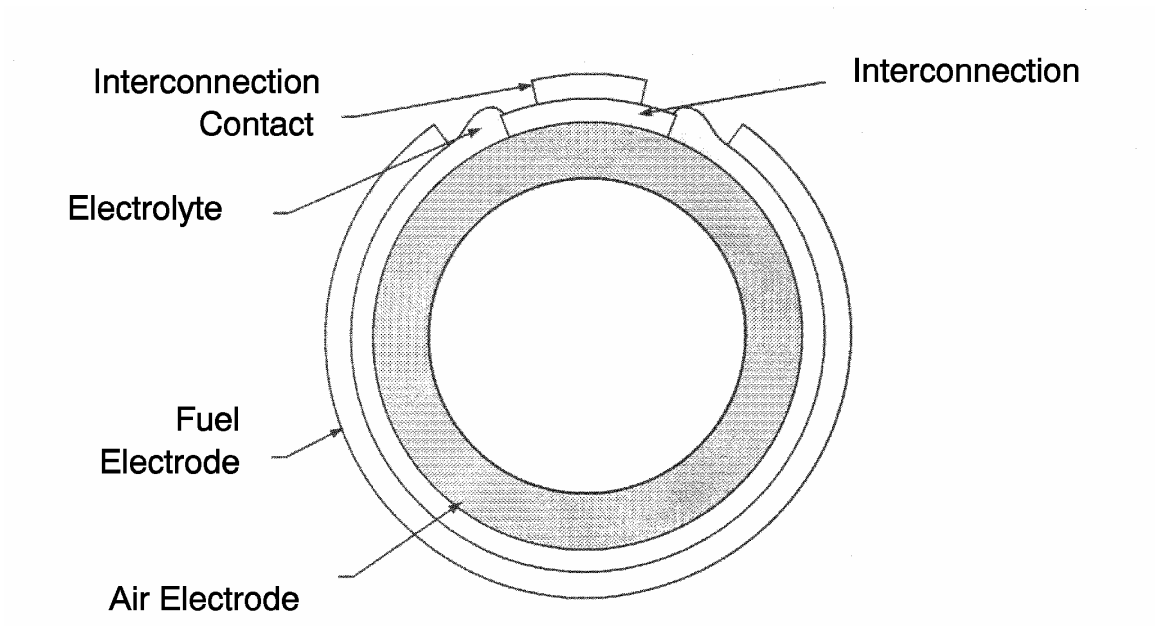

Figure 7-9 Cross Section of a Tubular Cell

The solid oxide electrolyte must be nonporous in order to prevent gas diffusion from one side of the electrolyte layer to the other, and it should be thin to minimize ohmic loss. In addition, the electrolyte must have a transport number for $O^{=}$ as close to unity as possible and a transport number for electronic conduction as close to zero as possible. Zirconia-based electrolytes are suitable for SOFCs because they exhibit pure anionic conductivity over a wide range of O_2 partial pressures (1 to 10^{-20} atmospheres). The other cell components should permit only

electronic conduction, and interdiffusion of ionic species in these components at 1,000°C should not have a major effect on their electronic conductivity. Other severe restrictions placed on the cell components are that they must be stable in the gaseous environments in the cell and that they must be capable of withstanding thermal cycling. The materials listed in Table 7-2 appear to meet these requirements.

The resistivities of typical cell components at 1,000°C under fuel cell gaseous environments (18) are 10 ohm-cm (ionic) for the electrolyte (8-10 mol % Y_2O_3 doped ZrO_2), 1 ohm-cm (electronic) for the cell interconnect (doped $LaCrO_3$), 0.01 ohm-cm (electronic) for the cathode (doped $LaMnO_3$), and 3 x 10^{-6} ohm-cm (electronic) for the anode (Ni/ZrO_2 cermet). It is apparent that the solid oxide electrolyte is the least conductive of the cell components, followed by the cell interconnect. Furthermore, an operating temperature of about 1,000°C is necessary if the ionic conductivity of the solid electrolyte (i.e., 0.02/ohm-cm at 800°C and 0.1/ohm-cm at 1,000°C) is to be within even an order of magnitude of that of aqueous electrolytes. The solid electrolyte in SOFCs must be only about 25-50 :m thick if its ohmic loss at 1,000°C is to be comparable to that of the electrolyte in PAFCs (19). Fortunately, thin electrolyte structures of about 40 :m thickness can be fabricated by EVD, as well as by tape casting and other ceramic processing techniques.

The successful operation of SOFCs requires individual cell components that are thermally compatible so that stable interfaces are established at 1,000°C, i.e., CTEs for cell components must be closely matched to reduce thermal stress arising from differential expansion between components. Fortunately, the electrolyte, interconnect, and cathode listed in Table 7-1 have reasonably close CTEs (i.e., ~10^{-5} cm/cm°C from room temperature to 1,000°C). An anode made of 100% nickel would have excellent electrical conductivity. However, the CTE of 100% nickel would be 50% greater than the ceramic electrolyte, or the cathode tube, which causes a thermal mismatch. This thermal mismatch has been resolved by mixing ceramic powders with Ni or NiO. The trade-off in the amounts of Ni (to achieve high conductivity) and ceramic (to better match the CTE) is approximately 30/70 Ni/YSZ by volume (20).

7.1.2 Cell Configuration Options

Two different design configurations are being developed for solid oxide fuel cells motivated by 1) considerations of how to seal the anode and cathode compartments, 2) ease of manufacturing, and 3) minimizing losses due to electric resistance. The two principal types are tubular and planar. Examples of these two basic configurations are presented in Figure 7-8 (21). The tubular SOFC has undergone development since the late 1950s. Operating between 900-1,000°C, the long tubes have relatively high electrical resistance but are simple to seal. Some tubular designs eliminate the need for seals and allow for thermal expansion. Several tubular units are presently operating in the field, with tens of thousands of hours of demonstrated operation. In the tubular configuration, bundles of tubes that are closed at one end are arranged in parallel. Air is introduced to the inside of each tube while fuel flows over the outside of the cells. Oxygen ions migrate through the electrolyte to react with fuel; the flow of ions produces electricity.

The PSOFC is composed of flat, thin ceramic plates. The PSOFC operates at 800°C or even less. Ultra-thin electrode/electrolyte sheets have low electrical resistance in order to achieve high efficiency. Operation at temperature lower than the tubular SOFC enables less exotic materials of construction, thus saving on cost.

In the planar configuration, the anode, electrolyte, and cathode form thin, flat layers that are sintered together, and then separated by bipolar plates similar to the design of other types of fuel cells. The plates can be either rectangular, square, circular, or segmented in series and can be manifolded externally or internally. Many of the PSOFCs use metallic bipolar plates and are operated at a lower temperature than the all-ceramic tubular design.

Planar SOFCs: The flat-plate design is shown in Figure 7-4 (2) for a cross-flow stack configuration. The unit shown has a pitch of 5 unit cells per inch. The most common plate shape is rectangular (square), although circular disks and segmented-in-series cells are also being developed. A recent development has been to use a bipolar interconnect made of ferritic stainless steel; this cannot be used in the manufacture higher-temperature fuel cells, because most steels oxidize quite readily at temperatures above 800°C.

To limit corrosion on the air side, the operating temperature of the PSOFC must be maintained below 800°C. However, the conductivity of the electrolyte decreases with falling temperature. There are two options for mitigating decreased performance in this case. The well-established YSZ electrolyte can be used at temperatures as low as 700°C when the thickness is about 15 micrometers. To go to even lower temperatures, more conductive electrolytes such as lanthanum gallate, scandium doped zirconia, or gadolinium doped ceria (GDC) can be used (4,22,23,24). Also, at significantly-reduced operating temperature, the lanthanum manganite cathode material becomes kinetic rate limiting to the point that it must be modified or replaced.

Multiple types of PSOFC stack configurations are under development. The conventional method has been the electrolyte-supported concept. This design has a thick electrolyte with thin anode and cathode layers. This was the first type of PSOFC, and is still in use by many developers today. These stacks operate at temperatures ranging from 900 - 1,100°C. The primary disadvantage of this design is that the high operating temperature requires specialized and exotic materials for the interconnect and other stack components. This leads to high material and production costs. These high temperatures also present a problem for long term operation and reliability due to material oxidation problems as well as integrating the balance of plant (BOP).

A newer stack configuration is the anode-supported concept. This design has a thick anode, which acts as the supporting structure. The electrolyte and cathode are very thin in comparison. These stacks operate within a temperature range of 700 - 800°C. Each individual cell is "sandwiched" or held between metal interconnecting plates that act as air and fuel flow channels as well as the electrical connection between each cell in a stack. This concept is illustrated in Figure 7-4. Most recently, this stack configuration is being explored. The advantage of this concept is the fact that metals are more durable than ceramics. By using the metallic bipolar plate as the main load-bearing component of the stack, the fracture resistance and thermal stress tolerance might be improved.

In order to produce significant amounts of power, cells are assembled into a stack analogous to a multi-layered sandwich. Cell membrane assemblies, each including an anode, electrolyte, and cathode are stacked, with metal interconnecting plates between them. The metal plates are shaped to permit the flow of fuel and air to the membranes, as shown in Figure 7-4 (2). The

electrolyte layer is made by tape casting. The electrodes are applied by the slurry method, by screen-printing, or by plasma spraying. Stacks of 10 kW electrical capacity and measuring 15 x 15 cm have been built and tested by several organizations. One major technical difficulty with these structures is their brittleness; the tensile strength is only about 20% of their compressive strength.

A new generation of intermediate temperature (650-800°C) SOFCs is being developed under the U.S. Department of Energy's SECA (Solid-State Energy Conversion Alliance) program. Fuel processing by an autothermal, steam, or partial oxidation reformer that operates between 500-800°C enables fuel cell operation on gasoline, diesel fuel, and other hydrocarbon fuels.

Reducing the temperature of the SOFC stack is one of the significant objectives being pursued to reduce the cost of SOFC stacks and the balance of plant (BOP). However, both beneficial and detrimental effects result from operating at reduced temperatures. The most significant obstacle is that a set of fully compatible materials has not yet been developed for operation at reduced temperature.

Benefits include:

- Reforming, Sulfur Removal, and Carbon Tolerance – A better thermal match exists with conventional reforming and sulfur removal processes. It should be noted that the optimal reformer temperature depends on the composition of the fuel. Thermodynamic conditions at the reduced temperatures do not favor carbon deposition.

- Sintering and Creep – Milder temperatures result in less sintering and creep of the stack materials. This helps maintain geometric stability and high surface area for reaction.

- Thermal Stress – Reduced temperature cycling reduces thermal expansion and contraction, thus maintaining geometric stability. This allows use of less construction material, which in turn improves area-specific resistance (ASR) and allows a wider range of sealing options.

- Material Flexibility – The range of potential construction materials is greater at lower temperatures. In particular, metals can be incorporated in SOFC stack designs.

- Balance of Plant – The BOP costs less if the stack fuel and oxidant exit temperature are less than 800°C; for the same reasons the stack should cost less.

- Heat Loss – Reduced heat loss from the stack at lower operating temperature. In particular, radiation losses can be significantly less, since these are a function of T^4. This can have a significant effect on the thermal efficiency of the stack.

- Time to Reach Operating Temperature – Assuming the same rate of heat-up as higher-temperature SOFCs, start-up time is reduced at lower operating temperature; this is obviously a benefit. Potential use of metals can also impact start-up time in a beneficial way, because metals can be heated at a faster rate than ceramics with no adverse thermal stress.

- Thermally Activated Processes – Thermally activated processes such as chromium vaporization, elemental inter-diffusion and migration, metallic corrosion, and ceramic aging become problematic at higher temperatures. The lower the operating temperature is maintained, the less damage these processes will cause to the fuel cell.

Some negative effects also result from reducing the operating temperature of the SOFC:

- Cell Voltage – For an equivalent stack, the overall cell voltage will be lower as temperature decreases due to the decreased kinetics, diffusion, and ionic conductivity. These effects offset the increased theoretical open circuit voltage of the electrochemical reaction at the lower temperature.

- Stack Materials – The only proven set of materials is functional between approximately 800 - 1,100°C. A proven material set in the intermediate temperature range (650 - 800°C) does not yet exist.

- Sulfur resistance decreases with temperature. However, recent work has shown that addition of certain materials provide adequate sulfur tolerance at lower temperatures.

- Lower temperatures generally require a planar configuration to minimize resistance losses. This is accomplished using ultra-thin electrode and electrolyte membranes. In turn, effective seals for the planar configuration are needed.

***Tubular SOFCs*:** Schematic representations of the gas manifold design and cross section of a typical tube bundle (25) are presented in Figures 7-10 and 7-11, respectively. In this design, the tubular cathode is formed by extrusion. Then the electrolyte and the cell interconnect are deposited by electrochemical vapor deposition (EVD) and plasma spraying, respectively, on the cathode. The anode is subsequently formed on the electrolyte by slurry deposition. A major advantage of this design over earlier designs is that relatively large single tubular cells can be constructed in which the successive active layers can be deposited without chemical or material interference with previously deposited layers. The support tube is closed at one end, which eliminates gas seals between cells.

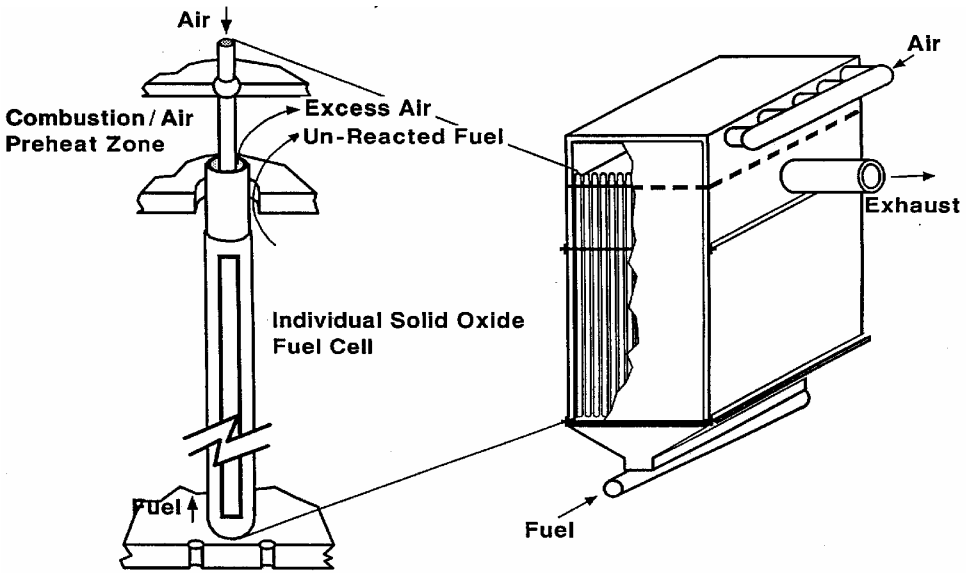

Figure 7-10 Gas Manifold Design for a Tubular SOFC

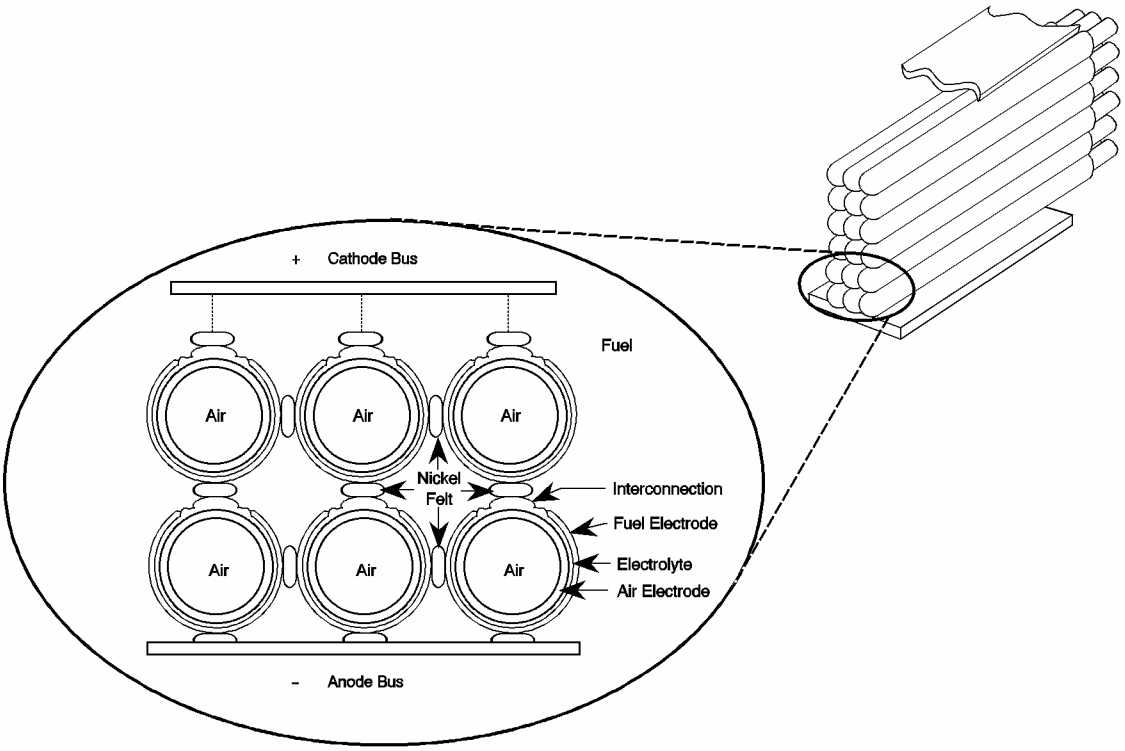

Figure 7-11 Cell-to-Cell Connections in a Tubular SOFC (25)

The oxidant is introduced via a central $A1_2O_3$ injector tube and the fuel gas is supplied to the exterior of the closed-end cathode tube. In this arrangement, the $A1_2O_3$ tube extends to the proximity of the closed end of the tube, and the oxidant flows back past the cathode surface to

the open end. The fuel gas flows past the anode on the exterior of the cell and in a parallel direction (co-flow) to the oxidant gas. The spent gases are exhausted into a common plenum where any remaining fuel reacts. The heat generated serves to preheat the incoming oxidant stream and/or drive an expander. One attractive feature of this arrangement is that it eliminates the need for leak-free gas manifolding of the fuel and oxidant streams. However, the seal-less tubular design results in a relatively long current path around the circumference of the cell to the interconnect, limiting performance. The length of the cell has been gradually increased from 30 cm to 150 cm. The cell has a diameter of 1.27 cm. Figure 7-11 shows a bundle of eighteen cells that features 3 cells in series with 6 cells in parallel. Also shown are the nickel felts that are used to make electrical connections. The cells are connected in a series-parallel array by nickel felt strips that are exposed to the reducing fuel gas. In this arrangement, the nickel felt strips and cell interconnects extend the length of the cell. Because the current flows in the circumferential direction of the electrodes, a relatively large ohmic loss exists, which places an upper limit on the tube diameter.

7.1.3 Development Status

For the current YSZ electrolyte to provide sufficient oxygen conductivity, it must be heated to a high temperature (900 - 1,000°C). This means, however, that expensive high temperature alloys must be used to house the fuel cell, increasing its cost substantially. These costs could be reduced if the operating temperature was lowered to between 600 - 800°C, allowing the use of less expensive structural materials such as stainless steel. A lower operating temperature would also ensure a greater overall system efficiency and a reduction in the thermal stress in the ceramic structure, leading to a longer service life for the fuel cell.

To lower the operating temperature, either the conductivity of the YSZ must be improved by producing thinner electrolytes, or alternative electrolytic materials must be developed that can replace YSZ. A concerted effort is being made by researchers around the world to find an optimal solution.

Planar Solid Oxide Fuel Cells: Worldwide, a number of developers, especially from the United States, Australia, Japan, and Europe, are involved in tubular and PSOFC technology; Table 7-3 summarizes several developers. Table 7-4 presents a list of U.S. participants and their roles in the PSOFC development effort. That list includes universities, national laboratories, industrial participants, and government agencies.

Table 7-3 Leading PSOFC Developers – World Wide

U.S.	Europe	Japan	Other
• General Electric* • MSRI** (GRI, EPRI, and University of Utah) • SOFCo (LBL, EPRI) • Siemens AG (Westinghouse) • Cummins • DOE • DOD • NIST	• Forschungszentrum Julich GmbH • Sulzer Hexis Ltd. • Rolls Royce	• Chubu Electric Power Company (Mitsubishi Heavy Industries, MHI) • Tokyo Gas Co. • Osaka Gas Co. (Murata Mfg. Co.) • Mitsui Engineering & Shipbuilding Co. • Other	• Ceramic Fuel Cells Limited (CFCL) (Australia) • Global Thermoelectric Inc. (GTI) (Canada, "license" of Julich technology)

* Formerly Honeywell
** Materials and Systems Research Inc.

Previous development of the PSOFC was based largely on work for solid oxide fuel cell operation at temperatures up to 1,000°C. The principal electrolyte material was YSZ. Reducing the operating temperature by 200°C extends component life and reduces manufacturing costs. However, reduced temperature also significantly reduces electrolyte conductivity and electrode kinetics. To overcome those performance reductions, recent cell and stack development have focused on the following:

- Thin-film electrode production
- Thin-film electrolyte production
- Enhanced oxygen ion transport through the electrolyte
- Enhanced electrode kinetics
- Develop inexpensive automated manufacturing technique
- Development of proton-conducting electrolytes

Present fuel cell designs make use of thin film concepts where films of electrode and electrolyte material are deposited on one another and sintered, forming a cell structure. The fabrication techniques differ according to the type of cell configuration and developer. After the electrode has been prepared, the electrode is coated with the electrolyte. The coating may be applied using a variety of techniques, including tape calendering, dip-coating, spray-coating, electrophoretic deposition, or spin coating. In each case, developers strive for a thin, dense, pinhole-free electrolyte coating.

Table 7-4 U.S. Participants Involved in PSOFC Research and Development

Developer	PSOFC Development Role
University of Florida (16)	Develop bi-layer ceria, bismuth oxide electrolyte for low temperature operation. Develop ionic conduction model.
Northwestern University/Applied Thin Films (9,16)	Develop segmented in series SOFC design. Develop internally reforming anode as discussed in "Nature".
Georgia Institute of Technology (16)	Development of ultra-low (500°C) temperature SOFC materials. Development of *in situ* FTIR emission spectroscopy for evaluation of gas-solid interactions in fuel cells.
NexTech Materials, Ltd. (11,12,26)	Development of cathode supported SOFC designs. Development of manufacturing techniques for low temperature SOFC materials.
SOFCo (27,28) (LBL, EPRI)	Interconnects. Development of low temperature material set. Demonstrate electrolyte-supported cell.
Oak Ridge National Lab (16,29)	SOFC material property and reliability evaluations Power electronics evaluation.
Pacific Northwest National Laboratory (13,16,30)	Component material development modeling. Prototype stack testing.
Lawrence Berkley National Laboratory (16)	Development of inexpensive metal alloy electrodes.
Argonne National Lab (16,31)	Low temperature cathode materials. Sulfur tolerant anode materials. Metallic bipolar plates.
University of Missouri – Rolla (16,32)	Development of parallel pore channel electrodes.
University of Utah (16,33,34) (MRSI, GRI, EPRI, NIST)	Demonstrate University of Utah PSOFC technology-anode supported cell.
General Electric (35,36,37)	Demonstrate a fuel flexible 3-to-10kw PSOFC system-anode supported cell.
Siemens Westinghouse (38)	Develop "planar" seal-less SOFCs for high temperature operation (850°C to 1,000°C) – cathode supported cell.
University of Texas, Austin (4)	Evaluation of lanthanum gallate for electrolyte applications.
University of Pennsylvania (39)	Performance of thin-film YSZ for operation between 600°C and 800°C.

To reduce the resistivity of the electrolyte, development has focused on reducing its thickness from 150 :m to less than 20 :m. Wang, et al., (39) at the University of Pennsylvania, fabricated thin-film YSZ electrolytes between 3 and 10 :m. Wang also reported significant improvement in cell performance with mixed conducting-doped YSZ electrodes; Tb- and Ti-doped YSZs increased power densities between 15 – 20%. Other examples of this approach are also available in the literature (4,16,23,24,33).

Ball and Stevens (23) report that gadolinium doped ceria is a good candidate for use as an alternative electrolyte when compared to zirconia, due to its higher conductivity at lower temperatures. However, doped ceria has a number of disadvantages, such as electronic

conductivity and reduced strength. Recent results indicate that an increase in strength can be produced in the ceria by addition of zirconia particles that is dependent on the particle size and heat treatment.

Research at the University of Texas at Austin (4) has also sought to develop electrolytes that have higher conductivity than YSZ. Goodenough and Huang (40) identified a system of LaSrGaMgO (LSGM) as a superior oxide-ion electrolyte with performance at 800°C comparable to YSZ at 1,000°C (40). LSGM lacks the toughness of YSZ, which makes it more difficult to fabricate as an ultra-thin film, but its superior ionic conductivity allows thicker films to be used. Figure 7-12 illustrates the performance of a single cell based on a LSGM electrolyte.

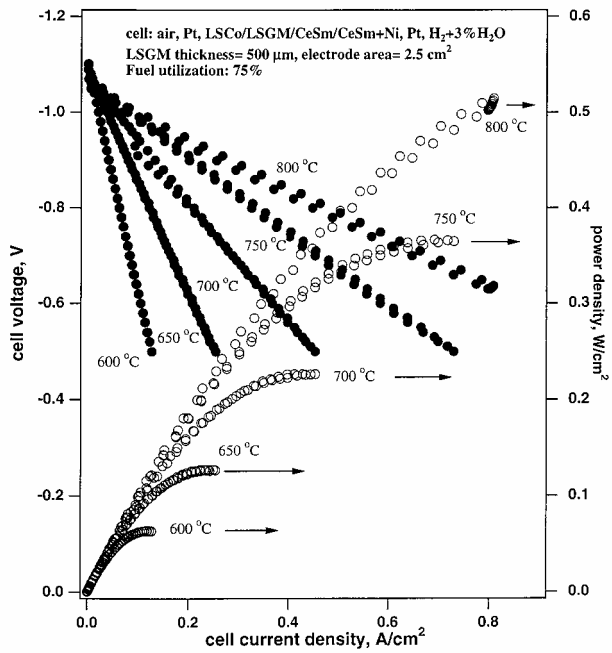

Figure 7-12 Single Cell Performance of LSGM Electrolyte (50 :m thick)

Barnett, Perry, and Kaufmann (24) found that fuel cells using 8 :m thick yttria-stabilized zirconia (YSZ) electrolytes provide low ohmic loss. Furthermore, adding thin porous yttria-doped ceria (YDC) layers on either side of the YSZ yielded much-reduced interfacial resistances at both LSM cathodes and Ni-YSZ anodes. The cells provided higher power densities than previously reported below 700°C, e.g., 300 and 480 mW/cm^2 at 600 and 650°C respectively (measured in 97% H_2 and 3% H_2O and air), and also provided high power densities at higher temperatures, e.g., 760 mW/cm^2 at 750°C. Recent data (Figure 7-13) from the University of Utah (16) show power densities of 1.75 W/cm^2 with H_2/air and 2.9 W/cm^2 with H_2/O_2 at 800°C for an anode-supported cell. However, no data is presented with regard to electrodes or electrolyte thickness and composition.

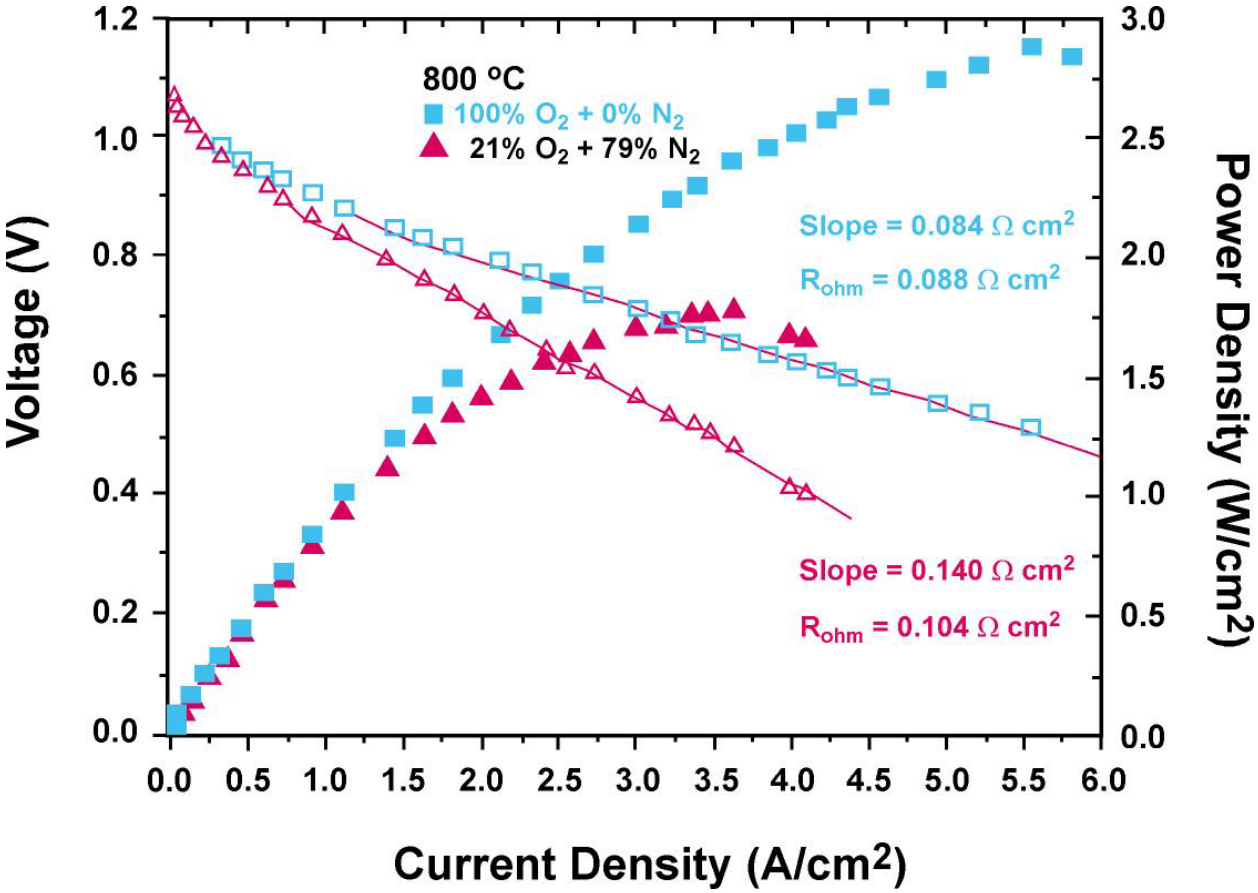

Figure 7-13 Effect of Oxidant Composition on a High Performance Anode-Supported Cell

Bhide, et al., at the University of Utah (33) examined joint chemical stability and proton conductivity of mixed perovskite conductors. Bhide identified $Ba_3CaNb_2O_9$ as a potential proton-conducting electrolyte for PSOFCs.

Doped barium cerate is also a well-known proton conducting oxide (44). It has been proposed as a fuel cell electrolyte, offering high conductivity at temperatures lower than those used in zirconia-based fuel cells. It has been observed, however, that exposure to CO_2 in the fuel cell causes degradation in barium carbonate and cerium oxide. By contrast, barium zirconate is quite stable in the presence of CO_2, but is undesirable as a fuel cell electrolyte because of its relatively low proton conductivity. Ryu, et al. (42), at the California Institute of Technology investigated conductivity and stability of doped barium cerate as a function of zirconium substitution onto the cerium site. Ryu observed a composition window at which both the chemical stability and proton conductivity were sufficiently high to meet the requirements of fuel cell applications.

Visco, et al., at Lawrence Berkeley National Laboratory (43) explored thin-film electrolyte fabrication as well as alternate electrolyte materials to promote oxygen transport. Single cells have produced 0.51V at a current density of 710 mA/cm^2 at 700°C. YSZ electrolyte performance was compared against scandia-stabilized zirconia (SSZ), samaria doped ceria

(SDC), and gadolinium doped ceria (GDC) alternatives. Although the SSZ electrolyte had significantly higher conductivity than YSZ between 600-700°C, improved fuel cell performance was not observed; this was attributed to possible poor electrode microstructure, in which an $La_{3.85}Sr_{0.15}MnO_3$ (LSM) electrode was used. Visco observed good performance for cobaltite perovskite electrodes such as $La_{0.60}Sr_{0.40}Co_{0.98}Ni_{0.02}O_3$ (LSCN) well below 800°C, and recommends their use with ceria electrolytes.

Other alternative material research includes investigating materials that exhibit 1) polarizable (easily weakened) metal oxygen bonds, 2) open, layered structures for greater ion mobility, and 3) lower coordination numbers for the mobile ions. These are important criteria for high conductivity (44). This approach to electrolyte development is to stabilize a very conductive oxide by compound formation or by solid solution formation with more stable oxides. Conductivity of 10^{-1}/ohm-cm has been obtained with Zn-doped $La_{1-x}Bi_xA1O_3$ compared to 1.8 x 10^{-2}/ohm-cm for YSZ at 700°C (45).

The conventional high temperature SOFC anode material, Ni-YSZ, remains a leading candidate for intermediate temperature operation due to its highly conductive nickel phase. Two factors, however, can decrease the performance of this anode over long-term operation. First, most fuels considered for SOFC applications contain a significant amount of sulfur, which is known to poison the catalytic activity of the anode at levels as low as 1 ppm. Sulfur removal technology prior to fuel introduction to the fuel cell will add to the size, complexity, and cost of the total system. Development of sulfur tolerant anodes would greatly alleviate or even eliminate this problem. The second factor relates to the stability of the anode if it is exposed to oxidizing environments during repetitive start-up and shutdown cycles.

As mentioned previously, one of the most significant changes resulting from operation at 800°C or below is the move from ceramic to metallic interconnects (2,12,26). Metal interconnects would almost certainly reduce the cost of the stack. They would also improve the mechanical strength of the stack and allow better thermal management during operation. Development of metallic interconnects is still at an early stage. The most significant problems that they face are oxidation of the metal or alloy on the air side of the bipolar plate, and the volatization of hydrous chromium oxide. New alloys and protective coatings are being developed to overcome these problems.

The successful operation of PSOFCs requires individual cell components that are thermally compatible, meaning that component interfaces are closely matched to reduce stresses arising from differential thermal expansion (13,16). Ideally, the electrolyte, interconnect, and electrodes have reasonably close coefficients of thermal expansion (i.e., ~10^{-5} cm/cm°C) over a wide temperature range. For example, an anode made of pure nickel will be 50% greater than a ceramic electrolyte and cause a thermal mismatch. Several organizations are investigating mixed conduction materials for the cathode and anode that have both good conductivity and thermal expansion coefficients matched to the electrolyte. Lanthanum strontium ferrite (LSF) is more active than LSM cathodes on zirconia electrolytes, and lanthanum strontium cobaltite is even better, but can only be used on ceria electrolytes (41).

Other concerns regarding the commercialization of PSOFCs include ease of manufacturing, manufacturing cost, and lightweight materials to minimize thermal mass for quick startup. Although these are not yet primary objectives of component R&D, the developers do consider these factors in their fuel cell designs.

Recent data on the performance of PSOFCs is presented in Figures 7-14 and 7-15 (35,38). The first of these shows the performance of anode-supported thin electrolyte cells. As seen from Figure 7-14, high power densities (e.g., 0.9 W/cm^2 at 650°C) have been achieved at temperatures less than 650°C. Figure 7-15 presents the estimated performance of the Siemens Westinghouse seal-less planar design versus that of the current 2.2 cm cylindrical design. A comparison of the current seal-less cross section with that of the seal-less planar design is shown in Figure 7-16. As seen from Figure 7-16, the new planar design has the following features:

- Maintains the seal-less design
- Reduction in resistance and cell cost
- Increase in cell power (power density and surface area)
- More compact stack

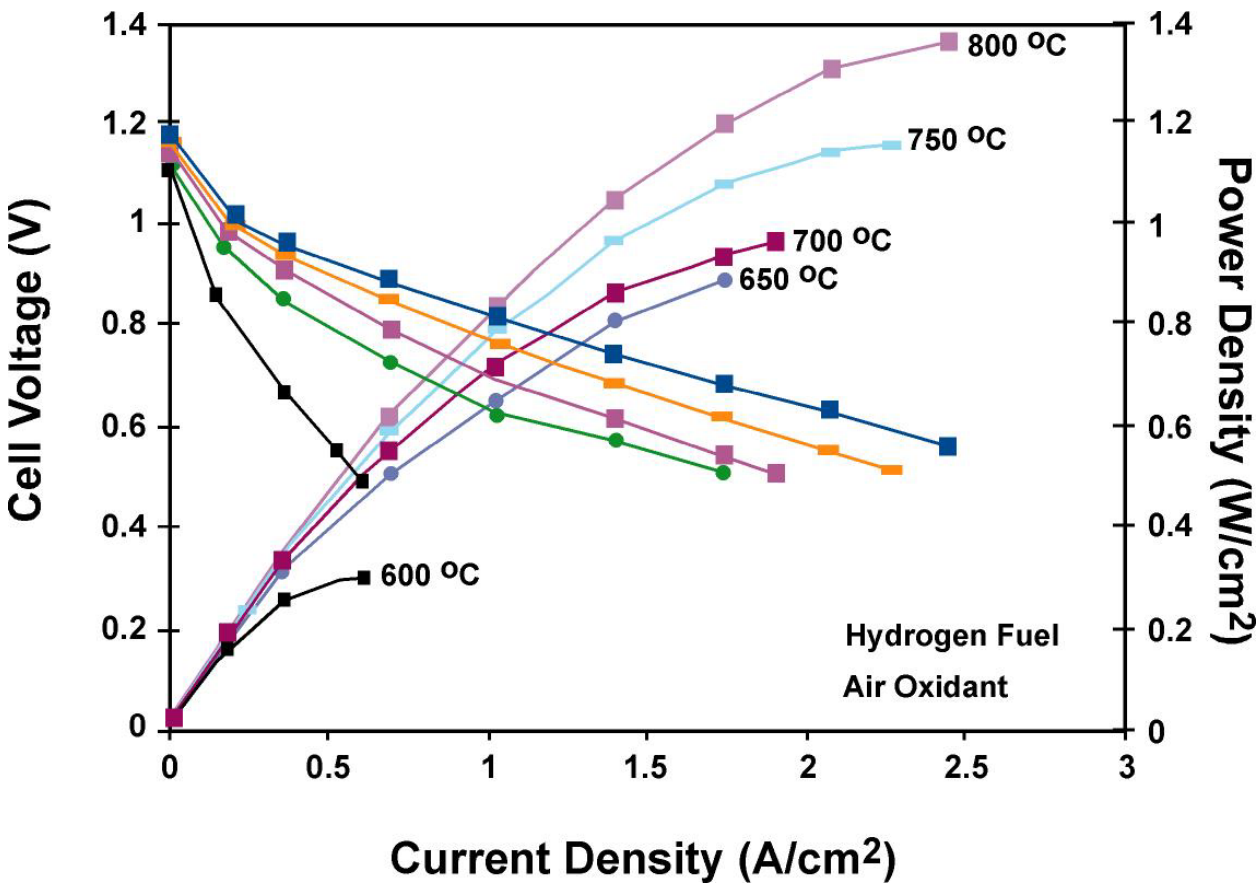

Figure 7-14 Performance of PSOFC at Reduced Temperatures

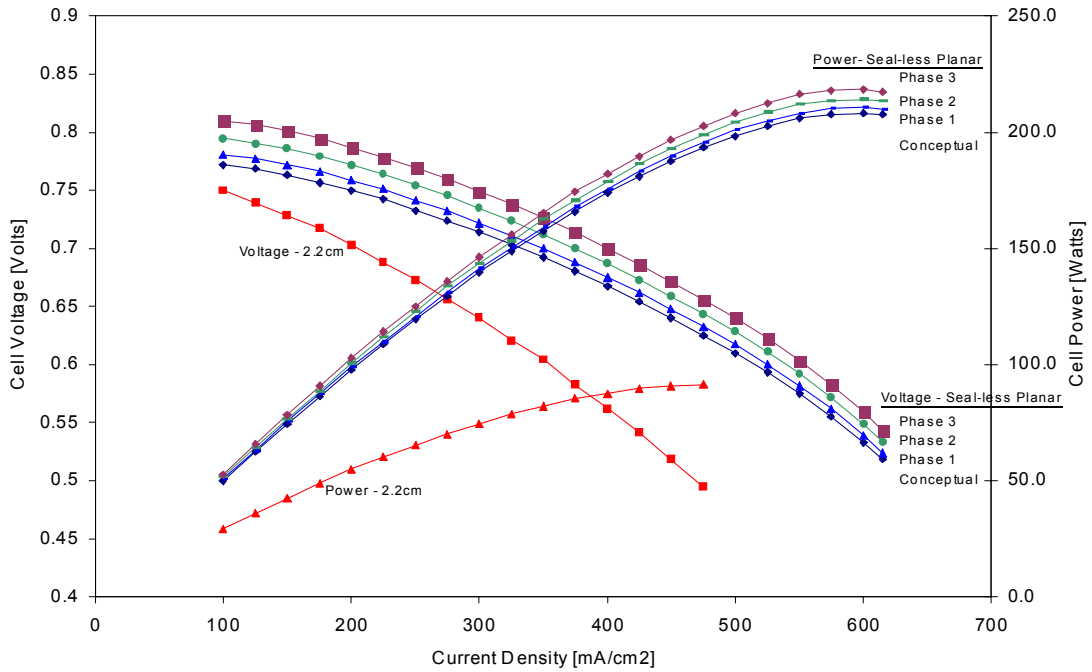

Figure 7-15 Projected Performance of Seal-less Planar Design with Current Seal-less Cylindrical Design

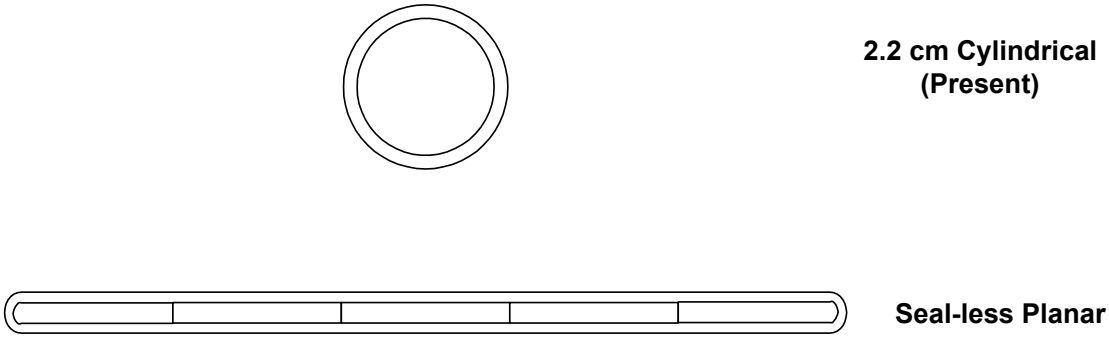

Figure 7-16 Planar Seal-less Design

As apparent from the discussion above, many organizations are involved in the development of PSOFC technology, including universities, national laboratories, industrial participants, and government agencies. The industrial participants are focused primarily on commercializing the technology. At this point, most development efforts are focused on the electrolyte and methods for supporting PSOFCs.

Tubular SOFCs: The major issue for improving tubular SOFC technology has been to develop materials that sustain good performance while withstanding the high operating temperature (900-1,000°C). Related critical issues are 1) that the present materials and cell designs must operate at high temperature to obtain performance due to their intrinsic high resistivity, and 2) high temperatures are required in the fabrication of ceramic components, which adds complexity, hence cost.

Siemens Westinghouse has developed its cell technology to the extent that a fabrication facility is being built to construct full size cell stacks that will be integrated into a power unit, as discussed at the 3rd Annual SECA Workshop (Solid-State Energy Conversion Alliance), Washington, DC, March 2002 (46). Recent work has focused on cost reduction, product definition, manufacturing expansion, and prototype production and testing.

7.2 Performance

This section provides empirical information that can be used to estimate the relative performance of SOFCs based on various operating parameters. The SOFCs being developed, particularly the planar types, have unique designs, are constructed of various materials, and are fabricated by different techniques. This development process will result in further evolution of the performance trends summarized here. The electrochemical reactions associated with hydrogen fuel are expressed in equations (7-4) to (7-6):

$$H_2 + O^{=} \rightarrow H_2O + 2e^- \tag{7-4}$$

at the anode, and

$$\tfrac{1}{2}O_2 + 2e^- \rightarrow O^{=} \tag{7-5}$$

at the cathode. The overall cell reaction is

$$H_2 + \tfrac{1}{2}O_2 \rightarrow H_2O \tag{7-6}$$

The corresponding Nernst equation for the reaction in equation 7-6 is

$$E = E^\circ + \frac{RT}{2F} \ln \frac{P_{H_2} P_{O_2}^{1/2}}{P_{H_2O}} \tag{7-7}$$

In addition to hydrogen, carbon monoxide (CO) and other hydrocarbons such as methane (CH_4) can also be used as fuels. It is feasible that the water gas shift reaction involving CO ($CO + H_2O \rightarrow H_2 + CO_2$) and the steam reforming of CH_4 ($CH_4 + H_2O \rightarrow 3H_2 + CO$) in the high temperature environment of SOFCs produce H_2 that is easily oxidized at the anode. The direct oxidation of CO in fuel cells is also well established. Because of the increased number of chemical species and competing reactions, however, derivation of cell performance as a function of temperature, pressure, and composition effects is not straightforward. Recent data by Crucian, et al. (47), presents results for the direct oxidation of hydrocarbons on copper/ceria.

The thermodynamic efficiency of SOFCs operating on H_2 and O_2 at open circuit voltage is lower than that of MCFCs and PAFCs because of the lower free energy at higher temperatures. On the other hand, the higher operating temperature of SOFCs is beneficial in reducing polarization resistance.

The voltage losses in SOFCs are governed by ohmic losses in the cell components. The contribution to ohmic polarization (iR) in a tubular cell (assuming uniform current distribution in the electrolyte) is 45% from the cathode, 18% from the anode, 12% from the electrolyte, and 25% from the interconnect when these components have thicknesses of 2.2, 0.1, 0.04 and 0.085 mm, respectively, and specific resistivities (ohm-cm) at 1,000°C of 0.013, 3×10^{-6}, 10, and 1, respectively. The cathode iR dominates the total ohmic loss despite the higher specific resistivities of the electrolyte and cell interconnection because of the short conduction path through these components and the long current path in the plane of the cathode.

7.2.1 Effect of Pressure

SOFCs, like PAFCs and MCFCs, show enhanced performance by increasing cell pressure. The following equation approximates the effect of pressure on cell performance at 1,000°C:

$$\Delta V_p(\text{mV}) = 59 \log \frac{P_2}{P_1} \tag{7-8}$$

where P_1 and P_2 are different cell pressures. The above correlation was based on the assumption that overpotentials are predominately affected by gas pressures and that these overpotentials decrease with increased pressure.

Siemens Westinghouse, in conjunction with Ontario Hydro Technologies, tested air electrode supported (AES) cells at pressures up to 15 atmospheres on both hydrogen and natural gas (48). Figure 7-17 illustrates the performance at various pressures:

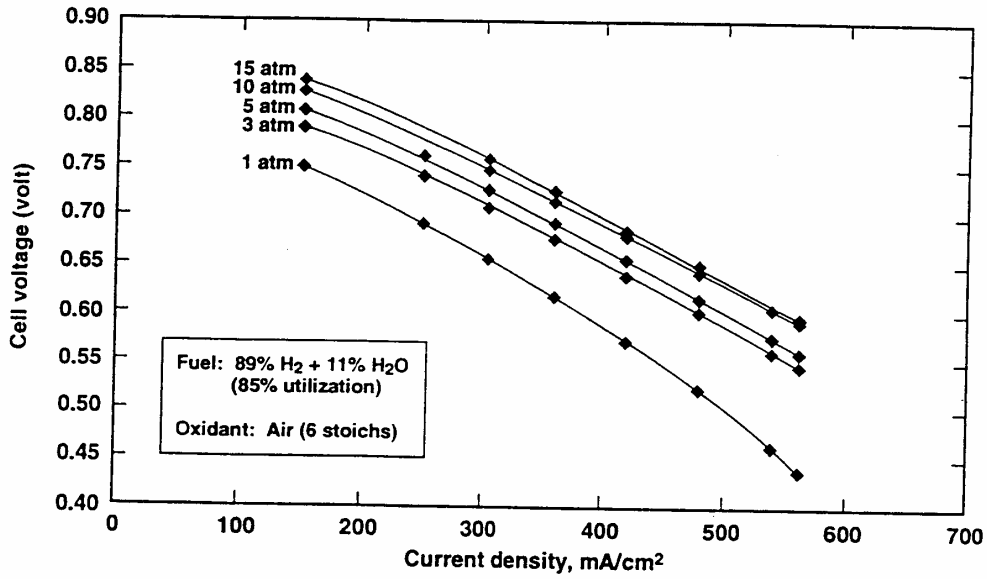

Figure 7-17 Effect of Pressure on AES Cell Performance at 1,000°C (2.2 cm diameter, 150 cm active length)

7.2.2 Effect of Temperature

The dependence of SOFC performance on temperature is illustrated in Figure 7-18 for a two-cell stack using air (low utilization) and a fuel of 67% H_2/22% CO/11% H_2O (low utilization). The sharp decrease in cell voltage as a function of current density at 800°C is a manifestation of the high ohmic polarization (i.e., low ionic conductivity) of the solid electrolyte at this temperature. The ohmic polarization decreases as the operating temperature increases to 1,050°C, and correspondingly, the current density at a given cell voltage increases. The data in Figure 7-18 show a larger decrease in cell voltage with decreasing temperature between 800 - 900°C than that between 900 - 1,000°C, at constant current density. This and other data suggest that the voltage gain with respect to temperature is a strong function of temperature and current density. One reference (49) postulates the voltage gain as:

$$\Delta V_T(\text{mV}) = 1.3(T_2 - T_1)(^\circ\text{C}) \tag{7-9}$$

for a cell operating at 1,000°C, 160 mA/cm^2, and a fuel composition of 67% H_2/22% CO/11% H_2O. In light of the strong functionality with respect to current density, it might be more appropriate to describe the voltage gain with the following relationship:

$$\Delta V_T(\text{mV}) = K(T_2 - T_1)(^\circ\text{C}) * J \tag{7-10}$$

where J is the current density in mA/cm^2.

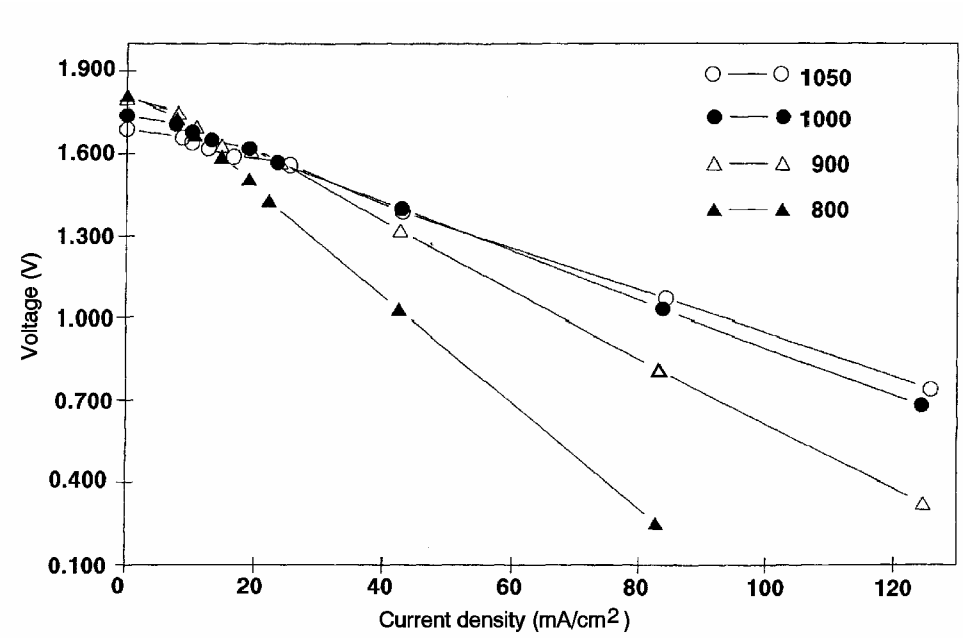

Figure 7-18 Two-Cell Stack Performance with 67% H_2 + 22% CO + 11% H_2O/Air

The following values of K have been deduced from several references using a fuel composition of 67% H_2/22% CO/11% H_2O, and an air oxidant.

Table 7-5 K Values for ΔV_T

K	Temperature (°C)	Ref.
0.008	~1000	49
0.006	1000 - 1050	50
0.014	900 - 1000	
0.068	800 - 900	
0.003	900 - 1000	51
0.009	800 - 900	

As can be seen, there is a reasonably large range in the value of K between these references. As the SOFC technology matures, these differences may reconcile to a more cohesive set of values. In the interim, the following expressions may help the reader if no other information is available:

$$\Delta V_T(mV) = 0.008(T_2 - T_1)(°C) * J(mA/cm^2) \qquad 900°C \leq T \leq 1050°C \qquad (7\text{-}11)$$

$$\Delta V_T(mV) = 0.040(T_2 - T_1)(°C) * J(mA/cm^2) \qquad 800°C \leq T \leq 900°C \qquad (7\text{-}12)$$

$$\Delta V_T(mV) = 1.300(T_2 - T_1)(°C) * J(mA/cm^2) \qquad 650°C \leq T \leq 800°C \tag{7-13}$$

Equations (7-11) and (7-12) are for a fuel composed of 67% H_2/22% CO/11% H_2O. Experiments using different fuel combinations, such as 80% H_2/20% CO_2 (51) and 97% H_2/3% H_2O (50,52), suggest that these correlations may not be valid for other fuels. Equation (7-13) is based on the average value of the data shown in Figure 7-14, i.e., an anode-supported PSOFC with a thin electrolyte using hydrogen as a fuel and air as an oxidant. This approach is indicative of the current development path being pursued in SOFC technology: planar, electrode supported cells featuring thin (<10 μm) electrolytes of YSZ. It has been noted that new electrode and electrolyte materials are also under development.

Figure 7-19 presents a set of performance curves for a fuel of 97% H_2/3% H_2O at various temperatures (49). Voltage actually increases with decreasing temperature for current densities below approximately 65 mA/cm^2. Other data (53) show that this inverse relationship can extend to current densities as high as 200 mA/cm^2.

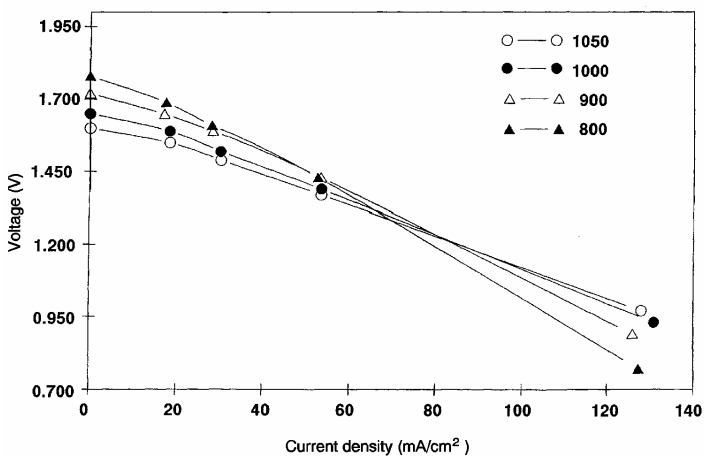

Figure 7-19 Two Cell Stack Performance with 97% H_2 and 3% H_2O/Air (49)

7.2.3 Effect of Reactant Gas Composition and Utilization

Because SOFCs operate at high temperature, they are capable of internally reforming fuel gases (i.e., CH_4 and other light hydrocarbons) without the use of a reforming catalyst (i.e., anode itself is sufficient), and this attractive feature of high temperature operation of SOFCs has been experimentally verified. Another important aspect of SOFCs is that recycle of CO_2 from the spent fuel stream to the inlet oxidant is not necessary because SOFCs utilize only O_2 at the cathode.

Oxidant: The performance of SOFCs, like that of other fuel cells, improves with pure O_2 rather than air as the oxidant. With a fuel of 67% H_2/22% CO/11% H_2O at 85% utilization, the cell voltage at 1,000°C shows an improvement with pure O_2 over that obtained with air (see Figure 7-20). In the figure, the experimental data are extrapolated by a dashed line to the theoretical Nernst potential for the inlet gas compositions (51). At a target current density of

160 mA/cm^2 for the tubular SOFC operating on the above-mentioned fuel gas, a difference in cell voltage of about 55 mV is obtained. The difference in cell voltage with pure O_2 and air increases as the current density increases, which suggests that concentration polarization plays a role during O_2 reduction in air. More recent data for planar cells at 800°C are presented in Figure 7-13. These data suggest that concentration polarization at open circuit conditions is not a significant factor with the new generation of cells. However, as expected, the differences in voltage between air and oxygen increases with increasing current density.

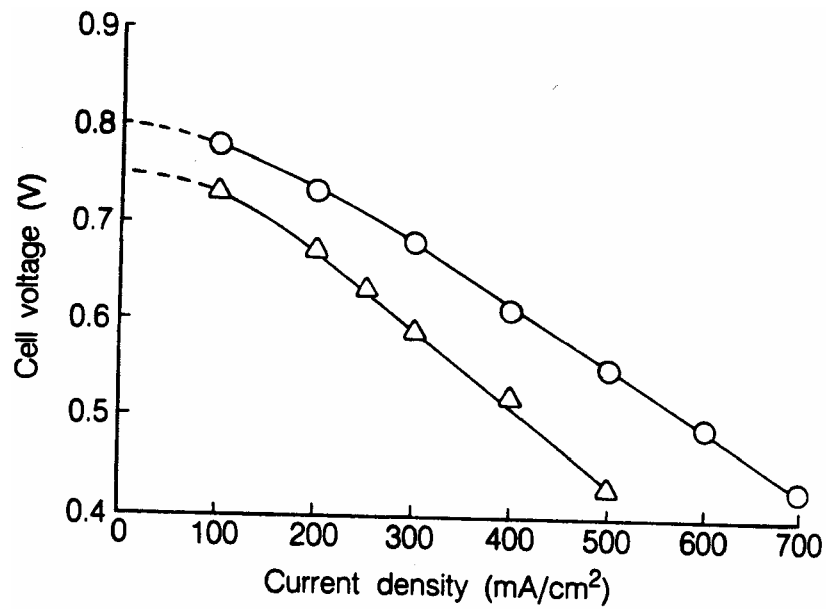

Figure 7-20 Cell Performance at 1,000°C with Pure Oxygen (o) and Air (Δ) Both at 25% Utilization (Fuel (67% H_2/22% CO/11%H_2O) Utilization is 85%)

Based on the Nernst equation, the theoretical voltage gain due to a change in oxidant utilization at T = 1,000°C is

$$\Delta V_{Cathode} = 63 \log \frac{(\overline{P}_{O_2})_2}{(\overline{P}_{O_2})_1} \tag{7-14}$$

where $\overline{P}_{O_2}$ is the average partial pressure of O_2 in the system. Data (49) suggest that a more accurate correlation of voltage gain is described by

$$\Delta V_{Cathode} = 92 \log \frac{(\overline{P}_{O_2})_2}{(\overline{P}_{O_2})_1} \tag{7-15}$$

Fuel: The influence of fuel gas composition on the theoretical open circuit potential of SOFCs is illustrated in Figure 7-21, following the discussion by Sverdrup, et al. (19). The oxygen/carbon (O/C) atom ratio and hydrogen/carbon (H/C) atom ratio, which define the fuel

composition, are plotted as a function of the theoretical open circuit potential at 1,000°C. If hydrogen is absent from the fuel gas, H/C = 0. For pure CO, O/C = 1; for pure CO_2, O/C = 2. The data in the figure show that the theoretical potential decreases from about 1 V to about 0.6 V as the amount of O_2 increases, and the fuel gas composition changes from CO to CO_2. The presence of hydrogen in the fuel produces two results: 1) the potential is higher, and 2) the O/C ratio corresponding to complete oxidation extends to higher values. These effects occur because the equilibrium composition obtained by the water gas shift reaction in gases containing hydrogen (H_2O) and carbon (CO) produces H_2, but this reaction is not favored at higher temperatures. In addition, the theoretical potential for the H_2/O_2 reaction exceeds that for the CO/O_2 reaction at temperatures of about 800°C; consequently, the addition of hydrogen to the fuel gas will yield a higher open circuit potential in SOFCs. Based on the Nernst equation, the theoretical voltage gain due to a change in fuel utilization at T = 1,000°C is

$$\Delta V_{Anode} = 126 \log \frac{(\overline{P}_{H_2} / \overline{P}_{H_2O})_2}{(\overline{P}_{H_2} / \overline{P}_{H_2O})_1} \tag{7-16}$$

where $\overline{P}_{H_2}$ and $\overline{P}_{H_2O}$ are the average partial pressures of H_2 and H_2O in the fuel gas.

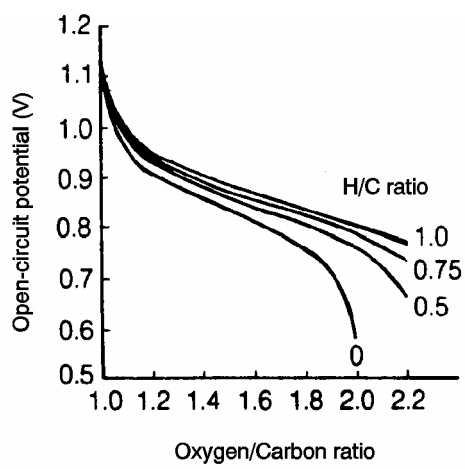

Figure 7-21 Influence of Gas Composition of the Theoretical Open-Circuit Potential of SOFC at 1,000°C

The fuel gas composition also has a major effect on the cell voltage of SOFCs. The performance data (54) obtained from a 15-cell stack (1.7 cm^2 active electrode area per cell) of the tubular configuration at 1,000°C illustrates the effect of fuel gas composition. With air as the oxidant and fuels of composition 97% H_2/3% H_2O, 97% CO/3% H_2O, and 1.5% H_2/3% CO/75.5% CO_2/20% H_2O, the current densities achieved at 80% voltage efficiency were ~220, ~170, and ~100 mA/cm^2, respectively. The reasonably close agreement in the current densities obtained with fuels of composition 97% H_2/3% H_2O and 97% CO/3% H_2O indicates that CO is a useful fuel for SOFCs. However, with fuel gases that have only a low concentration of H_2 and CO (i.e.,

1.5% H_2/3% CO/75.5% CO_2/20% H_2O), concentration polarization becomes significant and the performance is lower.

A reference fuel gas used in experimental SOFCs had a composition of 67% H_2/22% CO/11% H_2O. With this fuel (85% utilization) and air as the oxidant (25% utilization), individual cells (~1.5 cm diameter, 30 cm length and ~110 cm^2 active surface area) delivered a peak power of 22 W (55). Figure 7-22 (51) shows the change in cell voltage with fuel utilization for a SOFC that operates on this reference fuel and pure O_2 or air as oxidant (25% utilization). The cell voltage decreases with an increase in the fuel utilization at constant current density. Insufficient data are available in the figure to determine whether temperature has a significant effect on the change in cell voltage with utilization. However, the data do suggest that a larger voltage decrease occurs at 1,000°C than at 800 or 900°C. Based on this and other data (55,56), the voltage gain at T = 1,000°C and with air is defined by Equation (7-17):

$$\Delta V_{Anode} = 172 \log \frac{(\bar{P}_{H_2} / \bar{P}_{H_2O})_2}{(\bar{P}_{H_2} / \bar{P}_{H_2O})_1} \tag{7-17}$$

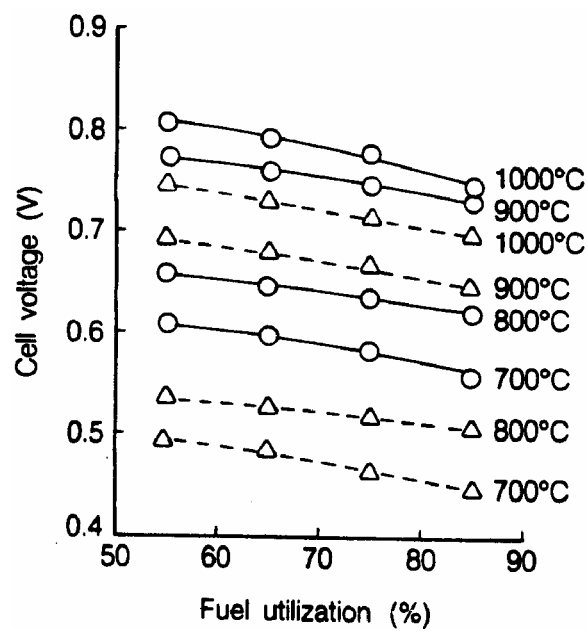

Figure 7-22 Variation in Cell Voltage as a Function of Fuel Utilization and Temperature (Oxidant (o - Pure O_2; Δ - Air) Utilization is 25%. Current Density is 160 mA/cm^2 at 800, 900 and 1,000°C and 79 mA/cm^2 at 700°C)

7.2.4 Effect of Impurities

Hydrogen sulfide (H_2S), hydrogen chloride (HCl) and ammonia (NH_3) are impurities typically found in coal gas. Some of these substances may be harmful to the performance of SOFCs. Early experiments (57) used a simulated oxygen-blown coal gas containing 37.2% CO/34.1% H_2/0.3% CH_4 /14.4% CO_2/13.2% H_2O/0.8% N_2. These experiments showed no degradation in the presence of 5,000 ppm NH_3. An impurity level of 1 ppm HCl also showed no detectable degradation. H_2S levels of 1 ppm resulted in an immediate performance drop, but this loss soon

stabilized into a normal linear degradation. Figure 7-23 shows the performance of the experimental cell over time (57). Additional experiments showed that removing H_2S from the fuel stream returned the cell to nearly its original level. It was also found that maintaining an impurity level of 5,000 ppm NH_3 and 1 ppm HCl, but decreasing the H_2S level to 0.1 ppm eliminated any detrimental effect due to the presence of sulfur, even though, as mentioned above, 1 ppm H_2S caused virtually no degradation.

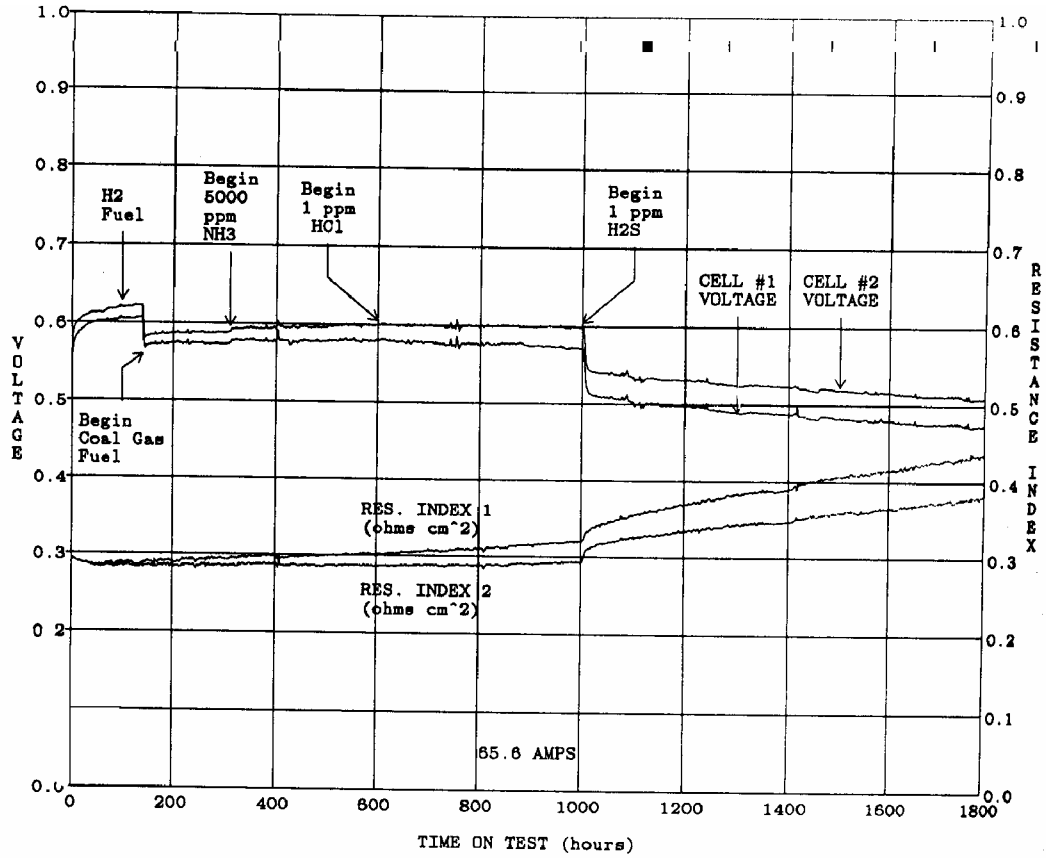

Figure 7-23 SOFC Performance at 1,000°C and 350 mA/cm^2, 85% Fuel Utilization and 25% Air Utilization (Fuel = Simulated Air-Blown Coal Gas Containing 5,000 ppm NH_3, 1 ppm HCl and 1 ppm H_2S)

In addition, silicon (Si), which also can be found in coal gas, has been studied (57) as a contaminant. It is believed to accumulate on the fuel electrode in the form of silica (SiO_2). The deposition of the Si throughout the cell has been found to be enhanced by high (~50%) H_2O content in the fuel. Si is transported by the following reaction:

$$SiO_2\ (s) + 2H_2O\ (g) \rightarrow Si(OH)_4\ (g) \qquad (7\text{-}18)$$

As the CH_4 component of the fuel reforms to CO and H_2, H_2O is consumed. This favors the reversal of Equation (7-18), which allows SiO_2 to be deposited downstream, possibly on exposed

nickel surfaces. Oxygen-blown coal gas, however, has a H_2O content of only ~13%, and this is not expected to allow for significant Si transport.

7.2.5 Effect of Current Density

The voltage level of a SOFC is reduced by ohmic, activation, and concentration losses, which increase with increasing current density. The magnitude of this loss is described by the following equation that was developed from information in the literature (50,58,59,60,61,62):

$$\Delta V_j(mV) = -0.73\Delta J \qquad (T = 1000°C) \qquad (7\text{-}19)$$

where J is the current density (mA/cm^2) at which the cell is operating. Air electrode-supported (AES) cells by Siemens Westinghouse exhibit the performance depicted in Figure 7-24.

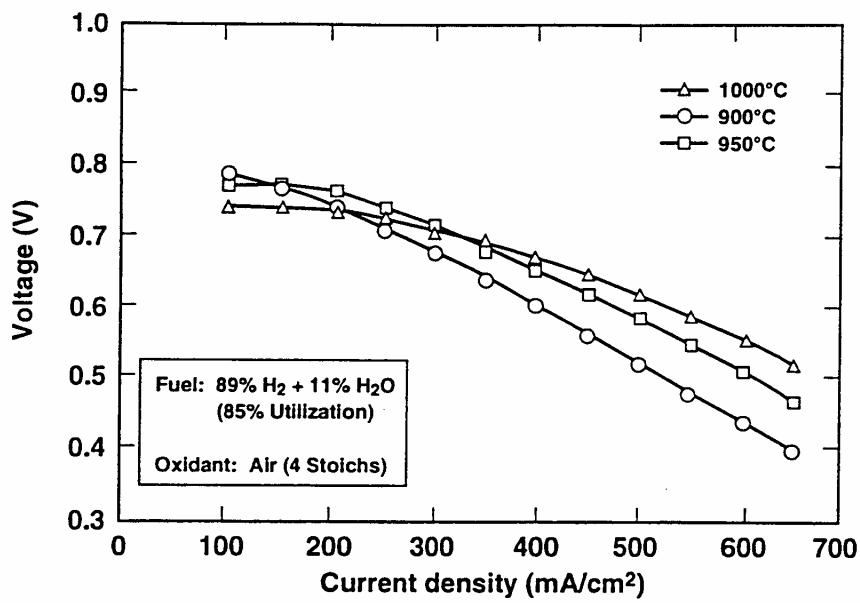

Figure 7-24 Voltage-Current Characteristics of an AES Cell (1.56 cm Diameter, 50 cm Active Length)

7.2.6 Effect of Cell Life

The endurance of the cell stack is of primary concern for SOFCs. As SOFC technology has continued to approach commercialization, research in this area has increased and improvements made. The Siemens Westinghouse state-of-the-art tubular design has been validated by continuous electrical testing of over 69,000 hours with less than 0.5% voltage degradation per 1,000 hours of operation. This tubular design is based on the early calcia-stabilized zirconia porous support tube (PST). In the current technology, the PST has been eliminated and replaced by a doped lanthanum manganite air electrode tube. These air electrode-supported (AES) cells have shown a power density increase of approximately 33% over the previous design. Siemens Westinghouse AES cells have shown less than 0.2 % voltage degradation per 1,000 hours in a

25 kW stack operated for over 44,000 hours (48,63), and negligible degradation in the 100 kW stack operated in the Netherlands and Germany (>16,000 hours).

7.3 Summary of Equations for SOFC

The preceding discussion provided parametric performance based on various referenced data at different operating conditions. It is suggested that the following set of equations could be used for performance adjustments unless the reader prefers other data or correlations.

Parameter	Equation	Comments	
Pressure	$\Delta V_p(mV) = 59 \log \frac{P_2}{P_1}$	1 atm $\leq$ P $\leq$ 10 atm	(7-8)
Temperature	$\Delta V_T(mV) = 0.008(T_2 - T_1)(°C) * J$[1]	900°C $\leq$ T $\leq$ 1050°C	(7-11)
	$\Delta V_T(mV) = 0.04(T_2 - T_1)(°C) * J$[1]	800°C $\leq$ T $\leq$ 900°C	(7-12)
	$\Delta V_T(mV) = 1.3(T_2 - T_1)(°C) * J$	650°C $\leq$ T $\leq$ 800°C	(7-13)
Oxidant	$\Delta V_{Cathode}(mV) = 92 \log \frac{(\overline{P}_{O_2})_2}{(\overline{P}_{O_2})_1}$	$0.16 \leq \frac{\overline{P}_{O_2}}{\overline{P}_{Total}} \leq 0.20$	(7-15)
Fuel	$\Delta V_{Anode} = 172 \log \frac{(\overline{P}_{H_2} / \overline{P}_{H_2O})_2}{(\overline{P}_{H_2} / \overline{P}_{H_2O})_1}$	$0.9 \leq \overline{P}_{H_2} / \overline{P}_{H_2O} \leq 6.9$ T = 1000°C, with air	(7-17)
Current Density	$\Delta V_J(mV) = - 0.73\Delta J$	50 < J < 400 mA/cm^2 P = 1 atm., T = 1000°C	(7-19)

7.4 References

1. Wright, J.D., "SOFC Stack Performance Goals," Proceedings of the Fuel Cells '97 Review Meeting.
2. Report to DOE FETC, "Assessment of Planar Solid Oxide Fuel Cell Technology," Reference 39463-02, Arthur D. Little, Inc., October 1999.
3. Buckkremer, H.P., et al., "Advances in the Anode-Supported Planar SOFC Technology," Electrochemical Proceedings, Vol. 97-18.
4. Goodenough, J.B. and K. Huang, "Lanthanum Gallate as a New SOFC Electrolyte," Proceedings of the Fuel Cells '97 Review Meeting. http://www.netl.doe.gov/publications/proceedings/97/97fc/FC5-5.pdf
5. Wang, S., T. Kobayashi, M. Dokiya, and T. Hashimoto, J. Electrochemical Society, p. 3606, v. 147 (10), (2000).
6. Huang, K., R.S. Tichy, and J. B. Goodenough, J. American Ceramics Society, p. 2565, v. 81 (10), (1998).

[1] Where J = mA/cm^2, for fuel composition of 67% H_2/22% CO/11% H_2O

7. Arachi, Y., H. Sakai, O. Yamamoto, Y. Takeda, and N. Imanishi, Solid State Ionics, p. 133, v. 122, (1999).
8. Global Thermoelectric, Inc. Website. http://www.globalte.com/index.htm
9. Fuel Cells, DOE/METC-86/0241, Technology Status Report, Morgantown Energy Technology Center, Morgantown, WV, 1986.
10. Lai, G.Y., "High Temperature Corrosion of Engineering Alloys," ASM 1990.
11. NexTech Materials, Ltd. Website. http://www.fuelcellmaterials.com
12. Swartz, S.L., "Low Cost Manufacturing of Multi-Layer Ceramic Fuels," paper presented at Solid State Energy Conversion Alliance 2nd Annual Workshop Proceedings, March 2001. http://www.netl.doe.gov/publications/proceedings/01/seca/swartz.pdf
13. Stevenson, J.W. and P. Singh, "Low Cost Modular SOFC Development," Technical Progress Report, Part 1: Development of Advanced Materials and Fabrication Techniques for SOFC Components, March 2002.
14. Kim, J. and A. Vikar, in "Solid Oxide Fuel Cells – VI," S. Singhal and M. Dokiya, eds., Electrochemical Society, Pennington, NJ, PV 99-19 (1999) 830.
15. Product Literature, Amethyst Galleries, Inc,. Dublin, Ohio.
16. Surdoval, W.A., "SECA Core Technology Program," presented at Solid State Energy Conversion Alliance 3rd Annual Workshop Proceedings, March 2002. http://www.netl.doe.gov/publications/proceedings/02/SECA/SECA3Surdoval.pdf
17. Isenberg, A.O., Proceedings of the Symposium on Electrode Materials on Processes for Energy Conversion and Storage, edited by J.D.E. McIntyre, S. Srinivasan, and F.G. Will, The Electrochemical Society, Inc., Pennington, NJ, p. 682, 1977.
18. Fee, D.C., S.A. Zwick, J.P. Ackerman, in Proceedings of the Conference on High Temperature Solid Oxide Electrolytes, held at Brookhaven National Laboratory, BNL 51728, compiled by F.J. Salzano, October, 1983.
19. Sverdrup, E.F., C.J. Warde, and A.D. Glasser, in "From Electrocatalysis to Fuel Cells," edited by G. Sandstede, University of Washington Press, Seattle, WA, 1972.
20. Minh, N.Q., "Ceramic Fuel Cells," J. Am. Ceram. Soc., p. 76 [3], 563-88, 1993.
21. Fuel Cell Handbook, DOE/NETL – 2000/1110, 5th Edition, National Energy Technology Laboratory, Morgantown, WV/Pittsburgh, PA, 2000.
22. Silver, M.N., "Recent Advances in SOFC Electrolyte, Cathode, and Anode Ceramic Materials," paper presented at the 26th Annual International Conference on Advanced Ceramics and Composites, Cocoa Beach, FL, January 13 – 18, 2002.
23. Ball, R.J. and R. Stevens, "Novel Composite Electrolytes for Solid Oxide Fuel Cell Applications," paper presented at the 26th Annual International Conference on Advanced Ceramics and Composites, Cocoa Beach, FL, January 13 – 18, 2002.
24. Barnett, S., Erica Perry and D. Kaufmann, "Application of Ceria Layers to Increase Low Temperature SOFC Power Density," Proceedings of the Fuel Cells '97 Review Meeting. http://www.netl.doe.gov/publications/proceedings/97/97fc/FC6-6.pdf
25. Courtesy of Siemens Westinghouse.
26. Swartz, S.L., M.M. Seabaugh, K. Hasinka, B.E. McCormick and W.J. Dawson, "Low Cost Manufacturing of Planar Solid Oxide Fuel Cells," paper presented at the 26th Annual International Conference on Advanced Ceramics and Composites, Cocoa Beach, FL, January 13 – 18, 2002.

27. Elangovan, S., et al., "Planar SOFC Integrated System Technology Development," Proceedings of the Fuel Cells '97 Review Meeting. http://www.netl.doe.gov/publications/proceedings/97/97fc/fc6-2/pdf
28. Cable, T.L., E.A. Barrington, and S. Elangovan, "Status of AMPS, The SOFC Planar Solid Oxide Fuel Cell," paper presented at the 26th Annual International Conference on Advanced Ceramics and Composites, Cocoa Beach, FL, January 13 – 18, 2002.
29. Kosacki, I., P.F. Becher, C.M. Rouleau, D.H. Lowndes, and T.R. Armstrong, "Effects of Film Thickness on the Ionic Conductivity in Epitaxial YSZ Films," paper presented at the 26th Annual International Conference on Advanced Ceramics and Composites, Cocoa Beach, FL, January 13 – 18, 2002.
30. Stevenson, J.W., "Solid Oxide Fuel Cell Development at PNNL (Invited)," paper presented at the 26th Annual International Conference on Advanced Ceramics and Composites, Cocoa Beach, FL, January 13 – 18, 2002.
31. Wang, X., J.M. Ralph, J.T. Vaughey, and M. Krumpelt, "Cathode Materials for Solid Oxide Fuel Cells," Argonne National Laboratory, paper presented at Joint Fuel Cell Technology Review Conference, 1999. http://www.netl.doe.gov/publications/proceedings/99/99fuelcell/fc7-5.pdf
32. Beeaf, D.R., and G.E. Hilmas, "Development of Parallel Pore Channel Electrodes for Solid Oxide Fuel Cells," paper presented at the 26th Annual International Conference on Advanced Ceramics and Composites, Cocoa Beach, FL, January 13 – 18, 2002.
33. Bhide, S.V., W. Meng, and A.V. Virkar, "Stability of Mixed Perovskite Proton Conductors," paper presented at Joint Fuel Cell Technology Review Conference, 1999. http://www.netl.doe.gov/publication/proceedings/99/99fuelcell/fc7-4.pdf
34. Virkar, A.V., J.W. Kim, K. Mehta, and K.Z. Fung, MSRI, "Low Temperature, High Performance, Planar Solid Oxide Fuel Cells and Stacks," Proceedings of the Fuel Cells '97 Review Meeting. http://www.netl.doe.gov/publications/proceedings/97/97fc/fc6-5.pdf
35. Minh, N., "SECA Solid Oxide Fuel Cell Program," presented at Solid State Energy Conversion Alliance 3rd Annual Workshop Proceedings, March 2002. http://www.netl.doe.gov/publications/proceedings/02/seca/seca3minh.pdf
36. Minh, N., "Solid Oxide Fuel Cell System Development," presented at Solid State Energy Conversion Alliance 3rd Annual Workshop Proceedings, March 2001. http://www/netl.doe.gov/publications/proceedings/01/seca/honeywell.pdf
37. Minh, N., K. Barr, P. Kelly, and K. Montgomery, "Allied Signal Solid Oxide Fuel Cell Technology," General Electric Co. Program and Abstracts, 1996 Fuel Cell Seminar.
38. George, R. "SECA Solid Oxide Fuel Cell Project," presented at Solid State Energy Conversion Alliance 3rd Annual Workshop Proceedings, March 2002. http://www.netl.doe.gov/publications/proceedings/02/seca/seca3george.pdf
39. Wang, C., W.L. Worrell, S. Park, J.M. Vohs, and R.J. Gorte, "Fabrication and Performance of Thin Film YSZ SOFCs Between 600 and 800°C," paper presented at the Joint Fuel Cell Technology Review Conference, 1999. http://www.netl.doe.gov/publications/proceedings/99/99fuelcell/fc7-1.pdf
40. Goodenough, J., "Solid Oxide Fuel Cells with Gallate Electrolytes," summary data on research supported by EPRI, 1998.
41. Ralph, J. M., et al., "Solid Oxide Fuel Cells - VII," H. Yokokawa and S. Singhal, eds., Electrochemical Society, Pennington, NJ, PV 2001-16 (2001) 466.

42. Ryu, K.H., S.M. Haile, G. Staneff, and S. Jamindar, "Influence of Zirconium Substitution on the Chemical Stability and Conductivity of $BaCeO_3$-based Proton Conductors," paper presented at the Joint Fuel Cell Technology Review Conference, 1999. http://www.netl.doe.gov/publications/proceedings/99/99fuelcell/fc7-3.pdf
43. Visco, S.J., C.P. Jacobson, and L.C. DeJonghe, "Influence of Zirconium Substitution on the Chemical Stability and Conductivity $BaCeO_3$-based Proton Conductors," paper presented at Joint Fuel Cell Technology Review Conference, 1999. http://www/netl.doe.gov/publications/proceedings/99/99fuelcell/fc6-7.pdf
44. Bloom, I., et al., "Electrolyte Development for Intermediate Temperature Solid Oxide Fuel Cells," Fuel Cell Program and Abstracts, 1992 Fuel Cell Seminar, Tucson, AZ, November, 1992.
45. Bloom, I., and M. Krumpelt, " Intermediate Temperature Electrolytes for SOFC," proceedings of the Fourth Annual Fuel Cells Contractors Review Meeting, U.S. DOE/METC, July, 1992.
46. Voigt, T., "The Challenge for Small-Scale, Ultra-Low Cost SOFC Power Systems," presented at the Solid State Energy Conversion Alliance, 3rd Annual Workshop Proceedings, March, 2002.
47. Crucian, R. J.M. Vohs, and R.J. Gorte, "Direct Oxidation of Hydrocarbons in Solid Oxide Fuel Cells," J. Electrochemical Society, p. 3603, v. 149, (1999).
48. Singhal, S.C., "Recent Progress in Tubular Solid Oxide Fuel Cell Technology," Proceedings of the Fifth International Symposium on Solid Oxide Fuel Cells (SOFC – V), The Electrochemical Society, Inc., Pennington, NJ, 1997.
49. Ide, H., et al., "Natural Gas Reformed Fuel Cell Power Generation Systems – A Comparison of Three System Efficiencies," Proceedings of the 24th Intersociety Energy Conversion Engineering Conference, The Institute of Electrical and Electronic Engineers, Washington, D.C., 1989.
50. Data from Allied – Signal Aerospace Company, 1992.
51. Zeh, C., private communication, 2nd Edition of Handbook, April, 1987.
52. Sammells, A., "Perovskite Electrolytes for SOFC," Proceedings of the Third Annual Fuel Cells Contractors Review Meeting, U.S. DOE/METC, May, 1991.
53. Khandkar, A., S. Elangovan, "Planar SOFC Development Status," Proceedings of the Second Annual Fuel Cells Contractors Review Meeting, U.S. DOE/METC, May, 1990.
54. Warde, C.J., A.O. Isenberg, and J.T. Brown, "High Temperature Solid Electrolyte Fuel Cells Status and Programs at Westinghouse," in Program and Abstracts, ERDA/EPRI Fuel Cell Seminar, Palo Alto, CA, June, 1976.
55. Dollard, W.J., and J.T. Brown, "Overview of the Westinghouse Solid Oxide Fuel Cell Program," Fuel Cell Abstracts, 1986 Fuel Cell Seminar, Tucson, AZ, October, 1986.
56. Uchuyama, F., et al., "ETL Multi-Layer Spray Coating for SOFC Component," The International Fuel Cell Conference Proceedings, NEDO/MITI, Tokyo, Japan, 1992.
57. Maskalick, N., "Contaminant Effects in Solid Oxide Fuel Cell," Proceedings of the Fourth Annual Fuel Cells Contractors Review Meeting, U.S. DOE/METC, July, 1992.
58. Minh, N., et al, "Monolithic Solid Oxide Fuel Cell Development: Recent Technical Progress," Fuel Cell Seminar Program and Abstracts, Fuel Cell Seminar, Tuscon, AZ, November, 1992.
59. Yashida, Y., et al, "Development of Solid Oxide Fuel Cell," paper provided by Mitsubishi Heavy Industries, Ltd.

60. Khandkar, A., et al., “Planar SOFC Technology Status and Overview,” Ceramatec, Inc., Fuel Cell Seminar Program and Abstracts, 1992 Fuel Cell Seminar, Tuscon, AZ, November, 1992.
61. “Research and Development on Fuel Cell Power Generation Technology,” FY 1990 Annual Report, NEDO, April, 1991.
62. Nakanishi, T., “Substrate Type, Planar Solid Oxide Fuel Cell,” Fuji Electric, Fuel Cell Seminar Program and Abstracts, 1992 Fuel Cell Seminar, Tucson, AZ, November, 1992.
63. Forbes, C., Private Communication, (2002).

8. FUEL CELL SYSTEMS

Although a fuel cell produces electricity, a fuel cell power system requires the integration of many components beyond the fuel cell stack itself, for the fuel cell will produce only dc power and utilize only certain processed fuel. Various system components are incorporated into a power system to allow operation with conventional fuels, to tie into the ac power grid, and often, to utilize rejected heat to achieve high efficiency. In a rudimentary form, fuel cell power systems consist of a fuel processor, fuel cell power section, power conditioner, and potentially a cogeneration or bottoming cycle to utilize the rejected heat. A simple schematic of these basic systems and their interconnections is presented in Figure 8-1.

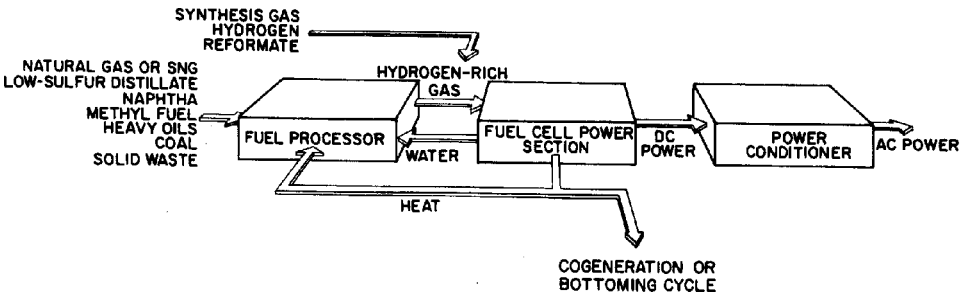

Figure 8-1 A Rudimentary Fuel Cell Power System Schematic

8.1 System Processes

The design of a fuel cell system involves more than the optimizing of the fuel cell section with respect to efficiency or economics. It involves minimizing the cost of electricity (or heat and electric products as in a cogeneration system) within the constraints of the desired application. For most applications, this requires that the fundamental processes be integrated into an efficient plant with low capital cost. Often these objectives are conflicting, so compromises, or design decisions, must be made. In addition, project-specific objectives, such as desired fuel, emission levels, potential uses of rejected heat (electricity, steam, or heat), desired output levels, volume or weight criteria (volume/kW or weight/kW), and tolerance for risk all influence the design of the fuel cell power system.

8.1.1 Fuel Processing

Fuel processing is defined in this Handbook as the conversion of a commercially available gas, liquid, or solid fuel to a fuel gas reformate suitable for the fuel cell anode reaction. Fuel processing encompasses the cleaning and removal of harmful species in the fuel, the conversion of the fuel to the fuel gas reformate, and downstream processing to alter the fuel gas reformate according to specific fuel cell requirements. Examples of these processes are:

- Fuel Cleaning – Removal of sulfur, halides, and ammonia to prevent fuel processor and fuel cell catalyst degradation.
- Fuel Conversion – Converting a fuel (primarily hydrocarbons) to a hydrogen-rich gas reformate.
- Reformate Gas Alteration – Converting carbon monoxide (CO) and water (H_2O) in the fuel gas reformate to hydrogen (H_2) and carbon dioxide (CO_2) via the water-gas shift reaction; selective oxidation to reduce CO to a few ppm, or removal of water by condensing to increase the H_2 concentration.

A fuel processor is an integrated unit consisting of one or more of the above processes, as needed for the fuel cell requirements[41] and the fuel, that function together to be cost effective for the application. Design considerations may include high thermal efficiency, high hydrogen yield (for some fuel cells hydrogen plus carbon monoxide yield), multi-cycling, compactness, low weight, and quick starting capability, depending on the application.

Figure 8-2 depicts the Processing steps needed for a low temperature cell.[42] Most fuel processors make use of the chemical and heat energy left in the fuel cell effluent to provide heat for fuel processing thus enhancing system efficiency.

41. Primarily determined by the cell's operating temperature.
42. Requires relatively complex fuel processing.

Figure 8-2 Representative Fuel Processing Steps & Temperatures

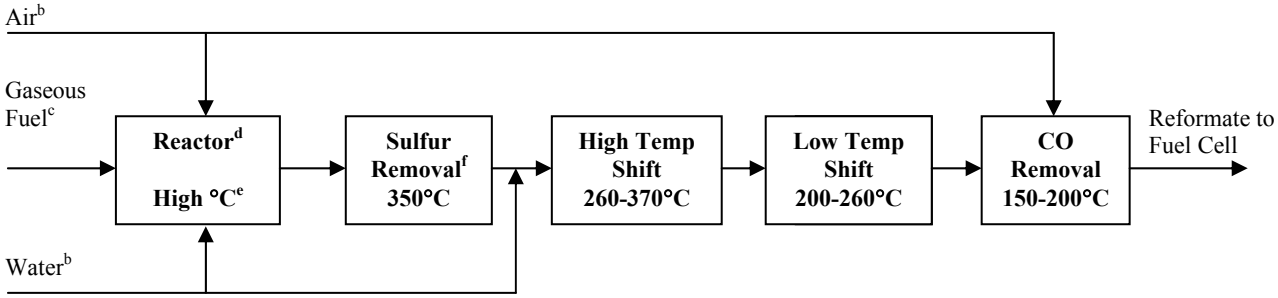

a) - For MCFC & SOFC, no high temperature shift, low temperature shift, or CO removal required.
   - For PAFC and circulating AFC, no CO removal required after low temperature shift.
   - For PEFC, all components required except that for high temperature CO removal eliminated or reduced in complexity.
b) Possible to use residual air, water, and heat of fuel effluent from fuel cell and other downstream components.
c) Vaporizer required for liquid fuels.
d) Non-catalytic POX fuel processor does not require water.
e) Temperature dependent on fuel, sulfur content of fuel, and type of reactor.
f) Can be located prior to, within, or after the reactor; liquid desulfurizer located prior to the vaporizer.

Fuel conversion and alteration catalysts are normally susceptible to deactivation by impurities,[43] thus the fuel cleaning process takes place upstream or within the fuel conversion process. The fuel conversion and reformate gas alteration processes can take place either external to the fuel cell or within the fuel cell anode compartment. The former is referred to as an external reforming fuel cell and the latter is referred to as an internal reforming fuel cell. Cells are being developed to directly react commercially available gas and liquid fuels, but the chemically preferred reaction of present fuel cells is via hydrogen-rich gas. This discussion will address external reforming fuel processors only. Descriptions of internal reforming are contained within the specific fuel cell sections. The system calculation section provides examples of heat and material balances for both externally and internally reforming fuel cells.

Fuel processors are being developed to allow a wide range of commercial fuels suitable for stationary, vehicle, and military applications. Technology from large chemical installations has been successfully transferred to small, compact fuel cells to convert pipeline natural gas, the fuel of choice for small stationary power generators. Several hundred multi-kWe commercial fuel cell units are operating that contain fuel processors (see Section 1.6). Cost is an issue, as it is with the entire fuel cell unit, for widespread commercial application. Scaling of existing fuel processing technology to larger fuel cell power plants will reduce the specific cost of the fuel processor.

Natural gas fuel reforming for fuel cells is essentially mature. Recent fuel processor research and development has focused on fuels for transportation and military applications.

43. Referred to as poisoning in catalysis literature. Ni-based fuel processing catalysts are poisoned by "physiadsorbtion" of S onto the Ni surface, thus reducing performance. Pt catalysts are less susceptible to S poisoning because S does not physiadsorb as strongly as it does on Ni; thus affecting performance less.

The issue with transportation is how to match a plausible commercial fuel infrastructure with the requirements of the fuel cell unit to be competitive. Economics drive the fuel of choice toward existing infrastructure, such as gasoline. Fuel cell requirements drive the fuel toward methanol or a "fuel cell friendly" gasoline. Environmental concerns drive the fuel of choice toward pure hydrogen[44]. Gasoline is a complex fuel, requiring high conversion temperature, and it has high levels of impurities that affect catalytic activity (see Appendix A). Methanol fuel processors (regarded by some as a necessary step towards an eventual liquid transportation fuel) are easier to develop than processors capable of converting gasoline. However, use of methanol or hydrogen would require major changes to the fuel supply infrastructure. Processors for both methanol and gasoline have been tested up to the 50 kWe level for vehicle application. What fuel to use onboard the vehicle is open to question at this time, but recent research in the fuel cell community points toward a modified gasoline tailored for fuel cell use that could be supplied through the existing fuel infrastructure (1).

The U.S. military has a substantial fuel supply infrastructure in place. The two predominant fuel types in this infrastructure are diesel and jet fuel, a kerosene. It is highly improbable that the U.S. military would change these fuels to accommodate fuel cells. Use of a fuel more suitable to the fuel cell would limit the technology's military use (there is R&D activity for fuel cell power packs to provide man-portable soldier power using hydrogen cartridges, or other hydrogen-containing forms, as well as methanol). Diesel and jet fuel are two of the most difficult conventional fuels to convert to a hydrogen-rich gas. They contain large amounts of sulfur that deactivate catalysts and require high conversion temperature. Fuel processors that convert diesel and jet fuel to a hydrogen-rich gas are in the early stages of development. The technology has been demonstrated at a 500 W size; 50 kWe units are being developed. Argonne National Laboratory (ANL) has operated a 3 kWe autothermal reformer with direct injection of diesel-like hydrocarbons – hexadecane and dodecane. Experiments with real diesel are anticipated shortly (2).

Fuel Processing Issues

Major issues that influence the development of a fuel processor are 1) choice of commercially available fuels suitable for specific applications; 2) fuel flexibility; 3) catalyst tolerance; 4) fuel cell size, and 5) vaporization of heavy hydrocarbons. Heavy hydrocarbons, such as diesel, require vaporization temperatures much in excess of 350-400°C, at which temperature some of the heavier fuels pyrolyze.

Fuel Choice and Flexibility: The fuel cell is a power generation technology that is in the early stages of commercial use. As a result, it is paramount to target applications that have the potential for widespread use (to attract adequate financial investment) with the simplest technology development (to minimize development cost). There is a strong relation between viable applications and the infrastructure of available fuels.

44. The US FreedomCAR program is focused primarily towards hydrogen and secondarily towards "gasoline" as the onboard fuel.

High-value niche markets drove early fuel cell technology development. These included the use of fuel cells for on-board electric power in space vehicles, and to demonstrate that fuel cells are an efficient, environmentally-friendly technology for stationary on-site commercial power.

The technology of choice for on-board electric power on mid-length space vehicle missions (several days to a year), including the important man-moon mission, was the fuel cell. This was because the use of batteries for more than a couple of days proved too heavy, combustion engines and gas turbines required too heavy a fuel supply, and the use of a nuclear reactor was only suitable for missions of a year or more. There was a simple choice of fuel for space fuel cells: it was hydrogen because it doesn't require a fuel processor other than storage and pressurization, it is relatively lightweight when stored under pressure, and it was the best fuel for the early-developed alkaline fuel cell. Fuel flexibility was not an issue.

It was logical to exploit fuel cell space development for terrestrial use. The initial terrestrial application was to increase power generation efficiency (in reaction to the oil crisis of the early 1970s) and to improve the environment by lowering fossil-fueled power generation exhaust emission. Although coal-derived gas was recognized as a viable fuel, early fuel cell development was based on conveniently accessible pipeline gas prior to turing attention to coal-derived gas. One of the major fuel cell sponsors at the time was the natural gas industry.

Pipeline gas consists primarily of methane that is relatively easy to purify. The technology to convert methane to a H_2-rich gas existed for large chemical plants. Developers had only to adapt existing technology to small fuel cell units, not easy due to several magnitudes of scale-down. Owners of stationary power plants usually desire fuel flexibility. Fortunately, the fuel processor on these early plants could convert a light distillate, such as naphtha, with minor changes (e.g., add a vaporizer, change-out the fuel nozzles).

Once the niche markets were exploited to start fuel cells on their development path, it became necessary to target widespread potential applications while keeping technology development as simple as possible. General application areas of present interest to the fuel cell community are multi-kWe residential, commercial, and light industrial stationary power, transportation prime and auxiliary power, and military uses.

In summary, these are the applications and coupled fuel choices of interest to fuel cell technology to date:

- H_2 is preferable for a closed environment such as space vehicle application. There are sources of H_2-rich gases, such as an off-gas at a chemical plant, that require only fuel cleaning. Fuel flexibility is not applicable in either case.
- The fuel choice for small, stationary power plants is pipeline gas due to its availability for multiple commercial, light-industrial, and residential applications. Some users request that the fuel processor convert at least one additional fuel, i.e., a light distillate.
- Light vehicles is a key commercial target due to the large number of potential units; the fuel choice is open to question. Some proponents support the use of on-board hydrogen. There is a strong argument for liquid fuels due to on-board volume restrictions and existing fuel supply infrastructure. Candidate liquid fuels for light vehicles could be available gasoline or

a new gasoline, if driven by the infrastructure. Methanol may have an edge if it proves too difficult to process gasoline, provided the use of methanol compares favorably on a cost and environmental basis with present internal combustion engine (ICE) gasoline. Fuel flexibility in processors should be considered because of the indecision on fuel type and because the public is accustomed to a selection of different octane liquid fuels and diesel.

- The present infrastructure fuel for heavy vehicles is high sulfur diesel (now ~500 ppm sulfur by weight) but this may change to a nearly sulfur-free diesel as proposed by the EPA. Beginning June 1, 2006, refiners must produce a diesel containing a maximum of 15 ppm sulfur (3). The fuel for this sector could also be a gasoline if such a fuel cell system could compete.
- On-board vehicle auxiliary power is increasing dramatically to satisfy consumer convenience demands. Fuel selection for these applications parallel light and heavy vehicle fuels.
- The military will continue with its fuel infrastructure of high sulfur diesel (up to 1,000 ppm sulfur by weight) and jet fuel (JP-8, up to 300 ppm by weight). Sulfur specification will remain high because the military has to consider worldwide fuel sources. High sulfur diesel and JP-8 are close in characteristics, so no fuel flexibility is required. However, there is a possibility that some parts of the military or the Coast Guard (a military service within the DOT) could use fuels more compatible to the fuel cell in limited applications.
- As environmental regulation becomes more stringent for megawatt-size power stations and fuel cells are scaled larger in size, there is the possibility to use the U.S.'s most plentiful, indigenous fuel, coal. The term, coal, covers a broad spectrum of solid fuels that complicate fuel processing, particularly cleanup.
- There is the possibility of using other available fuels such as light distillates, ethanol, anaerobic digester gas, biomass, and refuse-derived fuel.

The market that has the greatest impact on fuel processor development at this time is in the light vehicle application sector, due to the potential large number of units. Some fuel processor developers are focusing on the development of methanol fuel processing either as the fuel of choice or as a development step toward processing gasoline. Others consider that it is best to develop a vehicle that uses the most environmentally attractive fuel, hydrogen. There are numerous opinions reagarding fuel and infrastructure best-suited for the light vehicle transportation market.

Methanol is unquestionably the easiest of the potential liquid fuels to convert to hydrogen for vehicle use. Methanol disassociates to carbon monoxide and hydrogen at temperatures below 400°C and can be catalytically steam reformed at 250°C or less. This provides a quick start advantage. Methanol can be converted to hydrogen with efficiencies of >90 %. But methanol is produced primarily from natural gas, requiring energy, and it is less attractive than gasoline on a well-to-wheels efficiency basis (5, 6).

Gasoline has many advantages over methanol, but conversion to H_2 requires temperatures in excess of 650°C and produces greater amounts of CO, methane (CH_4), and possibly coke. Without catalyst, the conversion temperature is 1,000°C or higher. High temperatures require special materials of construction and significant preheating. Petroleum-derived fuels contain more sulfur and trace amounts of metal that could be harmful to the fuel cell. Natural gas is not

good for transportation because of its low relative energy density and 700°C or higher processing temperature (7).

ExxonMobil has presented a position paper (8) for liquid fuels that addresses the pros and cons of methanol versus gasoline. Paraphrased excerpts from this are:

- Fuels that are most directly suited to the fuel cell are the most difficult and costly to produce and distribute. Gasoline and methanol are the leading candidates to power fuel cell engines. Both the gasoline and methanol fuel cell vehicles should be more fully developed prior to making a commercial decision on fuel choice.
- Due to methanol's corrosivity and its affinity for water, it cannot be readily distributed in today's fuel infrastructure. Methanol burns with a nearly invisible flame. Available luminosity additives won't reform in the low-temperature methanol steam reformers. Methanol is more acutely toxic than gasoline. Additives that are likely to be needed for safety and health reasons will impact the fuel processor's performance and cost.
- Gasoline fuel processing has the ability to utilize the existing infrastructure, a major advantage. It is inherently more flexible than the low temperature methanol processor, allowing multiple fuel use in the same system. The gasoline processor is also more tolerant of contaminants or additives contained in the fuel. Due to the higher energy density of gasoline, the gasoline system offers the potential for up to twice the vehicle range of the methanol system. Today's mid-sized passenger cars are about 15 to 18 % "well-to-wheels" energy efficient as indicated in Figure 8-3.[45] Despite the increased vehicle efficiency of a methanol fuel-based system, the resultant "well-to-wheel" efficiency would be only 20 to 28%, lower than either gasoline hybrids or gasoline fuel cell vehicles.
- A customized gasoline for fuel cells could offer better performance and be produced at lower cost because many of conventional gasoline's more expensive ingredients would not be required. Naphtha is a common refinery stream that is an inexpensive alternative to conventional gasoline. Although its octane is too low for today's ICE, naphtha is ideal for fuel cells and could be supplied to retail stations within the existing gasoline infrastructure.

Fuel Cell and Fuel Processor Catalyst Tolerance: There are major fuel requirements for the gas reformates that must be addressed. These requirements result from the effects of sulfur, carbon monoxide, and carbon deposition on the fuel cell catalyst. The activity of catalysts for steam reforming and autothermal reforming can be affected by sulfur poisoning and coke formation; this commonly occurs with most fuels used in fuel cells of present interest. Other fuel constituents can also prove detrimental to various fuel cells. Examples of these are halides, hydrogen chloride, and ammonia.

---

45. Editor's note - The gasoline-fueled ICE well-to-wheel efficiency values apply to today's technology and are averaged over the entire driving cycle. Advanced IC engine/vehicles are more efficient over the entire operating cycle than 18 % (up to 20 some odd %). This implies that future IC engine/vehicle efficiency for light vehicles can be in excess of the 15 to 18 % quoted in the ExxonMobil paper. Vehicle miles per gallon increase when the ICE is combined with a battery in developmental vehicles with very low drag coefficients. For example, the 60+ mpg for the Honda Insight, 40 to 50+ mpg for the Toyota Prius, 70+ mpg for the Ford Prodigy, and ~80 mpg for the GM Precept. The overall well-to-wheel efficiency over a standard city/highway driving cycle for a four passenger, production hybrid vehicle has been estimated to be about 25-30 %, close to a fuel cell vehicle. The fuel cell engines for lightweight vehicles are likely to be hybrids, and therefore the projected efficiencies must be carefully considered.

There are discrepancies in the tolerance for harmful species specified by fuel cell developers, even for similar type fuel cells. These discrepancies are probably due to electrode design, microstructure differences, or in the way developers establish tolerance. In some cases, the presence of certain harmful species causes immediate performance deterioration. More often, the degradation occurs over a long period of time, depending on the developer's permissible exposure to the specific harmful species. Here, the developer establishes an estimated cell life based on economics. The permissible amount of the harmful constituent is then determined based on economic return vs. fuel cell life expectancy.

Figure 8-3 "WELL-TO-WHEEL" EFFICIENCY FOR VARIOUS VEHICLE SCENARIOS (9)

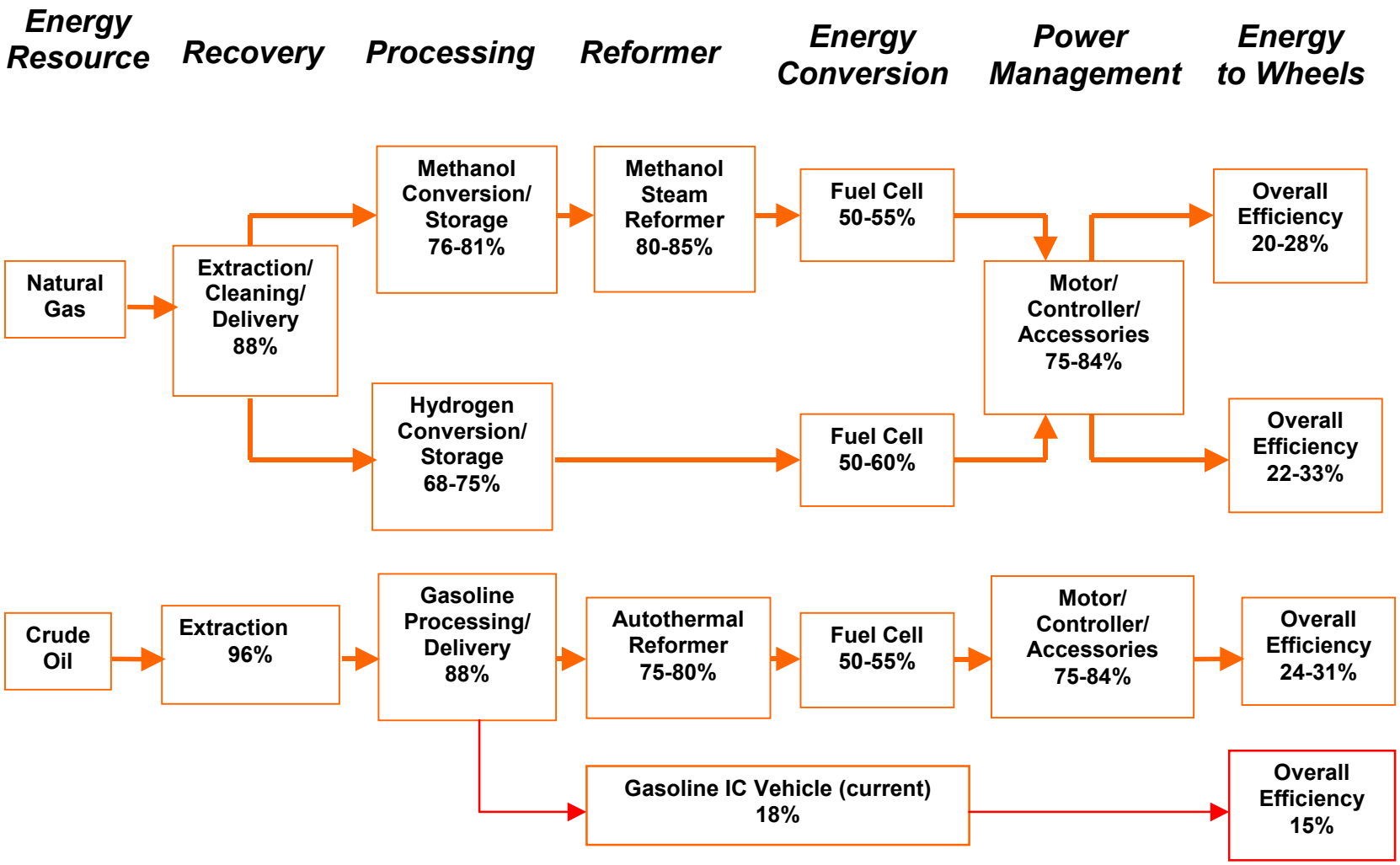

Sulfur Effects

Present gasolines contain approximately 300 ppm by weight of sulfur. New government standards will reduce the sulfur concentration to an average of 30 ppm and a maximum of 80 ppm by 2006; however fuel gas produced from these gasolines may contain as high as 3-8 ppm of H_2S. No. 2 fuel oil contains 2,200 to 2,600 ppm of sulfur by weight. Even pipeline gas contains sulfur-containing odorants (mercaptans, disulfides, or commercial odorants) for leak detection. Metal catalysts in the fuel reformer can be susceptible to sulfur poisoning, requiring that the sulfur in the fuel reformate be removed. Some researchers have advised limiting the sulfur content of the fuel from a steam reformer to less than 0.1 ppm, but note that the limit may be higher in an autothermal reformer (10).

Sulfur poisons catalytic sites in the fuel cell also. The effect is aggravated when there are nickel or iron-containing components, including catalysts that are sensitive to sulfur and noble metal catalysts such as found in low temperature cell electrodes. Sulfur tolerances are described in the specific fuel cell sections of this handbook.[46] In summary, the sulfur tolerances of the cells of interest, by percent volume in the cleaned and altered fuel reformate gas to the fuel cells from published data, are:

- PEFC - <50 ppm sulfur as H_2S (11), poisoning is cumulative and not reversible.
- PAFC - <50 ppm sulfur as H_2S + COS or <20 ppm sulfur as H_2S at the anode. Poisoned anodes can be re-activated by polarization at high potentials.
- MCFC - <0.5 ppm sulfur as H_2S (at the cathode) equates to <10 ppm at the anode because of fuel exhaust being sent to the cathode in an MCFC (same amount of sulfur, more gas at the cathode), poisoning is reversible.
- SOFC - <1 ppm sulfur as H_2S, poisoning is reversible for the tubular SOFC. H_2S levels of 1 ppm result in an immediate performance drop, but this loss soon stabilizes into a normal linear degradation. Tests show that high temperature planar SOFCs with all-ceramic components can tolerate up to 3,000 ppm of sulfur. Sulfur, in H_2S form, has been used as a fuel for an external reforming, all-ceramic SOFC operating at 1,000°C (12). However, developers want to reduce the cell temperature to allow less expensive metal components, primarily interconnects, and improve cycle efficiency. There is a requirement to lower sulfur significantly if metal parts are used in an SOFC. For planar SOFCs, claims for sulfur tolerance vary among the developers. The range of sulfur has been published as 10 to 35 ppm. Planar SOFC sulfur tolerance probably will be secondary to the fuel processor catalyst that, as mentioned, may be as low as 0.1 ppm.

46. There is ambiguity in the way sulfur is reported in fuel cell literature that has caused confusion in the amount that can be tolerated. Reports often fail to distinguish whether the sulfur is measured by weight, as it would be before vaporization of a liquid fuel, or by volume, as it would be in a gas fuel or fuel gas reformate. An approximate rule of thumb is that the amount (by volume) of sulfur in a vaporized fuel is one-tenth the amount of sulfur measured by weight in the liquid fuel. 300 ppm sulfur (by weight) in the liquid fuel equates to 30 ppm sulfur (by volume) when the fuel is converted to a gaseous reformate.

Carbon Monoxide Effects

Carbon monoxide, a fuel in high temperature cells (MCFC and SOFC), is preferentially absorbed on noble metal catalysts that are used in low temperature cells (PAFC and PEFC) in proportion to the H_2:CO partial pressure ratio. A particular level of carbon monoxide yields a stable performance loss. The coverage percentage is a function of temperature, and that is the sole difference between PEFC and PAFC (13). Cell limits are:

- PEFC – Consensus tolerance is <50 ppm into the anode.
- PAFC – Major US manufacturer set tolerance limit as <1.0 % into the anode.
- MCFC – CO and H_2O shift to H_2 and CO_2 in the cell as the H_2 is consumed by the cell reaction due to a favorable temperature and catalyst.
- SOFC – CO can be a fuel. However, if the fuel gas contains H_2O, the shift reaction ($CO + H_2O \rightarrow H_2 + CO_2$) is chemically favored.

Carbon Deposition Effects

The processing of hydrocarbons always has the potential to form coke (soot). If the fuel processor is not properly designed or operated, coking is likely to occur (7). Carbon deposition not only represents a loss of carbon for the reaction, but more importantly results in deactivation of catalysts in the processor and the fuel cell due to deposition at the active sites. Thermo-dynamic equilibrium provides a first approximation of the potential for coke formation. The governing equations are:

$C + CO_2 \leftrightarrow 2CO$	(Boudouard)	(8-1)
$C + 2H_2 \leftrightarrow CH_4$	(carbon-hydrogen)	(8-2)
$C + H_2O \leftrightarrow CO + H_2$	(carbon-steam or gasification)	(8-3)

The possible formation of carbon using a particular fuel can be determined by the simultaneous solution of the above equations using their equilibrium coefficients.[47] No solid graphitic carbon exists at low temperatures (~600°C) in binary mixtures containing at least 2 atoms of oxygen or 4 atoms of hydrogen per atom of carbon (14).

Fuel Cell Unit Size: The size of the fuel cell is a characteristic that impacts fuel processor selection. There is a lower level of power output at which it is no longer advantageous to incorporate a fuel processor. The decision is also application-specific. It is likely that releasing H_2 by chemical reaction from a solid compound when mixed with water is economical for small portable units (below 100 W). An H_2 storage cartridge can be replaced in seconds (15). Actually the power level at which the tradeoff is likely to occur changes as processing and storage technology advances. One fuel processor developer has produced a 100 W partial oxidation (POX) methane reactor the size of a coffee can. The unit includes a reforming zone, shift reactors, and all heat exchangers. H_2 is 36% (assume dry) and the CO level can be reduced to 1%. The unit runs on methane, propane, and ethanol (16). Another research project is investigating methanol reformers for sub-watt fuel cell power sources for the Army.

47. Carbon is slightly less likely to be deposited than equilibrium coefficient calculations indicate, due to kinetics.

Fuel Processing Techniques

The generic term most often applied to the process of converting liquid or gaseous light hydrocarbon fuels to hydrogen and carbon monoxide is "reforming". There are a number of methods to reform fuel. The three most commercially developed and popular methods are 1) steam reforming, 2) partial-oxidation reforming, and, 3) autothermal reforming.

Steam reforming (SR) provides the highest concentration of hydrogen and can obtain a conversion efficiency. Partial oxidation (POX) is a fast process, good for starting, fast response, and a small reactor size. Non-catalytic POX operates at temperatures of approximately 1,400°C, but adding a catalyst (catalytic POX or CPOX) can reduce this temperature to as low as 870°C. Combining steam reforming closely with CPOX is termed autothermal reforming (ATR).

Steam Reforming: Historically, steam reforming has been the most popular method of converting light hydrocarbons to hydrogen. The fuel is heated and vaporized, then injected with superheated steam into the reaction vessel. The steam-to-carbon molar ratio is usually in the neighborhood of 2.5:1 but developers strive for lower ratios to improve cycle efficiency. Excess steam is used to force the reaction to completion as well as to inhibit soot formation. Like most light hydrocarbons, heavier fuels can be reformed through high temperature reaction with steam. Steam reforming is usually carried out using nickel-based catalysts. Cobalt and noble metals are also active, but more expensive. The catalytic activity depends on metal surface area. For nickel, the crystals sinter quickly above the so-called Tamman temperature (590°C), approaching a maximum size related to the pore diameter of the support. The crystal growth results in loss of surface area and activity (17). The steam reformer can operate with or without a catalyst. Most commercial applications of steam reforming use a catalyst to enhance reaction rates at decreased temperatures. Lower temperatures favor high CO and hydrogen concentration. The reforming catalyst also promotes the water-gas shift reaction. Steam reforming is endothermic, thus favored by high temperatures. But it is a slow reaction and requires a large reactor (4). As a result, rapid start and transients cannot be achieved by steam reforming due to its inherently slower indirect heating (18). Steam reforming suits pipeline gas and light distillate stationary fuel cell power generation well.

The exothermic water-gas shift reaction occurs in the steam reformer reactor. The combined reaction, steam reforming and water gas shift, is endothermic. As such, an indirect high temperature heat source is needed to operate the reactor. This heat source usually takes the form of an adjacent, high-temperature furnace that combusts a small portion of the fuel or the fuel effluent from the fuel cell. Efficiency improves by using rejected heat from other parts of the system. Note that the intrinsic water-gas shift in the reactor may not lower the CO content to the fuel cell requirement, and additional shifting will be needed for lower temperature fuel cells.

Steam reforming of higher hydrocarbons can be used to produce methane suitable for use in high temperature internal reforming fuel cells. Steam pre-reforming of hydrocarbons, as a process step in the manufacture of hydrogen, ammonia, methanol, carbon monoxide, and syngas, is an established technology. All higher hydrocarbons are converted over a nickel-based catalyst into a gas mixture containing hydrogen, methane, and carbon oxides. Establishment of methanation and shift reaction equilibria at the process conditions determines the composition of the pre-

reformed gas. By proper design of fuel processing systems, a wide variety of fuels may be converted to a suitable reformate. This reformate can then be used to promote internal reforming for high temperature fuel cell systems. For each type of fuel, optimum operating parameters such as temperature, steam/carbon ratio, and catalyst must be established (19).

Partial Oxidation: A substoichiometric amount of air or oxygen is used to partially combust the fuel. Partial oxidation is highly exothermic, and raises the reactants to a high temperature. The resulting reaction products, still in a reduced state, are then quenched through the introduction of superheated steam. The addition of steam promotes the combined water-gas shift and steam reforming reactions, which further cools the gas. In most cases, and with sufficient pre-heating of the reactants, the overall reaction is exothermic and self-sustaining. For some applications however, particularly small-scale configurations, a catalyst can be used to increase reaction rates at lower reaction temperatures. As with steam reforming, additional, water-gas shift may be necessary to satisfy the fuel cell requirements.

POX reactor temperatures vary widely. Noncatalytic processes for gasoline reforming require temperatures in excess of 1,000°C. These temperatures require the use of special materials and significant preheating and integration of process streams. The use of a catalyst can substantially reduce the operating temperature, allowing the use of more common construction materials such as steel. Lower temperature conversion leads to less carbon monoxide (an important consideration for low temperature fuel cells), so that the shift reactor can be smaller. Lower temperature conversion will also increase system efficiency.

For some heavy hydrocarbon fuels, typical values range from as low as 870°C for catalytic POX upwards to 1,400°C for non-catalytic POX. For sulfur-bearing diesel fuel, a catalytic POX reactor will usually operate at approximately 925°C. This relatively elevated temperature is needed to overcome catalyst degradation due to the presence of sulfur. Non-catalytic POX reactors operate at around 1,175°C on diesel fuel.

Advantages of POX that make this type of fuel conversion suitable for transportation power are:

- POX does not need indirect heat transfer (across a wall), so the processor is more compact and lightweight (7).
- Contrary to widely-held opinion, POX and ATR are capable of higher reforming efficiencies than are steam reformers (20).

Partial oxidation should be reacted so that the overall reaction is exothermic, but at a low oxygen-to-fuel ratio to favor higher hydrogen yields.

It is a widely-held opinion that POX leads to lower efficiency than steam reforming due to the POX reaction being exothermic. However, a thorough examination of the thermodynamics shows that POX and ATR have higher reforming efficiencies than steam reformers. This raises the question why there is a need to use steam reforming or an ATR if the POX's efficiency is higher. The minimum allowable oxygen to carbon (O/C) ratio is 1 for the POX process. This generates high heat that leads to undesirable high temperatures (low H_2, CO_2 selectivity, materials of construction constraints, etc.). The steam reformer and ATR allow lower O/C ratios, keep the temperature down, and result in higher CO_2 and H_2 selectivity (more H_2 yield per mole of fuel).

Autothermal Reforming: The coupling of SR with POX is termed autothermal reforming (ATR). Some define ATR as a SR reaction and a POX reaction that take place over microscopic distances at the same catalytic site, thus avoiding complex heat exchange (21). Others have the less restrictive definition that ATR occurs when there is no wall between a combined SR reaction and catalytic POX reaction. ATR is carried out in the presence of a catalyst that controls the reaction pathways and thereby determines the relative extents of the POX and SR reactions. The SR reaction absorbs part of the heat generated by the POX reaction, limiting the maximum temperature in the reactor. The net result can be a slightly exothermic process.

Autothermal reforming provides a fuel processor compromise that operates at a lower O/C and lower temperature than the POX; is smaller, quicker starting, and quicker responding than the SR, and results in high H_2 concentration.. A catalytic POX reaction must be used to reduce the temperature to a value compatible with the SR temperature.

Other Reforming Combinations: There have been fuel processor configurations where a non-catalytic POX is placed in series with a steam reformer. Without catalyst, the POX reaction must be at a higher temperature than the steam reformer reaction. These reactions must take place in separate compartments with heat exchange and a wall between them (18). This configuration is not considered within the definition of autothermal reforming.

State-of-the-Art Components

Developers have brought fuel processing technology to the point where conversion of all fuels of interest to fuel cells have been demonstrated to a degree. Natural gas steam reforming is used in commercial fuel cell units. There has been equal success with steam reforming light distillates, although these fuels are not commonly used. Tests have been performed on reactors and complete small fuel processors using methanol, gasoline, and diesel, all suitable for vehicle use. These tests have not advanced to operation over prolonged periods. However, there have been tests that indicate these fuels can be processed in POX and ATR reactors with high levels of sulfur. Water-gas shift and methods to lower CO even to a few ppm have been developed, but the final CO cleanup processes are in an early stage of development. All fuel processors need additional engineering development to reduce volume, weight, and cost to allow widespread fuel cell power unit use. The state-of-the-art information below is based primarily on U.S. or closely-related fuel cell programs.

State-of-the-Art Components - Conversion of Fuels

Generic Fuel Conversion: Considering the spectrum of fuel conversion from steam reforming to partial oxidation should convey a basic understanding of the reforming processes. An elegant, general equation published by the ANL describes fuel conversion throughout the spectrum. Autothermal reforming falls within this spectrum so that the equation encompasses processes of interest to fuel cells. The equation does not apply to complete combustion, but that conversion process is not relevant to fuel cells (20, 22, 23). The general, idealized equation is:

$$C_nH_mO_p + x(O_2 + 3.76N_2) + (2n - 2x - p)H_2O = nCO_2 + (2n - 2x - p + m/2)H_2 + 3.76xN_2 \qquad (8\text{-}4)$$

where x is the molar ratio of oxygen-to-fuel. This ratio is very important because it determines:

- The minimum amount of water that is required to completely convert the carbon in the fuel to carbon dioxide ($2n - 2x - p$). Excess water is used in practice to ensure the conversion, resulting in water in the reformate (right side of the equation). Typically, one or two moles of water for every mole of oxygen are used.
- The maximum hydrogen yield ($2n - 2x - p + m/2$)
- The maximum concentration (percentage) of hydrogen in the reformate $\{[2n - 2x - p + m/2]/[n + (2n - 2x - p + m/2) + 3.76x]$ all times 100$\}$
- The heat of reaction $\{\Delta H_r = n(\Delta H_{f,CO_2}) - (2n - 2x - p)\Delta H_{f,H_2O} - \Delta H_{f,fuel}\}$.

Decreasing the oxygen-to-fuel ratio, x, results in increasing demand for water (water-to-fuel ratio), with commensurate increases in the yield and concentration of hydrogen in the reformate gas. When $x = 0$, the equation reduces to the strongly endothermic steam reforming reaction. The reaction becomes less endothermic with increasing oxygen. It becomes thermoneutral[48] at $x = x_0$ (0.44 for methane). Above this point, the reaction becomes increasingly exothermic. At $x = 1$ with methane, the pure POX reaction, the feed contains sufficient oxygen to convert all of the carbon in the fuel to CO_2. No water needs to be added. The equation is a mix of the steam reforming reaction and the POX reaction at values of x between 0 and n.

Beyond $x = [n - (p/2)] = n$ (when $p = 0$), where water is a product, the heat of reaction is determined by the phase of the product water. At still higher values, the excess oxygen oxidizes the hydrogen to produce water. Finally, at stoichiometric combustion, all carbon and hydrogen are converted to carbon dioxide and water. Here, $x = Xc = [n - (p/2) + (m/4)]$. The value of x reduces to 2 with CH_4 as the fuel.

Equation 8-4 depicts a total reaction where the fuel input is converted to carbon dioxide. Actually, the initial reforming step is carried out at elevated temperatures, where a mixture of carbon monoxide and carbon dioxide is formed. In the subsequent reformate conversion step, the carbon monoxide is converted via the water-gas shift to carbon dioxide:

$$CO + H_2O \leftrightarrow H_2 + CO_2 \qquad (8\text{-}5)$$

48. The thermoneutral point (of oxygen-to-carbon ratio) is where the enthalpy of the reaction is zero, ($\Delta H_{f,298} = 0$).

There may be additional, downstream inputs of water/steam and oxygen/air for water-gas shift and selective oxidation to further reduce CO, if needed.

When the function of a fuel processor is to convert a fuel to hydrogen, the fuel conversion efficiency is

$$\text{Efficiency} = \frac{\text{Lower Heating Value of Anode Fuel(s) Produced}}{\text{Lower Heating Value of Fuel Used}} \tag{8-6}$$

The fuel conversion efficiency for methane conversion to hydrogen is 93.9% at the thermoneutral point, $x = 0.44$ (an ATR reaction) and 91.7% at $x = 0$ (the SR reaction). The difference between the two efficiency values is exactly equivalent to the loss represented by the latent heat of vaporization of the H_2O that escapes with the combustions products in the SR burner exhaust. The concentration of hydrogen is 53.9% at $x = 0.44$ (ATR) and 80% at $x = 0$ (SR).

Equation 8-4 and related heats of reaction can be manipulated to show that the maximum efficiency is a state point function, regardless of path (steam reforming, partial oxidation, or autothermal reforming), and is achieved at the thermoneutral point. In practice, x is set slightly higher than the thermoneutral point so that additional heat is generated to offset heat losses from the reformer. Table 8-1 presents efficiencies at the thermoneutral point for various hydrocarbon fuels.

Table 8-1 Calculated Thermoneutral Oxygen-to-Fuel Molar Ratios (x_o) and Maximum Theoretical Efficiencies (at x_o) for Common Fuels (23)

$C_nH_mO_p$	n	m	p	$\Delta H_{f,fuel}$ (kcal/gmol)	m/2n	X_o, $\Delta H_r = 0$	Efficiency (%)
Methanol $CH_3OH(l)$	1	4	1	-57.1	2	0.230	96.3
Methane CH_4	1	4	0	-17.9	2	0.443	93.9
Iso-Octane $C_8H_{18}(l)$	8	18	0	-62.0	1.125	2.947	91.2
Gasoline $C_{7.3}H_{14.8}O_{0.1}(l)$	7.3	14.8	0.1	-53.0	1.014	2.613	90.8

Because the components and design of a fuel processor depend on the fuel type, the following discussion is organized by the fuel being processed.

Hydrogen Processing: When hydrogen is supplied directly to the fuel cell, the fuel processing section is no more than a storage and delivery system. However, in general applications, hydrogen must be generated from other fuels and processed to meet the system requirements.

Natural Gas Processing: The major constituents of pipeline gas are methane, ethane, propane, CO_2, and, in some cases, N_2. Sulfur-containing odorants (mercaptans, disulfides, or commercial odorants) are added for leak detection. Because neither fuel cells nor commercial reformer

catalysts are sulfur tolerant, the sulfur must be removed. This is usually accomplished with a zinc oxide sulfur polisher and the possible use of a hydrodesulfurizer, if required. The zinc oxide polisher is able to remove the mercaptans and disulfides. However, some commercial odorants, such as Pennwalt's Pennodorant 1013 or 1063, contain THT (tetrahydrothiophene), more commonly known as thiophane, and require the addition of a hydrodesulfurizer before the zinc oxide sorbant bed. The hydrodesulfurizer will, in the presence of hydrogen, convert the thiophane into H_2S that is easily removed by the zinc oxide polisher. The required hydrogen is supplied by recycling a small amount of the natural gas reformed product. Although a zinc oxide reactor can operate over a wide range of temperatures, a minimum bed volume is achieved at temperatures of 350 to 400°C (660 to 750°F).

The CH_4 in the natural gas is usually converted to H_2 and CO in a SR reactor. Steam reforming reactors yield the highest percentage of hydrogen of any reformer type. The basic SR reactions for methane and a generic hydrocarbon are:

$$CH_4 + H_2O \leftrightarrow CO + 3H_2 \tag{8-7}$$
$$C_nH_m + nH_2O \leftrightarrow nCO + (m/2 + n)\ H_2 \tag{8-8}$$
$$CO + H_2O \leftrightarrow CO_2 + H_2 \tag{8-9}$$

In addition to natural gas, steam reformers can be used on light hydrocarbons such as butane and propane, and on naphtha with a special catalyst. Steam reforming reactions are highly endothermic and need a significant heat source. Often the residual fuel exiting the fuel cell is burned to supply this requirement. Fuels are typically reformed at temperatures of 760 to 980°C (1,400 to 1,800°F).

A typical steam reformed natural gas reformate is presented in Table 8-2.

Table 8-2 Typical Steam Reformed Natural Gas Reformate

Mole Percent	Reformer Effluent	Shifted Reformate
H_2	46.3	52.9
CO	7.1	0.5
CO_2	6.4	13.1
CH_4	2.4	2.4
N_2	0.8	0.8
H_2O	37.0	30.4
Total	100.0	100.0

A POX reformer also can be used to convert gaseous fuels, but does not produce as much hydrogen as the steam reformers. For example, a methane-fed POX reformer would produce only about 75% of the hydrogen (after shifting) that was produced by an SR. Therefore, partial oxidation reformers are typically used only on liquid fuels that are not well suited for steam reformers. Partial oxidation reformers rank second after steam reformers with respect to their hydrogen yield. For illustration, the overall POX reaction (exothermic) for methane is

$$CH_4 + \frac{1}{2}O_2 \rightarrow CO + 2H_2 \quad (8\text{-}10)$$

When natural gas fuels are used in a PAFC or a PEFC, the reformate must be water-gas shifted because of the high CO levels in the reformate gas. A PAFC stack can tolerate about 1% CO in the cell before having an adverse effect on cell performance due to catalyst poisoning. The allowable CO level in the fuel gas for a PEFC is considerably lower. The shift conversion is often performed in two or more stages when CO levels are high. A first high-temperature stage allows high reaction rates, while a low-temperature converter allows for a higher conversion. Excess steam is used to enhance the CO conversion. A single-stage shift reactor is capable of converting 80 to 95% of the CO (24). The water gas shift reaction is mildly exothermic, so multiple stage systems must have interstage heat exchangers. Feed temperatures of high- and low-temperature shift converters range from approximately 260 to 370°C (500 to 700°F) and 200 to 260°C (400 to 500°F), respectively. Hydrogen formation is enhanced by low temperature, but is unaffected by pressure.

When used in a PEFC, the reformate must pass through a preferential CO catalytic oxidizer, even after being shifted in a shift reactor. Typically, the PEFC can tolerate a CO level of only 50 ppm. Work is being performed to increase the CO tolerance level in PEFC.

At least two competing reactions can occur in the preferential catalytic oxidizer:

$$CO + \frac{1}{2}O_2 \rightarrow CO_2 \quad (8\text{-}11)$$
$$H_2 + \frac{1}{2}O_2 \rightarrow H_2O \quad (8\text{-}12)$$

The selectivity of these competing reactions depends upon the catalyst and determines the quantity of required oxygen (25).

Liquid Fuel Processing: Liquid fuels such as distillate, naphtha, diesel oils, and heavy fuel oil can be reformed in partial oxidation reformers. All commercial POX reactors employ noncatalytic POX of the feed stream by oxygen in the presence of steam with reaction temperatures of approximately 1,300 to 1,500°C (2,370 to 2,730°F) (24). For illustration, the overall POX reaction for pentane is

$$C_5H_{12} + 5/2O_2 \rightarrow 5CO + 6H_2 \quad (8\text{-}13)$$

The overall reaction is exothermic, and largely independent of pressure. The process is usually performed at 20 to 40 atmospheres to yield smaller equipment (24). A typical fuel composition for a fuel oil fed POX reformer is presented in Table 8-3. The CO contained in this reformate may need to be converted with a shift converter or selective catalytic converter, depending upon the specific fuel cell being fed.

Table 8-3 Typical Partial Oxidation Reformed Fuel Oil Reformate (24)

Mole Percent (dry, basis)	Reformer Effluent
H_2	48.0
CO	46.1
CO_2	4.3
CH_4	0.4
N_2	0.3
H_2S	0.9
Total	100.0

Alcohols are steam-reformed at lower temperatures (<600°C) while alkanes[49] and unsaturated hydrocarbons require slightly higher temperatures. Cyclic hydrocarbons and aromatics have also been reformed at relatively low temperatures, however a different mechanism appears to be responsible for their reforming. Blended fuels like gasoline and diesel, that are mixtures of a broad range of hydrocarbons, require temperatures of >700°C maximum hydrogen production. Methanol, one of the fuels being considered for transportation applications, can be converted into hydrogen by steam reforming:

$$CH_3OH = CO + 2H_2 \quad (8\text{-}14)$$
$$CO + H_2O = CO_2 + H_2 \quad (8\text{-}15)$$

The equivalent overall result of these two specific reactions is:

$$CH_3OH + H_2O = CO_2 + 3H_2 \quad (8\text{-}16)$$

The optimum choice of operating conditions is close to a steam to methanol ratio of 1.5 and a temperature range of 250°C to 399°C. Pressure does not influence the reaction rate, but very high pressures limit the equilibrium conversion, which otherwise is better than 99% at the preferred range of 5 to 15 bars. The Cu/Zn/Al and Cu/Zn/Cr based catalysts have been used in industrial units for many years (17).

Coal Processing: The numerous coal gasification systems available today can be reasonably classified as one of three basic types: 1) moving-bed, 2) fluidized-bed, and 3) entrained-bed. All three of these types use steam and either air or oxygen to partially oxidize coal into a gas product. The moving-bed gasifiers produce a low temperature (425 to 650°C; 800 to 1,200°F) gas containing devolatilization products such as methane and ethane, and hydrocarbons including naphtha, tars, oils, and phenol. Entrained-bed gasifiers produce a gas product at high temperature (>1,260°C; >2,300°F composed almost entirely of hydrogen, carbon monoxide, and carbon dioxide. The fluidized-bed gasifier product gas falls between these two other reactor types in composition and temperature (925 to 1,040°C; 1,700 to 1,900°F).

49. Alkanes are saturated hydrocarbons, i.e., no double carbon bonds. Examples are CH_4, C_2H_6, C_3H_8, and C(n)H(2n+2). Alkenes have carbon-carbon double bonds such as ethene C_2H_4 and C(n)H(2n).

The heat required for gasification is supplied by the partial oxidation of coal. Overall, the gasification reactions are exothermic, so waste heat boilers often are used at the gasifier effluent. The temperature, and therefore composition, of the product gas depends upon the amount of oxidant and steam, as well as the design of the reactor.

Gasifiers typically produce contaminants that must be removed before entering the fuel cell anode. These contaminants include H_2S, COS, NH_3, HCN, particulates, tars, oils, and phenols. The contaminant levels depend on both the fuel composition and the gasifier employed. There are two families of cleanup that remove the sulfur impurities: hot and cold gas cleanup systems. Cold gas cleanup technology is commercial, has been proven over many years, and provides the system designer with several choices. Hot gas cleanup technology is still developmental and would likely need to be joined with low temperature cleanup systems to remove the non-sulfur impurities in a fuel cell system. For example, tars, oils, phenols, and ammonia could all be removed in a low temperature water quench followed by gas reheat.

A typical cold gas cleanup process following an entrained gasifier would include the following subprocesses: heat exchange (steam generation and regenerative heat exchange), particulate removal (cyclones and particulate scrubbers), COS hydrolysis reactor, ammonia scrubber, acid gas (H_2S) scrubbers (Sulfinol, SELEXOL), sulfur recovery (Claus and SCOT processes), and sulfur polishers (zinc oxide beds). All of these cleanup systems increase process complexity and cost, while decreasing efficiency and reliability. In addition, many of these systems have specific temperature requirements that necessitate the addition of heat exchangers or direct contact coolers.

For example, a COS hydrolysis reactor operates at about 180°C (350°F), the ammonia and acid scrubbers operate in the vicinity of 40°C (100°F), while the zinc oxide polisher operates at about 370°C (700°F). Thus, gasification systems with cold gas cleanup often become a maze of heat exchange and cleanup systems.

Typical compositions for several oxygen-blown coal gasification products are shown in Table 8-4.

Table 8-4 Typical Coal Gas Compositions for Selected Oxygen-Blown Gasifiers

Gasifier Type	Moving-Bed	Fluidized-Bed	Entrained-Bed			
Manufacturer	**Lurgi (20)**	**Winkler**	**Destec**	**Koppers-Totzek**	**Texaco**	**Shell**
Coal	Illinois No. 6	Texas Lignite	Appalachian Bit.	Illinois No. 6	Illinois No. 6	Illinois No. 6
Mole Percent						
Ar	trace	0.7	0.8	0.9	0.9	1.1
CH_4	3.3	4.6	0.6	-	0.1	-
C_2H_4	0.1	-	-	-	-	-
C_2H_6	0.2	-	-	-	-	-
CO	5.8	33.1	45.2	43.8	39.6	63.1
CO_2	11.8	15.5	8.0	4.6	10.8	1.5
COS	trace	-	-	0.1	-	0.1
H_2	16.1	28.3	33.9	21.1	30.3	26.7
H_2O	61.8	16.8	9.8	27.5	16.5	2.0
H_2S	0.5	0.2	0.9	1.1	1.0	1.3
N_2	0.1	0.6	0.6	0.9	0.7	4.1
NH_3+ HCN	0.3	0.1	0.2	-	-	-
Total	100.0	100.0	100.0	100.0	100.0	100.0

Reference Sources: (26, 27)
Note: All gasifier effluents are based on Illinois No. 6, except the Winkler, which is based on a Texas Lignite, and the Destec, which is based on an Appalachian Bituminous.

Other Solid Fuel Processing: Solid fuels other than coal can be utilized in fuel cell systems. For example, biomass and RDF (refuse-derived-fuels) can be integrated into a fuel cell system as long as the gas product is processed to meet the requirements of the fuel cell. The resulting systems would be very similar to the coal gas system with appropriate gasifying and cleanup systems. However, because biomass gas products can be very low in sulfur, the acid cleanup systems may simply consist of large sulfur polishers.

State-of-the-Art Components - Cleaning and Reformate Gas Alteration (Removal Of Contaminants): Besides their basic fuel reforming function, fuel processors require the removal of impurities that degrade the fuel processor or fuel cell performance. Sulfur is the major contaminant encountered. Carbon monoxide reduction for low temperature fuel cells and avoidance of carbon deposition are also addressed. A typical processing chain for a low temperature fuel cell will have a hydrodesulfurizer, a halogen guard, a zinc oxide sulfur absorber, a catalytic reformer, a high temperature shift converter, a second halogen guard, and low temperature shift converter. Figure 8-2 provides insight into how these may be arranged. The function of all these components, except the reformer, is to remove impurities. For the PEFC, an additional device is necessary to remove essentially all CO, such as a preferential oxidizer (28).

Sulfur Reduction: There are high temperature and low temperature methods to remove sulfur from a fuel reformate. Low temperature cleanup, such as hydrodesulfurizing (limited to fuels with boiling end points below 205°C), is less difficult and lower in cost so should be used where possible, certainly with low temperature fuel cells. Sulfur species in the fuel are converted to

H_2S, if necessary, then the H_2S is trapped on zinc oxide. A minimum bed volume of the zinc oxide reactor is achieved at temperatures of 350 to 400°C. Thermodynamic and economic analyses show that it is appropriate to use high temperature cleanup with high temperature fuel cells.

There is a vast difference between removing sulfur from a gaseous fuel and a liquid fuel. The sulfur in a liquid fuel is usually removed after it is converted to a gas. This by removing the sulfur in the reforming reactor at high temperature, or by incorporating sulfur resistant catalysts. Sulfur resistant catalysts are being developed, but none are mature enough for present use. ANL is developing catalysts to reform gasoline, and have demonstrated that their catalyst can tolerate sulfur. The ANL catalyst has been shown to tolerate (100s of hours) sulfur present in natural gas in an engineering scale reformer.

At least one developer has a liquid-phase fuel desulfurizer cartridge that will be used to remove sulfur prior to fuel vaporization. Other developers remove the sulfur immediately after vaporization and prior to reforming. Hydrogen must be recirculated to the removal device to convert the sulfur species to H_2S so that it can be entrapped on zinc oxide. Zinc oxide beds are limited to operation at temperatures below 430°C to minimize thermal cracking of hydrocarbons that can lead to coke formation. Thermodynamics also favor lower temperatures. At higher temperatures, the H_2S cannot be reduced to levels low enough for shift catalyst or to reach fuel cell limits. For sulfur removal in the reformer, the presence of significant concentrations of steam in the fuel gas has a negative impact on the reaction equilibrium, leading to a higher concentration of H_2S than could be achieved with a dry fuel gas.

Carbon Monoxide Reduction: The use of CO as a fuel in high temperature cells and water-gas shift reactions to lower carbon monoxide to conditions suitable for a PAFC or a PEFC have been previously described. Fuel gas reformate contains 0.5 to 1% by volume of CO even after the shift reactions. Present PEFCs operate below 100°C. At these temperatures, even small amounts of CO are preferentially adsorbed on the anode platinum (Pt) catalysts. This blocks access of H_2 to the surface of the catalyst, degrading cell performance (29). Reformate for PEFC stacks must contain very low (<50 ppm) CO to minimize Pt absorption to a reasonable value to maintain sufficient active sites for the oxidation of H_2. This can be achieved in two ways, by air injection into the anode at up to about 4% of the reformate feed rate or by reducing CO concentration prior to the cell: even at 50 ppm, catalyst poisoning by CO must be mitigated by the injection of some air at the anode. For the latter approach, a preferential oxidizer (PROX) is used to reduce CO concentration prior to the cell. It has highly dispersed supported Pt or Pt-Ru (ruthenium) catalyst. Such catalysts act on the principle of selective adsorption of CO onto the active Pt or Pt-Ru (relative to H_2), leading to CO being selectively oxidized by stoichiometric amounts of air co-fed to the catalyst bed. As the CO is oxidized, the gas temperature rises, which decreases the selectivity of CO adsorption on the catalyst and also increases the kinetics of the reverse water-gas shift reaction. In practice, the PROX process is carried out in stages to permit cooling between stages. The PROX is a relatively large unit that operates at 100 to 180°C (22). Preferential gas cleanup by selective oxidation results in 0.1 to 2% H_2 lost (30).

Carbon Deposition Avoidance: The processing of hydrocarbons always has the potential to form coke. Coke formation is influenced by the composition of the fuel, the catalyst, and the

process conditions (e.g., partial pressure of steam). Coke causes the greatest problems in gas flow paths and on catalyst. Carbon deposition not only represents a loss of carbon for the reaction, but more importantly also results in deactivation of the catalyst due to deposition at the active sites. Thermal cracking[50] in over-heated preheaters and manifolds can easily form carbon. If the fuel conversion reactor is not properly designed or operated, coking is likely to occur. Thermo dynamic equilibrium provides a first approximation of the potential for coke formation. Free carbon in hydrocarbon fuels forms according to the three equations, (8-1), (8-2), and (8-3). Figures 8-4 and 8-5 show the effect of increasing steam on carbon deposition for methane and octane, respectively. Increasing steam, hydrogen, and carbon dioxide concentrations alleviates carbon deposition. Low contents of aromatics and alkenes help to maintain the activity of the catalyst (10). No carbon deposits at low temperatures (~600°C) in mixtures containing at least two atoms of oxygen and four atoms of hydrogen per atom of carbon. At these conditions, all carbon is present as CO_2 or CH_4 (7).

Higher hydrocarbon fuels show a greater tendency for carbon formation than does methane. One method to alleviate carbon deposition problems in the fuel processor is to use special catalysts either containing alkali or based on an active magnesia support. With a highly active catalyst, the limit permitted on the final boiling point of the hydrocarbon feedstock is related mainly to the possibility of desulfurizing the feed to below 0.1 ppm, rather than to the reactivity of the hydrocarbons. With proper desulfurization, it has been possible to convert light oil into syngas with no trace of higher hydrocarbons in the reformate gas (17).

Coke formation resulting from higher hydrocarbon fuels can also be eliminated with an adiabatic pre-reformer. The adiabatic reformer is a simple fixed bed reactor. By adiabatic pre-reforming, all higher hydrocarbons are converted at low temperature (below ~500°C) with steam into methane, hydrogen, and carbon oxides at conditions where carbon formation does not occur. It is possible to use a high pre-heating temperature (650°C or above) for internal reforming in MCFC and SOFC without the risk of carbon formation. For natural gas containing only minor amounts of higher hydrocarbons, adiabatic pre-reforming at a steam to carbon ratio as low as 0.25 mole/atom has been demonstrated. For heavier feedstocks such as naphtha, operation at a steam to carbon ratio of 1.5 has been proven in industry. Pilot tests have been carried out at a steam to carbon ratio of 1.0 with reformate recycle.

50. Thermal cracking is the breaking of a hydrocarbon carbon-carbon bond through the free-radical mechanism. Cracking may result in the formation of lower chained hydrocarbons, the original "cracked" hydrocarbon, or further cracking of the hydrocarbon to soot.

Figure 8-4 Carbon Deposition Mapping of Methane (CH_4)
(Carbon-Free Region to the Right of Curve)

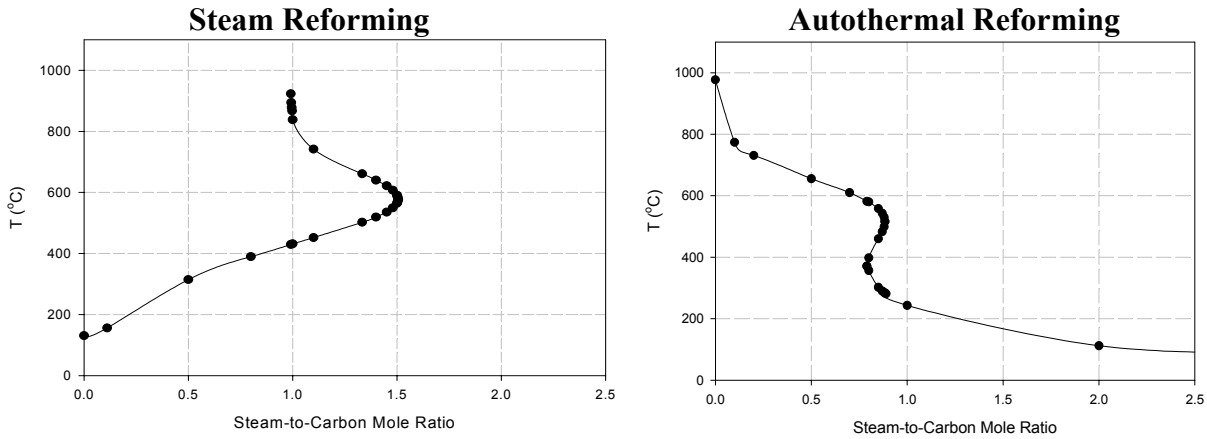

Figure 8-5 Carbon Deposition Mapping of Octane (C_8H_{18})
(Carbon-Free Region to the Right and Above the Curve)

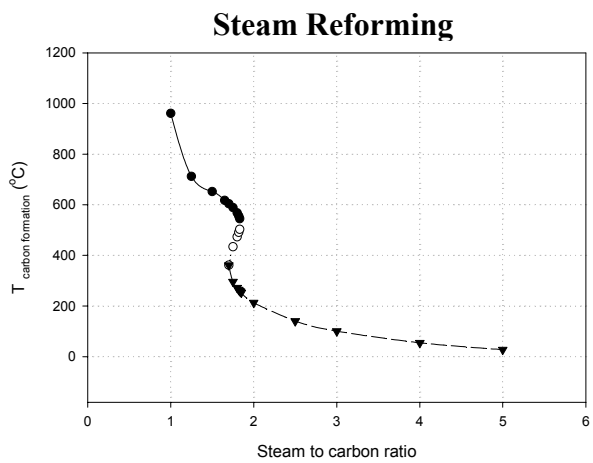

Coking can be also be avoided by operating at high temperatures and at high oxygen-to-carbon ratios, where the ratio is based on the total atoms of oxygen contained in the steam and air feeds. For a given O/C ratio in the feed, it is preferable that the oxygen comes from water. Thus, for a given O/C, SR is preferred over ATR, which is preferred over POX; "preferred" meaning that coke formation can be avoided while still operating at a lower temperature (20, 23, 31).

Other Impurities Reduction: Halides in fuels such as naphtha have deleterious effects on steam reforming and low temperature shift, thus halogen guards must be included in fuel processing.

There are many types of coal with different compositions, including harmful species. One common constituent, HCl, will cause formation of stable chlorides and corrosion in a MCFC. There has not been much work in SOFC yet on this topic. It is doubtful whether low temperature cells will be fueled by coal.

Research & Development Components
There are two major areas where fuel processor developers are focusing their research and development efforts, catalyst development and process/engineering development. A smaller, long term effort on novel processing schemes is in the early stages of investigation.

Catalyst Development. Performance targets for the fuel processor for transportation fuel cell systems will require that the reforming catalysts used in these processors exhibit a higher activity and better thermal and mechanical stability than reforming catalysts currently used in the production of H_2 for large-scale manufacturing processes. To meet these targets, reforming catalysts will have to process the feed at a space velocity of 200,000/hr (based on the volumetric flow of the feed in the gaseous state at 25°C and 1 atm) with a fuel conversion of >99% and a H_2 selectivity of >80% (moles of H_2 in product/moles of H_2 "extractable" from the feed), and have a lifetime of 5,000 hr. Given the potential market for transportation applications, many of the major catalyst producers, such as Johnson-Matthey, Engelhard Corporation, and dmc^2 division of OM Group, Inc., have begun to develop new reforming catalysts (32). An ANL program is focused on improving long-term stability (minimize deactivation), an important, immediate goal, reducing coke formation for higher hydrocarbons, and improving catalyst sulfur tolerance while addressing cost issues. A major issue is to demonstrate that the catalyst can operate for 40,000+ hours in stationary applications and 4,000+ hours in transportation applications. It is believed that no one has successfully demonstrated these targets. Another issue is that coke formation will be problematic with higher hydrocarbons, especially diesel. Most industrial reforming catalysts are operated steam-rich to minimize coke formation. However, this increases the size of the reformer as well as the energy needed to vaporize the water. This option may not be viable for reformers used with fuel cells. Finally, <20 ppb of S is the target for use with nickel steam reforming catalyst. Most fuels being considered contain either sulfur at the ppm level, such as gasoline, or added as an odorant for safety reasons, such as to natural gas. The ability of the catalyst to process fuels containing ppm levels of sulfur would be beneficial. The ANL catalysts are based on solid oxide fuel cell technology, where a transition metal is supported on an oxide- ion-conducting substrate, such as ceria, zirconia, or lanthanum gallate, that has been doped with a small amount of a non-reducible element, such as gadolinium, samarium, or zirconium. Platinum was the transition metal used in the first generation of the ANL catalyst. Because of concerns over the cost associated with using a precious metal-based catalyst, work has begun on reducing the cost of the catalyst either by replacing Pt with a less expensive non-noble metal or by using a combination of a noble metal, at a considerably lower metal loading, and with a base metal without sacrificing performance. Work is proceeding on catalysts based on Ni, Rh, and combinations of Ni and Rh. Süd-Chemie, Inc. currently produces reforming catalysts based on this technology under a licensing agreement with Argonne (32).

There is also a need to develop better water gas shift catalysts (7, 33, 34), especially catalysts that operate at temperatures ranging from 200-300 ^{o}C. Commercial shift catalysts based on FeCr and CuZn oxides are available, but are not designed for the rapid startups and frequent exposure to oxidizing conditions that will be experienced during normal operation of fuel processors developed for transportation applications. These commercial catalysts have fixed size, high density, and are susceptible to contaminant poisoning by ingredients found in infrastructure fuels. Of primary concern is the need to reduce these catalysts in a well-controlled manner that minimizes temperature rise in order to achieve maximum catalyst activity and to prevent the

exposure of the catalyst in the reduced state to oxidizing conditions. For example, the CuZn catalysts will sinter if exposed to >270 ^{o}C and are pyrophoric when exposed to air in the reduced state. Present commercial catalysts are developed for process plant service where transient conditions are not a concern. There is a need for highly active catalysts that can be supported on a low density monolith that do not require reduction in order to be active and are stable when exposed to oxidizing conditions. ANL is developing a more robust shift catalyst that will work better under transient operating conditions than present catalysts developed for process plant service. The advantage of this catalyst over standard catalysts is that it is air stable, which is needed for many start-up and shutdown cycles. There is a trade-off of a moderate reduction in activity (35).

There is also a need to demonstrate that the low-temperature, PROX catalysts have high selectivity toward CO and long term stability.

Process/Engineering Development Numerous engineering and process issues are being addressed by fuel processor developers (20, 31, 36). Several major issues are:

- As the size of the catalyst bed increases, the segregation within an ATR reactor bed toward over-oxidation and catalyst overheating in the front of the bed, and air starvation and carbon formation in the back end of the bed are important to consider. Maintaining a good temperature distribution in the bed, especially with a large reactor, is identified as one of the challenges facing this approach.
- Fuel processor tests have been on the order of 40 hours, although the fuel processors have been tested for 1,000 hours on natural gas. There is a need is to show similar results at realistic operating conditions and further engineering development to enhance the catalyst activity and make the fuel processor lighter and smaller.
- There is a need to investigate improved and simplified fuel processor designs. Examples are combining the reformer and the desulfurizer in a single stage to reduce weight and volume, producing an integrated vaporizer design, and designing for a wide variation of fuel vaporization temperatures to allow fuel flexible operation.
- Transient issues are important in transport applications and should be addressed early by testing. The challenge is to demonstrate the operation at high sulfur content over the full operating envelope of the vehicle – start-up, transients, shutdown, sulfur spikes in the fuel, etc. using the same processor.

Novel Processing Schemes: Various schemes have been proposed to separate the hydrogen-rich fuel in the reformate for cell use or to remove harmful species. At present, the separators are expensive, brittle, require large pressure differential, and are attacked by some hydrocarbons. There is a need to develop thinner, lower pressure drop, low cost membranes that can withstand separation from their support structure under changing thermal loads. Plasma reactors offer independence of reaction chemistry and optimum operating conditions that can be maintained over a wide range of feed rates and H_2 composition. These processors have no catalyst and are compact. However, results are preliminary and have only been tested at a laboratory scale.

Other: Although not R&D, it should prove beneficial for fuel cell developers to provide fuel tolerance specifications to fuel processor developers. Tolerances should be established by

standard definition, determination methods, and measurement procedures. This would aid the fuel processor developer to deliver products compatible with various fuel cell units. Of particular importance are sulfur and CO limits.

8.2 Power Conditioning

Power conditioning is an important enabling technology necessary for converting the DC electrical power generated by a fuel cell into usable AC power for stationary loads, automotive applications, and interfaces with electric utilities. Fuel cells are emerging as an attractive power source by virtue of their inherently clean, efficient, and reliable nature (37, 38). As the demand for various applications such as remote generation, backup power generation, distributed generation, and automotive applications increase, their prices are expected to decrease, thus furthering their penetration into the market (37). Further, unlike batteries, fuel cells can continuously provide power as long as reactants are supplied.

It should be noted that the electrical attributes of a fuel cell are far from an ideal electric power source. A typical fuel cell stack has a DC output voltage that varies widely (2:1) with the load current and age of the fuel cell, and has limited overload capability. Furthermore, a fuel cell stack is slow to respond to load changes (if the fuel supply is adjusted for best efficiency), needs considerable parasitic power for pumps and blowers, and may possibly be slow to start up due to heating requirements. Low cost power-conditioning units are essential for fuel cell systems to be cost competitive (39, 40, 41). Furthermore, the power conversion technology must create, as well as supply, the market demand in a cost effective manner for fuel cell technology to be viable. The aim of this section is to explore several possible power conversion approaches to interface a variety of fuel cell power sources for the following applications:

- Fuel cell power conversion for supplying a dedicated load in an isolated/remote location
- Fuel cell power conversion for supplying backup power (uninterrupted power supply) to a load connected to a local utility
- Fuel cell power conversion for supplying a load operating in parallel with the local utility (utility interactive)
- Fuel cell power conversion for connecting directly to the local utility
- Power conversion for automotive fuel cell applications
- Power conversion for a fuel cell turbine hybrid interfaced to local utility

Fundamentals of various power conversion stages such as DC-DC, DC-AC and AC-AC are essential for processing the electric energy generated by fuel cells. Section 8.2.1 is intended for those who need to understand the basics of power conversion building blocks. After examining basic power conversion blocks, Sections 8.2.2 to 8.2.8 delve into power conversion architectures suitable to serve a few kW to several MW power levels. Numerous power electronics books and scientific papers are available to provide additional details (42, 43, 44, 45).

8.2.1 Introduction to Fuel Cell Power Conditioning Systems

The purpose of this section is to provide an introduction to various power conversion blocks such as DC to DC, and DC to AC employed in fuel cell power conditioning systems. The section also includes a brief review of modern power semiconductor devices, gate drive requirements, packaging, and cooling methods. Figure 8-6 shows a block diagram of a fuel cell power plant.

Figure 8-7 illustrates a block diagram of a modern power conditioning system for processing fuel cell power to AC output. Figure 8-8 shows a typical variation of the output voltage of a fuel cell stack in response to changes in load current. Since the dc voltage generated by a fuel cell stack varies widely (Figure 8-8a) and is low in magnitude (<50V for a 5-10kW system, <350V for a 300kW system), a step-up DC to DC converter stage is essential to generate a regulated higher voltage dc (400V typical for 120/240V AC output). The DC to DC conversion stage is responsible for drawing power from the fuel cell, and therefore should be designed to match the fuel cell ripple current specifications. Further, the DC to DC converter should not introduce any negative current into the fuel cell. A DC to AC conversion stage is essential for converting the DC to useful AC power at 60Hz or 50Hz frequency. An output filter stage connected to the inverter filters the switching frequency harmonics and generates a high quality sinusoidal AC waveform suitable for the load.

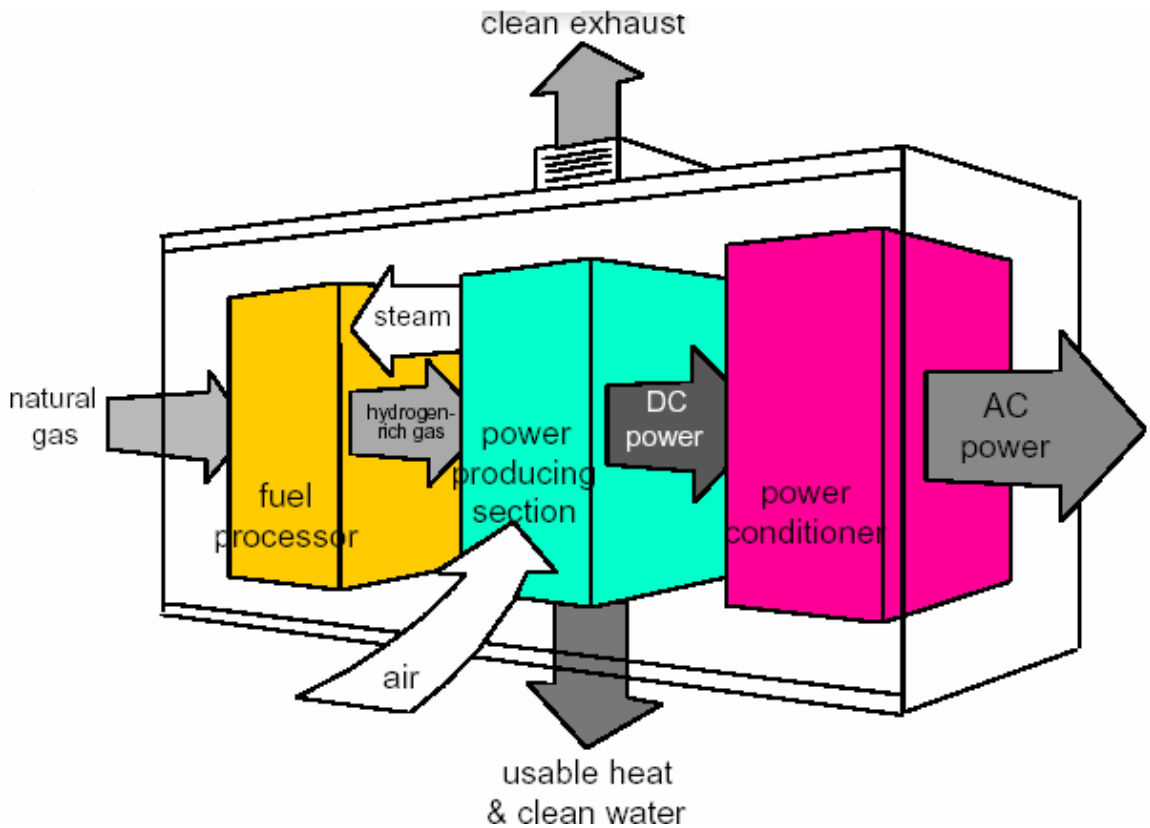

Figure 8-6 Block diagram of a fuel cell power system

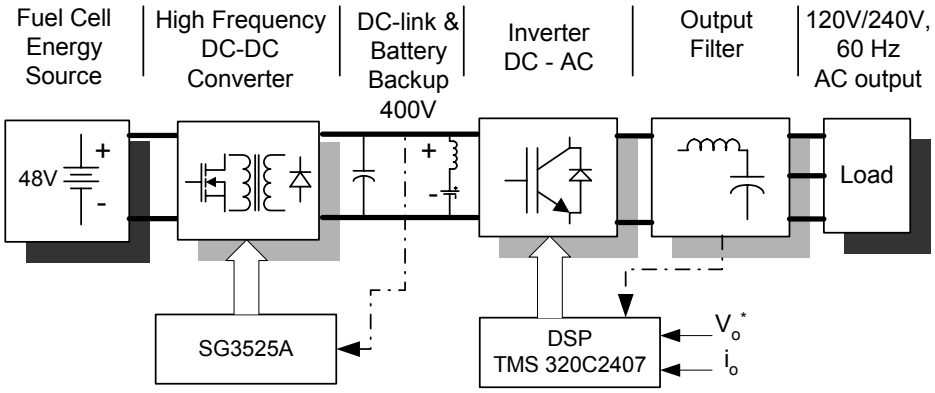

Figure 8-7 Block Diagram of a typical Fuel Cell Power Conditioning Stage

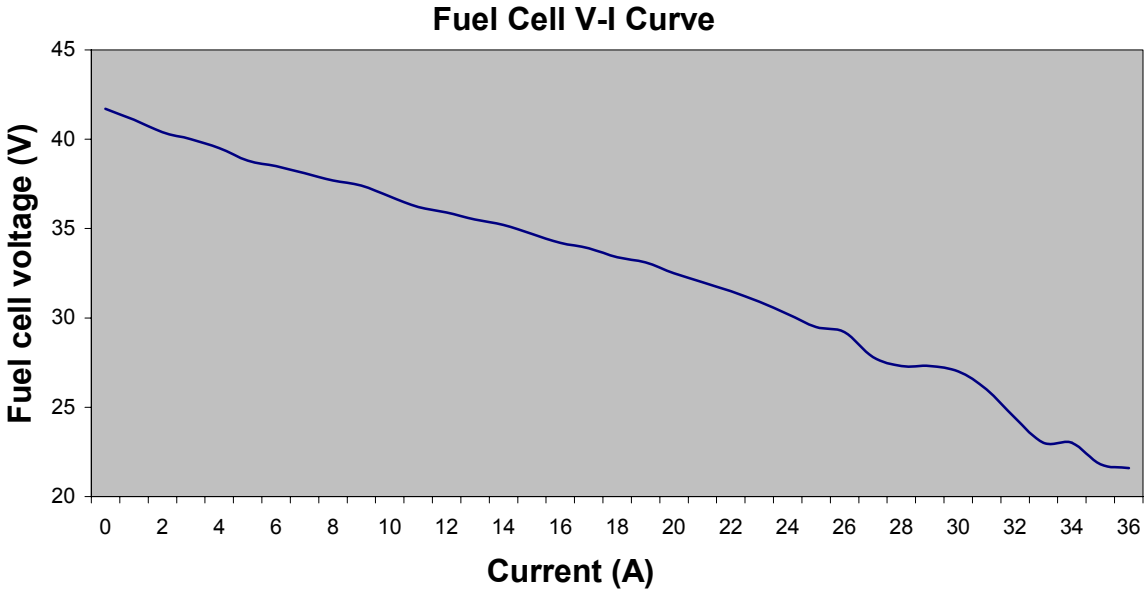

Figure 8-8a Typical fuel cell voltage / current characteristics (46)

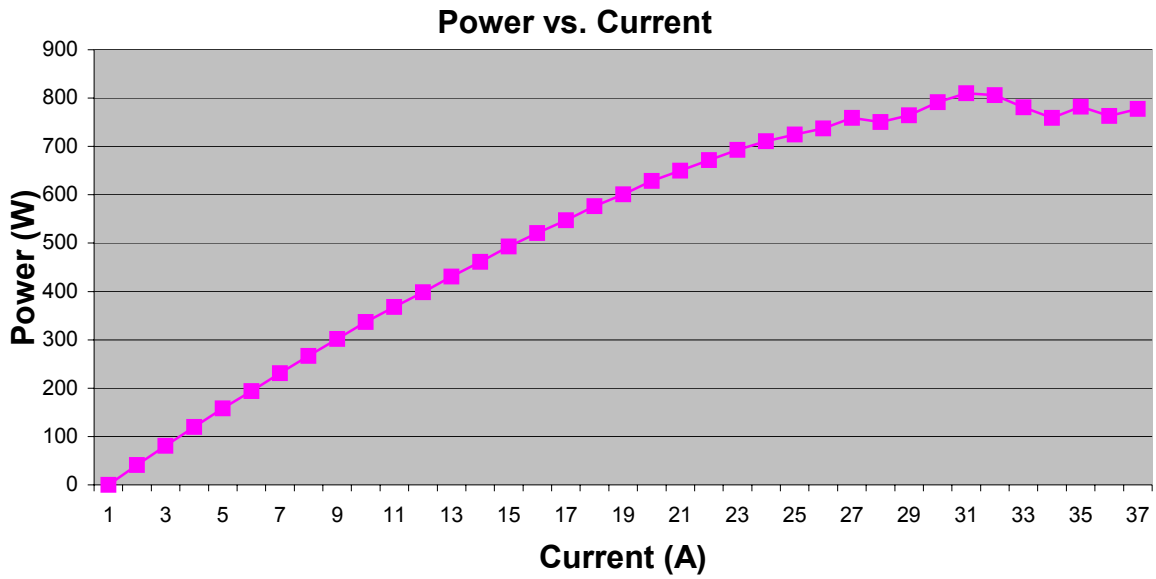

Figure 8-8b Fuel cell, power vs. current curve (46)

Power Semiconductor Devices: Power semiconductor devices are a critical element of "smart" power electronics technology, and are essential circuit components of a DC to DC converter, DC to AC converter, etc. A thorough understanding of the power semiconductor device characteristics is essential for a reliable, cost effective power conversion design. Today's commercial power semiconductor devices are almost exclusively based on silicon material, and can be classified as:

- Diodes
- Thyristors or silicon controlled rectifiers (SCRs)
- Power MOSFET
- Insulated gate bipolar transistor (IGBT)
- Integrated gate-commutated thyristor (IGCT)

Silicon carbide based power semiconductor devices, such as diodes and MOSFETs, are becoming commercially available and are not reviewed in this section. The reader is referred to reference (47, 48) for further information.

Power Diodes: Power diodes provide uncontrolled rectification of power and are used in many power conditioning systems such as DC-DC, DC-AC, and AC-DC conversion. Figure 8-9 shows the diode symbol and its volt-ampere characteristics. In the forward biased condition, the diode can be represented by a junction offset drop and a series-equivalent resistance that gives a positive slope in the V-I characteristics. The typical forward conduction drop is 1.0 V. This drop will cause conduction loss, and the device must be cooled by an appropriate heat sink to limit the junction temperature.

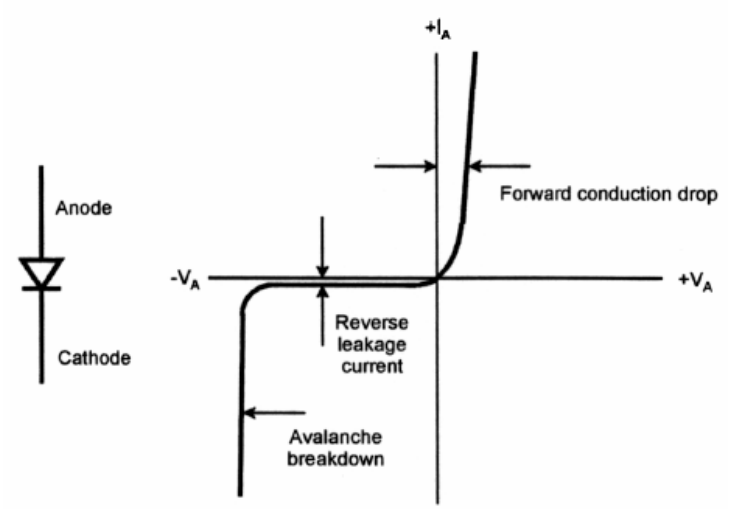

Figure 8-9 Diode symbol and volt-ampere characteristics

Power diodes can be classified as: 1) standard or slow recovery diode; 2) fast recovery diode; or 3) Schottky diode. The standard slow recovery diodes are used in line frequency (50/60Hz) power rectification. A Schottky diode has a lower forward conduction drop (0.5V typical) and faster switching time, but the limitations are lower blocking voltage (200V typical). Their main use in fuel cell power conditioning systems will be in the DC to DC converter rectifier stage, snubber circuits, etc.

Thyristors or Silicon Controlled Rectifiers (SCRs): Thyristors or silicon-controlled rectifiers (SCR) were introduced in 1950s, and the technology of solid state power conversion has became a reality since then. Figure 8-10 shows the thyristor symbol and its volt-ampere characteristics. Basically, it is a three-junction P-N-P-N device, where P-N-P and N-P-N component transistors are connected in a regenerative feedback mode. The device blocks the voltage in both the forward and reverse directions. When the anode is positive, the device can be triggered into conduction by a short positive gate pulse bust once the device is conducting, and the gate loses its control to turn off the device. Modern thyristors are available with very large voltage (several kV) and current (several kA) ratings. In the context of fuel cell power conditioning, they have limited application, such as in the area of high power static bypass switches (solid state AC switch) to interface inverters to the electric utility and/or in uninterrupted power supply (UPS) systems.

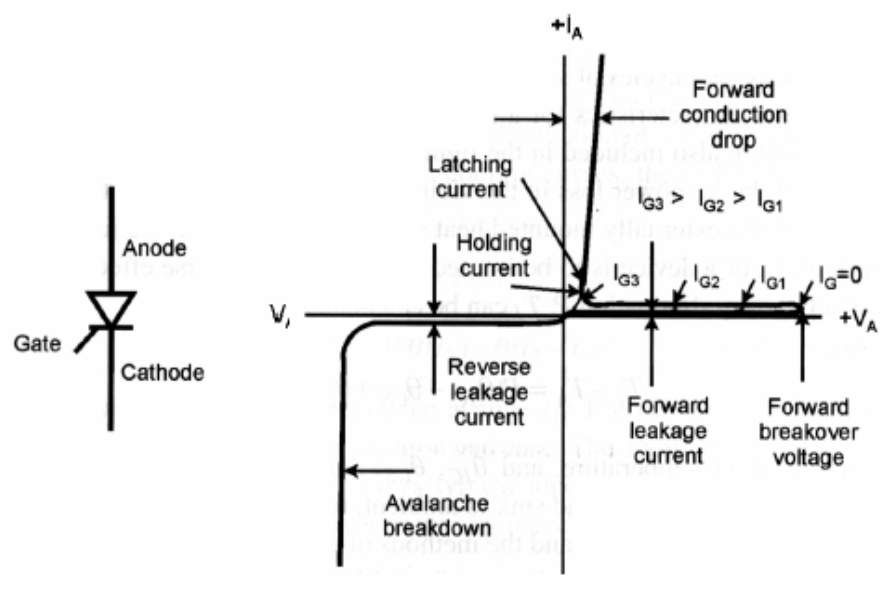

Figure 8-10 Thyristor symbol and volt-ampere characteristics

Power MOSFET: A power MOSFET (metal-oxide semiconductor field- effect transistor) is a unipolar, majority carrier, "zero junction," voltage-controlled device. Figure 8-11a shows the symbol of an N-type MOSFET and Figure 8-11b shows its volt-ampere characteristics. If the gate voltage is positive and beyond a threshold value, an N -type conducting channel will be induced that will permit current flow by majority carrier (electrons) between the drain and the source. Although the gate impedance is extremely high at steady state, the effective gate-source capacitance will demand a pulse current during turn-on and turn-off. The device has asymmetric voltage-blocking capability, and has an integral body diode, as shown, which can carry full current in the reverse direction. The diode is characterized by slow recovery, and is often bypassed by an external fast-recovery diode in high-frequency applications.

The V-I characteristics of the device have two distinct regions, a constant resistance *($R_{DS(on)}$)* region and a constant current region. The $R_{DS(on)}$ of a MOSFET is an important parameter that determines the conduction drop of the device. For a high voltage MOSFET, the longer conduction channel makes this drop large. It is interesting to note that modern trench gate technology tends to lower the conduction resistance (49). The positive temperature coefficient of this resistance makes parallel operation of MOSFET easy. In fact, large MOSFETS are fabricated by parallel connection of many devices.

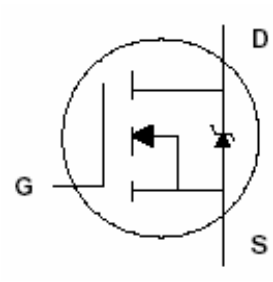

(a)

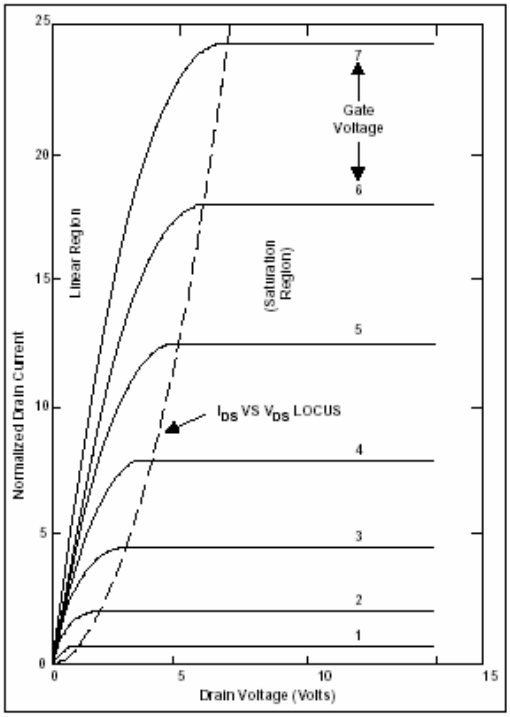

(b)

Figure 8-11(a) Power MOSFET symbol, (b) Normalized volt-ampere characteristics

Insulated Gate Bipolar Transistor (IGBT): The introduction of IGBTs in the mid-1980s was another important milestone in power conditioning. The device has become very popular due to its superior operating characteristics in medium power conversion applications (few kWs to a few MWs). Figure 8-12 shows the IGBT device structure, device symbol and device equivalent circuit, respectively. An IGBT is virtually identical to a power MOSFET. Both devices share a similar polysilicon gate structure and P wells with N+ source contacts. However, in spite of the many similarities, the physical operation of the IGBT is closer to that of a bipolar transistor than to that of a power MOSFET. This is due to the P+ substrate, which is responsible for the minority carrier injection into the N-region and the resulting conductivity modulation. In a power MOSFET, which does not benefit from conductivity modulation, a significant share of the conduction losses occur in the N-region, typically 70% in a 500V device. As shown in the equivalent circuit of Figure 8-12c, the IGBT consists of a PNP driven by an N-Channel MOSFET in a pseudo Darlington configuration. The absence of the integral reverse diode gives the user the flexibility of choosing an external fast recovery diode to match a specific requirement or to purchase a “co-pak,” i.e. an IGBT and a diode in the same package. The lack of an integral diode can be an advantage or a disadvantage, depending on the frequency of operation, cost of diodes, current requirement, etc.

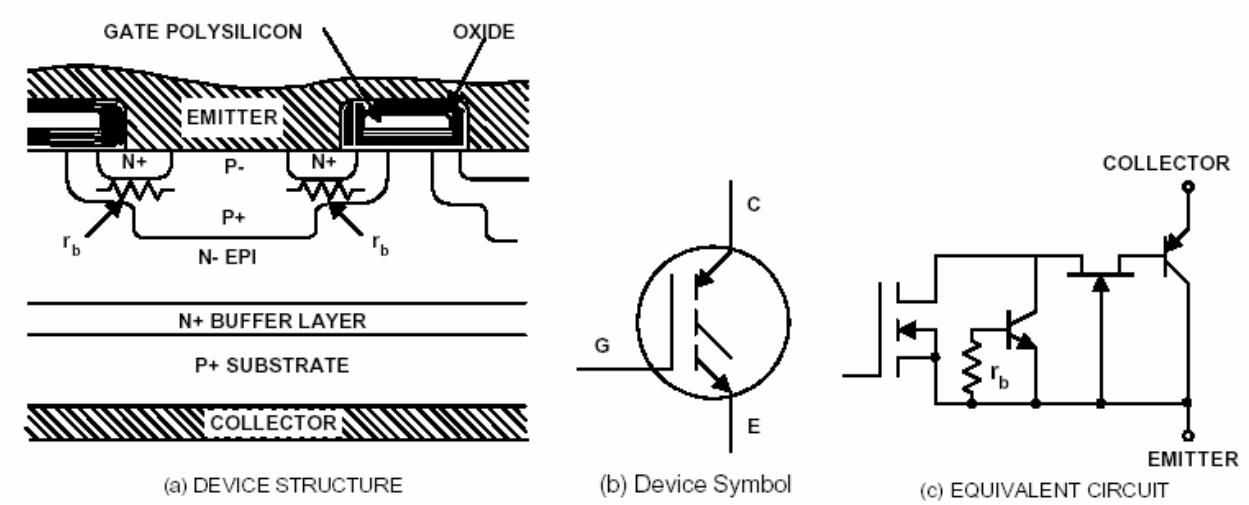

Figure 8-12 Silicon cross-section of an IGBT with its equivalent circuit and symbol

The collector is, actually, the emitter of the PNP. In spite of its similarity to the cross-section of a power MOSFET, operation of the two transistors is fundamentally different, the IGBT being a minority carrier device.

MOSFETs and IGBTs: Similar but Different: IGBT technology is certainly the device of choice for breakdown voltages above 1000V, while the MOSFET is certainly the device of choice for device breakdown voltages below 250V, such as in DC-DC converters. Between 250 to 1000V, there are many technical papers available from manufacturers of these devices, some preferring MOSFETs, some IGBTs. However, choosing between IGBTs and MOSFETs is very application-specific, and cost, size, speed, and thermal requirements should all be considered.

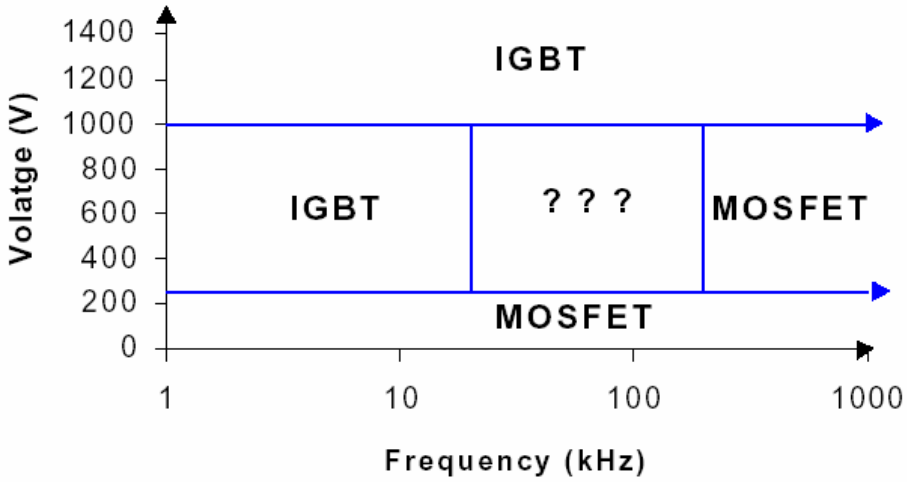

Figure 8-13 Preferred application of IGBTs and MOSFETs

Figure 8-13 shows some of the boundaries where it is fairly clear as to which is preferred, the MOSFET or IGBT (50). IGBTs have been the preferred device under these conditions: low duty cycle; low frequency (<20kHz); narrow or small line or load variations; high-voltage

applications (>1000V); operation at high junction temperature is allowed (>100°C); greater than 5kW output power.

Typical IGBT applications include:

- DC-AC inverters for motor control: Frequency <20kHz, short circuit/in-rush limit protection
- DC-AC inverters in uninterruptible power supply (UPS): Constant load, typically low frequency
- Welding: high average current, low frequency (<50kHz), ZVS circuitry
- Low-power lighting: Low frequency (<100kHz)

MOSFETs are preferred in:

- High frequency applications (>200kHz). Example: DC-DC converters
- Wide line or load variations
- Long duty cycles
- Low-voltage applications (<250V)
- < 500W output power

Typical MOSFET applications include:

- Switch mode power supplies (SMPS): Hard switching above 200kHz
- Switch mode power supplies (SMPS): ZVS below 1000 watts
- Battery charging

Integrated Gate-Commutated Thyristor (IGCT): The integrated gate-commutated thyristor (IGCT) is the newest member of the power semiconductor family, and was introduced in 1997 (51). IGCT is a high-voltage, high-power, hard-driven, asymmetric-blocking gate turn off thyristor (GTO) with unity turnoff current gain. This means that a 4500 V IGCT with a controllable anode current of 3000 A requires turnoff negative gate current of 3000 A. Such a gate current pulse of very short duration and very large *di/dt* has small energy content and can be supplied by multiple MOSFETS in parallel with ultra-low leakage inductance in the drive circuit. The gate drive circuit is built-in on the device module (Figure 8-14). The device is fabricated with a monolithically integrated anti-parallel diode. The conduction drop, turn on *di/dt,* gate driver loss, minority carrier storage time, and turn-off *dv/dt* of the device are shown to be superior. Table 8-5 shows a comparison between a high voltage IGBT and an IGCT. The device has found commercial applications in power distributions systems installations. Some example systems include: Medium voltage static transfer switches and Medium voltage industrial drive systems (52, 53).

Table 8-5 Comparison of high voltage devices

Features of 3.3 kV Types	IGBT	GTO	IGCT
Device on state	100%	70%	50%
Device turnoff loss	100%	≈100%	100%
Device turn on losses	100%	30%	5%
Gate drive power	≈ 1%	100%	50%
Short circuit current	Self limited	External limited (choke)	External limited (choke)
dv/dt snubber	No	Yes	No
di/dt snubber	No	Yes	Yes
Switch chip	Discrete	Monolithic	Monolithic
Diode chip	Discrete	Monolithic	Monolithic
Chip mount	Solder	Pressure	Pressure

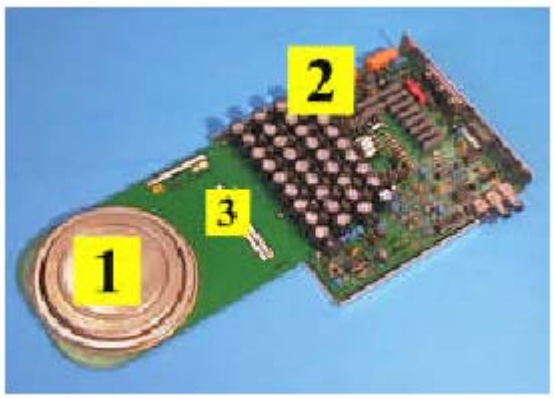

Figure 8-14a A 4.5kV, 3kA IGCT and the gate drive unit.

Figure 8-14b A 30MW Medium voltage power management system and the 9MVA IGCT power electronic building block (51)

Benefits of Silicon Carbide (SiC) Power Conditioning Systems: Recent theoretical studies have shown that once silicon carbide semiconductor technology becomes sufficiently developed,

SiC power devices will greatly outperform silicon power devices. In short, SiC power devices could operate at higher voltages and respond faster with lower parasitic resistance and be physically much smaller than silicon power devices. Faster switching speed not only increases power system conversion efficiency, but it also enables the use of smaller transformers and capacitors to further shrink the overall size and weight of the system. Furthermore, the high temperature capability of SiC greatly reduces cooling requirements that are also a substantial portion of the total size and cost of a power conversion and distribution system. SiC devices are therefore expected to drastically improve the distribution and efficient usage of power conditioning systems in the 21st century (47, 48).

DC to DC Converter: The DC electrical output of a fuel cell varies with the load current (Figure 8-8). This often necessitates a DC to DC converter to regulate the voltage. Since a majority of the present day fuel cell systems are designed for lower voltage (12V to 100V), a DC to DC boost converter is often required to increase the fuel cell voltage to higher voltage levels for further processing into AC via a DC to AC inverter stage. In this section, several DC to DC converter topologies are examined that can be employed in fuel cell systems.

Single Switch Boost Converter (42, 43, 44, 45): Figure 8-15 depicts a simplified schematic of a boost converter. The circuit consists of a control block, a switch (Q1), a diode (D1), inductor (L1) and output capacitor (C1).

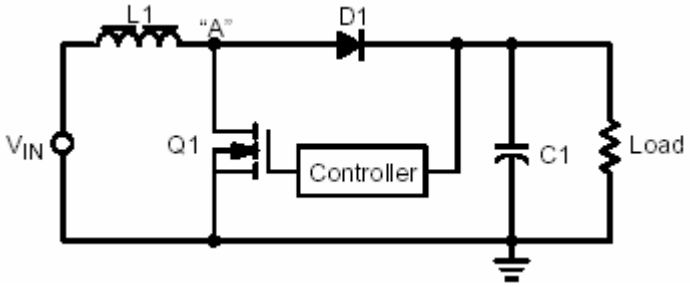

Figure 8-15 Single switch boost converter schematic

During normal operation the switch (Q1) is switched between the "on" and "off" state by the controller to boost the input voltage to a desired output voltage level. In the "on" state of the switch (Q1), energy is stored in inductor (L1), D1 is reversed biased and the load current is supplied by the output capacitor (C1). Conversely, during the "off" state of the switch, stored energy in the inductor is transferred to the load through the diode (D1). The boost converter has two distinct modes of operation, characterized by the current waveform of the inductor. These modes are referred to as continuous–conduction mode (CCM) or discontinuous–conduction mode (DCM). In CCM, the inductor current is greater than zero after each switching cycle, and in DCM the inductor current falls to zero after each switching cycle. Figure 8-16a shows the topological circuit state diagrams for the boost converter operating in CCM, followed by Figure 8-17 which shows typical idealized waveforms of the inductor current, switch current, diode current, and switch off–state voltage (node "A").

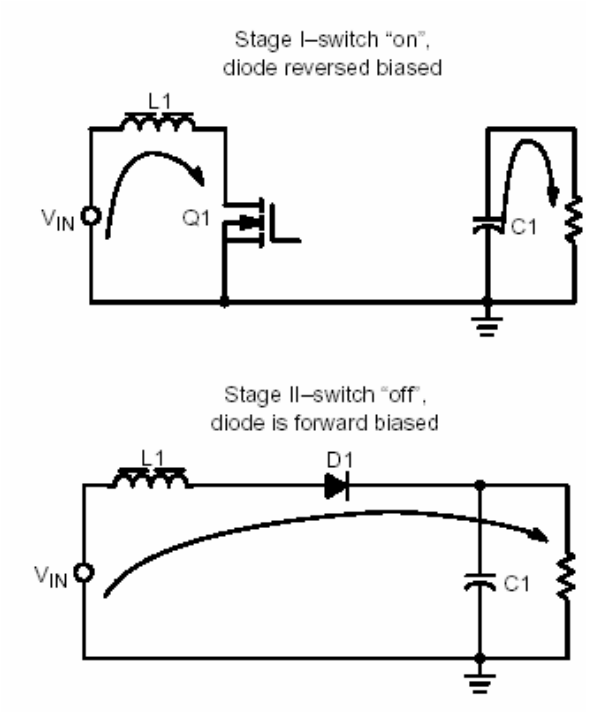

Figure 8-16 Boost converter states

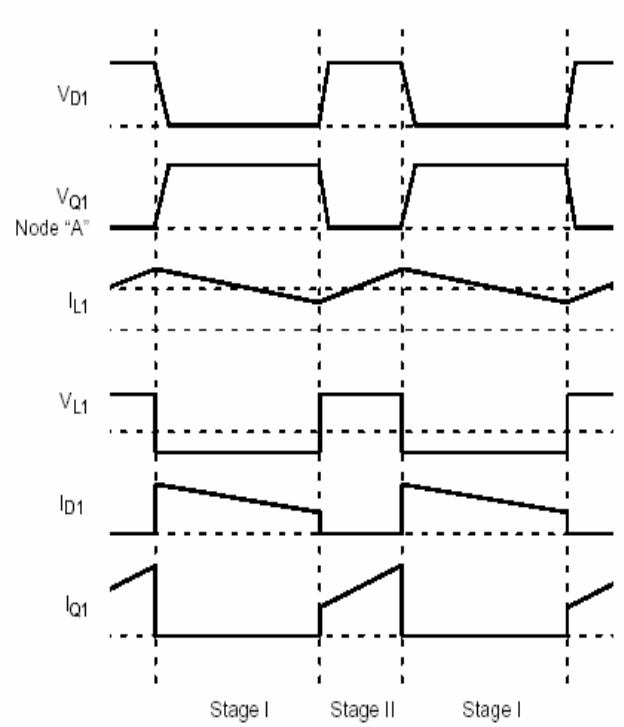

Figure 8-17 Idealized boost converter waveforms

An expression relating the input and output voltage may be derived using fundamental circuit parameters. In CCM, the inductor current increase during the "on" state, neglecting any loss terms, is given by:

$$\Delta I_L(+) = \frac{V_{IN}}{L} * t_{on} \tag{8-17}$$

As previously mentioned, during this circuit state the load current is supplied by the output capacitor. When the switch (Q1) is turned off, the inductor current continues to flow through diode (D1) since the inductor current can not change instantaneously. In order for this to occur, the voltage polarity across the inductor reverses due to a decreasing inductor current. The voltage across the inductor during the switch "off" time is V_O–V_{IN}. The inductor current, which decreases during the "off" time is, given by:

$$\Delta I_L = (\frac{V_O - V_{IN}}{L}) * t_{OFF} \tag{8-18}$$

The ripple current in the inductor during the on state ($\Delta I_{L(+)}$) and off state ($\Delta I_{L(-)}$) are equal in steady state. Equating (8-17) and (8-18) and solving for V_O yields the CCM boost–converter voltage conversion ratio (V_O/V_{IN}):

$$\frac{V_{IN}}{L} * t_{ON} = (\frac{V_O - V_{IN}}{L}) * t_{OFF} \tag{8-19}$$

$$\frac{V_O}{V_{IN}} = (\frac{t_{ON} + t_{OFF}}{t_{OFF}}) \tag{8-20}$$

Since the continuous–conduction mode only has two states, the sum of the "on" and "off" times is the switching period.

$$T_S = t_{ON} + t_{OFF} \quad (8\text{-}21)$$

The switch duty cycle is the ratio of "on" time to the switching period (Ts):

$$\alpha = t_{ON} / T_S \quad (8\text{-}22)$$

An expression for the off–time (t_{OFF}) can be derived from the two expressions above in terms of the duty cycle:

$$t_{OFF} = (1-\alpha) * T_S \quad (8\text{-}23)$$

Substituting this expression for t_{OFF}, t_{ON} and the switching period Ts into the voltage conversion ratio equation yields:

$$\frac{V_o}{V_{IN}} = \frac{1}{1-\alpha} \quad (8\text{-}24)$$

A plot of the non–linear voltage conversion ratio (M = VO/VIN) of a boost converter in CCM is shown in Figure 8-18.

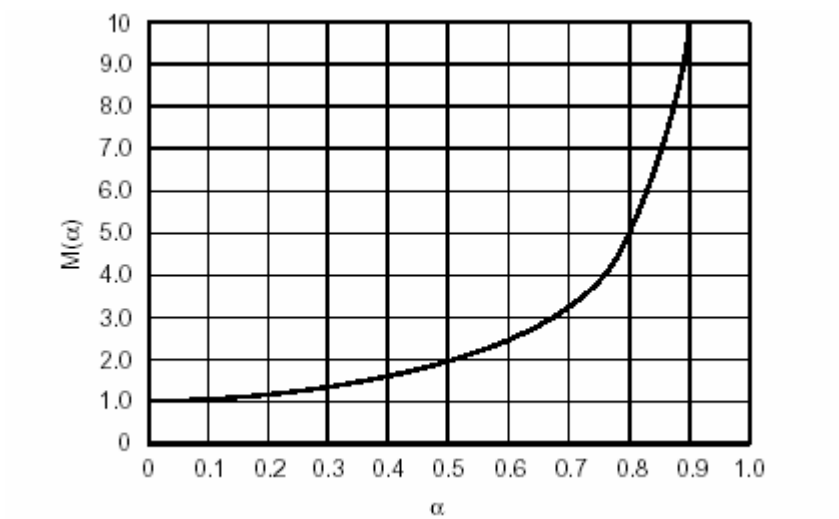

Figure 8-18 Voltage gain as a function of duty cycle.

The voltage conversation ratio graph illustrates that the output voltage is always greater than or equal to the input voltage, since the duty ratio is a quantity bounded between 0 and 1. In practical circuits, typically the duty ratio is constrained to values below 80%, which sets an upper bound on the set–up voltage conversion ratio. The converter will operate in the discontinuous–mode (DCM) at light loads. The boundary condition between CCM and DCM is determined by the input and output voltage, inductance, switch frequency, and load current. An expression for this boundary condition can be found in (8-25) and is given by:

$$\frac{M-1}{2*M^3} = \frac{L_c * f_S}{R_L} \quad (8\text{-}25)$$

Where, $M = \frac{V_o}{V_{IN}}$, L_c is the critical inductance, f_s is the switching frequency, and R_L is the load resistance.

Converter Design: The design of the boost converter can be divided into two parts: one is the selection of the switching frequency and controller IC, and the other is the calculation of the inductor and capacitor values.

PWM Control: Voltage–mode control in switch–mode power supplies is characterized by a single control loop that senses the output voltage, and compares it to a reference voltage. The output of this error amplifier stage is then applied to a PWM comparator that compares the error voltage to a fixed frequency triangle wave. The output of the PWM comparator is a square–waveform that is then applied to a driver stage to control the switching element. Figure 8-19 below illustrates a simplified voltage mode control loop.

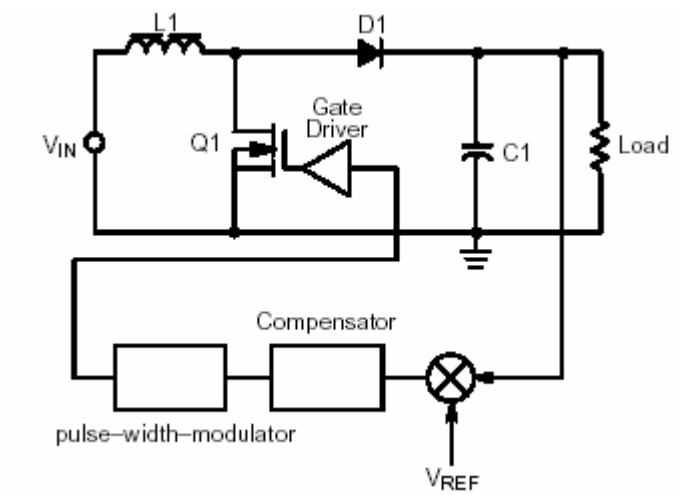

Figure 8-19 Closed loop control

Several variations of this basic control method exist, which include steering logic, blanking delays, pulse by pulse current limiting, etc.

Switching Frequency: The switching frequency can be chosen arbitrarily to minimize the size of the boost inductor and limit the loss of the semiconductor devices. At higher frequencies, the switching losses in the MOSFET increase, and therefore reduce the overall efficiency of the circuit. At lower frequencies, the required output capacitance and boost inductor size increases, and the volumetric efficiency of the supply degrades.

Boost Inductor: Once a switching frequency is chosen, the boost inductor value may be optimally determined to set the converter operating–mode in the required load and line range. The critical inductance is defined as the inductance at the boundary edge between continuous and discontinuous modes and is defined as:

$$L_C = \frac{V_O * T_S}{I_O} * \frac{M-1}{2 * M^3} \qquad (8\text{-}26)$$

Where I_o is the output current, V_O is the output voltage, T_s is the switching period, and M is the voltage conversion ratio (V_O/V_{IN}). To ensure continuous conduction mode for the operating conditions, the inductance has to be chosen at a value greater than the critical inductance.

Component Selection: The main switching element is chosen to handle the worst–case current and voltage stresses. The peak off–state voltage stress on the MOSFET is given as the sum of maximum input voltage and output voltage.

$$V_{DS(max)} = V_{IN(max)} + V_o \tag{8-27}$$

In CCM mode, the current waveform through the switch resembles a ramp on a step (refer to Figure 8-20). The worst–case peak switch current occurs when the input voltage is minimum and with maximum load. An expression for the peak and step current in CCM is given as:

$$I_{pk} = I_o * \left[M + (\frac{1}{2 * \tau_L}) * (\frac{M-1}{M^2}) \right] \tag{8-28}$$

$$I_{STEP} = I_o * \left[M - (\frac{1}{2 * \tau_L}) * (\frac{M-1}{M^2}) \right] \tag{8-29}$$

Where τ_L is given as:

$$\tau_L = \frac{I_o * L}{V_o * T_S} \tag{8-30}$$

Substituting values into these expressions yields the worst–case peak current stress in the MOSFET.

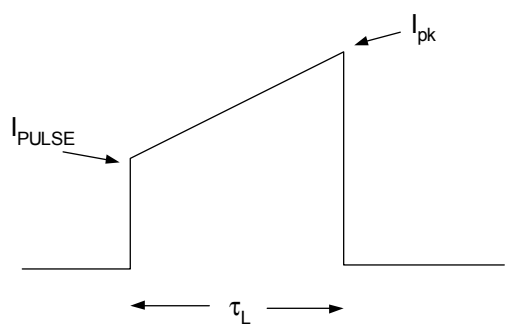

Figure 8-20 Current waveform.

The RMS (root mean squared) of the waveform shown in Figure 8-12 may be expressed in general terms by the following expression:

$$I_{T(rms)} = I_o * \sqrt{M * (M-1) + \frac{1}{3} * (\frac{1}{2 * \tau_L})^2 * (\frac{M-1}{M^2})^3} \tag{8-31}$$

The worst–case conduction loss of this MOSFET is given as:

$$P_{cond} = I_{T(rms)}^{\ 2} * r_{DS_{(ON)}} \tag{8-32}$$

The worst–case conduction loss in the Schottky diode is given as:

$$P_D = I_D * v_f \tag{8-33}$$

The output filter capacitor is chosen to meet the output voltage ripple specifications, as well as its ability to handle the required ripple current stress. Two important criteria in selecting a

capacitor are its capacitance and equivalent–series–resistance (ESR). An approximate expression for the required capacitance as a function of ripple voltage requirement (ΔV_O), peak inductor current (I_{pk}), boost inductance (L), input (V_{IN}) and output voltage (V_O) is given as:

$$Cr \geq \frac{I_{pk}^{2} * L}{2 * \Delta V_O * (V_O - V_{IN})} \tag{8-34}$$

Where ΔV_O is chosen depending on the desired output voltage regulation, and the worst case peak current is calculated from the equation shown above. An expression to compute the required RMS ripple current rating of the output capacitor(s) is given as:

$$I_C = I_O * \sqrt{(M-1) + \frac{1}{3} * (\frac{1}{2 * \tau_L})^2 * (\frac{M-1}{M^2})^2 * (\frac{1}{M})} \tag{8-35}$$

Application of this design in an example fuel cell-powered UPS is detailed in Section 8.2.3 in DC-DC Converter Design.

Push Pull Type DC to DC Converter (42, 43, 44, 45, 54): Figure 8-21a shows the basic topology of a push-pull converter. The push-pull topology utilizes a center-tapped primary winding. The transformer is used as a stepping up function to increase the output voltage. The fuel cell positive terminal is connected to the transformer center-tap, and a power switch is connected to both ends of the winding as shown. The secondary voltage is full-wave-rectified via four diodes, and the output is filtered via a *L-C* filter. The power switches do not simultaneously conduct, but alternate back and forth on alternate cycles. The two sides of the primary are wound in the same sense (or direction), but the current flows in the opposite direction. This results in the flux generated within the core material being driven in both the positive and negative flux polarities. This utilizes the core material in a more efficient manner, which can reduce the required core size. If properly designed, the push-pull topology is capable of generating many hundreds of watts as its output.

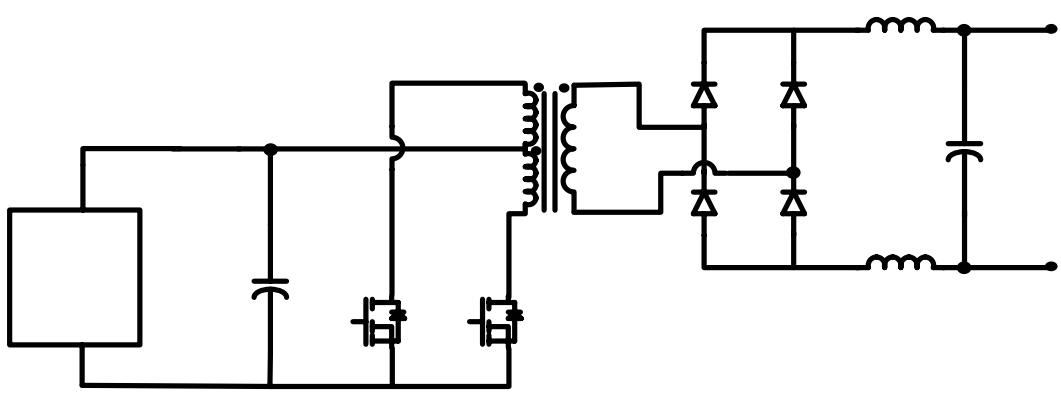

Figure 8-21a Push-pull DC-DC Converter

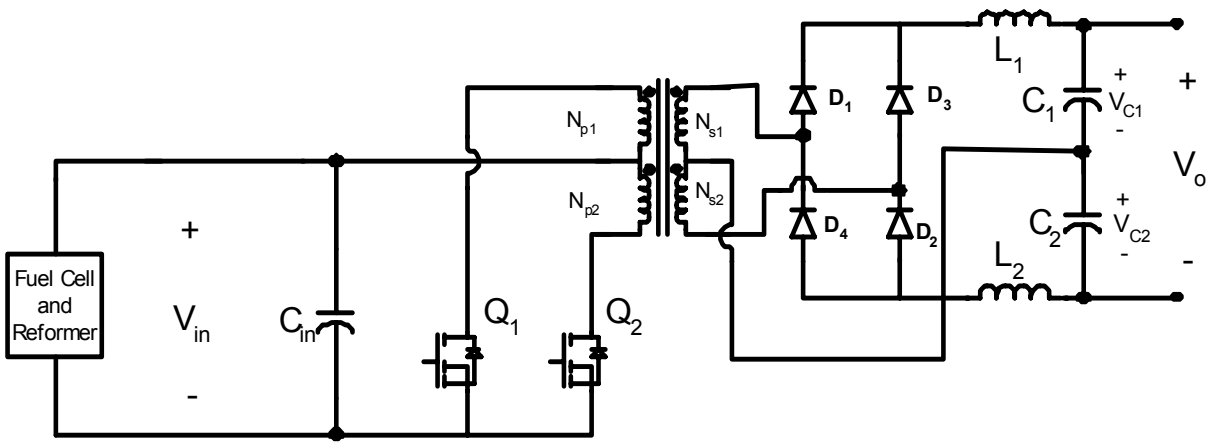

Figure 8-21b Push-pull DC-DC converter with voltage doubling center-tapped DC output

Figure 8-21b shows a voltage doubling output rectifier configuration. In this scheme a center-tapped secondary winding is employed to achieve twice the amount of dc-voltage. Furthermore, the charge on the dc-link capacitors is maintained evenly, and refreshed during each switching instant. It is critical that the power switches on the transformer primary not conduct at the same time, since this causes an effective short- circuited turn within the transformer and may result in their failure due to over-current.

The output DC voltage (V_o) is given by

$$V_o = \left[V_{in} * \frac{N_S}{N_P} \right] * \frac{4T_{on}}{T} \qquad \text{and} \quad 0 < T_{on} < 0.5T \qquad (8\text{-}36)$$

Transformer Flux Imbalance and Corrective Measures: Although the push-pull topology is one of the oldest and can handle several kilowatts, it suffers from transformer flux imbalance due to inherent mismatches in circuit operation. Specifically, the two halves of a center-tapped winding cannot be equal or symmetrically wound, and the power switch on/off times as well as their forward voltage drops are never equal. These irregularities, which exist in practice, can contribute to transformer core saturation and result in the converter failure. In order to overcome this deficiency, several corrective measures can be deployed:

- Gapping the core: an air gap is introduced in the core to avoid saturation. This increases the size of the converter.
- Adding primary resistance: this approach contributes to higher losses
- Using current mode control: This is by far the best solution to the flux imbalance problem. In this approach, the current in each switch is monitored and forced to have equal amplitude.

Flyback Current-Fed Push-Pull Topology (55, 56, 57): In this topology (Figure 8-22a), a flyback converter is in series with a push-pull converter. The output voltage is regulated by width modulating the input switches Q_1 and Q_2 on time. This circuit has many valuable attributes suitable for processing power from a fuel cell. It has less dissipation, cost, volume, and greater reliability. No output inductor is employed. Further, due to high source impedance of the flyback transformer primary, the flux imbalance problem of a voltage-fed push-pull does not exist. This approach is suitable for usage in the 1 to 10kW power levels.

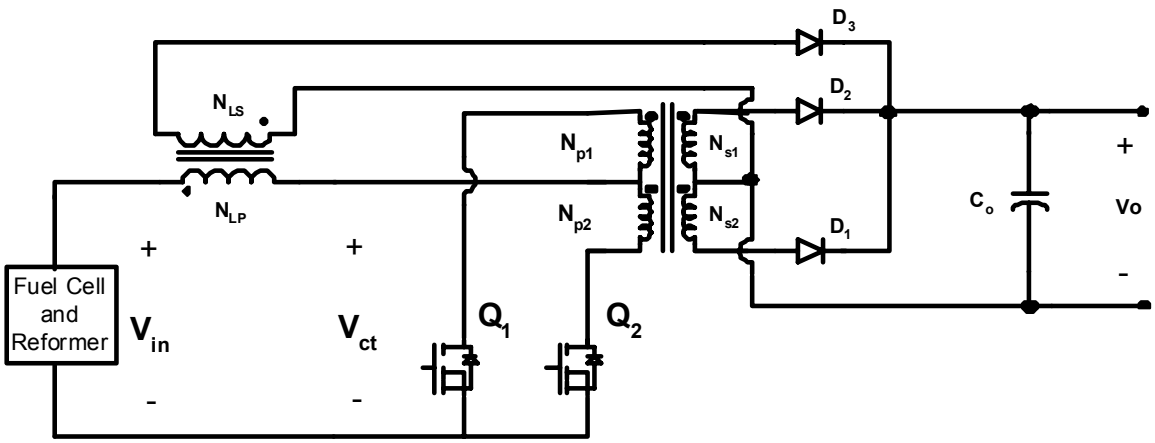

Figure 8-22a Flyback current fed push-pull topology. Clamp diode D_3 is connected to the output (44)

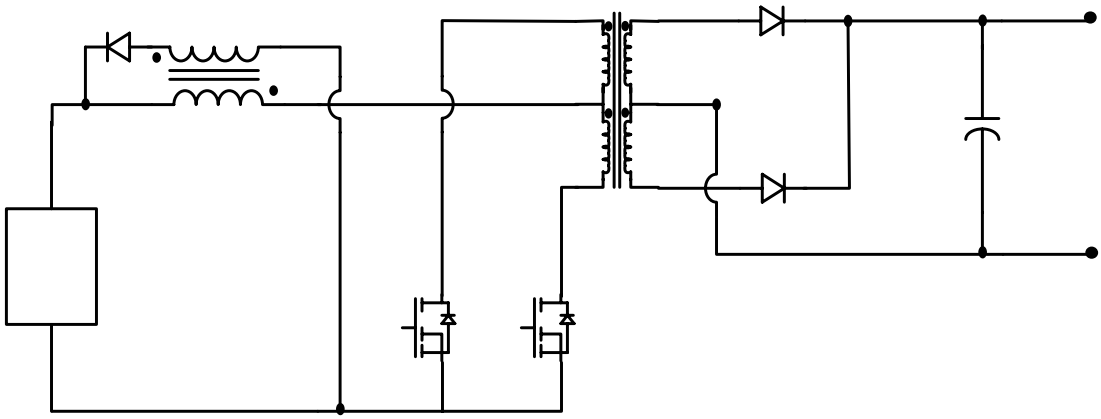

Figure 8-22b Flyback current fed push-pull topology. Clamp diode D_3 is connected to the input

The circuit is capable of operating over a wide input voltage range, particularly suitable for fuel cell systems experiencing 2:1 change in generated voltage. Further, two significantly different modes: non-overlapping (duty cycle <50%) and overlapping mode (duty cycle >50%) of operation are possible. In non-overlapping mode $(\frac{t_{on}}{T} < 0.5)$, it is difficult to accommodate a large ratio of maximum to minimum DC input variation such as from a fuel cell. Since the maximum on time is 0.5T at minimum DC, then at high DC inputs, on time will be small fraction of the period and may approach 1 μs at 100kHz switching frequency. By operating with over-lapping on times $(\frac{t_{on}}{T} > 0.5)$, it is possible to design the system for a larger variation of fuel cell output voltage. For over-lapping mode, the output voltage V_o is given by

$$V_o = \left(\frac{V_{dc}}{2\frac{N_P}{N_S}(1-D)} \right) - V_d \qquad (8\text{-}37)$$

Where V_d is the diode forward voltage drop.

Figure 8-22b shows another variation in this topology when the diode D_3 is returned to input voltage. In this configuration, the input current ripple is minimized, which makes it attractive for fuel cell systems.

Full Bridge DC to DC Converters: Figure 8-23 shows voltage-fed and current-fed full bridge dc to dc converter topologies. The switches Q1, Q2 and Q3, Q4 are turned on and off alternatively to impress a positive and negative voltage at the transformer primary. The maximum on time of each pair is designed not to exceed 80% of half switching period (T/2). This ensures a 0.2T/2 dead time between the turnoff of one switch pair and the turn on of the other. During the dead time, all four switches are off and the two output diodes (D1, D2) conduct current to the inductor L_o. The output voltage is given by

$$V_o = 2 * \frac{N_S}{N_P} * D * V_{in} \quad , D = t_{on} / T_s \ \ and \ \ 0 < D < 0.5 \qquad (8\text{-}38)$$

Similar to the voltage fed push-pull converter (Figure 8-23a) the voltage fed full bridge converter also suffers from several deficiencies such as transient over voltages during turn on and turnoff due to transformer leakage and output rectifier recovery. Further, flux imbalance due to mismatches in MOSFET transistors is also a possibility, especially at higher power (>1000W) and higher output voltages (>200V).

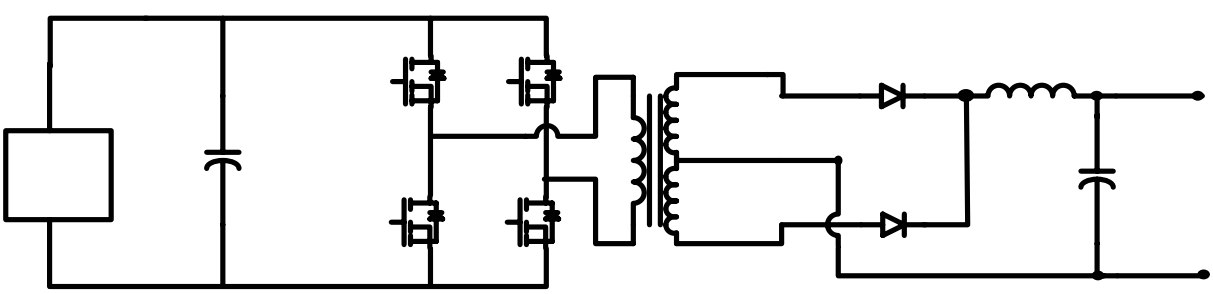

Figure 8-23a Full bridge DC to DC Converter (voltage-fed)

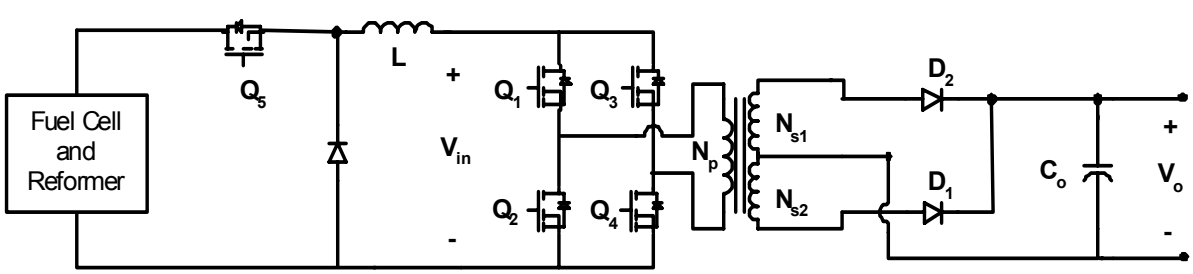

Figure 8-23b A Buck current-fed full bridge DC to DC converter

Figure 8-23b shows a current fed full bridge DC to DC converter with a buck regulator preceding the full bridge. A simple buck regulator (Q5) precedes a full bridge whose output is rectified to a capacitor (C2). In this approach, the full bridge MOSFET transistors are not width modulated. Diagonally opposite transistors (Q1-Q2; Q3-Q4) are operated simultaneously on at alternate half cycles, but deliberately kept on slightly greater than half period such that an overlap occurs. The slight overlap is essential due to the current source nature of the input. The buck MOSFET transistor Q5 suffers from a large spike of power dissipation at the instant of either turn on or turnoff due to continuous conduction of the inductor current. A turn on snubber circuit therefore becomes necessary. A loss less turn-on snubber for this topology can also be configured.

This topology is particularly suitable for widely changing input voltage (2:1), such as fuel cell systems, and high output power at high output voltages. A good design should yield efficiencies greater than 95%.

DC to AC Inverter (42, 43, 54): DC to AC inverter is an essential part in fuel cell power conditioners for generating single phase and three phase AC output. Four varieties of DC to AC inverter outputs are generally required to power most loads:

- Single phase AC output for domestic loads (120V, 60Hz in US and 240V, 50Hz for EU);
- Single phase AC dual output for powering homes (120V/240V 60Hz in US for domestic/industrial loads);
- Three phase fixed voltage, fixed frequency AC output for utility interface and backup power systems (208V, 230V, 480V, 60Hz in US and 400V, 50Hz in EU);
- Three phase variable voltage, variable frequency output suitable for adjustable speed AC motor loads such as in automotive traction applications.

In this section, DC to AC inverter basics are examined in the context of fuel cell power conversion.

Basic Half Bridge DC to AC Inverter: Figure 8-24 shows a single phase inverter input/output four quadrant operating characteristics. During the interval 1-3 (Figure 8-24c) the instantaneous power flow ($p_o = v_o * i_o$) is from DC to AC side (positive) and in 1-4 the instantaneous power flow is from AC to DC side (negative). The switch mode inverter (Figure 8-24a) must be capable of operating in all four quadrants (Figure 8-24d).

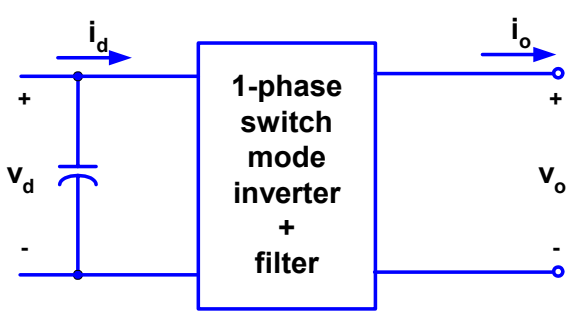

Figure 8-24a Inverter block diagram

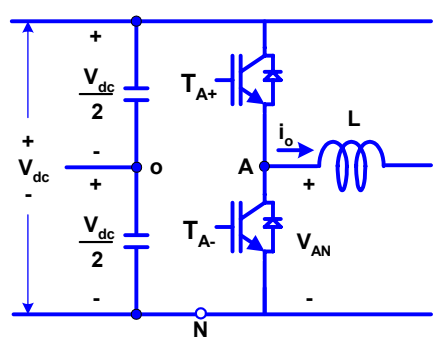

Figure 8-24b Basic half bridge PWM inverter

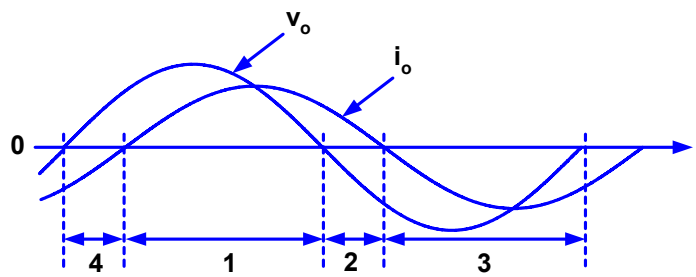

Figure 8-24c Voltage & current

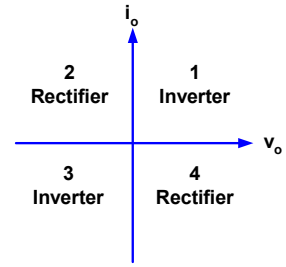

Figure 8-24d

Figure 8-24 Single inverter basic operation

Figure 8-24b shows the basic two switch half bridge DC to AC inverter configuration. The input DC is assumed to be split dc-link ($\pm V_d/2$). The AC output terminals are "a" and "o," and the load is usually inductive. All DC to AC inverters are derived from this basic half bridge inverter configuration. Understanding the operation of this inverter is therefore important. The inverter switches (IGBTs) are turned on and off at a fixed switching frequency, and on-off times are pulse width modulated (PWM) for shaping the output voltage (V_{AO}).

Pulse width modulated (PWM) scheme: The inverter is required to produce a sinusoidal AC output voltage at a desired frequency. In order to accomplish this, a sinusoidal control signal of the desired frequency is compared with a triangular carrier frequency as shown in Figure 8-25. The frequency of the triangular waveform (carrier) establishes the inverter switching frequency and is generally kept constant along with its amplitude (V_{tri}). From Figure 8-25 the following quantities can be defined,

$$m_a = \frac{V_{control}}{V_{tri}} \quad ; \quad m_f = \frac{f_s}{f_1} \qquad (8\text{-}39)$$

Where m_a is the modulating signal, defined as the ratio of the magnitude of the sinusoidal modulation signal to the magnitude of the triangular carrier signal, and m_f is the frequency modulation ratio, defined as the ratio of the frequency of the triangular carrier to the frequency of the sinusoidal modulating signal.

In the half bridge inverter (Figure 8-24b) the switches T_{A+} and T_{A-} are controlled based on the comparison of sinusoidal modulating signal and the triangular carrier. The following conditions apply

$v_{control} > v_{tri}$, T_{A+} is on, and the inverter output voltage $v_{Ao} = ½\ V_d$

$v_{control} < v_{tri}$, T_A - is on, and the inverter output voltage $v_{Ao} = -\ ½\ V_d$

Since the two switches are never off simultaneously, the output voltage v_{Ao} fluctuates between $½\ V_d$ and $-½ V_d$ as shown in Figure 8-25. The output voltage v_{Ao} is a switched waveform whose width is sinusoidally modulated (PWM) and therefore contains harmonic components including the fundamental. Figure 8-25 shows the harmonics (magnitude and frequency) present in the AC output voltage $v_{Ao.}$

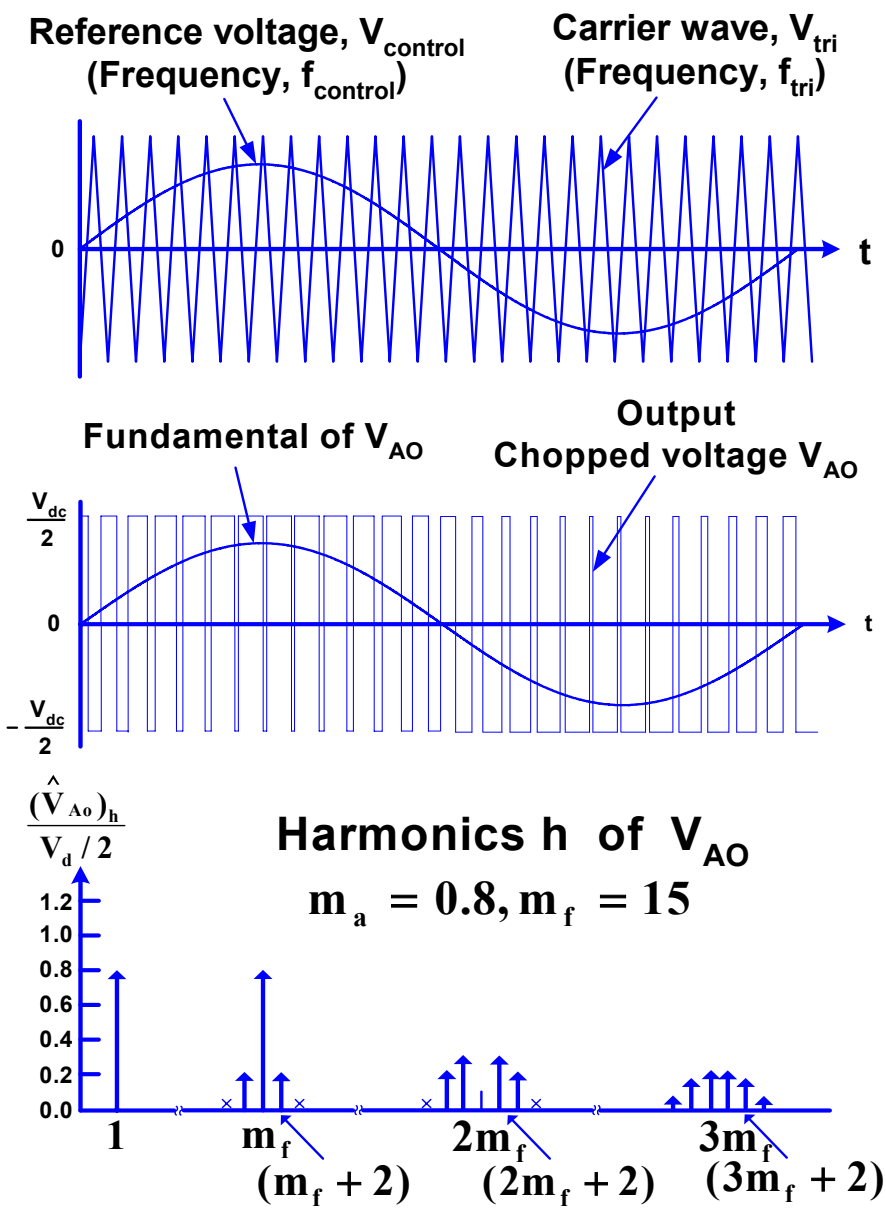

Figure 8-25 Pulse width modulation (PWM)

Table 8-6 Harmonics of v_{Ao} assuming m_f is large

m_a	0.2	0.4	0.6	0.8	1.0
m_f $m_f \pm 2$ $m_f \pm 4$	1.242 0.016	1.15 0.061	1.006 0.131	0.818 0.220	0.601 0.318 0.018
$2m_f \pm 1$ $2m_f \pm 2$ $2m_f \pm 4$	0.190	0.326 0.024	0.370 0.071	0.314 0.139 0.013	0.181 0.212 0.033
$3m_f$ $3m_f \pm 2$ $3m_f \pm 4$ $3m_f \pm 6$	0.335 0.044	0.123 0.139 0.012	0.083 0.203 0.047	0.171 0.176 0.104 0.016	0.113 0.062 0.157 0.044

Example:

In the half bridge inverter shown in Figure 8-24b, if $V_d = 400V$, $m_a = 0.8$, $m_f = 333$ (switching frequency $f_s \approx$20kHz), from Table 8-6 the following expression can be written for the output voltage v_{Ao},

$$v_{Ao} = 0.8 * \frac{V_d}{2} sin(wt) + 0.818 * \frac{V_d}{2} sin(m_f wt) + 0.22 * \frac{V_d}{2} sin((m_f \pm 2)wt) + ... \quad (8\text{-}40)$$

Where $w = 2\pi f$ and f is the fundamental frequency (60Hz). Substituting $V_d = 400V$ in Equation (8-40),

$$v_{Ao} = 160 * sin(wt) + 163.6 * sin(333 * wt) + 44 * sin((333 \pm 2)wt) + ... \quad (8\text{-}41)$$

It is clear from Equation (8-41) that the inverter output voltage v_{Ao} consists of 160V (peak) sinusoidal voltage at fundamental frequency (60Hz) and 163.6V of 20kHz harmonic voltage, etc. An output filter is usually employed to filter the higher frequency harmonics in the inverter output. From Table 8-6 and Equation (8-40) it is clear that the fundamental component in the inverter output V_{Ao} is given by

$$V_{Ao,1} = m_a * \frac{V_d}{2} sin(wt) \quad (8\text{-}42)$$

For an output voltage 120V (rms), $V_{Ao,1}$ =120*√2 = 170V , substituting this value in (8-42) yields

$m_a = 0.85$

Full Bridge DC to AC Inverter (54): Figure 8-26a shows the topology of a full bridge DC to AC inverter, which consists of four switches. For the control of the inverter switches, two reference sinusoidal signals 180^0 out of phase from each other are used to intersect the same triangular carrier signal (see Figure 8-26b and Figure 8-26c). The following switching sequence is followed:

- The switch T_{A+} is on when $V_{control} > V_{tri}$
- The switch T_{B-} is on when $-V_{control} < V_{tri}$ (8-43)
- The switch T_{B+} is on when $-V_{control} > V_{tri}$
- The switch T_{A-} is on when $V_{control} < V_{tri}$

The resultant PWM AC output voltage of the inverter (Figure 8-26a) is shown in Figure 8-26d

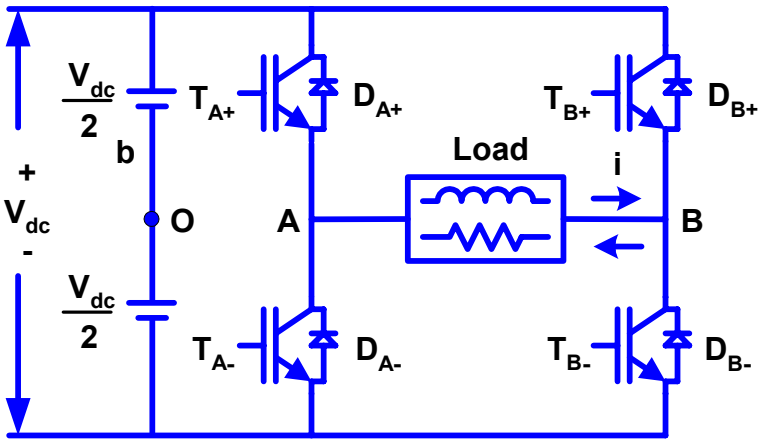

Figure 8-26a Single Phase full bridge DC to AC Inverter

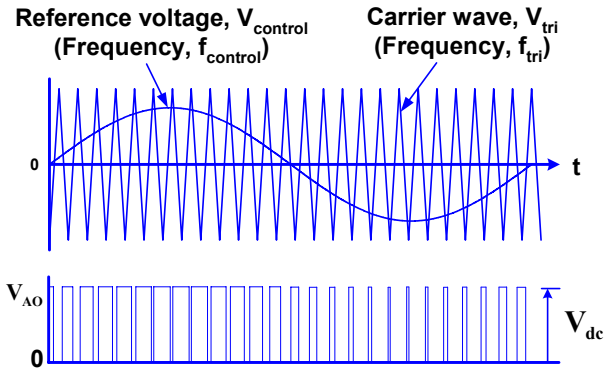

Figure 8-26b

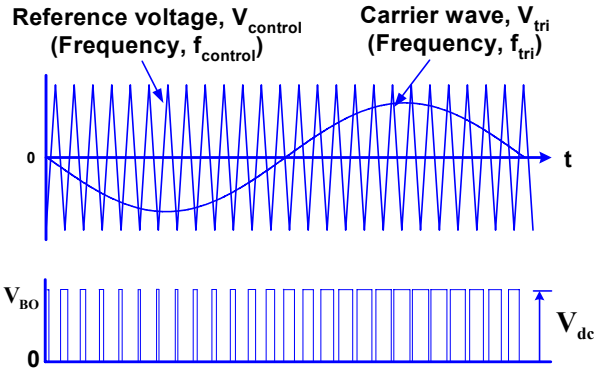

Figure 8-26c

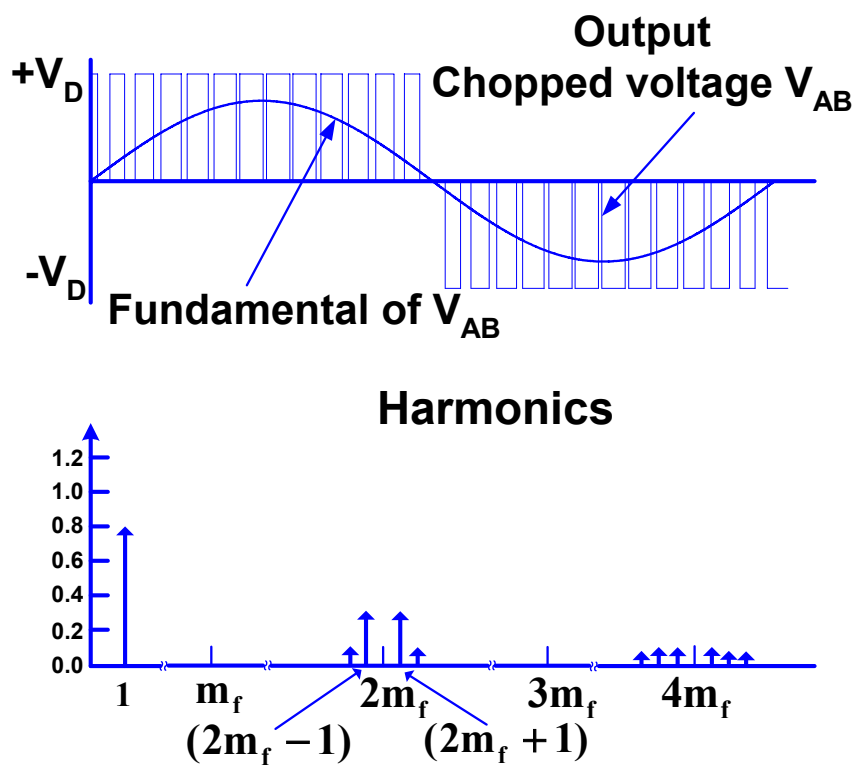

Figure 8-26d Full bridge inverter output voltage V_{AB} and its frequency spectrum.

Following the switching sequence given in (8-43), the output voltage of the full bridge inverter can be expressed as,

$$V_{AB} = V_{Ao} - V_{Bo} \qquad (8\text{-}44)$$

Example:

In the full bridge inverter shown in Figure 8-26a, if $V_d = 400V$, $m_a = 0.8$, $m_f = 333$ (switching frequency $f_s \approx 20$kHz), from Table 8-6 and (8-41)

$$v_{Ao} = 0.8 * \frac{V_d}{2} sin(wt) + 0.818 * \frac{V_d}{2} sin(m_f wt) + 0.22 * \frac{V_d}{2} sin((m_f \pm 2)wt) + ... \qquad (8\text{-}45)$$

Since v_{Bo} modulating signal is 180° phase shifted with respect to v_{Ao} (see Figure 8-26b and Figure 8-26c) and assuming m_f is even,

$$v_{Bo} = -0.8 * \frac{V_d}{2} sin(wt) + 0.818 * \frac{V_d}{2} sin(m_f wt) + 0.22 * \frac{V_d}{2} sin((m_f \pm 2)wt) + ... \qquad (8\text{-}46)$$

Substituting (8-45) and (8-46) in (8-44) yields

$$v_{AB} = 0.8 * V_d \, sin(wt) + ... \qquad (8\text{-}47)$$

The magnitude of the fundamental voltage component at the output V_{AB} is given by

$$V_{AB,1} = m_a * V_d \, sin(wt) \qquad (8\text{-}48)$$

In order to generate an output voltage 120V (rms.), $V_{AB,1}$ =120*√2 = 170V , substituting this value in (8-48) yields

$m_a = 0.85$ for a dc-link voltage $V_d = 200V$

Therefore, a full bridge inverter (Figure 8-26) requires half the voltage (i.e. 200V) of a half bridge inverter (Figure 8-24b, 400V) to generate a required AC output voltage (120V, rms). It is interesting to note that the harmonics at m_f and $m_f \pm 2$ frequencies are cancelled. Figure 8-26d shows the full bridge inverter output voltage v_{AB} and its corresponding frequency spectrum. It is clear from this figure that the voltage v_{AB} has harmonics around $2m_f$, $4m_f$, etc. Substituting $V_d = 200V$ in (8-47) yields, $V_{AB,1} = 160V$. Therefore, a full bridge inverter requires half the dc-link voltage of a half bridge inverter for a given AC output.

Dual Output Voltage DC to AC Inverter (39)]: In residential / commercial fuel cell applications, often times it is required to produce dual output voltages (120V/240V) with respect to a common neutral. In this section, two single phase inverter topologies are discussed that meet these requirements.

Four Switch Dual Output Voltage Inverter: Figure 8-27 shows a four switch inverter topology with a split dc-link configuration. The capacitor midpoint "o" is a common point between the two outputs (V_{Ao} , V_{Bo}). This terminal also becomes the neutral terminal output of the inverter.

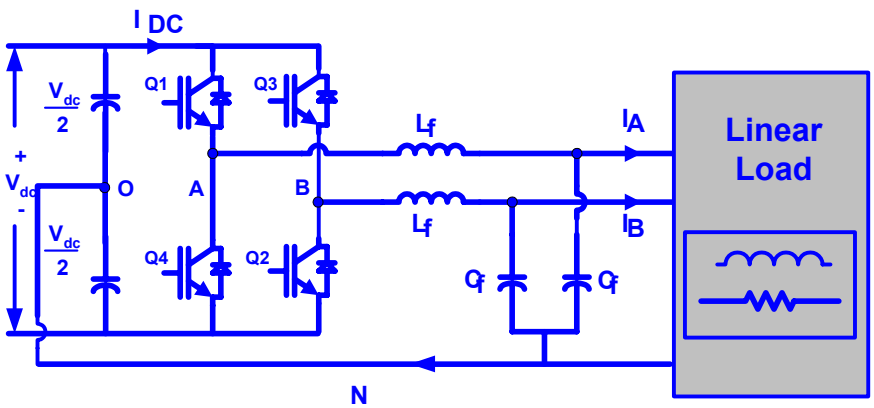

Figure 8-27 Dual output voltage inverter with four switches

This topology consists of two half bridge inverters, which can be controlled independently of each other. Switches Q1, Q4 are controlled in PWM fashion to generate an output voltage V_{Ao} (120V, 60Hz) and Q3, Q2 generate the second phase V_{Bo} (120V, 60Hz) that is 180° out of phase with V_{Ao}. The full bridge inverter modulation strategy discussed in the previous section can be employed. In terms of number of switches used, this approach is a minimum switch topology and could result in lower cost. Some disadvantages of this approach include larger size of dc-link capacitors and output L-C filter. A detailed design of a single phase fuel cell inverter based on this configuration is detailed in Section 8.2.3.

Basic Equations: Since the required output voltage of each phase is 120V (rms), (8-40) to (8-42) have shown that a dc-link voltage of 400V with ± 200V is essential. For $m_a = 0.85$, substituting these values in (8-42) yields

$$V_{Ao,1} = 170 \sin(wt) = 120\sqrt{2} \sin(wt) \quad (8\text{-}49)$$

From (8-46),

$$V_{Bo,1} = -170 \sin(wt) = -120\sqrt{2} \sin(wt) \quad (8\text{-}50)$$

From (8-48), (8-49) and (8-50),

$V_{AB} = 240\sqrt{2}\ sin(wt)$ (8-51)

Therefore, the inverter topology in Figure 8-27 is capable of producing dual output voltage suitable for residential systems. The required dc-link voltage is 400V DC. Since typical fuel cell systems do not output DC voltage in this range, suitable DC-DC converters discussed in Section 8.2.2 become necessary.

Operating Waveforms (39): Figure 8-28a and Figure 8-28b show the operating waveforms of the dual output voltage inverter for linear and nonlinear loads.

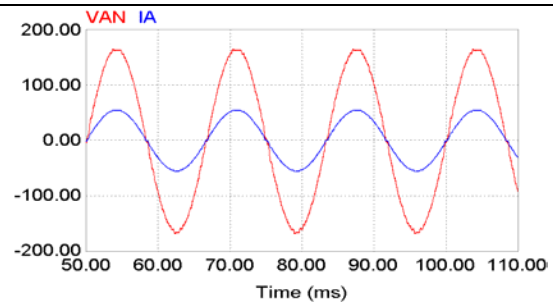

Figure 8-28a Dual voltage inverter output voltage & current on phase V_{An} for linear load (5kW)

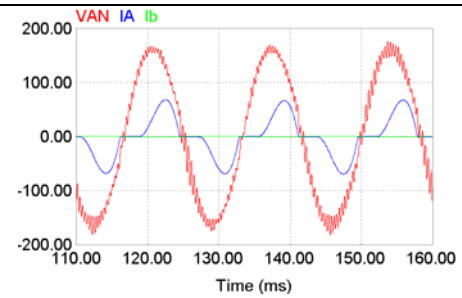

Figure 8-28b Dual voltage inverter output voltage & current on phase V_{An} for nonlinear load (5kW)

Six Switch Dual Output Voltage Inverter: Figure 8-29a shows the topology of a six switch dual output voltage inverter. Three half bridge inverters are combined together. Switches Q3, Q6 are controlled in PWM fashion to generate an output voltage V_{Ao} (120V, 60Hz) and Q5, Q2 generate the second phase V_{Bo} (120V, 60Hz) that is 180° out of phase with V_{Ao} similar to the 4-switch topology (Figure 8-27). The switches Q1, Q4 are modulated to generate zero fundamental voltage, i.e., to form a neutral terminal "n" (i.e. $V_{no,1} = 0$, $m_a = 0$, average voltage zero). Since the capacitor mid-point terminal "o" is not available (or does not exist, due to the non-use of spit dc-link), the output voltage V_{An} and V_{Bn} are 120V each with 180° phase shift between them. The voltage V_{AB} is therefore rated for 240V. The full bridge inverter modulation strategy discussed in the previous section can be employed. Figure 8-29b and Figure 8-29c show the operating waveforms for this topology. Table 8-7 shows a comparison between Figure 8-27 and Figure 8-29a dual output voltage inverters.

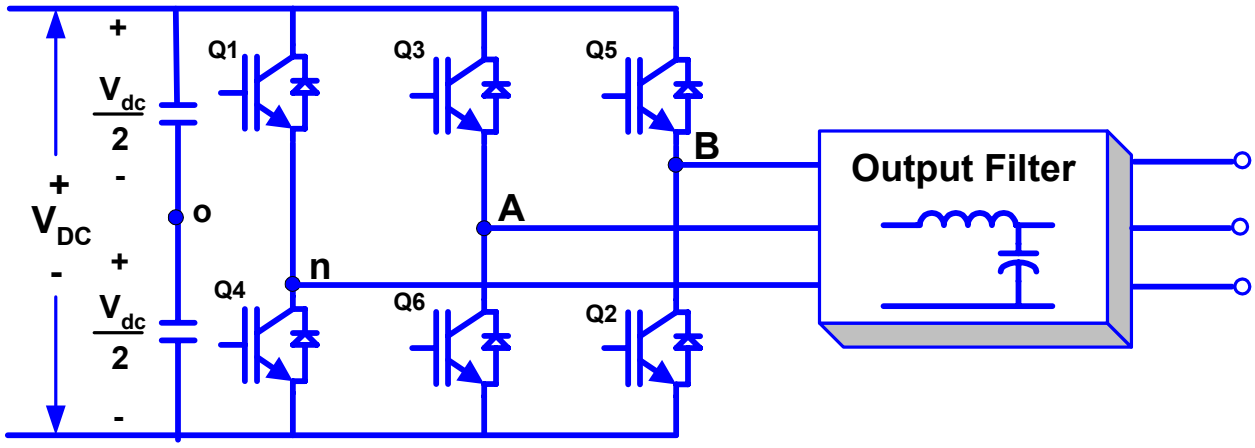

Figure 8-29a Six switch dual output voltage inverter topology

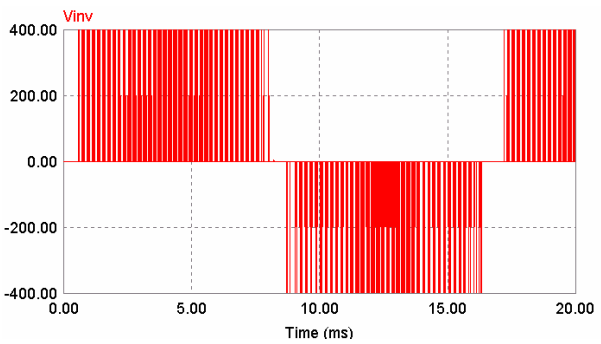

Figure 8-29b Output voltage V_{an}

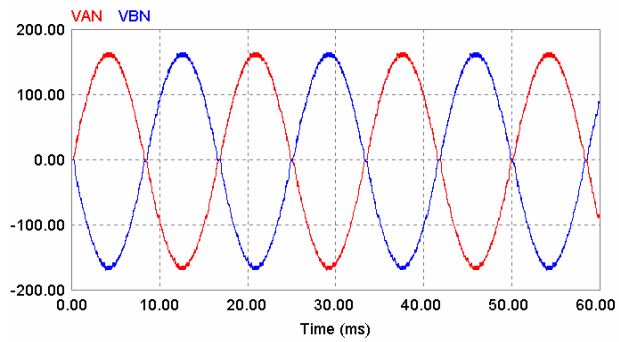

Figure 8-29c Filtered output voltage V_{an} and V_{bn}

Table 8-7 Comparison between Figure 8-27 and Figure 8-29a dual output voltage inverters for 120V/240V single phase output with a common neutral

Items	Fig. 8-27 Dual output voltage inverter	Fig. 8-29a Dual output voltage inverter
Number of switches (IGBTs)	4	6
Dc-link voltage	400V	400V
Switch voltage/current ratings	Same	Same
Number of dc-link capacitors	Two (split dc-link), each rated for 200V	One, rated for 400V
Dc-link capacitor voltage unbalance	Yes (a real possibility, requires active charge maintenance across each dc-link capacitor in order to maintain balance)	No (no such requirement)
Dc-link capacitor ripple current	High (lowest frequency component is 60Hz currents, since the midpoint supports one of the output phase terminals)	Low (lowest frequency component is 120Hz, even under unbalanced output loading)
Output filter size	Relatively larger (required to filter PWM switching frequency harmonics at m_f)	Relatively smaller (required to filter only twice the inverter switching frequency ($2m_f$) harmonics)
Inverter size	Relatively larger	Relatively smaller
Cost	Low	High

From Table 8-7, it is clear that both 4 switch and 6 switch configurations meet the required output criteria. The six-switch topology (Figure 8-29a) exhibits many superior performance attributes. However, this approach necessitates two additional switches, which contribute to higher cost.

Three phase Inverters: Three phase inverters are essential for generating three phase AC power from a given DC source. Figure 8-29a shows the basic topology of a six switch three phase inverter. Switches Q1 to Q6 are suitably pulse width modulated to generate balanced three phase output voltages: V_{AB}, V_{BC}, V_{CA}, respectively. Figure 8-30 illustrates a PWM strategy for control. This consists of comparing three sinusoidal modulating signals with appropriate 120° phase shift with a triangular carrier signal, and switches Q1 to Q6 are controlled in PWM fashion.

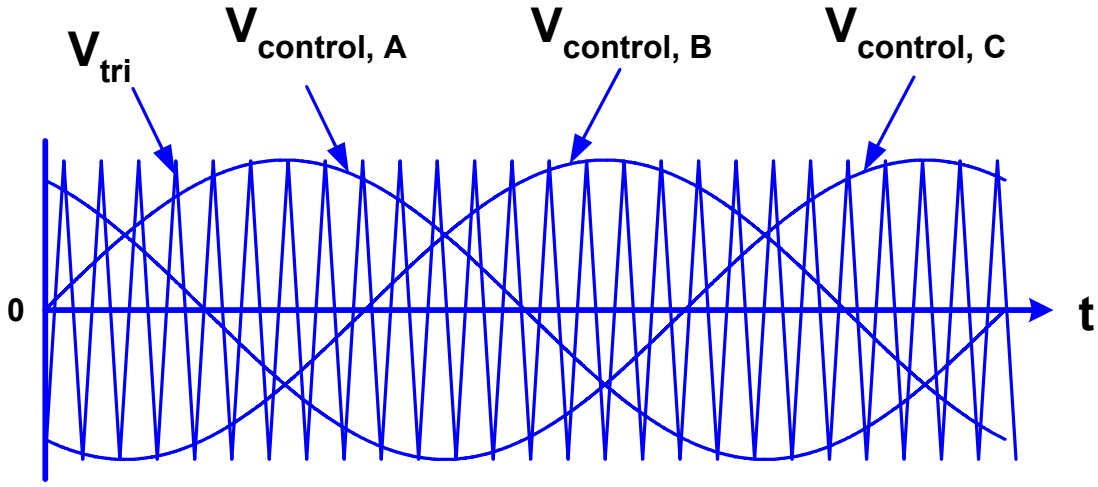

Figure 8-30 Three phase PWM signal generation

Following the basic equations presented for the operation of a half bridge inverter (8-39) to (8-42), the following equations can be written for a 3-phase inverter controlled via three phase PWM control (Figure 8-30). The fundamental component in V_{Ao} and V_{Bo} voltages are (see equation 8-42)

$$V_{Ao,1} = m_a * \frac{V_d}{2} sin(wt) \tag{8-52}$$

$$V_{Ao,1} = m_a * \frac{V_d}{2} sin(wt - 120^0) \tag{8-53}$$

Since the line to line output voltage $V_{AB} = V_{Ao} - V_{Bo}$,

$$V_{AB,1} = \sqrt{3} * m_a * \frac{V_d}{2} sin(wt + 30^0) \tag{8-54}$$

Similarly the fundamental component in V_{BC} phase can be shown to be

$$V_{BC,1} = \sqrt{3} * m_a * \frac{V_d}{2} sin(wt - 90^0) \tag{8-55}$$

Example Calculation: In order for the inverter to generate three phase 480V AC (rms) line to line voltage (i.e. $V_{AB,1} = \sqrt{2}*480$) the required dc-link voltage V_d can be computed from (8-54) as

$$V_d = * \frac{2 * |V_{AB,1}|}{\sqrt{3} * m_a} \tag{8-56}$$

Substituting $V_{AB,1}$ = 480V and m_a = 1.0 , V_d = 784V DC

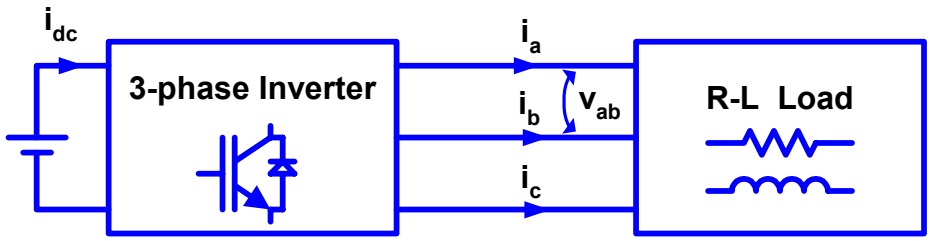

Figure 8-31a Three phase inverter supplying a three phase R-L load.

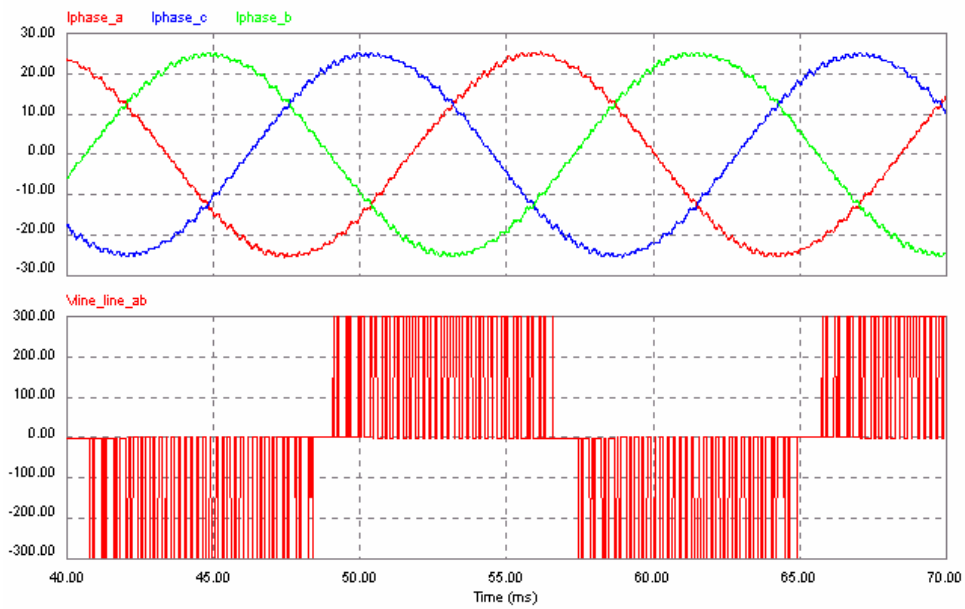

Figure 8-31b Three phase inverter waveforms (first screen: line currents, second screen: PWM line to line voltage V_{AB})

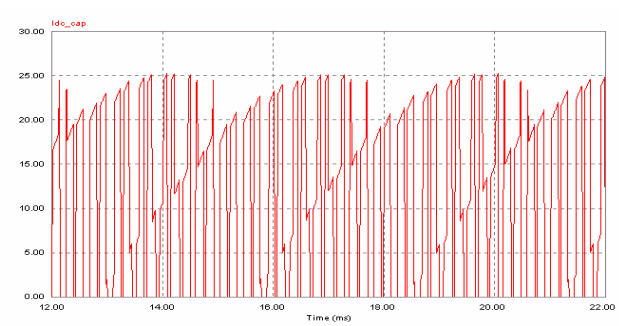

Figure 8-31c Dc-link current I_{dc}

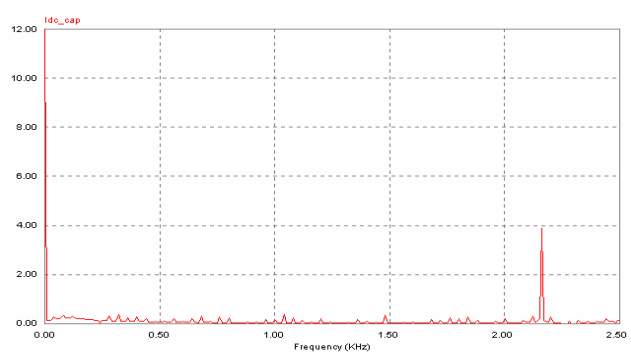

Figure 8-31d Frequency spectrum of I_{dc}

Figure 8-31 shows the operating waveforms of a three-phase PWM inverter.

Three Phase Four-Wire Inverters (54): In some industrial applications and UPS systems, its is required to generate a three phase 4-wire output, which essentially means that a neutral terminal must be available. Since the topology shown in Figure 8-31 generates three phase 3-wire output, alternative schemes must be explored for this purpose. Figure 8-32a shows a simple modification to the three phase six switch topology to generate a 4-wire output. A center-tapped dc-link is added to form the neutral connection. Figure 8-32b shows another possible approach, in which two additional IGBTs are added to form a neutral connection. This approach is similar to the one described in Section 8.2.3 for dual voltage inverters.

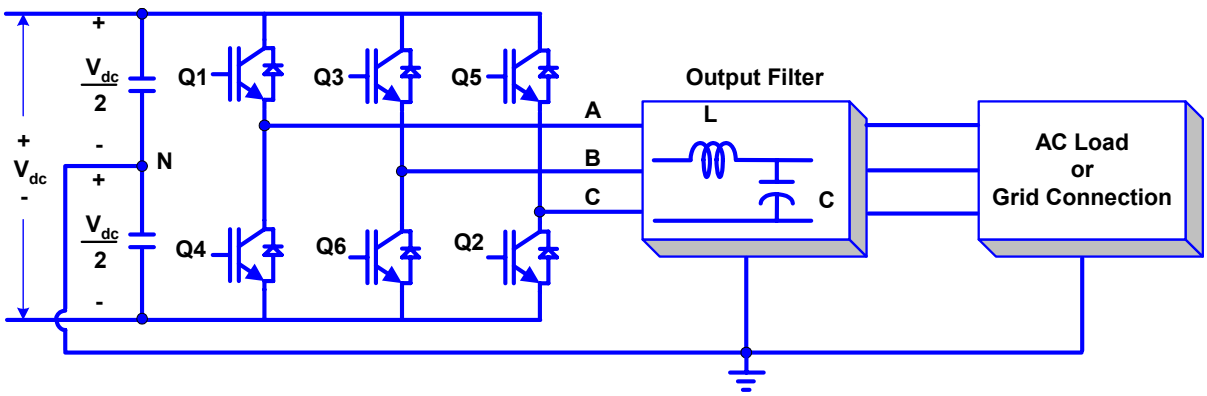

Figure 8-32a Three phase 4-wire DC to AC Inverter topology with a center-tapped dc-link

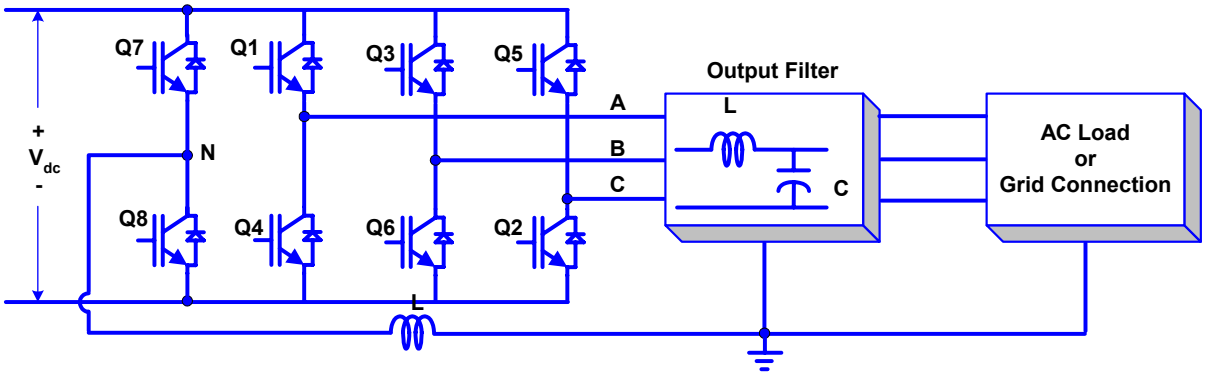

Figure 8-32b Three phase 4-wire DC to AC Inverter topology with 8-IGBT devices

Multilevel Three Phase Inverters (52, 53, 54): So far the discussion on DC to AC inverters has centered on two level inverters based on a half bridge cell (Figure 8-24b). For higher power (megawatt range) fuel cell hybrid systems, the fundamental AC output voltage from an inverter must be increased to medium voltage levels (2300V, 4160V, 6600V, 11,000V in US) in order to keep the current levels low. In order to accomplish this, the corresponding dc-link voltage (V_{DC}) must be increased and the power semiconductor devices must be connected in series. This necessitates the use of matched pair of devices and complicated dynamic voltage sharing schemes. Multilevel inverter topologies have the advantage of generating higher voltage AC output with simultaneous voltage sharing of series connected devices with clamped diodes.

Figure 8-33a shows the topology of a neutral point clamped (NPC) inverter circuit. Commercial NPC type inverters with IGBT / IGCT devices are currently available from a number of vendors (ABB, Siemens, etc.) for powering medium voltage adjustable speed AC motor drive systems (52, 53). In the NPC inverter (Figure 8-33a) the dc-link capacitor has been split to create a neutral point "o". A pair of devices with bypass diodes are connected in series with an additional diode connected between the neutral point and the center of the pair, as shown. The devices Q11 and Q14 function as main devices and Q12 and Q13 function as auxiliary devices which help to clamp the output potential to the neutral point with the help of clamping diodes D1 and D2. Freewheeling diodes cross each IGCT device, as they are an integral part of the device. A clamping circuit is installed in the dc-link with capacitors C_{c1}, C_{c2} and inductors L_{c1} , L_{c2} to limit the reverse recovery current of the freewheeling diodes, and plays an important role in the commutation of IGCT (51). Two additional IGCT devices VS1 and VS2 are installed in the dc-link path to provide rapid disconnect of fault current in the event of a short circuit. The NPC inverter output A,B,C is filtered via an L-C output filter and clean medium voltage sinusoidal voltage is generated suitable for utility interface. An output isolation transformer is normally employed to protect the fuel cell systems against utility induced faults. Figure 8-33b shows the voltage V_{Ao} of the NPC inverter and Figure 8-33c shows the line to line voltage V_{AB} after the L-C filter. Notice the high quality nature of the generated output sinusoidal voltage.

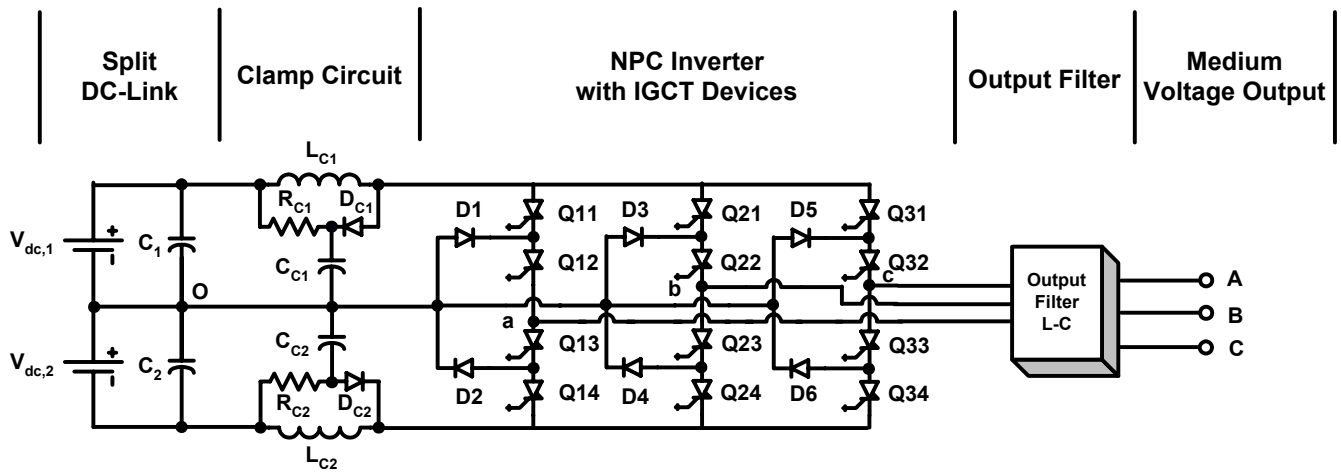

Figure 8-33a Circuit topology of neutral point clamped (NPC) inverter topology

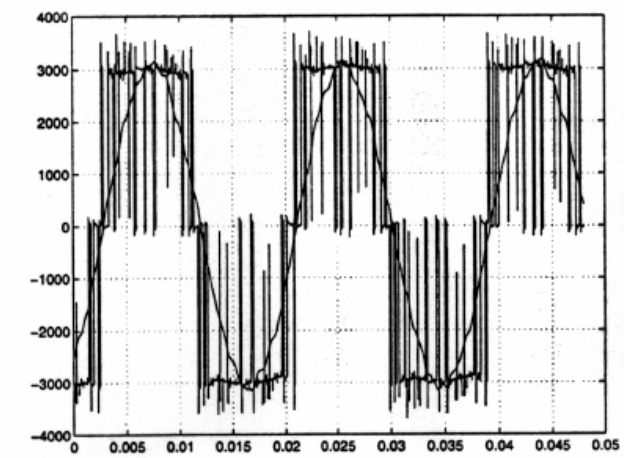

Figure 8-33b Phase "a" to dc-link midpoint "o" voltage

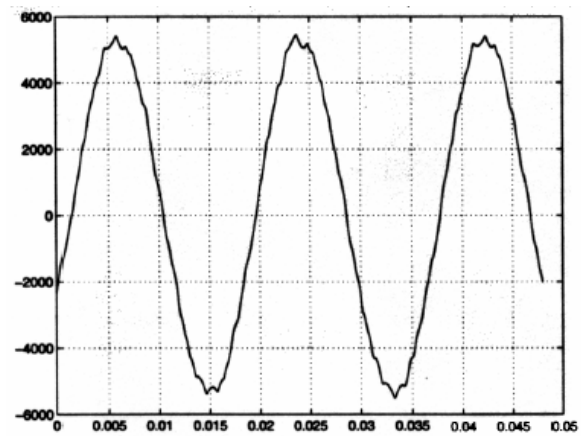

Figure 8-33c NPC Inverter line to line output voltage (V_{AB}) after the L-C filter

8.2.2 Fuel Cell Power Conversion for Supplying a Dedicated / Stand-Alone Load (58, 39, 40)

In this section, a fuel cell power conversion scheme for a 10kW stand-alone load is discussed. Figure 8-8 shows the variation of fuel cell output voltage vs. load. It is noted that fuel cell output DC voltage exhibits nearly 2:1 voltage range (Figure 8-8a). The power conversion unit must be capable of operating in this range and, in particular, be able to deliver rated power while regulating output voltage. Output from the power conversion unit is expected to be high quality power with less than 5% total harmonic distortion (THD). For domestic loads, a 5:1 or better peak to average power capability for tripping breakers and starting motors is also desired. This puts an additional constraint in the design of the power conditioning unit for stand-alone loads. Table 8-8 shows a typical specification for a stand-alone fuel cell powered power conditioning unit.

Table 8-8 Specifications of a typical fuel cell power-conditioning unit for stand-alone domestic (US) loads

Continuous output power:	10 kW continuous
Output Phase (s):	Split single-phase, each output rated for 0 to 5000 VA, not to exceed 10000 VA total
Output voltage:	120V, 240V Sinusoidal AC. Output voltage tolerance no wider than ±6% over the full allowed line voltage and temperature ranges, from no-load to full-load. Frequency 60±0.1 Hz.
Output frequency:	60Hz (US) or 50Hz (Europe) with enough precision to run AC clock accuracy
Fuel Cell Current Ripple: (Fuel cell dependent)	▪ ***120 Hz ripple: < 15% from 10% to 100% load*** ▪ 60 Hz ripple: < 10% from 10% to 100% load ▪ 10 kHz and above: < 60% from 10% to 100% load
Output THD:	< 5%
Protection:	Over current, over voltage, short circuit, over temperature, and under voltage. No damage caused by output short circuit. The inverter must shut down if the input voltage dips below the minimum input of 42 V. Inverter should not self-reset after a load-side fault. IEEE Std. 929 is a useful reference.
Acoustic Noise:	No louder than conventional domestic refrigerator. Less than 50 dBA sound level measured 1.5 m from the unit.
Environment:	Suitable for indoor installation in domestic applications, 10°C to 40°C possible ambient range.
Electromagnetic Interference	Per FCC 18 Class A -- industrial
Efficiency:	Greater than 90% for 5kW resistive load
Safety:	The system is intended for safe, routine use in a home or small business by non-technical customers.
Life:	The system should function for at least ten years with routine maintenance when subjected to normal use in a 20°C to 30°C ambient environment.

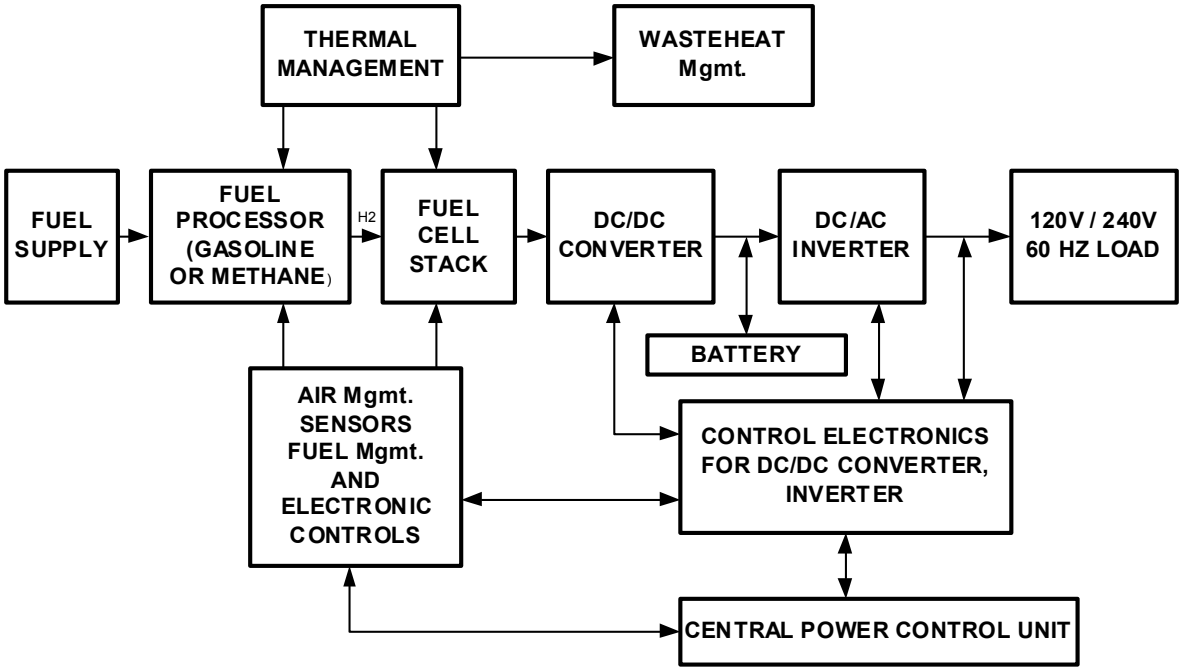

Figure 8-34a Block diagram of a typical fuel cell powered unit for supplying a load (120V/240V)

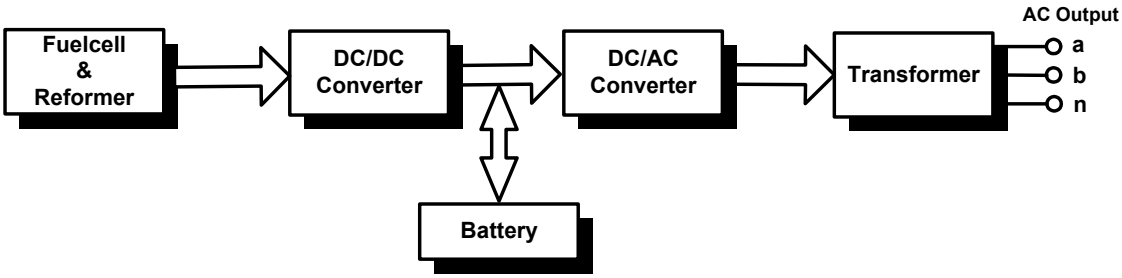

Figure 8-34b Block diagram of the power conditioning stage with line frequency transformer

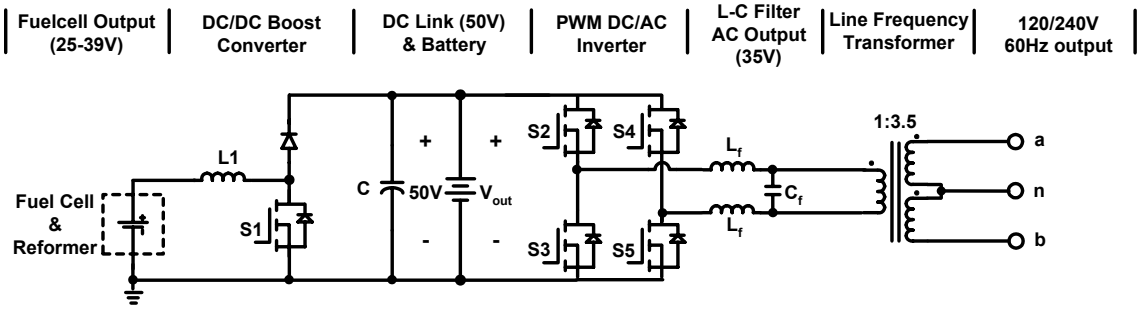

Figure 8-34c Circuit topology of the power conditioning stage with line frequency transformer

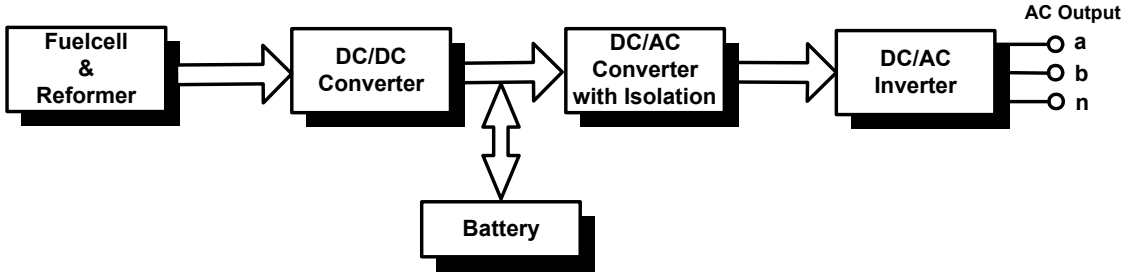

Figure 8-35a Block diagram of the power conditioning stage with high frequency isolation transformer within the DC-DC converter stage

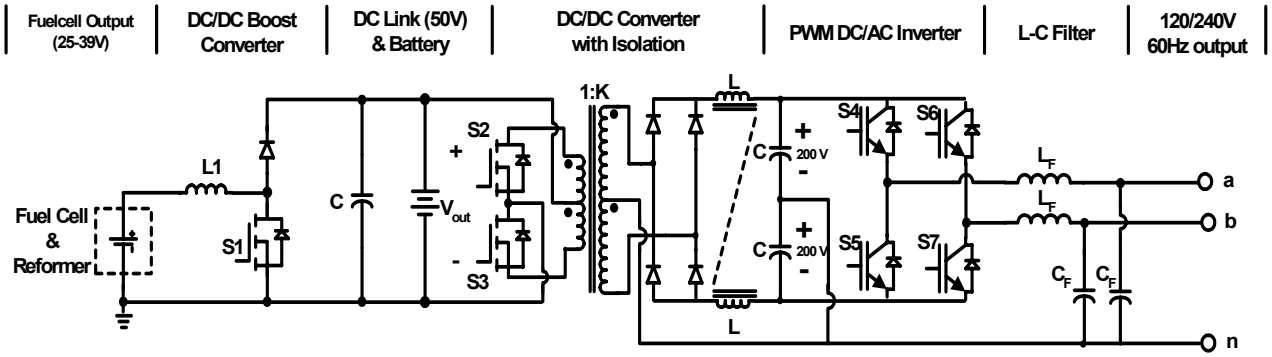

Figure 8-35b Circuit topology of the power conditioning stage with high frequency isolation transformer within the DC-DC converter stage

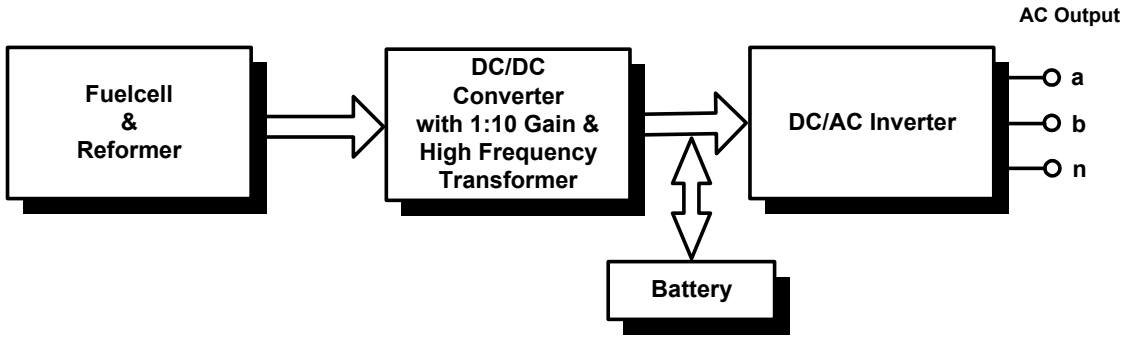

Figure 8-36a Block diagram of the power conditioning scheme with fewer power conversion stages in series path of the power flow

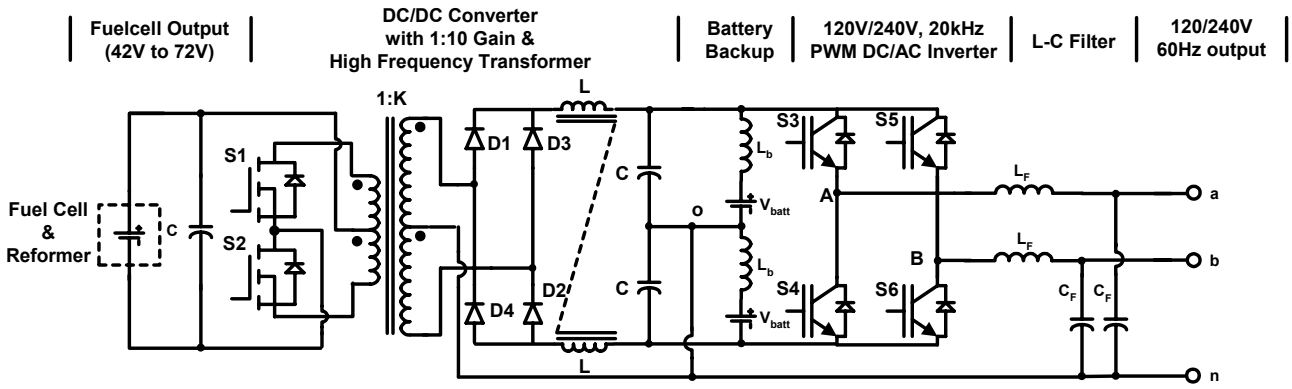

Figure 8-36b Circuit topology of the power conditioning scheme with fewer power conversion stages in series path of the power flow

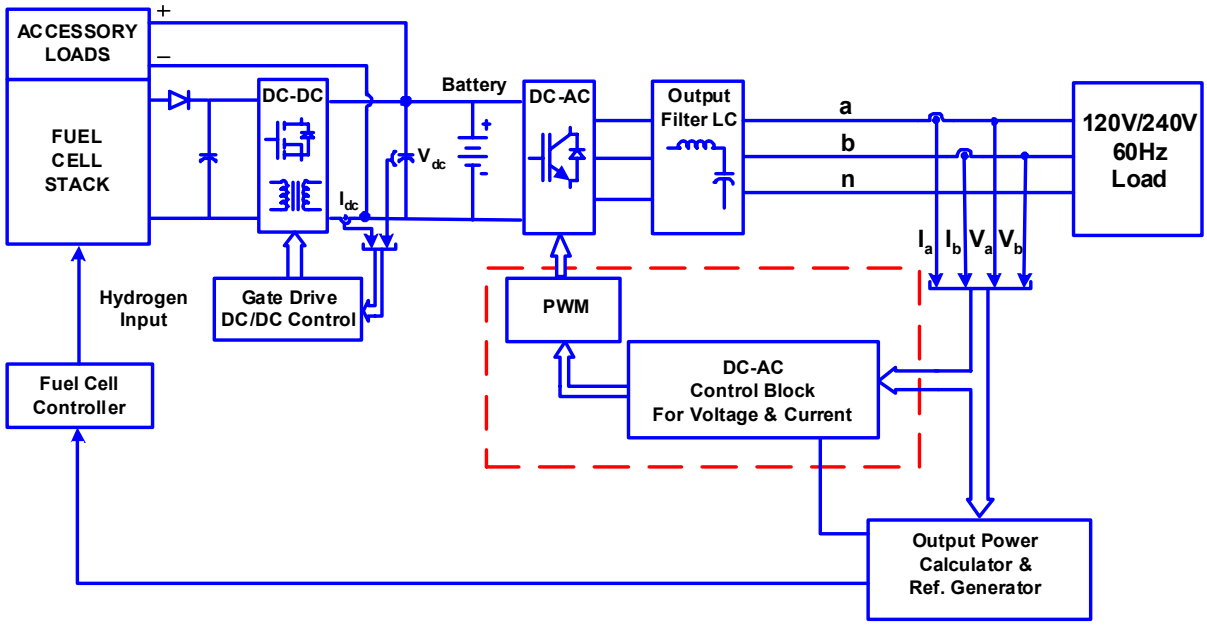

Figure 8-36c Fuel cell power conditioner control system for powering dedicated loads

Currently, fuel cell suppliers are focusing on supplying only average power from the fuel cell. Thus, peak power must be supplied from some other energy source, such as a battery or supercapacitor (59, 60). The power conditioning stage must therefore provide means for interfacing a battery and also ensure its charge maintenance. Figure 8-34a shows a block diagram of a typical fuel cell powered unit for supplying a load along with a battery interface. Figure 8-34 to Figure 8-37 show three possible block diagrams and circuit topologies of power conversion stages for this application.

Power Conditioning Stage With Line Frequency Transformer: Figure 8-34b shows the block diagram and Figure 8-34c shows the circuit topology of the power conditioning stage. In Figure 8-34c the fuel cell output DC (say 29V to 39V) is converted to a regulated dc output (say 50V) by means of a simple DC-DC boost converter. The output of the DC-DC converter is

processed via a PWM DC to AC inverter to generate a low voltage sinusoidal AC of ± 35 V AC (rms). A line frequency isolation transformer with a turns ratio of 1:3.5 is then employed to generate 120V/240V AC output as shown (Figure 8-34b). A 42-48V battery is connected to the output terminals of the DC-DC converter to provide additional power at the output terminals for motor startups, etc. During steady state, the DC-DC converter regulates its output to 50V and the battery operates in a float mode. The fuel cell and the DC-DC converter are rated for steady state power (say 10kW), while the DC-AC inverter section is rated to supply the motor starting VA. Assuming a motor starting current of 3 to 5 times the rated value, the DC-AC inverter rating will be in the 15kVA to 25kVA range. The DC-DC boost converter is operated in current mode control. During motor startup, the current mode control goes into saturation and limits the maximum current supplied from the cell. During this time, the additional energy from the battery is utilized. During steady state operation, the fuel cell energy is utilized to charge the battery when the output load is low.

Efficiency Calculation (Approximate): Referring to Figure 8-34b, assume

DC-DC converter efficiency $= \eta_1$

DC-AC inverter efficiency $= \eta_2$

Line frequency isolation transformer efficiency = η_3

The overall conversion efficiency of the power conditioning stage: $\eta = \eta_1 * \eta_2 * \eta_3$

Assuming $\eta_1 = 0.95$ (95%) ; $\eta_2 = 0.95$ (95%); $\eta_3 = 0.98$ (98%); $\eta = 0.88$ (88%).

The main limitation of this system is the low voltage nature of the entire power conditioning stage, which results in higher currents and lower overall efficiency. Another disadvantage is the presence of a line frequency isolation transformer which is bulky, large in size, and heavy (10kg/kw). Figure 8-34c shows the circuit topology of the power conditioning stage.

Power Conditioning Stage With High Frequency Isolation Transformer: Figure 8-35a shows a similar power conditioning block diagram. In this design, the low frequency isolation transformer has been eliminated by employing an additional DC-DC conversion stage. The 50V to 400V DC-DC conversion stage includes high frequency isolation. In this design, the fuel cell and the first DC-DC converter are rated for steady state conditions. The second DC-DC converter, along with the DC to AC inverter, is rated for steady state and transient conditions. Figure 8-35b shows the circuit topology of the power conditioning stage. This approach also suffers from three power conversion stages in the power flow path, which contributes to a lower efficiency.

Power Conditioning Stage With High Frequency Isolation With Fewer Power Processing Stages (39, 40): Figure 8-36a shows a power conditioning stage with fewer power processing stages in series. In this approach, a push-pull type boost converter with a 1:10 gain employing a high-frequency isolation transformer is used. The output of the push-pull DC-DC converter is set to 400V with ± 200V. The DC-DC converter output is connected to two half bridge dual voltage DC-AC inverters to obtain 120/240V AC output. It is economical to install a ± 200V battery at the output of the DC-DC converter stage and regulate the push-pull DC-DC converter output to ± 200V. The fuel cell and the push-pull DC-DC converter is rated to supply steady state load (10kW), while the DC-AC inverter stage is rated to supply the steady state as well as transient load demands such as motor starting, etc. Figure 8-36b illustrates the possible circuit topology

for this approach. Assuming conversion efficiency of the DC-DC and DC-AC stages to be 96% each, an overall efficiency of 92% can be realized with this approach. Figure 8-36c shows the fuel cell power conditioner control system block diagram for powering a load. The DC-DC and DC-AC control blocks are controlled separately. The power consumed by the load is first computed by the reference signal generator block, and suitable reference signals for the DC-AC inverter and the fuel cell controller are generated. The DC-DC converter controller regulates the dc-link and draws power from the fuel cell. This block has the appropriate protection circuitry and limits to protect both the fuel cell and the dc-link against over current and over voltage, respectively. Fuel cell accessory loads are supplied via the dc-link. The battery also provides start-up operation of this unit.

Design Example (39, 40): In this section, a design example of the power conversion stage (Figure 8-36b) is discussed for the specifications outlined in Table 8-8. The objective of the design example is to outline step by step calculations of switch voltage/current ratings, dc-link capacitor values, and L-C output filter values to meet the specifications.

Push-Pull DC-DC Converter Design: Inverter power output = 10000W
Assuming an overall efficiency of 90%, power input can be computed as

$$P_{in} = \frac{10000W}{0.9} = 11111W \tag{8-57}$$

A nominal fuel cell input voltage, V_{in} = 48V DC, is assumed. An output voltage, V_o = 400V DC and the switching frequency is set at 40kHz, with the two input switches in the push-pull converter to operate in duty ratio control. The fuel cell current is calculated for its lowest voltage condition (V_{in} = 42V DC) as

$$I_{in} = \frac{11111W}{42V} = 265A \tag{8-58}$$

The push-pull DC/DC converter shown in Figure 8-21a comprises two switches, S1 and S2. At the maximum duty ratio of 0.5 rms current rating, I_T of the switches is

$$I_T = \frac{I_{in}}{\sqrt{2}} = 188A \tag{8-59}$$

Two MOSFET devices in parallel, rated at 100V, 100A each are selected for S1 and S2.

High frequency transformer: To obtain an output voltage of 400V DC for the push-pull converter, a turns ratio of K = 5 is selected for the transformer. Center taps are available on both the primary and secondary sides. The VA rating of the transformer is defined as the sum of the total primary and secondary winding VA divided by two,

$$VA_{Tr} = \frac{1}{2}\left(\frac{V_{in}}{\sqrt{2}} \cdot \frac{I_{in}}{\sqrt{2}} \cdot 2 + V_{in} \cdot K \cdot \frac{I_{in}}{K} \cdot 2\right) = 1.5 V_{in} \cdot I_{in} = 1.5 \cdot 42 \cdot 265 = 16695W \cong 17.0kVA$$

(8-60)

Voltage ratings of the transformer are: Primary voltage = 80V, Secondary voltage = 400V, Diode (D1 to D4) ratings are calculated as follows:
The reverse blocking voltage is equal to the DC link voltage, 400V. Current rating (rms) of each diode, I_D is,

$$I_D = \frac{I_{in}}{K \cdot \sqrt{2}} = 37.5A \tag{8-61}$$

Designing the push-pull transformer is a long and cumbersome. Reference (44) provides more information on this topic.

Core Saturation Issues: A challenge that arises with the push-pull topology is that the transformer core may saturate if the characteristics of the forward-voltage drop and conduction times of the transistors are not precisely matched. Small imbalances can cause the DC component of voltage applied to the transformer-primary to be nonzero. Consequently, during every switching period, there is a net increase in the magnetizing current. If this imbalance continues, then the magnetizing current can eventually become large enough to saturate the transformer. Core saturation results in rapid thermal runaway and destruction of one of the MOSFET transistors. To ensure that there is no significant imbalance between the two switch currents, a coupled inductor is employed on the secondary of the transformer (Figure 8-36b). The coupled inductor balances the currents in the two halves of the center-tapped transformer. Additionally, it is designed to filter switching frequency components in the DC output and helps generate a clean ± 200VDC voltage for the inverter stage.

Control of Push-Pull DC to DC Converter: There are a number of commercially available low cost DC to DC control circuits (61). Motorola SG3525A Pulse Width Modulator controller can be used to control this type of DC-DC converter. The SG3525A is particularly suited for push-pull converter application because it has two output terminals. The two output terminals are suitable for the two transistors used in this converter design. The block diagram of the Motorola SG3525A is shown in Figure 8-37.

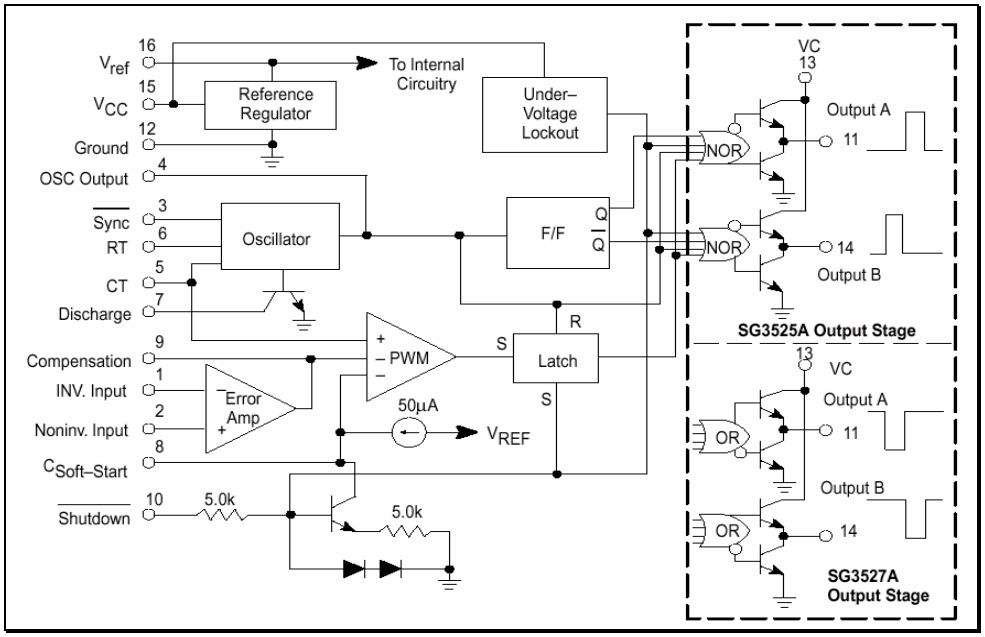

Figure 8-37 Motorola SG3525A Control chip for push-pull DC-DC converter stage

The Motorola SG3525A provides this design with other features that enhance control and safety. The SG3525A provides for an input under-voltage lockout that automatically shuts off the chip

in case of low voltage. The modulator has a soft start capability, which protects it from capacitor inrush currents.

DC to AC Inverter Stage Design (54, 39, 40): Since the DC-DC converter maintains equal ± 200V on the dc-link capacitors, two inverter legs are sufficient to generate 120V/240V AC output. The inverter consists of two half bridge modules, each PWM controlled to generate the required output voltage. An LC filter is used to filter out switching frequency harmonics generated by the inverter PWM. Consider the case when one of the phases (say B) is not loaded and Phase-A carries full load (5000W). The fundamental component in $V_{Ao,1}$ is given by Equation (8-42), and is

$$V_{AO1} = m_a \cdot \frac{V_{DC}}{2} sin(w_1 t) \qquad 0 < m_a < 1 \tag{8-62}$$

The switching function sw_1 of the half bridge inverter is [15]

$$sw_1 = 0.5 + \frac{m_a}{2} sin(wt) + \text{higher frequency terms} \tag{8-63}$$

The inverter is assumed to supply nonlinear load, which predominantly contains a large magnitude of third harmonic component (52). The inverter Phase-A current can be expressed as (51)

$$i_A = \sqrt{2} I_1 \, sin(w_1 t - \phi_1) + \sqrt{3} I_3 \, sin(3w_1 t - \phi_3) + ... \tag{8-64}$$

The current through the inverter IGBT switch Q1 is given by

$$\begin{aligned} i_{sA} &= sw_1 \cdot i_A \\ &= \frac{\sqrt{2}}{2} I_1 \, sin(wt - \phi_1) + \frac{\sqrt{3}}{2} I_3 \, sin(3wt - \phi_3) + ... \\ &+ \frac{m_a}{4} \sqrt{2} I_1 [cos\,\phi_1 - cos(2wt - \phi_1] + \frac{m_a}{4} \sqrt{2} I_3 [cos\,\phi_3 - cos(3wt - \phi_3)] + ... \end{aligned} \tag{8-65}$$

Neglecting higher frequency terms, the rms value of the Phase-A output current, I_{rms} is

$$I_{rms} = \sqrt{I_1^2 + I_3^2} \tag{8-66}$$

Assuming $I_3 = 0.7 * I_1$ which is typical of single phase rectifier type nonlinear loads,

$$I_{rms} = 1.22 \cdot I_1 \tag{8-67}$$

When supplying full load of 5000W at unity power factor,

$I_{rms} = \frac{5000}{120} = 41.7A$. Substituting this value in Equation (8-32) yields: $I_1 = \frac{41.7}{1.22} = 34A$

Therefore, the largest component of the capacitor current i_c is the fundamental frequency current, the rms value of which equals

$$i_{c,rms} = \frac{1}{2} \cdot I_1 = 17A \tag{8-68}$$

For a voltage ripple ΔV_c less than 5% or 10V,

$$\Delta V_c = \frac{i_{c,rms}}{\omega C} \tag{8-69}$$

The required dc-link capacitor value can be calculated as

$$C = \frac{i_{c,rms}}{\omega \Delta V_c} = \frac{17}{10 \cdot 2\pi \cdot 60} \cong 4500 \mu F \tag{8-70}$$

Two dc-link capacitors of 4500μF each are selected for this design.

Inverter Switch Ratings: The rms current i_{sA} is 41.7A. Thus, rms current rating of each switch is

$$I_T = \frac{41.7}{\sqrt{2}} = 30A \tag{8-71}$$

Voltage rating of the IGBTs is 600V.

DC-AC Inverter Output Filter (L-C) Selection: The function of the output filter is to effectively eliminate PWM switching frequency harmonics at the inverter output and to maintain output voltage distortion (THD) below 5%. Accomplishing this task when supplying nonlinear loads of crest factor 3, requires careful design (54).

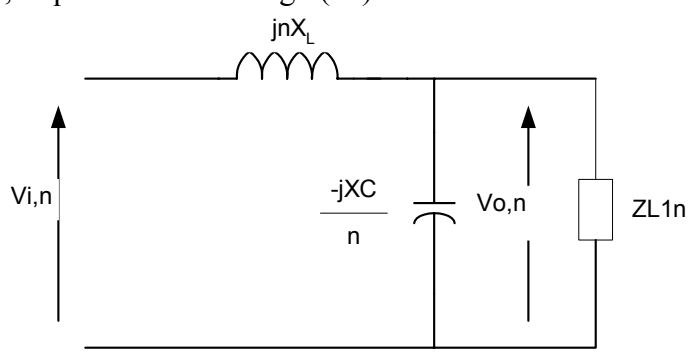

Figure 8-38 DC-AC Inverter Output Filter

The transfer function (gain) for this type of filter is given by.

$$H_n = \frac{V_{o,n}}{V_{i,n}} = -\frac{jX_C \cdot Z_{L,n}}{nX_L X_C + jZ_{L,n}(n^2 X_L - X_C)}. \tag{8-72}$$

Where n is the ratio of the switching frequency to the fundamental frequency,

$$n = m_f = \frac{f_s}{f} \tag{8-73}$$

Since the gain of the filter at fundamental frequency (H_1) should equal to 1, as $H_1 \to 1$; the condition $X_L << X_C$ must be satisfied. Substituting this in (8-73) yields,

$$H_1 \le \frac{-jX_C \cdot Z_{L,1}}{-jZ_{L,1} \cdot X_C} \cong 1. \tag{8-74}$$

Also, for no load condition, the output load impedance: $Z_{L,1} \to \infty$, substituting this in (8-72) results

$$|H_n| = -\frac{X_C}{n^2 X_L - X_C} = \frac{1}{n^2 \cdot \frac{X_L}{X_C} - 1} \tag{8-75}$$

Equation (8-73) depicts the gain of the filter (at $n = m_f = \frac{f_s}{f}$). To satisfy the THD requirement of less than 5% set the gain $H_n = 0.045$. Substituting this in (8-75) yields

$$\frac{1}{n^2 \cdot \frac{X_L}{X_C} - 1} \leq 0.045 \quad ; \quad \frac{X_L}{X_C} \geq \frac{23.22\bar{2}}{n^2} \tag{8-76}$$

Since the output filter should be capable of handling nonlinear loads (which are predominantly 3rd harmonic in nature for single phase systems) the filter equivalent circuit for this condition should be considered (Figure 8-39), where I_h is the harmonic current drawn by the load.

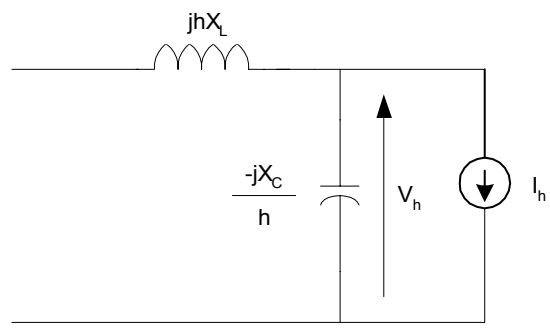

Figure 8-39 Equivalent Circuit for a Non-Linear Load

The transfer function for this condition is described by

$$V_h = \frac{jhX_L \cdot X_C}{X_C - n^2 X_L} \cdot I_h \tag{8-77}$$

Where,

$$|V_h| = \frac{hX_L}{1 - n^2 \frac{X_L}{X_C}} \cdot I_h \tag{8-78}$$

If the inverter switching frequency f_s = 20kHz and the fundamental frequency f = 60Hz, then from (8-73), n=333.33. Substituting this value in (8-76) yields

$\frac{X_L}{X_C} \geq 2.1*10^{-4}$ for this we can deduce: $n^2 \frac{X_L}{X_C} << 1$. Substituting this in (8-78),

$$|V_h| \leq hX_L \cdot I_h \tag{8-79}$$

Assuming the nonlinear load drawn predominantly third harmonic, the value of $h = 3$. Substituting this into (8-79) yields

$$\frac{|V_3|}{V_1} = \frac{3X_L \cdot I_3}{V_1} \tag{8-80}$$

Equation (8-80) gives the ratio of the third harmonic voltage V_3 at the inverter output with respect to the fundamental V_1. Limiting this to a reasonably low value will yield a lower THD. Therefore setting the ratio $\frac{|V_3|}{V_1} = 0.03$ in Equation (8-80) yields

$$X_L = \frac{0.03 \cdot V_1}{3 * I_3} \tag{8-81}$$

From (8-81) the output filter inductor can be determined.

Output Filter Component Selection:

For a 10 KW inverter (5 KW per Phase) with $V_{Ao,1} = 120V$, $I_{rms} = 41.67A$, third harmonic current $I_3 = 25.95A$. From (8-81), $X_L = 0.046$ which yields $L = 123\mu H$. From equation (8-72), $X_C = 221.26$, which yields $C = 12\mu F$

The output filter resonant frequency can be computed as

$$\frac{f_r}{f_1} = \sqrt{\frac{X_C}{X_L}} \leq \sqrt{\frac{n^2}{23.222}} \leq 69.17 \tag{8-82}$$

Experimental Results (39, 40): The fuel cell inverter design presented in this section was designed and tested in DOE sponsored future energy challenge competition in 2001 by a Texas A&M University team (39). Figure 8-40 shows the fuel cell inverter operating waveforms on a 1.5kW fuel cell at the DOE NETL facility.

Figure 8-40a. Texas A&M Inverter operating on DOE NETL Fuel Cell on August 14, 2001

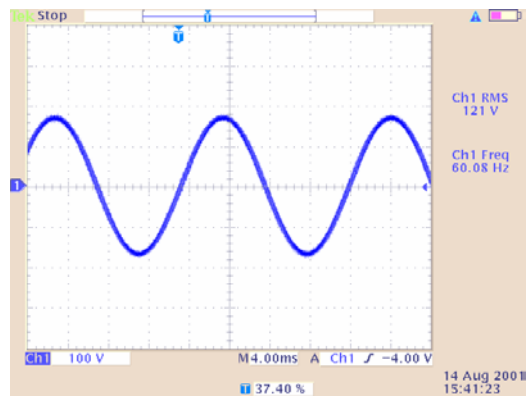

Figure 8-40b. Inverter output voltage waveform when running off the fuel cell at NETL on August 14, 2001

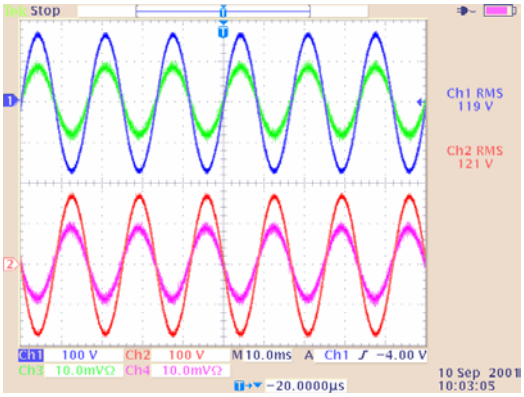

Figure 8-40c. Inverter output waveforms (voltage & current) when supplying 800W/phase. Both Phase-A and Phase-B were loaded equally.

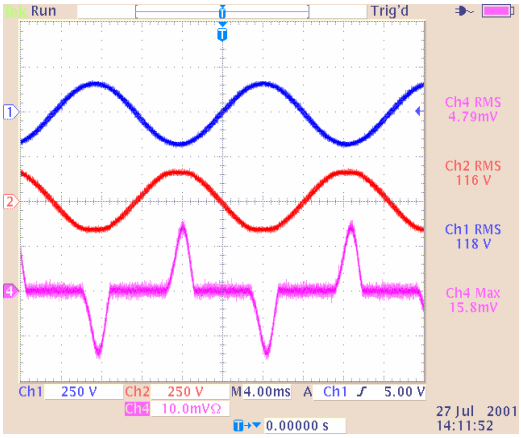

Figure 8-40d. Inverter output waveforms with Phase A on 800W/phase and Phase B on 150W switching power supply load.

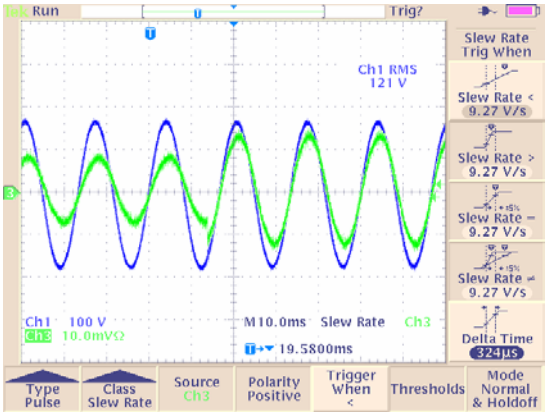

Figure 8-40e Inverter output waveforms (voltage & current) when a step change in load was applied from 360W to 610W on Phase A

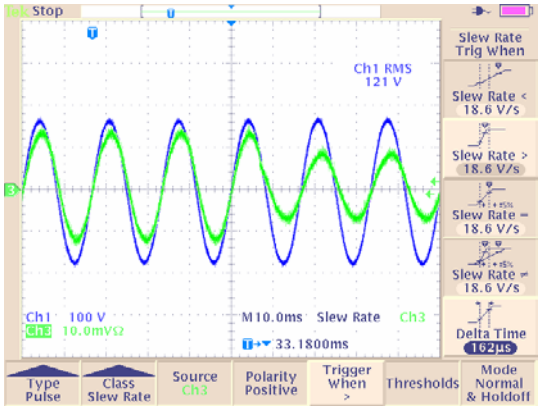

Figure 8-40f Inverter output waveforms (voltage & current) when a step change in load was applied from 610W to 360W on Phase A.

8.2.3 Fuel Cell Power Conversion for Supplying Backup Power (UPS) to a Load Connected to a Local Utility

Conventional uninterruptible power supply systems (UPS) employ engine generators and/or batteries as power sources to provide electric power for critical functions or loads when the normal supply, i.e. utility power, is not available (62). Typical UPS system consists of rechargeable batteries such as sealed lead-acid (SSLA) or nickel cadmium (Ni-Cd). However, these batteries contain toxic heavy metals such as cadmium, mercury, and lead, and may cause serious environmental problems if they are discarded without special care (62). Further, unlike batteries, fuel cells continuously provide power as long as reactants are supplied. This feature is especially useful when the duration of the power outage is uncertain.

Among the various kinds of fuel cells, Proton Exchange Fuel Cells (PEFC) are compact and lightweight, provide a high output power density at room temperature, and are easy to start-up and shut down in system operation (46, 63, 64).

In this section, design considerations for a 1-kW fuel cell powered line-interactive UPS system with one hour of backup power employing modular (fuel cell and power converter) blocks is discussed (Figure 8-41). Two commercially available PEFC (25-39V, 500W) modules (46) along with suitable DC-DC and DC-AC power electronic converter modules are considered. Commercially available supercapacitors (59) are chosen for supplying transient power at the output terminals. Two possible power-conditioning architectures are investigated.

Table 8-9 Example specifications for the 1kW fuel cell powered back power (UPS) unit. (65, 66)

Continuous output power:	1 kW continuous for 1hr
Peak power:	2kW for 20 seconds
Output Phase (s):	Single-phase, not to exceed 1000 VA total
Output voltage:	120V, Sinusoidal AC. Output voltage tolerance no wider than ±6% over the full allowed line voltage and temperature ranges, from no-load to full-load. Frequency 60±0.1 Hz.
Output frequency:	***60Hz (US) or 50Hz (Europe) with enough precision to run AC clock accuracy***
Transfer time (typical/max):	4/6 milliseconds
Load power factor (PF) range & crest factor (CF):	PF: 0.6 to 1; CF: 3
Fuel Cell Current Ripple: (Fuel cell dependent)	▪ ***120 Hz ripple: < 15% from 10% to 100% load*** ▪ 60 Hz ripple: < 10% from 10% to 100% load
Output THD:	< 5%
Protection:	Over current, over voltage, short circuit, over temperature, and under voltage. No damage caused by output short circuit. The inverter must shut down if the input voltage dips below the minimum specified fuel cell voltage (29V). Inverter should not self-reset after a load-side fault. IEEE Std. 929 is a useful reference.
Acoustic Noise:	No louder than conventional domestic refrigerator. Less than 50 dBA sound level measured 1.5 m from the unit.
Environment:	Suitable for indoor installation in domestic applications, 10°C to 40°C possible ambient range.
Electromagnetic Interference	Per FCC 18 Class A -- industrial
Efficiency:	Greater than 90%
Safety:	The system is intended for safe, routine use in a home or small business by non-technical customers.
Life:	The system should function for at least ten years with routine maintenance when subjected to normal use in a 20°C to 30°C ambient environment.

Table 8-10 Specifications of 500W PEFC Stack available from Avista Labs (46)

Power Output (Continuous)	500 [W]
Output Voltage	25-39 DC
Fuel Source	Hydrogen
Fuel Consumption	7.0L/min @500W(<1.0L/min @ no load)
System Start Time	7 minutes @room temperature
Turndown Ratio	500W to no load, infinity
Operating Temperature Range	41°F to 95°F (5°C to 35°C)
Dimension (W x D x H)	22.3” x 24.2” x 13.6” (0.056m x 0.0615m x0.0345m)
Weight	97 lbs w/cartridges (44kg w/cartridge)

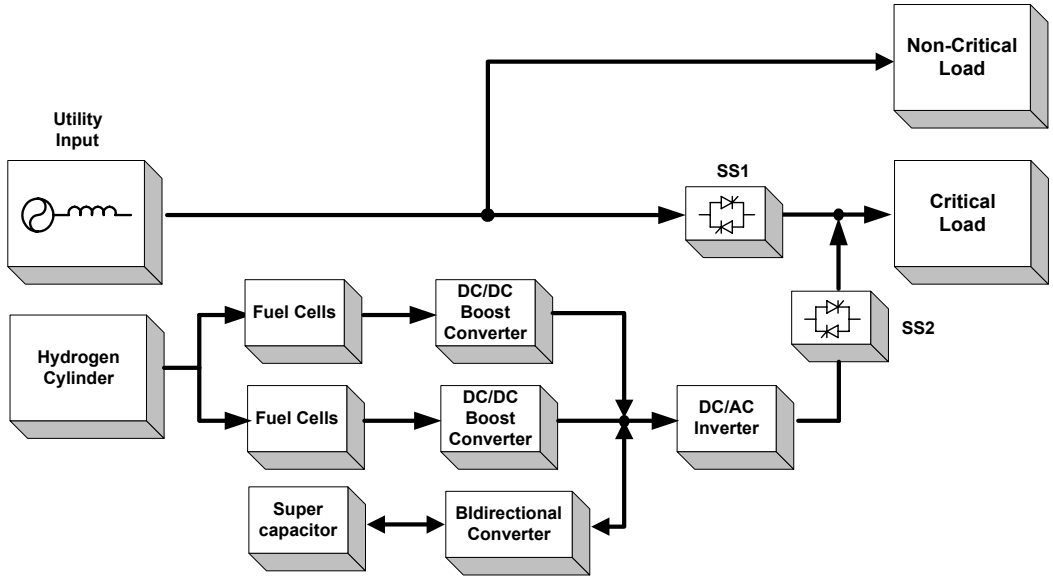

Figure 8-41 One line diagram of a modular fuel cell power conversion system for supplying backup power (UPS) to a load connected to a local utility (65, 66)

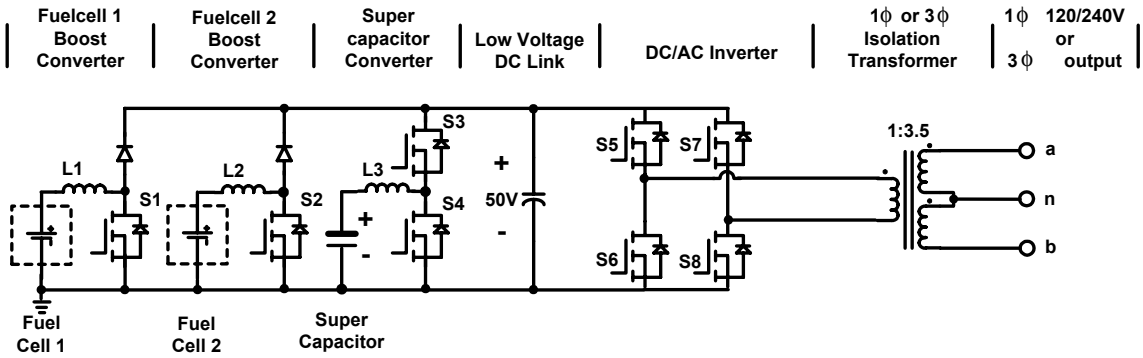

Figure 8-42 Modular power conditioning circuit topology employing two fuel cell power sources to supply a load via a line frequency isolation transformer (65, 66)

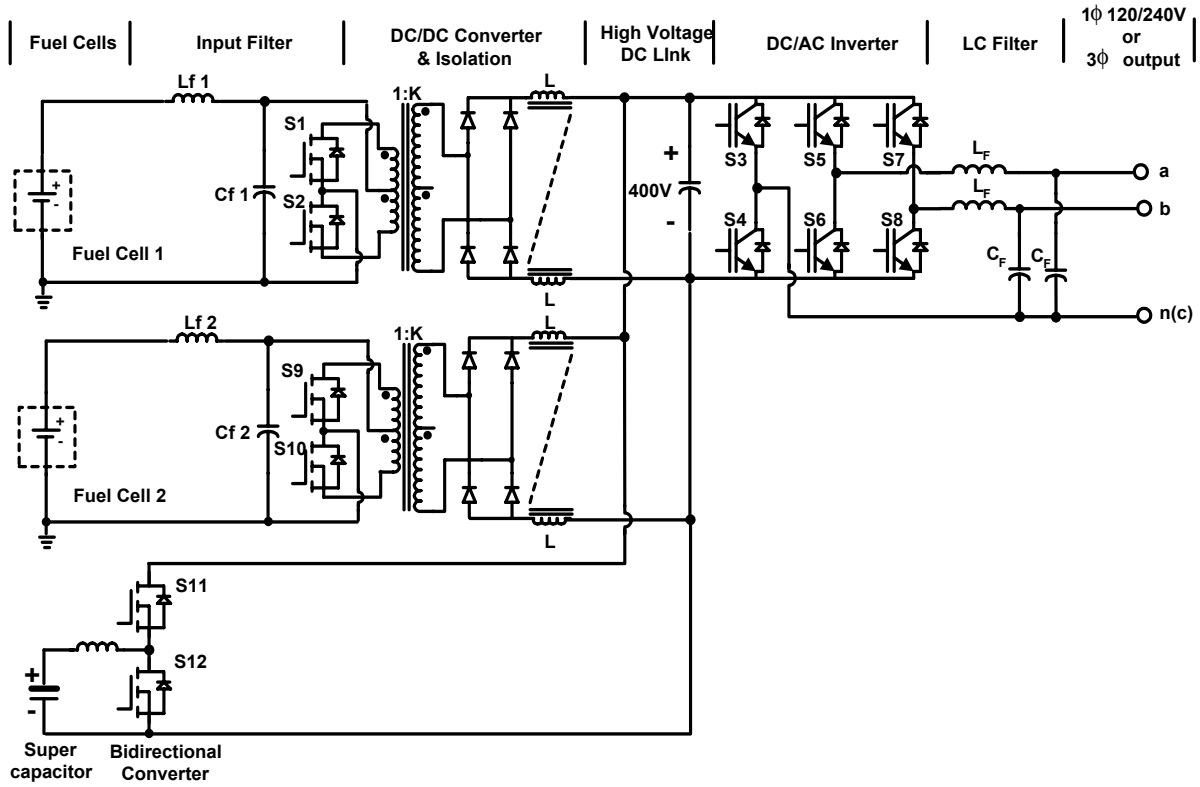

Figure 8-43 Modular power conditioning circuit topology employing two fuel cell power sources using a higher voltage (400V) dc-link (65, 66)

Figure 8-41 shows a one-line diagram of a line interactive UPS, whose main function is to provide backup power to a load connected to a local utility. The load is connected via two static transfer switches SS1 and SS2 either to the utility or to the fuel cell source. Normally the fuel cell inverter side static switch SS2 is rated for inverter output. However, the utility side SS1 is rated for 1500% for approximately 15 milliseconds to provide current to open the down stream or load side circuit breaker in case of a short circuit (62). Two commercially available 500W fuel cell stacks (see Table 8-10) are considered in this example design (Figure 8-41). The use of a supercapacitor is explored to supply inrush current to the load (2kW for 20 seconds). A static bypass switch is configured to disconnect the utility in case of its failure and/or out of specified voltage range for the load. In steady state, the fuel cell power source is assumed to be in hot standby mode, i.e. supply 10% of its capacity, this allows the fuel cell subsystem to be ready to supply the load during a utility shutdown. It is assumed that pure hydrogen is available to supply the rated output power (1kW) for a 1hr utility outage. Figure 8-42 and Figure 8-43 show two possible circuit topologies for this application. The approach in Figure 8-43 is more suitable, as it employs modular DC-DC converters to interface each fuel cell output to a 400V dc-link. A 42V supercapacitor module (59, 60) is also connected to the dc-link via a bi-directional DC-DC converter. The bi-directional DC-DC converter module allows quick discharge and charging of the supercapacitor modules to supply inrush current demanded by the load.

Design Example (65, 66):
In this section a design example is presented to compute the amount of hydrogen necessary to meet the specifications outlined in Table 8-10. Further, the rating of the supercapacitor is determined to supply the inrush current demanded by the load. All calculations are based on the low voltage dc-link architecture detailed in Figure 8-42.

Example Hydrogen fuel calculation to supply 1kW for 1hr during a power outage (65, 66, 67)
The purpose of this section is to present a calculation method (to serve as a design guide) to compute the amount of hydrogen necessary to supply 1kW of power for one hour. The basic chemical equation for a fuel cell (PEFC) reaction can be expressed as (67)

$$2H_2 + O_2 = 2H_2O \tag{8-83}$$

The rate of Hydrogen fuel usage in a single cell is related to current by

$$Q_{_H_2} = \frac{I}{Z \cdot F} \; [moles / sec] \tag{8-84}$$

where,

$Q_{_H2}$:	Hydrogen flow rate
F:	Faraday constant 96485 [coulombs/mole]
Z:	Number of electrons participating in the reaction

Thus, Hydrogen flow rate required to generate 1 ampere for one cell can be calculated as,

$$Q_{U_H_2} = \frac{I}{Z * F * I * K} = \frac{1[\frac{coulomb}{sec}] * 60[\frac{sec}{min}] * 22.4[\frac{SL}{mol}]}{2 * 96485[\frac{coulombs}{mol}] * 1[A] * 1[cell]} = 0.007\,[\frac{SLM}{A \cdot Cell}] \tag{8-85}$$

where,

K	: Number of cells
SLM	: Standard liter per minute

Considering parasitic power to run the control system of the fuel cell, the fuel cell is required to generate about 10% more power than needed. Thus, the hydrogen flow rate needed for 1kW fuel cell can be calculated as follows.

$$Q_{T_H2} = Q_{U_H_2} * \frac{P * 1.1}{V_{cell}} * N * S = 0.007 * \frac{1000 * 1.1}{34} * 48 * 1.2 = 13\,[SLM] \tag{8-86}$$

where,

$Q_{_T_H2}$:	Hydrogen flow rate needed to generate total power
V_{cell}:	Fuel cell nominal output voltage
N:	Number of cells
S:	Stoichiometry

Therefore, the total amount of the Hydrogen to be consumed for a 1kW UPS system during a 1-hour power outage can be calculated as,

$$Q_{T_H2}\,[SLM] * 60\,[min] = 13 * 60 = 780\,[L] \tag{8-87}$$

If the Hydrogen is stored in a cylinder as a compressed gas at 25°C (298.15[K]), its weight and volume at 150 atm (2205 [psi]) can be calculated:

$$\frac{780[L]*2[\frac{g}{mole}]}{22.4[\frac{L}{mole}]}=70[g] \tag{8-88}$$

Since Hydrogen gas normally takes up 3 weight percent when it is contained in a cylinder as a compressed gas, total weight of the compressed Hydrogen gas and its cylinder is

$$\frac{70[g]}{3[wt\%]}=2333[g] \tag{8-89}$$

Number of moles of Hydrogen in a certain volume (780[L] in this case) can be calculated as

$$n=\frac{P\cdot V}{R\cdot T}=\frac{1[atm]*780[L]*10^3[cm^3/L]}{82.06[\frac{cm3\cdot atm}{mol\cdot K}]*298.15[K]}=31.88[moles] \tag{8-90}$$

where

n:	Number of moles
P:	Pressure [atm]
V:	Volume of the gas [cm^3]
R:	Gas constant
T:	Temperature [K]

The volume of one mole of Hydrogen at 150[atm] can be calculated from the virial equation of state:

$$V_U=\frac{R\cdot T}{P}+B=\frac{82.06[\frac{cm3\cdot atm}{mol\cdot K}]*298.15[K]}{150[atm]}+15.4[\frac{cm3}{mol}]=178.5[\frac{cm^3}{mole}] \tag{8-91}$$

where,

V_U:	Volume of one mole of Hydrogen at a certain pressure
B:	Virial constant at 298.15[K]

Thus, the total volume of the Hydrogen at 25[°C] at 150 [atm] is

$$V_U*n=178.5[\frac{cm^3}{mole}]*31.88[mole]*10^{-3}[\frac{L}{cm^3}]=5.7[L] \tag{8-92}$$

The proposed line-interactive UPS system requires 780 liters of hydrogen at standard temperature and pressure (STP) (Equation (8-87)) to supply 1kW for 1hr. Assuming the UPS supplies 10% of the load along with the utility power in steady state, the hydrogen required can be calculated as 78-liters per hour at STP.

DC-DC Converter Design (57): In this section, an example design of various components of a DC-DC boost converter module shown in Figure 8-41 is detailed. Since the DC-DC converter is

required to convert the fuel cell output voltage of 25-39V to a 50V dc-link, a gain ≈ 2 is required. A standard single switch boost converter (described in section 8.2.1) is selected.

The DC/DC converter is designed to the following specifications:
Fuel Cell output voltage $(V_s) = 25 \text{ to } 39\ [V]$; Nominal: 34[V] (see Table 8-10)
Output voltage $(V_o) = 50\ [V]$
Output power of each converter $(P_o) = 500\ [W]$

Rated output current $(I_o) = \frac{P_o}{V_o} = 10\ [A]$ (8-93)

Maximum fuel cell input current $(I_s) = \frac{P_o}{V_{s,min}} = \frac{500}{25} = 20\ [A]$ (8-94)

Switching frequency $(f_s) = 100\,[\text{kHz}]$

Converter Gain (M) $= \frac{\text{Maximum output voltage}}{\text{Input voltage}} = \frac{50}{25} = 2$ (8-95)

Output voltage ripple $(V_{ripple}) = V_o * 0.01 = 0.5\ [V]\ ;\ \text{about } 1\%$ (8-96)

Critical load current above which continuous current is desired $(I_{critical}) = I_o * 0.1 = 1[A] : \text{i.e. for } 10\%$ load and higher DC-DC converter to operate in continuous current mode

Minimum inductance $L_1 = \frac{V_o * (M - 1)}{(I_{critical} * f_s * 2 * M^3)} = 32.15\ [\mu H]$ (8-97)

Worst case peak current $(I_{pk}) = I_o * [M + (\frac{V_o}{2 * I_o * L_c * F_s}) * (\frac{M - 1}{M^2})] = 22[A]$ (8-98)

Output dc capacitance $(C_o) = \frac{(I_{pk2} * L_c)}{[2 * V_r * (V_o - V_s)]} = 600\ [uF]$ (8-99)

Sizing Supercapacitor for Supplying Load Inrush Current (60, 64, 65):
In the recent past, supercapacitors have emerged as viable energy storage devices (59, 60). Super capacitors possess a number of unique characteristics that enable in a wide range of applications (e.g., hybrid electric vehicles/electric vehicles (HEVs/EVs), uninterruptible power supply (UPS) systems, ASD ride-through applications). Some of these features include the following:

- Energy densities 100 times greater than conventional capacitors and power densities 10 times greater than conventional batteries
- Specific energy range of 1.12–2.48 Wh/kg
- Charge and discharge times from fractions of a second to several minutes
- Rated capacitance range of 0.043–2700 F;
- Nominal voltage ranging from 2.3 to 100 V;
- Rated current ranging from 3 to 600 A, Power range 5–100 kW
- Cycle life greater than 100 000, Operating temperature range of 20 C–55 C;
- Modular and stackable, Maintenance-free operation, Environmentally safe.

The capabilities listed above offer to meet the inrush power demands required in power conditioning applications. The energy stored (W_j) in a supercapacitor is given by:

$$W_j = \frac{1}{2} C V^2 \tag{8-100}$$

Since the energy stored in a supercapacitor is directly proportional to the square of the voltage, a drop in 30% of its voltage (1pu to 0.7pu) represents the release of 50% of the stored energy. Further, losses in the DC-DC boost converter powering the supercapacitor along with the internal losses due to electrostatic resistance (ESR) also need to be accounted for. Adopting this discharge strategy, the following equation can be written:

$$\frac{1}{2}\left[CV_{sup}^2 - C(0.7V_{sup})^2\right] * \kappa = P_{in-rush} * t \tag{8-101}$$

Where C is the required capacitance of the supercapacitor, κ is the efficiency (which is less than 1 due to losses), $P_{in\text{-}rush}$ is the amount of inrush power (Watts) and "*t*" is the specified duration for the inrush current.

For the example system described in Table 8-9, we have: $P_{in\text{-}rush} = 1kW$; $t = 20$ seconds and let $\kappa = 0.9$. Assuming a supercapacitor of 42V rating, the required capacitance can be calculated by substituting these values in Eqn. (8-101)

$$C = \frac{4 * P_{in-rush} * t}{\kappa * V_{sup}^2} = \frac{4 * 1000 * 20}{0.9 * 42^2} = 50.4\ [F] \tag{8-102}$$

Therefore, a 42V, 50F supercapacitor will be sufficient to provide 1kW of additional power for 20 seconds.

8.2.4 Fuel Cell Power Conversion for Supplying a Load Operating in Parallel With the Local Utility (Utility Interactive)

Figure 8-44 shows the block diagram of a fuel cell power conversion scheme supplying a load in parallel with the utility. In this configuration, the peak power (as well as the inrush current) demanded by the load is provided by the utility. By paralleling the fuel cell power output to the utility, the following advantages can be realized:

- Power conversion rating is same as the fuel cell
- Peak power (as well as the inrush current) demanded by the load is provided by the utility
- A constant fuel cell power level can be set.

While in the utility connect mode, the voltage is set by the utility and current control is used to manage the power flow from the fuel cell.

In the event of a utility failure, the fuel cell system does not have the ability to supply inrush current to loads such as for motor starting, etc. Special circuit breakers to isolate loads up to the capacity of the fuel cell are necessary. Furthermore, the utility interconnection must conform to the IEEE standard P1547 to prevent energizing a section of the utility by the fuel cell source under utility fault conditions (islanding).

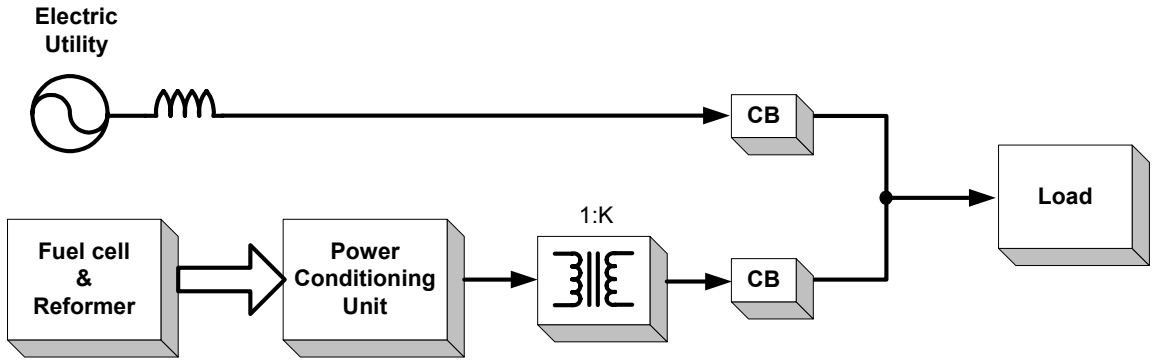

Figure 8-44 Fuel cell supplying a load parallel with the utility

8.2.5 Fuel Cell Power Conversion for Connecting Directly to the Local Utility

Fuel cell power systems can be connected directly to the utility to supply power (Figure 8-45). IEEE Standard P1547 (68), which is in the development stage, outlines the criteria and requirements for connecting distributed resources (DR) such as a fuel cell power plant to the electric power system. It provides requirements relevant to the performance, operation, testing, safety, and maintenance of the interconnection. Islanding should be avoided at any cost: a condition in which a fuel cell power plant energizes a portion of the electric power system (EPS) when the utility power is disconnected. In other words, the fuel cell connected to the utility must be disconnected immediately in case of utility failure. In general, a fuel cell power converter that has to be interfaced with the utility should meet the following requirements:

- When a DR such as fuel cell is synchronized with the utility, it should not cause the area electric power system (EPS) voltage fluctuation greater than ±5%
- The paralleling device, static switch / mechanical circuit breaker, should be capable of withstanding twice the nominal peak utility voltage
- Unintentional islanding: the fuel cell power conditioner must detect the islanding operation and cease to energize the area EPS within 2 seconds of formation of an island.

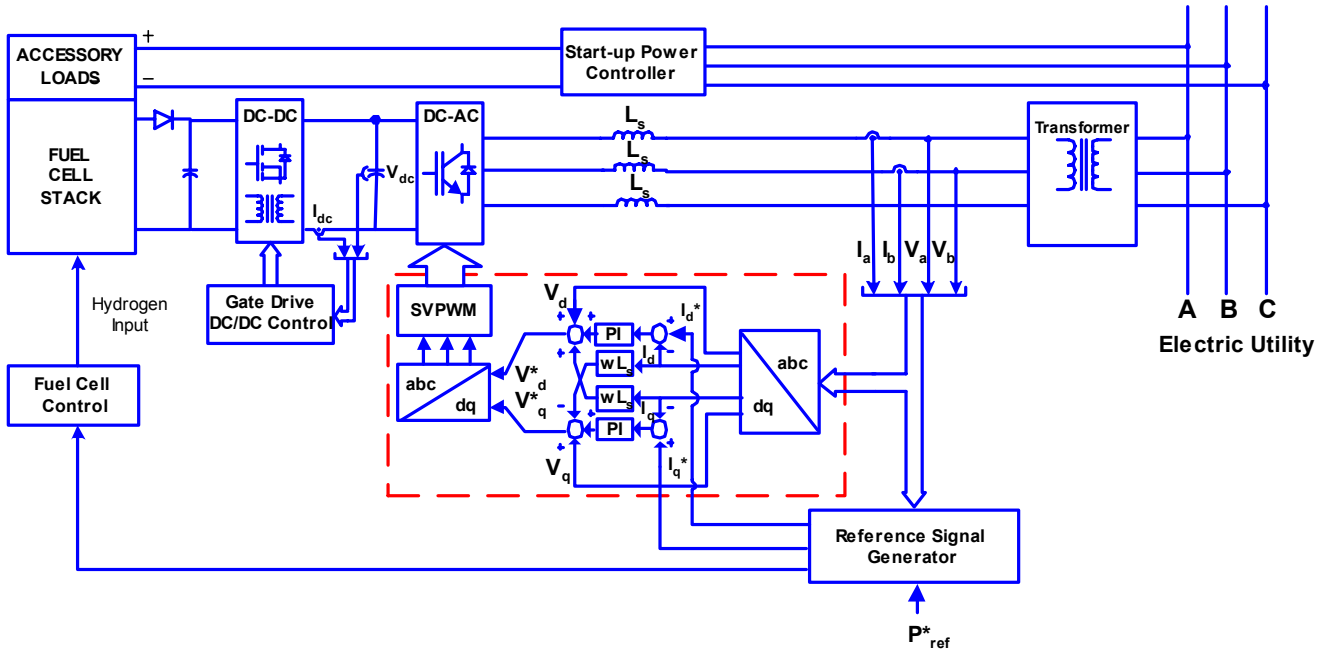

Figure 8-45 Fuel cell power conditioner control system for supplying power to the utility (utility interface)

Figure 8-44 shows the general connection diagram of the fuel cell and its associated power conditioning hardware. Figure 8-45 shows the fuel cell power conditioner control system for supplying power to the utility. The DC-DC converter and the DC-AC inverter are controlled separately. The required electric power to be injected into the utility grid is set by P^*_{ref} signal, the signal generator block then generates appropriate reference signals for the DC-AC inverter and the fuel cell controller to generate more power. The DC-AC inverter control block shows a "d-q" control with space vector PWM. A line frequency isolation transformer is shown to match the output AC voltage of the fuel cell with that of the utility. Utility power can be used initially to perform the fuel cell startup operation. Upon satisfactory startup, current control of the fuel cell power conditioning unit can be used to set the power level to the utility. Higher power fuel cell systems in the 50kW to 500kW range (69, 70, 71) are characteristic of commercial installations such as industrial facilities, hospitals, hotels, fast food outlets, etc. At these power levels 480V, three phase AC output is the preferred output (in the U.S.). It should be noted that a minimum dc-link voltage of 784V DC is essential to generate 480V AC output from a three phase power electronic inverter. The fuel cell voltage must be sufficiently high or a suitable DC-DC converter can be employed to increase the dc-link voltage. If the fuel cell stack voltage can be boosted to 800V DC then a transformer-less system can be envisioned. It should be emphasized that using an isolation transformer in higher voltage / higher power fuel cell systems interconnected to utility offer an effective means of meeting the requirements of domestic and international safety standards for electronic equipment. In the United States, for example, such standards are set by the Occupational Safety and Health Administration (OSHA), with product testing performed according to appointed laboratories, such as Underwriters Laboratories (UL). Throughout Europe, safety standards are established by the International Electro-technical Commission (IEC).

8.2.6 Power Conditioners for Automotive Fuel Cells

A recent announcement by the Secretary of Energy stated that $1.5 billion in U.S. government subsidies would be re-allocated to further develop fuel cell technologies for automotive applications. A number of requirements are necessary for fuel cell vehicles to effectively commercialize (72, 73). Most important of these are the need to further develop hydrogen-reforming technologies and the availability of low cost/ reliable power conditioning systems. In view of this, it is motivating to explore common power conditioning systems that have dual use: both for stationary and automotive fuel cell applications. Development of common standards would be beneficial for the overall fuel cell market.

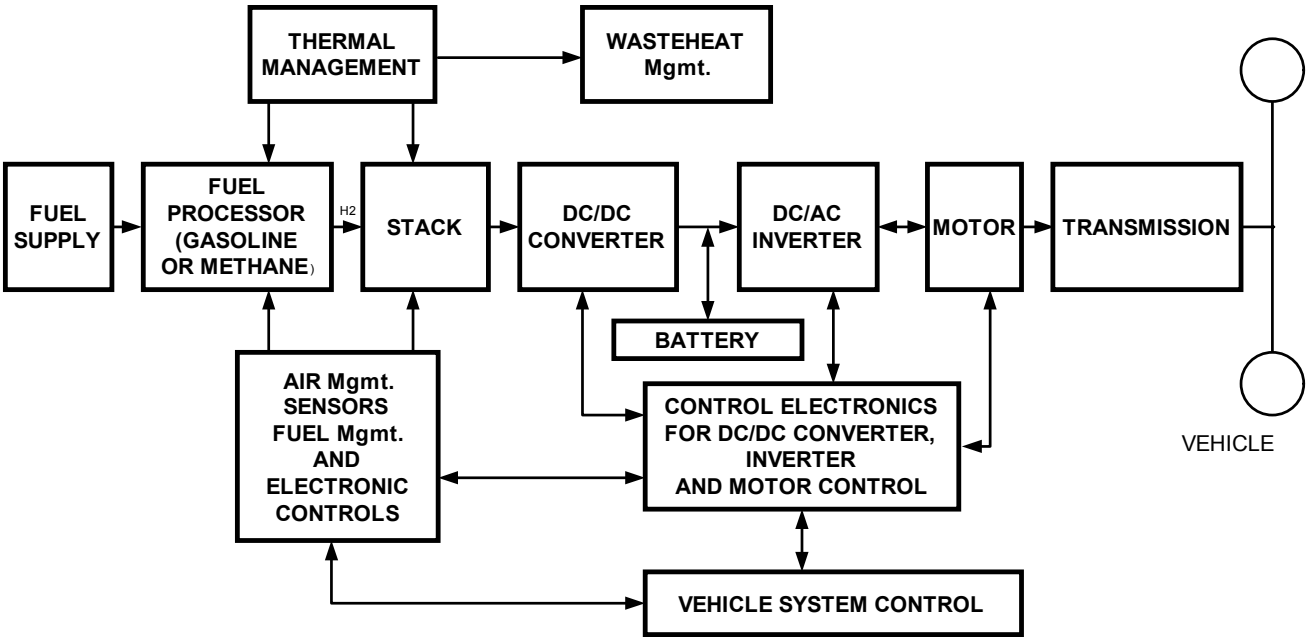

Figure 8-46 A typical fuel cell vehicle system (72)

Figure 8-46 shows a typical fuel cell vehicle system block diagram (72). A fuel cell vehicle system consists of three main components: 1) fuel processor; 2) fuel cell stack, and 3) power conditioning unit (DC to DC or DC to AC) to power a traction motor (AC or DC). A fuel cell system designed for vehicular propulsion applications must have weight, volume, power density, start-up, and transient response similar to the present internal combustion engine vehicles. Polymer electrolyte (PEFC) fuel cells are gaining importance as the fuel cell for vehicular applications (72, 73) because of their low operating temperature, higher power density, specific power longevity, efficiency, and relatively high durability. One problem in PEFC-based technology is that the carbon (CO) concentration in fuel should be reduced to less than 10 parts per million (PPM). Higher CO content in hydrogen contributes to deterioration of cell performance.

Fuel Cell Vehicle Configurations:

Fuel cell vehicles can be classified as either fuel cell electric or fuel cell hybrid vehicles (72, 73). A fuel cell electric vehicle uses the fuel cell system as the power source without the use of the battery. A fuel cell hybrid vehicle consists of a battery or a supercapacitor (72) in addition to the

fuel cell system. This configuration enables most efficient use of both the fuel cell and battery for vehicle propulsion. The battery (or Supercapacitor) provides power during starting/acceleration and the fuel supplies the steady state load. A range extender type fuel cell vehicle can also be designed with low power fuel cell whose function is only to charge the batteries. In this case, the battery is designed to provide full power and the fuel cell is employed as an onboard battery charger.

Power Conditioning System for the Fuel Cell Hybrid Vehicle:
Figure 8-47 shows a typical topology of a power conditioning unit for a fuel cell hybrid powering a three phase variable speed AC traction motor load. The bi-directional converter S2 and S3 can be eliminated if a 42V battery is employed. Figure 8-48 shows the fuel cell converter control system block diagram. The reference signal from the vehicle power controller is used to generate the current reference (I_{ref}) as shown. The current reference I_{ref} is used to control the hydrogen input to the fuel cell stack. Also I_{ref} regulates the current output of the DC to DC boost converter, which powers the DC to AC inverter stage. Accessory loads are powered from the battery. The battery power is also used for system start-up to bring the fuel cell stack voltage to a nominal value.

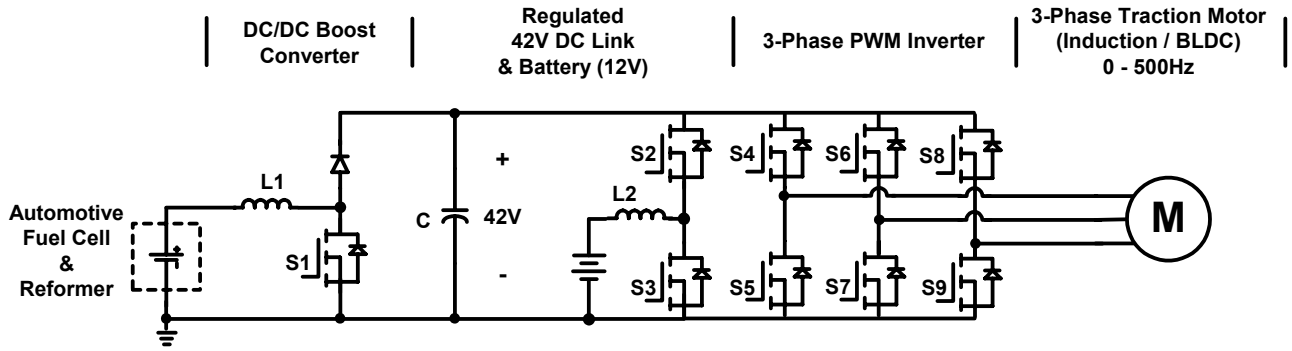

Figure 8-47 Power conditioning unit for fuel cell hybrid vehicle

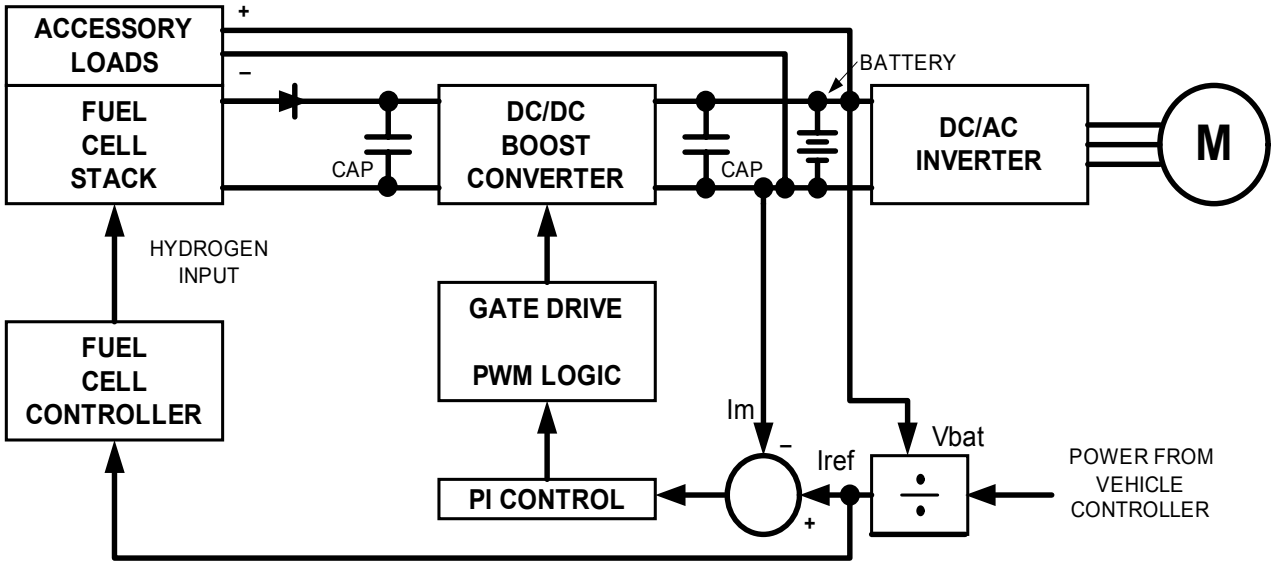

Figure 8-48 Fuel cell power conditioner control system (72)

It is important to note that the vehicle power train for fuel cell powered system is similar to that of battery powered vehicles. The cost of the fuel cell systems, power conditioning unit and the motor drive system must be reduced significantly. The power conditioning system requirements for vehicles include low EMI, high efficiency, low cost, and suitable for intermittent use over a 10-15 year period.

8.2.7 Power Conversion Architectures for a Fuel Cell Turbine Hybrid Interfaced to Local Utility

System studies to date indicate that fuel cell/turbine hybrids could realize a 25 percent increase in efficiency and 25 percent reduction in cost for a comparably sized fuel cell (70, 71). The synergy realized by fuel cell / turbine hybrids derives primarily from using the rejected thermal energy and combustion of residual fuel from a fuel cell in driving the gas turbine. This leveraging of the thermal energy makes the high-temperature molten carbonate and solid oxide fuel cells (SOFC) ideal candidates for hybrid systems. Use of a recuperator contributes to thermal efficiency by transferring heat from the gas turbine exhaust to the fuel and air used in the system. Integrating a pressurized SOFC with an microturbine generator (MTG) to yield a system with a nominal capacity of 250kW has shown a power generating efficiency approaching 60% (70, 71). During normal steady state operation, the SOFC will produce about 80% of the electrical power and the MTG will produce the remaining 20%. Effectively, for this design the fuel cell supplants the combustor of the MTG, providing the added benefit of eliminating combustion and combustion byproduct formation by MTG. For hybrid systems to become popular, the chief hurdle is cost and reliability. The cost of the power conditioning sub-system plays an important role.

Figure 8-49 shows the block diagram of the power conditioning architecture of a typical 250kW fuel cell turbine hybrid system. Three 100kW SOFC stacks, each generating 200V each, are connected in series to generate 600V DC. A DC to DC boost converter is employed to convert the 600V DC generated by SOFC to a 750V dc-link. The 750V dc-link is then connected to the

360kVA three phase PWM inverter to generate 480V, 60Hz output (Figure 8-49). The MTG typically operates at high speed (96,000 rpm rated speed) and is connected to a 3-phase brush-less permanent magnet (PM) generator (74). Utility supplies the necessary startup power for both SOFC and MTG.

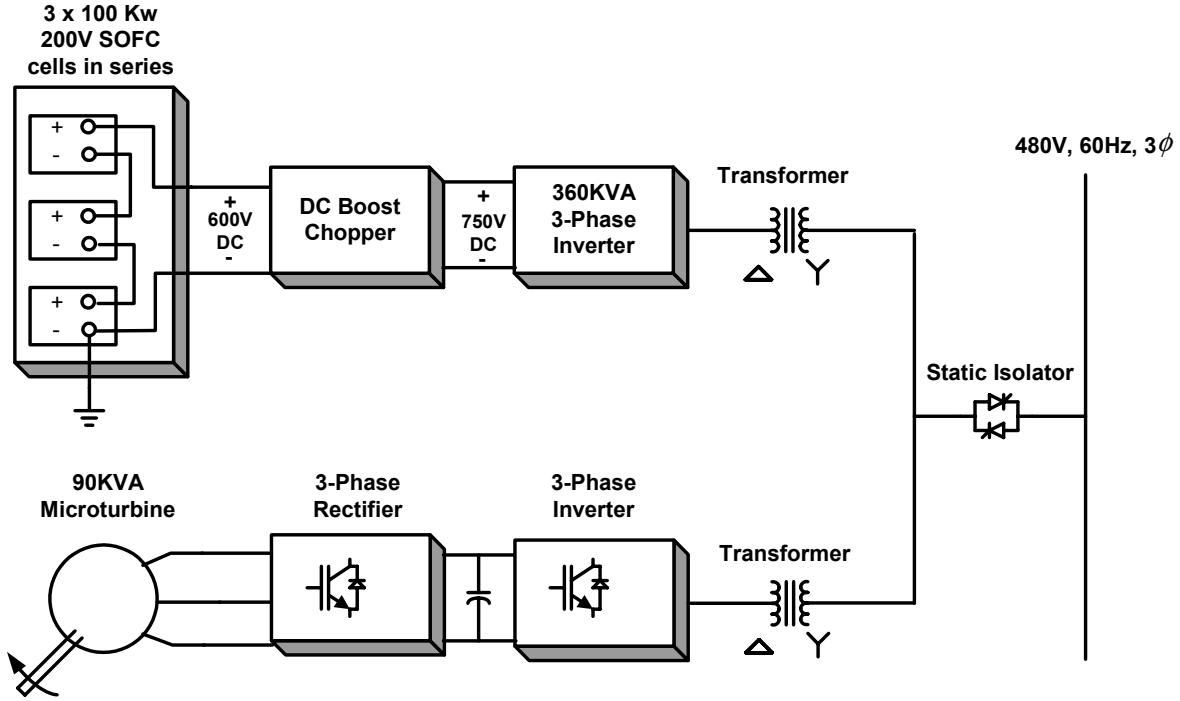

Figure 8-49 Power conditioning architecture for the 250kW fuel cell turbine hybrid system

The electric power generated by the MTG PM generator is at higher frequency (1.6kHz at rated speed) and is converted to DC via a 3-phase PWM rectifier. The DC power is then converted to AC by means of a 3-phase PWM inverter unit (Figure 8-49). The AC electrical outputs of both the SOFC and MTG are combined as shown (Figure 8-49) and connected to the utility. A line frequency isolation transformer is employed at the output terminals of the SOFC and MTG power conditioning units. The transformer provides isolation as well as voltage matching with the utility. The hybrid power generating system is connected to the utility via a static isolator to facilitate rapid disconnection in the event of a fault.

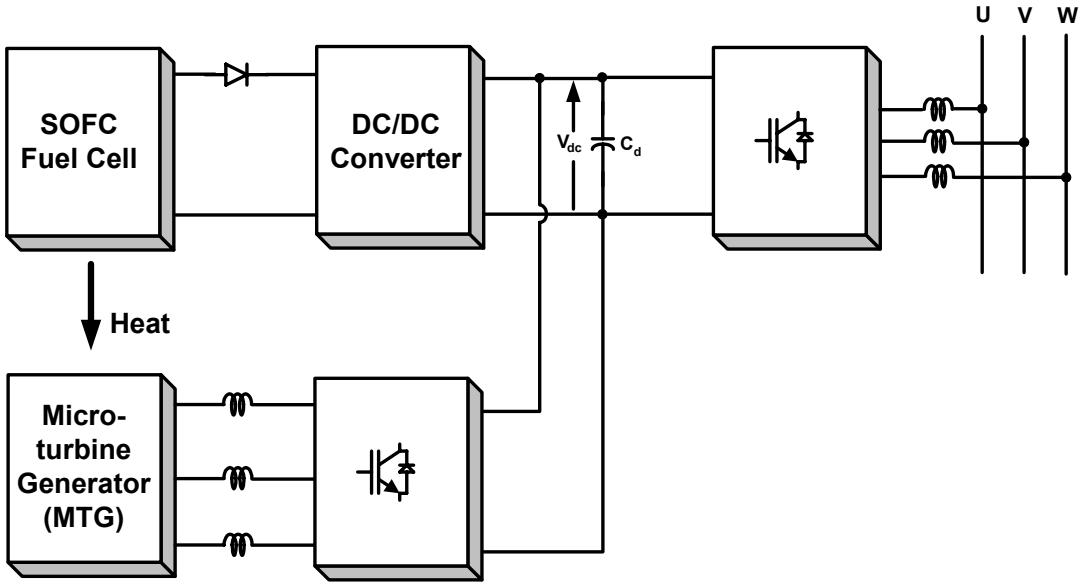

Figure 8-50 Alternative power conditioning architecture for the fuel cell turbine hybrid system with shared dc-link (41)

Shared DC-Link Power Conditioning Architecture (41): Figure 8-50 shows an alternative power conditioning architecture for the fuel cell turbine hybrid system. In this approach, a common dc-link system is envisioned. The SOFC DC-DC converter and the MTG PWM rectifier stages output are paralled together to form a common dc-link. The main advantage of this approach is that one common DC to AC power conditioning unit is necessary. This architecture has the potential to reduce the cost of the power conditioning stage of a hybrid system.

Power Conditioning Architectures for MW Range Fuel Cell Turbine Hybrid Systems (41): A multi-megawatt fuel cell turbine hybrid system is detailed in DOE's Vision 21 program. FuelCell Energy, Inc. (FCE) is developing ultra high efficiency fuel cell/turbine hybrid power plants (75). One hybrid system is based on an innovative power cycle utilizing an indirectly heated gas turbine to supplement fuel cell generated power. System development is being conducted under the Department of Energy's Vision 21 Program through the Office of Fossil Energy, and managed by the National Energy Technology Laboratory (NETL). The project objectives are to design a 40 MW system utilizing the internally reformed Direct FuelCell (DFC) technology being commercialized by FCE (75).

The power conditioning architecture for multi-megawatt fuel cell hybrid systems must operate at medium voltage levels (2300V, 4160V, 6600V or 11000V in the U.S.). Medium voltage power conditioner architectures employing IGCT type devices and/or modular systems employing high voltage IGBTs are possible candidates.

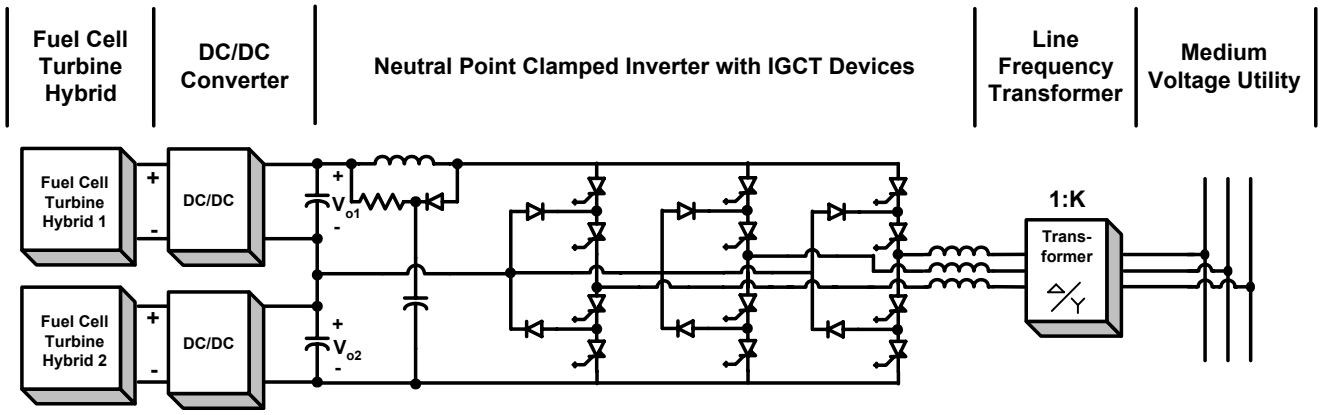

Figure 8-51 Possible medium voltage power conditioning topology for megawatt range hybrid fuel cell systems (41)

Figure 8-51 shows a possible power conditioning topology employing high voltage IGCT devices. It is envisioned that two fuel cell turbine hybrid systems with common dc-link are connected in series via their respective DC to DC Converter stages to form a high voltage dc-link (6000V). A neutral point clamped (NPC) type PWM inverter with 12 IGCT devices is employed to generate 4160V three-phase AC voltage that is suitable for utility interface. Commercial IGCT based NPC inverters are widely available for powering variable speed medium voltage induction motors (52, 53). The stated technology is therefore viable.

8.2.8 Fuel Cell Ripple Current (76)

An important variable in the design of the power conditioner for fuel cell is the amount of ripple current the fuel cell can withstand. Since the reactant utilization is known to impact the mechanical nature of a fuel cell, it is suggested (35) that the varying reactant conditions surrounding the cell (due to ripple current) govern, at least in part, the lifetime of the cells. Both the magnitude and frequency of the ripple current is important. For fuel cells powering single phase loads (60Hz), the ripple current of concern is twice the output frequency i.e. 120Hz. A limit of 0.15 per-unit (i.e. 15% of its rated current) from 10% to 100% load is specified (58). In case of single phase inverters with dual output voltage (120V/240V) there is a possibility of 60Hz ripple current in the fuel cell under unbalanced loading conditions (i.e. one output phase loaded and the other unloaded, Figures 8-40e and f). A limit of 0.1 per-unit is specified for 60Hz ripple current from 10% to 100% load (58). Further, the magnitude of the low frequency ripple current drawn from the fuel cell by the DC-DC converter is largely dependent on the voltage loop response characteristics. Also the dc-link capacitor size determines the 120Hz voltage ripple on dc-link, which in turn has an impact on the input current drawn from the fuel cell. It should be noted that switching frequency components in the DC-DC converter can be easily filtered via a small, high frequency capacitive filter. For balanced three phase AC loads at the inverter output, the possibility of low frequency components in the fuel cell input current is low.

Corrective Measures for Limiting Fuel Cell Ripple Current: The following corrective measures are suggested for limiting the fuel cell ripple current (especially for power conditioners with single phase AC output):

- Install an input filter to filter the 120Hz component of the ripple current to 0.15 per-unit: this approach contributes to additional size, weight and cost of the unit.
- Increase the size of dc-link capacitor in the DC to AC inverter: size, weight, cost is of concern.
- Reduce the response time of the voltage loop of the DC-DC converter: this will affect the regulation of the dc-link and impact the quality of inverter AC output, and possibly increase the size of output AC filter.

8.2.9 System Issues: Power Conversion Size, Cost

400V DC is required to produce 120V/240V AC at the output (Eqn. 8-51). If the fuel cell can produce 400V DC, then only a inverter stage is required, resulting in lowest cost for power conditioning. Present day commercially available fuel cells produce low voltage (12V to 100V), therefore a line frequency transformer to increase the ac voltage, or a DC to DC converter to boost the DC voltage is required, adding to cost/weight and volume. Figure 8-52 shows a representative cost per kW of the power conditioning unit as the voltage and current are varied for a certain power level. It is clear from this figure that extremes of voltage at low power and high current at high power levels does not result in an optimum design. In general, higher voltage levels are required at higher power outputs to minimize the cost of power conditioning hardware.

The other issue is power density and size of power conditioning unit. Using higher switching frequency for power conversion should result in smaller size. However, the switching losses are higher, and a design compromise becomes necessary. Employing power semiconductor devices with lower losses, combined with active cooling methods, should yield an optimum size. Power integrated circuits can also be considered for further size reduction, and become viable if the fuel cell systems are produced in high volume.

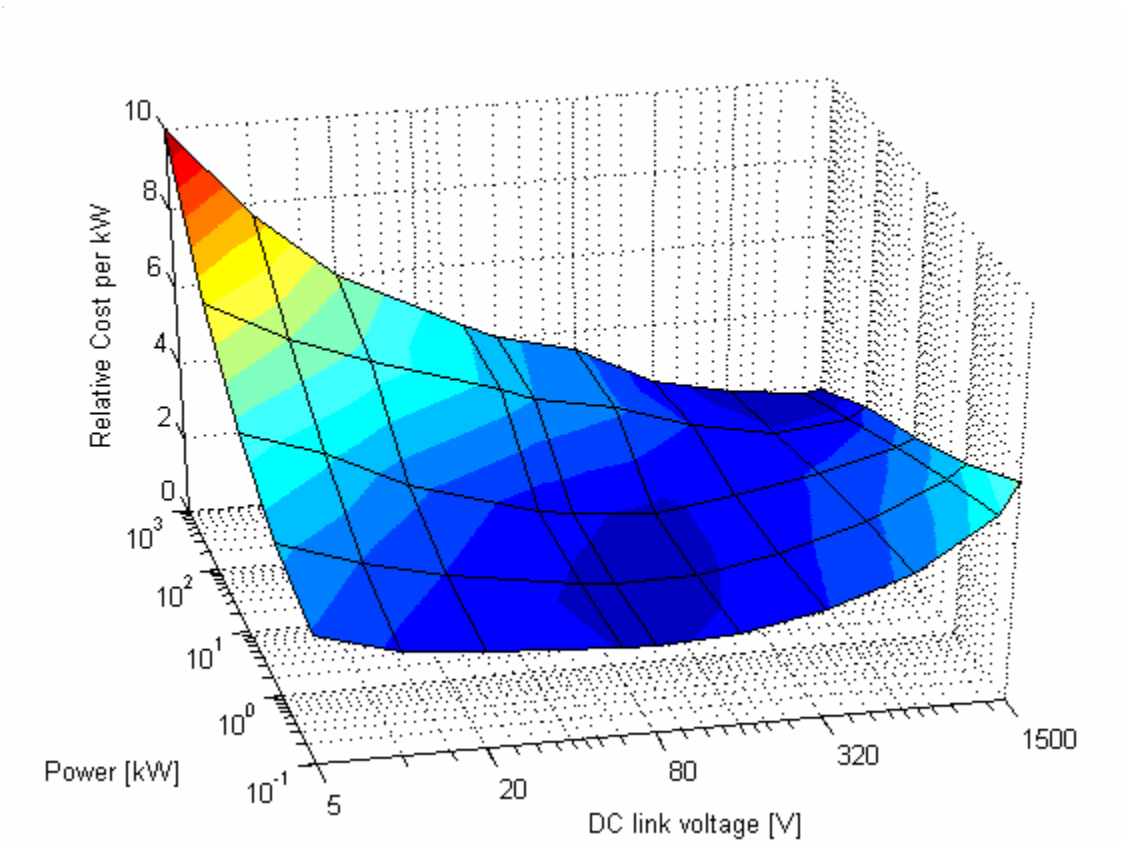

Figure 8-52 Representative cost of power conditioning as a function of power and dc-link voltage

8.3 References (sections 8.1 and 8.2)

1. J.P. Kopasz, S. Ahmed, M. Krumpelt, P. Devlin, "Challenges in Reforming Gasoline: All Components Are Not Created Equal," SAE Technical Paper Series 2001-0101915, International Spring Fuels and Lubricants Meeting and Exhibition, May 7-9, 2001.
2. Communication with Argonne National Laboratory, Argonne, Illinois, August 2000.
3. Federal Register, Volume 66, Number 12, p. 5001, January 18, 2001.
4. P.G. Gray and J.C. Frost, "Impact of Catalysis on Clean Energy in Road Transportation," Johnson Matthey, Energy&Fuels, Vol. 12, No. 6, pp. 1121 - 1129, 1998.
5. General Motors Corporation, Argonne National Laboratory, BP, ExxonMobil, and Shell, 2001, Well-to-Wheel Energy Use and Greenhouse Gas Emissions of Advanced Fuel/Vehicle Systems - North American Analysis - Volume 1, Executive Summary Report, June.2001.
6. M. Wang, "Well-to-Wheels Analysis of Fuel-Cell Vehicle/Fuel Systems" presented at the AIChE Spring National Meeting, March 10-14, New Orleans, LA, 2002.
7. S. Ahmed, R. Kumar, and M. Krumpelt, "Fuel Processing for Fuel Cell Power Systems," ANL, *Fuel Cells Bulletin*, Elsevier Scientific, Ltd., ISSN 1464-2859, No. 12, September 1999.
8. J. Holmes, "Fuel Choices for Fuel Cell Powered Vehicles," statement before Subcommittee on Energy and Environment of the Committee on Science, U.S. House of Representatives, on behalf of The American Petroleum Institute, Exxon Corporation, October 5, 1999.

9. P. Devlin, DOE-OTT and R. Sutton, ANL, "Program Overview," DOE Fuels for Fuel Cell Program, 2000.
10. Communication with Forschungszentrum Jillich, Rilich, Germany, July 2000.
11. F. Uribe, et al., DOE 2002 Review, Fuel Cell for Transportation Program, Golden, CO. May 9-10, 2002.
12. Communication with Ceramatec, Salt Lake City, UT, April 2000.
13. Communications with IFC, South Windsor, CT, September 2000 and June 2002.
14. Probstein and Hicks, "Synthetic Fuels," McGraw-Hill Book Company, 1982.
15. U. Bossel, "Portable Self-Sufficient 12 Volt PEFC Power Source with Integrated Chemical Hydrogen Generator," Pg. 742, *Fuel Cell Seminar Abstracts*, Courtesy Associates, Inc., November 1998.
16. J.C. Cross, et al., "Fuel Processing Technology for Premium Power Fuel Cell Systems," Epyx/ADL, Pg. 749, *Fuel Cell Seminar Abstracts*, Courtesy Associates, Inc., November 1998.
17. J.R. Rostrup-Nielsen, L.J. Christiansen, and K. Aasberg-Petersen, "Fuel Processing for High Efficiency Fuel Cell Systems," Haldor Topsoe A/S, Grove III Fuel Cell Symposium, September 1993.
18. T.J. Flynn, R. Privette, et al., "Compact Fuel Processor for Fuel Cell-Powered Vehicles," McDermott Technology, Inc. and Catalytical Advanced Technologies, Paper 1999-01-0536, Society of Automotive Engineers, Inc., 1999.
19. K. Ahmed and K. Föger, "Steam pre-reforming of propane to a methane-rich fuel for internal reforming in solid oxide fuel cells," Ceramic Fuel Cells Ltd., 4th EUROSOFC, Lucerne/Switzerland, July 2000.
20. "Gasoline to Hydrogen - A New Route for Fuel Cells," ANL, Electric & Hybrid Vehicle Technology of '97, 1997.
21. Communication with Johnson Matthey Technology Centre, Reading, England, February 2000.
22. S. Ahmed, et al., “Catalytic Partial Oxidation Reforming of Hydrocarbon Fuels,” ANL, Pg. 242, *Fuel Cell Seminar Abstracts*, Courtesy Associates, Inc., November 1998.
23. S. Ahmed, M. Krumpelt, “Hydrogen from hydrocarbon fuels for fuel cells,” ANL, for *International Journal of Hydrogen Energy*, Elsevier, 26 (2001) p. 291-301, 2001.
24. Chemical Process Industries, fourth edition, R. Shreve and J. Brink, McGraw-Hill, 1977.
25. D. Wilkinson, A. Steck, "General Progress in the Research of Solid Polymer, Fuel Cell Technology at Ballard," 1997 Proceedings of the Second International Symposium on New Materials for Fuel Cells and Modem Battery Systems, Montreal, Quebec Canada, July 1997.
26. Coal Gasification Systems: A Guide to Status, Applications and Economics, prepared by Synthetic Fuels Associates, Inc., EPRI AP-3109, Project 2207, Final Report; June 1983.
27. Coal Gasification Guidebook: Status, Applications and Technologies, EPRI TR- 102034, December 1993.
28. J. Appleby and F. Foulkes, "Fuel Cell Handbook," Texas A&M University, Van Nostrand Reinhold, New York (out of print), republished by Krieger Publishing Co., Melbome, FL, 1989.
29. S. Lee, R. Kumar, M. Krumpelt, "Removal of CO from Reformate for PEFC Application," ANL, Pg. 578, Fuel Cell Seminar Abstracts, Courtesy Associates, Inc., November 1998.

30. W. Mitchell, "Development of an Integrated Reformer/Fuel Cell Power System for Petroleum and Alcohol-Fueled Vehicles, Part I - Brassboard Demonstration," Epyx, Pg. 230, Fuel Cell Seminar Abstracts, Courtesy Associates, Inc., November 1998.
31. J. Hirschenhofer and J. White, "Preliminary Assessment of Planar Solid Oxide Fuel Cells for Transportation Power Applications," Parsons Corporation, for ANUDOE, to be published, October 2000.
32. M. Krumpelt, T. R. Krause, J. D. Carter, J. P. Kopasz, S. Ahmed, "Fuel Processing for Fuel Cell Systems in Transportation and Portable Power Applications," Argonne National Laboratory, 9700 South Cass Ave., Argonne, IL 60439. To be submitted for publication in *Catalysis Today*.
33. C. Pereira, R. Wilkenhoener, S. Ahmed, and M. Krumpelt, "Catalytic Reforming of Gasoline and Diesel Fuel," ANL, AlChE Spring 2000 Meeting, March 2000.
34. J. Mauzey, and R. Woods, "Fuel-Flexible Fuel Processor," J. Cuzens, Hydrogen Burner Technology, Pg. 234 Fuel Cell Seminar Abstracts, Courtesy Associates, Inc., November 1998.
35. C. Pereira, S. Ahmed, S.H.D. Lee, M. Krumpelt, "Integrated Fuel Processor Development," Society of Automotive Engineers, Inc., 02FCC-161, 2002.
36. J. Cuzens, J. Mauzey, and R. Woods, "Fuel-Flexible Fuel Processor," Hydrogen Burner Technology, Pg. 234 Fuel Cell Seminar Abstracts, Courtesy Associates, Inc., November 1998.
37. Department of Energy, "Fuel Cells: Opening New Frontiers in Power Generation," November, 1999.
38. J. Larminie and A. Dicks, *"Fuel Cell System Explained"*. John Wiley & Sons LTD, 2000
39. Ned Mohan, et al, "Power electronics: converters, applications & design," John Wiley & Sons, Second Edition, 1995. ISBN: 0471584088
40. P. Krein, "Elements of power electronics," New York: Oxford, 1998
41. A.I. Pressman, "Switching power supply design," McGraw-Hill, 1991
42. R. W. Erickson and D. Maksimovic, " Fundamental of Power Electronics: Second Edition," Kluwer Academic Publisher, 2001
43. N. Hingorani and K. Stahlkopf, "High-Power Electronics" Scientific American, November 1993
44. B. J. Baliga, "Power ICs In The Saddle," IEEE Spectrum, vol. 32, no. 7, pp. 34-49, July 1995.
45. Application notes: International Rectifiers, Inc: http://www.irf.com
46. C. Blake and C. Bull, "MOSFETs or IGBTs Choose wisely" International Rectifiers, Application notes
47. E. Carrol, N. Galster "IGBT or IGCT: Considerations for very high power applications," ABB Technical article. http://www.abb.com
48. A.H. Weinberg, P.R. Boldo, "A high power high frequency DC to DC converter for space applications," IEEE PESC Conference, 1992, pp.1140 to 1147
49. W.A. Peterson and S.L. Plaskon, "Dual charge mode control of a current fed boost-buck push-pull converter," IEEE IAS Conference, 1998, pp. 1596 to 1603
50. P. Enjeti, "Switching power supply design," ELEN-689, Course notes, Texas A&M University, 1998
51. P. Enjeti, "Rectifier and Inverter Circuits," ELEN-613, Course notes, Texas A&M University, 2000

52. DOE Future energy challenge: 2001, Low cost fuel cell inverter design competition.
53. "Analysis & design of a low cost fuel cell inverter for fuel cell systems," Texas A&M University Report to DOE, August 2001
54. R. Gopinath, S.S. Kim, P. Enjeti, et al, "Development of a low cost fuel cell inverter with DSP control," IEEE PESC Conference record, June 2002
55. P. Enjeti, P. Krein, J. Lai, "Power conditioning approaches to fuel cells and gas turbine hybrids," NTU short course (Sponsored by DOE), March 2002
56. A. Kusko, "Emergency/Standby power systems," Mc-Graw-Hill Book company, 1989, ISBN: 0-07-035688-0
57. Avistalabs, "SR-12 Modular PEM Generator Operator's Manual," 2000
58. E.Santi, et al, "A Fuel Cell Based Domestic Uninterruptible Power Supply," IEEE Applied Power Electronics Conference and Exposition, APEC '02 Proceedings P 605-613, 2002
59. Sukumara, G.V.; Parthasarathy, A.; Shankar, V.R, "Fuel cell based uninterrupted power sources," Power Electronics and Drive Systems, Proceedings Volume: 2 Page(s): 728 –733, 1997
60. W. Choi, P. Enjeti, "Design of a modular fuel cell based UPS system," paper submitted to IEEE APEC'03
61. P. Enjeti and J. Howze, "A 2kW fuel cell based UPS system," Texas state energy conservation office and DOE sponsored project, Texas A&M University, 2002
62. Montena, "http://www.montena.com/," PC2500 Ultracapacitor Datasheet
63. Christopher C. Boyer, "Special Topics: Fuel Cell Technology," CHEN 689 Class Notes, Texas A&M University, 2002
64. J. L. Durán-Gómez, P. Enjeti and A. von Jouanne, "An Approach to Achieve Ride-Through of an Adjustable Speed Drive with Flyback Converter Modules Powered by Super Capacitors," *IEEE Transactions on Industry Applications,* Vol. 38, No. 2, March/April 2002, pp 514-522
65. IEEE standard P1547 document: http://www.ieee.org
66. "220kW solid oxide fuel cell / microturbine generator hybrid proof of concept demonstration report," March 2001, California Energy Commission
67. H.G. Ayagh, J.M. Daly, et al. "Critical Components for Direct Fuel Cell/Turbine Ultra-Efficiency System," Presented at Turbine power systems conference and conditioning monitoring workshop, Galveston, TX, Feb 2002. Authors affiliation: Fuel Cell Energy Inc. Danbury, CT
68. 30kW Capstone microturbine generator, http://www.capstone.com
69. P. Lataire, "White paper on the new ABB medium voltage drive system, using IGCT power semiconductors and direct torque control," EPE journal, Vol. 7, No. ¾, December 1998, pp 40-45
70. J.P. Lyons. V. Vlatkovic, P.M. Espelage, F.H. Boettner, E. Larsen, (*GE*), "Innovation IGCT Main Drives," IEEE IAS, Conf. Rec. 1999
71. Randall S. Gemmen, "Analysis for the Effect of Inverter Ripple Current on Fuel Cell Operating Condition," ASME 2001 International Mechanical Engineering Congress and Exposition, November 11, 2001, New York
72. McDermott Technology, Inc. and Northern Research and Engineering Corporation , "Fuel Cell/Micro-Turbine Combined Cycle," Final Report for U.S. Department of Energy, December 1999

73. Siemens Westinghouse Power Corporation, "A High Efficiency PSOFC/ATS-Gas Turbine Power System," Final Report for U.S. Department of Energy, February 2001
74. "Switchmode: A design guide for switching power supply circuits & components," Motorola publications, Ref: SG79/D, REV5, 1993
75. K. Rajashekara, "Propulsion system strategies for fuel cell vehicles," Fuel cell power for transportation 2000 conference, SAE 2000 World congress, March 2000, Ref: 2000-01-0369
76. T. Matsumoto, et al, "Development of fuel cell hybrid vehicle," Fuel cell power for transportation 2002 conference, SAE 2002 World congress, March 2000, Ref: 2002-01-0096

8.4 System Optimization

The design and optimization of a fuel cell power system is very complex because of the number of required systems, components, and functions. Many possible design options and trade-offs affect unit capital cost, operating cost, efficiency, parasitic power consumption, complexity, reliability, availability, fuel cell life, and operational flexibility. Although a detailed discussion of fuel cell optimization and integration is not within the scope of this section, a few of the most common system optimization areas are examined.

From Figure 8-53, it can be seen that the fuel cell itself has many trade-off options. A fundamental trade-off is determining where along the current density voltage curve the cell should operate. As the operating point moves up in voltage by moving (left) to a lower current density, the system becomes more efficient but requires a greater fuel cell area to produce the same amount of power. That is, by moving up the voltage current density line, the system will experience lower operating costs at the expense of higher capital costs. Many other parameters can be varied simultaneously to achieve the desired operating point. Some of the significant fuel cell parameters that can be varied are pressure, temperature, fuel composition and utilization, and oxidant composition and utilization. The system design team has a fair amount of freedom to manipulate design parameters until the best combination of variables is found.

8.4.1 Pressure

Fuel cell pressurization is typical of many optimization issues, in that there are many interrelated factors that can complicate the question of whether to pressurize the fuel cell. Pressurization improves process performance at the cost of providing the pressurization. Fundamentally, the question of pressurization is a trade-off between the improved performance (and/or reduced cell area) and the reduced piping volume, insulation, and heat loss compared to the increased parasitic load and capital cost of the compressor and pressure-rated equipment. However, other factors can further complicate the issue. To address this issue in more detail, pressurization for an MCFC system will be examined.

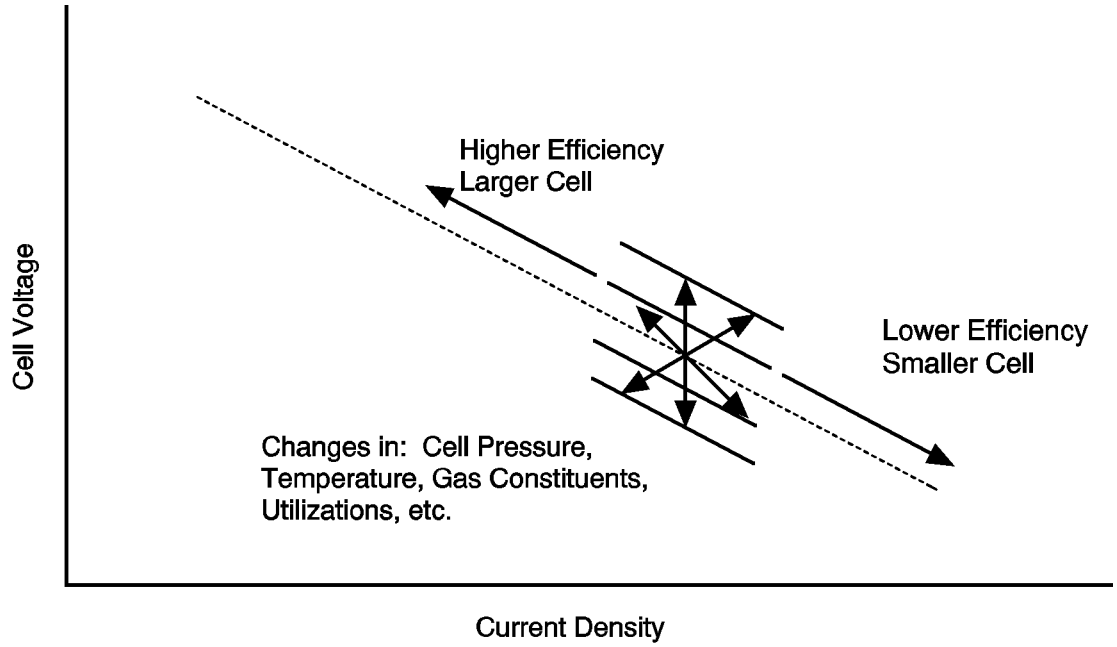

8-

Figure 8-53 Optimization Flexibility in a Fuel Cell Power System

In an MCFC power system, increased pressure can result in increased cathode corrosion. Cathode corrosion is related to the acidity of the cell, which increases with the partial pressure of CO_2, and therefore with the cell pressure. Such corrosion is typified by cathode dissolution and nickel precipitation, which can ultimately result in a shorted cell, causing cell failure (1). Thus, the chosen pressure of the MCFC has a direct link to the cell life, economics, and commercial viability.

Increasing the pressure in a MCFC system can also increase the likelihood of soot formation and decrease the extent of methane reforming. Both are undesirable. Furthermore, the effect of contaminants on the cell and their removal from a pressurized MCFC system have not been quantified. The increased pressure also will challenge the fuel cell seals (1).

The selection of a specific fuel cell pressure will affect numerous design parameters and considerations such as the current collector width, gas flow pattern, pressure vessel size, pipe and insulation size, blower size and design, compressor auxiliary load, and the selection of a bottoming cycle and its operating conditions.

These issues do not eliminate the possibility of a pressurized MCFC system, but they do favor the selection of more moderate pressures. For external reforming systems sized near 1 MW, the current practice is a pressurization of 3 atmospheres.

The performance of an internal reforming MCFC also would benefit from pressurization, but unfortunately, the increase is accompanied by other problems. One problem that would need to be overcome is the increased potential for poisoning the internal reforming catalyst resulting from the

increase in sulfur partial pressure. The current practice for internal reforming systems up to 3 MW is atmospheric operation.

Pressurization of an SOFC yields a smaller gain in fuel cell performance than either the MCFC or PAFC. For example, based on the pressure relationships presented earlier, changing the pressure from one to ten atmospheres would change the cell voltage by ~150, ~80, and ~60 mV for the PAFC, MCFC, and SOFC, respectively. In addition to the cell performance improvement, pressurization of SOFC systems allows the thermal energy leaving the SOFC to be recovered in a gas turbine, or gas turbine combined cycle, instead of just a steam bottoming cycle. Siemens Westinghouse is investigating the possibilities associated with pressurizing the SOFC for cycles as small as 1 to 5 MW.

Large plants benefit the most from pressurization, because of the economy of scale on equipment such as compressors, turbines, and pressure vessels. Pressurizing small systems is not practical, as the cost of the associated equipment outweighs the performance gains.

Pressurization in operating PAFC systems demonstrates the economy of scale at work. The IFC 200 kWe and the Fuji Electric 500 kWe PAFC offerings have been designed for atmospheric operation, while larger units operate at pressure. The 11 MWe plant at the Goi Thermal Power Station operated at a pressure of 8.2 atmospheres (2), while a 5 MWe PAFC unit (NEDO / PAFCTRA) operates at slightly less than 6 atmospheres (3). NEDO has three 1 MWe plants, two of which are pressurized while one is atmospheric (3).

Although it is impossible to generalize at what size a plant would benefit by pressurization, when plants increase in size to approximately 1 MW and larger, the question of pressurization should be evaluated.

8.4.2 Temperature

Although the open circuit voltage decreases with increasing temperature, the performance at operating current densities increases with increasing temperature due to reduced mass transfer polarizations and ohmic losses. The increased temperature also yields higher quality rejected heat. An additional benefit to an increased temperature in the PAFC is an increased tolerance to CO levels, a catalyst poison. The temperatures at which the various fuel cells can operate are, however, limited by material constraints. The PAFC and MCFC are both limited by life shortening corrosion at higher temperatures. The SOFC has material property limitations. Again, the fuel cell and system designers should evaluate what compromise will work best to meet their particular requirements.

The PAFC is limited to temperatures in the neighborhood of 200ºC (390ºF) before corrosion and lifetime loss become significant. The MCFC is limited to a cell average temperature of approximately 650ºC (1200ºF) for similar reasons. Corrosion becomes significant in an MCFC when local temperatures exceed 700ºC (1290ºF). With a cell temperature rise on the order of 100ºC (180ºF), an average MCFC temperature of 650ºC (1200ºF) will provide the longest life, highest performance compromise. In fact, one reference (4) cites "the future target of the operating temperature must be 650°C $\pm$30°C (1290°F $\pm$55°F)."

The high operating temperature of the SOFC puts numerous requirements (phase and conductivity stability, chemical compatibility, and thermal expansion) on material selection and development (5). Many of these problems could be alleviated with lower operating temperatures. However, a high temperature of approximately 1000°C (1830ºF), i.e., the present operating temperature, is required in order to have sufficiently high ionic conductivities with the existing materials and configurations (5).

8.4.3 Utilization

Both fuel and oxidant utilizations[51] involve trade-offs with respect to the optimum utilization for a given system. High utilizations are considered to be desirable (particularly in smaller systems) because they minimize the required fuel and oxidant flow, for a minimum fuel cost and compressor/blower load and size. However, utilizations that are pushed too high result in significant voltage drops. One study (6) cites that low utilizations can be advantageous in large fuel cell power cycles with efficient bottoming cycles because the low utilization improves the performance of the fuel cell and makes more heat available to the bottoming cycle. Like almost all design parameters, the selection of optimum utilization requires an engineering trade-off that considers the specifics of each case.

Fuel Utilization: High fuel utilization is desirable in small power systems, because in such systems the fuel cell is usually the sole power source. However, because the complete utilization of the fuel is not practical, except for pure H_2 fuel, and other requirements for fuel exist, the selection of utilization represents a balance between other fuel/heat requirements and the impact of utilization on overall performance.

Natural gas systems with endothermic steam reformers often make use of the residual fuel from the anode in a reformer burner. Alternatively, the residual fuel could be combusted prior to a gas expander to boost performance. In an MCFC system, the residual fuel often is combusted to maximize the supply of CO_2 to the cathode while at the same time providing air preheating. In an SOFC system, the residual fuel often is combusted to provide high-temperature air preheating.

The designer has the ability to increase the overall utilization of fuel (or the oxidant) by recycling a portion of the spent stream back to the inlet. This increases the overall utilization while maintaining a lower per pass utilization of reactants within the fuel cell to ensure good cell performance. The disadvantage of recycling is the increased auxiliary power and capital cost of the high temperature recycle fan or blower.

One study by Minkov, et al. (6) suggests that low fuel and oxidant utilizations yield the lowest COE in large fuel cell power systems. By varying the fuel cell utilization, the electric power generation split between the fuel cell, steam turbine, and gas turbine are changed. The low fuel utilization decreases the percentage of power from the fuel cell while increasing the fuel cell performance. The increased power output from the gas turbine and steam turbine also results in their improved performance and economy of scale. The specific analysis results depend upon the assumed stack costs. The optimal power production split between the fuel cell and the gas and steam turbines is approximately 35%, 47%, and 17% for a 575 MW MCFC power plant. The

[51]. Utilization - the amount of gases that are reacted within the fuel cell compared to that supplied.

associated fuel utilization is a relatively low 55%. It remains to be seen whether this trend will continue to hold for the improved cells that have been developed since this 1988 report was issued.

Oxidant Utilization: In addition to the obvious trade-off between cell performance and compressor or blower auxiliary power, oxidant flow and utilization in the cell often are determined by other design objectives. For example, in the MCFC and SOFC cells, the oxidant flow is determined by the required cooling. This tends to yield oxidant utilizations that are fairly low (~25%). In a water-cooled PAFC, the oxidant utilization based on cell performance and a minimized auxiliary load and capital cost is in the range of 50 to 70%.

8.4.4 Heat Recovery

Although fuel cells are not heat engines, heat is still produced and must be removed. Depending upon the size of the system, the temperature of the available heat, and the requirements of the particular site, this thermal energy can be either rejected, used to produce steam or hot water, or converted to electricity via a gas turbine or steam bottoming cycle or some combination thereof.

Cogeneration: When small quantities of heat and/or low temperatures typify the waste heat, the heat is either rejected or used to produce hot water or low-pressure steam. For example, in a PAFC where the fuel cell operates at approximately 205°C (400°F), the highest pressure steam that could be produced would be something less than 14 atmospheres (205 psia). This is obviously not practical for a steam turbine bottoming cycle, regardless of the quantity of heat available. At the other end of the spectrum is the TSOFC, which operates at ~1000°C (~1800°F) and often has a cell exhaust temperature of approximately 815°C (1500°F) after air preheating. Gas temperatures of this level are capable of producing steam temperatures in excess of 540°C (1000°F), which makes it more than suitable for a steam bottoming cycle. However, even in an SOFC power system, if the quantity of waste heat is relatively small, the most that would be done with the heat would be to make steam or hot water. In a study performed by Siemens Westinghouse of 50 to 2000 kW TSOFC systems, the waste heat was simply used to generate 8 atmosphere (100 psig) steam (7).

Bottoming Cycle Options: Whenever significant quantities of high-temperature rejected heat are available, a bottoming cycle can add significantly to the overall electric generation efficiency. Should the heat be contained within a high-pressure gas stream, then a gas turbine potentially followed by a heat recovery steam generator and steam turbine should be considered. If the hot gas stream is at low pressure, then a steam bottoming cycle is logical.

If a steam bottoming cycle is appropriate, many design decisions need to be made, including the selection of the turbine cycle (reheat or non-reheat) and the operating conditions. Usually, steam turbines below 100 MW are non-reheat, while turbines above 150 MW are reheat turbines. This generalization is subject to a few exceptions. In fact, a small (83 MW) modern reheat steam turbine went into operation (June 1990) as a part of a gas turbine combined cycle repowering project (8).

8.4.5 Miscellaneous

Compressor Intercooling: Whether a compressor should be intercooled or not depends on the trade-off between the increased efficiency of the intercooled compressor and its increased capital cost. In general, intercooling is required for large compressors with pressure ratios that exceed approximately 5:1 (9). The designer also should consider whether the heat is advantageous to the process. For example, when near the 5:1 pressure ratio, it may not be appropriate to intercool if the compressed stream will subsequently require preheating as it would with the process air stream of an MCFC or SOFC system.

Humidification/Dehumidification: Water often is added or removed in fuel cell systems to promote or prevent certain chemical reactions. For some reactions, excess water can help to drive the reaction, while too much requires larger equipment and can even reduce the yield of a reaction or decrease the performance of a fuel cell. Excess water often is utilized to increase the yield of reforming reactions and the water gas shift.

In a natural gas fueled PAFC, water is condensed out of the fuel stream going to the fuel cell to increase the partial pressure of hydrogen. In a coal gasification MCFC, water often is added to the fuel stream prior to the fuel cell to prevent soot formation. The addition of excess steam not only prevents soot formation, but also causes a voltage drop of approximately 2 mV per each percentage point increase in steam content (10). The use of zinc ferrite hot gas cleanup can aggravate the soot formation problem because of the catalytic effect of the sorbent on carbon formation, and requires even higher moisture levels (11).

Maintaining the proper quantity of water within a PEFC is very important for proper operation. Too much, and the cell will flood; too little, and the cell membrane will dehydrate. Either will severely degrade cell performance. The proper balance is achieved only by considering water production, evaporation, and humidification levels of the reactant gases. Achieving the proper level of humidification is also important. With too much humidification, the reactant gases will be diluted, with a corresponding drop in performance. The required humidification level is a complex function of the cell temperature, pressure, reactant feed rates, and current density. Optimum PEFC performance is achieved with a fully saturated, yet unflooded membrane (12).

8.4.6 Concluding Remarks on System Optimization

System design and optimization encompass many questions, issues, and trade-offs. In the process of optimizing a power plant design, the engineer will address the selection of fundamental processes, component arrangements, operating conditions, fuel cell and bottoming cycle technologies and associated power production split, system integration, and capital and life cycle costs. The design will be governed by criteria such as output, weight, fuel basis, emissions, and cost objectives. Site and application specific criteria and conditions may strongly influence the cycle design criteria and resulting design.

The objective of this system optimization discussion was not to present a detailed review of the subject of optimization, but simply to present select issues of system optimization as they apply to fuel cell power systems.

8.5 Fuel Cell System Designs

The following five cycles are examples of current fuel cell offerings that reflect manufacturers' anticipated commercialization plans. These cycles are based on information available in relevant literature and may differ from the ultimate size of the commercial offering.

8.5.1 Natural Gas Fueled PEFC System

A natural gas PEFC power plant configuration is shown in Figure 8-54 and is a slight simplification of a cycle published in 1997 by a Ballard Researcher (13). In light of the PEFC sensitivity to CO, CO_2 and methane, the fuel processing represents a significant portion of the cycle. Natural gas fuel enters a fuel compressor and a fuel cleanup device. (The reference document does not describe the cleanup device, but it is assumed to be a sulfur polisher to prevent poisoning of the fuel cell catalyst.) The cleaned gas is mixed with water in a vaporizer, which evaporates the liquid water into water vapor with waste heat from the reformer. This humidified fuel is reformed in the steam reformer. Because natural gas reformate is high in CO, the reformate is sent to a shift converter and selective oxidizer to reduce the CO to 10 to 50 ppm. This hydrogen rich/carbon monoxide lean fuel is fed to the PEFC stack where it reacts electrochemically with compressed air.

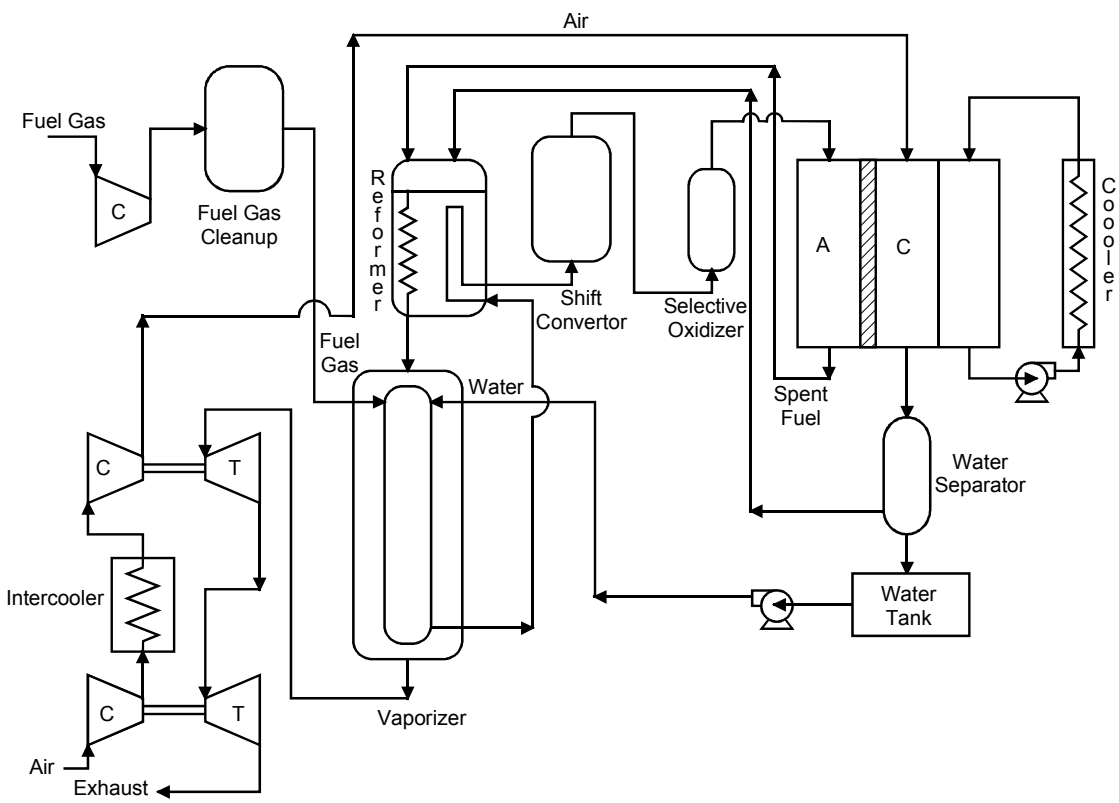

Figure 8-54 Natural Gas Fueled PEFC Power Plant

Ambient air is compressed in a turbocharger, powered by the expansion of the hot pressurized exhaust gases. Following this first compression stage, the air is intercooled by a fin fan air cooler and fed into a second turbocharger. The high-pressure air is fed directly to the PEFC

stack. The fuel cell water product is liberated to the oxidant gas stream. The spent oxidant stream exits the fuel cell where a water separator removes much of this water, which is subsequently used to humidify the fuel gas prior to the entering the reformer. The spent oxidant and fuel streams are combusted in the reformer burner to provide heat for the endothermic reforming reactions. The reformer exhaust also provides heat to the vaporizer. Finally, the residual heat and pressure of this exhaust stream are used in the turbochargers to drive the air compressor.

The fuel cell itself liberates heat that can be utilized for space heating or hot water. The reference article did not list any operating conditions of the fuel cell or of the cycle. The PEFC is assumed to operate at roughly 80ºC. Another recent article (14) published by Ballard shows numerous test results that were performed at 3 to 4 atmospheres where fuel utilizations of 75 to 85% have been achieved. Performance levels for an air fed PEFC are now in the range of 180 to 250 mW/cm^2. Ballard Power Systems has performed field trials of 250 kW systems with select utility partners. Commercial production of stationary power systems is anticipated for the year 2002. Similarly sized transportation cycles also are anticipated for commercial production in the same year.

8.5.2 Natural Gas Fueled PAFC System

IFC has been marketing the PC25, a 200 kW atmospheric PAFC unit, since 1992. Details of this commercial cycle are proprietary and not available for publication. In order to discuss an example PAFC cycle, a pressurized (8 atm) 12 MW system will be presented (15). This cycle is very similar to the 11 MW IFC PAFC cycle that went into operation in 1991 in the Tokyo Electric Power Company system at the Goi Thermal Station, except that two performance enhancements have been incorporated. Limited data are available regarding the Goi power plant. However, it is understood that the average cell voltage is 750 mV and the fuel utilization is 80% (16). The enhanced 12 MW cycle presented here utilizes values of 760 mV and 86%. This enhanced cycle (Figure 8-55) is discussed below with selected gas compositions presented in Table 8-11.

Natural gas (stream 100) is supplied at pressure and contains sulfur odorants for leak detection. A small hydrogen-rich recycle stream (stream 117) is mixed with the natural gas to hydrolyze the sulfur compounds to facilitate sulfur removal. The fuel stream (stream 102) is heated to 299ºC (570ºF) before entering the sulfur removal device. Superheated steam (stream 1) is mixed with the heated fuel to provide the required moisture for the reforming and the water gas shift reactions. The humidified stream (stream 105) is heated to approximately (705ºC) 1300ºF before entering the reformer. The effluent fuel stream (stream 107) leaves the reformer at approximately 760ºC (1400ºF) and is cooled in the heat exchanger used to preheat the humidified natural gas stream. This stream (stream 108) enters the high temperature shift converter (HTSC) at approximately 360ºC (680ºF), while leaving (stream 109) at about 415ºC (780ºF). The HTSC effluent is cooled in two heat exchangers before proceeding to the low temperature shift converter. A two-stage approach is utilized, allowing the HTSC to proceed at a faster rate, while the LTSC yields higher hydrogen concentrations.

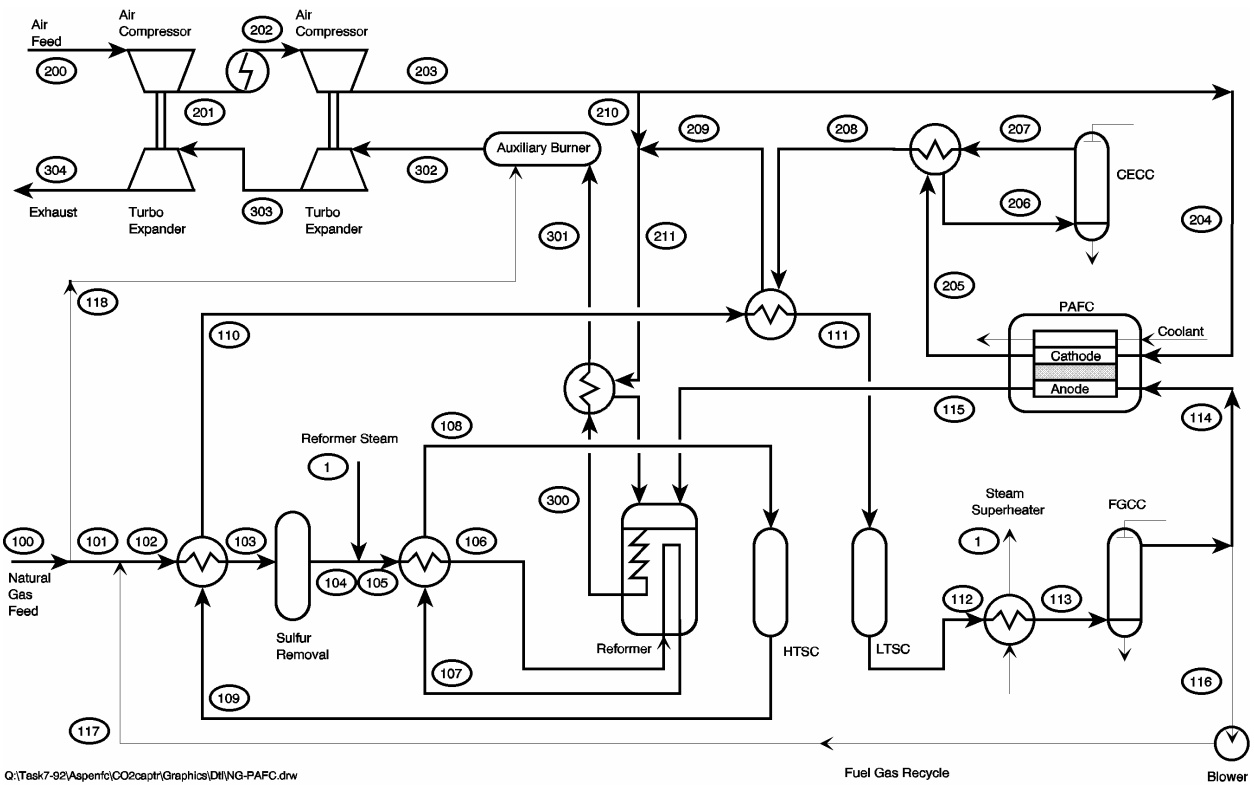

Figure 8-55 Natural Gas fueled PAFC Power System

Table 8-11 Stream Properties for the Natural Gas Fueled Pressurized PAFC

Strm No.	Description	Temp. C	Press. atm	Mole Flow Kgmol/hr	Mass Flow kg/hr	MW	Ar %	CH4 %	C2H6 %	CO %	CO2 %	H2 %	H2O %	N2 %	O2 %	Total %
1	Reformer Steam	243.3	10.00	418.8	7,545	18.02							100.0			100.0
100	NG Feed	15.6	13.61	115.1	1,997	17.34		90.0	5.0					5.0		100.0
106	Reformer Feed	712.8	9.93	562.6	9,846	17.50		18.3	1.0	trace	1.0	4.0	74.5	1.1		100.0
107	Reformer Effluent	768.3	9.59	755.9	9,846	13.03		2.4	trace	7.1	6.5	46.3	37.0	0.8		100.0
112	LTSC Effluent	260.0	8.72	755.9	9,846	13.03		2.4		0.5	13.1	52.9	30.4	0.8		100.0
114	Anode Feed	60.6	8.55	506.6	5,557	10.97		3.3		0.7	18.3	74.5	2.0	1.1		100.0
115	Anode Exhaust	207.2	7.95	181.4	4,901	27.02		9.3		1.9	51.2	28.8	5.7	3.1		100.0
118	NG to Aux Burner	15.6	13.61	1.59	27.5	17.34		90.0	5.0					5.0		100.0
200	Air Feed	15.6	1.00	1,156.5	33,362	28.85	0.9				trace		1.1	77.2	20.7	100.0
204	Cathode Feed	192.8	8.27	1,120.8	32,332	28.85	0.9				trace		1.1	77.2	20.7	100.0
205	Cathode Exhaust	207.2	8.09	1,283.4	32,987	25.70	0.8				trace		26.3	67.5	5.4	100.0
208	Cath. Gas to Heat Exch.	151.7	7.85	1,045.3	28,697	27.45	1.0				trace		9.5	82.8	6.7	100.0
209	Cath. Gas to Ref. Burner	243.9	7.81	1,045.3	28,697	27.45	1.0				trace		9.5	82.8	6.7	100.0
211	Cath. Gas to Heat Exch.	242.2	7.81	1,081.0	29,727	27.50	1.0				trace		9.2	82.6	7.1	100.0
301	Reformer Exhaust	380.6	7.71	1,234.6	34,629	28.05	0.9				9.2		15.9	72.8	1.2	100.0
302	Aux. Burner Exhaust	410.6	7.68	1,236.2	34,656	28.03	0.9				9.3		16.1	72.7	1.0	100.0
304	Exhaust	180.0	1.03	1,236.2	34,656	28.03	0.9				9.3		16.1	72.7	1.0	100.0

The LTSC effluent (stream 112) is utilized to superheat the steam required for the reformer and water gas shift reactions. The saturated steam sent to the superheater is supplied by the fuel cell water cooling circuit. The cooled stream (stream 113) is further cooled in a fuel gas contact

cooler (FGCC) to remove the excess moisture levels. This raises the partial pressure of hydrogen in the fuel before entering the fuel cell. Some of the hydrogen-rich fuel is recycled back, as mentioned previously, to the incoming natural gas, while the majority of the fuel (stream 114) proceeds to the fuel cell anode. Approximately 86% of the hydrogen in the fuel stream reacts in the fuel cell, where the hydrogen donates an electron and the resulting proton migrates to the cathode, where it reacts with oxygen in the air to form water. Key cell operating parameters are summarized in Table 8-12. The overall performance is summarized in Table 8-13. The spent fuel is combusted in the reformer burner and supplies heat for the endothermic reforming reactions.

Table 8-12 Operating/Design Parameters for the NG fueled PAFC

Operating Parameters	Value
Volts per Cell (V)	0.76
Current Density (mA/cm^2)	320
No of stacks	12
Cell Operating Temp. (ºC)	207
Cell Outlet Pressure (atm)	8.0
Overall Fuel Utilization (%)	86.2
Overall Oxidant Utilization (%)	70.0
DC to AC Inverter efficiency	97.0%
Auxiliary Load	4.2%

Table 8-13 Performance Summary for the NG fueled PAFC

Performance Parameters	Value
LHV Thermal Input (MW)	25.42
Gross Fuel Cell Power (MW)	
Fuel Cell DC Power	13.25
Inverter Loss	(0.40)
Fuel Cell AC Power	12.85
Auxiliary Power	0.54
Net Power	12.31
Electrical Efficiency (% LHV)	48.4
Electrical Efficiency (% HHV)	43.7
Heat Rate (Btu/kWh, LHV)	7,050

Note: The net HHV efficiency for the Goi Thermal Power Station is 41.8% (HHV) (1).

Ambient air (stream 200) is compressed in a two-stage compressor with intercooling to conditions of approximately 193ºC (380ºF) and 8.33 atmospheres (122.4 psia). The majority of

the compressed air (stream 203) is utilized in the fuel cell cathode; however, a small amount of air is split off (stream 210) for use in the reformer burner. The spent oxidant (stream 205) enters a recuperative heat exchange before entering a cathode exhaust contact cooler, which removes moisture to be reused in the cycle. The dehumidified stream (stream 207) is again heated, mixed with the small reformer air stream, and sent to the reformer burner (stream 211). The reformer burner exhaust (stream 300) preheats the incoming oxidant and is sent to the auxiliary burner, where a small amount of natural gas (stream 118) is introduced. The amount of natural gas required in the auxiliary burner is set so the turbine shaft work balances the work required at the compressor shaft. The cycle exhaust (stream 304) is at approximately 177ºC (350ºF).

Some of the saturated steam generated by the fuel cell cooling water is utilized to meet the reformer water requirements. Approximately 3,800 kg/hr (8,400 lb/hr) of 12.2 atmospheres (180 psi) saturated steam is available for other uses.

Cycle performance is summarized in Table 8-13. The overall net electric conversion efficiency is 43.7% based on HHV input, or 48.4% on LHV.

8.5.3 Natural Gas Fueled Internally Reformed MCFC System

Fuel Cell Energy is developing initial market entry MCFC power systems, with mature megawatt class units projected to be available in 2004. These units will be produced in various sizes. Preliminary cycle information was received from FCE for a nominal 3 MW power plant. This cycle is presented in Figure 8-56 and is described below.

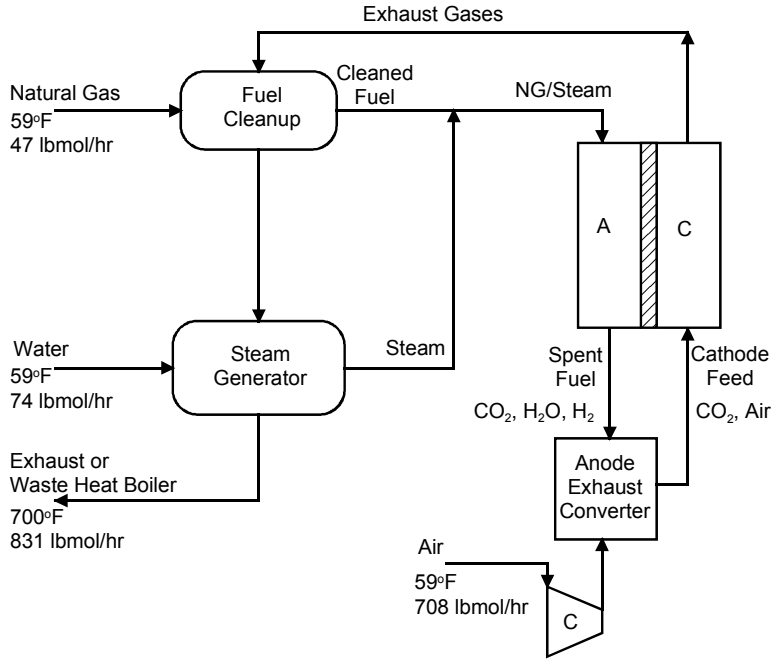

Figure 8-56 Natural Gas Fueled MCFC Power System

Natural gas is cleaned of its sulfur contaminants in a fuel cleanup device. Steam is added to the fuel stream prior to being fed to the internally reforming fuel cell. The fuel reacts electrochemically with the oxidant within the fuel cell to produce 3 MW of dc power.

The spent fuel is completely combusted in the anode exhaust converter. This flue gas mixture is fed directly to the fuel cell cathode. The cathode exhaust has significant usable heat, which is utilized in the fuel cleanup and in steam generation. The residual heat can be utilized to heat air, water, or steam for cogeneration applications. Design parameters for the IR-MCFC are presented in Table 8-14. Overall performance values are presented in Table 8-15.

Table 8-14 Operating/Design Parameters for the NG Fueled IR-MCFC

Operating Parameters	Value
Volts per Cell (V)	unknown
Current Density (mA/cm^2)	unknown
Operating Temperature (ºC)	unknown
Cell Outlet Pressure (atm)	1.0
Fuel Utilization (%)	78.%
Oxidant Utilization (%)	75.%
Inverter Efficiency	95.%

Table 8-15 Overall Performance Summary for the NG Fueled IR-MCFC

Performance Parameters	Value
LHV Thermal Input (MW)	4.8
Gross Fuel Cell Power (MW)	
Fuel Cell DC Power	3.0
Inverter Loss	(0.15)
Fuel Cell AC Power	2.85
Auxiliary Power (MW)	0.05
Net Power (MW)	2.80
Electrical Efficiency (% LHV)	58%
Heat Rate (Btu/kWh, LHV)	5,900

8.5.4 Natural Gas Fueled Pressurized SOFC System

This natural gas fuel cell power system is based on a pressurized TSOFC combined with a combustion turbine developed by Siemens Westinghouse[52] (17). Most TSOFC power plant concepts developed to date have been based on atmospheric operation. However, as shown in

[52]. The referenced Siemens Westinghouse publication presented the cycle concept and overall performance values. Neither specific stream information nor assumptions were presented. The stream data and assumptions presented here were developed by Parsons. The stream data were developed using an ASPEN simulation which yielded performance numbers in general agreement with the publication.

Section 7, the cell voltage increases with cell pressure. Thus, operating with an elevated pressure will yield increased power and efficiency for a given cycle. In addition, the use of a pressurized SOFC will also allow integration with a combustion turbine. The combustion turbine selected for integration by Siemens Westinghouse is the unique 1.4 MW Heron reheat combustion turbine, a proposed product of Heron (18).

A flow diagram for the natural gas fueled 4.5 MW class cascaded[53] TSOFC power cycle is presented in Figure 8-57. A brief process description is given below, followed by a performance summary. Selected state point values are presented in Table 8-16.

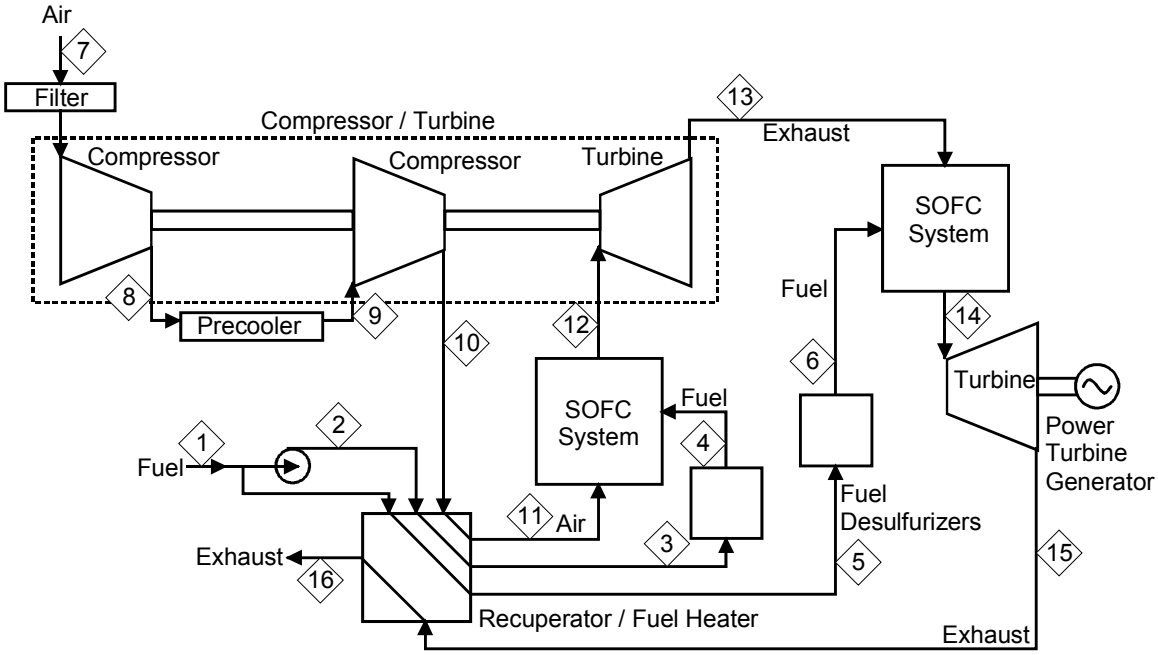

Figure 8-57 Schematic for a 4.5 MW Pressurized SOFC

[53]. The term "cascaded" fuel cells is used here to describe a fuel cell system where the exhaust of a high-pressure fuel cell is utilized as an oxidant feed stream in a low-pressure fuel cell after passing through an expander.

Table 8-16 Stream Properties for the Natural Gas Fueled Pressurized SOFC

Strm No.	Description	Temp C	Press. atm	Mass Flow kg/hr	Mole Flow kgmol/hr	MW	Ar %	CH4 %	CO2 %	H20 %	N2 %	O2 %	Total %
1	Fuel feed	15	8.85	508	30.9	16.44		97.4	0.4		0.9		100.0
2	Pressurized Fuel	21	9.53	508	30.9	16.44		97.4	0.4		0.9		100.0
3	Heated HP Fuel	399	9.42	508	30.9	16.44		97.4	0.4		0.9		100.0
4	Cleaned HP Fuel	399	9.32	281	17.1	16.44		97.4	0.4		0.9		100.0
5	Heated LP Fuel	399	9.42	227	13.8	16.44		97.4	0.4		0.9		100.0
6	Cleaned LP Fuel	399	3.13	227	13.8	16.44		97.4	0.4		0.9		100.0
7	Air Feed	15	0.99	18,536	642.3	28.86	0.9		trace	1.0	77.2	20.8	100.0
8	Compressed Air	135	2.97	18,536	642.3	28.86	0.9		trace	1.0	77.2	20.8	100.0
9	Intercooled Air	27	2.69	18,351	635.9	28.86	0.9		trace	1.0	77.2	20.8	100.0
10	HP Air	160	8.80	18,351	635.9	28.86	0.9		trace	1.0	77.2	20.8	100.0
11	Heated Air	555	8.66	18,167	629.5	28.86	0.9		trace	1.0	77.2	20.8	100.0
12	HP FC Exhaust	860	8.39	18,448	646.5	28.53	0.9		2.7	6.2	75.2	15.0	100.0
13	HPT Exhaust	642	3.11	18,631	653.1	28.53	0.9		2.7	6.2	75.2	15.0	100.0
14	LP FC Exhaust	874	2.83	18,859	667.0	28.28	0.9		4.7	10.2	73.7	10.6	100.0
15	LPT Exhaust	649	1.01	18,859	667.0	28.28	0.9		4.7	10.2	73.7	10.6	100.0
16	Cycle Exhaust	258	1.00	19,044	673.4	28.28	0.9		4.6	10.1	73.7	10.7	100.0

Reference Source: (30).

The natural gas feed to the cycle (stream 1) is assumed to consist of 95% CH_4, 2.5% C_2H_6, 1% CO_2, and 1.5% N_2 by volume along with trace levels of sulfur odorants. The odorants must be reduced to 1 ppmv before entrance into the fuel cell to prevent performance and cell life deterioration. Because the desulfurization requires elevated temperatures, the fuel (streams 3 and 5) is fed through a heat exchanger that recovers heat from the fuel cell exhaust stream (stream 15). The hot desulfurized fuel stream (stream 4) enters the anodes of the high-pressure fuel cell at approximately 399ºC (750ºF) and 9.3 atmospheres. The fuel entering the low-pressure fuel cell (stream 6) is approximately 399ºC (750ºF) and 3.1 atmospheres. Ambient air (stream 7) is compressed to 3.0 atmospheres and 135ºC (275ºF) (stream 8), subsequently intercooled to 27ºC (81ºF) (stream 9), compressed again to 8.8 atmospheres and 160ºC (320ºF) (stream 10), and heated to 555ºC (1031ºF) prior to entering the high-pressure fuel cell cathode (stream 11).

The hot desulfurized fuel and the compressed ambient air are electrochemically combined within the high-pressure fuel cell module with fuel and oxidant utilizations of 78% and 20.3%, respectively. The SOFC high-pressure module was assumed to operated at 0.63 volts per cell. The spent fuel and air effluents of the Siemens Westinghouse tubular geometry SOFC are combusted within the module to supply heat required for the endothermic reforming reaction within the pre-reformer. The majority of the reforming takes place within the tubular fuel cell itself. The heat for internal reforming is supplied by the exothermic fuel cell reaction. A gas recirculation loop provides water for the internal reforming and to prevent soot formation.

The combusted air and fuel stream (stream 12) from the high-pressure fuel cell are expanded (stream 13) in a turbine expander. The work of this turbine is used to drive the low- and high-pressure air compressors. The reduced pressure exhaust stream (stream 13) is utilized as the low-pressure fuel cell oxidant stream. Although vitiated, it still has 15% oxygen. The low-pressure TSOFC operates at 0.62 volts per cell, and fuel and air utilizations of 78 and 21.9%, respectively. The spent air and fuel effluents are combusted and sent (stream 14) to the low-pressure power turbine. The turbine generator produces approximately 1.4 MW AC. The low-pressure exhaust (stream 15) still has a temperature of 649ºC (1200ºF) and is utilized to

preheat the fuel and oxidant streams. The resulting cycle exhaust stream (stream 16) exits the plant stack at approximately 258ºC (496ºF).

Operating parameters are summarized in Table 8-17. Cycle performance is summarized in Table 8-18. The overall net electric LHV efficiency is 67%.

The high efficiency of this TSOFC/Heron combined cycle is a result of synergism that exists between the SOFC and the Heron turbine. The TSOFC is able to fully replace the gas turbine combustor. That is, the waste heat of the SOFC exhaust is able to completely eliminate the need for the gas turbine combustor at the design point. As seen in Table 8-19, the Heron combustor design temperature of roughly 860ºC (1580ºF) is well within the TSOFC operating temperature range. Conversely, the Heron cycle is able to act as an efficient bottoming cycle without requiring a waste heat boiler or steam turbine. In simple cycle mode, the Heron cycle has a respectable LHV net electric efficiency of 42.9%. Together, the TSOFC/Heron cycle operates at an efficient 67%. Another advantage of this cycle is the low NOx emissions, because only the spent fuel is fired at the design point. The majority of the fuel reacts within the fuel cell. Overall NOx levels of less than 4 ppmv are expected.

Table 8-17 Operating/Design Parameters for the NG Fueled Pressurized SOFC

Operating Parameters	HP FC	LP FC
Volts per Cell (V)	0.63*	0.62*
Current Density (mA/cm^2)	NA	NA
Cell Operating Temp. (ºC)	1000*	1000*
Cell Outlet Pressure (atm)	8.4*	2.9*
FC Fuel Utilization (%)	78.0*	78.0*
FC Oxidant Utilization (%)	20.3*	21.9*
DC to AC Inverter Effic. (%)	96.0	
Generator Efficiency (%)	96.0*	
Auxiliary Load (% of gross)	1.0*	

Note: * assumed by Parsons to reasonably match the reference paper.

Table 8-18 Overall Performance Summary for the NG Fueled Pressurized SOFC

Performance Parameters	Value
LHV Thermal Input (MW)	6.68
Gross Fuel Cell Power (MW) Fuel Cell DC Power Inverter Loss Fuel Cell AC Power	 3.22 (0.13) 3.09
Gross AC Power (MW) Fuel Cell AC Power Turbine Expander Gross AC Power	 3.09 1.40 4.49
Auxiliary Power	0.04
Net Power	4.45
Electrical Efficiency (% LHV)	66.6
Electrical Efficiency (% HHV)	60.1
Heat Rate (Btu/kWh, LHV)	5,120

Table 8-19 Heron Gas Turbine Parameters

Performance Parameters	Value
Compressor Air Flow (kg/h)	18,540
HP Combustor Temperature (ºC) LP Combustor Temperature (ºC)	861 863
Compressor Pressure Ratio	8.8:1
Power Turbine Exhaust Temp. (ºC)	620

The cycle discussed here is based on a Siemens Westinghouse publication for a 4.5 MWe plant. Recent information from Siemens Westinghouse, plans for commercialization of a scaled down 1 MWe version of this dual pressure TSOFC/Heron cycle. A 1 MW cycle was not available in the literature.

8.5.5 Natural Gas Fueled Multi-Stage Solid State Power Plant System

The fuel cell system presented below is based on an innovative solid state fuel cell system developed by U.S.DOE (19). Conventional fuel cell networks, in order to effectively use the supplied fuel, often employ fuel cell modules operating in series to achieve high fuel utilization[54] or combust the remaining fuel for possible thermal integration such as cogeneration steam or a steam bottoming cycle. Both of these conventional approaches utilize fuel cell modules at a single state-of-the-art operating temperature. In conventional fuel cell networks, heat exchangers are utilized between the fuel cell modules to remove heat so the subsequent fuel cell can operate at the desired temperature.

In the multi-stage fuel cell, the individual stages are designed to operate at different temperatures, so that heat exchangers are not required to cool the effluent gases between stages. Each stage is designed to accommodate the next higher temperature regime. In addition, the multi-stage fuel cell concept does not attempt to maximize the fuel utilization in each stage, but allows lower utilizations in comparison to the state-of-the-art design. The number of stages and the fuel utilization per stage in the multi-stage concept is a matter of design choice and optimization. An example of the fuel utilization for a five stage concept is presented in Table 8-20.

Table 8-20 Example Fuel Utilization in a Multi-Stage Fuel Cell Module

	Fuel Balance for 100 Units of Fuel			Fuel Utilization	
Stage	Fuel Feed	Fuel Out	Fuel Used	per Stage	Cumulative
1	100.0	81.0	19.0	19.0 %	19.0 %
2	81.0	62.0	19.0	23.5 %	38.0 %
3	62.0	43.0	19.0	30.6 %	57.0 %
4	43.0	24.0	19.0	44.2 %	76.0 %
5	24.0	6.0	18.0	75.0 %	94.0 %
Overall	100.0	6.0	94.0		94.0 %

A flow diagram for a natural gas fueled, 4 MW class, solid state fuel cell power cycle is presented in Figure 8-58. A brief process description is given below, followed by a performance summary. Selected state point values are presented in Table 8-21.

[54]. Current state-of-the-art SOFCs have fuel utilizations of 75 to 85%. By utilizing a second fuel cell in series, the total utilization could be theoretically increased to 93 to 98%. Note: Two cascaded fuel cells operating with a fuel utilization of 85% will have an overall utilization of 98%. $1-(0.15)^2 = 1-0.02 = 0.98$ or 98%.

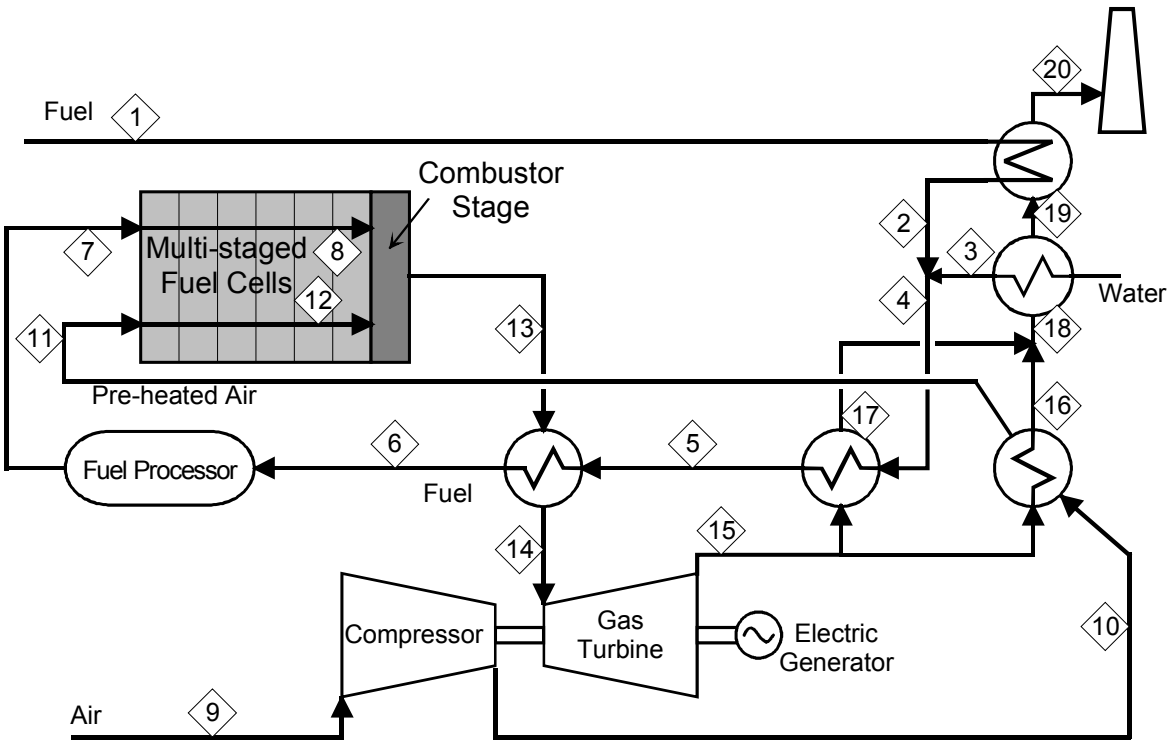

Figure 8-58 Schematic for a 4 MW Solid State Fuel Cell System

Table 8-21 Stream Properties for the Natural Gas Fueled Solid State Fuel Cell Power Plant System

Strm No.	Description	Temp. C	Press. atm	Mass Flow kg/hr	Mole Flow kgmol/hr	MW	CH4 %	C2H6 %	C3H8+ %	CO %	CO2 %	H2 %	H20 %	N2 %	O2 %	Total %
1	Fuel feed	25	3.74	373	21.64	17.23	93.9	3.2	1.1		1.0			0.8		100
2	Heated fuel	84	3.67	373	21.64	17.23	93.9	3.2	1.1		1.0			0.8		100
3	Humidification water	275	3.93	614	34.09	18.02							100.0			100
4	Humidified fuel	192	3.67	987	55.73	17.71	36.5	1.3	0.4		0.4		61.2	0.3		100
5	Heated fuel	725	3.60	987	55.73	17.71	36.5	1.3	0.4		0.4		61.2	0.3		100
6	Heated fuel	725	3.60	987	55.73	17.71	36.5	1.3	0.4		0.4		61.2	0.3		100
7	Processed fuel	494	3.53	987	63.70	15.50	29.1	0.0		0.6	6.0	##	41.6	0.3		100
8	Spent Fuel	999	3.46	2,319	98.40	23.57	1.1			0.3	21.7	0.6	76.1	0.2		100
9	Air feed	25	1.00	7,484	259.42	28.85								79.0	21.0	100
10	Compressed air	175	3.47	7,484	259.42	28.85								79.0	21.0	100
11	Heated air	725	3.40	7,484	259.42	28.85								79.0	21.0	100
12	Spent air	999	3.33	6,149	217.69	28.25								94.1	5.9	100
13	FC exhaust	1119	3.33	8,471	315.78	26.83					7.2		24.7	65.0	3.2	100
14	Cooled exhaust	1119	3.33	8,471	315.78	26.83					7.2		24.7	65.0	3.2	100
15	Expanded exhaust	856	1.04	8,471	315.78	26.83					7.2		24.7	65.0	3.2	100
16	Cooled exhaust	328	1.02	6,438	239.99	26.83					7.2		24.7	65.0	3.2	100
17	Cooled exhaust	333	1.02	2,033	75.79	26.83					7.2		24.7	65.0	3.2	100
18	Combined exhaust	329	1.02	8,471	315.78	26.83					7.2		24.7	65.0	3.2	100
19	Cooled exhaust	152	1.01	8,471	315.78	26.83					7.2		24.7	65.0	3.2	100
20	Cycle exhaust	147	1.00	8,471	315.78	26.83					7.2		24.7	65.0	3.2	100

Reference Source: (20).

The natural gas feed to the cycle (stream 1) is typical of pipeline quality natural gas within the U.S. containing both sulfur odorants and higher hydrocarbons (C_2H_6, C_3H_8, etc.). The odorants

must be removed before entrance into the fuel cell to prevent performance and cell life deterioration. Higher hydrocarbons are assumed to be pre-reformed to hydrogen and carbon monoxide in a mild reformer[55] to avoid "sooting" or carbon deposition within the fuel cell. Because both the desulfurization and reforming require elevated temperatures, the fuel is fed through a series of heat exchangers that recover heat from the fuel cell exhaust stream (streams 13 to 20). Humidification steam (stream 3) is added to the fuel to provide the required moisture for the reforming and water-gas shift reactions. The heated and humidified fuel is desulfurized in a sorbent bed and partially reformed in a mild reformer catalyst bed. The balance of the reforming will occur between the stages of the multi-stage fuel cell module. The hot desulfurized and partially reformed fuel stream (stream 7) enters the fuel cell anode at approximately 500ºC (930ºF).

Ambient air (stream 9) is compressed to 3.5 atmospheres and 175ºC (347ºF) (stream 10), and subsequently heated to 500ºC (932ºF) prior to entering the fuel cell cathode (stream 11).

The hot processed fuel and the compressed ambient air are electrochemically combined within the fuel cell module. The fuel hydrocarbons still remaining after the mild reformer are reformed within the fuel cell. The heat required for the endothermic steam reforming reactions is supplied by the exothermic fuel cell reactions. The overall reactions are exothermic, and the fuel and oxidant temperatures rise to 999ºC (1830ºF) (streams 8 and 12). The fuel cell is capable of utilizing both H_2 and CO as fuel and has an overall fuel utilization of 94%.

The spent fuel (stream 8) and oxidant (stream 12) are combusted upon exiting the multi-stage fuel cell module. The resulting exhaust stream (stream 13) has a temperature of 1119ºC (2046ºF) before being cooled in a fuel heater and expanded to 1.04 atmospheres and 856ºC (1573ºF) (stream 15). This nearly atmospheric exhaust stream passes through several additional heat exchangers before leaving the plant stack at 147ºC (300ºF).

Operating parameters are summarized in Table 8-22. Cycle performance is summarized in Table 8-23. The overall net electric LHV efficiency is 80.1%.

One advantage of this concept is the elimination of heat exchangers between fuel cell modules. This will minimize the cycle complexity, cost, and losses. Another advantage of the concept is the minimization of unreacted fuel leaving the fuel cell. By having discrete fuel cell stages, each operating with its own voltage and current density, fuel utilization can be pushed to very high levels without hurting the performance of the entire module. The voltage and performance degradation resulting from the low fuel concentrations (high utilization) is isolated to the latter fuel cell stage(s) whereas a single fuel cell module, the entire fuel cell performance is degraded. Experiencing a reduced voltage, power, and efficiency level in the latter stages of a multi-stage module is acceptable because it minimizes the heat released in the combustion stage, which is largely passed to the bottoming cycle, which typically has an efficiency of roughly 40%. That is, 60% of the heat liberated to the bottoming cycle is wasted. Thus, the minimization of heat

[55]. A "mild reformer" is assumedto eliminate of the higher hydrocarbons prior to entering the fuel cell to prevent sooting. This reformer is called a "mild reformer" to indicate that the reforming reactions are not pushed to completion, for it is desired that the methane be reformed in the fuel cell for better temperature management. Some of the methane, however, will be reformed with the higher hydrocarbons in the mild reformer.

passed to the bottom cycle is desirable, even at the "cost" of reduced efficiency in a fraction of the fuel cell module.

One obstacle for this concept is the uncertainty of fuel cell performance in a high utilization multi-stage concept. No testing has been performed to date utilizing a fuel cell in this manner. The exact loss of performance in the latter stages is not known. The reference document (21) for this multi-stage fuel cell concept did not attempt to specify the number of stages nor the fuel cell performance within each stage. Instead, an average fuel cell performance was assumed. This assumption may or may not represent of how a multi-stage fuel cell will perform. Additional development work of this novel and efficient concept is required.

Table 8-22 Operating/Design Parameters for the NG fueled Multi-Stage Fuel Cell System

Operating Parameters	Value
Volts per Cell (V)	0.800
Current Density (mA/cm^2)	unspecified
Number of Stages	to be determined
Cell Operating Temperature (ºC)	multiple temps (~650 to 850ºC)
Cell Outlet Pressure (atm)	3.3
Overall Fuel Utilization (%)	94.0%
Overall Oxidant Utilization (%)	81.5%
Steam to Carbon Ratio	1.5:1
DC to AC Inverter efficiency	97.0%
Generator efficiency	98.0%
Fuel Cell Heat Loss (% of MW_{dc})	1.7%
Auxiliary Load	1.0%

Table 8-23 Overall Performance Summary for the NG fueled Multi-StageFuel Cell System

Performance Parameters	Value
LHV Thermal Input (MW)	4.950
Gross Fuel Cell Power (MW)	
Fuel Cell DC Power	3.579
Inverter Loss	(0.108)
Fuel Cell AC Power	3.471
Gross AC Power (MW)	
Fuel Cell AC Power	3.471
Net Compressor/Expander	0.534
Gross AC Power	4.005
Auxiliary Power	0.040
Net Power	3.965
Electrical Efficiency (% LHV)	80.10%
Electrical Efficiency (% HHV)	72.29%
Heat Rate (Btu/kWh, LHV)	4,260

8.5.6 Coal Fueled SOFC System (Vision 21)

The coal fueled solid oxide fuel cell power system presented here is based on work performed for the Department of Energy's Vision 21 Program (22) to develop high efficiency, low emission, fuel flexible (including coal) processes. This cycle is a coal-fueled version of the Siemens Westinghouse TSOFC cycle presented in Section 9.3.5 consists of a Destec gasifier, cascaded SOFCs at two pressure levels, an integrated reheat gas turbine, and a reheat steam turbine bottoming cycle. The high-pressure portion of the cycle is designed to operate at 15 atmospheres to capitalize on a reasonable gas turbine expansion ratio and an advanced, but not unrealistic, fuel cell pressure. An operating pressure of 30 atmospheres would yield better fuel cell and gas turbine performance, but has been conservatively limited to 15 atmospheres; this is lower than the typical Destec design pressure. Higher pressure operation is feasible and would have better performance. The coal analysis is presented in Table 8-25.

A flow diagram for the coal fueled 500 MW class cascaded TSOFC power cycle is presented in Figure 8-59. A brief process description is given below, followed by a performance summary. Selected state point values are presented in Table 8-26.

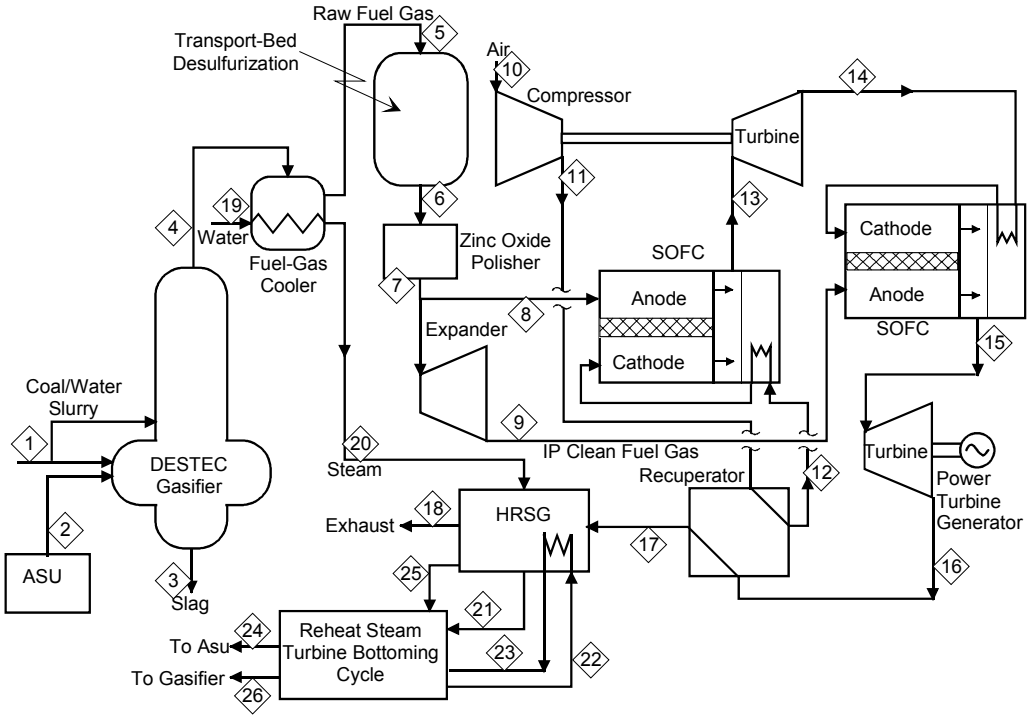

Figure 8-59 Schematic for a 500 MW Class Coal Fueled Pressurized SOFC

Table 8-24 Stream Properties for the 500 MW Class Coal Gas Fueled Cascaded SOFC

Strm No.	Description	Temp C	Press atm	Mass Flow t/h	Mole Flow kgmol/hr	MW	CH4 %	CO %	CO2 %	H2 %	H20 %	H2S %	N2+Ar %	NH3 %	O2 %	Total %
1	Coal Slurry Feed	18	23.8	151.2	-	NA										
2	ASU Oxygen	179	23.8	83.3	2,583	32.23							5.0		95.0	100.0
3	Slag Waste	93	19.1	11.6	-	NA										
4	Gasifier Effluent	1043	18.6	237.6	12,280	19.35	0.3	42.3	9.5	35.8	9.6	0.7	1.5	0.2		100.0
5	Raw Fuel Gas	593	17.6	237.6	12,280	19.35	0.3	42.3	9.5	35.8	9.6	0.7	1.5	0.2		100.0
6	Desulfurized Gas	593	16.6	236.2	12,280	19.23	0.3	42.3	9.6	35.8	10.3	trace	1.5	0.2		100.0
	Recycle to Gasifier	399	15.0	9.4	491	19.23	0.3	42.3	9.6	35.8	10.3	trace	1.5	0.2		100.0
7	Polished Gas	399	15.0	226.7	11,789	19.23	0.3	42.3	9.6	35.8	10.3	trace	1.5	0.2		100.0
8	HP Fuel Gas	399	15.0	108.8	5,659	19.23	0.3	42.3	9.6	35.8	10.3	trace	1.5	0.2		100.0
9	IP Fuel Gas	221	3.7	117.9	6,130	19.23	0.3	42.3	9.6	35.8	10.3	trace	1.5	0.2		100.0
10	Ambient Air	17	0.98	1,270.1	44,024	28.85			trace		1.1		78.1		20.8	100.0
11	Compressed Air	409	15.1	1,146.2	39,732	28.85			trace		1.1		78.1		20.8	100.0
12	Heated Air	579	15.0	1,146.2	39,732	28.85			trace		1.1		78.1		20.8	100.0
13	HP SOFC Exhaust	979	14.7	1,255.1	43,181	29.07			6.9		7.1	trace	72.1	trace	13.9	100.0
14	HPT Exhaust	645	3.6	1,296.3	44,609	29.06			6.6		6.9	trace	72.3	trace	14.1	100.0
15	IP SOFC Exhaust	982	3.3	1,414.2	48,346	29.25			12.7		12.3	trace	66.9	0.1	8.0	100.0
16	IPT Exhaust	691	1.01	1,477.7	50,547	29.23			12.2		11.8	trace	67.4	0.1	8.6	100.0
17	Cooled Exhaust	573	0.99	1,477.7	50,547	29.23			12.2		11.8	trace	67.4	0.1	8.6	100.0
18	Cycle Exhaust	126	0.98	1,477.7	50,540	29.24			12.2		11.8		67.5		8.6	100.0
19	Gas Cooler Water	306	107.4	244.6	13,580	18.02					100.0					100.0
20	Gas Cooler Steam	317	107.4	244.6	13,580	18.02					100.0					100.0
21	HP Steam	538	99.6	301.4	16,730	18.02					100.0					100.0
22	Cold Reheat	359	29.3	298.4	16,563	18.02					100.0					100.0
23	Hot Reheat	538	26.4	298.4	16,563	18.02					100.0					100.0
24	ASU Steam	538	26.4	3.9	218	18.02					100.0					100.0
25	LP Steam	310	6.1	15.6	865	18.02					100.0					100.0
26	Gasifier Steam	307	5.4	32.0	1,774	18.02					100.0					100.0

Reference Source: (30)

The Destec entrained bed gasifier is fed both a coal water slurry (stream 1) and a 95% pure oxygen stream (stream 2) and operates with a cold gas conversion efficiency[56] of 84%. The gasifier fuel gas product (stream 4) is cooled in a radiant heater, which supplies heat to the bottoming cycle. The cooled fuel gas is cleaned (stream 6) in a hot gas desulfurizer at 593ºC (1100ºF) and a polisher (stream 7) at 399ºC (750ºF) to less than 1 ppmv of sulfur prior to entering the high-pressure fuel cell (stream 8). Part of the polished fuel is expanded to 3.7 atmospheres and 220ºC (429ºF) before being sent to the low-pressure fuel cell (stream 9).

Ambient air (stream 10) is compressed to 15.1 atmospheres and 409ºC (275ºF) (stream 11), and subsequently heated to 579ºC (1075ºF) prior to entering the high-pressure fuel cell cathode (stream 12).

The hot clean fuel gas and the compressed ambient air are electrochemically combined within the high-pressure fuel cell with fuel and oxidant utilizations of 90% and 24.5%, respectively. The SOFC module is set (sized) to operate at 0.69 volts per cell.[57] The spent fuel and air effluents of the SOFC are combusted within the module to supply heat for oxidant preheating. Unlike the natural gas case, the fuel does not require a pre-reformer with only 0.3% methane along with 36% hydrogen and 43% carbon monoxide. The carbon monoxide will be either water gas shifted to hydrogen or utilized directly within the fuel cell. A gas recirculation loop for the

[56]. Cold gas conversion efficiency is the ratio of the gasifier fuel gas total heating value [i.e., (heating value)(mass flow)] to that of the coal feed, [(heating value)(mass flow)].

[57]. Siemens Westinghouse provided TSOFC performance values for the HP and LP conditions, which Parsons incorporated into the systems analysis.

fuel cell has not been assumed, for water is not required for pre-reforming nor internal reforming.

The combusted air and fuel stream (stream 13) from the high-pressure fuel cell is expanded (stream 14) in a turbine expander. The work of this turbine is used to drive the low- and high-pressure air compressors. The reduced pressure exhaust stream (stream 14) is utilized as the low-pressure fuel cell oxidant stream. Although vitiated, it still has 14% oxygen. The low-pressure SOFC operates at 0.69 volts per cell and fuel and air utilizations of 90 and 34.7%, respectively (23). The spent air and fuel effluents are combusted and sent (stream 15) to the low-pressure power turbine. The turbine generator produces approximately 134 MWe. The low-pressure exhaust (stream 16) has a temperature of 691ºC (1276ºF) and is utilized to preheat the high-pressure oxidant. The resulting cooled exhaust stream (stream 17) still has a temperature of 573ºC (1063ºF) and is utilized to supply heat to a steam bottoming cycle.

Steam generated in the bottoming cycle is utilized in a reheat turbine to produce 118 MWe, as well as to supply the steam required by the air separation unit (ASU) and the gasifier coal slurry heater. The cycle exhaust exits the heat recovery steam generator at 126ºC (259ºF) and 0.98 atmospheres.

Operating parameters are summarized in Table 8-26. Cycle performance is summarized in Table 8-27. The overall cycle net HHV efficiency is 59%, and is very near the 60% Vision 21 goal.

Table 8-25 Coal Analysis

Coal Parameters	Value
Source	Illinois No. 6
Ultimate Analysis, (wt %, a.r.)	
Moisture	11.12
Carbon	63.75
Hydrogen	4.50
Nitrogen	1.25
Chlorine	0.29
Sulfur	2.51
Ash	9.70
Oxygen (by difference)	6.88
Total	100.00
HHV (Btu/lb)	11,666
LHV (Btu/lb)	11,129

Table 8-26 Operating/Design Parameters for the Coal Fueled Pressurized SOFC

Operating Parameters	HP FC	LP FC
Volts per Cell (V)	0.69	0.69
Current Density (mA/cm^2)	312	200
Cell Operating Temp. (ºF)	1794	1800
Cell Outlet Pressure (atm)	14.7	3.3
Overall Fuel Utilization (%)	90%	90%
Overall Oxidant Utilization (%)	18.7%	20.4%
DC to AC Inverter Efficiency	97.0%	
Generator Effic. - ST, GT	98.5%	
Generator Effic. - Expander	98.0%	
Auxiliary Load	7.2%	

Table 8-27 Overall Performance Summary for the Coal Fueled Pressurized SOFC

Performance Parameters	Value
LHV Thermal Input (MW)	875.8
Gross Fuel Cell Power (MW)	
Fuel Cell DC Power	310.9
Inverter Loss	(9.3)
Fuel Cell AC Power	301.6
Gross AC Power (MW)	
Fuel Cell AC Power	301.6
Combustion Turbine	133.7
Steam Turbine	118.1
Fuel Expander	9.6
Gross AC Power	562.9
Auxiliary Power	40.3
Net Power	522.6
Electrical Efficiency (% HHV)	59.7%
Electrical Efficiency (% LHV)	62.6%
Heat Rate (Btu/kWh, HHV)	5,720

This configuration has the potential to yield a very competitive cost of electricity. For example, for a fuel cell stack cost of $300 to $400/kW, it is estimated that the COE would range from 3.5 to 3.9 cents/kWh (Assuming 20% equity at 16.5%, 80% debt at 6.3%, and a levelized carrying charge of 0.12.)

8.5.7 Power Generation by Combined Fuel Cell and Gas Turbine System

In general, the oxidation of H_2, CO, CH_4, and higher hydrocarbons in fuel cells to produce power also produces reject heat. This heat arises from two sources:

- the entropy decrease, ΔS, resulting from the overall oxidation reaction -- accompanying the usual decrease in the number of mols of gas, from reactants to products; and

- the loss in work, or a conversion of "reversible" work from the oxidation process to heat, due to irreversible processes occurring in the operation of the cell.

Heat from these two sources must be rejected from the fuel cell in order to maintain its temperature at a desired level. The heat can be removed and recovered by transferring it across a bounding surface to a heat transfer fluid, but care must be taken to maintain the cell at its desired temperature in this and adjacent regions. Alternatively, heat can be removed in one of the reactant streams passing through the cell -- most practically the air, oxidant stream.

Also in the operation of a practical fuel cell, some unburned fuel must remain in the combustion products leaving the cell in order to maintain a significant generated voltage throughout the cell.

In order to obtain the highest possible efficiency in electrical generation, both the thermal energy in the heat and the unburned fuel rejected from the cell must be recovered and converted into additional electrical energy. This can be accomplished by means of a heat engine cycle making use of a gas turbine operating in a regenerative Brayton or combined Brayton-Rankine cycle or a steam turbine operating in a Rankine cycle. The relative merits of these three heat engine cycles depend on their overall efficiencies and on the practical aspects of integration, operation, and cost of the power generation plant as a whole.

8.5.8 Heat and Fuel Recovery Cycles

Simple representations of three fuel cell based heat and fuel recovery cycles are shown in Figures 8-60, 8-61, and 8-64.

Regenerative Brayton Cycle: The regenerative Brayton cycle, Figure 8-60, shows a gas turbine compressor for the air flow to the cell. The flow then passes through a countercurrent, recuperative heat exchanger to recover heat from the combustion product gases leaving the gas turbine. The air and the fuel streams then pass into the cathode and anode compartments of the fuel cell(s). The air and fuel streams leaving the cell(s) enter the combustor where they mix and the residual fuel burns. The combustion products enter the turbine, expand, and generate additional power. The turbine exhaust gases pass through the recuperative exchanger to the stack.

The most significant variables characterizing the cycle are the fuel cell operating temperature range and the temperature and pressure at the gas turbine expander inlet. These variables are directly related to certain operating variables: the air/fuel ratio entering the fuel cell, the fraction of the fuel leaving the cell unburned, and the temperature difference between the combustion products and air at the high temperature end of the recuperative heat exchanger. The operating variables must be selected and controlled to allow effective operation of the fuel cell, combustor, and gas turbine. There may well be an optimal quantity of unburned fuel leaving the fuel cell, depending on the acceptable fuel cell operating temperature range and turbine inlet temperature.

Further insight can be gained from the idealized T - S diagram for the cycle, Figure 8-60. The compression of the air and fuel streams is represented here as a single adiabatic reversible (constant S) process in which the temperature of the gases rises above ambient. The heating of

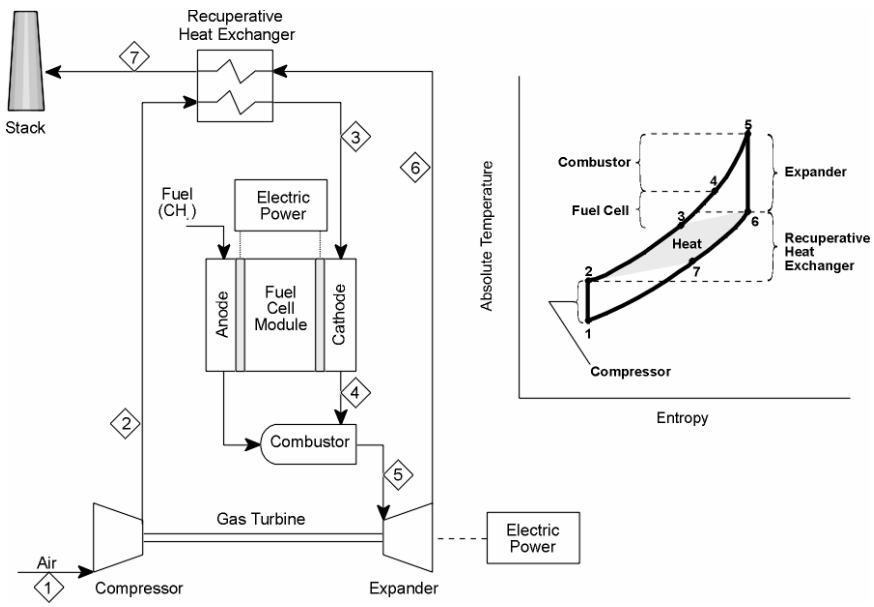

Figure 8-60 Regenerative Brayton Cycle Fuel Cell Power System

the air and also the fuel streams first in the recuperative exchanger, then in the fuel cell and finally in the combustor is assumed to occur along a single line of constant pressure. The subsequent expansion of the combustion gases in the turbine is also represented as an adiabatic reversible (constant S) process in which the temperature of the gases drops to a value close to that of the gases entering the fuel cell. The pressure ratio (PR) of the turbine (and of the compressor) is therefore established by the turbine nozzle inlet temperature (NIT) and the fuel cell operating temperature. In general, the pressure ratio of a regenerative Brayton cycle is low compared with that of a combined Brayton-Rankine cycle. A low pressure ratio allows a low outlet temperature of the exhaust gases from the recuperative exchanger as heat is transferred to the air leaving the compressor (and possibly also the fuel) and consequently results in low heat rejection and a high cycle efficiency.

The practical aspects of the cycle involve the efficiencies of the gas compressors, the turbine expander, and the fuel cell; the pressure losses as the gases flow through the system; and the temperature differences and the difference in heat capacities of the streams flowing through the recuperative heat exchanger. Other aspects of the fuel cell operation must be considered in greater detail for the design and evaluation of the power system. These include the possible need for fuel reforming external to the cell and the recycle of combustion product streams to provide the steam required to carry out the reforming process, to avoid carbon deposition, and to provide H_2 for effective cell operation.

Table 8-28 Performance Calculations for a Pressurized, High Temperature Fuel Cell (SOFC) with a Regenerative Brayton Bottoming Cycle; Approach Delta T=30F

COMPRESSOR EFF =	0.83	n = number of moles	
TURB EXPANDER EFF =	0.89	Cp = specific heat	
FUEL CELL EFF=	56.9	Hf = heat of formation at standard conditions	
CYCLE EFF=	82.1	So = entropy at standard conditions	

STREAM #	1	2	3	4	5	6	7	Cycle
p, PRESSURE, atm	1	1.48	1.48	1.48	1.48	1	1	
T, TEMPERATURE, K	298	337	1200	1311	1332	1216	352	
CH4, n	1	1	1	0.07	0	0	0	
CO, n								
H2, n								
CO2, n	0	0	0	0.93	1	1	1	
H2O, n	0	0	0	1.86	2	2	2	
O2, n	16.23	16.23	16.23	14.37	14.23	14.23	14.23	
N2, n	64.92	64.92	64.92	64.92	64.92	64.92	64.92	
SUM(n)	82.15	82.15	82.15	82.15	82.15	82.15	82.15	
SUM(nCp)	629.72	629.72	629.72	628.97	628.92	628.92	628.92	
SUM(nHf)	-17.9	-17.9	-17.9	-196.181	-209.6	-209.6	-209.6	
SUM(nSo)	3813.11	3813.11	3813.11	3811.99	3811.91	3811.91	3811.91	
GAMMA	1.350				1.351			
Q, HEAT, kcal/molCH4	0.0	543.5	0.0	-0.2	0.0	543.5		1086.8
W, WORK, kcal/molCH4	-24.4	0.0	109.1	0.0	72.7	0.0		157.4

The performance of a solid electrolyte fuel cell (SOFC) system (Hirschenhofer et al., 1994) operating with a regenerative Brayton bottoming cycle for heat and fuel recovery has been calculated. Table 8-28 illustrates the results. The work from the fuel cell burning CH_4 is assumed to be 60% the theoretical maximum; the corresponding fuel cell voltage is 0.63 volts. The efficiencies of the fuel and air compressors are 83%; and the expander of the turbine, 89%. It is assumed that the cell makes direct use of CH_4 fuel, or that oxidation and reforming are coincident; operation of the cell thus provides both the heat and the H_2O required for CH_4 reforming. Pressure losses in the fuel cell, combustor, recuperative exchanger, and the ducts of the system are ignored.

The results of the performance calculations are summarized in Table 8-29. The efficiency of the overall power system, work output divided by the lower heating value (LHV) of the CH_4 fuel, is increased from 57% for the fuel cell alone to 82% for the overall system with a 30 F difference in the recuperative exchanger and to 76% for an 80 F difference. This regenerative Brayton cycle heat rejection and heat-fuel recovery arrangement is perhaps the simplest approach to heat recovery. It makes minimal demands on fuel cell heat removal and gas turbine arrangements, has minimal number of system components, and makes the most of the inherent high efficiency of the fuel cell.

Table 8-29 Performance Computations for Various High Temperature Fuel Cell (SOFC) Heat Recovery Arrangements

General Conditions

SOFC, solid oxide fuel cell

Operating temperature, 1700-1900 F

Fuel cell output: 60% of theoretical maximum from CH4 fuel

Gas turbine compressor, expander efficiences: 83, 89%

Steam turbine efficiency: 90%

Notes

PR = pressure ratio of the gas turbine

NIT = nozzle inlet temperature of the turbine expander

Heat Recovery Arrangement	Work Output, %			Overall System Eff., %	Remarks
	Fuel Cell	Gas Turbine	Steam Turbine		
Regenerative Brayton Cycle	69.3	30.7	n/a	82.1	30 F Approach in Recuperative Exchanger Gas Turbine PR=1.48, NIT=1938 F
Regenerative Brayton Cycle	74.5	25.5		76.3	80 F Approach in Recuperative Exchanger Gas Turbine PR=1.35, NIT=1938 F
Combined Brayton-Rankine Cycl	75.3	10.3	14.3	75.6	Gas Turbine PR=12, NIT=2300 F Steam Turbine: 1600 psia, 1000 F, 1.5" Hg
Rankine Cycle	79.1		20.9	72.4	Steam Turbine: 1600 psia, 1000 F, 1.5" Hg

Combined Brayton-Rankine Cycle: The combined Brayton-Rankine cycle, Figure 8-61, again shows the gas turbine compressor for the air flow to the cell. This flow passes through a heat exchanger in direct contact with the cell; it removes the heat produced in cell operation and maintains cell operation at constant temperature. The air and fuel streams then pass into the cathode and anode compartments of the fuel cell. The separate streams leaving the cell enter the combustor and then the gas turbine. The turbine exhaust flows to the heat recovery steam generator and then to the stack. The steam produced drives the steam turbine. It is then condensed and pumped back to the steam generator.

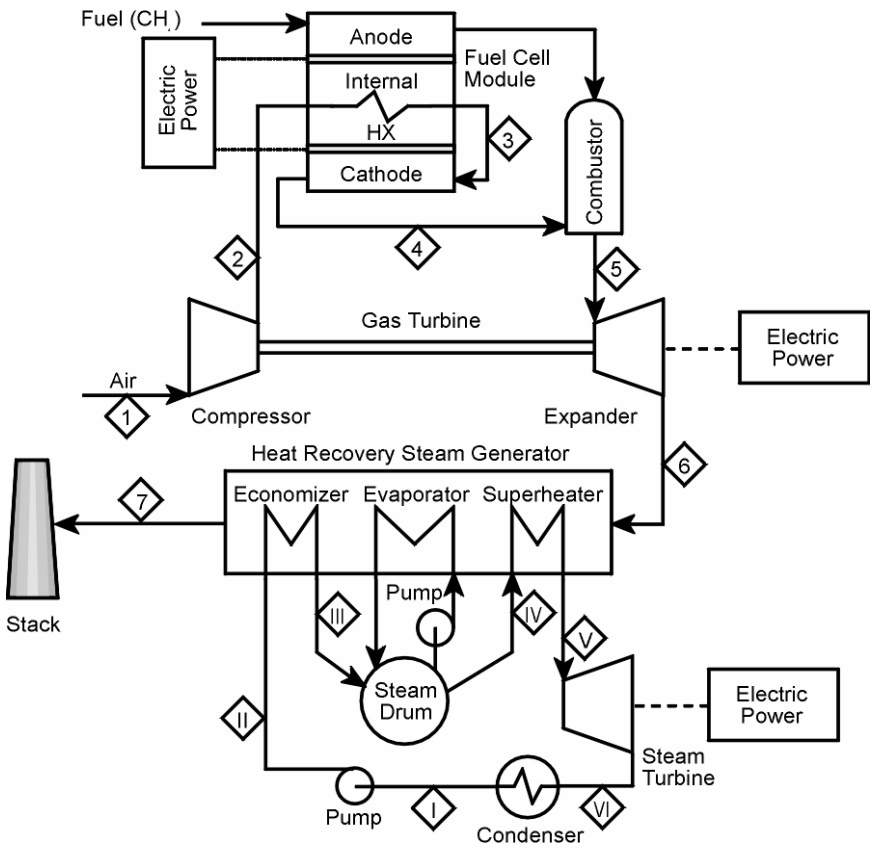

Figure 8-61 Combined Brayton-Rankine Cycle Fuel Cell Power Generation System

The air/fuel ratio entering the fuel cell and the fraction of the CH_4 fuel consumed in the cell are selected to achieve the desired fuel cell operating temperature range and gas turbine NIT and PR. These are selected to correspond with those of a conventional, large-scale, utility gas turbine.

Further insight can be gained from an idealized T- S diagram for the cycle, Figure 8-62, in which both the Brayton and the Rankine cycles are illustrated. Both the pressure and the temperature increase during fuel and air compression in this combined cycle will be significantly greater than in the regenerative Brayton cycle described above. The heating of the air and fuel, the operation of the fuel cell, and the burning of the residual fuel are assumed to occur at constant pressure. The expansion of the combustion product gases in the gas turbine again is represented as an adiabatic, reversible (constant S) process. Next, heat is removed from these gases at nearly constant pressure in the heat recovery steam generator; and they pass out through the stack.

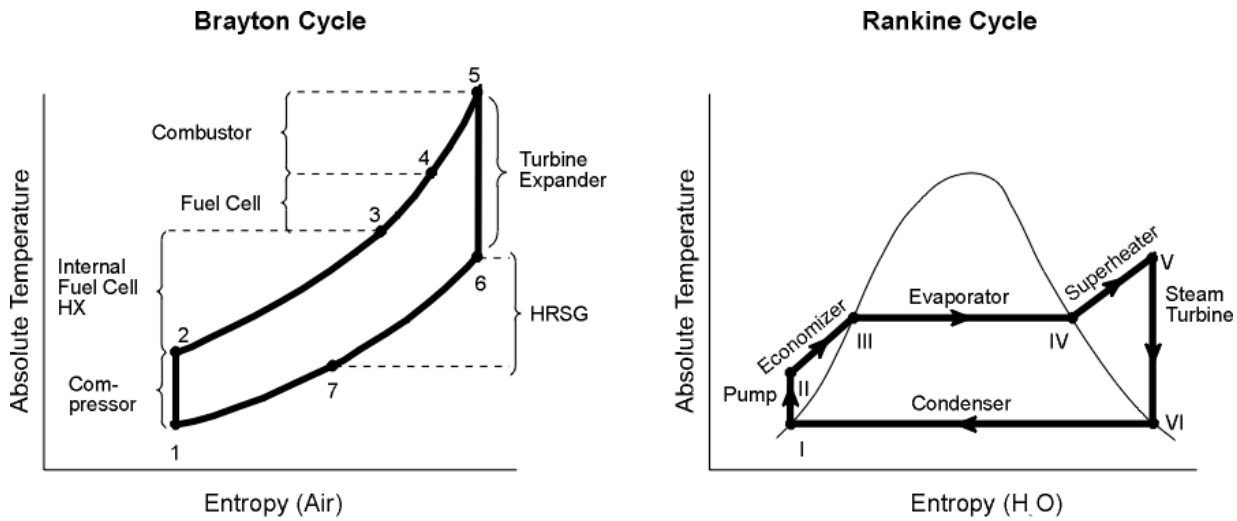

Figure 8-62 Combined Brayton-Rankine Cycle Thermodynamics

The Rankine cycle diagram placed adjacent the Brayton cycle in Figure 8-62 is indicated as a simple steam cycle with superheat, but no reheat and no multi-pressure steam generation. The thermodynamic advantage of the Rankine bottoming cycle is the lowered temperature of heat rejection, in the steam condenser, from the overall combined cycles.

The performance of a SOFC system with a Brayton-Rankine bottoming cycle for heat and fuel recovery has been calculated. Gas turbine compressor and expander efficiencies of 83% and 89% and a steam turbine efficiency of 90% have been assumed.

The significant operating conditions of the gas and steam turbines and the results of the computations are summarized in Table 8-29. The principal result is that the efficiency of the overall system, work output divided by the CH_4 LHV, is increased from 57% for the fuel cell alone to 75% for the overall system. This combined Brayton-Rankine cycle heat-fuel recovery arrangement is significantly more complex and less efficient than the simple regenerative Brayton cycle approach. It does, however, eliminate the requirement for a large, high temperature gas to gas heat exchanger.

The key link between the Brayton and the Rankine cycles is the heat recovery steam generator whose operation is illustrated by the temperature-heat (T-Q) plot in Figure 8-63. The temperatures of the gases and of the water, T, are plotted as a function of the heat, Q, transferred from the combustion product gases to the water-steam between their entrance and any point in the steam generator. The area between the temperature curves for the two flowing streams is an indication of the irreversibility, or loss in available work, resulting from the transfer of heat over a finite temperature difference. Reducing this area, moving the gas and steam curves closer, requires increased heat transfer surface area in the steam generator. Steam reheat and multi-pressure level heat recovery boilers are frequently proposed to minimize the loss in available work.

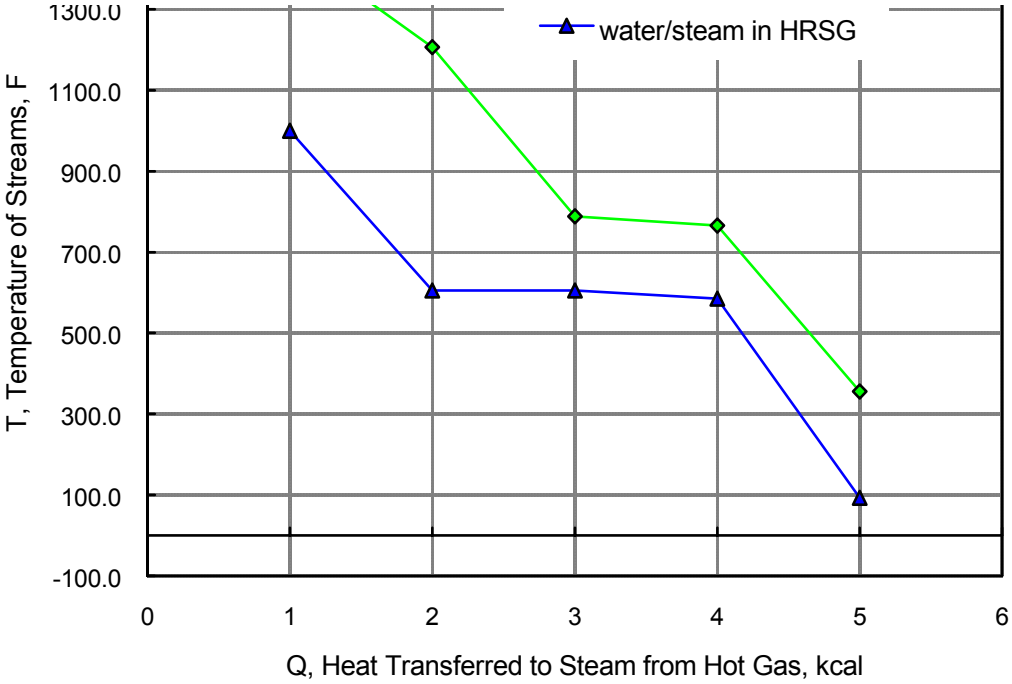

Figure 8-63 T-Q Plot for Heat Recovery Steam Generator (Brayton-Rankine)

Rankine Cycle: The fuel cell Rankine cycle arrangement in Figure 8-64 employs a heat recovery steam generator operating on the exhaust combustion product stream from the fuel cell and combustor at atmospheric pressure. This exhaust stream first provides the heat required to preheat and reform the CH_4 fuel, providing CO and H_2 at temperature to the fuel cell. Partially combusted fuel from the cell is recycled to provide the H_2O required for reforming the fuel. Depleted air from the cell exhaust is recycled to the air feed stream to raise its temperature to the desired value at the cell inlet. The operating conditions and the T - S diagram for the Rankine cycle are identical to those illustrated for the combined Brayton-Rankine cycle in Figure 8-62 and Table 8-29.

The results of the performance calculations for the fuel cell, Rankine cycle heat recovery system, summarized in Table 8-29, indicate that the efficiency of the overall system is increased from 57% for the fuel cell alone to 72% for the overall system. This Rankine cycle heat-fuel recovery arrangement is less complex but less efficient than the combined Brayton-Rankine cycle approach, and more complex and less efficient than the regenerative Brayton approach. It does, however, eliminate the requirement for a large, high temperature gas to gas heat exchanger. And in applications where cogeneration and the supply of heat is desired, it provides a source of steam.

The T - Q plot for the heat transfer processes involved in this fuel cell Rankine cycle arrangement is shown in Figure 8-65. Because heat is removed from the exhaust gases to heat and reform the CH_4 fuel feed, the temperature of the hot gas entering the heat recovery steam generator in this

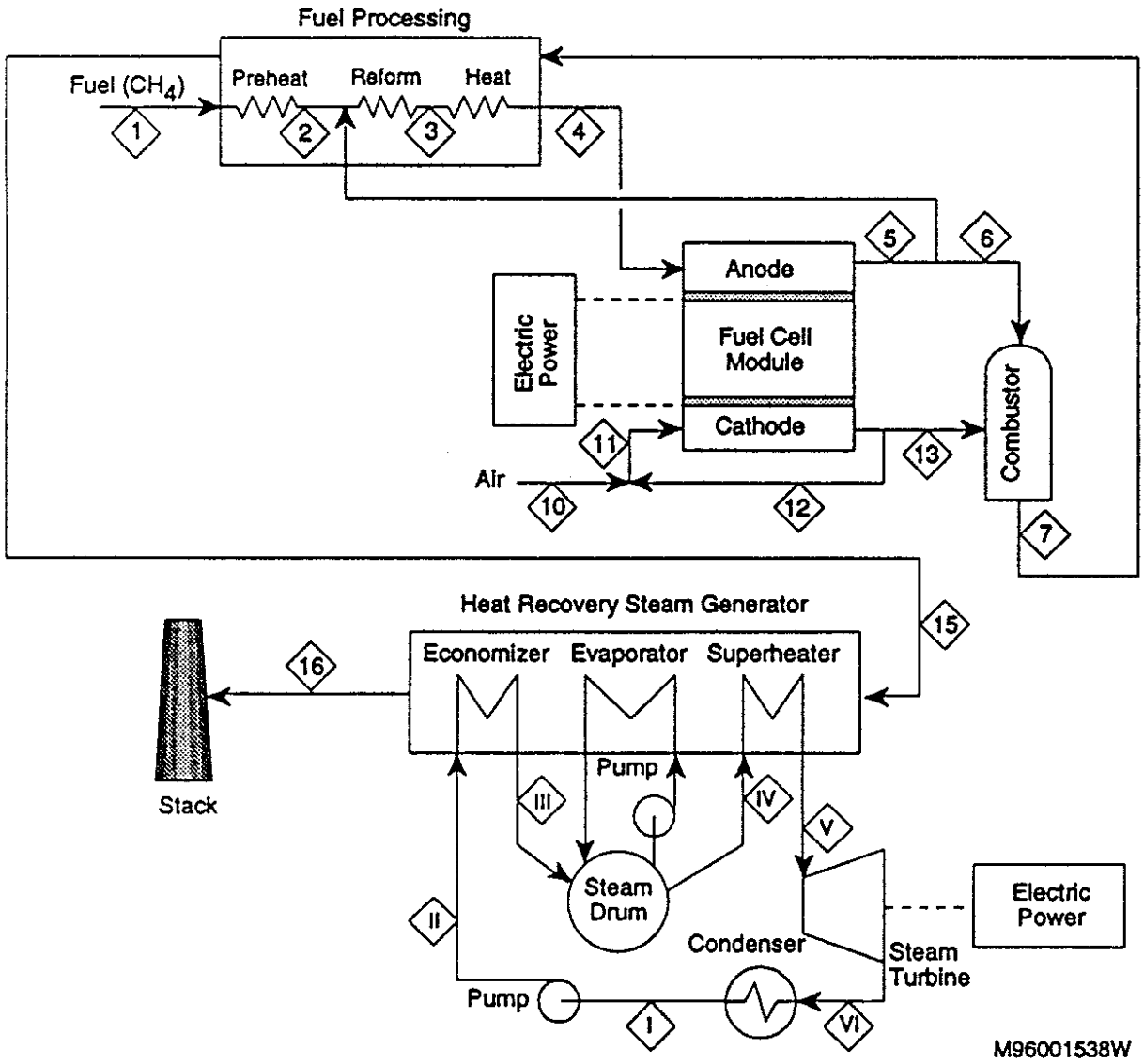

Figure 8-64 Fuel Cell Rankine Cycle Arrangement

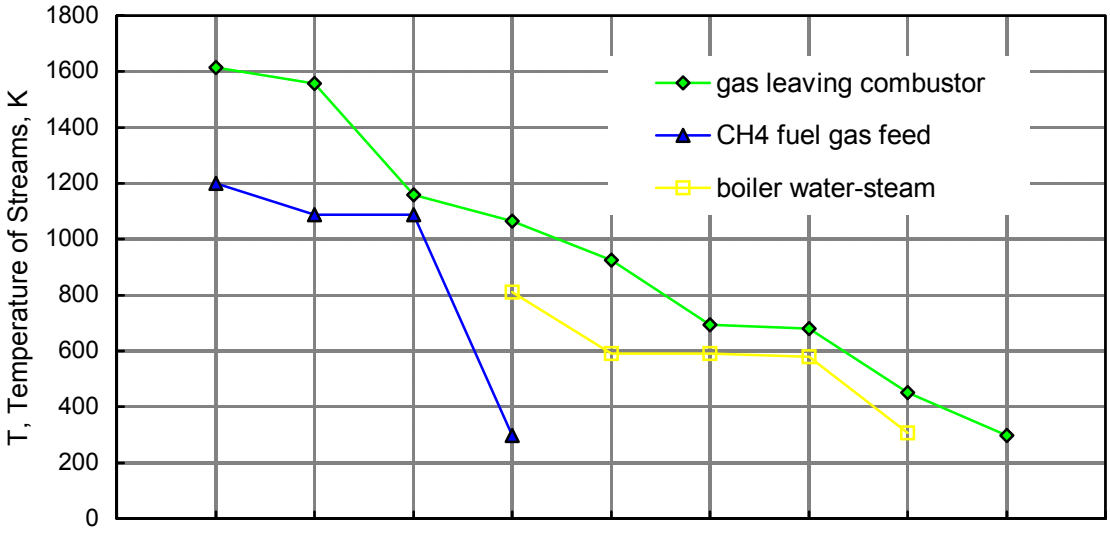

Figure 8-65 T-Q Plot of Heat Recovery from Hot Exhaust Gas

particular Rankine cycle fuel cell arrangement is significantly lower than in the previous combined Brayton-Rankine cycle arrangement. Increased surface area is, therefore, required in the heat recovery steam generator for this fuel cell Rankine cycle arrangement.

These three approaches to reject heat and exhaust fuel recovery with power generation apply primarily to the higher temperature, solid oxide (1800 F) and molten carbonate (1200 F), fuel cell systems operating on CH_4 fuel. The lower operating temperatures of the phosphoric acid (400 F) and polymer electrolyte (175 F) fuel cells severely limit the effectiveness of thermal cycle based power generation as a practical means of heat recovery.

All three of the heat recovery arrangements have calculated overall efficiencies greater that 70% as indicated in Table 8-29. None have been optimized in any sense -- in terms of efficiency, capital and operating costs, maintainability or availability. Each of the arrangements has its advantages and disadvantages. It appears, however, that the regenerative Brayton cycle has the advantage of greatest simplicity and highest potential overall efficiency over the combined Brayton-Rankine and Rankine cycle approaches.

The consideration of heat recovery and use in such fuel cell systems requires some consideration of heat generation and transfer within the cells of the system. Direct oxidation of CH_4 at the anode of the cell, if possible, would implement the overall process:

$$CH_4 + 2O_2 = CO_2 + 2H_2O\ (v)$$

This reaction, having equal number of mols of gas reactants and products, has a negligible change in entropy and thus a negligible heat effect if carried out reversibly at constant temperature. The maximum work available from a fuel cell under these circumstances would then be approximately the enthalpy change of the reaction, i.e., the heat of combustion of the

CH_4; the efficiency of the fuel cell power generation process could, therefore, approach 100%. However, work is lost and a corresponding quantity of heat is produced by irreversibilities both in fuel cell operation --

- the electrical resistance of the electrolyte to ion flow and of the electrodes, current collectors, and leads to electron flow;
- the kinetics of the processes involving reactants, ions, and electrons at the anode and cathode of the cell;
- the transport, or diffusion, of reactants within the anode and cathode chambers to the electrode;
- and also in overall system operation –
- the preheating of the air and fuel streams;
- the pretreating, or reforming, of the CH_4 fuel to provide more reactive H_2 and to prevent the deposition of carbon (C).

The heat resulting from these irreversibilities must then be removed in order to maintain the fuel cells at a desired operating temperature. Irreversibilities and the resulting quantity of heat produced can be reduced, in general, by increasing the active area of the fuel cells, heat exchangers, and fuel reformer; but increased equipment costs result.

In general, reforming of the CH_4 fuel with excess H_2O outside the cell has been practiced both in molten carbonate and solid oxide fuel cell systems in order to produce H_2, more reactive on a fuel cell anode, and to avoid the possible deposition of C. This reforming reaction

$$CH_4 + H_2O = CO + 3H_2$$

is associated with an increase in entropy and absorbs heat. Excess H_2O produces additional H_2 and reduces the CO content of the reformed gases, which may adversely affect anode reactions, by the shift reaction

$$H_2O + CO = H_2 + CO_2.$$

This reaction is thermally neutral. The heat absorbed in the CH_4 reforming reaction is released by the subsequent reaction of the H_2 product at the anode of the fuel cell. If, therefore, the reforming process can be carried out in close proximity to and in thermal contact with the anode process, the thermal neutrality of the overall CH_4 oxidation process can be approximated. And the heat removal and recovery process for the fuel cell system can deal merely with the heat produced by its operational irreversibilities.

Heat removal from fuel cells, and cell batteries, can be accomplished:

- directly through the flow of reactants to and products from them.
- indirectly through heat transfer surfaces in contact with the cell or included within a battery.

A specific fuel cell system is viewed here as having a fixed range of operating temperature between a maximum and minimum; heat must therefore be removed in such a manner to maintain the temperature within these limiting values. If heat is removed directly by reactant flows, then the quantity of flow must be adjusted so that inlet and outlet temperatures (as well as

the intermediate temperatures) of the cell and of the flow streams are within the permissible range. Practically, the air stream is adjusted to achieve this result, since the purpose of the fuel cell is to consume the fuel in the production of electrical energy. Increasing the fuel flow to remove heat from the cell increases the quantity of unburned fuel in the exhaust from the cell. If heat is removed from the fuel cell indirectly through adjacent or embedded surface, then the flow and temperature of the coolant stream can be selected somewhat independent of the cell operating temperature. But the distribution of heat transfer surface in the cell (or battery) and the rate of heat transfer across that surface must be carefully adjusted and controlled to maintain the temperature throughout the cell (or battery) within the prescribed temperature range.

The regenerative Brayton cycle, as presented, depends primarily on its fuel cell component for conversion of the fuel and thus for its overall efficiency. The gas turbine merely provides the means for recovery of the waste heat and residual fuel in the combustion product stream. The gas turbine operates, therefore, at a temperature only slightly elevated above that of the cell by the combustion of the residual fuel. The pressure ratio selected for the turbine in this regenerative cycle is determined by the ratio of the temperature of the gases leaving the auxiliary combustor to the temperature of the reactant gases entering the fuel cell. In general, for either molten carbonate or solid oxide cells, this selected pressure ratio will be less than two. The proposed method of cell cooling is air flow, which will be increased significantly, by a factor of 4-8 above that required for oxidation of the fuel. The feasibility of this cycle will depend on the availability of air compressor and turbine expander units with:

- the pressure ratio and temperature capability compatible with the fuel cell operation.
- a capacity appropriate to market applications.

The effectiveness of the regenerative Brayton cycle performance will depend on the efficiency of the fuel cell, compressor, and turbine units; the pressure loss of gases flowing through the system; the approach temperatures reached in the recuperative exchanger; and, most importantly, the cost of the overall system.

The combined Brayton-Rankine cycle depends on both the fuel cell and the gas turbine components for conversion of the fuel and thus for its overall efficiency. The extent of conversion of the fuel occurring in the fuel cell increases as the cell operating temperature and the range of coolant temperature rise increase. For this reason, the cycle as presented is based on indirect heat removal from the cell, heating the air stream temperature from the compressor outlet to the cell operating temperature. This provision maximizes the cell contribution to the energy output of the combined cycle. The PR and NIT of the turbine are those selected to match those of the current utility scale equipment -- a PR of 12 and an NIT of 2300 F -- resulting in a combined cycle efficiency of perhaps 45-50%, not considering the electrical energy output of and the fuel input to the fuel cell. The fuel combustion occurring in the combustor and overall air/fuel ratio is then determined by the combination of the cell and the turbine inlet temperatures.

The fuel cell Rankine cycle arrangement has been selected so that all fuel preheating and reforming are carried out external to the cell and air preheating is accomplished by mixing with recycled depleted air. The air feed flow is adjusted so that no heat transfer is required in the cell or from the recycled air. Consequently, the internal fuel cell structure is greatly simplified, and the requirement for a heat exchanger in the recycle air stream is eliminated.

Summary

Advantages, Disadvantages of Various Fuel Cell, Power Cycles

Regenerative Brayton

Advantages:

- simple cycle arrangement, minimum number of components.
- relatively low compressor and turbine pressure ratio, simple machines.
- relatively low fuel cell operating pressure, avoiding the problems caused by anode/cathode pressure differential and high pressure housing and piping.
- relatively low turbine inlet temperatures, perhaps 1950 F for solid oxide and 1450 F for molten carbonate fuel cell systems. Turbine rotor blade cooling may not be required.
- relatively simple heat removal arrangements in fuel cells, accomplished by excess air flow. No internal heat transfer surface required for heat removal.
- fuel conversion in cells maximized, taking full advantage of fuel cell efficiency.
- adaptability to small scale power generation systems.

Disadvantages:

- tailoring of compressor and turbine equipment to fuel cell temperature and cycle operating pressure required. (It is not clear to what extent available engine supercharging and industrial compressor and turbine equipment can be adapted to this application.)
- large gas to gas heat exchanger for high temperature heat recuperation required.
- efficiency and work output of the cycle sensitive to cell, compressor, and turbine efficiencies; pressure losses; and temperature differentials.

Combined Brayton-Rankine

Advantages:

- integrated plant and equipment available for adaptation to fuel cell heat recovery.
- high efficiency system for heat recovery.

Disadvantages:

- complex, multi component, large scale system for heat recovery.
- adaptation of existing gas turbine required to provide for air take off and return of hot depleted air and partially burned fuel.
- high pressure operation of the bulky fuel cell system required.
- precise balancing of anode and cathode pressures required to prevent rupture of fuel cell electrolyte.
- indirect heat removal required from fuel cells with compressed air, initially at low temperature, to enable significant conversion of the fuel flow in the cells.

Rankine

Advantages:

- ambient pressure operation within the fuel cell.
- heat recovery in a boiler, avoiding the high temperature gas to gas exchanger of a regenerative Brayton cycle.
- no gas turbine required, only fans for air and exhaust product gas flow.

- steam available for cogeneration applications requiring heat.

Disadvantages:

- inherently lower efficiency than regenerative Brayton and combined Brayton-Rankine cycles.
- requirement for cooling and feed water.
- greater complexity than regenerative Brayton cycle arrangement.

8.6 Fuel Cell Networks

8.6.1 Molten Carbonate Fuel Cell Networks: Principles, Analysis and Performance

The U.S. Department of Energy's National Energy Technology Laboratory (NETL) sponsors the research and development of engineered systems which utilize domestic fuel supplies while achieving high efficiency, economy and environmental performance. One of the most promising electric power generation systems currently being sponsored by NETL is the molten carbonate fuel cell (MCFC).

NETL looked at improving upon conventional MCFC system designs, in which multiple stacks are typically arranged in parallel with regard to the flow of reactant streams. As illustrated in Figure 8-66a, the initial oxidant and fuel feeds are divided into equal streams which flow in parallel through the fuel cell stacks.

In an improved design, called an MCFC network, reactant streams are ducted such that they are fed and recycled among multiple MCFC stacks in series. Figure 8-66b illustrates how the reactant streams in a fuel cell network flow in series from stack to stack. By networking fuel cell stacks, increased efficiency, improved thermal balance, and higher total reactant utilizations can be achieved. Networking also allows reactant streams to be conditioned at different stages of utilization. Between stacks, heat can be removed, streams can be mixed, and additional streams can be injected.

Stacks in series approach reversibility. MCFC stack networks produce more power than conventional configurations because they more closely approximate a reversible process. To illustrate this fact, consider Figure 8-67, which compares the maximum power that could be generated by three different MCFC systems having identical feed stream compositions[1].

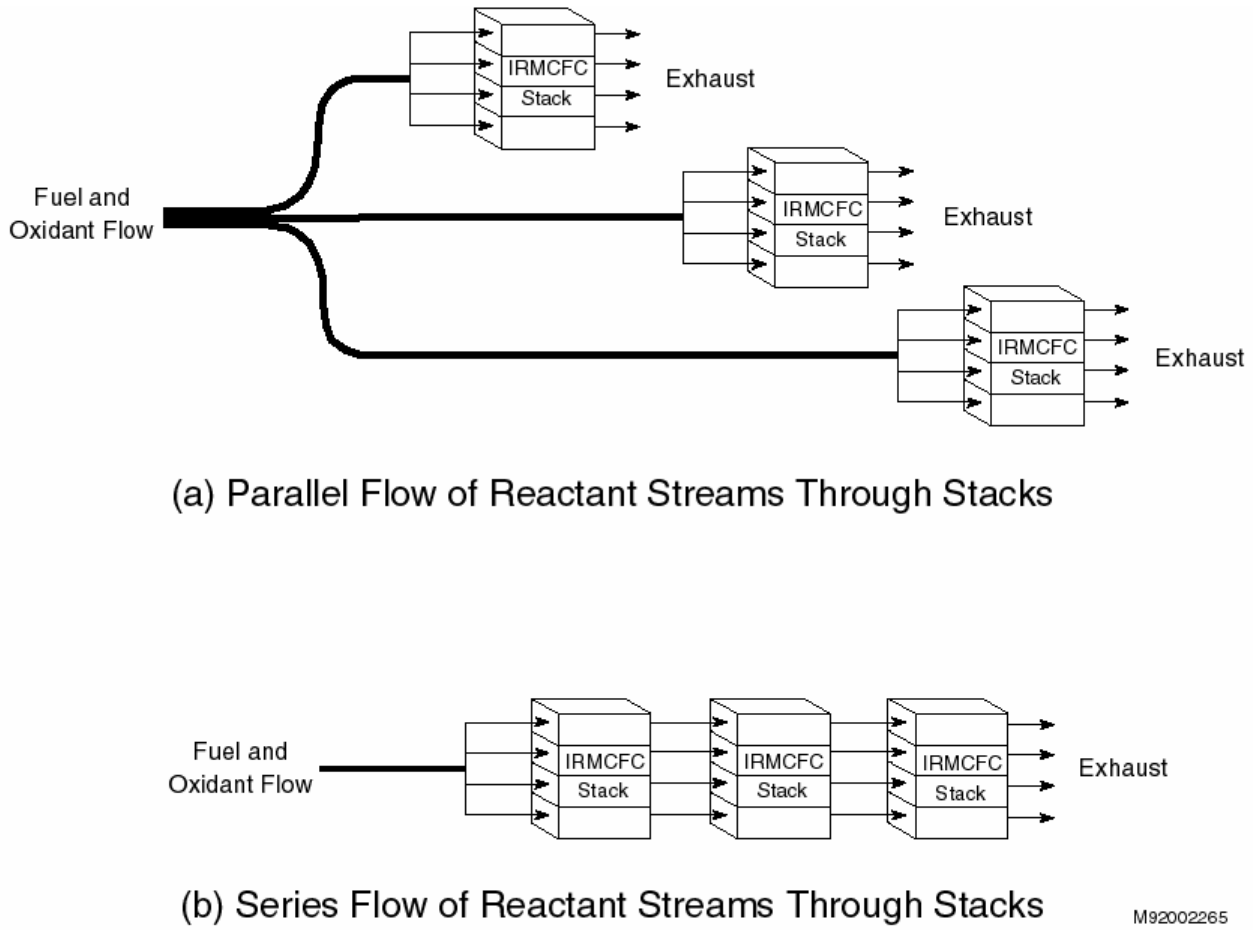

Figure 8-66 MCFC System Designs

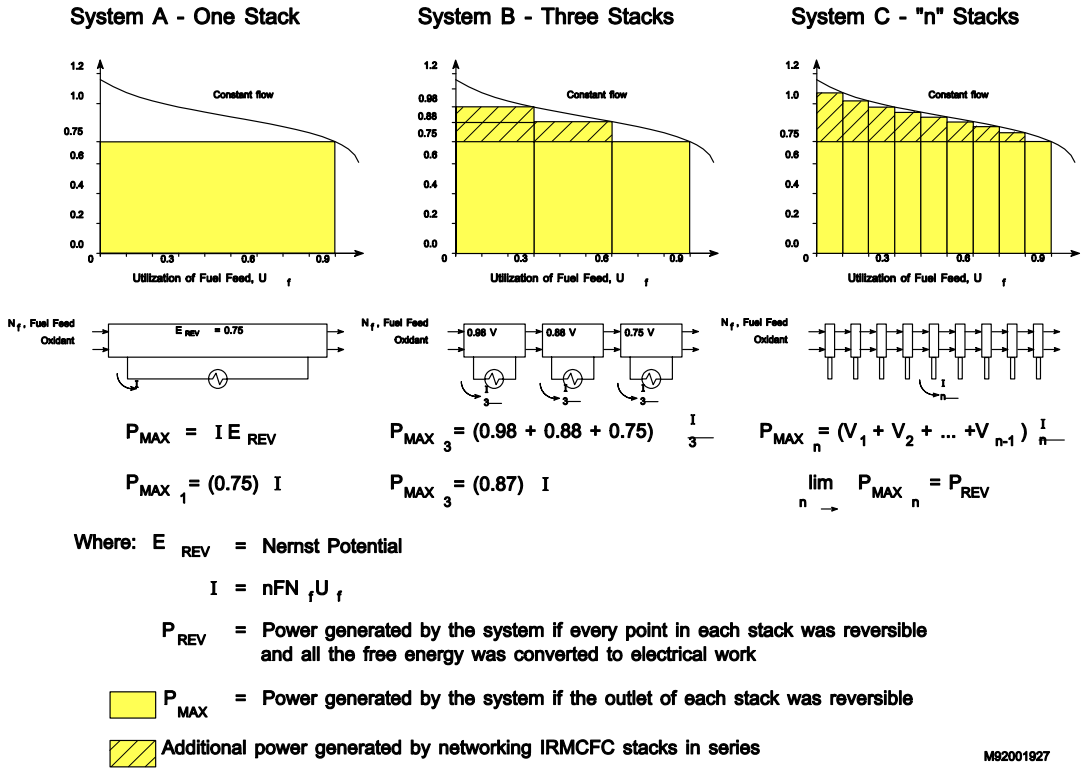

Figure 8-67 Stacks in Series Approach Reversibility

A graph of Nernst potential versus fuel utilization for the given feed stream compositions (60) was duplicated three times in Figure 8-67. The Nernst potential is the voltage which drives reversible electrode reactions. This reversible voltage, generated by the overall cell reaction, is a function of the local temperature, pressure, and reactant concentrations. As reactants are utilized, their concentrations change. Since Nernst potential is dependent upon the concentrations of reactants, it varies with the degree of utilization.

Fuel utilization is directly proportional to the charge transferred across the electrolyte. Therefore, the shaded areas of the graphs represent power -- the product of voltage and current. If reversibility is assumed at the outlet of each stack, no voltage losses are deducted from the Nernst potential. Therefore, each shaded area represents the maximum power, which each cell could generate.

System A in Figure 8-67 is composed of a single stack. Three stacks are arranged in series in system B. System C features many, or "n," stacks configured in series. In all three systems, the voltage of each stack corresponds to reactant concentrations at its outlet.

For comparison, each system is assumed to have the same total stack membrane area. That is, the area of each stack in system B is one third the area of the stack in system A. Similarly, the

area of each stack in system C is one "nth" the area of the single stack in system A. For simplicity, each stack is considered to contain only one cell.

Since each system achieves the same total fuel utilization (90%) across the same total area, each stack has the same average current density. Irreversible voltage loss is mainly a function of current density and stack temperature. Since these parameters are equivalent in each stack, it is assumed that the Nernst potential of each stack would be reduced by the same amount.

In system A, 90% of the fuel is utilized in a single stack, and all the current is generated at a single voltage. The power that this system can achieve is represented by the graph's shaded region.

In system B, three stacks in series each utilize 30% of the fuel. The current generated by each stack in system B is one third of the current generated in system A. Each stack in system B produces a different voltage. At the exit of the first stack, a high Nernst potential is generated because 70% of the fuel is still unburned. Likewise, at the exit of the second stack, 40% of the fuel remains unburned, generating another improved Nernst potential. Only ten percent of the fuel remains at the exit of the third stack, yielding the same Nernst potential that the single stack in system A produced. The three stack network can produce more power because two-thirds of the total charge is transferred at increased voltages. Comparing the shaded areas of the graphs illustrates the additional power that can be produced by arranging stacks in series.

In system C, many stacks are connected in series. Very small currents are generated at still higher voltages. As the number of stacks in series is increased, the maximum achievable power quickly approaches the power which a reversible system would generate, i.e. complete conversion of the available free energy. (A reversible system is reversible at every point in each stack, not just at the stack outlets.) The shaded area in the graph nearly fills the entire area under the curve - the reversible power.

Each system in Figure 8-66 converts an equivalent amount of free energy (90% fuel utilization) into heat and electrical work. The key difference, however, is that the systems with MCFC stacks networked in series transfer charge at higher voltages, thus converting more of the free energy directly into electrical work, and less into heat. As the number of stacks in series is increased, a reversible process is approached which would convert all the free energy into work and none into heat. Although heat that is produced from free energy can be reconverted into electrical work (e.g. via a steam turbine), an MCFC stack's direct conversion of free energy is intrinsically more efficient. Therefore, networking MCFC stacks in series results in more efficient power production even when waste heat is recovered.

Although each stack added to a series network would improve the system's efficiency, the incremental benefit obtained with each additional stack diminishes. A finite number of stacks could adequately, but not exactly, approach a reversible process. In a practical network, the number of stacks would be limited by economic, space, and design constraints.

In a similar study, Liebhafsky and Cairns (26) compared two arrangements of tubular, calcia-stabilized solid oxide fuel cells. In one arrangement, hydrogen and air were supplied to a single,

30-cm cell. In the other arrangement, the same cell was segmented into three, 10-cm cells which were ducted such that the same reactant streams flowed through them in series. Each arrangement had a total fuel utilization of 90% and each cell had the same average current density. Each cell in the series arrangement accomplished one-third of the total fuel utilization. Calculations showed that the series arrangement produced 5% more power than the single cell, and that further sectioning would produce greater improvements. It was concluded that the increase in irreversibility associated with changes in gas composition has nothing to do with electrode kinetics, but is rooted in the Nernst equation.

8.6.2 MCFC Network

When designing an MCFC power system, several requirements must be met. An MCFC system must properly condition both the fuel and oxidant gas streams. Methane must be reformed into the more reactive hydrogen and carbon monoxide. Carbon deposition, which can plug gas passages in the anode gas chamber, must be prevented. To supply the flow of carbonate ions, the air oxidant must be enriched with carbon dioxide. Both oxidant and fuel feed streams must be heated to their proper inlet temperatures. Each MCFC stack must be operated within an acceptable temperature range. Excess heat generated by the MCFC stacks must be recovered and efficiently utilized.

Figure 8-68 shows an MCFC network. The arrangement of stacks in series, as well as a unique recycle scheme, allows an MCFC network to meet all the requirements of an MCFC power system, while achieving high efficiency.

8.6.3 Recycle Scheme

In the network's recycle scheme, a portion of the spent fuel (Stream 5) and oxidant (Stream 4) is mixed and burned. The products of combustion (Stream 3) are then recycled through the cathode in order to provide the necessary carbon dioxide to the stacks. This eliminates the need for an external source of pure carbon dioxide. The cathode-cathode recycle (Stream 4) is large enough to cool the stacks, transferring excess energy to the heat recovery boilers. During the transfer of heat, enough energy is left in the oxidant recycle to heat the fresh air feed to the designated cathode inlet temperature. A second portion of the spent fuel (Stream 1) is recycled through the anode to provide enough steam to prevent carbon deposition and internally reform methane. This eliminates the need for steam to be supplied from another source. The anode-anode recycle also heats the fresh fuel feed to the designated anode inlet temperature.

8.6.4 Reactant Conditioning Between Stacks in Series

When MCFC stacks are networked in series, reactant streams can be conditioned between the stacks -- at different stages of utilization. The composition of reactant streams can be optimized between stacks by injecting a reactant stream (see Figure 8-66) or by mixing the existing reactant streams.

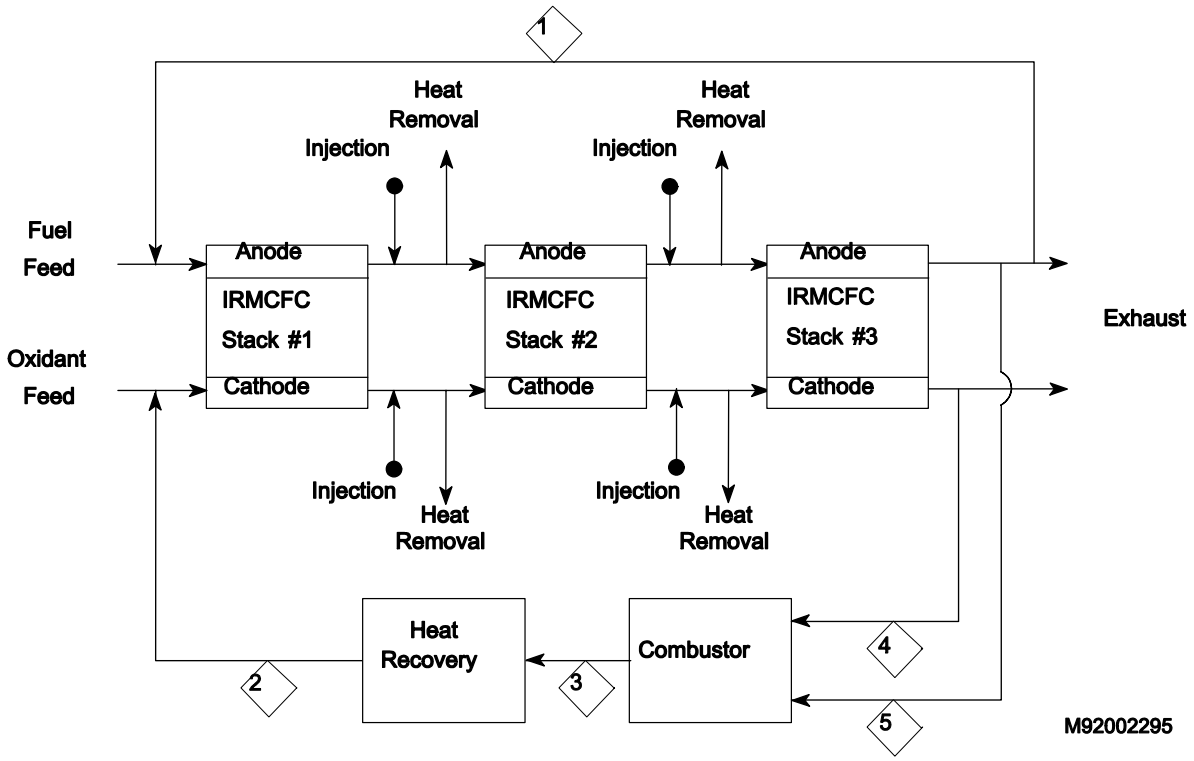

Figure 8-68 MCFC Network

Between stacks networked in series, heat can be removed from the reactant streams to assist in controlling stack temperatures. The heat in a network reactant stream can be transferred to a cooler process stream in a heat exchanger or hot and cold reactant streams can be mixed directly. The recovered heat may be utilized in a combined cycle or for cogeneration.

Methane can be injected into fuel streams between stacks networked in series. Since the reforming of methane into hydrogen is endothermic, its careful distribution among stacks in series is expected to improve the thermal balance of the system by allowing waste heat to be more evenly consumed throughout the total utilization of reactants. Improved thermal balance should allow stacks to be operated nearer their maximum temperature, reducing ohmic voltage losses. However, injecting portions of the fuel feed between stacks in series decreases the Nernst potential of every stack except the last one, since less fuel passes through each stack. (The amount of fuel which passes through the last stack does not change.) Optimizing the system requires an evaluation of the point at which the benefits of improved thermal balance outweigh the reduction in Nernst potential associated with such fuel redistribution.

8.6.5 Higher Total Reactant Utilization

The optimum total reactant utilization of stacks networked in series is higher than that of conventional, parallel stacks. Conventional designs avoid high utilization, because that would result in low voltages. In conventional configurations, the total utilization of reactants is accomplished in one stack. Therefore, when high utilizations are attempted, the low voltage which is generated adversely affects the total power production. In networks, however, the

utilization of reactants is accomplished incrementally, and the low voltage associated with high utilization is restricted to stacks which produce only a portion of the total power.

Manifolding problems can further limit the practical reactant utilization of conventional MCFC systems. Ideally, fuel and oxidant streams are distributed equally among individual cells in a stack. Today's manifolds, however, have not been able to achieve this, and cells are typically supplied with unequal reactant flows. This causes the composition of outlet reactant streams to be variable among the cells. At high utilizations, this variability leads to a significant reduction in stack voltage. Therefore, conventional systems avoid such high utilizations. However, when stacks are networked in series, reactant streams can be thoroughly mixed between cells. This reduces the variability in reactant composition and helps to minimize the stack voltage loss.

Another study (7) maximized the efficiency of conventional and series-connected fuel cell systems by optimizing cell voltage and current density. The study found that the optimum fuel utilization in the series-connected system was higher than that in the conventional system. Most importantly, the higher fuel utilization and lower current density of the series-connected system combined to give more efficient performance than the conventional system.

8.6.6 Disadvantages of MCFC Networks

For recycling to improve the performance of an MCFC network, it must provide benefits that outweigh its inherent disadvantages. If carbon dioxide is not separated from the anode-anode recycle, the concentration of carbon dioxide in the anode is increased. This reduces the Nernst potential. The Nernst potential is similarly reduced by the anode-cathode recycle if steam is not condensed out, since recycled steam dilutes reactant concentrations in the oxidant. In addition, part of the power generated by the network is consumed by the equipment necessary to circulate the recycle streams. Such circulation equipment, along with the additional ducting required by recycling, also increases the capital cost of the MCFC network.

Given the same initial feed streams, the flowrate of reactants through stacks networked in series is much larger than the flowrate of reactants through stacks in a conventional system. Conventional fuel cell systems divide the initial feed streams among many stacks arranged in parallel. However, the initial feed streams in an MCFC network are not divided, but fed directly into the first of a series of many stacks. Perhaps the greatest disadvantage of MCFC networks is that this increased flowrate creates larger pressure drops.

Another potential disadvantage of an MCFC network is the interdependence of the stacks in series. A problem with one stack could alter the performance of succeeding stacks. Furthermore, bypassing or isolating a problematic stack in a network could be a difficult control process. In the conventional parallel configuration, stack performance is not so interrelated.

8.6.7 Comparison of Performance

Two ASPEN (Advanced System for Process Engineering, public version) simulations compare the performance of conventional and networked fuel cell systems having identical recycle schemes and steam bottoming cycles. Each simulated system was composed of three MCFC stacks operating at the same temperature and pressure. The Nernst potential of each MCFC in both systems was reduced by 0.3 volts due to activation, concentration and ohmic voltage

polarizations. (This is a conservative estimate, representing a much higher outlet voltage polarization than would be expected.) Simple, single-pressure steam cycles produce secondary power.

When the total fuel utilization of each system was optimized for maximum efficiency, the efficiency of the fuel cell stacks networked in series was nearly 10% greater than that of the stacks arranged in parallel (44.9% vs. 35.4%, LHV). When the power generated by each system's steam bottoming cycle was considered in addition to its fuel cell power, the gap in efficiency narrowed to 5.5%. The efficiency of the total networked system is 56.8%, while that of the total conventional system was 51.3%.

The fuel cell network which was simulated was not fully optimized. Optimization of flow geometry, operating pressure, stack fuel utilization and current, reactant conditioning, and other parameters would be expected to yield further significant increases in total system efficiency.

8.6.8 Conclusions

Key to the concept of networking is the arrangement of multiple fuel cell stacks relative to the flow of reactant streams. Conventional fuel cells systems have been designed such that reactant streams flow in parallel through fuel cell stacks. In a fuel cell network, however, reactant streams are ducted such that they are fed and recycled through stacks in series.

Arranging fuel cell stacks in series offers several advantages over conventional fuel cell systems. Stacks networked in series more closely approach a reversible process, which increases the system efficiency. Higher total reactant utilizations can be achieved by stacks networked in series. Placing stacks in series also allows reactant streams to be conditioned at different stages of utilization. Between stacks, heat can be consumed or removed, (methane injection, heat exchange) which improves the thermal balance of the system. The composition of streams can be adjusted between stacks by mixing exhaust streams or by injecting reactant streams.

Computer simulations have demonstrated that a combined cycle system with MCFC stacks networked in series is significantly more efficient than an identical system with MCFC stacks configured in parallel.

8.7 Hybrids

This section present hybrids for generating electricity or for providing power in automotive vehicles. Hybrid systems that incorporate gas turbines build upon the outstanding performance of the fuel cell by utilizing the exhausted fuel cell heat. Hybrid electric vehicles utilize fuel cells to provide electric power to augment or replace exiting power sources. These systems are highly efficient and deliver superior environmental performance. Presented below is a general discussion of hybrid technology as well as specific initiatives in the gas turbine / fuel cell and electric power hybrid vehicle areas.

8.7.1 Technology

Advanced power generation cycles that combine high-temperature fuel cells and gas turbines, reciprocating engines, or another fuel cell are the hybrid power plants of the future. These conceptual systems have the potential to achieve efficiencies greater than 70 % and be

commercially ready by the year 2010 or sooner. The hybrid fuel cell/turbine (FC/T) power plant will combine a high-temperature, conventional molten carbonate fuel cell (MCFC) or a solid oxide fuel cell (SOFC) with a low-pressure-ratio gas turbine, air compressor, combustor, and in some cases, a metallic heat exchanger (27). The synergistic effects of the hybrid fuel cell/turbine technology will also provide the benefits of reduced greenhouse gas emissions. Nitrous (NOx) emissions will be an order of magnitude below those of non-fuel cell power plants and carbon monoxide emissions will be less than 2 parts per million (ppm) (28). There will also be a substantial reduction in the amount of carbon dioxide produced compared to conventional power plants.

The hybrid system is key to the Department of Energy's Vision 21 plants. The Vision 21 program has set power plant goals of achieving efficiencies greater than 75 % (LHV) for natural gas. The higher efficiencies play a key role in reducing emissions, another target in Vision 21 plants. As a comparison, conventional coal-burning power plants are typically 35 % efficient and natural gas fired plants are now 40 to 50 % efficient. Figure 8-69 shows the estimated efficiency ranges of current and future power generation systems.

The combination of the fuel cell and turbine operates by using the rejected thermal energy and residual fuel from a fuel cell to drive the gas turbine. The fuel cell exhaust gases are mixed and burned, raising the turbine inlet temperature while replacing the conventional combustor of the gas turbine. Use of a recuperator, a metallic gas-to-gas heat exchanger, transfers heat from the gas turbine exhaust to the fuel and air used in the fuel cell. Figure 8-70 illustrates an example of a proposed fuel cell/turbine system.

There can be many different cycle configurations for the hybrid fuel cell/ turbine plant. In the topping mode described above, the fuel cell serves as the combustor for the gas turbine while the

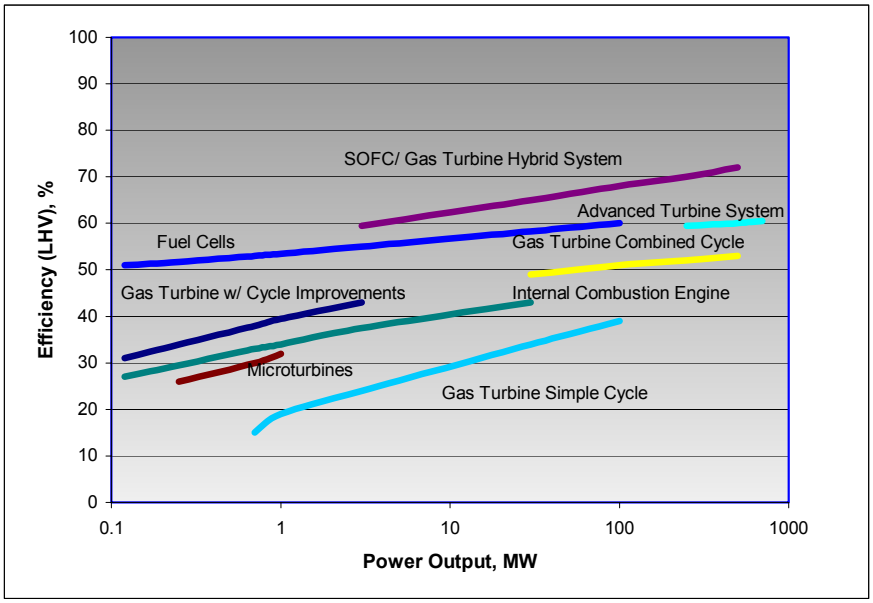

Figure 8-69 Estimated performance of Power Generation Systems

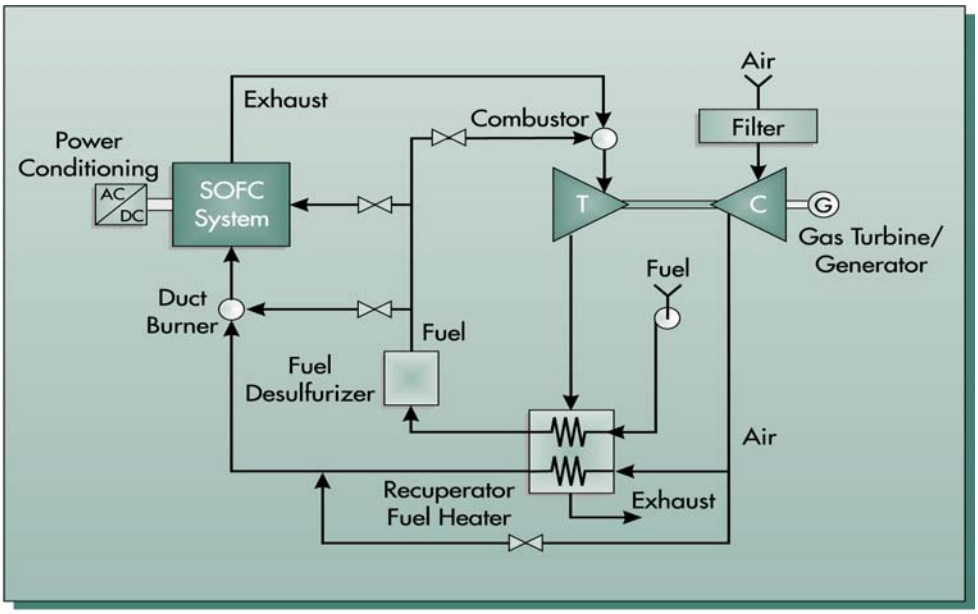

Figure 8-70 Diagram of a Proposed Siemens-Westinghouse Hybrid System
(Taken from DOE Project Fact Sheet – Fuel Cell/ ATS Hybrid Systems)

gas turbine is the balance-of-plant for the fuel cell, with some generation. In the bottoming mode, the fuel cell uses the gas turbine exhaust as air supply while the gas turbine is the balance of plant. In indirect systems, high temperature heat exchangers are used (29).

The hybrid plants are projected to cost 25 % below comparably sized fuel cells, (30) and be capable of producing electricity at costs of 10 to 20 % below today's conventional plants (27). Operation of the plant is almost totally automatic. Therefore, it can be monitored and managed remotely with the possibility of controlling hundreds of the power plants from a single location (28).

Initial systems will be less than 20 MW, with typical system sizes of 1-10 MW. Future systems, in the megawatt class size, will boost efficiency even further by combining two solid oxide fuel cell modules with more advanced gas turbines and introducing sophisticated cooling and heating procedures. Another possibility of a hybrid power plant is to combine a solid oxide fuel cell with a polymer electrolyte (PEFC) fuel cell. The SOFC would produce both electric power and hydrogen. This hydrogen would then be utilized by the PEFC to generate more electric power (28).

8.7.2 Projects

In 1997, a Program Research and Development Announcement (PRDA) was issued by the Department of Energy for conceptual feasibility studies of high-efficiency fossil power plants (HEFPPs). The terms of the conceptual power plant must be less than 20 MW in size, operate on natural gas and contain a high-temperature fuel cell. By late 1998, DOE awarded contracts to determine the feasibility of the highly efficient hybrid power plants.

FCE, of Danbury, CT, teamed with Allison Engine Company to evaluate a carbonate fuel cell combined with a gas turbine and a steam turbine generator. The system was operated at ambient pressure. The net power of the hybrid system was 20.6 MW and the NOx levels were less than 1 ppm. The process showed a 65 % efficiency with off-the-shelf turbomachinery and 72 % efficiency with cycle specific machinery. The COE is predicted to be comparable to present day alternatives.

Siemens-Westinghouse Power Corporation, of Pittsburgh, PA, with a subcontract to Allison Engine Company, evaluated a pressurized solid oxide fuel cell coupled with conventional gas turbine technology without a steam plant. The system was operated at a pressure of 7 atm. The fuel cell generated 16 MW of power and the gas turbine generated 4 MW of power. The process showed 67 % efficiency as developed. An efficiency of 70 % is deemed achievable with improvement in component design. The COE is predicted to be comparable to present day alternatives. NOx levels were less than 1 ppm.

McDermott Technology, Inc., of Alliance, OH, developed a conceptual design of a high efficiency power plant system that joins planar solid oxide fuel cell technology with micro-turbine technology in a combined cycle. The system was operated at atmospheric conditions. The power plant had a combined cycle output of 700 kW with the turbine supplying 70 kW. The results indicate 70 % efficiency is possible and the COE is comparable to present day alternatives.

Siemens-Westinghouse Power Corporation, Pittsburgh, PA, and Solar Turbines developed a conceptual design of an economically and technically feasible 20-MW, 70-% efficient natural gas-fueled power system that employs solid oxide fuel cells operating at elevated pressure in conjunction with an Advanced Turbine System gas turbine. The fuel cell, operated at 9 atm pressure, generated 11 MW of power. Two Solar Mercury 50 gas turbines were used to generate 9 MW of power. The results of the study indicated a system efficiency near 60 %. A low COE relative to conventional power generation is predicted.

In March of 1999, FCE, of Danbury, CT, with Allison Engine Company, Indianapolis, IN, and Capstone Turbine Corp., Woodland Hills, CA. was awarded a project under the Vision 21 program to create a fuel cell/turbine system that provides efficiencies and emissions targets that meet or exceed stringent Vision 21 goals. The 3-year program will include four steps:

- Development of a high-utilization fuel cell,
- Development of key system components,
- Tests of the fuel cell/hybrid system to assess integration and system operation of an existing 250-kilowatt fuel cell stack with a commercially available micro-turbine, and
- Preparation of a conceptual design of a 40 MW ultra-high efficiency power plant.

A unique feature of the proposed system will allow the fuel cell and turbine modules to operate at independent pressures. The fuel cell will be operated at ambient pressure. This can increase the fuel cell stack life and save on piping and vessel costs. The turbine can then operate at its optimum pressure ratio.

Countries around the world are developing interest in the high-efficiency hybrid cycles. A 320 kW hybrid (SOFC and gas turbine) plant will enter service in Germany, operated by a consortium under the leadership of RWE Energie AG. This will be followed by the first 1 MW plant, which will be operated by Energie Baden-Wurttemberg AG (EnBW), Electricite de France (EDF), Gaz de France, and Austria's TIWAG (29).

Another project under development at the NETL is an advanced power plant system that combines a multistaged fuel cell with an extremely efficient turbine. Preliminary estimates show efficiencies greater than 80% (LHV). Studies showed that natural gas to electricity LHV efficiencies could break through an 80% barrier, while remaining cost competitive for a 4-MW solid oxide plant (tubular or plarnar). The Advanced Fuel Cell concept directly coincides with the long-term goals of the 21st Century Fuel Cell Program. These include system costs of $400/kW and efficiencies of 70-80 percent or more (LHV to AC electricity), with fuel flexibility and a stack-life of 40,000 hours. They are intended for commercial application in 2015, maintaining ultra-low emissions.

8.7.3 World's First Hybrid Project

Siemens-Westinghouse Power Corporation of Pittsburgh, PA developed and fabricated the first advanced power plant to combine a solid oxide fuel cell and a gas turbine. The microturbine generator was manufactured by Northern Research and Engineering Corporation of Woburn, Mass. The factory acceptance test was completed in April 2000. Southern California Edison is operating the new hybrid plant at The National Fuel Cell Research Center at the University of California-Irvine. A year of testing in a commercial setting will be performed at this site. The system cycle is expected to generate electric power at 55 % efficiency.

The pressurized system will generate 220 kilowatts of power and be operated at 3 atm of pressure. The fuel cell is made up of 1152 individual tubular ceramic cells and generates about 200 kilowatts of electricity. The microturbine generator will produce an additional 20 kilowatts of electricity at full power. No sulfur dioxide pollutants will be released into the air. Nitrogen oxide emissions are likely to be less than 1 ppm.

A 320-kilowatt hybrid system is also in the planning stages. An initial commercial offering of a one MW fuel cell-microturbine power plant in late 2002 will be the end results of this Department of Energy/Siemens Westinghouse partnership program (31).

8.7.4 Hybrid Electric Vehicles (HEV)

Hybrid Electric Vehicles (HEVs) typically combine the conventional internal combustion engine of the automobile with an energy storage device, such as a battery. However, there are many different arrangements for the HEV. The key components to an HEV are the energy storage system (batteries, ultracapacitors, and flywheels), the power unit (spark ignition engines, compression ignition direct injection engines, gas turbines and fuel cells) and the vehicle propulsion system (electric motor). The benefits of HEVs, much like the hybrid power plants, are increased efficiency and lower emissions.

Fuel cell hybrid cars are not a new concept. In the early 1970s, K. Kordesch modified a 1961 Austin A-40 two-door, four-passenger sedan to an air-hydrogen fuel cell/battery hybrid car (32).

This vehicle used a 6-kW alkaline fuel cell in conjunction with lead acid batteries, and operated on hydrogen carried in compressed gas cylinders mounted on the roof. The car operated on public roads for three years and about 21,000 km.

In 1994 and 1995, H-Power (Belleville, New Jersey) headed a team that built three PAFC/battery hybrid transit buses(33, 34). These 9 meter (30 foot), 25 seat (with space for two wheel chairs) buses used a 50 kW fuel cell and a 100 kW, 180 amp-hour nickel cadmium battery.

Recently, the major activity in transportation fuel cell development has focused on the PEFC. In 1993, Ballard Power Systems (Burnaby, British Columbia, Canada) demonstrated a 10 m (32 foot) light-duty transit bus with a 120 kW fuel cell system, followed by a 200 kW, 12 meter (40 foot) heavy-duty transit bus in 1995 (35). These buses use no traction batteries. They operate on compressed hydrogen as the on-board fuel. In 1997, Ballard provided 205 kW (275 HP) PEFC units for a small fleet of hydrogen-fueled, full-size transit buses for demonstrations in Chicago, Illinois, and Vancouver, British Columbia. Working in collaboration with Ballard, Daimler-Benz built a series of PEFC-powered vehicles, ranging from passenger cars to buses (36). The first such vehicles were hydrogen-fueled. A methanol-fueled PEFC A-class car unveiled by Daimler-Benz in 1997 has a 640 km (400 mile) range. Plans are to offer a commercial vehicle by 2004. A hydrogen-fueled (metal hydride for hydrogen storage), fuel cell/battery hybrid passenger car was built by Toyota in 1996, followed in 1997 by a methanol-fueled car built on the same RAV4 platform (37).

Other major automobile manufacturers, including General Motors, Volkswagen, Volvo, Honda, DaimlerChrysler, Nissan, and Ford, also have announced plans to build prototype polymer electrolyte fuel cell vehicles operating on hydrogen, methanol, or gasoline (38). Honda's FCX, a fuel cell prototype sedan, includes both hydrogen- and methanol-based systems. Honda hopes to have this car on the road by 2003. The GM Precept will use a hydrogen hydride storage system to help it to attain a 108 miles per gallon gasoline equivalent (39).

The Department of Energy's Transportation Fuel Cell program is a collaboration between government and industry that supports the Partnership for a New Generation of Vehicles. Domestic automakers, fuel cell developers, national labs, universities, component suppliers and the fuel industry have created a Fuel Cell Alliance. This alliance helps in collaborating government sponsored research and development within the auto industry. Some of the goals of the program include developing fuel cell stack systems that are greater than 57 % efficient at 25 % peak power, more than 100 times cleaner than EPA Tier 2 emissions, and capable of operating on hydrogen or hydrogen-rich fuel from gasoline, methanol, ethanol and natural gas. By 2004, the program hopes to have fuel cell power systems that are reliable, safe and cost competitive with internal combustion engines (40).

California has started a Fuel Cell Partnership with oil companies, automakers and fuel cell companies. They hope to have 50 fuel cell vehicles, both passenger cars and transit buses, on the road by 2003. The goals of the program include demonstrating vehicle performance, identifying fuel infrastructure issues and addressing commercialization challenges (41).

DOD is interested in new or novel advanced power and propulsion systems that will reduce fuel consumption, improve performance, extend vehicle range, reduce emissions, and reduce support costs. The Navy and Army are considering hybrids for ships, land vehicles, helicopters, and battlefield power requirements.

In 1997, the Office of Naval Research (ONR) initiated an advanced development program to demonstrate a ship service fuel cell (SSFC) power generation module. During Phase 1, competitive conceptual designs of 2.5 MW SSFC were prepared, along with critical component demonstrations. Phase 2 of the development program, scheduled for completion in 2002, will result in a nominal 500 kW fuel cell ship service generator demonstration module to be constructed and tested in a laboratory setting. The baseline concept is fueled by logistic fuel which is reformed in an adiabatic reformer designed and built by International Fuel Cells. Downstream of the reformer is a series of components that remove CO and H_2S before the gas is sent to the fuel cell. The spent fuel and air are mixed and burned to drive a turbocompressor and recover compression work.[58]

The Army has two programs that are looking at hybrids using fuel cells. In 1999, the Land Warrior Operational Combat System was approved. The goal is to develop a portable hybrid fuel cell system that weighs less than one kilogram and meets the power demand of the Land Warrior Power requirements. The second program is the Future Combat System. This program plans to develop technologies and systems for a lightweight, overwhelming lethal, strategically deployable, self-sustaining combat systems.[59]

8.8 References

1. James M. Douglas, *Conceptual Design of Chemical Processes*, McGraw-Hill, Inc., New York, NY, 1988.
2. Max S. Peters, and Klaus D. Timmerhaus, *Plant Design and Economics for Chemical Engineers*, 3rd Edition, McGraw-Hill, Inc., New York, NY, 1980.
3. Warren L. McCabe, Julian C. Smith, Peter Harriot, *Unit Operations of Chemical Engineering*, 4th Edition, 1985.
4. M.C. Williams, and T.J. George, "Research Issues in Molten Carbonate Fuel Cells: Pressurization," *presented at the 1992 IECEC*, Vol. 3, pp. 263-267.
5. "Overview of 11 MW Fuel Cell Power Plant," non-published information from Tokyo Electric Power Company, September 1989.
6. T. Koshimizu, et al., "Development of 5000 kW and 1000 kW PAFC Plants," *presented at the JASME-ASME Joint Conference (ICOPE-93)*, Tokyo, September 1993.
7. R. Shreve and J. Brink, *Chemical Process Industries*, fourth edition, McGraw-Hill, 1977.
8. T. Okado, et al., "Study of Temperature Control in Indirect Internal Reforming MCFC Stack," presented at 25th IECEC, pp. 207-212, 1990.
9. N.Q. Minh, "High-Temperature Fuel Cells, Part 2: The Solid Oxide Cell," Chemtech, Vol. 21, February 1991.

[58] R.M. Privette, et al., "2.5 MW PEFC System for Navy Ship Service Power," paper presented at the 1999 Review Conference on Fuel Cell Technology, Chicago, Illinois, August 3-5, 1999.

[59] J.C. Stephens, K. Gardner, and R. Jacobs, "US Army CECOM Fuel Cell Program," presented at the World Association for Case Method Research and Application, Lucerne, Switzerland, January 5-7, 2000.

10. V. Minkov, et al., "Topping Cycle Fuel Cells Effective Combined with Turbines," Power Engineering, July 1988, pp. 35-39. "Design and Economics of Large Fuel Cell Power Plants," presented at 1986 Fuel Cell Seminar, Tucson, AZ, p 255.
11. F.G. Baily, "Steam Turbines for Advanced Combined Cycles," *presented at the 35th GE Turbine State-of-the-Art Technology Seminar*, 1991.
12. M.S. Peters, and K.D. Timmerhaus, *Plant Design and Economics for Chemical Engineers*, Third Edition, McGraw-Hill, 1980.
13. M. Farooque, "Development of Internal Reforming Carbonate Fuel Cell Stack Technology," Performed under Contract No. DE-AC21-87MC23274, DOE/MC/23374-2941, October 1990.
14. M. Farooque, et al., "Comparative Assessment of Coal-Fueled Carbonate Fuel Cell and Competing Technologies," *presented at the 25th IECEC*, Vol. 3, pp.193-200, 1990.
15. Dawn M. Bernardi, "Water-Balance Calculations for Solid-Polymer-Electrolyte Fuel Cells," Journal of Electrochemical Society, Vol. 137, No. 11, November 1990.
16. David P. Wilkinson, (Ballard Power Systems) and David Thompsett (Johnson Matthey Technology Centre), "Materials and Approaches for CO and CO_2 Tolerance for Polymer Electrolyte Membrane Fuel Cells," *presented at the 1997 Proceedings of the Second International Symposium on New Materials for Fuel Cells and Modern Battery Systems*, Montreal, Quebec, Canada, July 6-10, 1997.
17. David P. Wilkinson, and Alfred E. Steck, "General Progress in the Research of Solic Polymer Fuel Cell Technology at Ballard," *presented at the 1997 Proceedings of the Second International Symposium on New Materials for Fuel Cells and Modern Battery Systems*, Montreal, Quebec Canada, July 6-10, 1997.
18. Thomas L. Buchanan, John H. Hirschenhofer, David B. Stauffer, and Jay S. White, "Carbon Dioxide Capture in Fuel Cell Power Systems," September 1994, G/C Report 2981.
19. "Overview of 11 MW Fuel Cell Power Plant," Non-published information from Tokyo Electric Power Company, September 1989.
20. F. P. Bevc, W. L. Lundberg and D. M. Bachovchin, "Solid Oxide Fuel Cell Combined Cycles," ASME Paper 96-GT-447, *presented at International Gas Turbine and Aeroengine Congress & Exhibition*, Birmingham, UK, June 1996.
21. R. Hendricks, "Heron Turbine Prototype Test Results," 20th International Congress on Combustion Engines, International Council on Combustion Engines (CIMAC), London, 1993.
22. T.J. George, K.D Lyons, and R. James III, "Multistaged Oxide Fuel Cell Power Plant Concept," May 1998.
23. Fax Transmittal from J. Hirschenhofer of Parsons Energy & Chemicals Group to Tom George of USDOE/FETC, dated August 26, 1998, Re: Aspen Analysis Results of the Multistaged SOFC Concept.
24. Parsons Energy & Chemical, work for the U.S. DOE, Spring 1998.
25. Appleby, A.J.; Foulkes F.R. *Fuel Cell Handbook*; Van Nostrand Reinhold: New York, 1989.
26. " Fuel-Flexible Fuel Processor," J. Cuzens, J. Mauzey, and R. Woods, Hydrogen Burner Technology, Pg. 234 Fuel Cell Seminar Abstracts, Courtesy Associates, Inc., November 1998.
27. Theory and Application; Paper presented at the 1992 AIChE Annual Meeting: Miami Beach, FL, 1-6 November, 1992.
28. "Developing Power Systems for the 21st Century – Fuel Cell/ATS Hybrid Systems," U.S. Dept. of Energy, National Energy Technology Center & Office of Industrial Technologies,

Project facts for Advanced Clean/ Efficient Power Systems, PS031.1099.
29. U. Eberl, "Fuel Cells and Gas Turbines: A Marriage of Efficiency," Research and Innovation, January 2000.
30. R. Gemmen, et al, "Technical Development Issues and Dynamic Modeling of Gas Turbine and Fuel Cell Hybrid Systems," *Proceedings of the 1999 Review Conference on Fuel Cell Technology*, August 1999.
31. "Fuel Cells- Opening New Frontiers in Power Generation," U.S. Department of Energy, Office of Fossil Energy, National Energy Technology Center, November 1999.
32. DOE Techline Press Release, "Department of Energy Announces World's First "Hybrid" Fuel Cell-Turbine," April 2000.
33. "Auto Show Attendees get a Glimpse of Future Concept Cars," Alternative Fuel News, Vol.4 No.1, US Department of Energy, Office of Energy Efficiency and Renewable Energy.
34. K.V. Kordesh, "City Car with H2-Air Fuel Cell and Lead Battery," *6th Intersociety Energy Conversion Engineering Conference*, SAE Paper No. 719015, 1971.
35. A. Kaufman, "Phosphoric Acid Fuel Cell Bus Development," *Proceedings of the Annual Automotive Technology Development Contractors' Coordination Meeting*, Dearborn, MI, October 1994, SAE Proceedings Volume P-289, pp. 289-293, 1995.
36. R.R. Wimmer, "Fuel Cell Transit Bus Testing & Development at Georgetown University," *Proceedings of the Thirty Second Intersociety Energy Conversion Engineering Conference*, July 1997, Honolulu, HI, pp. 825-830.
37. N.C. Otto, P.F. Howard, "Transportation Engine Commercialization at Ballard Power Systems," Program *and Abstracts 1996 Fuel Cell Seminar*, November 1996, Orlando, FL, pp.559-562.
38. F. Panik, "Fuel Cells for Vehicle Applications in Cars – Bringing the Future Closer," J. Power Sources, 71, pp.36-38, 1998.
39. S. Kawatsu, "Advanced PEFC Development for Fuel Cell Powered Vehicles," J. Power Sources, 71, pp. 150-155, 1998.
40. *Fuel Cell Technology: Powering the Future*, Electric Line, November/December 1996.
41. J. Milliken, "The DOE Transportation Fuel Cell Program: Recent Accomplishments and Future Plans," U.S. Dept. of Energy, Office of Transportation Technologies. "Questions and Answers – California Fuel Cell Partnership," www.drivingthefuture.org.

9. SAMPLE CALCULATIONS

This section presents sample problems to aid the reader in understanding the calculations behind a fuel cell power system. The sample calculations are arranged topically with unit operations in Section 9.1, system issues in Section 9.2, supporting calculations in Section 9.3, and cost calculations in Section 9.4. A list of conversion factors common to fuel cell systems analysis is presented in Section 9.5 and a sample automotive design calculation is presented in Section 9.6.

9.1 Unit Operations

The following examples are presented for individual unit operations found within a fuel cell system. Unit operations are the individual building blocks found within a complex chemical process. By analyzing example problems for each unit operation, one can learn about the underlying scientific principles and engineering calculation methods that are applied to various processes. This approach will provide the reader with a better understanding of fuel cell power system building blocks as well as the interactions between the unit operations. For example, the desired power output from the fuel cell unit will determine the fuel flow requirement from the fuel processor. This section starts by examining the fuel cell unit operation, and continues on to the fuel processor and power conditioner.

9.1.1 Fuel Cell Calculations

Example 9-1 Fuel Flow Rate for 1 Ampere of Current (Conversion Factor Derivation)

What hydrogen flow rate is required to generate 1.0 ampere of current in a fuel cell? (This exercise will generate a very useful conversion factor for subsequent calculations.)

Solution:

For every molecule of hydrogen (H_2) that reacts within a fuel cell, two electrons are liberated at the fuel cell anode. This is most easily seen in the PAFC and PEFC because of the simplicity of the anode (fuel) reaction, although the rule of two electrons per diatomic hydrogen molecule (H_2) holds true for all fuel cell types. The solution requires knowledge of the definition of an ampere (A) and an equivalence of electrons.[60]

$H_2 \rightarrow 2H^+ + 2e^-$

The moles of hydrogen liberated to generate one amp can be calculated directly:

[60] One equivalence of electrons is 1 g mol of electrons or 6.022 x10^{23} electrons (Avagadro's number). This quantity of electrons has the charge of 96,487 coulombs (C) (Faraday's constant). Thus, the charge of a single electron is 1.602 x10^{-19} C. One (1) ampere of current is defined as 1 C/sec.

$$n_{H_2} = (1.0\text{ A})\left(\frac{1\text{ coulomb/sec}}{1\text{ A}}\right)\left(\frac{1\text{ equivalence of e}^-}{96{,}487\text{ coulombs}}\right)\left(\frac{1\text{ g mol H}_2}{2\text{ equiv. of e}^-}\right)\left(\frac{3600\text{ sec}}{1\text{ hr}}\right) = 0.018655\,\frac{\text{g mol}}{\text{hr - A}}\,H_2$$

$$m_{H_2} = \left(0.018655\,\frac{\text{g mol}}{\text{hr - A}}\,H_2\right)\left(\frac{2.0158\text{ g}}{1\text{ g mol H}_2}\right)\left(\frac{1\text{ kg}}{1000\text{ g}}\right) = 37.605\text{x}10^{-6}\,\frac{\text{kg H}_2}{\text{hr - A}}\text{ or }0.037605\,\frac{\text{kg H}_2}{\text{hr - kA}}$$

The result of this calculation, 0.037605 kg H_2 per hour per kA (0.08291 lb H_2 per hour per kA), is a convenient factor that is often used to determine how much fuel must be provided to supply a desired fuel cell power output, as illustrated in the next example.

Example 9-2 Required Fuel Flow Rate for 1 MW Fuel Cell
A 1.0 MW_{DC} fuel cell stack is operated with a cell voltage of 700 mV on pure hydrogen with a fuel utilization, U_f of 80%. (a) How much hydrogen will be consumed in lb/hr? (b) What is the required fuel flow rate? (c) What is the required air flow rate for a 25% oxidant utilization, U_{ox}?

Solution:
(a) The solution of this problem will be simplified by assuming that the individual fuel cells are arranged in parallel. That is, the fuel cell stack voltage is the same as each individual cell voltage, and the fuel cell stack current is equal to the current of an individual cell times the number of cells.

Recalling that power (P) is the product of voltage (V) and current (I),

P = I x V

Therefore, the current through the fuel cell stack can be calculated as

$$I = \frac{P}{V} = \left(\frac{1.0\text{ MW}}{0.7\text{ V}}\right)\left(\frac{10^6\text{ W}}{1\text{ MW}}\right)\left(\frac{1\text{ VA}}{1\text{ W}}\right)\left(\frac{1\text{ kA}}{1000\text{ A}}\right) = 1429\text{ kA}$$

The quantity of hydrogen consumed within the fuel cell stack is

$$m_{H_2,\text{consumed}} = (1429\text{ kA})\left(\frac{0.08291\text{ lb H}_2}{\text{hr - kA}}\right) = 118.4\,\frac{\text{lb H}_2}{\text{hr}}$$

Note that without the simplifying assumption that the fuel cells were arranged in parallel, the same hydrogen mass flow could have been calculated with a few extra steps. For example, if the fuel cell stack was composed of 500 cells in series, then the stack voltage would have been 350 volts [(500 cells)(0.7 V/cell)], and the stack current would have been 2.858 kA/cell [1429 kA / 500 cells]. Because this stack current passes through 500 cells arranged in series, the hydrogen consumption is calculated as

$$m_{H_2,\text{consumed}} = \left(2.858\,\frac{\text{kA}}{\text{cell}}\right)\left(\frac{0.08291\text{ lb H}_2}{\text{hr - kA}}\right)(500\text{ cells}) = 118.4\,\frac{\text{lb H}_2}{\text{hr}}$$

Thus, the reader may find it more expedient and less error prone to envision parallel arrangement when calculating the mass flow requirement of hydrogen.

(b) The utilization of fuel in a fuel cell is defined as

$$U_f = \frac{H_{2,\,consumed}}{H_{2,in}}$$

Therefore the fuel flow rate required togenerate1 MW_{DC} can be calculated as

$$H_{2,\,in} = \frac{H_{2,\,consumed}}{U_f} = \frac{118.4\,\frac{lb\,H_2}{hr}}{80\,\%} = 148.0\,\frac{lb\,H_2}{hr}$$

(c) To determine the air requirement, first observe that the stoichiometric[61] ratio of hydrogen to oxygen is 2 to 1 for H_2O. Thus, the moles of oxygen required for the fuel cell reaction are determined by

$$n_{O_2,\,consumed} = \left(118.4\,\frac{lb\,H_2}{hr}\right)\left(\frac{1\,lb\,mol\,H_2}{2.0158\,lb\,H_2}\right)\left(\frac{1\,lb\,mol\,O_2}{2\,lb\,mol\,H_2}\right) = 29.38\,\frac{lb\,mol\,O_2}{hr}$$

If 25% utilization is required, then the air feed must contain four times the oxygen that is consumed

$$n_{O_2,\,supplied} = \left(29.38\,\frac{lb\,mol\,O_2\ consumed}{hr}\right)\left(\frac{1\,lb\,mol\,O_2\ supplied}{0.25\,lb\,mol\,O_2\ consumed}\right) = 117.5\,\frac{lb\,mol\,O_2}{hr}$$

Because dry air contains 21% O_2 by volume, or by mole percent, the required mass flow rate of dry air is

$$m_{air,\,supplied} = \left(117.5\,\frac{lb\,mol\,O_2\ supplied}{hr}\right)\left(\frac{1\,lb\,mol\,air}{0.21\,lb\,mol\,O_2}\right)\left(\frac{28.85\,lb\,dry\,air}{1\,lb\,mol\,of\,air}\right) = 16{,}142\,\frac{lb\,dry\,air}{hr}$$

Example 9-3 PAFC Effluent Composition

A PAFC, operating on reformed natural gas (900 lb/hr) and air, has a fuel and oxidant utilization of 86% and 70% respectively. With the fuel and oxidant composition and molecular weights listed below, (a) How much hydrogen will be consumed in lb mol/hr? (b) How much oxygen is consumed in lb mol/hr? (c) What is the required air flow rate in lb mol/hr and lb/hr? (d) How

[61] The stoichiometric ratio is the ratio of atoms in a given molecule.

much water is generated? (e) What is the composition of the effluent (spent) fuel and air streams in mol %?

Fuel Data	mol %
CH_4	4.0
CO	0.4
CO_2	17.6
H_2	75.0
H_2O	3.0
Total	100.0
MW	10.55

Air Data	mol %, dry	mol %, wet
H_2O	0.00	1.00
N_2	79.00	78.21
O_2	21.00	20.79
Total	100.00	100.00
MW	28.85	28.74

Solution:

(a) To determine the lb mol/hr of hydrogen, first determine the molar fuel flow

$$n_{\text{fuel, supplied}} = \left(900\frac{\text{lb fuel}}{\text{hr}}\right)\left(\frac{1\text{ lb mol fuel}}{10.55\text{ lb fuel}}\right) = 85.29\frac{\text{lb mol fuel}}{\text{hr}}$$

Thus,

$$n_{H_2\text{ consumed}} = \left(85.29\frac{\text{lb mol fuel}}{\text{hr}}\right)\left(\frac{75\text{ lb mol }H_2}{100\text{ lb mol fuel}}\right)\left(\frac{86\text{ lb mol }H_2\text{ consumed}}{100\text{ lb mol }H_2\text{ supplied}}\right) = 55.01\frac{\text{lb mol }H_2}{\text{hr}}$$

(b) To determine how much oxygen is consumed, it is useful to note the overall fuel cell reaction

$$H_{2\,(g)} + \tfrac{1}{2}\,O_{2\,(g)} \rightarrow H_2O_{\,(g)}$$

Therefore,

$$n_{O_2\text{, consumed}} = \left(55.01\frac{\text{lb mol }H_2}{\text{hr}}\right)\left(\frac{\tfrac{1}{2}\text{ lb mol }O_2}{1\text{ lb mol }H_2}\right) = 27.51\frac{\text{lb mol }O_2}{\text{hr}}$$

(c) The required air flow will be determined on a wet air basis, thus

$$n_{\text{air, required}} = \left(27.51\frac{\text{lb mol }O_2}{\text{hr}}\right)\left(\frac{100\text{ lb mol }O_2\text{ supplied}}{70\text{ lb mol }O_2\text{ consumed}}\right)\left(\frac{100\text{ lb mol wet air}}{20.79\text{ lb mol }O_2}\right) = 189.01\frac{\text{lb mol wet air}}{\text{hr}}$$

$$m_{air,\,required} = \left(189.01\frac{\text{lb mol wet air}}{\text{hr}}\right)\left(\frac{28.74\text{ lb wet air}}{1\text{ lb mol wet air}}\right) = 5{,}433\frac{\text{lb wet air}}{\text{hr}}$$

(d) Per the overall fuel cell reaction above, the water generated is equal to the moles of hydrogen consumed

$$n_{H_2O\text{ generated}} = n_{H_2\text{ consumed}} = 55.01\frac{\text{lb mol } H_2}{\text{hr}}$$

(e) The composition of the effluent is developed in the table below, by working from the left to right. The composition is determined by converting the composition to moles, accounting for the fuel cell reaction, and converting back to the desired units, mol %. (Note: mol % is essentially equivalent to volume % for low pressure gases.)

Spent Fuel Effluent Calculation

	mol %	lb mol/hr			mol %
Gas	**FC inlet**	**FC inlet**	**FC reaction**	**FC outlet**	**FC outlet**
CH_4	4.0	3.41		3.41	11.27
CO	0.4	0.34		0.34	1.13
CO_2	17.6	15.01		15.01	49.58
H_2	75.0	63.97	-55.01	8.96	29.58
H_2O	3.0	2.56		2.56	8.45
Total	**100.0**	**85.29**	**-55.01**	**30.28**	**100.00**

In the PAFC, only the moles of hydrogen change on the anode (fuel) side of the fuel cell. The other fuel gas constituents simply pass through to the anode exit. These inert gases act to dilute the hydrogen, and as such will lower the cell voltage. Thus, it is always desirable to minimize these diluents as much as possible. For example, to reform natural gas, significant quantities of steam are typically added to maximize the reforming reactions. The wet reformer effluent would commonly have a water composition of 30 to 50%. The reformate gas utilized in this example has been "dried" to only 3% moisture via condensation in a contact cooler.

The spent oxidant composition is calculated in a similar manner. Note that in both the PAFC and PEFC the water is generated on the cathode (air) side. This can be seen from the cathode reaction listed below and the following table listing the fuel cell reaction quantities.

$$\tfrac{1}{2}O_2 + 2H^+ + 2e^- \rightarrow H_2O$$

Spent Air Effluent Calculation

	mol %	lb mol/hr			mol %
Gas	**FC inlet**	**FC inlet**	**FC reaction**	**FC outlet**	**FC outlet**
H_2O	1.00	1.89	55.01	56.90	26.28
N_2	78.21	147.82		147.82	68.27
O_2	20.79	39.30	-27.51	11.79	5.44
Total	**100.00**	**189.01**	**27.51**	**216.51**	**100.00**

Example 9-4 MCFC Effluent Composition - Ignoring the Water Gas Shift Reaction
An MCFC operating on 1,000 lb/hr of fuel gas and a 70% air/30% CO_2 oxidant has a fuel and oxidant utilization of 75% and 50% respectively. With the fuel and oxidant composition and molecular weights listed below, (a) How much hydrogen will be consumed in lb mol/hr? (b) How much oxygen is consumed in lb mol/hr? (c) What are the required air and oxidant flow rates in lb mol/hr? (d) How much CO_2 is transferred from the cathode to the anode? (e) What is the composition of the effluent (spent) fuel and oxidant streams in mol % (ignoring the water gas shift reaction)?

Fuel Data	Mol %
CH_4	0.0
CO	0.0
CO_2	20.0
H_2	80.0
H_2O	0.0
Total	100.0
MW	10.42

	Air	Air + CO_2
Oxidant Data	**mol %, wet**	**Mol %, wet**
CO_2	0.00	30.00
H_2O	1.00	0.70
N_2	78.21	54.75
O_2	20.79	14.55
Total	100.00	100.00
MW	28.74	33.32

Solution:
(a) To determine the lb mol/hr of hydrogen, first determine the molar fuel flow

$$n_{\text{fuel, supplied}} = \left(1000\frac{\text{lb fuel}}{\text{hr}}\right)\left(\frac{1\text{ lb mol fuel}}{10.42\text{ lb fuel}}\right) = 96.02\frac{\text{lb mol fuel}}{\text{hr}}$$

Thus,

$$n_{H_2\text{ consumed}} = \left(96.02\frac{\text{lb mol fuel}}{\text{hr}}\right)\left(\frac{80\text{ lb mol }H_2}{100\text{ lb mol fuel}}\right)\left(\frac{75\text{ lb mol }H_2\text{ consumed}}{100\text{ lb mol }H_2\text{ supplied}}\right) = 57.61\frac{\text{lb mol }H_2}{\text{hr}}$$

(b) To determine how much oxygen is consumed, it is useful to note the overall fuel cell reaction

$H_{2\,(g)} + ½\, O_{2\,(g)} \rightarrow H_2O_{(g)}$
Therefore,

$$n_{O_2,\,\text{consumed}} = \left(57.61\frac{\text{lb mol } H_2}{\text{hr}}\right)\left(\frac{½\text{ lb mol } O_2}{1\text{ lb mol } H_2}\right) = 28.81\frac{\text{lb mol } O_2}{\text{hr}}$$

(c) The required air flow will be determined on a wet air basis:

$$n_{\text{air, required}} = \left(28.81\frac{\text{lb mol } O_2}{\text{hr}}\right)\left(\frac{100\text{ lb mol } O_2\text{ supplied}}{50\text{ lb mol } O_2\text{ consumed}}\right)\left(\frac{100\text{ lb mol wet air}}{20.79\text{ lb mol } O_2}\right) = 277.11\frac{\text{lb mol wet air}}{\text{hr}}$$

The oxidant flow rate will be calculated knowing that air is 70% of the total oxidant flow:

$$n_{\text{oxidant, required}} = \left(277.11\frac{\text{lb mol wet air}}{\text{hr}}\right)\left(\frac{100\text{ lb mol oxidant}}{70\text{ lb mol wet air}}\right) = 395.86\frac{\text{lb mol oxidant}}{\text{hr}}$$

(d) Per the overall fuel cell reaction presented below, the quantity of CO_2 transferred from the cathode to the anode side of the fuel cell equals the moles of hydrogen consumed:

$$H_{2,\text{ anode}} + \tfrac{1}{2}O_{2,\text{ cathode}} + CO_{2,\text{ cathode}} \rightarrow H_2O_{,\text{ anode}} + CO_{2,\text{ anode}}$$

Therefore,

$$n_{CO_2\text{ transferred}} = n_{H_2\text{ consumed}} = 57.61\frac{\text{lb mol}}{\text{hr}}$$

(e) The composition of the fuel effluent is developed in the table below, by working from left to right. The composition is determined by converting the composition to moles, accounting for the fuel cell reaction, and converting back to the desired units, mol %.

Spent Fuel Effluent Calculation

	mol %	lb mol/hr			Mol %
Gas	**FC inlet**	**FC inlet**	**FC reaction**	**FC outlet**	**FC outlet**
CH_4	0.0	0.00		0.00	0.00
CO	0.0	0.00		0.00	0.00
CO_2	20.0	19.20	57.61	76.82	50.00
H_2	80.0	76.82	-57.61	19.20	12.50
H_2O	0.0	0.00	57.61	57.61	37.50
Total	**100.0**	**96.02**	**-57.61**	**153.63**	**100.00**

The oxidant effluent composition is calculated in a similar manner. Note that in the MCFC, both oxygen and carbon dioxide are consumed on the cathode (air) side. This can be seen from the cathode reaction listed below and the following table listing the fuel cell reaction quantities.

$\frac{1}{2}O_2 + CO_2 + 2e^- \rightarrow CO_3^=$ (MCFC cathode reaction)

Spent Oxidant Effluent Calculation

	mol %	lb mol/hr			Mol %
Gas	**FC inlet**	**FC inlet**	**FC reaction**	**FC outlet**	**FC outlet**
CO_2	30.00	83.13	-57.61	25.52	13.38
H_2O	0.70	1.94		1.94	1.02
N_2	54.70	151.71		151.71	79.56
O_2	14.6	40.33	-28.81	11.52	6.04
Total	**100.00**	**277.11**	**-86.42**	**190.69**	**100.00**

Example 9-5 MCFC Effluent Composition - Accounting for the Water Gas Shift Reaction
For the above example, determine the composition of the effluent (spent) fuel stream in mol % including the effect of the water gas shift reaction. Assume an effluent temperature of 1200ºF and that the water gas shift reaction proceeds to equilibrium.

Solution:
For convenience, the water gas shift reaction is presented below:

$CO + H_2O \Leftrightarrow CO_2 + H_2$

The double headed arrow is used to indicate that the reaction is in equilibrium. That is, the reaction does not proceed completely to the left or to the right. Instead, the reaction proceeds to an equilibrium point, where both "products" and "reactants" remain. The equilibrium composition depends on the initial composition and final temperature and pressure. Fortunately, the equilibrium concentrations can be determined by a temperature dependent equilibrium constant, K, and the following equation:

$$K = \frac{[CO_2][H_2]}{[CO][H_2O]}$$

The quantities in brackets represent the thermodynamic activities of the reacting species. Because the reaction is equimolar, the quantities in brackets are also equal to the mole fractions of the respective components. At 1200ºF, the equilibrium constant is 1.967[62]. A check of the

[62] Equilibrium constants can be calculated from fundamental chemical data such as Gibbs free energy, or can be determined from temperature dependent tables or charts for common reactions. One such table has been published by Girdler Catalysts (1). The following algorithm fits this temperature dependent data to within 5% for 800 to 1800ºF, or within 1% for 1000 to 1450ºF: $Kp= e^{(4,276/T -3.961)}$. Kp(1200ºF or 922K) equals 1.967.

compositions from the preceding example shows that those concentration levels are not in equilibrium.

$$\frac{[CO_2][H_2]}{[CO][H_2O]} = \frac{[0.50][0.125]}{[0.0][0.375]} = \infty \neq 1.967$$

Because the numerator contains the products of the reaction and the denominator contains the reactants, it is clear that the reaction must proceed more towards the reactants. By introducing a variable, x, to represent the extent of the reaction to proceed to the right and rewriting the equilibrium equation as:

$$K = \frac{[CO_2][H_2]}{[CO][H_2O]} = \frac{[0.50 + x][0.125 + x]}{[0.0 - x][0.375 - x]} = 1.967$$

This can be solved algebraically as follows:

$$K = \frac{[CO_2 + x][H_2 + x]}{[CO - x][H_2O - x]}$$

can be written as

$$K[CO - x][H_2O - x] = [CO_2 + x][H_2 + x]$$

which can be expanded as

$$K\left\{x^2 - ([CO] + [H_2O])x + [CO][H_2O]\right\} = x^2 + ([CO_2] + [H_2])x + [CO_2][H_2]$$

which can be combined to

$$\underbrace{(1 - K)}_{a}x^2 + \underbrace{\left\{[CO_2] + [H_2] + K([CO] + [H_2O])\right\}}_{b}x + \underbrace{\left\{[CO_2][H_2] - [CO][H_2O]K\right\}}_{c} = 0$$

This is in the standard quadratic form of

$ax^2 + bx + c = 0$

which can be solved by the quadratic formula

$$x = \frac{-b \pm \sqrt{b^2 - 4ac}}{2a}$$

Substituting the appropriate values for K and the concentrations yields two roots of -0.0445 and 1.454. The larger root is physically impossible; it "wants to" react more CO and H_2O than are

initially present. The remaining root of -0.0445 is used to compute the equilibrium gas composition, which is shown in the following table.

Spent Fuel Effluent Calculation

	mol %	Lb mol/hr, assuming 100 lb mol/hr basis			Mol %
Gas	**FC outlet w/o shift.**	**FC outlet w/o shift**	**effect of shift rxn**	**FC outlet in shift equil.**	**FC outlet in shift equil.**
CO	0.00	0.00	4.45	4.45	4.45
CO_2	50.00	50.00	-4.45	45.55	45.55
H_2	12.50	12.50	-4.45	8.05	8.05
H_2O	37.50	37.50	4.45	41.95	41.95
Total	**100.0**	**100.00**	**0.00**	**100.00**	**100.00**

Example 9-6 SOFC Effluent Composition - Accounting for Shift and Reforming Reactions
An SOFC operates at 1800°F on 100 % methane (CH_4) and a fuel utilization of 85%. What is the composition of the effluent (spent) fuel in mol %? Assume that the methane is completely reformed within the fuel cell, and the moisture required for reforming is supplied by internal recirculation.

Solution:
There are many different ways to approach this problem, some of which may seem rather complex because of the simultaneous reactions (fuel cell, reforming, and water gas shift reactions) and the recycle stream supplying moisture required for the reforming reaction. The solution to this problem can be simplified by focusing on the fuel cell exit condition.

First, write the relevant reactions:

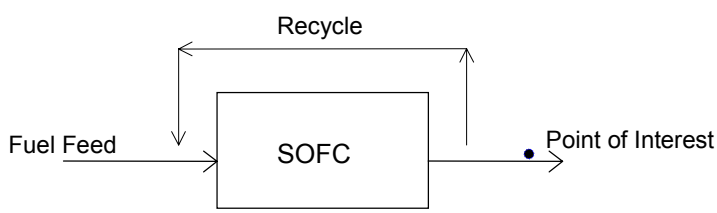

$CH_4 + 2H_2O \rightarrow 4H_2 + CO_2$ (Steam Reforming Reaction)

$H_{2,\ anode} + \frac{1}{2}O_{2,\ cathode} \rightarrow H_2O_{,\ anode}$ (Fuel Cell Reaction)

$CO + H_2O \Leftrightarrow CO_2 + H_2$ (Water Gas Shift Reaction)

Next combine the reforming reaction and the fuel cell reaction into an overall reaction for that portion of the fuel that is consumed (i.e., 85%). The combined reaction is developed by adding

the steam reforming reaction to 4 times the fuel cell reaction. The factor of four allows the hydrogen molecules to drop out of the resulting equation because it is fully utilized.

$CH_{4,\ anode} + 2H_2O_{,\ anode} \rightarrow 4H_{2,\ anode} + CO_{2,\ anode}$	(Steam Reforming Reaction)
$4H_{2,\ anode} + 2O_{2,\ cathode} \rightarrow 4H_2O_{,\ anode}$	(Fuel Cell Reaction)
$CH_{4,\ anode} + 2O_{2,\ cathode} \rightarrow 2H_2O_{,\ anode} + CO_{2,\ anode}$	(Combined Reforming and FC Reactions)

For ease of calculation, assume a 100 lb/hr basis for the methane.

$$n_{fuel,\,supplied} = \left(100\,\frac{\text{lb CH}_4}{\text{hr}}\right)\left(\frac{1\text{ lb mol CH}_4}{16.043\text{ lb CH}_4}\right) = 6.23\,\frac{\text{lb mol CH}_4}{\text{hr}}$$

Thus, 85%, or 5.30 lb mol CH_4 /hr, will be reformed and consumed by the fuel cell. The remainder will be reformed but not consumed by the fuel cell reaction. These changes are summarized in the following table:

Spent Fuel Effluent Calculation

	mol %	lb mol/hr				mol %
Gas	**FC inlet**	**FC inlet**	**Ref / FC rxn**	**Reforming**	**FC outlet**	**FC outlet**
CH_4	100.0	6.23	-5.30	-0.93	0.00	0.00
CO	0.0	0.00	0.00	0.00	0.00	0.00
CO_2	0.0	0.00	5.30	0.93	6.23	33.33
H_2	0.0	0.00	0.00	3.74	3.74	20.00
H_2O	0.0	0.00	10.60	-1.87	8.73	46.67
Total	**100.0**	**6.23**	**10.60**	**1.87**	**18.70**	**100.00**

This intermediate solution reflects only two out of three reactions. Now apply the water gas shift reaction to determine the true exit composition. Use the quadratic equation listed in Example 9-5 to determine how far the reaction will proceed, where x is the extent of the reaction in the forward direction as written:

$$CO + H_2O \xleftrightarrow{x} CO_2 + H_2$$

$$x = \frac{-b \pm \sqrt{b^2 - 4ac}}{2a}$$

The equilibrium constant, K, at 1800°F (1255°K) is

$$K = e^{(4276/1255-3.961)} = 0.574$$

$$a = (1-K) = (1-0.574) = 0.426$$

$$b = \{[CO_2] + [H_2] + K([CO] + [H_2O])\} = 0.3333 + 0.2000 + 0.574 * (0.00 + 0.4667) = 0.8012$$

$$c = \{[CO_2]\,[H_2] - [CO]\,[H_2O]K\} = (0.3333)(0.20) - (0.00)(0.4667)(0.574) = 0.0666$$

$$x = \frac{-b \pm \sqrt{b^2 - 4ac}}{2a} = \frac{-0.8012 \pm \sqrt{(0.8012)^2 - 4(0.426)(0.0666)}}{2(0.426)} = -0.0873 \text{ and } -1.794$$

The only root that is physically possible is x = -0.0873. The following table summarizes the effect of accounting for the water gas shift equilibrium:

Spent Fuel Effluent Calculation

	mol %	Lb mol/hr, assuming 100 lb mol/hr basis			Mol %
Gas	**FC outlet w/o shift.**	**FC outlet w/o shift**	**Effect of shift rxn**	**FC outlet in shift equil.**	**FC outlet in shift equil.**
CO	0.00	0.00	-(-8.73)	8.73	8.73
CO_2	33.33	33.33	-8.73	24.61	24.61
H_2	20.00	20.00	-8.73	11.27	11.27
H_2O	46.67	46.67	-(-8.73)	55.39	55.39
Total	**100.00**	**100.00**	**0.00**	**100.00**	**100.00**

Example 9-7 Generic Fuel Cell - Determine the Required Cell Area and Number of Stacks
Given a desired output of 2.0 MW_{DC} and the desired operating point of 600 mV and 400 mA/cm^2, (a) How much fuel cell area is needed? (b) Assuming a cell area of 1.00 m^2 per cell and 280 cells per stack, how many stacks are needed for this 2.0 MW unit?

Solution:

(a) Recalling that power is the product of voltage and current, first determine the total current for the fuel cell as

$$I = \frac{P}{V} = \left(\frac{2.0\text{ MW}}{0.600\text{ V}}\right)\left(\frac{10^6\text{ W}}{1\text{ MW}}\right)\left(\frac{1\text{ VA}}{1\text{ W}}\right)\left(\frac{1\text{ kA}}{1000\text{ A}}\right) = 3{,}333\text{ kA}$$

Because each individual cell will operate at 400 mA/cm^2, determine the total area as

$$\text{Area} = \frac{I}{\text{Current Density}} = \left(\frac{3{,}333\text{ kA}}{400\text{ mA / cm}^2}\right)\left(\frac{1000\text{ mA}}{1\text{ A}}\right)\left(\frac{1000\text{ A}}{1\text{ kA}}\right) = 8{,}333{,}333\text{ cm}^2$$

b) The number of required cells and stacks are calculated simply as

$$\text{No. of Cells} = \frac{\left(8{,}333{,}333\ \text{cm}^2\right)}{\left(1\ \text{m}^2\ \text{per cell}\right)}\left(\frac{1\ \text{m}^2}{10{,}000\ \text{cm}^2}\right) = 833\ \text{cells}$$

$$\text{No. of Stacks} = \frac{(833\ \text{cells})}{(280\ \text{cells per stack})} = 2.98\ \text{stacks} \cong 3\ \text{stacks}$$

9.1.2 Fuel Processing Calculations

Example 9-8 Methane Reforming - Determine the Reformate Composition

Given a steam reformer operating at 1400ºF, 3 atmospheres, pure methane feed stock, and a steam to carbon ratio of 2 (2 lb mol H_2O to 1 lb mol CH_4), (a) List the relevant reactions; (b) Determine the concentration assuming the effluent exits the reactor in equilibrium at 1400ºF; (c) Determine the heats of reaction for the reformer's reactions; (d) Determine the reformer's heat requirement assuming the feed stocks are preheated to 1400ºF; (e) Considering LeChâtelier's Principle, indicate whether the reforming reaction will be enhanced or hindered by an elevated operating temperature; (f) Considering LeChâtelier's Principle, indicate whether increased pressure will tend to promote or prevent the reforming reaction.

Solution:

(a) The relevant reactions for the steam reformer are presented below:

$CH_4 + H_2O \Leftrightarrow 3H_2 + CO$ (Steam Reforming Reaction)

$CO + H_2O \Leftrightarrow CO_2 + H_2$ (Water Gas Shift Reaction)

A third reaction is presented below; this reaction is simply a combination of the other two. Of the three reactions, any two can be used as an independent set of reactions for analysis, and can be chosen for the user's convenience.

$CH_4 + 2H_2O \Leftrightarrow 4H_2 + CO_2$ (Composite Steam Reforming Reaction)

(b) The determination of the equilibrium concentrations is a rather involved problem, requiring significant background in chemical thermodynamics, and will not be solved here. One aspect that makes this problem more difficult than Example 9-6, which accounted for the steam reforming reaction within the fuel cell, is that the reforming reaction cannot be assumed to proceed to completion as in the former example. In Example 9-6, hydrogen was consumed within the fuel cell, thus driving the reforming reaction to completion. Without being able to assume the reforming reaction goes to completion, two independent equilibrium reactions must be solved simultaneously. The solution to this problem is most easily accomplished with chemical process simulation programs using a technique known as the minimization of Gibbs free energy. To solve this problem by hand is an arduous, time-consuming task.

The ASPEN™ computer solution to this problem is provided below:

	Inlet Composition (lb mols/hr)	Effluent Composition (lb mols/hr)	Effluent Composition (mol fraction)
CH_4	100	11.7441	2.47
CO	0	64.7756	13.59
CO_2	0	23.4801	4.93
H_2	0	288.2478	60.49
H_2O	200	88.2639	18.52
Total	300	476.5115	100.00

(c) This problem is rather time-consuming to solve without a computer program, and will therefore be left to the ambitious reader to solve[63] from thermodynamic fundamentals. As an alternative, the reader may have access to tables that list heat of reaction information for important reactions. The following temperature-dependent heats of reaction were found for the water gas shift and reforming reactions in the Girdler tables (1).

$CH_4 + H_2O \Leftrightarrow 3H_2 + CO$ $\Delta H_r(1800^oF) = 97{,}741$ Btu/lb mol

$CO + H_2O \Leftrightarrow CO_2 + H_2$ $\Delta H_r(1800^oF) = -13{,}892$ Btu/lb mol

Note: a positive heat of reaction is endothermic (heat must be added to maintain a constant temperature), while a negative heat of reaction is exothermic (heat is given off).

(d) With knowledge of the equilibrium concentration and the heats of reaction, the heat requirement for the reformer can be approximated. Knowing that for each lb mol of CH_4 feed, 88.3% [(100-11.7)/100= 88.3%] of the CH_4 was reformed, and 26.6% [23.5/88.3= 26.6%] of the formed carbon monoxide shifts to carbon dioxide, then the overall heat generation for each lb mol of methane feed can be developed from

$$\left(1 \text{ lbmol } CH_4\right)\left(\frac{88.3\% \ CH_4 \text{ reacted}}{100\% \ CH_4 \text{ feed}}\right)\left(97{,}741 \ \frac{\text{Btu}}{\text{lbmol reformed } CH_4}\right) = 86{,}300 \ \frac{\text{Btu}}{\text{lbmol } CH_4 \text{ feed}}$$

$$\left(1 \text{ lbmol } CH_4\right)\left(\frac{88.3\% \ CH_4 \text{ rxtd.}}{100\% \ CH_4 \text{ feed}}\right)\left(\frac{1 \text{ lbmol CO}}{\text{lbmol } CH_4 \text{ rxtd}}\right)\left(\frac{26.6\% \text{ CO shifts}}{\text{lbmol CO feed}}\right)\left(\frac{-13{,}982 \text{ Btu}}{\text{lbmol CO rxn}}\right) = -3{,}300 \ \frac{\text{Btu}}{\text{lbmol } CH_4 \text{ feed}}$$

Summing these results, the heat requirement for the reformer is about 83,000 Btu/lb mol of CH_4 fed to the reformer. Because this value is positive, the overall reaction is endothermic and heat must be supplied. This approximate value neglects the change in sensible heat in taking the reactants from 1400° F to the reference temperature of 1800° F, and then the products from the reference temperature (1800° F) back to 1400° F.

[63] The reader can refer to Reference 2, Example 4-8 for the solution of a related problem.

(e) LeChâtelier's Principle simply states that "*if a stress is applied to a system at equilibrium, then the system readjusts, if possible, to reduce the stress*". In this reforming example, LeChâtelier's Principle dictates whether higher or lower temperatures will promote the reforming reaction just by knowing that the reaction is endothermic. To facilitate the application of the principle, write the endothermic reforming reaction (which is the dominant heat of reaction) with a heat term on the left side of the equation.

$CH_4 + H_2O + \text{Heat} \Leftrightarrow 3H_2 + CO$

Consider that raising the temperature of the system is the applied stress; the stress will be relieved when the reaction proceeds forward. Therefore, the reforming reaction is thermodynamically favored by high temperatures.

(f) To solve this application of LeChâtelier's Principle, write the reforming reaction in terms of the number of gaseous molecules on the left and right sides.

$CH_{4(g)} + H_2O_{(g)} \Leftrightarrow 3H_{2(g)} + CO_{(g)}$

$2\text{Molecules}_{(g)} \Leftrightarrow 4\text{Molecules}_{(g)}$

Now imagine the reformer at equilibrium, and increase the pressure (the applied stress), then the reaction will try to proceed in a direction that will reduce the pressure (stress). Because a reduction in the number of molecules will reduce the stress, elevated pressure will tend to inhibit the reforming reaction. (Note: reformers often operate at moderate pressures, for operation at pressure will reduce the equipment size and cost. To compensate for this elevated pressure, the designer may be required to raise the temperature.)

Example 9-9 Methane Reforming - Carbon Deposition
Given the problem above, (a) List three potential coking (carbon deposition, or sooting) reactions, and (b) Considering LeChâtelier's Principle, indicate whether excess steam will tend to promote or inhibit the coking reactions.

Solution:
(a) Three of the most common/important carbon deposition equations are presented below.

$CH_4 \Leftrightarrow C + 2H_2$ (Methane Coking)

$2CO \Leftrightarrow C + CO_2$ (Boudouard Coking)

$CO + H_2 \Leftrightarrow C + H_2O$ (CO Reduction)

(b) Considering LeChâtelier's Principle, the addition of steam will clearly inhibit the formation of soot from the CO Reduction reaction. The introduction of excess steam will encourage the reaction to proceed towards the reactants, i.e., away from the products, of which water is one. Since water does not participate in the other two reactions, excess steam does not have

a direct effect on either the Methane coking or the Boudouard coking reactions except that the presence of steam will dilute the reactant and product concentrations. Because neither reaction is equimolar with respect to gaseous species, the effect will be ambivalent; the Methane coking reaction will be driven forward while the Boudouard coking reaction will reverse. In addition, the reverse reaction of CO-reduction stimulated by excess steam will increase the presence of CO, driving the Boudouard coking reaction forward. Overall, the addition of steam is useful at preventing soot from ruining the expensive catalysts used in reformers and fuel cell systems. Too much steam, however, simply adds an unnecessary operating cost.

Determination of the minimum steam to carbon ratio that will inhibit carbon deposition is of interest to the fuel cell system designer. The interested reader is referred to references (4), (5), and (6).

The quantity of steam that would preclude the formation of soot based upon thermodynamic equilibrium could be calculated based on minimization of Gibbs free energy. However, it may not be necessary to add as much steam as is implied by this method. Although soot formation may be thermodynamically favored under certain conditions, the kinetics of the reaction can be so slow that sooting would not be a problem. Thus, the determination of sooting on a kinetic basis rather than equilibrium basis is of significant interest. The interested reader is referred to reference (6). When temperature drops to about 750ºC, kinetic limitations preclude sooting (7). However, above this point, the composition and temperature together determine whether sooting is kinetically precluded. Typically, steam reformers have operated with steam to carbon ratios of 2 to 3, depending on the operating conditions in order to provide an adequate safety margin. An example calculation presented in reference (6) reveals that conditions requiring a steam to carbon ratio of 1.6 on a thermodynamic basis can actually support a steam to carbon ratio of 1.2 on a kinetic basis.

9.1.3 Power Conditioners

Example 9-10 Conversion between DC and AC Power

Given a desired output of 1.0 MW_{AC}, and an inverter efficiency of 96.5%, what DC output level is required from the fuel cell stack?

Solution:

(a) The required DC power output level is found simply as the quotient of AC power and the inverter efficiency as demonstrated below.

$$MW_{DC} = \left(1.0\ MW_{AC}\right)\left(\frac{1\ MW_{DC}}{96.5\%\ MW_{AC}}\right) = 1.036\ MW_{DC}$$

9.1.4 Others

Numerous other unit operations and subsystems can be found in fuel cell processes. These operations and subsystems are well documented in many references (2,8,9,10). For convenience, the unit operations that are commonly found within fuel cell power system are listed below:

- heat exchangers
- pumps
- compressors
- expanders
- intercoolers
- direct contact coolers
- gasification
- gas clean up

9.2 System Issues

This section covers performance issues such as higher heating value (HHV), lower heating value (LHV), cogeneration efficiency, heat rate, and cogeneration steam duty calculations.

9.2.1 Efficiency Calculations

Example 9-11 LHV, HHV Efficiency and Heat Rate Calculations

Given a 2.0 MW_{AC} fuel cell operating on 700 lb/hr of methane, what is (a) the HHV[64] thermal input of the methane gas, (b) the LHV thermal input, (c) the HHV electric efficiency, (d) the LHV electric efficiency, and (e) the HHV heat rate? Assume the higher and lower heating value of methane as 23,881 and 21,526 Btu/lb respectively.

Solution:

(a) The HHV thermal input of the methane gas is

$$\text{HHV Thermal Input} = (700\ \text{lb/hr}\ \ CH_4)\left(\frac{23{,}881\ \text{Btu, HHV}}{1\ \text{lb}\ CH_4}\right)\left(\frac{1\ \text{MMBtu}}{10^6\ \text{Btu}}\right) = 16.716\ \text{MMBtu/hr}$$

or

$$\text{HHV Thermal Input} = (16.716\ \text{MMBtu/hr})\left(\frac{1\ \text{MW}}{3.412\ \text{MMBtu}}\right) = 4.899\ MW_t$$

(b) The LHV thermal input of the methane gas is

$$\text{LHV Thermal Input} = (700\ \text{lb/hr}\ \ CH_4)\left(\frac{21{,}526\ \text{Btu, LHV}}{1\ \text{lb}\ CH_4}\right)\left(\frac{1\ \text{MMBtu}}{10^6\ \text{Btu}}\right) = 15.068\ \text{MMBtu/hr}$$

or

$$\text{LHV Thermal Input} = (15.068\ \text{MMBtu/hr})\left(\frac{1\ \text{MW}}{3.412\ \text{MMBtu}}\right) = 4.416\ MW_t$$

(c) The HHV electrical efficiency is

[64] Heating values are expressed as higher or lower heating values (HHV or LHV). Both higher and lower heating values represent the amount of heat released during combustion. The difference between the HHV and LHV is simply whether the product water is in the liquid phase (HHV), or the gaseous phase (LHV).

$$\text{Electrical Efficiency (HHV)} = \left(\frac{\text{Output}}{\text{Input, HHV}}\right) = \left(\frac{2.0\ \text{MW}_{\text{AC}}}{4.899\ \text{MWt, HHV}}\right) = 40.8\%\ \text{HHV}$$

(d) The LHV electrical efficiency is

$$\text{Electrical Efficiency (LHV)} = \left(\frac{\text{Output}}{\text{Input, LHV}}\right) = \left(\frac{2.0\ \text{MW}_{\text{AC}}}{4.416\ \text{MWt, LHV}}\right) = 45.3\%\ \text{LHV}$$

Note: Because a fuel's LHV is less than or equal to its HHV value, the LHV efficiency will always be greater than or equal to the HHV efficiency.

(e) Heat rate is the amount of heat (Btu/hr) required to produce a kW of electricity. Alternatively it can be thought of as an inverse efficiency. Because 1 kW is equivalent to 3,412 Btu/hr, a heat rate of 3,412 Btu/kWh represents an efficiency of 100%. Note that as the efficiency goes up, the heat rate goes down. The HHV heat rate for this example can be calculated easily from either the HHV efficiency or the thermal input. Both methods are demonstrated below:

$$\text{Heat Rate (HHV)} = \left(\frac{3412\ \text{Btu/kWh}}{\text{Efficiency, HHV}}\right) = \left(\frac{3412\ \text{Btu/kWh}}{40.8\%}\right) = 8{,}360\ \frac{\text{Btu}}{\text{kWh}}\ \text{(HHV)}$$

or

$$\text{Heat Rate (HHV)} = \left(\frac{\text{Input, HHV}}{\text{Output}}\right) = \left(\frac{16{,}716{,}000\ \text{Btu/hr}}{2{,}000\ \text{kW}}\right) = 8{,}360\ \frac{\text{Btu}}{\text{kWh}}\ \text{(HHV)}$$

Note: The LHV to HHV ratio of 90% for methane (21,526/23,881 = 90%) is typical for natural gas, while this ratio is roughly 94% for fuel oils. Common coals typically have a LHV to HHV ratio of 92 to 96% depending upon the hydrogen and moisture content[65]. Typically, gas turbine based cycles are presented on an LHV basis. Conventional power plants, such as coal-, oil-, and gas-fired steam generator/steam turbine cycles are presented on an HHV basis within the U.S. and on an LHV basis throughout the rest of the world.

Example 9-12 Efficiency of a Cogeneration Fuel Cell System
Given the system described in Example 9-11, what is the combined heat and power efficiency assuming that cycle produces 2 tons/hr of 150 psia/400ºF steam? Assume a feedwater temperature of 60ºF.

Solution:
Before calculating the cogeneration efficiency, first determine the heat duty associated with

[65] The difference between the LHV and HHV heating values can be estimated by (1055 Btu/lb)*w, where w is the lbs moisture after combustion per lb of fuel. Thus, w can be determined from the fuel's hydrogen and moisture content by w= moisture + 18/2 * hydrogen. [e.g., for a fuel with 10% moisture and 4% hydrogen, the LHV to HHV difference is 485 Btu/lb, [i.e., 1055*(0.10 + 0.04*9)=485.]

steam production. This requires knowledge of the steam and feed water enthalpies, which can be found in the ASME Steam Tables (11) as indicated below:

	Temperature (ºF)	Pressure (psia)	Enthalpy (Btu/lb)
Steam	400	150	1219.1
Feedwater	60	180	28.6

The steam heat duty is calculated as

$$\text{Heat Duty} = (\text{mass flow})(\text{Change in enthalpy}) = (4000\ \text{lb/hr})(1219.1 - 28.6\ \text{Btu/lb})\left(\frac{1\ \text{MMBtu}}{10^6\ \text{Btu}}\right) = 4.762\ \text{MMBtu/hr}$$

Alternatively, this heat duty can be expressed as 1.396 MWt, [4.762 / 3.412 = 1.396 MW]. Thus, the combined heat and power efficiency is calculated as

$$\text{Combined Heat \& Electrical Efficiency (HHV)} = \left(\frac{\text{Output}}{\text{Input, HHV}}\right) = \left(\frac{2.00\ \text{MW}_{\text{AC}} + 1.396\ \text{MWt}}{4.899\ \text{MWt, HHV}}\right) = 69.3\%\ \text{HHV}$$

9.2.2 Thermodynamic Considerations

Example 9-13 Production of Cogeneration Steam in a Heat Recovery Boiler (HRB)
Given 10,000 lb/hr of 700ºF cycle exhaust gas passing through a heat recovery boiler (HRB) (a) How much 150 psia, 400ºF steam can be produced? (b) How much heat is transferred from the gas in the HRB? (c) What is the exhaust temperature of the gas leaving the HRB? and (d) Sketch the T-Q (temperature-heat) diagram for the HRB. Assume a gas side mean heat capacity of 0.25 Btu/lb-ºF, an evaporator pinch temperature of 30ºF, a feedwater temperature of 60ºF, and an evaporator drum pressure of 180 psia to allow for pressure losses.

Solution:

(a) Develop a solution strategy by examining a typical HRB T-Q diagram presented below. From this diagram, observe that the pinch point, the minimum temperature differential between the gas and saturated steam, limits the steam production. To produce more steam, the lower steam line would be stretched to the right until it "bumped" into the hot gas line. At the point of contact, both the hot gas and saturated steam would be at the same temperature. This is thermodynamically impossible, because heat will only "flow" from a higher temperature to a lower one. In practice, the temperature approach at the pinch point is kept large enough (15 to 40ºF) to prevent an unusually large and expensive evaporator. Because the pinch limits the steam production, the sensible heat available in the exhaust gas from 700° F to the pinch point will determine how much steam can be produced.

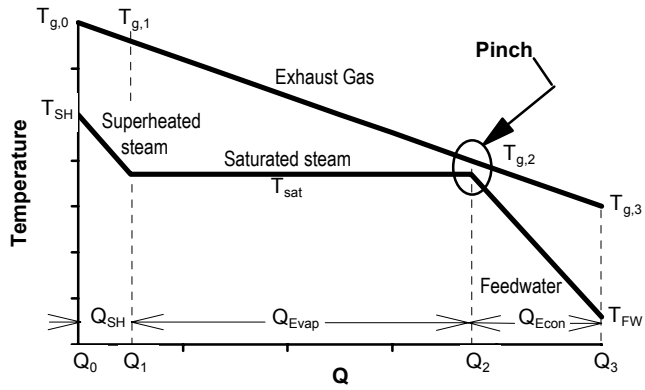

The governing equations for the heat available in the gas down to the pinch point ($T_{g,0}$ to $T_{g,2}$), and the corresponding heat absorbed by the superheated and saturated steam are presented below.

$$Q^{gas}_{SH+Evap} = (m_{gas})(C_p)(T_{g,0} - T_{g,2})$$

$$Q^{steam}_{SH+Evap} = (m_{steam})(h_{superheated} - h_f)$$

$$Q^{gas}_{SH+Evap} = Q^{steam}_{SH+Evap}$$

Calculate $Q^{gas}_{SH+Evap}$ based on the steam saturation temperature from the steam tables. By using the ASME steam tables (11), determine the saturation temperature and enthalpies of interest:

$h_{superheated}$ (150 psia, 400 ºF) = 1219.1 Btu/lb

h_f (180 psia, saturated water) = 346.2 Btu/lb

T_{sat} (180 psia, saturated steam/water) = 373.1ºF

$T_{g,2} = T_{sat} + 30 = 403.1°F$

Now solve for $Q^{gas}_{SH+Evap}$

$$Q^{gas}_{SH+Evap} = \left(10{,}000\,\frac{lb}{hr}\right)\left(0.25\,\frac{Btu}{lb^{o}F}\right)\left(700 - 403.1\ ^{o}F\right) = 742{,}000\,\frac{Btu}{hr}$$

Substitute this heat value into the steam side equation to solve directly for the steam mass flow rate:

$$m_{steam} = \frac{Q^{steam}_{SH + Evap}}{(h_{superheated} - h_f)} = \frac{742{,}000 \ \frac{Btu}{hr}}{\left(1219.1 - 346.2 \ \frac{Btu}{lb}\right)} = 850 \ \frac{lb}{hr}$$

(b) Knowing the water/steam mass flow rate, the HRB heat duty can be calculated using the following equations:

$h_{feedwater}$ (60 ºF) = 28.6 Btu/lb

$$Q^{steam}_{Total} = (m_{steam})(h_{superheated} - h_{feedwater}) = \left(850 \ \tfrac{lb}{hr}\right)\left(1219.1 - 28.6 \tfrac{Btu}{lb}\right) = 1{,}012{,}000 \ \frac{Btu}{hr}$$

(c) The gas temperature leaving the HRB ($T_{g,3}$) is now easily calculated, because the total heat transferred to the steam is equivalent to that lost by the gas stream:

$$Q^{gas}_{Total} = (m_{gas})(C_p)(T_{g,0} - T_{g,3})$$

Thus,

$$1{,}012{,}000 \frac{Btu}{hr} = \left(10{,}000 \frac{lb\ gas}{hr}\right)\left(0.25 \frac{Btu}{lb^{o}F}\right)\left(700\ F - T_{g,3}\right)$$

Solving, $T_{g,3}$ = 295ºF.

(d) Because a constant mean Cp was assumed for the exhaust gas over the temperature range of interest, simply draw a straight line from 700ºF to 295ºF, with the 295ºF corresponding to a transferred quantity of heat of 1.01 MMBtu/hr. On the steam side, separately determine the heat absorbed by the superheater, the evaporator, and the economizer. These heats are determined by the following equations:

$$Q^{steam}_{SH} = (m_{steam})(h_{superheated} - h_g)$$

$$Q^{steam}_{Evap} = (m_{steam})(h_g - h_f)$$

$$Q^{water}_{Econ} = (m_{water})(h_f - h_{feedwater})$$

Substitute the known flow and enthalpy data and solve for these three quantities:

h_g (180 psia, saturated steam) = 1196.9 Btu/lb

$$Q^{steam}_{SH} = (850 \tfrac{lb}{hr})(1219.1 - 1196.9 \tfrac{Btu}{lb}) = (850 \tfrac{lb}{hr})(22.2 \tfrac{Btu}{lb}) = 18{,}900 \frac{Btu}{hr}$$

$$Q_{Evap}^{steam} = (850\,\tfrac{lb}{hr})(1196.9 - 346.2\,\tfrac{Btu}{lb}) = (850\,\tfrac{lb}{hr})(850.7\,\tfrac{Btu}{lb}) = 723{,}100\,\frac{Btu}{hr}$$

$$Q_{Econ}^{water} = (850\,\tfrac{lb}{hr})(346.2 - 28.6\,\tfrac{Btu}{lb}) = (850\,\tfrac{lb}{hr})(317.6\,\tfrac{Btu}{lb}) = 270{,}000\,\frac{Btu}{hr}$$

Use these values to calculate cumulative heat duties:

$$Q_1 = Q_{SH}^{steam} = 18{,}900\,\frac{Btu}{hr} = 0.019\,\frac{MMBtu}{hr} \text{ at } 373.1^{o}\,F$$

$$Q_2 = Q_1 + Q_{Evap}^{steam} = 18{,}900 + 723{,}100\,\frac{Btu}{hr} = 742{,}000\,\frac{Btu}{hr} = 0.742\,\frac{MMBtu}{hr} \text{ at } 373.1^{o}\,F$$

$$Q_3 = Q_2 + Q_{Econ}^{water} = 742{,}000 + 270{,}000\,\frac{Btu}{hr} = 1{,}012{,}000\,\frac{Btu}{hr} = 1.012\,\frac{MMBtu}{hr} \text{ at } 60^{o}\,F$$

Plotting these points on the chart below yields the following T-Q diagram.

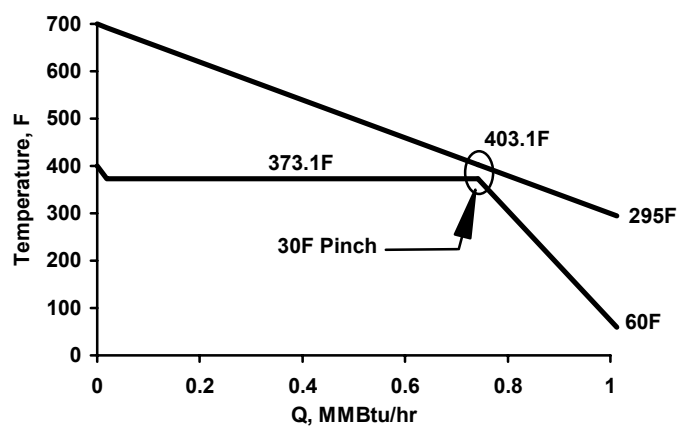

9.3 Supporting Calculations

Example 9-14 Molecular Weight, Density and Heating Value Calculations
Given the fuel gas composition presented below, what is (a) the molecular weight, (b) the higher heating value in Btu/ft^3? (c) the density of the gas in lb/ft^3 at 1 atm and 60ºF? (d) the higher heating value in Btu/lb, and (e) the lower heating value in Btu/ft^3?

Fuel Constituent	mol %
CH_4	4.0
CO	0.4
CO_2	17.6
H_2	75.0
H_2O	3.0
Total	100.0

Solution:

(a) Before determining the molecular weight of the fuel gas mixture, develop the molecular weights of each of the gas constituents in the following table:

Fuel Constituent	MW Derivation	MW
CH_4	(12.01) + 4*(1.008) = 16.04	16.04
CO	(12.01) + 1*(16.00) = 28.01	28.01
CO_2	(12.01) + 2*(16.00) = 44.01	44.01
H_2	2*(1.008) = 2.016	2.016
H_2O	2*(1.008) +1*(16.00) = 18.02	18.02

The molecular weight for the gas mixture is calculated below for a 100 lb mol basis:

		100 lb mol basis			1 lb mol
Fuel Constituent	mol %	lb mols	MW (lb/lb mol)	Weight (lb)	MW (lb/lb mol)
CH_4	4.0	4.0	16.04	64.16	
CO	0.4	0.4	28.01	11.20	
CO_2	17.6	17.6	44.01	774.58	
H_2	75.0	75.0	2.016	151.20	
H_2O	3.0	3.0	18.02	55.06	
Total	100.0	100.0		1056.2	10.56

b) The higher heating value of the fuel gas can be reasonably predicted from the composition. The following table presents the higher heating value for common fuel gas constituents:

Table 9-1 HHV Contribution of Common Gas Constituents

Gas	Higher Heating Value	
	Btu/lb	Btu/ft^3
H_2	60,991	325
CO	4,323	321
CH_4	23,896	1014
C_2H_6	22,282	1789
C_3H_8	22,282	2573
C_4H_{10}	21,441	3392
H_2O, CO_2, N_2, O_2	0	0

Reference (12)
HHV (Btu/ft^3) at 1 atm and 60ºF.

Using these HHV contributions, the gas composition, and the ideal gas law, calculate the overall HHV on a basis of 100 ft^3 in the following table:

Fuel Constituents	mol %	100 ft^3 Basis			1 ft^3 Basis
		Volume (ft^3)	HHV (Btu/ft^3)	Heat Input (Btu)	HHV (Btu/ft^3)
CH_4	4.0	4.0	1014	4056	
CO	0.4	0.4	321	128	
CO_2	17.6	17.6	0	0	
H_2	75.0	75.0	325	24,375	
H_2O	3.0	3.0	0	0	
Total	100.0	100.0		28,559	285.6

Thus, the higher heating value for the specified fuel gas is 285.6 Btu/ft^3.

(c) The density of any ideal gas can be calculated by modifying the ideal gas law, presented below:

$$PV = nRT$$

Because density is simply the mass of a substance divided by its volume, multiply both sides of the ideal gas equation by the molecular weight, MW, of the gas mixture. Recall that the moles of a substance, n, times its molecular weight equals its mass.

$$PV(MW) = n(MW)RT$$

$$PV(MW) = (mass)RT$$

Rearrange this equation to derive an ideal gas law equation that will calculate the density of any ideal gas given the temperature, pressure and MW:

$$\text{density} = \frac{\text{mass}}{\text{volume}} = \frac{P(MW)}{RT}$$

The selection of the ideal gas constant, R, in convenient units such as (atm-ft^3)/(lb mol-R) will simplify the density calculation in units of lbs per ft^3

$$\text{density} = \frac{P(MW)}{RT} = \frac{(1\,\text{atm})(10.56\,\frac{\text{lb}}{\text{lbmol}})}{(0.7302\,\frac{\text{atm-ft}^3}{\text{lbmol-R}})(60+460\,\text{R})} = 0.02781\,\frac{\text{lb}}{\text{ft}^3}\ (\text{at}\,1\,\text{atm},\,60^\circ\,\text{F})$$

(d) The HHV in Btu/lb can be calculated from the HHV in Btu/ft^3 and the density:

$$\text{HHV} = \left(285.6\,\frac{\text{Btu}}{\text{ft}^3}\right)\left(\frac{1\,\text{ft}^3}{0.02781\,\text{lb}}\right) = 10{,}270\,\frac{\text{Btu}}{\text{lb}}$$

(e) The LHV can be calculated by recalling that the fundamental difference between HHV and LHV is the state of the product water. That is, HHV is based on a liquid water product, while LHV is based on a gaseous water product. Because energy is consumed to evaporate liquid water into gaseous water, LHV values are always less than or equal to HHV values. To convert liquid water to water vapor at 1 atm and 60ºF requires approximately 1050 Btu/lb, or 50 Btu/ft^3 of water vapor. For a given gas mixture, the quantitative difference between the HHV and LHV is, obviously, a function of how much water is produced by the given fuel. So the first step in converting HHV to LHV is the determination of the amount of water produced by the fuel. This is done in the table below. The LHV to HHV adjustment is calculated by multiplying the water volume times the change in enthalpy going from liquid to vapor (50 Btu/ft^3):

Fuel Constituent	mol %	Basis: 1.0 ft^3 of Fuel Gas			
		Fuel Gas Volume (ft^3)	Stoichiometric Factor[66] for Gas to H_2O	Water Volume (ft^3)	LHV to HHV Adjustment (Btu/ft^3)
CH_4	4.0	0.04	2.0	0.08	4.0
CO	0.4	0.004	0.0	0.00	0.0
CO_2	17.6	0.176	0.0	0.00	0.0
H_2	75.0	0.75	1.0	0.75	37.5
H_2O	3.0	0.03	0.0	0.00	0.0
Total	100.0	1.00		0.83	41.5.

Thus, the LHV can be estimated from the HHV of 285.6 Btu/ft^3 as 246.1 Btu/ft^3 (285.6 - 41.5= 244.1 Btu/ft^3).

9.4 Cost Calculations

This section presents information on developing the Cost of Electricity (COE), as well as information for the development of capital costs.

9.4.1 Cost of Electricity

Three major components are considered in the computation of the COE for a fuel cell power plant: 1) capital cost, 2) fuel cost and 3) operation and maintenance costs. The cost of electricity ($/MWh) can be calculated using these parameters as follows:

$$COE = \frac{0.125CC}{H} + \frac{3.412\ FC}{\varepsilon_s} + \frac{O\&M}{H}$$

where 0.125 is a typical capital recovery rate (excluding taxes and insurance), CC is the capital cost ($/kW), FC is the fuel cost ($/$10^6$ Btu), 3.412 is the theoretical heat rate for 100% efficiency (3412 Btu/kWh) divided by 1000 for units consistency, ε_s is the fractional efficiency, H is the annual operating hours divided by 1000, and O&M is the operating and maintenance cost ($/kW-yr total, including fixed and variable costs).

Example 9-15 Cost of Electricity

Given a capital cost of $1000/kW, a fuel cost of $2 per MMBtu, a net plant efficiency of 40% (LHV), 6000 operating hours, and a total O&M cost of $20/kW-yr, what is the estimated cost of electricity?

[66] The stoichiometric factor is the number of water molecules produced per fuel molecule in complete combustion. For example, for CH_4, which combusts to 2 H_2O, the stoichiometric factor is two.

Solution:

$$COE = \frac{(0.125)(1000)}{6} + \frac{(3.412)\,(2)}{0.40} + \frac{(20)}{6}$$

$$COE = 20.8 + 17.1 + 3.3 = \$41.2 / MWh, \text{ or } 4.1 \text{ cents} / kWh$$

9.4.2 Capital Cost Development

There is a need for an easily understood, flexible, and reasonably accurate methodology for rapidly estimating the cost of conceptual fuel cell power plants.

One method proposed for estimating the cost of fuel cell power plants is to calculate distributive (bulk) costs as a function of the equipment cost using established factors based on conventional generating technologies. When applied to compensate for the differences associated with a fuel cell plant, this approach can yield reasonable results. Based on the international prominence of the Association for the Advancement of Cost Engineering (AACE), this approach is useful for conceptualizing the costs for fuel cell/turbine power plant systems.

Typical factors in common use are listed in Table 9-4. These factors apply to processes operating at temperatures in excess of 400° F at pressures of under 150 psig, and are taken from the AACE Recommended Practice No. 16R-90, *Conducting Technical and Economic Evaluations in the Process and Utility Industries*.

Table 9-2 Distributive Estimating Factors

Area	Material	Labor
Foundations	0.06	1.33
Structural Steel	0.05	0.50
Buildings	0.03	1.00
Insulation	0.02	1.50
Instruments	0.07	0.75
Electrical	0.06	0.40
Piping	0.40	0.50
Painting	0.005	3.00
Misc.	0.04	0.80

The suggested material factors are applied to direct equipment costs, whereas the labor factors apply to the corresponding material item. Because the distributive factors are based on large scale field-built plants, an alternative factory fabrication adjustment can be made to reflect a modular construction approach requiring less field fabrication, as would likely be the case with smaller plant configurations. This approach is illustrated in reference (16).

The approach discussed above does not preclude the use of alternate methodologies. One such alternate methodology, currently in the early stages of development, is based on the premise that fuel cell plant costs could be more accurately estimated using factors developed specifically for fuel cell applications, rather than factors based on conventional generating technologies. An overview of this approach along with a "first cut" at developing new fuel cell specific factors is presented in reference (18). Fuel cell specific factors developed to date are based on limited data and should be considered highly preliminary. Continued refinement will be required as additional fuel cell plant costing information becomes available.

9.5 Common Conversion Factors

To Convert From	To	Multiply by	To Convert From	To	Multiply by
A (amperes)	Faradays/sec	1.0363E-05	Joule (J)	V-coulomb	1
A/ft²	mA/cm²	1.0764			
atm	kg/cm²	1.0332			
atm	lb/in²	14.696			
atm	bar	1.01325	kg	lb	2.2046
atm	Pa	101,325	kg/cm²	lb/in²	14.223
Avagadro's number	particles/g mol	6.022E+23			
bar	atm	0.98692	Kcal	Btu	3.9686
bar	lb/in²	14.504	kPa	lb/in²	0.14504
bar	kg/cm²	1.0197	kW	Btu/hr	3412.1
bar	Nm²	100,000	kW	kcal/sec	0.23885
bar	Pa	100,000	kW	hp	1.3410
Btu	cal	251.98	lb	grams	453.59
Btu	ft-lb	778.17	lb	kg	0.45359
Btu	J (Joules)	1055.1			
Btu	kWh	2.9307E-04			
Btu/hr	W	0.29307	lb/in²	kg/cm²	0.070307
Btu/lb-°F	cal/g-°C	1.0000	lb/in²	Pa	6894.7
°C	°F	°C*(9/5)+32	l (liter)	m³	1.0000E-03
°C	°K	°C+273.16	m (meter)	ft	3.2808
cal	J	4.1868	m (meter)	in	39.370
cm	ft	0.032808	m²	ft²	10.764
cm	in	0.39370	m³	ft³	35.315
°F	°C	(°F-32)*(5/9)	m³	gal	264.17
Faradays	C (coulombs)	96,487	mA/cm²	A/ft²	0.92903
Faradays/sec	A	96,487	MMBtu/hr	MW	0.29307
ft	m	0.30480	MW	MMBtu/h	3.4121
ft	cm	30.480	Pa	lb/in²	1.4504E-04
ft²	cm²	929.03	R (gas constant)	atm-ft³/lbmol-R	0.73024

To Convert From	To	Multiply by	To Convert From	To	Multiply by
ft^2	m^2	0.092903	R (gas constant)	Btu/lb mol-R	1.9859
ft^3	liters	28.317	R (gas constant)	cal/g mol-K	1.9857
ft^3	m^3	0.028317	R (gas constant)	ft-lbf/lb mol-R	1545.3
ft^3	gal	7.4805	R (gas constant)	J/g mol-K	8.3144126
gal	liters	3.7854	R (gas constant)	l-atm/g mol-K	0.082057
grams (g)	lb	2.2046E-03	tonne	kg	1000.0
hp	ft-lb/sec	550.00	tonne	lb	2204.6
horsepower (hp)	kW	0.74570	Watts	Btu/hr	3.4121
hp	W	745.70	Watts	hp	1.3410E-03

9.6 Automotive Design Calculations

The total power, P, needed from a vehicle's power system must be sufficient for vehicle acceleration, aerodynamic drag losses, rolling resistance, changes in elevation, and auxiliary power for vehicle accessories (19, 20). These power terms are, respectively:

$$P = (mav + 0.5\kappa C_D A_F v^3 + mgC_R v + mgv \cdot \sin(2)) / 0 + P_{aux}$$

Where P = total power (W)
m = vehicle mass (kg)
a = vehicle acceleration (m/sec^2)
v = vehicle velocity (m/sec)
κ = air density (kg/m^3)
C_D = aerodynamic drag coefficient
A_F = vehicle area normal to direction of travel (m^2)
g = gravitation constant (9.8 m/sec^2)
C_R = coefficient of rolling resistance
2 = inclined angle of road (radians)
0 = efficiency of motor, controller, and gearing
P_{aux} = auxiliary power for lights, radio, wipers, air conditioner, cigarette lighter, etc. (W)

The power system may consist of the fuel cell plus peak power storage device(s). Criteria established by the Partnership for a New Generation of Vehicles (PNGV) specify that:

- The fuel cell system (without peak power device) must provide enough power to sustain a speed of 55 mph (24.58 m/sec) on a 6.5 % grade, and
- The output of the fuel cell system plus peak power device must allow acceleration for high speed passing of 3 mph/sec (1.34 m/sec^2) on a level road at 65 mph (29.05 m/sec)

These values are computed for a conventional mid-size passenger vehicle using the following assumptions:

$m = 1360$ kg (vehicle weight) + 272 kg (weight of passengers plus cargo)
$\kappa = 1.29$ kg/m^3 (at standard temperature and pressure)
$C_D = 0.3$
$A_F = 2.0$ m^2
$g = 9.8$ m/sec^2
$C_R = 0.0085$
$0 = 0.77$
$P_{aux} = 400$ W (= 400 kg-m^2/sec^3)

Substituting these values into the equation above, the minimum power needed by the fuel cell alone to sustain 24.58 m/sec on a 6.5 % grade (0.0649 radians) is

$$P_S = ((0.5)(1.29)(0.3)(2.0)(24.58)^3 + (1632)(9.8)(0.0085)(24.58) + (1632)(9.8)(24.58)\sin(0.0649))/0.77 + 400$$

$$P_S = 45{,}339 \text{ kg-m}^2/\text{sec}^3 = 4.53 \text{ kW}$$

The minimum power needed by the power system to accelerate on a level road at 1.34 m/sec^2 at 29.05 m/sec is

$$P_A = ((1632)(1.34)(29.05) + (0.5)(1.29)(0.3)(2.0)(29.05)^3 + (1632)(9.8)(0.0085)(29.05))/0.77 + 400$$

$$P_A = 100{,}355 \text{ kg-m}^2/\text{sec}^3 = 10.03 \text{ kW}$$

9.7 References

1. "Physical and Thermodynamic Properties of Elements and Compounds," Girdler Catalysts, Chemetron Corporation, Catalysts Division.
2. J. M. Smith, H. C. Van Ness, Introduction to Chemical Engineering Thermodynamics, Third Edition, McGraw-Hill, 1975.
3. Chemistry: Principles and Applications, M. J. Sienko, R. A. Plane, McGraw-Hill, New York, NY, 1979.
4. D. B. Stauffer, J. S. White, J. H. Hirschenhofer, "An ASPEN/SP MCFC Performance User Block," DOE Contract DE-AC21-89-MC25177, Task 7, July 1991.
5. D. B. Stauffer, R. R. Engleman Jr., J. S. White, J. H. Hirschenhofer, "An ASPEN/SP SOFC Performance User Block," DOE Contract DE-AC21-88-FE-61684, Task 14, September 1993.
6. E. S. Wagner, G. F. Froment, "Steam Reforming Analyzed," Hydrocarbon Processing, July 1992, pp. 69 -77.
7. Fuel Cell Systems, Edited by L. J. M. Blomen, M. N. Mugerwa, Plenum Press, New York, NY, 1993.

8. W. L. McCabe, J. C. Smith, P. Harriot, Unit Operations of Chemical Engineering, 4th Edition, 1985.
9. Chemical Engineers' Handbook, Edited by R. H. Perry, D. Green, 6th Edition, McGraw-Hill, 1984.
10. M. S. Peters, K. D. Timmerhaus, Plant Design and Economics for Chemical Engineers, 3rd Edition, McGraw-Hill, Inc., New York, NY, 1980.
11. C. A. Meyers, R. B. McClintok, G. J. Silvestri, R. C. Spencer, Jr., 1967 ASME Steam Tables, New York, 1967.
12. Combustion, Fossil Power: A Reference Book on Fuel Burning and Steam Generation, 4th Edition, edited by J. G. Singer, P.E., Combustion Engineering, 1991.
13. B. J. McBride, "Coefficients for Calculating Thermodynamic and Transport Properties of Individual Species," NASA Technical Memorandum 4513, October 1993.
14. B. J. McBride, "Thermodynamic Data for Fifty Reference Elements," NASA Technical Paper 3287, January 1993.
15. H. M. Spencer, *Ind. Eng. Chem.*, 40:2152 (1948), as presented in Introduction to Chemical Engineering Thermodynamics, Third Edition, J. M. Smith and H. C. Van Ness, McGraw-Hill, 1975.
16. T. J. George, R. James III, K. D. Lyons, "Multi-Staged Fuel Cell Power Plant (Targeting 80% Lower Heating Value Efficiency)," *Power Generation International 1998 Conference*, December 9-11, 1998, Orange County Convention Center, Orlando, Florida.
17. Recommended Practice No. 16R-90, *Conducting Technical and Economic Evaluations in the Process and Utility Industries*.
18. L. L. Pinkerton, "Express Method for Estimating the Cost of Fuel Cell Plants," *1998 Fuel Cell Seminar*, November 16-19, 1998, Palm Springs Convention Center, Palm Springs, California.
19. J. M. Ogden, M. M. Steinbugler, and T. G. Kreutz. 1999. "A Comparison of Hydrogen, Methanol, and Gasoline as Fuels for Fuel Cell Vehicles: Implications for Vehicle Design and Infrastructure Development." Journal of Power Sources, 79 (1999) 143-168.
20. K. H. Hauer, D. J. Friedmann, R. M. Moore, S. Ramaswamy, A. Eggert, and P. Badranarayanan, March 6-9, 2000. "Dynamic Response of an Indirect-Methanol Fuel Cell Vehicle." Fuel Cell Power for Transportation 2000. Society of Automotive Engineers World Congress, Detroit, Michigan.

10. APPENDIX

10.1 Equilibrium Constants

Figure 10-1 presents the temperature dependence of the equilibrium constants for the water gas shift reaction,

$$CO_2 + H_2 = CO + H_2O \qquad (10\text{-}1)$$

the carbon deposition (Boudouard reaction) reaction,

$$2CO \rightarrow C + CO_2 \qquad (10\text{-}2)$$

the methane decomposition reaction,

$$CH_4 \rightarrow C + 2H_2 \qquad (10\text{-}3)$$

and the methane formation reaction,

$$CO + 3H_2 \rightarrow CH_4 + H_2O \qquad (10\text{-}4)$$

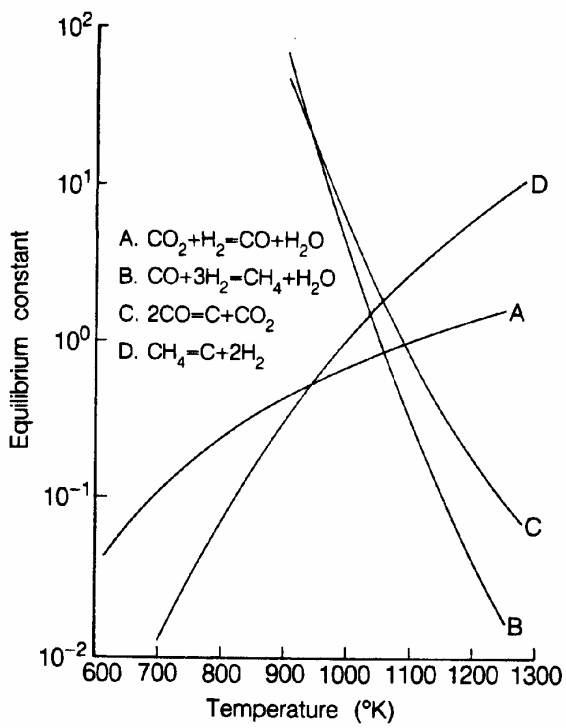

Figure 10-1 Equilibrium Constants (Partial Pressures in MPa) for (a) Water Gas Shift, (b) Methane Formation, (c) Carbon Deposition (Boudouard Reaction), and (d) Methane Decomposition (J.R. Rostrup-Nielsen, in Catalysis Science and Technology, Edited by J.R. Anderson and M. Boudart, Springer-Verlag, Berlin GDR, p.1, 1984.)

10.2 Contaminants from Coal Gasification

A list of contaminant levels that result from various coal gasification processes is presented in Table 10-1. The contaminant levels obtained after a first stage of hot gas cleanup with zinc ferrite also are listed.

Table10-1 Typical Contaminant Levels Obtained from Selected Coal Gasification Processes

Parameters	Coal Gasification Process		
	LURGI Fixed Bed	METC (raw gas) Fixed Bed	Cleaned Gas
Max. Product Temp. (EC)	750	1300	<800
Gasification	O_2 blown	Air blown	Regenerative
Pressure (psi)	435	220	150
Product Gas (EC)	600	650	<700
Methane (vol%)	11	3.5	3.5
Coal type	Sub-bitum. Navajo	Sub-bitum. New Mexico	(Humidified Output)
Particulates (g/l)	0.016	0.058	0.01 est.
Sulfur (ppm) (Total H_2S, COS, CS_2, mercaptans)	2,000	5,300	<10
NH_3 (vol%)	0.4	0.44	0.25
Trace metals (ppm)			
As	2	NS[a]	NS
Pb	0.8	2	1.7
Hg	0.4	NS	NS
Zn	0.4	NS	140
Halogens (ppm)	200	700	500
Hydrocarbons (vol%)			
C_2H_6	1	NS	NS
C_2H_4	1	0.3	NS
C_2H_2	1	NS	NS
Oil tar	0.09	NS	NS

a - Not specified

Source: A. Pigeaud, Progress Report prepared by Energy Research Corporation for U.S. Department of Energy, Morgantown, WV, Contract No. DC-AC21-84MC21154, June 1987.

10.3 Selected Major Fuel Cell References, 1993 to Present

Books on Fuel Cells:

1. A.J. Appleby, F.R. Foulkes, *Fuel Cell Handbook*, Van Norstand Reinhold, New York, N.Y., 1989. Republished by Krieger Publishing Company, Melborne, FL, 1993.

2. L.J. Blomen, M.N. Mugerwa, editors, *Fuel Cell Systems*, ISBN 0-306-44158-6, Kluwer Academic Publishers, 1994.

3. M. Corbett, Opportunities in Advanced Fuel Cell Technologies – Volume One – Stationary Power Generation 1998-2008, Kline & Company, Inc., Fairfeild, NJ, 1998.

4. EscoVale Consultancy Services, *Fuel Cells: The Source Book.*

5. S. Gottesfeld, T.A. Zawodzinski, "Polymer Electrolyte Fuel Cells," *Advances in Electrochemical Science and Engineering*, *Volume 5,* edited by R.C. Alkire, et al., Wiley-VCH, 1998.

6. G. Hoogers, *Fuel Cell Technology Handbook,* CRC Press, ISBN: 0849308771 August, 2002.

7. T. Koppel, *Powering the Future: The Ballard Fuel Cell and the Race to Change the World*, John Wiley & Sons, ISBN: 047-1646296, 2001.

8. K. Kordesch, G. Simander, *Fuel Cells and Their Applications*, VCH Publishers, New York, N.Y., ISBN: 3-527-28579-2, 1996.

9. J. Larminie, A. Dicks, *Fuel Cell Systems Explained,* John Wiley and Sons, ISBN: 0-471-49026-1, 2000.

CD's on Fuel Cells:

1. Fuel Cell Handbook, 5th Edition - November 2000. The latest technical specifications and description of fuel cell types. Prepared by EG&G Technical Services, Parsons, Inc., and Science Applications International Corporation for the National Energy Technology Laboratory.

2. Distributed Generation Primer – May 2002. This CD provides the background for decision makers to evaluate the options, market conditions, drivers and issues related to successful use of distribution generation. Prepared by Science Applications International Corporation and EG&G Technical Services for the National Energy Technology Laboratory.

3. Hybrid Fuel Cell Technology Overview - May 2001. Prepared by Energy and Environmental Solutions for the National Energy Technology Laboratory.

Periodicals and Newsletters:

1. Advanced Fuel Cell Technology – monthly. Published by Seven Mountains Scientific, Inc. Boalsburg, PA 16827. Online subscription available at http://www.7ms.com/fct/index.html

2. Alternative Fuel News – quarterly. Published by U.S. Department of Energy's Alternative Fuel Data Center and the Clean Cities Program. Available online at http://afdcweb.nrel.gov/documents/altfuelnews/

3. Clean Fuels and Electric Vehicles Report – Published 4 times per year. Published by Energy Futures, Inc. Boulder, CO 80306. Online subscription available at www.energy-futures.com/

4. Electrifying Times – 3 issues per year. Published by Bruce Meland, Bend, Oregon 97701. Table of contents and past issue archives available online at www.electrifyingtimes.com/

5. Fuel Cell Catalyst – quarterly. Published by U.S. Fuel Cell Council and National Fuel Cell Research Center and sponsored by National Energy Technology Laboratory. To subscribe http://lb.bcentral.com/ex/manage/subscriberprefs.aspx?customerid=9927

6. Fuel Cell Connection – monthly e-mail. Published by U.S. Fuel Cell Council and National Fuel Cell Research Center and sponsored by National Energy Technology Laboratory. To subscribe http://lb.bcentral.com/ex/manage/subscriberprefs.aspx?customerid=9927

7. Fuel Cell Industry Report – monthly. Published by Scientific American Newsletter, New York, NY 10003. To subscribe http://www.sanewsletters.com/fcir/FCIRinfo.asp

8. Fuel Cell Magazine – a supplement in March, June, September 2002 issues of Battery Power Products and Technology. Will be standalone bimonthly magazine in October 2002. To subscribe http://www.fuelcell-magazine.com

9. Fuel Cell Quarterly – quarterly. Published by Fuel Cells 2000, Washington DC 20006. Headlines available online at http://www.fuelcells.org/newsletter.htm

10. Fuel Cell Technology News – monthly. Published by Business Communications Company, Inc. Norwalk, CT 06855.

11. Fuel Cell World – quarterly (in German). Published by World Fuel Cell Council, Frankfurt am Main, Germany.

12. Fuel Cells Bulletin – monthly. Published by Elsevier Advanced Technology, Kidlington, Oxford OX5 1AS, United Kingdom. Online ordering information at http://www.elsevier.com/inca/publications/store/6/0/1/4/4/3/index.htt

13. Fuel Cells: From Fundamentals to Systems – Journal. Published by Wiley – VCH. Online ordering information at http://www.interscience.wiley.com/jpages/1615-6846/

14. Fuel Cell Industry Report – monthly. Published by Scientific American Newsletters, New York, New York 10010. Online ordering information at http://www.sanewsletters.com/fcir/FCIRinfo.asp

15. Hybrid Vehicles – bimonthly. Published by Energy Futures, Inc. Boulder, CO 80306. Online subscription available at www.energy-futures.com/

16. Hydrogen and Fuel Cell Letter – monthly. Published by Peter Hoffman, Rhinecliff, NY 12574. Headlines and ordering information available online at www.hfcletter.com/

17. The Hydrogen – Gazette – Newsletter published by HyWeb and the German Hydrogen Association. Available online at www.hydrogen.org

18. Hydrogen Mirror / Wasserstoff-Spiegel – bimonthly. Published by Deutscher-Wasserstoff-Verband (German Hydrogen Association). To subscribe http://www.dwv-info.de/wse.htm

19. International Journal of Hydrogen Energy – monthly. Published by Elsevier Advanced Technology, Kidlington, Oxford OX5 1AS, United Kingdom. Online ordering information at http://www.elsevier.com/inca/publications/store/4/8/5/index.htt

20. Journal of Power Sources - monthly. Published by Elsevier Advanced Technology, Kidlington, Oxford OX5 1AS, United Kingdom. Online ordering information at http://www.elsevier.com/inca/publications/store/5/0/4/0/9/3/index.htt

21. Platinum Metals Review – quarterly. Published by Johnson Matthey PLC, London, United Kingdom. Available online at http://www.platinum.matthey.com/publications/pmr.php

22. SCNG News – monthly. Published by the U.S. Department of Energy's Strategic Center for Natural Gas. Available online at http://www.netl.doe.gov/scng/news/news_toc.html

Proceedings and Abstracts from Major U.S. Fuel Cell Conferences:

1. *Fuel Cell Seminar, Programs and Abstracts*, Fuel Cell Seminars, sponsored by Fuel Cell Seminar Organizing Committee. Meetings held every two years at U.S. locations, annually starting in 2002, Courtesy Associates, Inc., Washington, D.C. For information visit web site at http://www.gofuelcell.com/:

   November /December 1994 – San Diego, California.
   November 1996 – Orlando, Florida.
   November 1998 – Palm Springs, California.
   November 2000 – Portland, Oregon.
   November 2002 - Palm Springs, California.
   2003 – Miami, Florida.

2. *Proceedings of the Annual Fuel Cells Review Meeting*. Meetings held annually at the U.S. DOE Morgantown Energy Technology Center (now the National Energy Technology Laboratory), Morgantown, WV, until 1998, then at U.S. locations:

   DOE/METC-94/1010, August 1994
   DOE/METC-95/1020, August 1995
   DOE/METC CD-ROM, August 1996
   DOE/FETC–98/1054 CD-ROM, August 1997
   Joint DOE/EPRI/GRI Workshop on Fuel Cell Technology, May 1998, San Francisco, CA
   Joint DOE/EPRI/GRI Workshop on Fuel Cell Technology, August 1999, Chicago, IL

3. *EPRI/GRI Fuel Cell Workshop on Technology Research and Proceedings*, Cosponsored by EPRI and GRI, Proceedings by EPRI, Palo Alto, CA, March 1994.

   March 1994, Atlanta, Georgia
   April 1995, Irvine, California.
   April 1996, Temple, Arizona
   In 1997, the EPRI/GRI Workshop joined with the DOE Annual Fuel Cells Contractors Meeting. See Item 2 for information in 1997 and beyond.

4. J.R. Selman, et al., ed. *Carbonate Fuel Cell Technology IV*, Proceedings Vol. 97-4, Montreal, Canada, The Electrochemical Society, Inc., Pennington, NJ, 1997.

5. K. Hemmes, et al., *Proceedings of the Fifth International Symposium on Molten Carbonate Fuel Cell Technology*, Honolulu, Hawaii, The Electrochemical Society, Inc., Pennington, NJ, October 1997.

6. S.C. Singhal, et al., *Proceedings at the Fourth International Symposium on Solid Oxide Fuel Cells*, Proceedings Vol. 95-1, Yokohama, Japan, The Electrochemical Society, Inc., Pennington, NJ, 1995.

7. S.C. Singhal, et al., *Proceedings of the Fifth International Symposium on Solid Oxide Fuel Cells*, Proceedings Vol. 97-40, Aachen, Germany, The Electrochemical Society, Inc., Pennington, NJ, 1997.

8. S.C. Singhal, et al., *Proceedings of the Sixth International Symposium on Solid Oxide Fuel Cells*, Proceedings Vol. 99-19, Honolulu, Hawaii, The Electrochemical Society, Inc., Pennington, NJ, 1999.

9. A.R. Landgrebe, S. Gottesfeld, *First International Symposium on Proton Conducting Membrane Fuel Cells*, Chicago, IL, Proceedings Vol. 95-23, The Electrochemical Society, Inc., Pennington, NJ, 1995.

10. S. Gotts, et al., *Second International Symposium on Proton Conducting Membrane Fuel Cells*, Boston, MA, The Electrochemical Society, Inc., Pennington, NJ, 1998.

11. *Proceedings of the Workshop on Very High Efficiency Fuel Cell/Gas Turbine Power Cycles*, edited by M.C. Williams, C.M. Zeh, U.S. DOE Federal Energy Technology Center, Morgantown, WV, October 1995.

12. *Proceedings of the National Hydrogen Association Meetings*, National Hydrogen Association, usually in Alexandria, VA, annually in spring.

13. *Proceedings of the Intersociety Energy Conversion Engineering Conference*. Sponsorship of meeting rotates among six technical societies. Meetings are held annually (usually in August) in different cities of the United States:

    29th - Part 2, Sponsor - American Institute of Aeronautics and Astronautics, Monterey, CA, August 1994.
    30th - Volume 3, Sponsor - American Society of Mechanical Engineers, Orlando, Fl, August 1995.
    31st - Volume 2, Sponsor - Institute of Electrical and Electronics Engineers, Washington, D.C., August 1996.
    32nd - Sponsor - American Institute of Chemical Engineers, Honolulu, Hawaii, July/August 1997.
    33rd - CD-ROM, Sponsor - American Nuclear Society, Colorado Springs, Colo., August 1998.
    34th - CD-ROM, Sponsor – Society of Automotive Engineers, Vancouver, BC, August 1999.
    35th – Sponsor - American Institute of Aeronautics and Astronautics, Las Vegas, NV, July 2000.
    36th – Sponser - American Society of Mechanical Engineers, Savannah, Georgia, July 2001.

14. *Proceedings of the 58th American Power Conference*, Volume 58-1, Sponsored by Illinois Institute of Technology, Chicago, IL, 1996.

15. *Proceedings of U.S. Russian Workshop on Fuel Cell Technologies*, Sandia National Laboratories, Albuquerque, N.M., September 1995.

16. *Lake Tahoe Fuel Cell Conference Proceedings*, Desert Research Institute, Energy & Environmental Engineering Center, P.O. Box 60220, Reno, NV 69506-0220, July 1998.

17. *Next Generation Fuel Cells Workshop: Workshop Proceedings* – National Energy Technology Laboratory (formerly Federal Energy Technology Center), Morgantown, WV, December 1998.

18. *Proceedings of the NETL Workshop on Fuel Cell Modeling*, National Energy Technology Center, Morgantown, WV, April 2000.

19. *Proceedings of the Second Annual Small Fuel Cells & Batteries Conference*, New Orleans, LA, The Knowledge Foundation, Brookline, MA, April 2000.

20. *Proceedings of the U.S. DOE Natural Gas/Renewable Energy Hybrids Workshops.* Morgantown, WV. Proceedings can be found online at http://www.netl.doe.gov/publications/proceedings/01/hybrids/hybrid01.html

21. *Proceedings of the Second DOE/UN International Conference and Workshop on Hybrid Power Systems.* April 16-17, 2002. Proceedings can be found online at http://www.netl.doe.gov/publications/proceedings/02/Hybrid/hybrid02.html

22. *Proceedings of the Solid State Energy Conversion Alliance Workshops,* SECA is coordinated by the National Energy Technology Center and Pacific Northwest National Laboratory. Proceedings can be found online at http://www.seca.doe.gov/Publications/workshops.htm

First Workshop	Baltimore, Maryland	June 2000
Second Workshop	Arlington, Virginia	March 2001
Third Workshop	Washington, DC	March 2002

23. *Proceedings of the Fuel Cell Summits on Codes and Standards*, Originated in the Department of Energy's Office of Building Equipment, State and Community Programs, but has now transferred to the Departments Office of Power Technologies. Results of the Summits can be found online at http://www.pnl.gov/fuelcells/summits.htm

Summit I	April 1997
Summit II	May 1998
Summit III	April 1999
Summit IV	May 2000
Summit V	May 2001
Summit VI	May 2002

Other Important Information on Fuel Cells:

1. U.S. DOE, *Fuel Cell Program Plans*, published each Fiscal Year by U.S. Department of Energy, Assistant Secretary of Fossil Energy:

   1994 - DOE/FE-0311P
   1995 - DOE/FE-0335
   1996 - DOE/FE-0350

2. NEDO, *Research and Development on Fuel Cell Power Generation Technology*, published yearly by the New Energy and Industrial Technology Development Organization, Tokyo, Japan.

3. *Fuel Cell RD&D in Japan*, Published annually by the Fuel Cell Development Information Center c/o The Institute of Applied Energy, Tokyo, Japan, usually in August.

4. *Proceedings of the Grove Anniversary Fuel Cell Symposium*, London, UK, September 1995, Journal of Power Sources, Elsevier Sequoia Science, The Netherlands, January 1995.

5. *Proceedings of the Grove Anniversary Fuel Cell Symposium*, London, UK, September 1997, Journal of Power Sources, Elsevier Sequoia Science, The Netherlands, March 1998.

6. *Proceedings of the 6th Grove Anniversary Fuel Cell Symposium*, London, UK, September 1999, Journal of Power Sources, Elsevier Sequoia Science, The Netherlands, March 2000.

7. *Proceedings of the 7th Grove Anniversary Fuel Cell Symposium*, London, UK, September 2001, Journal of Power Sources, Elsevier Sequoia Science, The Netherlands. For information see http://www.grovefuelcell.com/

8. U. Bossel, editor, *Proceedings of the European Solid Oxide Fuel Cell Forums*, European Fuel Cell Group and IEA Advanced Fuel Cell Programme, 1994, 1996, 1998.

9. Various Technical Reports Posted on the Strategic Center for Natural Gas Fuel Cell Reference Shelf. Available online at http://www.netl.doe.gov/scng/enduse/fc_refshlf.html

Selected Fuel Cell Related URLs:

Fuel Cell Developer Sites:

Avista Labs	www.avistalabs.com
Ballard Power Systems, Inc.	www.ballard.com
Ceramatec, Inc.	www.ceramatec.com
Dais-Analytic Corporation	www.daisanalytic.com
ElectroChem, Inc.	www.fuelcell.com
FuelCell Energy, Inc	www.fce.com
H-Power, Inc.	www.hpower.com
Honeywell	www.honeywell.com
McDermott Technologies, Inc.	www.mtiresearch.com
NexTech Materials, Ltd.	www.nextechmaterials.com
UTC Fuel Cells	www.internationalfuelcells.com
Plug Power L.L.C.	www.plugpower.com
Siemens Westinghouse	www.pg.siemens.com/en/fuelcells
Warsitz Enterprises, Inc.	www.warsitz-enterprises.com

Government Sites:

Argonne National Labs	www.anl.gov
Department of Defense	www.dodfuelcell.com
DOE Fossil Energy	www.fe.doe.gov
DOE R&D Project Summaries	www.osti.gov/rd/
Energy Efficiency/Renewable Energy Network	www.eren.doe.gov
FreedomCAR	www.cartech.doe.gov/

Los Alamos National Labs	www.lanl.gov
National Energy Technology Laboratory	www.netl.doe.gov
National Renewable Energy Laboratory	www.nrel.gov
Oak Ridge National Labs	www.ornl.gov
Pacific Northwest National Laboratory	www.pnl.gov
Partnership for a New Generation of Vehicles	www.ta.doc.gov/pngv
Sandia National Labs	www.sandia.gov
Solid State Energy Conversion Alliance	www.seca.doe.gov
Strategic Center for Natural Gas	www.netl.doe.gov/scng/index.html

Miscellaneous Sites:

California Fuel Cell Partnership	www.drivingthefuture.org
Electric Power Research Institute	www.epri.com
Fuel Cell 2000	www.fuelcells.org
FuelCellOnline.Com	www.fuelcellonline.com
Fuel Cell Today	www.fuelcelltoday.com
Gas Technology Institute	www.gri.org
Hydrogen and Fuel Cell Newsletter	www.hfcletter.com
HyWeb	www.hydrogen.org
International Energy Agency	www.ieafuelcell.com
National Fuel Cell Research Center	www.nfcrc.uci.edu
National Hydrogen Association	www.hydrogenus.com
NEDO (Japan)	www.nedo.go.jp/nedo-info/index-e.html
US Car	www.uscar.org
U.S. Fuel Cell Council	www.usfcc.com
World Fuel Cell Council	www.fuelcellworld.org

10.4 List of Symbols

Abbreviations:

®	registered
A.R.	as received
ABS	acrylonytril-butadiene-styrene
AES	air electrode supported
AFC	alkaline fuel cell
APU	auxiliary power unit
ASF	amps/ft2
ASR	area-specific resistance
ASU	air separation unit
CC	capital cost
COE	cost of electricity
CVD	chemical vapor deposition
DIR	direct internal reforming
DOE	Department of Energy

EMF	electromotive force
EVD	electrochemical vapor deposition
FC	fuel cost
FCE	Fuel Cell Energy
FEP	fluoro-ethylene-propylene
FETC	Federal Energy Technology Center
GDL	gas diffusion layer
HHV	higher heating value
HR	heat rate
IIR	indirect internal reforming
iR	ohmic loss
J-M	Johnson Mathey Technology Center
LHV	lower heating value
MCFC	molten carbonate fuel cell
MEA	membrane/electrode assembly
NETL	National Energy Technology Laboratory
O&M	operating and maintenance costs
ODS	oxide dispersion strengthened anode
OS/IES	on-site/integrated energy systems
PAFC	phosphoric acid fuel cell
PC	phthalocyanines
PEFC	polymer electrolyte fuel cell
PMSS	pyrolysis of metallic soap slurry
PR	pressure ratio
Pt	platinum
PTFE	polytetrafluoroethylene
RDF	refuse derived fuel
SOFC	solid oxide fuel cell
TAA	tetraazaannulenes
TBA	tetrabutyl ammonium
TFMSA	trifluoromethane sulfonic acid
THT	tetrahydrothiophene (thiophane)
TMPP	tetramethoxyphenylporphyrins
TPP	tetraphenylporphyrins
TZP	tetragonal phase
™	trade mark
U.S.	United States of America
WSF	watts/ft2
YSZ	yittria stabilized zirconia

Letter Symbols:

ΔE	potential difference
ΔG	Gibbs free energy
ΔH_c	heat available from combustion of fuel gas
ΔH_r	enthalpy of reaction

ΔS_r	entropy of reaction
ΔV	voltage difference
<D>	equilibrium pore size
a	$(-2.3RT/\alpha nF) \log i_o$
a	coefficient
AC	alternating current
b	$2.3RT/\alpha nF$
b	coefficient
b	Tafel slope
Btu	British Thermal Unit
c	coefficient
C_B	bulk concentration
C_p	heat capacity
C_S	surface concentration
D	diffusion coefficient
D	pore diameter
dBA	average decibles
DC	direct current
e^-	electron
E	equilibrium (reversible) potential
E°	standard potential
E_a	activation energy
F	Faraday's constant
f	gas flow rate
hrs	hours
I	current
i	current density
i_L	limiting current density
i_o	exchange current density
J	current density
K	equilibrium constant
k(T)	constant, function of temperature
kW	kilowatt
lb	pound
MM	million
mol	mole
MW	megawatt (1000 kW)
MWhr	megawatt-hour
n	number of electrons participating in a reaction
n_{max}	maximum stoichiometric value
P	pressure
P_i	partial pressure
ppm	parts per million
P_T	total pressure
R	cell resistance
R	universal gas constant

t	electrolyte thickness
T	temperature
U	utilization
V	cell voltage
v	rate at which reactant species are consumed
V	volume
V_c	voltage of single cell
vol	volume
W_{el}	maximum electrical work
wt	weight
X	mole fraction
yr	year

Greek Letter Symbols:

α	transfer coefficient
β	hydrogen utilization
Γ	mole fraction
γ	interfacial surface tension
γ	oxidant utilization
δ	diffusion layer thickness
η_{act}	activation polarization
η_{conc}	concentration polarization
η_{ohm}	ohmic polarization
θ	electrolyte contact angle
θ_{CO}	CO coverage

Subscripts:

a	anode
c	cathode
e	electrolyte
f	fuel
i	species
in	cell inlet
out	cell outlet
ox	oxygen or oxidant
p	pressure
t	temperature

10.5 Fuel Cell Related Codes and Standards

10.5.1 Introduction

The rapid development and application of fuel cells throughout the world has created the need for fuel cell technology related codes and standards. Several organizations and committees are currently working on the development of codes and standards related to fuel cells.

According to the National Fire Protection Agency (NFPA) Regulations Governing Committee Projects, codes and standards are defined as follows:

Code: A standard that is an extensive compilation of provisions covering broad subject matter or that is suitable for adoption into law independently of other codes and standards.

***Standard*:** A document, the main text of which contains only mandatory provisions using the word "shall" to indicate requirements and which is in a form generally suitable for mandatory reference by another standard or code or for adoption into law. Non-mandatory provisions shall be located in an appendix, footnote, or fine-printnote and are not to be considered a part of the requirements of a standard.

This section provides a brief overview of the existing and developing codes and standards related to fuel cell technologies. The discussion focuses on participating organizations, specific codes and standards and more generally applied codes and standards (e.g., the Uniform Building Code) that apply to system installation.

10.5.2 Organizations

Below is a listing and brief description of organizations involved in the development of codes and standards pertaining to fuel cell technology.

American National Standards Institute (ANSI): ANSI has served in its capacity as administrator and coordinator of the United States private sector voluntary standardization system for 80 years. The Institute is a private, nonprofit membership organization supported by a diverse constituency of private and public sector organizations. ANSI Z21.83 has been published and provides a means of testing and certifying the safety of stationary fuel cell power plants having a capacity of less than 1 MW.

American Society of Mechanical Engineers (ASME): ASME is an international engineering society that conducts one of the world's largest technical publishing operations. ASME International is a nonprofit educational and technical organization serving a worldwide membership. Its mission is to promote and enhance the technical competency and professional well being of engineers through programs and activities in mechanical engineering. To this end, ASME has developed the Boiler and Pressure Vessel Code, which is referenced as part of the AGA certification. Additionally, ASME is working on a fuel cell standard, ASME PTC 50, Performance Test Code for Fuel Cell Power System Performance. Publication of this standard is expected in 2002.

Institute of Electrical and Electronics Engineers (IEEE): The mission of IEEE is to advance global prosperity by promoting the engineering process of creating, developing, integrating, sharing and applying knowledge about electrical and information technologies. IEEE Standards Coordinating Committee 21 (SCC21) oversees the development of standards in the area of fuel cells, photovoltaics, distributed generation, and energy storage. SCC21 coordinates efforts in these fields among the various IEEE societies and other appropriate organizations to insure that all standards are consistent and properly reflect the views of all applicable disciplines. Working Group 1547 - Standard for Distributed Resources Interconnected with Electric Power Systems -

establishes criteria and requirements for interconnection by distributed resources with electric power systems. The purpose is to provide a uniform standard for interconnection of distributed resources with electric power systems and requirements relevant to the performance, operation, testing, safety considerations, and maintenance of the interconnection.

International Code Council (ICC): The International Code Council (ICC) was established in 1994 as a nonprofit organization dedicated to developing a single set of comprehensive and coordinated national model construction codes without regional limitations.

International Electrotechnical Commission (IEC): The IEC is the world organization that prepares and publishes international standards for all electrical, electronic and related technologies. The membership consists of more than 50 participating countries, including all of the world's major trading nations and a growing number of industrializing countries. The IEC's mission is to promote, through its members, international cooperation on all questions of electrotechnical standardization and related matters, such as the assessment of conformity to standards, in the fields of electricity, electronics and related technologies. The IEC charter embraces all electrotechnologies including electronics, magnetics and electromagnetics, electroacoustics, telecommunication, and energy production and distribution, as well as associated general disciplines such as terminology and symbols, measurement and performance, dependability, design and development, safety and the environment.

The National Fire Protection Association (NFPA): NFPA is non-profit organization that publishes the National Electrical Code®, the Life Safety Code®, the Fire Prevention Code™, the National Fuel Gas Code®, and the National Fire Alarm Code®. The mission of NFPA is to reduce the worldwide burden of fire and other hazards on the quality of life by providing and advocating scientifically based consensus codes and standards, research, training, and education. NFPA 853, "Standard for the Installation of Stationary Fuel Cell Power Plants" covers the design, construction, and installation of stationary fuel cells of at least 50 kW output.

Society of Automotive Engineers (SAE): SAE is a resource for technical information and expertise used in designing, building, maintaining, and operating self-propelled vehicles for use on land, sea, in air or in space. Comprised of nearly 80,000 engineers, business executives, educators, and students from more than 97 countries, the network of members share information and exchange ideas for advancing the engineering of mobility systems. Technical committees write more new aerospace and automotive engineering standards than any other standards-writing organization in the world. In late 1999, a Fuel Cell Standards Forum was created to establish standards and test procedures for fuel cell powered vehicles. It will address the safety, performance, reliability and recyclability of fuel cell systems in vehicles with an emphasis on efficiency and environmental impact.

Underwriters Laboratories Inc. (UL): UL is an independent, not-for-profit product safety testing and certification organization. UL has tested products for public safety for more than a century with more than 14 billion UL Marks applied to products worldwide. UL has developed a standard for inverters that can be applied to fuel cells.

10.5.3 Codes & Standards

A summary of existing and pending fuel cell related codes and standards is presented in Table 10-2. More detailed descriptions are provided subsequently based on their specific area of application.

Table 10-2 - Summary of Related Codes and Standards

CODE/STANDARD	ORGANIZATION	SUMMARY
1. PTC 50	ASME	***Performance Test Code*** - Will provide test procedures, methods and definitions for the performance characterization of fuel cell power systems.
2. IEEE SCC 21	IEEE	***Standards coordinating committee*** - fuel cells, photovoltaics, dispersed generation and energy storage
3. IEEE P1547	IEEE	***DG Interconnection Standard*** - Establishes criteria and requirements for interconnection of distributed resources with electric power systems
4. ANSI Z21.83-1998	ANSI	***Product Standard*** - Provides detailed test and examination criteria for fuel cell power plants that make use of natural and liquefied petroleum gases.
5. NFPA 853	NFPA	***Installation Standard*** - applies to installation of stationary fuel cell power plants.
6. NEC/NFPA 70 Article 690,691 & 705	NFPA	690 – Solar Photovoltaic Systems 691 – Fuel Cells 705 – Interconnected Power Production Sources
7. IEEE SCC 36	IEEE	***Standards Coordinating Committee*** - pertains to utility communications
8. UL 1741	UL	***Electric Inverters*** - Standard for testing, listing and safety certification for Inverters
9. SAE Standards Forum	SAE	***Vehicle Standards*** - In the early stages of developing standards for safety, performance, reliability and recyclability. Also establish testing procedures.
10. IEC TC 105	IEC	***Technical Committee 105*** – Seeking to expand the scope of ANSI Z21.83 for international basis and additional fuel cell technologies.
11. IMC 2000/ 924	ICC	***Installation Standard*** – Must be in compliance with ANSI Z21.83.

10.5.4 Codes and Standards for Fuel Cell Manufacturers

ANSI Z21.83: American National Standard - Fuel Cell Power Plants provides a means of testing and certifying the safety of stationary fuel cell power plants with a nominal electric capacity not exceeding 1.0 MW. This standard is intended for applications other than residential when installed outdoors and operated on a gaseous hydrocarbon as the reactant. The current version of the standard is based on two specific fuel cell technologies and is being revised to take into consideration the characteristics of additional fuel cell power plant technologies. Many state and local regulatory authorities have adopted this standard.

ASME PTC 50: ASME Performance Test Code 50 - Fuel Cell Power Systems provides test procedures, methods and definitions for the performance characterization of fuel cell power systems. The code specifies the methods and procedures for conducting and reporting fuel cell system ratings. Specific methods of testing, instrumentation, techniques, calculations and reporting are presented.

IEC TC 105: The International Electrotechnical Committee has established a Technical Committee charged with the preparation of an international standards regarding fuel cell technologies for all fuel cell applications including stationary power plants, transportation propulsion systems, transportation auxiliary power units and portable power generation systems. The standards will have five parts: Terminology and Definitions, Stationary Fuel Cell Systems, Fuel Cell Systems in Transportation, and Portable Fuel Cell Systems. The committee was established in 2000 and plans to have the standards approved and published in 2004.

IEEE SCC21/P1547: The Institute of Electrical and Electronic Engineers has established a Standards Coordinating Committee (SCC 21) chartered with the development of a standard for the interconnection of distributed resources. This standard focuses on electrical interface standards for the application of distributed generation technologies described as fuel cells, photovoltaics, dispersed generation and energy storage. The resulting standard will be IEEE P1547, which will establish criteria, and requirements for the interconnection of distributed resources with electric power systems.

IEEE SCC 36: This committee reviews, recommends and solicits the development of standards relevant to the gas, water, and electric utility industries on a worldwide basis with respect to utility communication architecture. This SCC coordinates standards-development activities with other relevant IEEE groups and sponsors standards-development activities that are appropriate to the needs of the utility industry.

IMC 2000/ 924.1**:** The International Code Council develops the International Mechanical Code. Section 924.1 of the IMC 2000 requires stationary fuel cell power plants not exceeding 1,000 kW to be tested and listed to ANSI Standard Z21.83.

ISO TC 197**:** The International Organization for Standardization has developed a committee to develop international safety standards for the production, storage, transport, measurement and use of hydrogen.

UL 1741: Underwriters Laboratory 1741 is a standard for the testing, listing and safety certification for electric inverters. This standard is for static inverters and charge controllers for use in photovoltaic power systems, but may be used for fuel cells.

10.5.5 Codes and Standards for the Installation of Fuel Cells

NFPA 853: National Fire Protection Association 853 - Standard for Fuel Cell Power Plants provides a standard for the design, construction and installation of stationary packaged, self contained and field constructed fuel cell power plants with a capacity greater than 50 kW.

NFPA 70: National Fire Protection Association 70 is also known as the National Electric Code (NEC). Revisions and addenda to the code are currently being developed that specifically address fuel cells. Article 690 - Solar Photovoltaic Systems has been targeted for revision to include fuel cells and alternate energy sources systems. This proposal is not expected to be approved since the technological and operational differences between fuel cells and photovoltaic systems are considerable. A new article, Article 692 deals with rules covering fuel cell systems for buildings or residential dwellings. This standard addresses the electrical interface between the fuel cell system and a building's electrical distribution panel. NFPA Article 705 - Interconnected Electrical Power Production Sources is also being revised to address fuel cell power sources.

10.5.6 Codes and Standards for Fuel Cell Vehicles

SAE has established a Fuel Cells Standard Forum that is chartered with the establishment of standards and test procedures for fuel cell powered vehicles. The committee was established in 1999. The standards will cover the safety, performance, reliability and recyclability of fuel cell systems in vehicles with emphasis on efficiency and environmental impact. The standards will also establish test procedures for uniformity in test results for the vehicle/systems/components performance, and define interface requirements of the systems to the vehicle. Working Groups have been formed in the areas of safety, performance, emissions, recyclability, interface and terminology. The working groups have created the following documents:

J2572 – Draft - Recommended Practice for Measuring the Exhaust Emissions, Energy Consumption and Range of Fuel Cell Powered Electric Vehicles Using Compressed Gaseous Hydrogen.
J2574 – Published March 2002 - SAE Information Report, Fuel Cell Electric Vehicle Terminology.
J2578 – Draft – Recommended Practices for General Fuel Cell Vehicle Safety.
J2579 – Draft – Recommended Practices for Hazardous Fluid Systems in Fuel Cell Vehicles.
J2594 – Draft – Fuel Cell Recyclability Guidelines.
J2600 – Draft – Compressed Hydrogen Vehicle Fueling Connection Devices.
J2601 – Draft – Compressed Hydrogen Vehicle Fueling Communication Devices.
J2615 – Draft – Performance Test Procedure of Fuel Cell Systems for Automotive Applications.
J2616 – Draft – Performance Test Procedure for the Fuel Processor Subsystem of Automotive Fuel Cell System.
J2617 – Draft – Performance Test Procedure of PEM Fuel Cell Stack Subsystem for Automotive Applications.

10.5.7 Application Permits

The installation of stationary fuel cells requires adherence to a variety of building codes. In April 2001, The National Evaluation Service published a "Protocol for Evaluation of Stationary Fuel Cell Power Plants." This is used by NES to facilitate the process of evaluating stationary fuel cell power plant technology for compliance to all codes. A few of the major codes are summarized below.

International Mechanical Code 2000: Published by the International Code Council. At the present time, it is the only code to provide specific guidance on stationary fuel cell power plants.

Uniform Building Code: The Uniform Building Code (UBC) is the most widely adopted model building code in the world and is a proven document meeting the needs of government units charged with enforcement of building regulation. Published triennially, the UBC provides complete regulations covering all major aspects of building design and construction relating to fire and life safety and structural safety. The requirements reflect the latest technological advances in the building and fire and life-safety industry.

Uniform Mechanical Code: Provides a complete set of requirements for the design, construction, installation and maintenance of heating, ventilating, cooling and refrigeration systems, incinerators, and other heat-producing appliances.

Uniform Plumbing Code: Published by the International Association of Plumbing and Mechanical Officials (IAPMO), the Uniform Plumbing Code covers all aspects of plumbing, including requirements for plumbing materials and IAPMO installation standards.

National Electric Code: The National Electrical Code (NFPA 70) provides "practical safeguarding of persons and property from hazards arising from the use of electricity." More specifically, the National Electric Code covers the installation of electric conductors and equipment in public and private buildings or other structures (including mobile homes, recreational vehicles, and floating buildings), industrial substations, and other premises (such as yards, carnivals, and parking lots). The National Electric Code also covers installations of optical fiber cable. Wiring, general electrical equipment, the use of electricity in specific occupancies (from aircraft hangars to health care facilities), and equipment (ranging from elevators to hot tubs) are covered, as well as special conditions (emergency and stand-by power, or conditions requiring more than 600 volts, for example) and communication systems.

National Fire Code: The National Fire Code consists of approximately 300 codes and standards as published by the National Fire Protection Association (NFPA). These codes address the practices to reduce the burden of fire on the quality of life by advocating scientifically based consensus codes and standards, research and education for fire and related safety issues. The most widely applied codes are:

(1.) NFPA 70 – National Electric Code
(2.) NFPA 101 – Life Safety Code
(3.) NFPA 30 – Flammable and Combustible Liquids Code

(4.) NFPA 13 – Standard for the Installation and Maintenance of Automatic Fire Sprinkler Systems

10.5.8 References

1. M. Glass, *Fuel Cell Codes and Standards Summit III Summary*, April 5-7, 1999, Pacific Northwest Labs.
2. ASME, *Object & Scope for the Proposed Code on Fuel Cell Power Systems*, August 2000, http://www.asme.org.
3. IEEE, *Distributed Resources and Electrical Power Systems Interconnection Working Group - Meeting Minutes*, June 7-8, 2000, http://grouper.ieee.org.
4. SAE, *SAE Initiates Activities in Area of Fuel Cells*, August 1999, http://www.sae.org.
5. UL, *Standard for Safety for Static Inverters and Charge Controllers for Use in Photovoltaic Power Systems*, 2000, http//:ulstandardsinfonet.ul.com.
6. National Evaluation Service*, National Evaluation Protocol for Stationary Fuel Cell Power Plant*, June 5, 2000, http://www.nateval.org.
7. International Electrotechnical Commission, IEC TC 105 Strategic Policy Statement, March 2000, CA/1719A/R, http://www.iec.ch.
8. R. Bielen, *Telephone Contact*, August 9, 2000, NFPA.
9. S. Kazubski, *Telephone Contact*, August 14, 2000, CSA International.
10. D. Conover, *Telephone Contact*, August 9, 2000, National Evaluation Service.

10.6 Fuel Cell Field Site Data

This section of the handbook contains field site information. Most of the worldwide summaries were extracted from an IEA paper[67] and updated with information taken from "Fuel Cell Technology News"[68]. Information on the U.S. Department of Defense (DoD) Fuel Cell Demonstration was taken from the following web site: www.dodfuelcell.com. Finally, updating the information for Fuel Cell Energy, IFC, and Siemens Westinghouse was taken from "Fuel Cell Technology News"[ii]. The IFC PAFC summary includes a number of projects reported by DoD. In the DoD demonstration program, a total of 30 PAFC units were installed at DoD sites across the United States. These were model B and C PC-25 units.

10.6.1 Worldwide Sites

Worldwide information reported in this handbook is for stationary application of fuel cells in different countries. Data on PEFC, PAFC, AFC, MCFC, and SOFC has been collected. The main worldwide projects are summarized below:

PEFC

Canada: Ballard 250 kWe stationary prototypes are developed by Ballard Generation Systems. The first prototype operating is in Vancouver, Canada. Ballard delivered a second 250-kilowatt

[67] K. Kono, "Implementing Agreement "Advanced Fuel Cells," Annex IX Fuel Cells for Stationary Applications, Subtask 2," draft IEA paper, April 1999.

[68] Fuel Cell Technology News, January 2002, published by Business Communications Company, Inc.

PEFC power system to Cinergy Technology. This is the first field trial unit built by Ballard. The unit runs on natural gas, and was commissioned in 1999 at the Naval Surface Warfare Center in Crane, Indiana. A third unit in Berlin, Germany at Bewag Treptow Heating Plant started operating the second half of 1999. In 2001, Ballard completed 10-kW and 60-kW engineering prototype stationary fuel cell generators.

Japan: 2 and 30 kWe PEFC pilot plants have been promoted in Japan as a part of New Sunshine Program. The 2 kWe plant is for residential use and will be developed by Sanyo Electric. The plant is scheduled for testing in 2000.

United States: Plug Power has installed over 300 residential systems for unattended operation. Plug Power delivered more than 106 5-kW grid-parallel systems, through October 31, 2001, against its milestone 125 to 150 units for the year. Deliveries included 44 units to the New York State Research & Development Authority and 57 systems to the Long Island Power Authority.

PAFC

Europe: The Energetic Utility of Milan, the National Agency for Energy, New Technology and Environment (ENEA), and Ansaido Ricerche designed, built, and tested 1.3 MWe PAFC system in Milan. The powerplant had an actual capacity of 930 kW and an energy efficiency of 38% (LHV). It has operated for over 5,000 hours.

Japan: Fuji Electric has developed a 100 kWe on-site system. To date, they have tested a 50 kW power plant using innovative cell design that improves electrolyte management. They tested this stack (154 cells) for about 2,000. They have tested 65, 50 kWe units for a total cumulative operating tome of over 1 million hours. They have tested 3, 500 kWe units for a total of 43,437 hours. Their latest design, FP100E, has been shown to have a net AC efficiency of 40.2% (LHV).

Mitsubishi Electric has developed a 200 kWe class on-site powerplant. To date, 11 units are being operated in the field with applications ranging from an electric utility to a brewery factory. Four of the units have operated more than 2,000 hours.

AFC

United Kingdom: ZeTek Power, an UK based company with plants in the US and Europe, is developing Alkaline fuel cells. They are putting AFCs in fleet vehicles and boats in Europe. AFCs are getting greater than 50% efficiency over most of the power curve (5-95%). Capital cost for the AFC stack is $300/kWe, and approximately $700 for the system.

MCFC

Japan: As part of the New Sunshine Program, 200 and 1,000 kWe test facilities are planned in Japan. This plan is promoted collectively by 10 electric power companies, 3 gas companies, Central Research Institute of Electric Power Industry, 7 manufacturers, and 2 research associations. The 1,000 kWe is located in Kawagoe, and the 200 kWe is located in Amagasaki. Both units are scheduled to begin operations in the first half of 1999.

Europe: Italy and Spain have been working on research and development of MCFC systems as a collaborative project called MOLCARE program. The project has a budget of 10 billion pesetas (35% by Spain and 65% by Italy). They have partnered with industry to develop and conduct a 1,000-hour test on a 100 kWe unit.

The European Direct Fuel Cell Consortium carries out the largest European program for the commercialization of MCFC. They are developing an innovative direct fuel cell process which is internally reformed and operates on humidified hydrocarbon fuels. They have successfully tested a 292 cell, 155 kW stack (60% of maximum power).

United States: FuelCell Energy is developing an externally manifolded internally reformed MCFC. FuelCell Energy has reached the 50 MW manufacturing capacity and plans to have 400 MW capacity by 2004. They have also constructed a 400 kWe test facility. They have successfully completed the manufacture and test of 16 stack (4 modules), 2 MWe test in Santa Clara, California, for 4,000 hours. Details on Fuel Cell Energy field site are found in Table 10-3.

SOFC

Japan: The Kansai Electric Company has tested a four-cell article and accumulated 10,529 hours of operation at high current densities and completed 101 thermal cycles. Tokyo Gas started research and development of a planner SOFC in 1993. They conducted a 1.7 kW module test with stable performance.

Australia: Ceramic Fuel Cells Limited was demonstrated a 5 kWe laboratory prototype fuel cell system in 1997. Their system has thin sheet steel components as interconnects in a planer fuel cell design. They are currently scaling up to a 25 kWe pre-commercial stack module.

Canada: Ontario Hydro has tested a single Siemens-Westinghouse cell for 1725 hours. Over 1425 of the hours were at elevated pressure of 5 atm.

Europe: The ELSAM/EDB project for a 100 kWe Siemens-Westinghouse SOFC field unit has operated from January 1998. The unit will operate until January 2000 with a total of 17,500 test hours according to the plan.

Spain: A consortium called SEGE is developing an intermediate temperature planner fuel cell.

United States: Siemens-Westinghouse projects on SOFC include a 250 kWe tubular prototype at the Irvine University campus (California), that will be operated by Southern California Edison Company. It is pressurized to 3.5 bar and thus is expected to give 200 kWe; a coupled microturbine gives an additional 50 kWe. The have operated a tubular SOFC at pressures up to 15 atm. Siemens-Westinghouse plans to deploy its fuel cell product line in the commercial market by fall 2003.

10.6.2 DoD Field Sites

DoD's Climate Change Fuel Cell program included purchasing and installing 30 ONSI PC25 200 kWe PAFC at DoD installations in addition to providing rebates of $1,000/kW (up to 1/3 of the installed cost). There are many factors that determine the availability and efficiency of

individual units; maintenance programs and application are two of many possible factors. The summary table, Table 10-2, does provide information on operating hours, efficiency, and availability. Logging onto can access additional information on individual units: www.dodfuelcell.com.

10.6.3 IFC Field Units

IFC provided DOE with information on their 59 fuel cell unit operating in North America. This information is provided in Table 10-4. As mention before, several of these units are operating on DoD field site and are report on Table 10-3.

10.6.4 FuelCell Energy

FuelCell Energy provided DOE with information on their fuel cell field units. This information is provided in Table 10-5.

10.6.5 Siemens Westinghouse

Siemens Westinghouse provided DOE with information on their fuel cell field units. This information is provided in Table 10-6.

Table 10-3 DoD Field Site

Through January 31, 2002

SITE NAME	SERVICE	START DATE	OPER. HOURS	MWHRS OUTPUT	AVG kWe	ELEC. EFF.	AVAIL.
MODEL B UNITS							
Naval Station Newport	Navy	1/23/95	42,375	6,387.537	150.7	30.2%	76.1%
U.S. Army Soldier Systems Center	Army	1/27/95	38,608	6,379.235	165.2	31.2%	61.2%
US Military Academy	Army	11/17/95	28,393	4,872.371	171.6	31.5%	63.0%
934th Airlift Wing	Air Force	2/1/95	26,777	4,653.232	173.8	29.7%	48.2%
Picatinny Arsenal	Army	10/11/95	32,053	5,316.291	165.9	30.9%	62.4%
Naval Hospital MCB Camp Pendleton	Marines	10/6/95	26,859	4,507.218	167.8	33.9%	55.1%
Naval Hospital MCAGCC Twentynine Palms	Marines	6/20/95	21,652	3,522.419	162.7	32.3%	44.6%
Nellis AFB	Air Force	9/23/95	19,996	3,383.481	169.2	32.5%	38.7%
Watervliet Arsenal	Army	10/29/97	28,875	4,117.735	142.6	31.4%	77.3%
Fort Eustis	Army	9/12/95	27,705	4,256.532	157.2	31.9%	50.7%
Kirtland AFB	Air Force	7/20/95	16,713	2,502.970	149.8	31.0%	32.5%
Naval Oceanographic Office	Navy	10/7/97	19,641	3,574.854	182.0	34.6%	51.4%
Pine Bluff Arsenal	Army	10/21/97	9,343	1,747.040	187.0	34.9%	39.6%
CBC Port Hueneme	Navy	9/18/97	18,001	3,332.808	185.1	34.3%	46.3%
B's TOTAL/AVG:			356,367	58,553.723	164.3	31.9%	53.8%
MODEL C UNITS*							
911th Airlift Wing	Air Force	12/18/96	35,234	6,037.038	171.3	31.6%	79.8%
Naval Hospital NAS Jacksonville	Navy	3/18/97	33,284	6,193.403	186.1	31.6%	78.4%
NAS Fallon	Navy	3/30/97	31,054	4,880.720	157.2	30.8%	80.1%
Subase New London	Navy	9/30/97	32,848	5,884.840	179.2	31.8%	84.8%
Fort Richardson	Army	12/17/96	30,593	5,617.251	183.6	31.5%	68.1%
Little Rock AFB	Air Force	8/17/97	23,104	4,336.428	187.7	31.7%	68.2%
Westover AFB	Air Force	9/19/97	32,844	6,316.483	192.3	30.7%	86.3%
Barksdale AFB	Air Force	7/24/97	28,554	5,289.629	185.2	31.1%	72.0%
Fort Huachuca	Army	7/28/97	31,776	5,744.980	180.8	32.4%	80.3%
Laughlin AFB	Air Force	9/16/97	29,558	5,584.936	188.9	32.4%	77.0%
US Naval Academy	Navy	9/22/97	37,928	4,736.374	124.9	27.9%	80.9%
Edwards AFB	Air Force	7/5/97	23,866	4,603.664	192.9	32.6%	59.9%
Fort Bliss	Army	10/10/97	23,973	3,936.077	164.2	32.0%	63.6%
Davis-Monthan AFB	Air Force	10/14/97	26,462	4,513.985	170.6	32.1%	71.5%
NDCEE	Other	8/14/97	17,167	2,083.041	121.3	30.5%	58.1%
C's TOTAL/AVG:			794,621	134,312.570	169.0	31.6%	63.5%
B+C TOTAL/AVG:			794,621	134,312.570	169.0	31.6%	63.5%

Disclaimer

Electrical efficiency calculations include fuel cell idle time (such as when the fuel cell is awaiting the return to operation of the utility grid, etc.). If values were adjusted for idle time, fuel cell electrical efficiencies would be higher. ONSI fuel cells passed DoD Fuel Cell Program electrical efficiency criteria during unit acceptance tests (range = 33.5% to 37.2%, Higher Heating Value).

Availability values are not adjusted for times when the fuel cell was down for extended periods unrelated to typical fuel cell operation (delays in maintenance personnel response, site operating conditions, etc.). Adjusting for these times would result in higher availability values.

Table 10-4 IFC Field Units

PC25 C Fuel
Cell Power Plant
(Run hours, etc.
as of 8/4/00)

North America

	Status	Country/State	Site	Start Date	Load hrs	MW-hrs	
1	Active	SOUTH WINDSOR, CT	PROTOTYPE FOR R&D	N/A	N/A	N/A	0
2	Active	DEL RIO, TX	HOSPITAL	9/6/97	20,143	3,743.4	37181
3	Active	LITTLE ROCK, AR	HOSPITAL	10/6/97	21,408	3,872.6	36024
4	Active	SHREVEPORT, LA	HOSPITAL	7/18/97	19,577	3,786.3	35954
5	Active	GROTON, CT	CENTRAL BOILER PLANT	9/27/97	23,175	4,044.2	24942
6	Active	ANNAPOLIS, MD	DORMITORY	9/20/97	20,274	2,945.9	11593
7	Active	STATEN ISLAND, NY	CHEMICAL PLANT	8/22/96	27,412	4,940.3	28415
8	Active	ANCHORAGE, AK	YMCA	11/18/96	21,589	3,572.0	25504
9	Active	JACKSONVILLE, FL	HOSPITAL	3/17/97	24,396	4,580.2	24704
10	Active	EL PASO, TX	LAUNDRY	10/7/97	16,775	2,870.1	26707
11	Active	STATEN ISLAND, NY	CHEMICAL PLANT	8/27/96	29,333	5,342.8	25001
12	Active	PITTSBURGH, PA	CENTRAL BOILER PLANT	12/16/96	28,105	4,988.9	25171
13	Active	SYRACUSE, NY	SCHOOL	1/22/97	27,222	2,802.1	34626
14	Active	CAPE COD, MA	COLLEGE	3/31/99	10,995	2,016.5	32982
15	Active	OMAHA, NE	BANK	3/25/99	11,084	1,569.1	32825
16	Active	YONKERS, NY	ANAEROBIC DIGESTER GAS	4/8/97	18,321	2,349.2	29169
17	Active	OMAHA, NE	BANK	3/24/99	11,030	1,565.1	32496
18	Active	ANCHORAGE, AK	ARMORY BUILDING	12/24/96	9,046	1,739.4	29658
19	Active	ANCHORAGE, AK	ARMORY BUILDING	12/11/96	22,321	4,061.2	18430
20	Active	DEER ISLAND, MA	ANAEROBIC DIGESTER GAS	9/4/97	2,760	395.7	34506
21	Being Installed	ANN ARBOR, MI	RESEARCH LAB		0	0.0	31842
22	Active	FALLON, NV	GALLEY BUILDING	2/28/97	25,781	4,211.7	30955
23	Active	OMAHA, NE	BANK	3/24/99	10,648	1,521.4	32128

24	Active	SPOKANE, WA	HOTEL	6/11/97	22,680	4,370.4	11799
25	Active	CHICOPEE, MA	CENTRAL BOILER PLANT	9/15/97	22,230	4,393.4	30078
26	Active	TUCSON, AZ	CENTRAL BOILER PLANT	10/18/97	20,577	3,644.0	11941
27	Active	ROSAMOND, CA	CENTRAL BOILER PLANT	6/19/97	19,325	3,367.7	29133
28	Active	SIERRA VISTA, AZ	BARRACKS	7/28/97	20,812	3,893.1	11961
29	Will be restarted Fall '00	JOHNSTOWN, PA	OFFICE/RESEARCH LAB	7/28/97	9,637	1,180.7	26736
30	Active	HARTFORD, CT	OFFICE BUILDING	6/18/97	26,023	4,800.7	29284
31	Active	WINDSOR LOCKS, CT	DATA CENTER	12/19/97	19,634	2,135.2	19838
32	Active	MERIDAN, CT	OFFICE BUILDING	9/21/97	20,987	3,991.5	31961
33	Being Installed	ALCORN STATE, MS	UNIVERSITY		0	0.0	29302
34	Active	BRAINTREE, MA	LANDFILL	9/10/99	5,211	906.2	25556
35	Being Installed	BRONX, NY	HOSPITAL		0	0.0	26786
36	Active	SOUTH WINDSOR, CT	INDUSTRIAL SPACE HEATING	3/9/98	19,689	3,771.9	26612
37	Active	PORTLAND, OR	WASTE WATER TREATMENT PLANT	5/21/99	7,259	1,051.5	28749
38	Active	OMAHA, NE	BANK	3/25/99	11,068	1,570.6	29117
39	Owner sold property; being relocated	HARVEY, LA	COMMERCIAL FACILITY	3/13/99	6,823	1,185.1	0
40	Active	HOUSTON, TX	MANUFACTURING	5/12/98	17,871	1,847.8	30063
41	Not Yet Installed	NY, USA	TBD		0	0.0	0
42	Active	GULFPORT, MI	DINING FACILITY	5/13/99	7,775	1,504.3	11956
43	Not Yet Installed	NJ, USA	COLLEGE		0	0.0	23561
44	Active	NEW YORK, NY	SKYSCRAPER OFFICE BUILDING	12/15/99	5,220	920.5	18165
45	Active	NEW YORK, NY	SKYSCRAPER OFFICE BUILDING	12/16/99	5,553	1,039.2	25284
46	Active	RAMAPO, NJ	COLLEGE	3/29/00	2,448	429.1	24466

47	Active	NEW YORK, NY	POLICE STATION	4/17/99	11,108	231.1	24929
48	Active	MESA, AZ	MUNICIPAL BUILDING	4/29/00	2,192	410.2	26467
49	Active	ANCHORAGE, AK	POST OFFICE DISTRIBUTION CENTER	6/28/00	3,396	475.2	13848
50	Active	ANCHORAGE, AK	POST OFFICE DISTRIBUTION CENTER	6/28/00	3,329	518.0	27416
51	Active	ANCHORAGE, AK	POST OFFICE DISTRIBUTION CENTER	6/28/00	3,939	612.0	0
52	Active	ANCHORAGE, AK	POST OFFICE DISTRIBUTION CENTER	6/28/00	4,123	614.1	0
53	Active	ANCHORAGE, AK	POST OFFICE DISTRIBUTION CENTER	6/28/00	3,563	531.4	0
54	Active	CALABASAS, CA	ANAEROBIC DIGESTER GAS	12/15/99	6,613	953.9	23010
55	Active	CALABASAS, CA	ANAEROBIC DIGESTER GAS	12/15/99	8,322	1,216.0	9431
56	Active	JOHNSTOWN, PA	RESEARCH LAB	1/6/00	3,655	497.9	18813
57	Active	SOUTH KINGSTOWN, RI	HOSPITAL	10/18/99	6,532	1,032.4	26779
58	Active	SYRACUSE, NY	HIGH SCHOOL	2/4/00	4,427	803.0	25143
59	Active	BELLAIR, TX	INDUSTRIAL BUILDING	5/24/00	1,867	364.7	22582

Table 10-5 FuelCell Energy Field Sites (mid-year 2,000)

Fuel Cell Type	Location	Status	Start Date	Operating Hours	MWhrs Output	Size, kw Design	Actual*	Eff. %	Avail. %
Direct Fuel Cell	Santa Clara, CA	Completed	3/1996	5,800	2,570	1,800	1,930	44	99**
Direct Fuel Cell	Danbury, CT	Completed	2/1999	11,800	1,906	250	263	45	93
Direct Fuel Cell	Bielefeld, Germany	Continuing	11/1999	4,300+	500+	250	225	45	90

* Maximum attained
** BOP availability

Table 10-6 Siemens Westinghouse SOFC Field Units (mid-year 2,002)

Year	Customer	Size, kWe	Fuel	Cell Type	Cell Length (cm)	Operating Hours	Cell Number	MWH (DC)
1986	TVA	0.4	H2+CO	TK-PST	30.0	1,760	24	0.5
1987	Osaka Gas	3.0	H2+CO	TK-PST	36.0	3,012	144	6
1987	Osaka Gas	3.0	H2+CO	TK-PST	36.0	3,683	144	7
1987	Tokyo Gas	3.0	H2+CO	TK-PST	36.0	4,882	144	10
1992	JGU-1	20.0	PNG	TK-PST	50.0	817	576	11
1992	Utilities–A	20.0	PNG	TK-PST	50.0	2,601	576	36
1992	Utilities-B1	20.0	PNG	TK-PST	50.0	1,579	576	26
1993	Utilities-B2	20.0	PNG	TK-PST	50.0	7,064	576	108
1994	SCE-1	20.0	PNG	TK-PST	50.0	6,015	576	99
1995	SCE-2	27.0	PNG/DF-JP-8	AES	50.0	5,582	576	118
1995	JGU-2	25.0	PNG	AES	50.0	13,194	576	282
1998	SCE-2/NFCRC	27.0	PNG	AES	50.0	3,394+	576	73+
1997	EDB/ELSAM-1	125.0	PNG	AES	150.0	4,035	1152	471
1999	EDB/ELSAM-2	125.0	PNG	AES	150.0	12,577	1152	1,153+
2000	SCE	180.0	PNG	AES	150.0	770+	1152	25+
2001	RWE	125.0	PNG		150.0	3,700+	1152	

PND = Pipeline Natural Gas
TK-PST = Thick Wall Porous Support Tube
TN-PST = Thin Wall Porous Support Tube
AES = Air Electrode Support
+ = Testing Continues

10.7 Hydrogen

10.7.1 Introduction

The use of hydrogen in the United States energy infrastructure has been considered for decades. For economic reasons, the hydrogen economy has not developed; for environmental reasons, the potential of hydrogen becoming a major commodity exists. In 1990, the United States Congress passed the Matsunaga Hydrogen Research and Development Act. The Act required the Department of Energy to develop critical hardware for hydrogen technology. The Act also established the Hydrogen Technical Advisory Panel, which is composed of experts from industry and academia, to advise the Secretary of Energy on the status and recommended direction of hydrogen energy development. In 1996, Congress passed the Hydrogen Future Act; the Act authorized the spending of $164.5 million between 1996 and 2001 on the research, development, and demonstration of hydrogen production, storage, transport, and use.

The demand for hydrogen has grown 23 percent per year between 1994 and 1999 and is projected to continue to grow by 14 percent per year through 2003. (3) Oil refining accounts for 67 percent of the current hydrogen usage in the United States. The manufacturing of petrochemicals accounts for 26 percent and the final 7 percent is used in the reduction of metals, electronics, glass, rocket fuel, food processing, laboratory use and power generation. Many believe that the demand for hydrogen will continue to grow for the following reasons:

- As domestic reserves of oil decline and heavier imported crude oil is refined, increased amounts of hydrogen will be required.
- As higher sulfur crude oils are refined, additional hydrogen for desulfurization to meet existing and more stringent future regulations will be required.
- The number of hydrogen-powered vehicles will increase.
- Electricity produced by hydrogen-fueled technology will increase.
- The increased use of hydrogen will reduce the dependency on imported oil.

The interest in hydrogen as pollution-free energy has sparked legislation. The following is some of the Federal and state legislation:

- The "Hydrogen Future Act of 1996" focuses Federal hydrogen research on the basic scientific fundamentals needed "to provide the foundation for private sector investment and development of new and better energy sources."
- California's "zero-emission" standard for passenger cars requires that 2 percent of new cars in the state be non-polluting.
- As part of California's Clean Transportation Fuels Initiative, the California Energy Commission (CEC) will assist in establishing publicly accessible clean-fuel refueling facilities to serve clean-fuel fleets and vehicles in California. Eligible projects include all non-petroleum fuels such as natural gas, alcohol and hydrogen (for fuel cell applications).
- In April 2000, the Arizona Legislature passed SB 1504 - an important piece of legislation for the alternative fuels movement and most particularly the hydrogen program. The Hydrogen Grant Program allows up to $500,000 for hydrogen programs that benefit the public.
- The State of Georgia offers an income tax credit of $5,000 for the purchase or lease of a zero emission vehicle (ZEV). ZEVs include battery-only electric vehicles (EVs) and hydrogen fuel cells.

- New York's Alternative-Fuel (Clean-Fuel) Vehicle Tax Incentive Program offers tax credits and a tax exemption for people who purchase alternative fuel vehicles (AFVs). Purchasers of compressed natural gas, liquefied petroleum gas, methanol, ethanol, and hydrogen-powered vehicles, as well as hybrid electric vehicles (HEVs), are eligible for a tax credit worth 60% of the incremental cost.
- In 1992, the state of Pennsylvania established a program to reduce Pennsylvania's dependence on imported oil and improve air quality through the use of alternative fuels. Eligible alternative motor fuels and fuel systems are compressed natural gas, liquefied natural gas, liquid propane gas, ethanol, methanol, hydrogen, hythane, electricity, coal-derived liquid fuels, fuels derived from biological materials, and fuels determined by the Secretary of the U.S. Department of Energy as meeting the requirements of Section 301 of the Energy Policy Act of 1992. After July 1, 2001, qualified projects will receive funding for 20% of eligible project costs.
- Effective January 1, 1996, Virginia's sales and use taxes were reduced by 1.5% for any motor vehicle that has been manufactured, converted, or retrofitted to operate on compressed natural gas, liquefied natural gas, liquefied petroleum gas, hydrogen, or electricity.
- The University of Wisconsin-Milwaukee Center for Alternative Fuels offers a Congestion Mitigation Air Quality Alternative Fuels Grant Program for the incremental cost of purchasing AFVs. Wisconsin municipalities, in an 11 county area (including Milwaukee, Waukesha, Racine, Kenosha, Walworth, Washington, Ozaukee, Sheboygan, Manitowoc, Kewaunee, and Door counties), are eligible to participate in the grant program. Eligible vehicles include dedicated, bi-fuel or flexible fuel vehicles. Eligible fuels include ethanol, methanol, hydrogen, compressed natural gas, liquefied natural gas, propane, biodiesel, and electricity. Grant awards are allocated through a competitive grant application process. The maximum grant award per passenger vehicle is $6,500 and $12,000 per truck, van or bus with a total of $50,000 per municipality.

The opportunities for R&D to advance hydrogen production, utilization, and storage hold great potential. "Much of the recent ferment over hydrogen and fuel cells has taken place in the auto industry. DaimlerChrysler has committed $1 billion over 10 years to fuel cell development, and is working with Ford and Ballard Power Systems to put transit fuel cell buses on the road in Europe in 2002. General Motors aims to be the first car company to sell one million fuel cell vehicles, beginning mass production in 2010, and in June announced major investments in two companies specializing in hydrogen storage and delivery. Toyota recently sent shock waves through the industry by announcing it would start selling its fuel cell car in Japan in 2003. The energy industry is also getting serious about hydrogen. Both Shell and BP have established core hydrogen divisions within their companies. ExxonMobil is teaming up with GM and Toyota to develop fuel cells. Texaco has become a major investor in hydrogen storage technology." (4) For additional information on industry announcements, see The Hydrogen and Fuel Cell Letter.

10.7.2 Hydrogen Production

A number of hydrogen manufacturing plants are sited (see Table 10-7) across the United States. Any carbonaceous material can be used to make hydrogen from steam reforming, but they are more likely to contain contaminants than natural gas, and would require cleanup before using. The main reason natural gas is used is that the supply of natural gas is abundant and the price continues to remain low. If the price of natural gas or restrictions on the use make using natural

gas impossible, water is the other abundant source. Several forms of energy can be used to make hydrogen:

- **Thermal:** Thermal decomposition of water into hydrogen and oxygen occurs at temperatures around 2,500 ^{o}C. The process isn't attractive because few materials can withstand that temperature. In the plasma arc process, water is heated to 5,000 ^{o}C by an electric field resulting in the cracking products H, H_2, O, O_2, OH, HO_2, and H_2O. A fraction of 50 percent by volume of H and H_2 is possible. The plasma gases are quenched with a cryogenic liquid to avoid the gases from recombining. This process consumes a lot of energy and is very expensive to operate.
- **Thermochemical:** Today, hydrogen is produced mainly from natural gas by steam methane reforming. Steam methane reforming (SMR) is not only the most common, but is also the least expensive method of producing hydrogen; almost 48 percent of the world's hydrogen is produced from SMR. (5) Refineries produced and used 2,500 billion scf in 1998. The chemical reaction of this process is:

$$CH_4 + 2\ H_2O = 4\ H_2 + CO_2$$

- **Electrochemical:** Water electrolysis passes a direct current between two electrodes in water. The water is made more conductive by adding an electrolyte such as potassium hydroxide. Hydrogen gathers around the negative electrode (cathode) and oxygen gathers around the positive electrode (anode). The gases are collected separately.
- **Photoelectrochemical:** Sunlight (photons) provides the source of energy for this process. Photons interact with dissolved chemicals to produce activated species, which in turn deactivate by releasing hydrogen from water. This is solar-powered electrolysis.
- **Photobiologial:** Sunlight provides the source of energy for this process. Living organisms, such as green algae, make enzymes. The pigment of algae absorbs the solar energy and the enzyme in the cell acts as a catalyst to split the water molecules.

For additional information on natural gas reforming, see U.S. Department of Energy, Office of Energy Efficiency and Renewable Energy Network

Table 10-7 Hydrogen Producers[1]

Producer	Capacity*
Merchant Cryogenic Liquid	
Air Products and Chemicals, New Orleans, LA	26,800
Air Products and Chemicals, Pace, FL	11,500
Air Products and Chemicals, Sacramento, CA	2,300
Air Products and Chemicals, Sarnia, Ont.	11,500
BOC, Magog, Quebec	5,900
HydrogenAL, Becancour, Quebec	4,600
Praxair, East Chicago, IN	11,500
Praxair, McIntosh, AL	11,500
Praxair, Niagara Falls, NY	15,000
Praxair, Ontario, CA	8,500
Total Merchant Cryogenic Liquid	109,100
Merchant Compressed Gas	
Air Liquide (11 locations)	67,960
Air Products and Chemicals (20 locations)	740,440
BOC (6 locations)	14,650
Brown Industries (3 locations)	460

General Hydrogen, Natrium, WV	200
Holox, Augusta, GA	400
Industrial Gas Products, Sauget, IL	1,500
Javelina, Corpus Christi, TX	35,000
Jupiter Chemicals, Westlake, LA	35,000
Lagus, Decatur, AL	9,000
Equistar, Channelview, TX	80,000
MG Industries (3 locations)	1,300
Praxair (22 locations)	425,960
Prime Gas, Delaware City, DE	200
Rohm and Haas, Deer Park, TX	n.a.
T&P Syngas Supply, Texas City, TX	32,400
Total Merchant Compressed Gas	1,444,470
Total Merchant Product	1,553,570

* Thousands standard cubic feet (SCF) per day merchant hydrogen from steam reforming of light hydrocarbons or recovered as by-product from chloralkali plants or chemical synthesis operations.

Hydrogen Utilization

Hydrogen can be used to power vehicles, run turbines or fuel cells to produce electricity, and generate heat and electricity for buildings. Hydrogen is used as a chemical in the petrochemical, electronics, and food industries. The zero-emission potential of using hydrogen as a fuel has sparked interest in the utility and transportation sectors.

10.7.3 DOE's Hydrogen Research

Concerns about air pollution, global warming and long-term fuel availability have focused international attention on the development of alternative fuels. Hydrogen will be an important part of future energy systems addressing these concerns. Whether processed in a fuel cell or burned in a combustion process, hydrogen represents an exceptionally clean energy source. Development is underway on processes that economically produce hydrogen from methane, water, and other abundant sources.

DOE's hydrogen research draws upon core competence in several engineering and technology areas, including systems engineering, safety and risk assessment, chemical and mechanical engineering, manufacturing and materials, sensors and controls, plasma processing, fuel cell technology, biotechnology engineering, and alternative fuel vehicle fueling infrastructure development. Hydrogen programs are managed at the Idaho National Engineering and Environmental Laboratory (INEEL) and the National Renewable Energy Laboratory (NREL). Promising technologies related to production, infrastructure, and utilization of hydrogen are:

- Thermal-plasma/quench process for converting methane to hydrogen, with solid carbon produced as a byproduct. (INEEL)
- Biotechnology processes for production of hydrogen from renewable resources. (INEEL)
- Photoconversion production uses either biological organisms (bacteria or algae) or semiconductors to absorb sunlight, split water, and produce hydrogen. (NREL)
- Thermochemical production uses heat to produce hydrogen from biomass and solid waste. (NREL)
- Low-pressure storage of hydrogen in the use of metal ion intercalated graphite fibers as a medium. (INEEL)

- Fleet and fueling systems engineering analysis of hydrogen-powered buses and supporting fueling stations. (INEEL)
- Safety and risk assessment of hydrogen as transportation fuel. (INEEL)
- Demonstration of hydrogen-powered vehicles and related transportation system infrastructure, including hydrogen production, storage, and fueling.
- Demonstration of hydrogen-fueled, small-scale power generation for local (distributed) electricity production.
- Since hydrogen can neither be seen nor smelled, as an added safety precaution for hydrogen-fueled vehicles, hydrogen sensors are being developed. To detect hydrogen, a very thin sensor that reacts to hydrogen by changing colors is applied to the end of a fiber optic cable. The sensors can be placed throughout the vehicle to relay information on leak detection to a central control panel. (6) (NREL)

As research and development progresses, collaboration with private sector partners to conduct demonstration testing of hydrogen-fueled vehicles, and demonstration testing of prototype hydrogen-fueled distributed electric power stations will be done. (7)

10.7.4 Hydrogen Storage

There are many methods for storing hydrogen; the four most common methods are:

- **Compressed gas in pressure vessels:** New materials have allowed pressure vessels and storage tanks to be constructed that can store hydrogen at extremely high pressures.
- **Hydrogen absorbing materials:**

1. A number of metals (pure and alloyed) can combine with hydrogen to make a metal hydride. The hydride releases hydrogen when heated. Hydrogen stored in hydrides under pressure has a very high energy density.
2. Hydrogen molecules that have been absorbed on charcoal can approach the storage density of liquid hydrogen.
3. Small glass spheres (microspheres), carbon nanotubes, and fullerenes can hold hydrogen if it is induced at high pressures and temperatures. The hydrogen is held captive in the solid matrix when the temperature lowers. Hydrogen can be released by heating the solid.

- **Liquid storage:** Hydrogen can be converted into a liquid by reducing the temperature to –253 ^{o}C. This can save cost in transportation, but requires additional energy and cost to keep the hydrogen at the lower temperature. Refrigerating hydrogen to liquid form uses the equivalent of 25 to 30 percent of its energy content. A concern of storing liquid hydrogen is minimizing loss of liquid hydrogen by boil-off.
- **Underground storage in depleted oil and natural gas reservoirs, aquifers, and salt cavities:** For underground storage of hydrogen, a large cavern of porous rock with an impermeable caprock above it is needed to contain the gas. As much as 50 percent of the hydrogen pumped into the formation will remain in the formation.

10.7.5 Barriers

A number of key barriers must be addressed by federal, state, and local governments along with industry and academia. These barriers (8) are listed below:

- The primary constraint on remote fuel cells generating electricity from hydrogen is economical. Power is inexpensive in the United States. For a fuel cell to compete with

other generation sources, its price must be reduced dramatically. Remote power applications offer the best opportunities for fuel cells to compete economically. Generally speaking, the cost of the hydrogen should be under $10/MMBtu to be competitive with other energy sources. Fuel cells at customer sites with a use for the waste heat must be acquired and installed at a cost under $2,000/kW.

- Research and development is required to improve the performance and lower the cost of renewables, storage, and fuel cell technologies. Technologies are needed that can produce hydrogen for the same price as gasoline. Storage technologies must be developed to allow cheap, safe hydrogen storage. Finally, fuel cell technology must advance to improve efficiency.
- Safety is a prime consideration for stationary fuel cells. As fuel cells come closer to the customer, codes must be written and building inspectors educated to allow the introduction of renewable fuel cell power systems. Standards are being developed for on-board hydrogen, but these efforts must be expanded to include standards in building codes and for on-site hydrogen production, storage, and use at industrial sites. Codes and standards activities along these lines are underway.
- Difficulty in obtaining insurance is of prime concern for siting hydrogen projects. Efforts must be undertaken for the government to provide a layer of insurance coverage. In addition, insurance companies must be educated as to the proper handling of hydrogen and the associated risks. This would allow for property, liability, and efficacy insurance to be offered at reasonable rates.
- Public outreach is necessary for the development of hydrogen technologies. The public perception is that hydrogen is dangerous. EPA lists hydrogen as a hazardous chemical. The public requires positive experiences in using hydrogen at work or in transportation to overcome negative perceptions. Children can be educated at school with a curriculum that includes studying hydrogen as a renewable, nonpolluting energy source.

10.8 The Office of Energy Efficiency and Renewable Energy work in Fuel Cells

The Office of Energy Efficiency and Renewable Energy (EERE), whose mission is to develop and deploy efficient and clean energy technologies, is part of the United States Department of Energy. Prior to 2002, it was organized around five energy sectors – industry, transportation, buildings, power and Federal Agencies. EERE was organized into five offices corresponding to the above sectors: Office of Industrial Technologies (OIT), Office of Transportation Technologies (OTT), Office of Building Technology, State and Community Programs (BTS), Office of Power Technologies (OPT), and Office of Federal Energy Management Programs (FEMP). EERE partners with the private sector, state and local governments, DOE national laboratories, and universities to conduct its program activities. To help accomplish its mission, EERE is aided by the Golden Field Office and six regional offices, each of which serves a specific geographic region of the United States and its territories.

In early 2002, the Office of Energy Efficiency and Renewable Energy reorganized. It is moving away from the sector organization and is streamlining the thirty-one existing programs of the above offices into eleven Program Offices. These offices include

1. Solar

2. Wind and Hydropower
3. Geothermal
4. Distributed Energy, Electricity Infrastructure and Reliability
5. Biomass
6. Industrial Technologies
7. FreedomCAR & Vehicle Technologies
8. Hydrogen, Fuel Cells and Infrastructure Technologies
9. Building Technologies
10. Weatherization and Intergovernmental Grants
11. Federal Energy Management Programs

EERE's fuel cell research is focused on low temperature fuel cells, including transportation applications, building applications and hydrogen technologies. The majority of fuel cell research will now be located in the Hydrogen, Fuel Cell and Infrastructure Technologies Program Office, including work that was previously in Office of Transportation Technologies and Distributed Energy Resources.

The information in the rest of the section is organized around the five energy sectors of EERE because this is how the budgets are reported.

10.8.1 The Office of Industrial Technologies

The Office of Industrial Technologies (OIT) is divided into five program activities, Industries of the Future (Specific), Industries of the Future (Crosscutting), Cooperative Programs with States, Energy Efficiency Science Initiative, and Management and Planning. The budget for the OIT for Fiscal Years 2001, 2002 and 2003 (requested) are $146.0 million, $148.9 million, and $138.3 respectively.

The Inventions and Innovation Program, funded within the Industries of the Future (Crosscutting) program activity, provides financial assistance to support the development of new energy efficient technologies. Several fuel cell technologies have been funded within this program in the last several years. Prototype development of an industrial fuel cell microgenerator, developed by Fuel Cell Technologies, Inc., is one such project. It is a new, low-cost, small-scale molten carbonate fuel cell power plant designed for continuous operation. It will be competitively priced for small-scale onsite power generation of 30 to 50 kW. The market application will be to businesses that depend on an uninterrupted and economical supply of power. The goal of the project is to design, build and test the balance of plant for a 40-kW carbonate microgenerator prototype to serve as a test bed for future demonstrations of the product.

Another project is the compact and efficient chemical reactor proposed by Mesoscopic Devices, LLC. The reactor will be used in producing syngas for fuel cells in the utility and automotive industries. The new design will improve heat transfer, chemical conversion rates and reactor size. The goal of the project is to develop and build a compact chemical reactor and demonstrate the performance improvements over standard reactor technology. The successful design will support the deployment of fuel cells in automobiles.

An Industries of the Future (Specific) fuel cell project in the area of mining is to produce fuel cell mining vehicles that are more energy efficient and have safety and environmental benefits for use in underground mines. Some of the project partners include Fuelcell Propulsion, Atlas Copco Wagner, Bituminous Coal Operator's Association, Joy Mining Machinery, Long-Airdox Company, and Sandia National Laboratory along with several foreign project partners.

Another area of fuel cell activity within the Office of Industrial Technologies is in the Energy Efficiency Science Initiative program. The program funds research and development that falls between fundamental exploratory science and pre-commercial applied R&D. It expands on existing cooperative efforts with the Office of Fossil Energy in fuel cell technologies and other areas.

10.8.2 The Office of Transportation Technologies

The Office of Transportation Technologies (OTT) is divided into eight program activities: Vehicle Technologies R&D, Fuels Utilization R&D, Materials Technologies, Technology Deployment, Biofuels Energy Systems, Cooperative Programs with States, Energy Efficiency Science Initiative, and Management and Planning. The budget for the OTT for Fiscal Years 2001, 2002 and 2003 (requested) are $297.5 million, $301.6 million, and $275.7 respectively.

Within the OTT, fuel cell R&D is funded mainly within the Vehicle Technologies program activity. The Fuel Cell Programs budgets for FY 2000, 2001 and 2002 (requested) in the Vehicle Technologies program activity are $36.6 million, 41.3 million, and 41.9 million, respectively. The Fuel Cell R&D Program develops highly-efficient, low- or zero-emission, cost-competitive automotive fuel cell power system technologies that operate on conventional and alternative fuels. The program combines the automotive industry, fuel cell and fuel processor developers, national laboratories, universities, and fuel suppliers in a customer-focused national program. The goal is to develop more fuel efficient, cleaner, and cost-effective vehicle power systems that meet the most stringent emission standards while retaining the same performance as today's vehicles. Specific goals and performance measures include:

- By 2005, reduce the cost of a 50 kW fuel cell system to $125/kW.
- By 2004, reduce the fuel cell stack platinum loading to 0.6g/peak kW.
- By 2010, reduce the cost of a 50 kW fuel cell system to $45/kW.
- By 2008, develop and validate fuel cell power system technologies that meet vehicle requirements in terms of: 1) cost competitiveness with internal combustion engines: and 2) performance, range, safety, and reliability.

Assuming all program goals are met, the benefits will include

- 0.00, 0.003, and 0.102 millions of barrels per day of petroleum displaced for years 2005, 2010, and 2020 respectively.
- 0, 6, and 201 trillion Btu of total primary energy displaced for years 2005, 2010, and 2020 respectively.
- 0, 64, and 1,655 millions of dollars in energy costs or savings for years 2005, 2010, and 2020 respectively.
- 0.00, 0.12, and 3.90 MMTCe carbon equivalent emissions displaced for years 2005, 2010, and 2020 respectively.

Accomplishments of the fuel cell program include the ongoing testing and evaluation of a fuel-flexible 50 kW integrated fuel cell power system. Planned accomplishments for Fiscal Year 2002 include the demonstrating and delivering an advanced 50 kW fuel processor for automotive fuel cell systems.

To a lesser extent, fuel cell R&D within the OTT is also funded through Fuels Utilization R&D, Materials and Technologies, Technology Deployment, Cooperative Programs with States, Energy Efficiency Science Initiative, and Management and Planning.

The Fuel Cells for Transportation Program has selected the polymer electrolyte fuel cell (PEFC) as the leading technology candidate because of its high power density, quick start-up capability, and simplicity of construction. Key research areas include fuel-flexible fuel processing and storage, fuels for fuel cells, high-efficiency, low-cost fuel cell stack and components, and integrated fuel cell systems and components.

The Progress Reports for Fiscal Year 2001 for Transportation Fuel Cell Power Systems and Fuels for Advanced CIDI Engines and Fuel Cells includes projects in the categories of Fuel Cell Power System Development, Fuel Processing Subsystem, Fuel Cell Stack Subsystem, PEFC Stack Component Cost Reduction, Air Management Subsystems, and Fuels for Fuel Cell Vehicles. Please refer to the Progress Reports on the Office of Transportation of Technologies web site for more specific information on projects listed within these categories. The Transportation Fuel Cell Power Systems Progress Report can be found at
http://www-db.research.anl.gov/db1/cartech/document/DDD/156.pdf – Part 1
http://www-db.research.anl.gov/db1/cartech/document/DDD/159.pdf – Part 2

The Fuels for Advanced CIDI Engines and Fuel Cells Progress Report can be found at
http://www-db.research.anl.gov/db1/cartech/document/DDD/186.pdf

The following projects have been selected by the Transportation Fuel Cell Power System Program to highlight some of the program accomplishments.

The Atmospheric Fuel Cell Power System, with partner International Fuel Cells.

- Description – A 50-kW gasoline fueled power plant, operating at near-ambient pressure, consisting of a 50-kW-equivalent, fuel flexible fuel processing system and a 50-kW polymer electrolyte membrane stack assembly.
- Accomplishments – The system was successfully tested and delivered during FY 2001. It was demonstrated using California Phase II reformulated gasoline. It operates at ambient pressure, requires no compressor, and includes all necessary ancillary equipment and control systems for automated operation. The nominal 50-kW power plant achieved a maximum net power output power of 53 kW with a maximum system efficiency of ~35% at a net power output of ~18kW. The second phase of the project will deliver and advanced gasoline-fueled 75-kW fuel cell power plant.

CO-Tolerant Electrodes, with partner Los Alamos National Laboratory.

- Description – Fuel cell electrodes that are tolerant to higher levels of Carbon Monoxide (CO) are needed. Reconfigured anodes with improved catalysts and optimized electrode structures have been developed.
- Accomplishments – Enhanced tolerance to CO in reformate fuel streams was achieved, along with reduced Platinum catalyst loading and air bleed. New reconfigured membrane electrode assemblies (MEAs) tolerate CO levels up to 100 parts per million (ppm) in reformate with a catalyst loading of only 0.1 mg/cm^2 with air bleed. New catalysts with a reconfigured anode demonstrate full tolerance to 500 ppm of CO reformate with less than 5% air bleed and improved transient behavior for system startup. Tolerance to 50 ppm CO was achieved with no air bleed.

Direct Methanol Fuel Cell, with partners U.S. Department of Defense and Los Alamos National Laboratory.

- Description – Direct methanol fuel cells use liquid methanol instead of hydrogen as the fuel that is oxidized directly at the anode. This eliminates the need for a hydrogen storage tank or reformer.
- Accomplishments – Focus is on reducing the required amount, or loading, of platinum catalyst without reducing the peak power. Platinum catalyst loadings have been reduced by over a factor of ten with peak power reduced only 30%. New hardware developed and used in a 30-cell fuel stack with a 50-cm^2 cross sectional area produced 80 W of power at near ambient conditions. Projected output at higher conditions (90 °C and 30 psig) is 200 W. A successful demonstration of a direct methanol fuel cell using factory-grade methanol without purification indicated that special "fuel cell grade" fuel will not be required.

Fuel Composition Effects on Processor Catalysts, with partner Argonne National Laboratory.

- Description – Microreactor was designed to test the effect of fuel composition on the ability of catalysts to autothermally reform fuels into hydrogen. Long-term tests of isooctane and a benchmark fuel mixture of the chemical compounds were performed on a Platinum catalyst.
- Accomplishments – Argonne National Laboratory developed and licensed a new class of autothermal reforming catalysts modeled after the internal anode materials used in solid oxide fuel cells. The rhodium catalyst has demonstrated very high conversions of iso-octane at temperatures as low as 500 °C.

Improved Water-Gas Shift Catalysts, with partner Argonne National Laboratory.

- Description – Explored alternative water-gas shift catalysts that did not need to be activated in situ, were not pyrophoric (did not need to be sequestered during system shutdown), and were tolerant to temperature excursions. Work focused on bifunctional catalysts, where one component adsorbs or oxidizes CO to CO_2, and another component dissociates water to H_2 and donor oxygen for oxidation. Three bifunctional catalysts have been tested: platinum/mixed oxide, non-precious metal/mixed oxide, and vanadium-cobalt oxides.
- Accomplishments – Argonne has developed platinum/mixed oxide and non-precious metal/mixed oxide catalysts that have greater activity than commercial LTS copper/zinc oxide. The catalysts are active up to 400 °C. The platinum/mixed oxide does not lose its activity when exposed to air at temperatures up to 550 °C and the non-precious metal/mixed oxide is tolerant to air up to 230 °C. The higher activity of the catalyst equates to a 30% reduction in catalyst volume when compared to conventional catalysts. The platinum/mixed

oxide catalyst has been able to reduce inlet 10% CO to exit concentrations of less than 1% CO from diesel, and to 1.1% CO from simulated reformate. During 2001, Argonne developed a copper/oxide catalyst that can operate above 250 °C, allowing it to be used in both the low-temperature shift and high-temperature shift stages. The Argonne copper/oxide catalyst reduced the total catalyst volume needed by 88% compared to commercial catalysts.

Integrated 50-kW Fuel Cell Stack System, with partners Argonne National Laboratory and Honeywell Engines & Systems.

- Description – Build and test an integrated 50-kW polymer electrolyte membrane stack system with subsystems for air, water, and thermal management. Overall system performance depends on successfully integrating subsystems with the fuel cell stack. The program involves fabricating and testing three generations of PEFC stacks (10-kW) leading up to the final 50-kW system.
- Accomplishments – The fuel cell stack demonstrated tolerance to Carbon Monoxide concentrations greater than 200 parts per million in the reformate without appreciable performance loss. This meets DOE's technical target for CO tolerance and is compatible with typical CO levels resulting from gasoline reformate cleanup systems (<50 parts per million). A 10-kW stack has consistently shown excellent performance for 250 hours while operating on reformate containing carbon monoxide. Uniform voltage distribution, a specific power of 0.87 kW/kg, and a power density of 1.6 kW/liter were also achieved.

Low-Cost Membrane Electrode Assemblies (3M Company).

- Description – 3M has developed integrated pilot processes to manufacture high-performance membrane electrode assemblies (MEA) with low platinum loading in high volume. A novel, five-layer MEA design employing a unique, proprietary nanostructured thin-film catalyst support system has been developed. Pilot plant, high-volume fabrication, employing vacuum coating of precious metal catalysts onto nanostructured substrate, has been demonstrated.
- Accomplishments – Novel 3M nanostructured MEA design concept has been extended to a six-cell stack, demonstrating the viability of the MEAs to be scaled in area and manufactured by the continuos process methods. Methods to screen the performance of new catalyst compositions and structures were developed and in-situ techniques for characterizing MEA properties were implemented. Optimal water management and operating conditions for the nanostructured MEAs were identified. Laboratory quantities (100-suare foot batches) of catalyzed electrode material, with low precious metal alloy loadings of 0.005 to 0.1 mg/cm^2 were prepared. Experimental MEAs with a catalyst loading of 0.1 mg Pt/cm^2 were fabricated and tested.

Molded Bipolar Separator Plates for Fuel Cells, with partners Argonne National Laboratory, Honeywell, Inc., Gas Technology Institute, PEFC Plates, LLC (collaboration of Stimsonite and ENDESCO Services), Superior Graphite Corporation.

- Description – Raw materials were selected, blended, and optimized to achieve electrical, chemical, and physical properties, as a substitute for conventional graphite bipolar plates, needed for fuel cell stacks. Moldable blends of graphite, resins and additives were identified and used for molding composite graphite bipolar plates. The expense associated with conventional machining and finishing of the typically complex separator plate shapes is

avoided by molding the plates. The new plates were manufactured in a pilot production molding line and then tested (as assembled fuel cell stacks) for functional performance and endurance under typical vehicle operating conditions.

- Accomplishments – The molded plates were shown to meet or exceed specified properties for conductivity, corrosion, and hydrogen (fuel) permeability. They also demonstrated good performance during crush strength, flexibility, total creep, flexural strength, and combustibility testing. Overall plate performance, measured in millivolts of electrical output, closely followed that of conventional, machined plates at typical current densities around 400 mA/cm^2. At higher currents, the molded plates actually performed better, because their hydrophilic nature accelerates draining of the by-product water produced during the electrochemical reaction inside the fuel cell stack. Researchers, using a pilot production line, have produced up to five plates per hour. Assuming a production level equal to at least 100 megawatts annually, which is the capacity needed for 2,000 fuel cell cars each with a 50-kW fuel cell engine, a full-size production line, incorporating less expensive materials and more efficient manufacturing processes, could reduce the cost of bipolar plates to $10/kW. Molded composite graphite plates were assembled into multicell stacks of 4, 7, 20, and 52 cells, which were tested under normal vehicle operating conditions during continuous and intermittent operation. The 20-cell fuel stacks achieved 2,300 operating hours and, some plates were reused with no changes in chemical or mechanical properties for over 5,000 hours.

Small, Efficient Microchannel Fuel Processors, with partners Defense Advanced Research Projects Agency and Pacific Northwest National Laboratory.

- Description – A new class of process technology, based on microfabricated heat exchangers and reactors, shows significant promise for use in compact, onboard hydrogen generation systems for fuel cell vehicles. Microchannel reactor-based fuel processors are small, efficient, modular, lightweight, and potentially inexpensive. These units operate more efficiently than larger conventional chemical reactors because of their unique heat transfer and mass transport properties.
- Accomplishments – Researchers at PNNL have demonstrated the technical feasibility of using microthermal and chemical systems for energy conversion and chemical processing:
    1. A microchannel steam reforming system, consisting of four-cell reactor, multistream heat exchangers, and water/fuel vaporizers, that supports a 20-kW fuel cell and achieves 83 – 85% fuel processor efficiency on iso-octane.
    2. Compact microchannel heat exchangers with extremely high convective heat transport coefficients and low-pressure drops.
    3. Microchannel catalytic reactors with millisecond residence times and reduced production of unwanted secondary reaction products.
    4. Microchannel separations units that reduce CO_2 and CO concentrations to very low levels.
    5. Low-cost lamination methods for fabricating microchannel devices.

In January of 2002, FreedomCAR was introduced. FreedomCAR is a government-industry research program, whose goal is to develop hydrogen-powered fuel cell cars and light trucks that are free from the dependence of foreign oil and harmful emissions. It is a cooperative effort between the U.S. Department of Energy and the U.S. Council of Automotive Research.

10.8.3 The Office of Power Technologies

The Office of Power Technologies (OPT) includes Renewable Energy Resources, Distributed Energy Resources and Management and Planning. The budget for the OPT for Fiscal Years 2001, 2002 and 2003 (requested) are $348.9 million, $376.2 million, and $394.4 respectively.

The Distributed Energy Resources (DER) is divided into three main activities toward the development and demonstration of distributed energy resources: Systems architecture and integration, Technology development, and Systems implementation and outreach. Fuel cell activity is under the technology development area, in the Fuel Cells for Buildings Program. DER is focusing its efforts on the Proton Exchange Membrane Fuel Cell. It has the appropriate size and operating characteristics for building use. The fuel cell will supply both the electric and thermal load of the buildings, maximizing the use of recoverable energy to integrate with Buildings Cooling, Heating and Power (BCHP).

The Fuel Cells for Building Program has the following performance targets:

- Target fuel to electricity conversion of 40-50% for stand-alone operations. For integration into BCHP 75-80% efficiency.
- Operating temperatures of 120°C to 150°C (Currently at 80°C) and pressures of less than 1.5 atmospheres (currently greater than 3 atm).
- Develop an economical process of fuel reforming of natural gas producing a hydrogen fuel that contains less than 10 ppm of carbon monoxide, for the low temperature fuel cell.
- Market clearing price of $1500/kW or less.
- Operating life greater than 40,000 hours.

In June 2001, the Department of Energy announced over $85 million in research awards given to 18 organizations and 5 universities. Eleven of the awards were in fuel cell research. The research will primarily focus on overcoming technical barriers, such as high component costs, size, weight and start-up time. The following is a short synopsis of each project.

Fuel Cell Membranes – 3M, St. Paul, Minnesota, will develop Membrane Electrode Assemblies (MEAs) with improved cathodes, high temperature membranes, and optimized gas diffusion layers. Improved flow fields as well as MEA fabrication methods will be developed.

Fuel Cell Membranes – DeNora North America, Somerset, New Jersey, will develop improved cathodes and high temperature membranes for PEFC. Advanced MEA fabrication methods will also be developed.

Fuel Cell Electrodes, Blowers and Sensors – International Fuel Cells, South Windsor, Connecticut, was selected for three contracts. They will develop polymeric membranes incorporating advanced cathode catalysts and capable of operating in PEFC at high operating temperatures. They will develop chemical and physical property sensors required for PEFC systems (physical property sensors include temperature, flow rate, pressure and humidification). They will also develop motor-blower technologies for ambient pressure fuel cell systems.

Fuel Cell Electrodes – Superior MicroPowders, Albuquerque, New Mexico, will develop new electrocatalysts and cathode structures with low platinum content to improve performance and lower the cost of PEFC.

Fuel Cell Bipolar Plates – Porvair Corporation, Hendersonville, North Carolina, will develop carbon/carbon composite bipolar plates for PEFC. They will also develop high-volume production methods for the composite bipolar plates.

Fuel Cell Fuel Processor – Catalytica Energy Systems, Mountain View, California, will develop a 50 kW fuel-flexible fuel processor capable of running on EPA Phase II Reformulated Gasoline.

Fuel Cell Fuel Processor – University of Michigan, Ann Arbor, Michigan, will develop microreactor fuel processing technology, which can lead to dramatic reductions in the size and start-up time of fuel-flexible processors for PEFC systems.

Fuel Cell Turbo-Compressor, Sensors, and Thermal/Water System – Honeywell, Torrance, California, was selected for three contracts. They will develop an automotive scale fuel cell air compressor, focusing on cost reduction and performance enhancements of a 50 kW rated fuel cell turbo-compressor. They will develop physical property sensors, including temperature, flow rate, pressure, and humidity, for automotive PEFC systems. They will also develop a low-cost, high-performance, thermal and water management system for PEFC with integrated lightweight heat exchanger technology and air management system.

Ethanol Fuel Cell System – Caterpillar Inc., Peoria, Illinois, will design and fabricate a 13 kW, integrated, ethanol-fueled PEFC power system producing three-phase electrical power. Durability testing of the power system will be performed.

Development of High Temperature H2/O2 Proton Exchange Membrane Fuel Cells – Pennsylvania State University, University Park, Pennsylvania, will develop a high temperature PEFC. Improvements in proton conductivity, electro-osmotic drag of water, thermal stability, and mechanical strength and the development of technologies for preparation of the membrane electrode assemblies using polyphosphazene membranes will allow the fuel cell to operate at elevated temperatures, maybe up to 250 °C.

Advanced Materials for PEFC-Based Material Systems – Virginia Polytechnic Institute and State University, Blacksburg, Virginia, will provide bridging science for the research and development of next-generation polymer electrolyte membranes, membrane electrode assemblies, and related fuel cell material systems.

The program is also working with Pacific Northwest National Laboratory, Argonne National Laboratory and the following companies:

- FuelCell Energy Inc
- Kse Inc
- Gas Technology Institute
- Arthur D. Little
- Honeywell

Plug Power Inc
Foster Miller Associates
Hydrogen Burner Technology
General Electric Corporation

10.8.4 Office of Building Technology, State and Community Programs

The fuel cells/ cogeneration work from that was once a part of the Office of Building Technology, State and Community Programs (BTS) was transferred to the Office of Power Technologies in FY 2002.

10.9 Rare Earth Minerals

10.9.1 Introduction

In an effort to reduce fuel cell manufacturing cost, lower priced rare earth minerals are being considered. Rare earth minerals such as lanthanum are used in making cathodes for the solid oxide fuel cell. Lower purity minerals such as lanthanide manganite are being tested determine whether if these new materials will perform without serious degradation of the fuel cell performance.

The rare earth minerals are composed of scandium, yttrium, and the lanthanides. The lanthanides comprise a group of 15 elements that include: lanthanum, cerium, praseodymium, neodymium, promethium, samarium, europium, gadolinium, terbium, dysprosium, holmium, erbium, thulium, ytterbium, and lutetium. Cerium is the most abundant element in the rare earth group at 60 ppm, followed by yttrium at 33 ppm, lanthanum at 30 ppm, and neodymium at 28 ppm. Thulium and lutetium are the least abundant at 0.5 ppm.

Molycorp, a wholly owned subsidiary of Unocal Corp., was the only company to mine rare earth minerals in the United States in 2001. Molycorp mined Bastnasite, a rare earth fluocarbonate mineral, as a primary product at Mountain Pass, California. The value of domestic ore production was estimated at $28 million; the estimated value of refined rare earth minerals was more than $1 billion. The end uses for rare earth products in 2000 were as follows: automotive catalytic, 22%; glass polishing and ceramics, 39%; permanent magnets, 16%; petroleum refining catalysts, 12%; metallurgical additives and alloys, 9%; rare earth phosphors for lighting, televisions, computer monitors, radar, and x-ray intensifying film, 1%; and miscellaneous, 1%.

Rare earth minerals are relatively abundant in the Earth's crust, but discovered minable concentrations are less common than for most other ores. U.S. and world resources are contained primarily in bastnasite and monazite. Bastnasite deposits in China and the United States constitute the largest percentage of the world's rare earth economic reserves, while monazite deposits in Australia, Brazil, China, India, Malaysia, South Africa, Sri Lanka, Thailand and the United States constitute the second largest segment. Xenotime, rare earth bearing clays, loparite, phosphorites, apatite, eudialyte, secondary monazite, cheralite, and spent uranium solutions make up most of the remaining resources. Undiscovered resources are thought to be very large relative to expected demand. Table 10-8 provides world mine production and reserves. (8)

Table 10-8 World Mine Production and Reserves

Country	Mine Production, 2001	Reserves
United States	5,000	13,000,000
Australia	--	5,200,000
Brazil	200	82,000
Canada	--	940,000
China	75,000	43,000,000
India	2,700	1,100,000
Malaysia	450	30,000
South Africa	--	390,000
Sri Lanka	120	12,000
Former Soviet Union	2,000	19,000,000
Other Countries	--	21,000,000
World Total (rounded)	85,500	100,000,000

Rare earth prices are quite competitive, causing product prices to be quoted on a daily basis. Table 10-9 shows Rhodia, Inc. quoted prices (10). For additional information on rare earth mineral price history, click USGS 1999 Mineral Yearbook.

Table 10-9 Rhodia Rare Earth Oxide Prices in 2,000

Product (oxide)	Percentage purity	Standard package quantity (kilograms)	Price (dollars per kilogram)
Cerium	96.00	25	19.20
Cerium	99.50	900	20.85
Dysprosium	99.00	3	120.00
Erbium	96.00	2	155.00
Europium	99.99	1	990.00[1]
Gadolinium	99.99	3	130.00
Holmium	99.90	10	440.00[2]
Lanthanum	99.99	25	23.00
Lutetium	99.99	2	3,500.00
Neodymium	95.00	20	28.50
Praseodymium	96.00	20	36.80
Samarium	99.90	25	360.00
Samarium	99.99	25	435.00
Scandium	99.99	1	6,000.00
Terbium	99.99	5	535.00
Thulium	99.90	5	2,500.00
Ytterbium	99.00	10	230.00
Yttrium	99.99	50	88.00

[1] Price for quantity greater than 40 kilograms is $900.00 per kilogram
[2] Price for quantity less than 10 kilograms is $485.00 per kilogram

10.9.2 Demand

The forecast growth in demand for rare earth minerals over the next 3-4 years is in the range of 4-9 percent per year. On this basis, total world demand could exceed 100,000 tons per year rare earth oxide (REO) for the first time by 2004. However, if the current slowdown in the telecommunications and computer industries continues then this milestone could be delayed, as these industries are major consumers of rare earth minerals. Growth in autocatalysts has been strong in response to legislation on lower emission levels, and between 1997 and 2000 the demand for rare earth magnets grew at 21% per year in spite of the uncertainties created by the financial crisis in Asia. Over the past 3-4 years China has increased its dominance of the world market, supplying an estimated 85-95% of world demand in 2000. China is thought to have mined ores containing 75,500 tons REO (compared with a global production equivalent to 85,900 tons), exported 47,000 tons REO of rare earth concentrates, chemicals and metals, and satisfied domestic demand of 19,200 tons REO (11).

World reserves are believed to be sufficient to meet forecast world demand well into the 21st century. Several world class rare-earth deposits in Australia and China have yet to be developed because world demand is currently being satisfied by existing production. The long-term outlook is for an increasing competitive and diverse group of rare-earth suppliers. As research and technology continue to advance the knowledge of rare earth minerals and their interactions with other elements, the economic base of the rare-earth industry is expected to continue to grow. New applications are expected to be discovered and developed.

10.10 References

1. K. Kono, "Implementing Agreement "Advanced Fuel Cells," Annex IX Fuel Cells for 2. Stationary Applications, Subtask 2," draft IEA paper, April 1999.
2. Fuel Cell Technology News, January 2002, published by Business Communications Company, Inc.
3. "Hydrogen," ChemExpo, Chemical Profile, January 29, 2001, web site http://www.chemexpo.com%2fnews%2fprofile010129.cfm
4. "Hydrogen Rising in Energy Policy Debate: Global race for "tomorrow's petroleum" heats up," Worldwatch News Release, August 2, 2001.
5. C Padro and V. Putsche, "Survey of the Economics of Hydrogen Technologies," NREL/TP-570-27079, September 1999.
6. National Renewable Energy Laboratory web site: http://www.nrel.gov/lab/pao/hydrogen.html
7. Idaho National Engineering and Environmental Laboratory web site: http://www.inel.gov/energy/fossil/hydrogen
8. National Hydrogen Association Near-term Hydrogen Implementation Plan 1999-2005; http://www.hydrogenus.com/impplan.htm
9. U.S. Geological Survey, Mineral Commodity Summaries, January 2002.
10. U.S. Geological Survey, Mineral Yearbook, 1999 edition.
11. Source: www.roskill.co.uk/rey.html

11. INDEX

acid, xii, 1-4, 1-7, 1-12, 1-27, 3-2, 3-7, 5-2, 5-3, 5-5, 5-6, 5-11, 5-13, 6-7, 10-12
alkali, 1-4, 6-5, 6-6, 6-8, 6-10, 6-31
alkaline, 1-3, 1-4, 1-7, 1-12, 1-27, 10-11
anode, 1-1, 1-2, 1-4, 1-5, 1-6, 1-12, 1-13, 3-4, 3-5, 3-6, 3-8, 3-11, 3-13, 3-16, 3-17, 5-1, 5-2, 5-9, 5-10, 5-11, 5-12, 5-13, 5-16, 5-17, 5-20, 6-1, 6-2, 6-3, 6-4, 6-5, 6-7, 6-9, 6-10, 6-16, 6-17, 6-18, 6-19, 6-20, 6-21, 6-23, 6-25, 6-27, 6-30, 6-32, 6-33, 6-34, 6-40, 7-25, 7-29, 9-1, 9-5, 9-7, 9-8, 9-12, 10-15
anodic, 5-16, 5-19, 6-30
Ansaldo, 1-15, 6-1
applications, 1-2, 1-3, 1-9, 1-11, 1-12, 1-13, 1-15, 1-28, 3-1, 3-4, 3-6, 3-11, 3-16, 3-17, 5-7, 8-1, 8-2, 9-30
availability, xii, 1-10, 1-16
balance, 1-2, 1-4, 3-5, 6-3
Ballard Power Systems, 1-17, 1-27, 1-28, 1-39, 10-10
bio-fuel, 1-12
bipolar, 3-6, 3-13, 5-4, 5-5, 6-9
bottoming cycle, 8-1
Cairns, 5-24, 6-44
carbon, 1-7, 3-10, 3-13, 5-1, 5-2, 5-3, 5-9, 5-10, 5-11, 5-12, 6-16, 6-17, 6-19, 6-35, 7-31, 9-9, 9-14, 9-16, 9-17, 9-18, 10-1
carbon black, 1-7, 5-1, 5-2, 5-3, 5-9, 5-10, 5-11
carbon composite, 3-10
carbon monoxide, 3-10, 9-16
catalyst, 1-2, 1-5, 1-12, 1-13, 3-6, 3-10, 3-11, 3-13, 3-14, 5-1, 5-8, 5-9, 5-10, 5-11, 5-13, 6-30, 6-33, 6-35, 7-29
catalysts loading, 1-4
cathode, 1-1, 1-2, 1-4, 1-5, 1-12, 1-13, 3-4, 3-5, 3-11, 3-13, 3-15, 5-1, 5-2, 5-6, 5-9, 5-11, 5-12, 5-13, 5-14, 5-18, 5-20, 6-1, 6-2, 6-3, 6-4, 6-5, 6-7, 6-9, 6-10, 6-11, 6-12, 6-14, 6-16, 6-18, 6-20, 6-21, 6-22, 6-23, 6-25, 6-30, 6-31, 6-32, 6-40, 7-25, 7-29, 9-6, 9-7, 9-8, 9-9, 9-12, 10-15
cathode dissolution, 6-11
cation, 3-2
Ceramatec, 1-22
ceramic, 1-4, 1-13, 6-6, 6-10, 7-1
cermet, 1-5
characteristics, 1-1, 1-9, 1-10, 1-13, 1-14, 1-17, 1-22, 3-5, 6-40
chemisorption, 3-4, 3-15
cleanup, 1-21, 5-10, 6-10, 6-13, 6-27, 6-29, 10-2
coal gasification, 6-27, 10-2
cogeneration, 1-9, 1-11, 1-12, 1-13, 1-14, 1-15, 5-1, 8-1, 8-2, 9-19, 9-21
coking, 9-17
commercialization, 1-20, 3-18, 6-32, 7-35
concentration losses, 5-20, 6-32, 7-34
contaminants, 1-10, 1-21, 3-10, 5-10, 5-13, 6-13, 6-26, 6-27, 6-32
converter, 1-10, 5-10, 8-9, 8-12, 8-19, 8-21, 8-22, 8-28, 8-29, 8-30, 8-31, 8-33, 8-34, 8-36, 8-37, 8-53, 8-54, 8-55, 8-56, 8-57, 8-58, 8-63, 8-65, 8-67, 8-68, 8-69, 8-70, 8-71, 8-73, 8-75, 8-77, 8-78, 8-82
cooling, 1-15, 3-6, 3-10, 3-12, 5-5
corrosion, 1-1, 1-4, 1-13, 5-3, 5-4, 5-9, 5-11, 5-12, 5-14, 6-3, 6-4, 6-7, 6-9, 6-21, 6-31
cost of electricity, 8-2, 9-28, 10-11
creepage, 6-4
crossover, 3-17, 6-12
current density, 3-11, 5-7, 5-12, 5-13, 5-14, 5-20, 6-7, 6-15, 6-18, 6-21, 6-30, 6-32, 6-39, 7-27, 7-30, 7-32, 7-34, 10-13
Daimler-Benz, 1-27
degradation, 1-1, 1-3, 3-16, 5-4, 5-8, 5-9, 5-10, 5-14, 5-20, 6-27, 6-32, 7-33, 7-35
demonstration, 5-3
desulfurization, 6-29
dielectric, 5-5
digester, xii
diluent, 1-12, 5-19
direct internal reforming, 6-33, 10-12
Dow Chemical, 3-7, 3-12
drag, 3-5
DuPont, 3-7, 3-12
efficiency, xii, 1-6, 1-9, 1-12, 1-14, 1-15, 1-19, 1-20, 1-21, 3-5, 3-16, 6-10, 6-12, 6-17, 6-27, 7-26, 8-1, 8-2, 9-18, 9-19, 9-20, 9-21, 9-28
electrocatalyst, 1-4, 1-7, 3-10, 3-16, 5-1, 5-2, 5-3, 5-6
electrochemical performance, 1-2
electrodes, 1-1, 1-3, 1-6, 1-7, 1-8, 1-13, 3-1, 3-5, 3-8, 3-11, 3-13, 3-14, 3-18, 5-1, 5-3, 5-10, 5-11, 5-16, 5-18, 5-19, 6-3, 6-4, 6-9, 6-10, 6-11
electrolyte management, 6-4
emissions, xii, 1-9, 1-21, 1-27
endothermic, 1-5, 3-4, 6-19, 6-33, 6-34, 9-16
equilibria, 6-23
equilibrium, 1-7, 6-3, 6-17, 6-19, 6-20, 6-22, 6-23, 6-25, 6-30, 6-31, 6-35, 7-31, 9-7, 9-9, 9-10, 9-13, 9-14, 9-15, 9-16, 9-17, 10-1, 10-13
Europe, xii, 1-27, 6-1
exchange current, 5-13, 10-13
exothermic, 1-6, 3-15, 6-19, 6-33, 6-34, 9-16
external, 1-1, 1-3, 1-5, 1-12, 3-4, 3-6, 6-12, 6-33, 6-34
Faraday, 6-40, 9-1, 10-13
flat plate, 1-8, 1-13, 5-7
flooded, 1-3, 1-7, 6-3
Foulkes, 1-2, 1-37, 10-4
Frequency, 1-15, 8-26, 8-31, 8-48, 8-51, 8-55, 8-63

fuel, xii, xiii, 1-1, 1-2, 1-3, 1-4, 1-5, 1-6, 1-7, 1-8, 1-9, 1-10, 1-11, 1-12, 1-13, 1-14, 1-15, 1-16, 1-17, 1-20, 1-21, 1-22, 1-23, 1-26, 1-27, 1-28, 1-37, 2-1, 3-4, 3-5, 3-6, 3-10, 3-11, 3-12, 3-13, 3-16, 3-17, 3-18, 5-1, 5-3, 5-4, 5-5, 5-9, 5-10, 5-11, 5-12, 5-15, 5-16, 5-17, 5-19, 5-20, 6-6, 6-7, 6-9, 6-10, 6-13, 6-17, 6-18, 6-19, 6-20, 6-21, 6-23, 6-25, 6-26, 6-27, 6-29, 6-30, 6-31, 6-32, 6-33, 6-34, 6-35, 6-38, 7-1, 7-25, 7-27, 7-28, 7-29, 7-31, 7-32, 7-33, 7-34, 7-35, 8-1, 8-2, 9-1, 9-2, 9-3, 9-4, 9-5, 9-6, 9-7, 9-8, 9-9, 9-11, 9-12, 9-14, 9-15, 9-18, 9-19, 9-20, 9-26, 9-27, 9-28, 9-29, 9-30, 10-11, 10-12, 10-15
fuel cell stacks, 1-16, 9-2
fuel electrode, 7-33
fuels, 1-1, 1-9, 1-12, 1-22, 1-26, 3-10, 5-15, 6-3, 6-17, 6-18, 6-31, 6-33, 7-29, 7-32, 8-1
Fuji Electric Corporation, 5-1
gas turbine, 1-9, 1-12, 1-20, 9-20
gasification, 9-19
gasified coal, 6-17
gasifiers, 1-21, 5-17
Germany, 1-38, 5-23, 10-7
Girdler, 9-10, 9-16, 9-32
graphite, 3-13, 5-3, 5-4, 5-5
Grove, 10-10
Grubbs, 3-2
Halides, 6-27, 6-31, 6-45
heat exchanger, 9-18
heat rate, 6-3, 9-19, 9-20, 9-28, 10-12
heat removal, 5-5
heat transfer, 3-10, 6-14, 9-23, 9-24
higher heating value, 9-24, 9-26, 10-12
Hitachi, 6-42
hybrid, 1-20, 1-27
hydrogen, 1-2, 1-3, 1-4, 1-5, 1-8, 1-11, 1-16, 1-22, 1-26, 1-27, 1-28, 1-37, 3-4, 3-10, 3-13, 3-18, 5-10, 5-16, 6-33, 6-34, 7-26, 7-31, 7-33, 9-1, 9-2, 9-3, 9-4, 9-5, 9-7, 9-8, 9-12, 9-15, 9-20, 10-14
impurities, 3-11, 5-11, 5-16, 5-17, 7-33
indirect internal reforming, 6-33, 10-12
interconnect, 1-3, 1-8, 7-26
interconnections, 8-1
internal, 1-3, 1-5, 1-11, 3-15, 6-13, 6-33, 6-34, 6-35, 9-11
internal manifolding, 6-13
internal reforming, 1-3, 1-5, 1-11, 6-33, 6-34, 6-35
International Fuel Cells Corporation (IFC), 1-15
inverter, 9-18
ionomer, 3-13
Japan, 1-15, 1-27, 5-1, 5-23, 5-24, 6-1, 6-33, 6-42, 10-7, 10-9, 10-11
Johnson Matthey, 3-18, 5-9
kinetics, 1-3, 1-11, 1-13, 5-13, 6-11, 9-17, 9-18
life, xii, 1-1, 1-3, 1-8, 1-13, 1-16, 3-7, 5-2, 5-4, 5-5, 5-7, 5-9, 5-11, 5-20, 6-3, 6-9, 6-12, 6-21, 6-27
logistic fuel, xii, 1-22, 1-23
loss, 3-13, 3-15, 3-16, 5-10, 5-11, 5-12, 5-14, 5-16, 5-17, 5-18, 5-20, 6-10, 6-12, 6-17, 6-21, 6-22, 6-26, 6-31, 6-32, 7-26, 7-33, 7-34
lower heating value, 1-9, 9-19, 9-25, 10-12
management, 1-4, 1-11, 3-7, 3-10, 3-13, 6-3, 6-35
manifold, 1-3, 5-5, 6-12
manufacturing, 1-15, 1-16, 3-8
M-C Power, 1-21, 6-43
membrane, 1-3, 1-4, 1-12, 3-1, 3-2, 3-5, 3-7, 3-8, 3-11, 3-13, 3-14, 3-15
membranes, 3-6, 3-7, 3-11, 3-12, 3-13
methanation, 3-11, 6-16, 6-19
methane (CH_4), 9-11
methanol, 1-8, 1-26, 1-28, 3-13, 3-14, 3-16, 3-17, 3-18
migration, 5-11, 6-4
Mitsubishi Electric Corporation, 5-1, 5-8
molten carbonate, xii, 1-3, 1-7, 6-3, 6-4, 6-7, 6-8, 6-9, 6-31, 6-33, 10-12
Nafion, 3-12, 3-13, 3-14
Nafion membranes, 3-14
natural gas, xii, 1-5, 1-8, 1-12, 1-14, 1-15, 1-16, 1-17, 1-20, 1-21, 1-22, 1-26, 1-37, 3-4, 3-13, 5-15, 6-13, 6-21, 6-35, 7-26, 9-4, 9-5, 9-20, 9-24, 9-25, 9-26
Nernst, 3-15, 5-14, 6-15, 6-20, 6-25, 7-25, 7-30, 7-31
nitrogen compounds, 5-19
ohmic, 3-15, 3-16, 5-12, 5-13, 5-20, 6-7, 6-12, 6-21, 6-32, 7-26, 7-27, 7-34, 10-12, 10-14
ohmic loss, 5-13, 6-7, 6-12, 7-26, 10-12
ohmic polarization, 6-7, 6-21, 7-26, 7-27, 10-14
ohmic resistance, 3-15, 6-7
ONSI, 1-21, 1-38, 10-10
overpotential, 5-14, 5-16, 6-11
oxidant, 1-1, 1-2, 1-3, 1-8, 5-5, 5-11, 5-12, 5-14, 5-15, 5-16, 5-19, 5-20, 6-14, 6-17, 6-20, 6-21, 6-22, 6-23, 6-25, 6-26, 6-28, 7-28, 7-29, 7-30, 7-32, 9-2, 9-4, 9-6, 9-7, 9-8, 9-9, 10-14, 10-15
oxidation, 1-2, 1-7, 3-4, 3-11, 3-13, 3-17, 5-13, 5-16, 5-17, 5-18, 6-1, 6-5, 6-33, 6-34, 7-25, 7-31
oxygen, 1-1, 1-2, 1-5, 1-8, 1-11, 1-12, 3-11, 3-12, 3-13, 3-15, 5-11, 5-12, 5-13, 5-16, 7-1, 7-31, 9-3, 9-4, 9-7, 9-8, 9-9, 10-15
phosphoric acid, xii, 1-3, 1-4, 5-1, 5-5, 5-9, 5-10, 5-11, 6-3, 10-12
planar, 1-13, 1-22
poison, 1-4, 1-12
polarization, 1-7, 3-16, 5-12, 5-13, 5-14, 5-16, 5-17, 5-18, 6-20, 6-21, 6-22, 6-26, 7-26, 7-27, 7-30, 7-32, 10-14
polymer, xii, 1-3, 1-4, 1-27, 1-28, 3-3, 3-5, 3-6, 3-10, 3-11, 3-18, 10-12
porous electrodes, 1-3, 1-7, 5-2, 5-3, 5-4, 6-3
potential, 1-11, 1-21, 3-15, 3-17, 5-3, 5-13, 5-14, 5-19, 6-2, 6-3, 6-4, 6-9, 6-12, 6-13, 6-15, 6-16, 6-17, 6-19, 6-20, 6-23, 6-25, 6-30, 6-32, 7-30, 7-31, 8-2, 9-17, 10-12, 10-13
power conditioning, 1-8
pressure, 1-3, 1-4, 1-6, 1-8, 1-12, 1-15, 1-37, 2-1, 3-5, 3-6, 3-11, 3-12, 3-14, 3-15, 3-17, 5-3, 5-8, 5-11, 5-12, 5-13, 5-14, 5-15, 5-16, 5-17, 5-21, 6-8, 6-11, 6-14, 6-15, 6-16, 6-17, 6-18, 6-20, 6-21, 6-27, 6-31, 6-34, 6-40, 7-26, 7-30, 9-5, 9-17, 9-21, 9-27, 10-13, 10-15
pressurization, 5-10, 5-13
processing, 1-8, 1-21, 3-10, 6-6
production, 1-2, 1-16, 3-5, 9-21
ramp, 1-16
Rare Earth Minerals, 10-46
reactants, 1-1, 1-2, 1-3, 1-7, 1-8, 3-10, 6-14, 6-16, 6-17, 9-9, 9-10, 9-17
reformate, 3-14, 3-16, 6-35, 9-5
reformer, 1-6, 1-22, 1-37, 3-18, 6-33, 9-5, 9-14, 9-15, 9-16
reservoir, 5-7

resistivity, 1-13, 3-11, 6-12
seals, 5-7
separator plate, 1-8
shift, 3-11, 3-13, 5-10, 5-16, 6-1, 6-17, 6-19, 6-20, 6-21, 6-23, 6-29, 6-30, 6-34, 7-25, 7-31, 9-7, 9-9, 9-11, 9-13, 9-14, 9-16, 10-1
Siemens Westinghouse, xiii, 1-20, 1-21, 1-22, 7-26, 7-34, 7-35
sintering, 5-13, 6-10
siting, 1-15
solid oxide, xii, 1-3, 1-8, 10-12
space, 1-2, 1-11, 1-13, 1-15, 1-27, 1-28, 3-7, 5-10
stability, 1-4, 1-13, 3-7, 5-2, 5-4, 5-9, 6-3, 6-7
stack, 1-8, 1-16, 1-21, 1-22, 3-6, 3-7, 3-10, 3-11, 3-12, 3-14, 5-4, 5-5, 5-6, 5-7, 5-8, 5-9, 5-13, 5-20, 6-5, 6-7, 6-10, 6-12, 6-13, 6-14, 6-15, 6-18, 6-21, 6-22, 6-26, 6-32, 6-40, 7-27, 7-31, 7-35, 8-1, 9-2, 9-14, 9-18
stacking, 1-16
stationary, 1-13, 1-14, 1-17, 1-21, 1-22, 3-1, 3-4, 5-1
steam reforming, 5-16, 6-23, 6-33, 6-34, 6-35, 7-25, 9-12, 9-15
steam turbine, 1-12, 9-20
structure, 1-1, 1-3, 1-7, 1-8, 3-5, 3-10, 3-13, 5-3, 5-5, 6-3, 6-4, 6-6, 6-7, 6-9, 6-10, 6-11, 6-12, 6-31
sulfonic, 1-4, 3-7, 10-12
sulfur, 5-16, 5-17, 5-19, 6-10, 6-27, 6-30, 6-31, 6-32, 7-33
system efficiency, 1-5, 1-9, 1-12, 6-10
Tafel, 10-13
tape casting, 6-6, 6-7
temperature, 1-3, 1-4, 1-5, 1-7, 1-8, 1-9, 1-10, 1-11, 1-12, 1-13, 1-14, 2-1, 3-1, 3-4, 3-5, 3-10, 3-14, 3-15, 3-16, 5-2, 5-4, 5-10, 5-11, 5-12, 5-13, 5-17, 5-19, 6-3, 6-8, 6-9, 6-10, 6-12, 6-14, 6-18, 6-19, 6-20, 6-21, 6-25, 6-27, 6-33, 6-34, 7-1, 7-25, 7-26, 7-27, 7-29, 7-32, 9-9, 9-10, 9-15, 9-16, 9-17, 9-18, 9-20, 9-21, 9-22, 9-23, 9-27, 10-1, 10-13, 10-14, 10-15
thermodynamic, 2-1, 6-3, 7-26, 9-16, 9-17, 9-18
three phase interface, 1-2, 5-3
Tokyo Electric Power, 5-7, 5-23
Toshiba Corporation, 1-15, 5-1
vehicle, xii, 1-11, 1-26, 1-27, 1-28, 3-17
voltage, 1-7, 3-15, 3-16, 3-17, 5-2, 5-3, 5-5, 5-10, 5-12, 5-13, 5-15, 5-16, 5-17, 5-20, 6-5, 6-7, 6-12, 6-14, 6-15, 6-17, 6-18, 6-19, 6-20, 6-21, 6-22, 6-26, 6-30, 6-31, 6-32, 6-39, 6-40, 7-26, 7-27, 7-29, 7-30, 7-31, 7-32, 7-34, 7-35, 9-2, 9-5, 9-14, 10-13, 10-14
voltage efficiency, 7-32
Westinghouse, 1-38, 5-24, 7-35
zirconia, 7-35, 10-12